EVALUATION AND MODELING OF HIGH-VOLTAGE CABLE INSULATION USING A HIGH-VOLTAGE IMPULSE

By

Thomas Owen Bialek

A Dissertation
Submitted to the Faculty of
Mississippi State University
in Partial Fulfillment of the Requirements
for the Degree of Doctor of Philosophy
in Electrical Engineering
in the Department of Electrical and Computer Engineering

Mississippi State, Mississippi

May 2005

EVALUATION AND MODELING OF HIGH-VOLTAGE CABLE INSULATION USING A HIGH-VOLTAGE IMPULSE

By

Thomas Owen Bialek

Approved:

Dr. Stanislaw Grzybowski Professor of Electrical and Computer Engineering (Major Advisor and Director of Dissertation)	Dr. Nicholas H. Younan Professor of Electrical and Computer Engineering (Committee Member and Graduate Coordinator)
Dr. Noel Schulz Associate Professor of Electrical and Computer Engineering (Committee Member)	Dr. Herb Ginn Assistant Professor of Electrical and Computer Engineering (Committee Member)

Dr. Kirk Schulz
Dean of College of Engineering

Name: Thomas Owen Bialek

Date of Degree: May 7, 2005

Institution: Mississippi State University

Major Field: Electrical Engineering

Major Professor: Dr. Stanislaw Grzybowski

Title of Study: EVALUATION AND MODELING OF HIGH-VOLTAGE CABLE INSULATION USING A HIGH-VOLTAGE IMPULSE

Pages in Study: 289

Candidate for Degree of Doctor of Philosophy in Electrical Engineering

Failure of underground cable on San Diego Gas & Electric's electric underground distribution system is an ever increasing problem. While there are a great number of cable diagnostic techniques available, none lend themselves to both an averaged and location specific, on-line implementation.

This dissertation demonstrates the development of an on-line suitable technique that utilizes transients and Fast Fourier Transforms to determine a cable section's impedance magnitude and phase angle as a function of frequency. Simultaneously a theoretical model was developed to simulate various scenarios that an in-service cable might experience.

Significant effort was expended developing and optimizing the measurement and data analysis technique. This includes a statistical approach for comparing performance of different cable samples.

Both the preliminary and final tests demonstrated the superiority of the frequency domain analysis over comparisons in the time domain. With the effort to date, there appears to be three distinct results: good cable, degraded cable and damaged cable. These differences are statistically significant at the 95% confidence level. Additionally, there appears to be good agreement between the theoretical model and actual test results. Consequently, this measurement methodology continues to hold promise for future practical development.

DEDICATION

To Safa, my wife, for all the years of sacrifice and stress that pursuing this degree has entailed. I did not expect for this to take so long; however, the end is in sight and we will finally be able to take vacations. To my parents Albert and Joan for starting me on this path.

ACKNOWLEDGEMENTS

I thank Dave Geier and Caroline Winn of San Diego Gas & Electric for their continuing support of this effort and belief in the potential value of this work. I would also like to thank all the staff at the San Diego Gas & Electric's Skills Training facility, in particular, Carolyn Alkire and Bill Haden for providing me with the needed support to arrange for the test measurements. I also thank John Hunter and Stephen (Skip) Mattes for their perseverance in performance of the tests. I would also like to take the opportunity to thank Jim Cobb and Jose Cervantes work on performing the physical measurements on the cable test samples.

I would also express my gratitude to Dr. Stanislaw Grzybowski for his support, guidance and encouragement in pursuing this opportunity. I would also like to thank the members of the Committee: Dr. Nicholas H. Younan, Dr. Noel Schulz and Dr. Herb Ginn for their involvement in providing direction for this dissertation and reviewing the work.

TABLE OF CONTENTS

CHAPTER Page

CHAPTER Page

LIST OF TABLES

LIST OF FIGURES

FIGURE Page

FIGURE Page

FIGURE Page

FIGURE Page

FIGURE Page

FIGURE Page

FIGURE Page

FIGURE Page

FIGURE Page

FIGURE Page

FIGURE Page

FIGURE Page

FIGURE Page

FIGURE Page

FIGURE Page

FIGURE Page

FIGURE Page

FIGURE Page

FIGURE Page

FIGURE Page

FIGURE Page

FIGURE Page

CHAPTER I

INTRODUCTION

Statement of Problem

San Diego Gas & Electric, SDG&E, has in-service, underground distribution cables of varying age. Because San Diego Gas & Electric has kept excellent records, engineers have been able to fit cumulative distribution functions to available cable failure data. However, these records are incomplete since information on some manufacturers and locations are missing.

Since capital investments are under great scrutiny, all potential cable replacements must be assessed and prioritized. In an ideal world, the cumulative probability of failure versus time would be known for all cable manufacturers, vintages and sizes and it would then be an easy matter to prioritize cable replacement upon choosing the appropriate failure percentage. Unfortunately, cable replacement prioritization can not be so conveniently determined. The decision regarding failure rate to replace cables has other associated problems such as available manpower, budgets and manufacturing capabilities. Therefore, it is critical to develop some methodology that takes these factors into account and also looks at the remaining performance capabilities of the cable.

Remaining cable life can be estimated with diagnostic tests. The diagnostic methods currently available are divided into two categories: off-line or on-line methods. Generally, these categories are identical with respect to the parameters being measured. However, the bandwidth and range of the measurement is typically reduced in on-line methods since the measurement devices have limited bandwidth due to the physical realization of the equivalent circuits and external noise sources. Some of these test methods provide information on the average condition while others provide location specific information. In all instances the measured quantities are voltage and current as functions of applied voltage, time and frequency. These quantities are then mathematically transformed to provide the desired diagnostic criteria. As for off-line measurements, the bandwidth of the signals is typically orders of magnitude higher than on-line methods; however, one major disadvantage is the need for utility operations to take a forced outage and remove other extraneous equipment.

Independent Contribution

This new approach to performing cable diagnostic measurements offers the convenience to test and diagnose underground cables as current methods without the key limitations of current on-line and off-line methods. This methodology as currently developed provides a measure of the overall average condition of the cable one of the key measures of cable insulation deterioration. The method appears to be suitable for indicating the presence of partial discharges, although this area is not the subject of this dissertation. Additionally, these measurements have the potential to be developed into an on-line test method a key limitation of current off-line measurement techniques.

However, since the measurement method does not incorporate time domain reflectometry it is therefore incapable of pin pointing the exact location of defects and deteriorated insulation.

While most of the techniques utilized in this new cable diagnostics method have been developed in typically various off-line forms, the proposed combination of these techniques applied to switching transient measurements for cables and the statistical analysis is unique and has not been developed by any other researcher. Currently, utilities measure or model cable systems to determine the magnitude of switching transients, completely ignoring the additional information that is contained in the voltage and current waveforms. The statistical methods are necessary to determine whether or not the measurement variability is due to either cable insulation deterioration or manufacturing variability on the part of cable manufacturers.

Dissertation Scope

This dissertation reviews cable design issues including defects in Chapter II. Next a review of existing cable diagnostic measurements which discussed the pros and cons of the different measurements is included in Chapter III. Next the dissertation covers the development of a theoretical model and measurement methodology, which are detailed in Chapter IV, and demonstrations for new and field aged cables, which is detailed in Chapter V. Key results and analytical deductions are presented in Chapter VI.

As mentioned earlier, the measurement methodology utilizes Fast Fourier Transforms to generate a cable's impedance magnitude and phase angle versus frequency

spectrum. The voltage and current waveforms are measured with a voltage divider and Rogowski coil when a high voltage impulse is applied to various cables. The measured waveform data is digitized and transformed to produce the impedance frequency spectra. The data is then analyzed in a statistical manner to account for manufacturing variations. The results are evaluated to determine suitability of this method for detecting cable deterioration. However, as previously stated, partial discharge measurement capabilities and the transition to an on-line test method including field testing and verification are not part of the scope for this dissertation.

CHAPTER II

HV CABLE DESIGN AND THE EFFECT OF DEFECTS

HV Cable Design

Figure 2.1 exemplifies a typical 12 kV rated single conductor cable with a taped neutral. The conductor is stranded with the conductor material and diameter dependant upon the ampacity of required application. Immediately adjacent to the conductor is an extruded semi-conducting screen to create a uniform electric field. Next the polymeric insulation is extruded over the conductor shield. Currently the insulation is typically either tree-retardant cross-linked polyethylene, TRXLPE, or ethylene propylene rubber, EPR, and the insulation thickness depends upon the utility's system voltage and design characteristics. Next there is an extruded semi-conducting insulation shield, to control the electric field enhancement created by the taped shield neutral conductor. Newer construction cables have a concentric neutral conductor as opposed to a taped shield. Current manufacturing capabilities allow the cable manufacturers to extrude all three layers simultaneously.

As might be excepted defects can be introduced or created during the extrusion process. Figure 2.2 which is a cross section portion of a cable provides a physical illustration of the type of defects and provides reference locations within the cable. An incomplete list of defects which can be introduced or created includes: a loose semi-

conductive screen, bubbles caused by gas evolution in the conductive screen, cavities due to shrinkage or gas-formation in the insulation, defects in the core screen, inclusion of foreign particles that separate gases, projections or points on the semi-conductive screen, splinters and fibers. All the defects affect the local electric field and in the presence of moisture, an applied electric field and given time can lead to the formation water trees. Figure 2.3 shows a cross section of a cable with a vented water tree growing from a protrusion of the conductor screen into the insulation. The water tree grew into an electrical tree which subsequently became an electrical failure site. The deterioration of the cable insulation over time is an important issue for utilities and their ability to provide electricity to their customers. Diagnostic testing may be performed on a cable section in an effort to determine the condition of the insulation and prevent an unplanned outage.

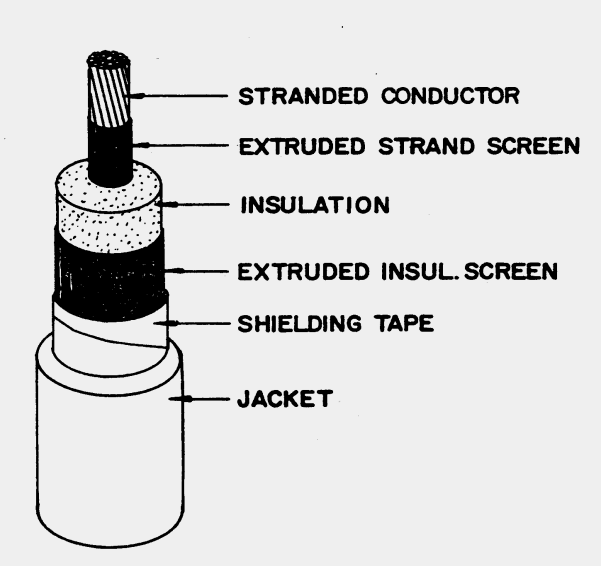

Figure 2. 1 Typical 12 kV, Single Conductor Cable with Taped Neutral

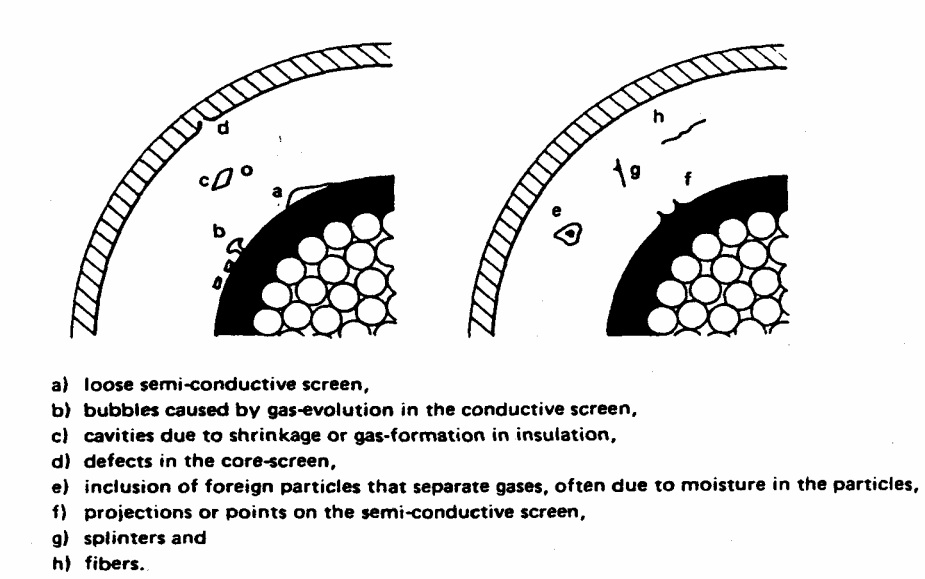

Figure 2. 2 Defects in Extruded Cable Dielectrics

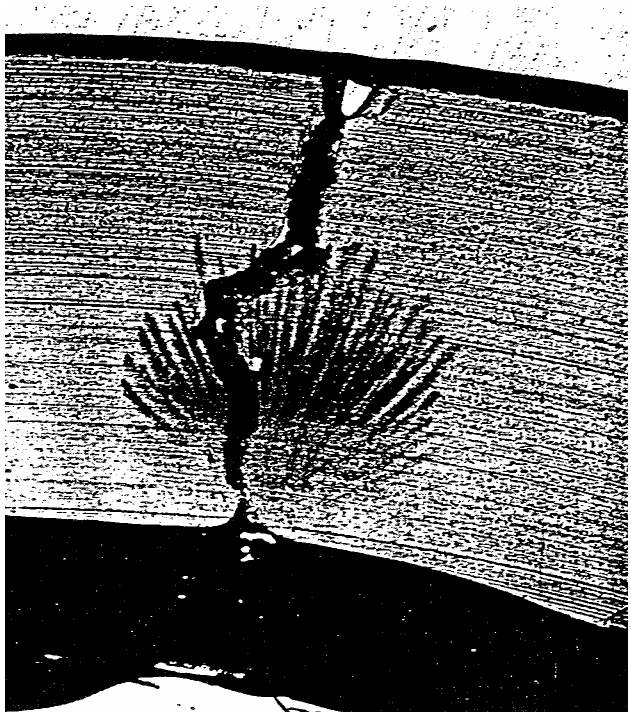

Figure 2. 3 Vented Water Tree Leading to Electrical Failure – Courtesy of SDG&E

Voltage Distribution in a Polymeric Cable

With the introduction of defects into the cable insulation, it is important for a diagnostic test that the voltage distribution and electric stresses in the cable under test be identical to what occurs in the field otherwise it will be necessary to correlate the test method with field experience. An example calculation of the electric stress and voltage distribution demonstrates depending upon the type of applied voltage that excessive voltage and electric stress can be impressed upon defects which may result in electrical failure locations at which the cable would not fail in service and these failures may be due to a number of other failure mechanisms. The results from such testing would obscure the goal of the test program, an estimation of remaining life.

Figure 2.4 displays the equivalent cross section of the cable in Figure 2.1 with a worst case, circumferential air bubble, 100 μm thick, throughout the insulation. The dimensions shown in Figure 2.4 are typical for a single conductor cable with 10 mm outer diameter, OD, Aluminum conductor and 5 mm of XLPE insulation.

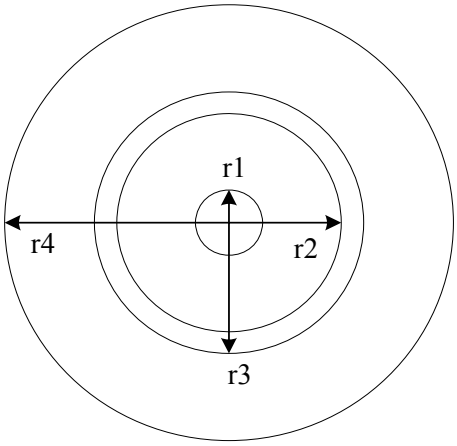

r1=5mm, r2=7.5mm, r3=7.6mm, r4=10mm

Figure 2. 4 Cross Section of Single Conductor Cable

Calculation of the electric field and voltage distribution for a three-layer, coaxial dielectric system is given in Appendix A. The final complete expressions for the maximum electric field within each dielectric layer are given in equations 2-1 to 2-3 respectively. Next the equations for the DC case are presented in equations 2-4 to 2-6. Lastly, the equations at 60 Hz are presented in 2-7 to 2-9.

$$E_{1max} = \frac{V}{r_1 \cdot \left[\ln\left(\frac{r_2}{r_1}\right) + \ln\left(\frac{r_3}{r_2}\right) \cdot \frac{\sqrt{(\gamma_1)^2 + (\omega \cdot \varepsilon_o \cdot \varepsilon_1)^2}}{\sqrt{(\gamma_2)^2 + (\omega \cdot \varepsilon_o \cdot \varepsilon_2)^2}} + \ln\left(\frac{r_4}{r_3}\right) \cdot \frac{\sqrt{(\gamma_1)^2 + (\omega \cdot \varepsilon_o \cdot \varepsilon_1)^2}}{\sqrt{(\gamma_3)^2 + (\omega \cdot \varepsilon_o \cdot \varepsilon_3)^2}} \right]} \quad (2\text{-}1)$$

$$E_{2max} = \frac{V}{r_2 \cdot \left[\ln\left(\frac{r_2}{r_1}\right) \cdot \frac{\sqrt{(\gamma_2)^2 + (\omega \cdot \varepsilon_o \cdot \varepsilon_2)^2}}{\sqrt{(\gamma_1)^2 + (\omega \cdot \varepsilon_o \cdot \varepsilon_1)^2}} + \ln\left(\frac{r_3}{r_2}\right) + \ln\left(\frac{r_4}{r_3}\right) \cdot \frac{\sqrt{(\gamma_2)^2 + (\omega \cdot \varepsilon_o \cdot \varepsilon_2)^2}}{\sqrt{(\gamma_3)^2 + (\omega \cdot \varepsilon_o \cdot \varepsilon_3)^2}} \right]} \quad (2\text{-}2)$$

$$E_{3max} = \frac{V}{r_3 \cdot \left[\ln\left(\frac{r_2}{r_1}\right) \cdot \frac{\sqrt{(\gamma_3)^2 + (\omega \cdot \varepsilon_o \cdot \varepsilon_3)^2}}{\sqrt{(\gamma_1)^2 + (\omega \cdot \varepsilon_o \cdot \varepsilon_1)^2}} + \ln\left(\frac{r_3}{r_2}\right) \cdot \frac{\sqrt{(\gamma_3)^2 + (\omega \cdot \varepsilon_o \cdot \varepsilon_3)^2}}{\sqrt{(\gamma_2)^2 + (\omega \cdot \varepsilon_o \cdot \varepsilon_2)^2}} + \ln\left(\frac{r_4}{r_3}\right) \right]} \quad (2\text{-}3)$$

For DC conditions $\omega=0$ therefore

$$E_{1max} = \frac{V}{r_1 \cdot \left(\ln\left(\frac{r_2}{r_1}\right) + \ln\left(\frac{r_3}{r_2}\right) \cdot \frac{\gamma_1}{\gamma_2} + \ln\left(\frac{r_4}{r_3}\right) \cdot \frac{\gamma_1}{\gamma_3} \right)} \quad (2\text{-}4)$$

$$E_{2max} = \frac{V}{r_2 \cdot \left(\ln\left(\frac{r_2}{r_1}\right) \cdot \frac{\gamma_2}{\gamma_1} + \ln\left(\frac{r_3}{r_2}\right) + \ln\left(\frac{r_4}{r_3}\right) \cdot \frac{\gamma_2}{\gamma_3} \right)} \quad (2\text{-}5)$$

$$E_{3max} = \frac{V}{r_3 \cdot \left(\ln\left(\frac{r_2}{r_1}\right) \cdot \frac{\gamma_3}{\gamma_1} + \ln\left(\frac{r_3}{r_2}\right) \cdot \frac{\gamma_3}{\gamma_2} + \ln\left(\frac{r_4}{r_3}\right) \right)} \quad (2\text{-}6)$$

For AC conditions $\omega\varepsilon_o\varepsilon_r >> \gamma$

$$E_{1max} = \frac{V}{r_1 \cdot \left(\ln\left(\frac{r_2}{r_1}\right) + \ln\left(\frac{r_3}{r_2}\right)\cdot\frac{\varepsilon_1}{\varepsilon_2} + \ln\left(\frac{r_4}{r_3}\right)\cdot\frac{\varepsilon_1}{\varepsilon_3}\right)} \quad (2\text{-}7)$$

$$E_{2max} = \frac{V}{r_2 \cdot \left(\ln\left(\frac{r_2}{r_1}\right)\cdot\frac{\varepsilon_2}{\varepsilon_1} + \ln\left(\frac{r_3}{r_2}\right) + \ln\left(\frac{r_4}{r_3}\right)\cdot\frac{\varepsilon_2}{\varepsilon_3}\right)} \quad (2\text{-}8)$$

$$E_{3max} = \frac{V}{r_3 \cdot \left(\ln\left(\frac{r_2}{r_1}\right)\cdot\frac{\varepsilon_3}{\varepsilon_1} + \ln\left(\frac{r_3}{r_2}\right)\cdot\frac{\varepsilon_3}{\varepsilon_2} + \ln\left(\frac{r_4}{r_3}\right)\right)} \quad (2\text{-}9)$$

Utilizing the dimensions in Figure 2.4, one can now solve equations 2-1 through 2-9 to determine the maximum electric fields and voltages across the layers. In solving the equations the values of γ_1, γ_2 and γ_3 are 10^{-14}, 10^{-18} and 10^{-14} S/m respectively. Additionally, the values of the dielectric constants ε_1, ε_2 and ε_3 are 3.2, 1 and 3.2 respectively. The results for the exact, DC and AC equations are shown in Tables 2-1 and 2-2 and plotted in Figures 2.5 and 2.6. The legend descriptors define which curves in the figures correspond to the various equations. The calculated values for the 0.1 Hz case were obtained by utilizing the exact equation. These results apply to the application of 6.9 kV_p DC, 6.9 kV_{rms} 0.1 Hz and 6.9 kV_{rms} 60 Hz voltages from the conductor to the shield. Tables 2.1 and 2.2 clearly demonstrate that testing a cable which is normally

energized with a 60 Hz voltage with DC will result in the dielectric layer 2 being drastically overstressed, causing a breakdown of the air gap and invalidating any correlation to operating conditions. Figures 2.5 and 2.6 show the voltage and electric field respectively as a function of radial distance from the conductor as calculated in Tables 2.1 and 2.2 but do not include the 0.1 Hz values since they are essentially the 60 Hz and exact values. The circumferential bubble is shown in the figures starting at a radius of 7.5 mm from the center of the conductor.

Table 2.1

Applied Voltage 6.9 kV_{rms} or 6.9 kV_{DCp}
Maximum Calculated Electric Stress with Different Types of Voltages Waveforms

Field in kV/mm	Exact Equation	DC Equation	0.1 Hz	AC Equation
E_{1max}	1.9184	1.0408×10^{-2}	1.9182	1.9184
E_{2max}	4.0296	69.387	4.0987	4.0296
E_{3max}	1.2621	6.8474×10^{-3}	1.262	1.2621

Table 2.2

Applied Voltage 6.9 kV_{rms} or 6.9 kV_{DCp}
Calculated Voltage Across Dielectric Layers with Different Types of Applied Voltages

Voltage in kV	Exact Equation	DC Equation	0.1 Hz	AC Equation
V1	3.8892	0.0211	3.889	3.8892
V2	0.4066	6.8928	0.4072	0.4066
V3	2.6324	0.0143	2.6322	2.6324

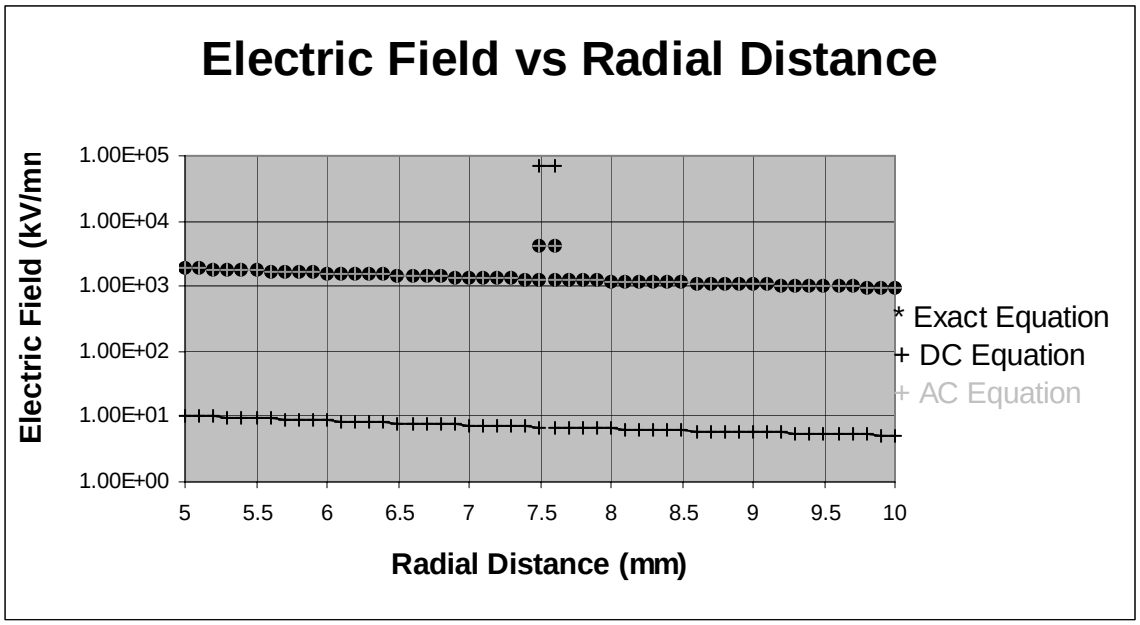

Figure 2. 5 Electric Field within Cable with Defect

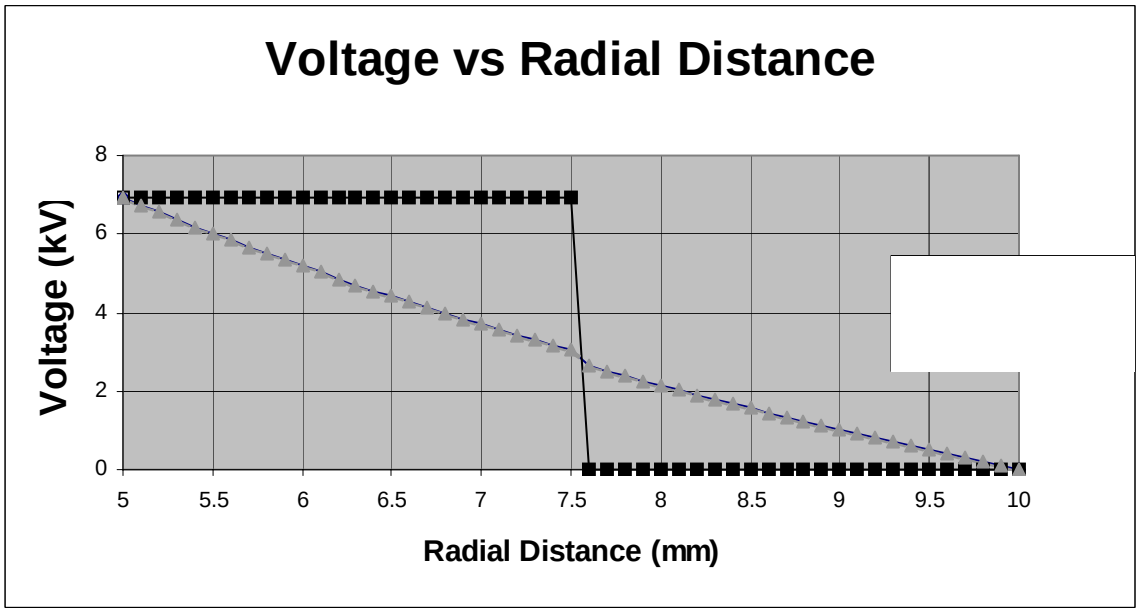

Figure 2. 6 Voltage Distribution within Cable with Defect

CHAPTER III

DISCUSSION OF EXISTING CABLE DIAGNOSTIC METHODS

Introduction

Chapter II explored cable design issues, the role defects play in degradation of the cable insulation and examined the impact of different types of voltage waveforms on the electric stress and voltage distribution within a defective cable dielectric that had a circumferential air bubble. With respect to performance of a cable installed in a utilities' underground distribution system, a diagnostic test method that can prioritize cables for replacement is a useful tool. While there is a variety of existing diagnostic test methods for evaluating the condition of an electrical equipment insulation system, some are more applicable to testing cables than others. There are two types of test methods: the cable system is de-energized and removed from service (off-line) and the cable remains in-service energized at operating system voltage (on-line). This chapter discusses the majority of cable diagnostic methods and the pros and cons of these methods based upon a literature review.

Alternating Current Testing 60 Hz

This diagnostic method creates the voltage and electric stress distributions within a cable dielectric that is similar to most conditions as would occur with a cable system energized in-service. Typically, the applied voltage is increased to a value above

operating voltage to ensure the cable insulation is adequate for the cable to be returned to service. This test can be combined with many of the other diagnostic measurements discussed below. If the test utilizes the actual system as the voltage source, then any additional diagnostic measurements can be performed on-line without experiencing a system outage.

The disadvantages of this method are the large capacitive current requirements for long cable runs in an off-line test. However, with a resonant test set one can overcome the capacitive current issues. This type of test is difficult to perform in the field and requires an equipment outage. In assessing the insulation condition voltages in excess of system operating voltage may be applied which may result in an insulation electrical failure occurring due to mechanisms which would not have occurred if the cable system test voltage was limited to operating voltage. A section of cable can also be subjected to a voltage that is increased in steps until failure occurs. This AC breakdown voltage is compared to results from new cables; however, interpretation of the results from the step stress test is problematic since the correlation to life time at operating voltage has not been definitively determined. An additional problem is that the difference in AC breakdown voltages between 30 and 40 years is negligible which makes this diagnostic method of limited value despite its wide applicability [53, 54].

Alternating Current Testing 0.1 Hz

This diagnostic method creates nearly the same voltage and electric stress distributions within a cable dielectric that are similar to most conditions as would occur with a cable system energized in-service. Typically, the applied voltage is also increased to a value above operating voltage to ensure the cable insulation is adequate for the cable to be returned to service. This test can be also combined with many of the other diagnostic measurements discussed below. Additionally, the test supply has smaller capacitive current requirements due to the 0.1 Hz operation which makes it small lightweight and portable [1,5,11,18].

However, there are some disadvantages which need to be considered. This method can only be utilized in an off-line test. The test time will also be longer to apply the same number of cycles which is important for noise reduction techniques. There are also problems correlating 0.1 Hz results to AC tests performed at 60 Hz since the slower voltage variation with time can affect space charge and electron movement within the cable and ultimately the cable breakdown voltage [1,27].

Direct Current Testing

The main advantages of this diagnostic method are that the equipment is small, lightweight and portable, the familiarity with field personnel with the equipment since it has been almost universally applied to evaluating all electrical equipment and the equipment is usually readily available. Because of these advantages there are proponents of DC cable testing today [15]. Typically, the applied voltage is increased to a value above operating voltage to ensure the cable insulation is adequate for the cable to be

returned to service. The leakage current is also measured and compared to that of a new cable either as a single point measurement or as a function of applied voltage.

This diagnostic method has major disadvantages. As shown in Chapter II for polyethylene based dielectrics, DC voltages will result in a voltage and electric field distribution within a dielectric with a circumferential air bubble such that there would be electrical failures of the air gap. There are also substantial published accounts of cable electrical failures occurring at locations which would be unaffected by service at 60 Hz [1,3,5,15,18,20]. DC testing, including thumping, also results in the injection of space charge into the insulation which results in worsened field performance under certain conditions [1,5,15,18]. Lastly this test method is an off-line test which requires an system outage.

Applied Combination Waveform Testing

The application of a variety of combined waveforms has been explored by many organizations as an alternative diagnostic test. These combination waveforms include but are not limited to a damped capacitive discharge test with an oscillation frequency of approximately 50 to 500 Hz and an AC 60 Hz voltage with a superimposed DC voltage [8,11,13,16,17,55]. The damped capacitive discharge test must be performed with the cable de-energized and removed from service although it is possible to modify this test for on-line application.

The superimposed DC test has successfully been implemented in Japan for a number of years as an on-line test for ungrounded, cross-linked polyethylene, XLPE, cable system applications [8,11,16]. A small DC voltage is applied between the cable

concentric neutral and the phase conductor. The DC leakage current through the cable insulation is monitored continuously. In general, the test results have been successful in determining cable deterioration due to water trees which causes an increased DC leakage current.

The major disadvantage for most applied combination diagnostic tests is the requirement for additional test equipment and more complex test arrangements. There is also a limited amount of experience testing cables with the capacitive discharge diagnostic methods. Currently, the damped capacitive discharge test is also an off-line test requiring system outages. While the superimposed DC test utilized by the Japanese is currently being performed on-line, it is only applicable to utilities with ungrounded underground distribution systems.

Cable Physical Measurements

Some utilities and researchers are strong proponents of physical measurements as a diagnostic test. A utility may chose to randomly test aged, in-service, high-voltage distribution cables or cable sections from the vicinity of an electrical failure which resulted in an electrical power outage to customers. Sections of a cable are dissected and then these physical measurements of insulation thickness, semi-conducting shield adhesion and other conductor measurements are performed to determine adherence to cable manufacturing specifications. Additionally, cross sections of the cable are dyed with a methylene blue dye and under a microscope the dimensions and number of protrusions, contaminants and water trees of all types are counted and classified. The microscopic measurements are once again compared to manufacturing specifications as

well as physical measurements of areas immediately adjacent to an electrical failure site. This physical measurement provides direct evidence of water trees in the insulation if they are present and there have been numerous studies on the effect of tree length on AC breakdown strength. Other chemical tests such as degree of polymerization and oxidation index can be performed. The goal of the physical measurements test is to obtain a subjective rating of the in-service cables' insulation condition.

The most obvious disadvantage of such a method is its destructive nature. The test is also conducted off-line requiring a system outage. Additionally, the physical measurement results are only valid for the cable section dissected and measured. Without performing a costly and time consuming random statistical sampling method there is no guarantee that even if either water trees of a certain size or type or other defects are found in the test sample that an adjacent run of cable will also have similar physical measurement results or vice versa.

Capacitance and Dissipation Factor Bridge Measurements

This measurement is performed with AC voltages typically in addition to a applied voltage withstand test. A standard capacitor and bridge are required to measure the test object capacitance and losses. The measurements can be performed as a function of applied voltage to provide additional information regarding the cable insulation condition. The advantages of this measurement include an accurate characterization of the cable capacitance and losses. Additionally, the results give an indication of average condition of the cable. Variants of this method can be performed both off-line and on-line [9].

There are also numerous disadvantages associated with this measurement. Foremost, there are difficulties associated with performing this test in the field which must be performed off-line with the test object must be removed from service. The measurement because it present an averaged result of the entire cable is not sensitive to localized defects within the insulation [3].

Partial Discharge Measurements

There has been much emphasis placed on this method in the past few years and there are currently three companies offering partial discharge measurement services. Testing can be performed at both 60 and 0.1 Hz. However, at lower frequencies the test time is longer in comparison to power frequency tests. This method measures electrical discharges associated with localized defects which are located with time domain reflectometry [12,21,22,23]. This method can be performed both off and on-line [12]. The measurements do not provide any indication of water tree degradation which is typically the precursor to any electrical discharge activity [3]. When significant electrical discharges do occur within cable insulation, electrical failure occurs very quickly making it difficult to find cable with partial discharges. Additionally, the entire cable system is tested including joints and terminations which tend to be the sites of most discharges [22].

Dielectric Spectroscopy Measurements

This method is nothing more than capacitance and dissipation factor over a range of frequencies to provide the complex dielectric constant amplitude and phase

response[2]. The test can either be performed in the frequency domain or in the time domain. Low frequency dielectric spectroscopy, from 0.001 to 100 Hz, gives good indication of water tree impacts based upon a limited amount of testing [2, 25,28,29,47]. This test method is currently available off-line but suitable for on-line tests [25].

Harmonic Analysis Measurements

Research work has shown that water treed cables tend to exhibit non-linear impedance behavior which manifests itself as a 60 Hz waveform with higher harmonic content [10,14,26,33]. The harmonic content not only provides an indication of degree of water treeing but also of the water tree length [26]. This method is currently available off-line but could clearly be developed into an on-line test [10].

DC Polarization Measurements

There are many distinct measurement methods associated with the application of a DC step voltage to a cable. An incomplete list includes the return voltage test, isothermal relaxation current analysis, and space charge measurement [19, 24, 31, 32]. Most of these methods are categorized by long test times since the DC voltage must be applied and then the cable shorted to ground. While most of these tests claim to provide an indication of degree of water tree degradation, they suffer from poor reproducibility since the cable typically has to be completely discharged prior to the DC voltage application. All of these tests must be performed off-line necessitating a system outage.

Literature Review Conclusions

The above summary of existing diagnostic tests and measurement methods demonstrates the response to an urgent industry need. However, it is clear from a theoretical perspective that the diagnostic technique must produce the same voltage distribution within the cable as occurs in service otherwise one risks unnecessarily replacing good cable. It is also clear that the effect of water trees, typically the precursor to failure, results in a modification of capacitance and resistance values of the cable impedance network which may necessitate the use of multiple diagnostics to detect average as well as localized cable system changes [3].

Test equipment can be expensive and bulky which typically makes performing diagnostic tests not cost effective. Parts of the increased costs are due to long setup times and for some tests long test times. Therefore, any diagnostic test which might be performed on a widespread basis should be performed as a on-line measurement, since it is too costly to take system outages.

An issue with any test is the measurement sensitivity required to discern differences between cables. The ambient noise levels in the field are high; therefore, there is need for various signal analysis techniques like those which have been developed for partial discharge measurements. There is also a need to examine the entire cable system, since a failure of cable system defined as failure of any components.

It is clear from the literature that substantial effort has developed test methods which can examine cable properties, both bulk and localized. It is also clear that one test alone is insufficient to provide clear evidence that a particular cable run should be

replaced. Based upon economics, it is usually more effective to replace the cable once a failure occurs. Therefore, any diagnostic test and measurement methods to be successful and utilized across a system must be low-cost and be able to be performed on-line. On-line test methods are a necessity since the costs associated with an off-line test can negate the value of the test.

Based upon the literature review of the existing diagnostic test and measurement methods conducted as part of this dissertation, it is claimed by various authors that the tests and methods demonstrate measuring a cable's properties as a function of frequency can discriminate between new and water treed cables on an average basis and can even track the length of water trees [2,10,14,25,26,28,29,33,47]. These methods can be adapted to on-line measurement [9,10]. Location specific techniques such as partial discharge are currently being performed on line [12]. In order to provide a conclusive decision on the state of a cable it is necessary to perform a multitude of tests and yet this should be performed on-line to be cost effective [3].

Proposed Solution

This dissertation demonstrates promising results for a potentially new, more effectual, cable diagnostics method with the potential capability to develop into an on-line diagnostic test and measurement method. This method utilizes Fourier Transforms to generate the impedance magnitude and phase angle of a cable section versus frequency (impedance magnitude and phase angles spectra) from voltage and current measurements of the cable section response to an applied high-voltage impulse; the resulting data is then analyzed in a statistical manner to account for manufacturing variability.

CHAPTER IV

THEORY AND MODELING

Concept

As shown in Figure 4.1, this dissertation proposes to measure high-voltage impulses created by switching a charged capacitor into a de-energized cable system with voltage dividers and a Rogowski coil which provide analog signals to a digital storage oscilloscope. These waveform forms are digitized and the data is transferred to a personal computer where Fast Fourier Transforms, FFTs, are performed to transform the time domain voltage and current waveforms into the frequency domain. The Fast Fourier Transform, FFT, of a digitized time domain signal produces both the amplitude and phase angle in the frequency domain with a continuum of frequency components (magnitude and phase angle spectra). Dividing the transformed current by the transformed voltage will allow derivation of the transfer function. Dividing the transformed voltage by the transformed current will produce the impedance magnitude and phase angle as function of frequency.

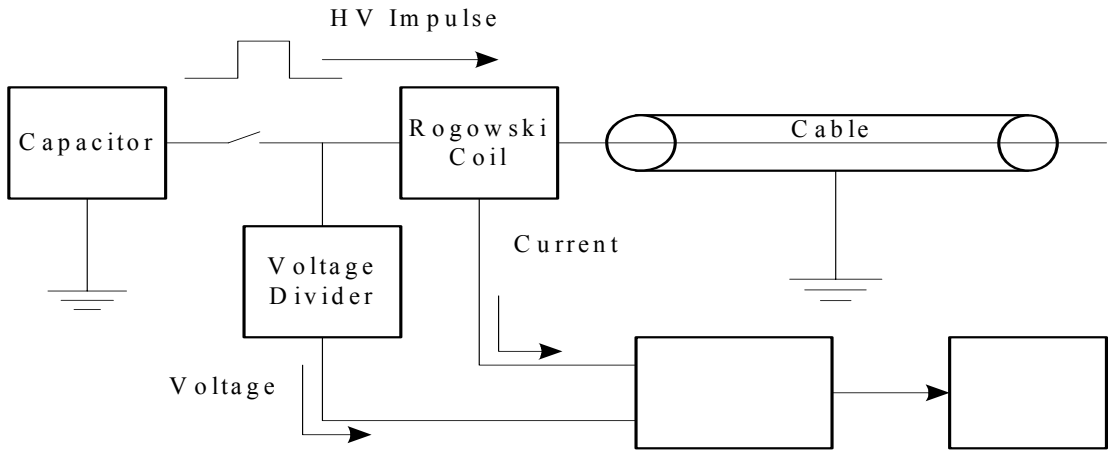

Figure 4. 1 Dissertation Concept Block Diagram

The transfer function and dielectric spectroscopy diagnostic measurements which are available today can be utilized with some modifications to subsequently compare new and field-aged cables to discern which cables are in need of replacement. This diagnostic test and measurement method could take the place of other existing methods since the Fourier Transform of a switching surge contains infinite number of frequencies in the frequency domain. If the magnitudes of frequency components of the surge are high enough it may also be possible to perform localized partial discharge measurements; however, this is not addressed at length in this program.

Next a short summary of transfer function and dielectric spectroscopy measurements is provided to demonstrate the current use of these measurements These summaries provide a bridge between this dissertation, existing practices, the theory behind the proposed methodology and finally the equivalent circuit modeling of the cable system under test.

Transfer Function and Dielectric Spectroscopy

The transfer function is a tool utilized for impulse testing of transformers where the impulse voltage and current measurements at reduced voltage are compared to the same measurements at rated voltage and if abnormalities exist then the transformer fails the test [34-36, 38-44]. The impulse testing measurements need to be capable of detecting single turn winding shorts caused by insulation failure [39]. This test is a comparison method which requires sensitive measurements unaffected by deviations in the applied voltage waveform [40].

The transfer function, the impulse current divided by impulse voltage, gives the transformer transadmittance as function of frequency in the frequency domain [39]. The transfer function is unaffected by variations in the applied voltage impulse waveform and allows reduced and full impulse waveforms to compared by superimposing one on the other in the frequency domain [35, 37, 39, 43]. In this comparison, changes in peak location with respect to frequency indicate a change in the impedance parameters of the transformer being tested [39, 41]. However, when changes in peak magnitude for a given frequency occur, this indicates partial discharge within the winding which is not a reason to fail the impulse test [39, 41, 43].

In order to calculate the transfer function, both the impulse voltage and current waveforms are recorded by a digital storage oscilloscope with a minimum of 10 bit vertical resolution and a sampling speed of at least 10 megasamples per second.[40] Next the stored waveforms are converted into the frequency domain utilizing a FFT. The current waveform as a function of frequency is divided by the voltage waveform as a

function of frequency to obtain the transfer function [41]. The FFT process requires a data reduction and filtering to produce the waveforms in the frequency domain with a minimum amount of noise [35, 39, 40, 41, 43-46].

The use of transfer function as an on-line measurement is currently being investigated with some success [34,35]. It is recognized although that the point on wave where the switching transient occurs is a random phenomena. Additionally, the actual load connected to the system is also a random variable. Therefore, the data can only be interpreted with statistical methods [34,35].

The measurement of a two terminal impedance at one frequency can not distinguish between a resistor and capacitor connected in series or parallel; however, measuring at many frequencies exposes the physical RC arrangement. Dielectric spectroscopy is the measurement of capacitance and dissipation factor, or impedance magnitude and phase angle, as a function of frequency. It has been shown to successful in detecting the presence of water trees [2, 25, 29, 47]. This measurement can be performed by either applying a voltage waveform and sweeping the frequency spectrum or by applying a step function and performing a Fast Fourier Transform [29, 32, 47]. It may be possible to obtain the same results by measuring cable switching transients and then applying a Fast Fourier Transform to the measured time domain waveforms to obtain the voltage and current waveforms in the frequency domain.

Step Response of a Simplified Cable Model

In order to be confident that the proposed diagnostic test and measurement method will provide an adequate continuum of frequency components in the frequency domain it is necessary to perform a theoretical evaluation of a cable system subject to step voltage. The first step is to develop solutions for the response of a cable model to a step voltage in the time domain and to then transform them into the frequency domain.

As shown in Figure 4.2, a cable system can be modeled a lumped parameter RLC circuit where the components are connected in series. The solution for current flowing due to a step voltage resulting from the closure of the switch can be derived by utilizing Laplace Transforms [52]. The complete derivation is shown in Appendix B, while the final equations for a series connected RLC arrangement are shown below. The first equation is the general solution for a RLC circuit and the remaining equations are reductions for the three roots of the second order differential equation which are shown below.

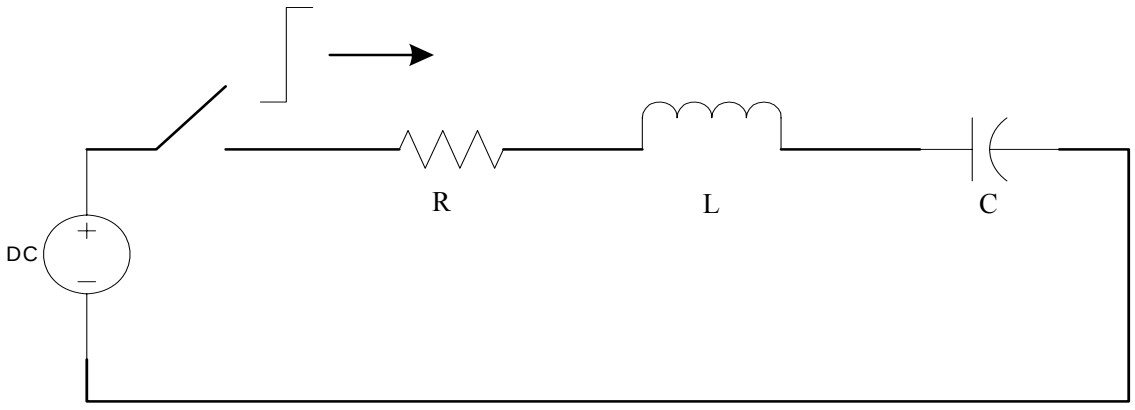

Figure 4. 2 Series Connected Lumped Circuit Model of Cable

General equation

$$I(t) = \frac{V}{L\cdot\sqrt{\frac{1}{(\tau_s)^2}-\frac{4}{T^2}}}\cdot\left(e^{a\cdot t}-e^{b\cdot t}\right) \tag{4-1}$$

Where: I(t)=the current as a function of time

$\lambda=Zo/R$, $\tau_s=L/R$, $Zo=\sqrt{(L/C)}$, $T^2=LC$

$$a = \frac{-1}{2\cdot\tau_s}+\frac{1}{2}\cdot\sqrt{\frac{1}{(\tau_s)^2}-\frac{4}{T^2}}$$

$$b = \frac{-1}{2\cdot\tau_s}-\frac{1}{2}\cdot\sqrt{\frac{1}{(\tau_s)^2}-\frac{4}{T^2}} \tag{4-2}$$

$\lambda < ½$, over-damped response

$$I(t) = \frac{V\cdot 2\cdot\tau_s\cdot e^{\frac{-t}{2\cdot\tau_s}}}{L\cdot\sqrt{\left(1-4\cdot\lambda^2\right)}}\cdot\sinh\left(\sqrt{1-4\cdot\lambda^2}\cdot\frac{t}{2\cdot\tau_s}\right) \tag{4-3}$$

$\lambda > ½$, under-damped response

$$I(t) = \frac{V\cdot 2\cdot\tau_s\cdot e^{\frac{-t}{2\cdot\tau_s}}}{L\cdot\sqrt{4\cdot\lambda^2-1}}\cdot\sin\left(\sqrt{4\cdot\lambda^2-1}\cdot\frac{t}{2\cdot\tau_s}\right) \tag{4-4}$$

$\lambda = ½$, critically-damped response

$$I(t) = \frac{V}{L}\cdot t\cdot e^{\frac{-t}{2\cdot\tau_s}} \tag{4-5}$$

Fourier Transforms of the Step Response of a Simplified Cable Model

Fourier transforms of the step response in the time domain provides the frequency domain solution for the current. For the series connected RLC circuit, the switching surge Fourier Transform of the current is given by Equations 4-6 to 4-7 for each root along with a generic plot of the magnitude of current versus frequency. In each equation $\lambda=Zo/R$, $Zo=1/\sqrt{(LC)}$ and $\tau_s=L/R$. The complete derivation of the Fourier Transform for all three roots is given in Appendix C. For each solution, the magnitude of current is symmetric around $\omega=0$. These plots demonstrate that from a theoretical perspective it is possible to obtain whatever frequency is desired for a diagnostic test.

For $\lambda< ½$ over damped case

$$I(j\omega) = \frac{V\cdot\tau_S}{L\cdot\sqrt{\left(1-4\cdot\lambda^2\right)}}\cdot\left[\frac{1}{\frac{\left(1-\sqrt{1-4\cdot\lambda^2}\right)}{2\cdot\tau_S}+j\cdot\omega}-\frac{1}{\frac{\left(1+\sqrt{1-4\cdot\lambda^2}\right)}{2\cdot\tau_S}+j\cdot\omega}\right] \tag{4-6}$$

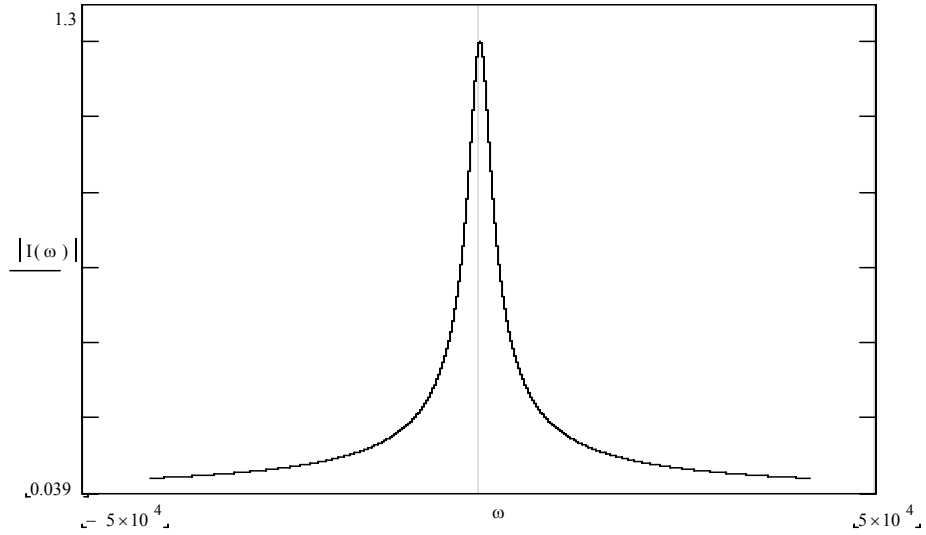

Figure 4. 3 Over Damped Response

For $\lambda > ½$ under damped case

$$I(j\omega) = \frac{V}{L} \cdot \frac{1}{\left[\left(\frac{1}{2 \cdot \tau_s} + j \cdot \omega\right)^2 + \left(\frac{\sqrt{1 - 4 \cdot \lambda^2}}{2 \cdot \tau_s}\right)^2\right]} \tag{4-7}$$

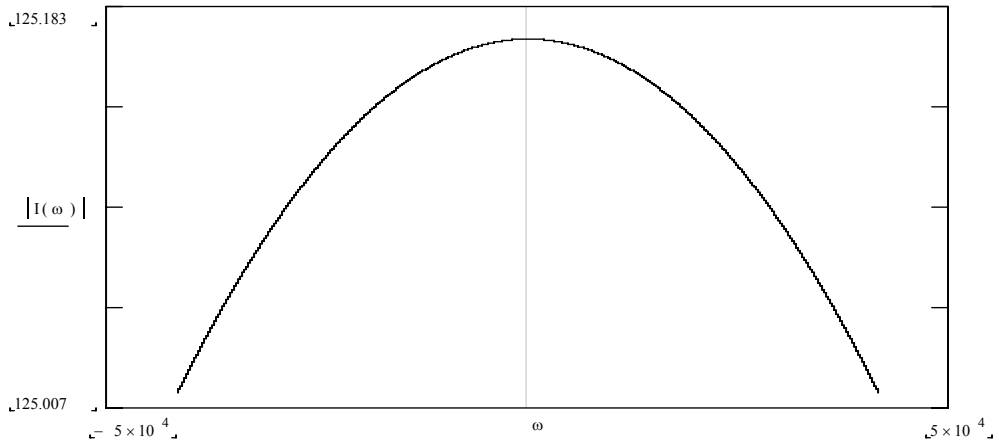

Figure 4. 4 Under Damped Response

For $\lambda = ½$ critically damped case

$$I(j\omega) = \frac{V}{L} \cdot \frac{1}{\left(\frac{1}{2 \cdot \tau_s} + j \cdot \omega\right)^2} \tag{4-8}$$

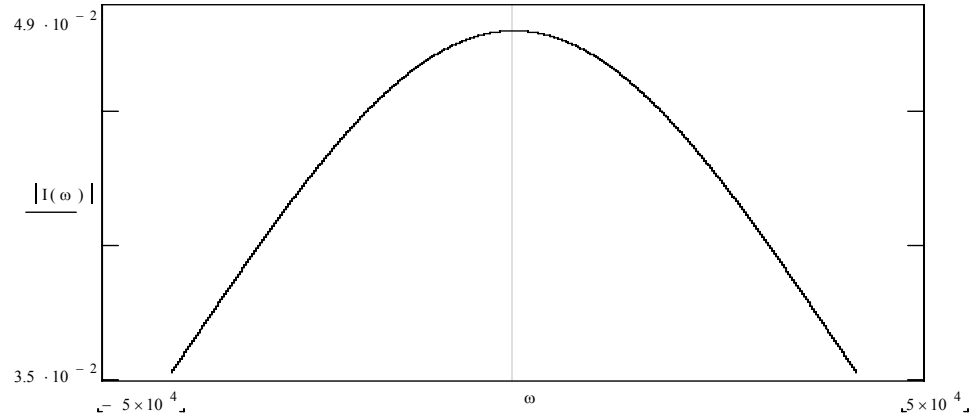

Figure 4. 5 Critically Damped Response

Development and Evaluation of an Equivalent Cable Model

The above solutions for the Fourier Transform of the step response current demonstrate that there are an adequate number of frequencies present to calculate diagnostic parameters such as capacitance and dissipation factor, or impedance and phase angle, and the transfer function as a function of frequency. The next step in the theoretical development is to evaluate the performance of field aged cable from a cable length, conductor size and insulation type and thickness perspective with a theoretical cable model that can be utilized as a proxy.

With this model it is possible to examine the effects of water tree degradation, the loss of the cable concentric neutral and the role that the length, conductor and insulation type have on a cable. The goal of a successful model is to be able to explain the impact of these parameters such that test results on known good cable can be modified to provide a baseline for any other piece of cable that would be tested.

Figure 4.6 a) shows the equivalent circuit of a length typical underground polymeric distribution cable and Figure 4.6 b) shows the equivalent physical circuit with a voltage source connected between the conductor and concentric neutral. The cable can be modeled by an impedance matrix where the capacitance, resistance and inductance of the cable is subdivided into discrete sections. Impedances Z5 and Z14 are the equivalent conductor resistance and inductance for the length of the cable being modeled. Impedances Z9 and Z18 are the equivalent concentric neutral resistance and inductance for the length of the cable being modeled. Impedances Z1, Z2, Z3,Z4, Z10, Z11, Z12, Z13, Z19, Z20, Z21 and Z22 are a parallel capacitance and resistance combination that

represents the insulation impedance between the conductor and the concentric neutral. Impedances Z6, Z7, Z8, Z15, Z16 and Z17 are also a parallel capacitance and resistance combination that represents the insulation impedance parallel to the conductor and concentric neutral. The cable was modeled in this fashion to allow the evaluation of the placement of water trees in numerous locations throughout the insulation. The number of discrete impedance elements was limited to 22 in order to avoid the use of higher level matrix functions in MathCAD, the commercially available software program that was utilized to solve the nine equations in nine unknowns.

The overall cable which is being modeled is 100 meters of 10.3 mm OD Aluminum conductor with 4.45 mm of insulation. With this type of cable the overall capacitance to ground is 32 nF, the insulation resistance to ground is 3 GΩ, the conductor resistance is 30 mΩ and the conductor inductance is 0.3 mH. The impedance magnitude and phase angle is calculated as a function of frequency with the insulation intact and with one portion, Z1, of the impedance affected by the presence of water trees. Water trees are simulated by a reduction in resistance and increase in dielectric constant.

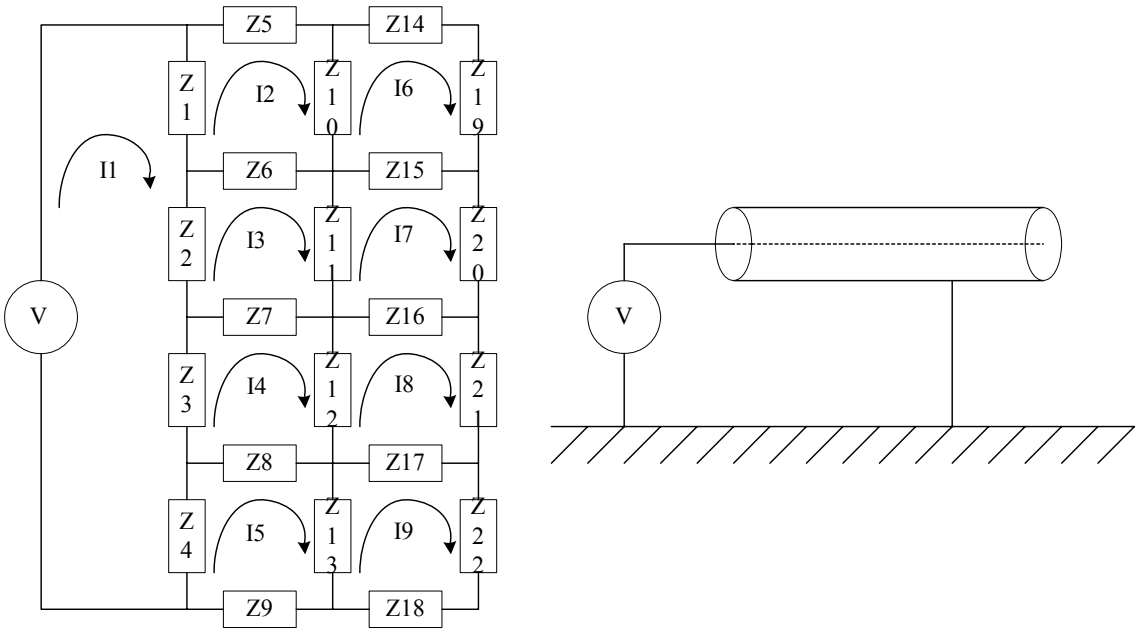

a) b)

Figure 4. 6 22 Element Equivalent Circuit of 100 m Cable Length

The detailed derivation of the equivalent circuit solution is shown in Appendix D. The solution requires solving nine equations in nine unknowns and this can be accomplished by utilizing Cramer's Rule. The voltage and current value of interest are the applied voltage, V, and the overall current, I_1. From these values the overall impedance magnitude and phase angle can be calculated.

Next the frequency is swept over a range of 6 kradians/sec to 3.1 Mradians/sec. These values were selected because they correspond to the actual test results.

Figure 4.7 shows the calculated impedance magnitude, in ohms, and phase angle, in radians, over this frequency range. The solution absent a water tree is represented by the solid curve in Figure 4.7 for the overall cable impedance magnitude and phase angle respectively. The modified solution which includes a water tree, Z1 in Figure 4.6, is

represented by the dashed curve in Figure 4.7 for the overall cable impedance magnitude and phase angle respectively.

As Figure 4.7 demonstrates the impedance value starts at a high initial value, 10 kilohms decreases to a minimum value then increases to another maximum. This behavior is repeated once more then the magnitude asymptotically decreases to approximately 80 ohms. Figure 4.7 shows the phase angle starting at -1.5 radians then changing in a step fashion to +1.5 radians followed by another step return to -1.5 radians. This negative to positive to negative step change sequence is repeated one additional time. The final value remains constant at -1.5 radians.

The observed behavior corresponds to an inductance/capacitance resonance pair. At resonance, the phase angle changes from capacitive, a negative value, to inductive, a positive value, and back to capacitive. This change is observed as a step change in the impedance phase angle frequency spectrum. It appears that there are two resonance pairs which occur, the first starting at approximately 500 kradians/sec and the second at approximately 1.4 Mradians/sec. There are impedance magnitude maxima and minima which correspond to the phase angle oscillations. The effect of the Z1 water tree on the impedance magnitude is to shift the maxima to a lower frequency, while modifying the magnitudes; higher for the first maxima and lower for the second maxima. The minima are unaffected in this instance. The phase angle shows commensurate changes with each resonance pair shifting from positive to negative and back (± 1.5 or $\pm \Pi/2$); however, the magnitude is unaffected.

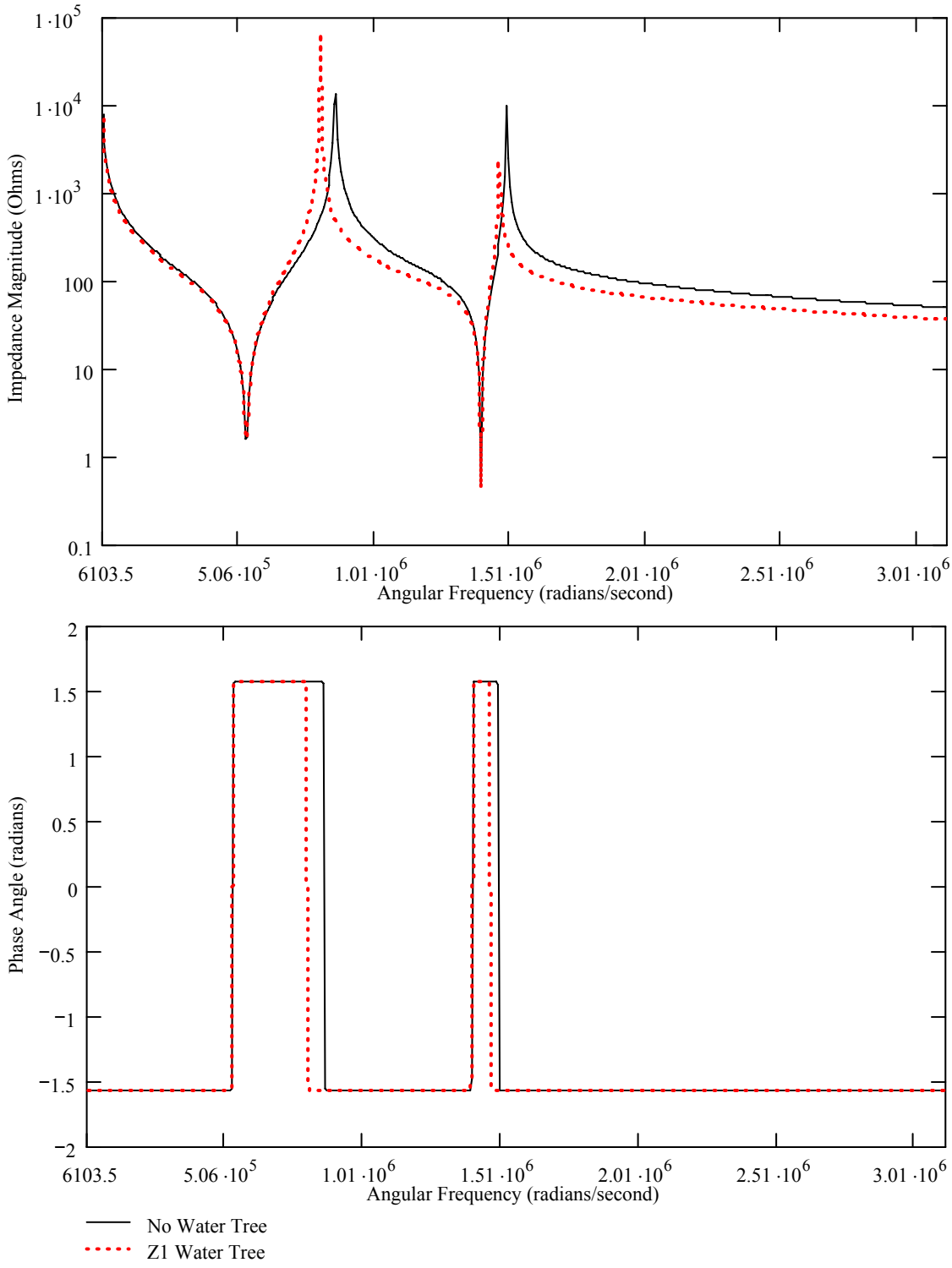

Figure 4.7 Calculated Impedance Magnitude and Phase Angle vs Frequency 22 Impedance Element Model, L=100 m, D=10.3 mm AL, 4.45 mm XLPE, Without vs With Z1 Water Tree

The equivalent circuit of Figure 4.6 models the conductor by two impedance sections, Z5 and Z14, and the concentric neutral by two impedance sections, Z9 and Z18. The insulation is modeled by 3 parallel sections with 4 series impedances each. One of the reasons for modeling the cable in this fashion is to place more emphasis on the insulation section but there are also computational limitations in MathCAD, a commercially available mathematics software package, for some definition functions which limited the maximum array as a 10x10 array, or 100 elements. Without invoking some higher level functions and to limit the computational time, this limits the model to two conductor impedance pairs.

It is possible by re-configuring the equivalent circuit model to obtain three conductor impedance sections. Now, Figure 4.8 a) shows the equivalent circuit of a typical length of underground polymeric distribution cable and Figure 4.8 b) shows the equivalent physical circuit with a voltage source connected between the conductor and concentric neutral. Here impedances Z5, Z12 and Z18 are the equivalent conductor resistance and inductance for the length of the cable being modeled. Impedances Z7, Z14 and Z21 are the equivalent concentric neutral resistance and inductance for the length of the cable being modeled. Impedances Z1, Z2, Z3,Z8, Z9, Z10, Z15, Z16, Z17, Z22, Z23 and Z24 are a parallel capacitance and resistance combination that represents the insulation impedance between the conductor and the concentric neutral. Impedances Z5, Z6, Z12, Z13, Z19 and Z20 are also a parallel capacitance and resistance combination that represents the insulation impedance parallel to the conductor and concentric neutral.

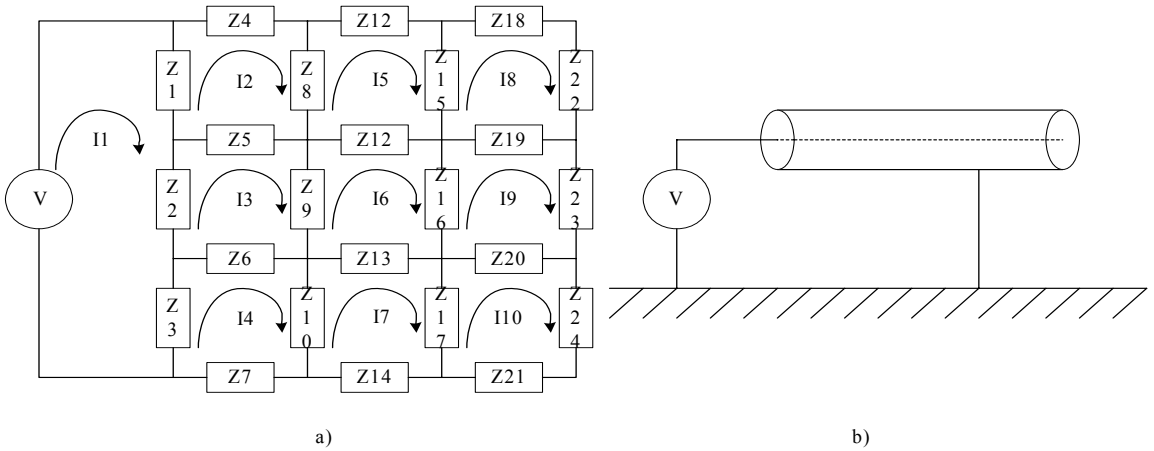

Figure 4. 8 24 Element Equivalent Circuit of 100 m Cable Length

The same effect of a water tree calculation as was conducted as previously for the two conductor impedance sections model was also solved for the three conductor impedance section model and the results of these calculations for the impedance magnitude, in ohms, and phase angle, in radians, are shown in Figure 4.9. The solution absent a water tree is represented by the solid curve in Figure 4.9 for the overall cable impedance magnitude and phase angle respectively. Once again, the modified solution includes a water tree, Z1 in Figure 4.8, and is represented by the dashed curve in Figure 4.9 for the overall cable impedance magnitude and phase angle respectively. Figure 4.9 shows an additional resonance peak pair. The first resonance pair starts at approximately 800 kradians/sec, the second at approximately 1.4 Mradians/sec and the third at approximately 2.2 Mradians/sec. The effect of the Z1 water tree is to shift the maxima to a lower frequency, while modifying the magnitudes; lower for all maxima. The minima are unaffected in this instance. The phase angle shows commensurate changes; however, the magnitude is unaffected, ±1.5 or ±Π/2. The effect of water trees in other locations is discussed further in one of the next sections.

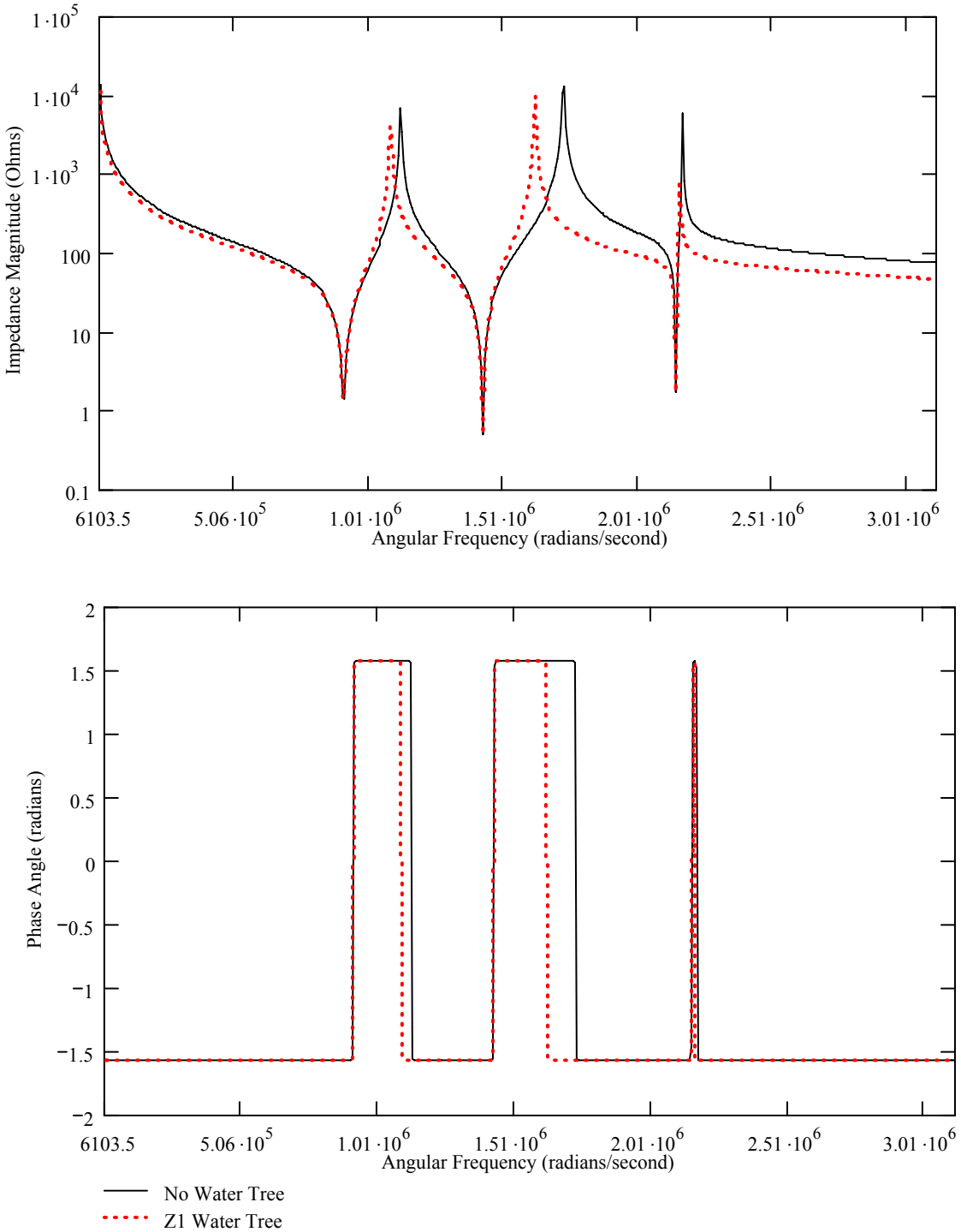

Figure 4. 9 Calculated Impedance Magnitude and Phase Angle vs Frequency 24 Impedance Element Model, L=100 m, D=10.3 mm AL,4.45 mm XLPE, Without vs With Z1 Water Tree

Further Results for the Equivalent Cable Model

The complete series of impedance magnitude, in ohms, and phase angle, in radians, graphs from calculations utilizing the theoretical, equivalent cable model represented by Figure 4.6 are provided in Appendix E. In all cases the calculation condition represented by the solid curve in the figure is the first description in the figure title, while the dashed curve is the calculation condition explained by the second description in the figure title.

Impacts of Varying Conductor Length and Diameter

It is possible with the theoretical model, to investigate for a fixed conductor diameter and fixed insulation thickness the effect of cable length as well as the effect of different cable diameters for a fixed length of cable and fixed insulation thickness.

Figure 4.10 compares the impedance magnitude, in ohms, and phase angle, in radians, over the frequency range of interest of a 100 versus 1000 m XLPE cable with an insulation thickness of 4.45 mm and an aluminum conductor of 10.3 mm OD. For a fixed conductor diameter and fixed insulation thickness, a longer cable run results in increased cable capacitance, resistance and inductance values. These increased parameters result in a shift of the resonance pairs to lower frequencies for the longer cable run. Compared to the 100 m cable, the 1000 m cable run associated impedance magnitude peaks are at a lower magnitude for both the 1^{st} and 2^{nd} maxima and higher magnitude for the 1^{st} and 2^{nd} minima respectively. Additionally, the 1000 m cable run phase angle step changes are shifted commensurate with the impedance magnitude peaks. However, there is no change in the phase angle values which remains at $\pm\Pi/2$.

Figure 4.11 compares the impedance magnitude, in ohms, and phase angle, in radians, over the frequency range of interest of a 100 versus 30 m XLPE cable with an insulation thickness of 4.45 mm and an aluminum conductor of 10.3 mm OD. For a fixed conductor diameter and fixed insulation thickness, a shorter cable run results in a decreased cable capacitance, resistance and inductance values. These decreased parameters result in a shift of the resonance pairs to higher frequencies for the shorter cable run. Compared to the 100 m cable , the 30 m cable run impedance magnitude has a higher magnitude for both the 1^{st} and 2^{nd} maxima and lower magnitude for the 1^{st} and 2^{nd} minima respectively, although the 2^{nd} maxima and minima are not shown in the figure. Additionally, the 30 m cable run phase angle step changes have been shifted commensurate with the impedance magnitude peaks. However, there is no change in the phase angle values which remains at $\pm\Pi/2$.

Figure 4.12 shows the calculated results of Figures 4.10 and 4.11 in one summary graph. This allows for a simpler visual summary of the impact of cable length on the impedance magnitude and phase angle versus frequency for a fixed conductor diameter.

Figure 4.13 compares for a XLPE cable length of 100 m, 4.45 mm insulation thickness the impedance magnitude, in ohms, and phase angle, in radians, over the frequency range of interest of a 10.3 mm OD aluminum, AL, conductor, versus 4.3 mm OD copper, CU, conductor. For a fixed cable length and identical insulation thickness, this smaller diameter conductor cable has a decreased capacitance to ground and increased conductor resistance and inductance values. Compared to the 10.3 mm OD, aluminum conductor diameter cable, the 4.3 mm OD copper conductor cable run

associated impedance magnitude has a higher magnitude for both the 1st and 2nd maxima and a lower and higher magnitude for the 1st and 2nd minima peaks respectively. Additionally, the 4.3 mm OD conductor cable run phase angle step changes have been shifted commensurate with the impedance magnitude peaks. However, there is no change in the phase angle values which remains at ±Π/2.

For a XLPE cable with an insulation thickness of 4.45 mm and a cable length of 100 m, Figure 4.14 compares the impedance magnitude, in ohms, and phase angle, in radians, over the frequency range of interest of a 10.3 mm OD aluminum conductor versus 28.4 mm OD aluminum conductor. For a fixed cable length and fixed insulation thickness, a larger diameter conductor has a increased capacitance to ground and decreased conductor resistance and inductance values. Compared to the 10.3 mm OD, aluminum conductor cable, the 28.4 mm OD conductor cable run associated impedance magnitude has a higher and lower magnitude for the 1st and 2nd maxima respectively and a lower and higher magnitude for the 1st and 2nd minima peaks respectively. Additionally, the 28.4 mm OD conductor cable run phase angle step changes have been shifted commensurate with the impedance magnitude peaks. However, there is no change in the phase angle values which remains at ±Π/2.

Figure 4.15 compares the calculated results of Figures 4.13, 4.14 and E.5 (Appendix E) in one graph. This allows for a simpler visual summary of how conductor size and insulation thickness impacts the impedance magnitude and phase angle versus frequency for a fixed cable length.

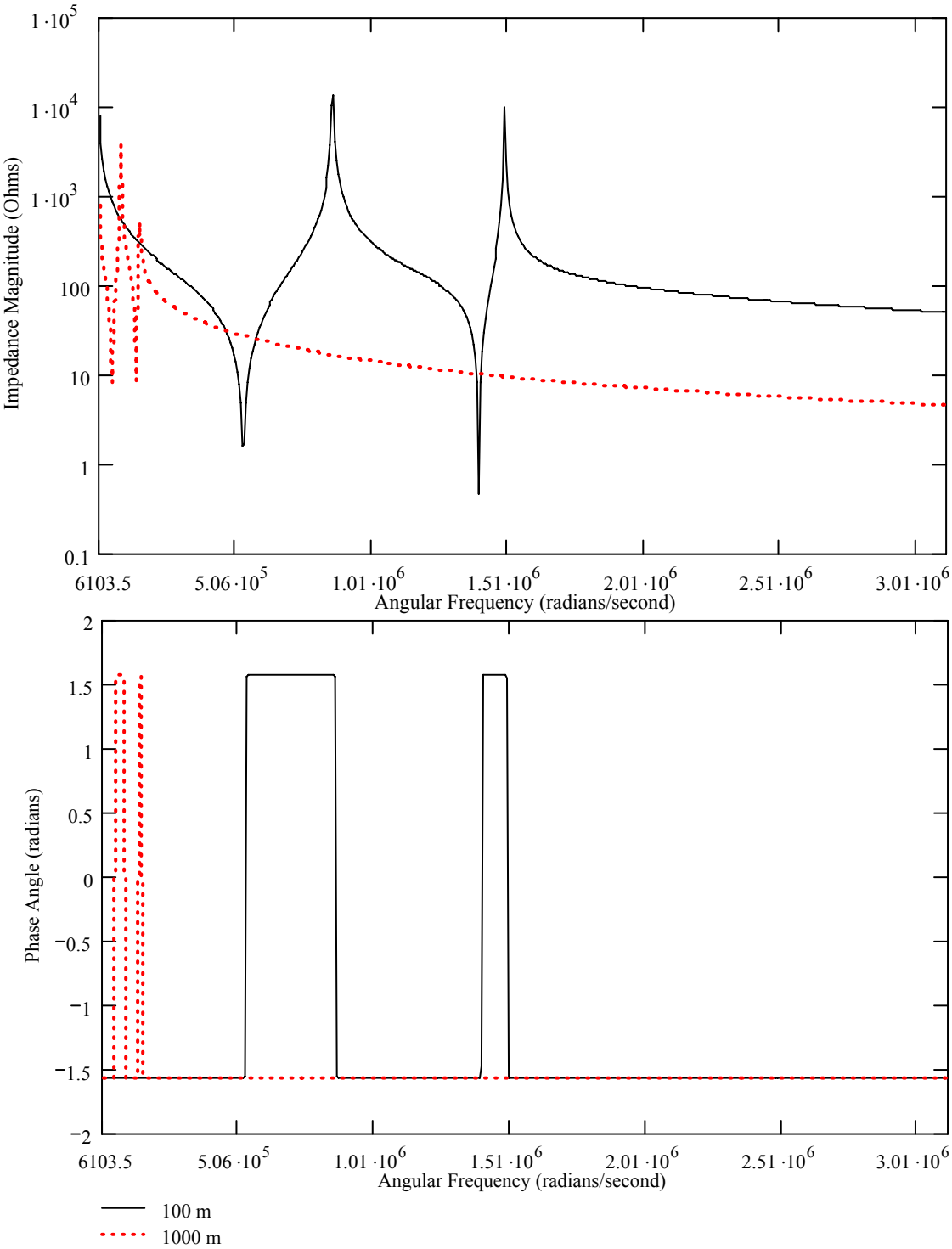

Figure 4.10 Calculated Impedance Magnitude and Phase Angle vs Frequency 22 Impedance Element Model, L=100 vs 1000 m, D=10.3 mm AL, 4.45 mm XLPE

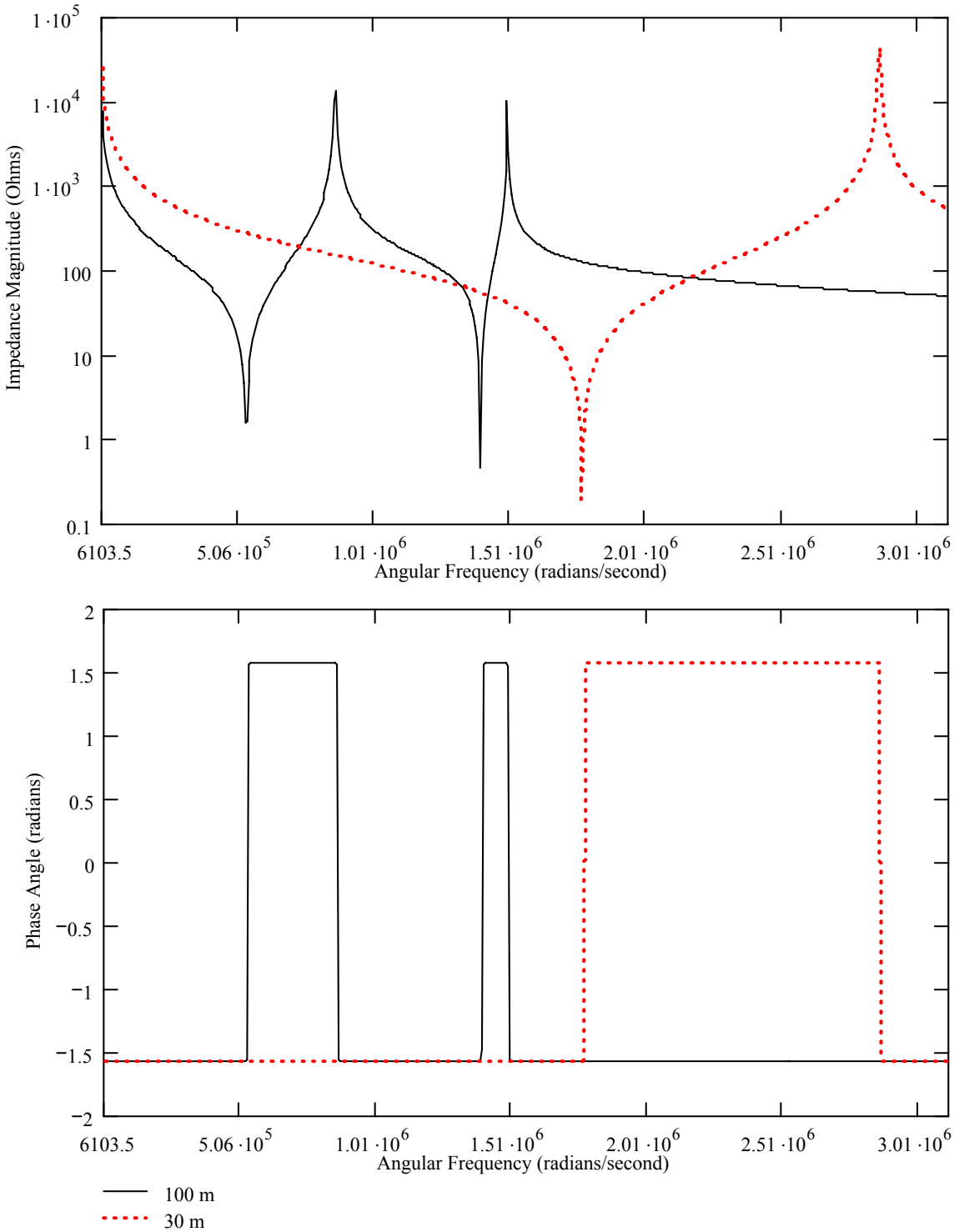

Figure 4.11 Calculated Impedance Magnitude and Phase Angle vs Frequency 22 Impedance Element Model, L=100 vs 30 m, D=10.3 mm AL, 4.45 mm XLPE

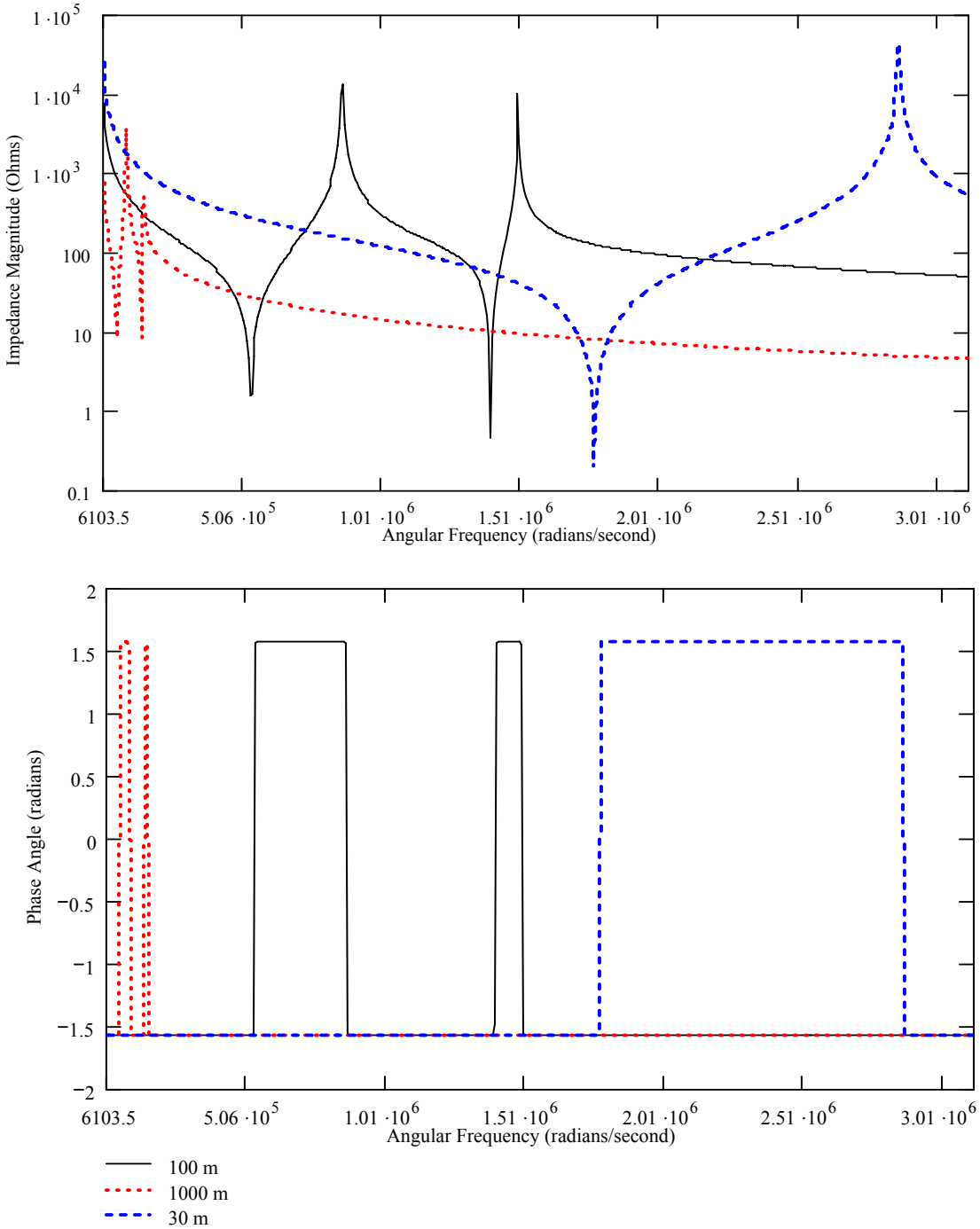

Figure 4.12 Calculated Impedance Magnitude and Phase Angle vs Frequency
22 Impedance Element Model, L=100, 30 & 1000 m, D=10.3 mm,
4.45 mm XLPE

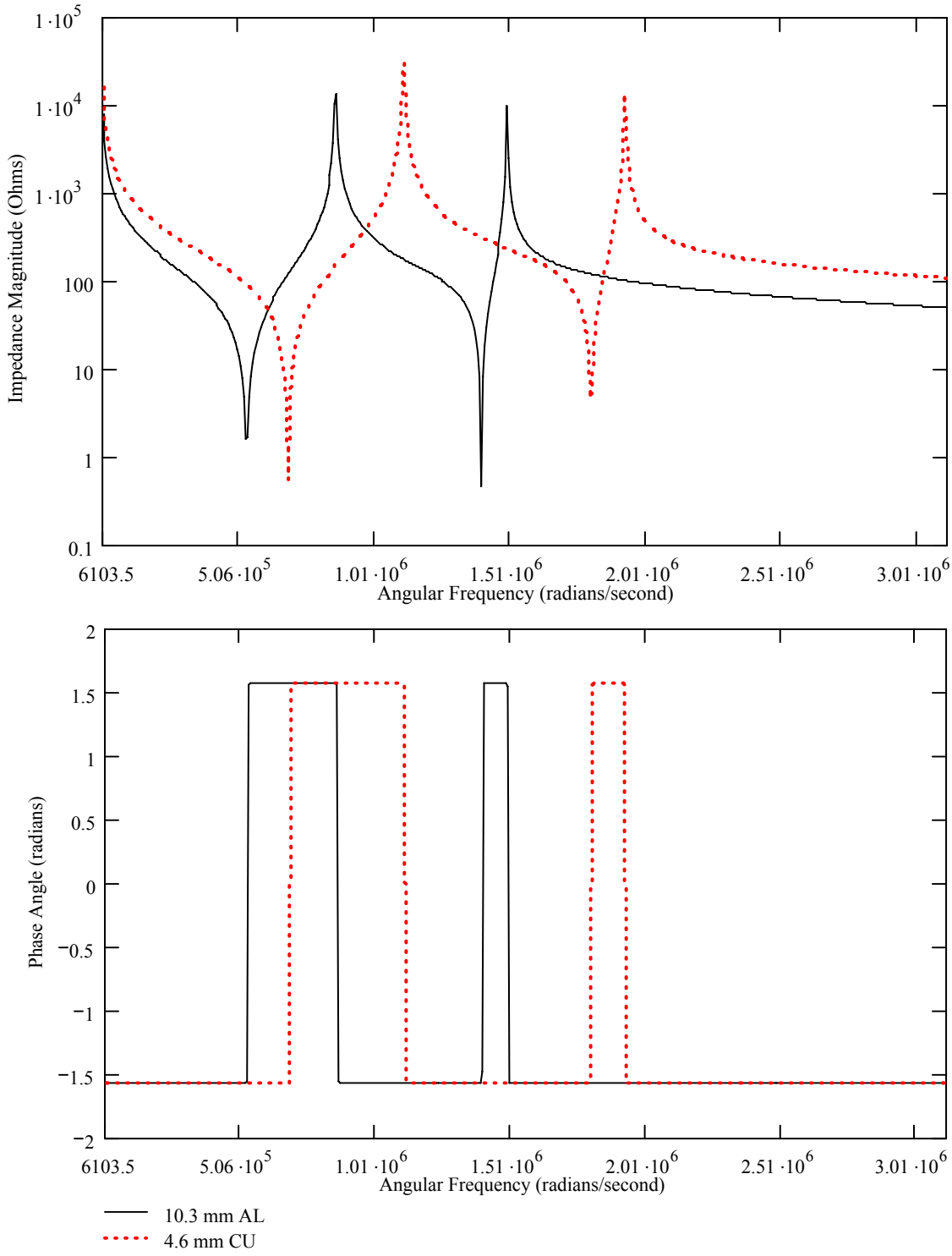

Figure 4.13 Calculated Impedance Magnitude and Phase Angle vs Frequency
22 Impedance Element Model, L=100 m, D=10.3 mm AL, 4.45 mm XLPE
vs D=4.6 mm CU, 5.59 mm HMWPE

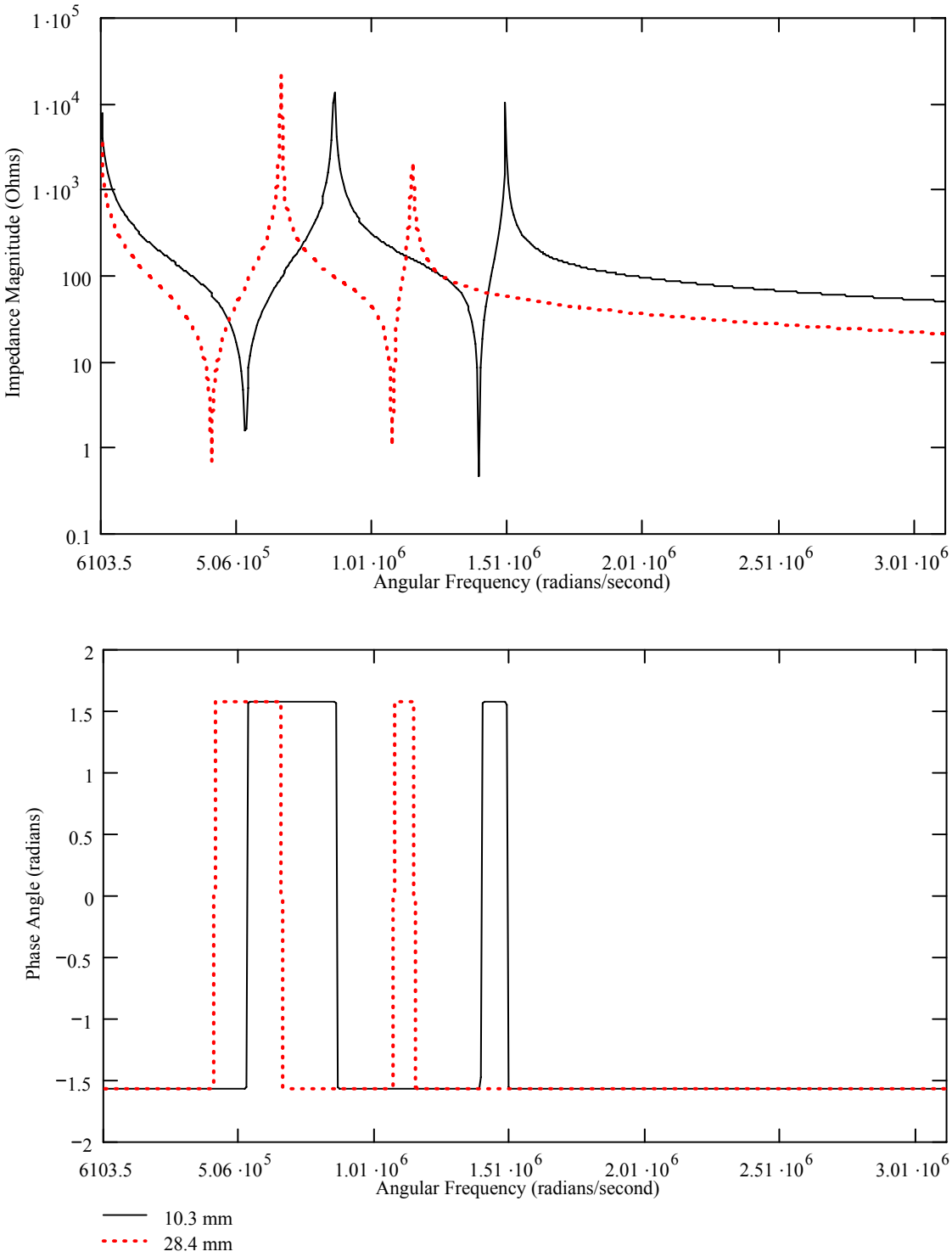

Figure 4.14 Calculated Impedance Magnitude and Phase Angle vs Frequency
22 Impedance Element Model, L=100 m, D=10.3 vs 28.4 mm AL,
4.45 mm XLPE

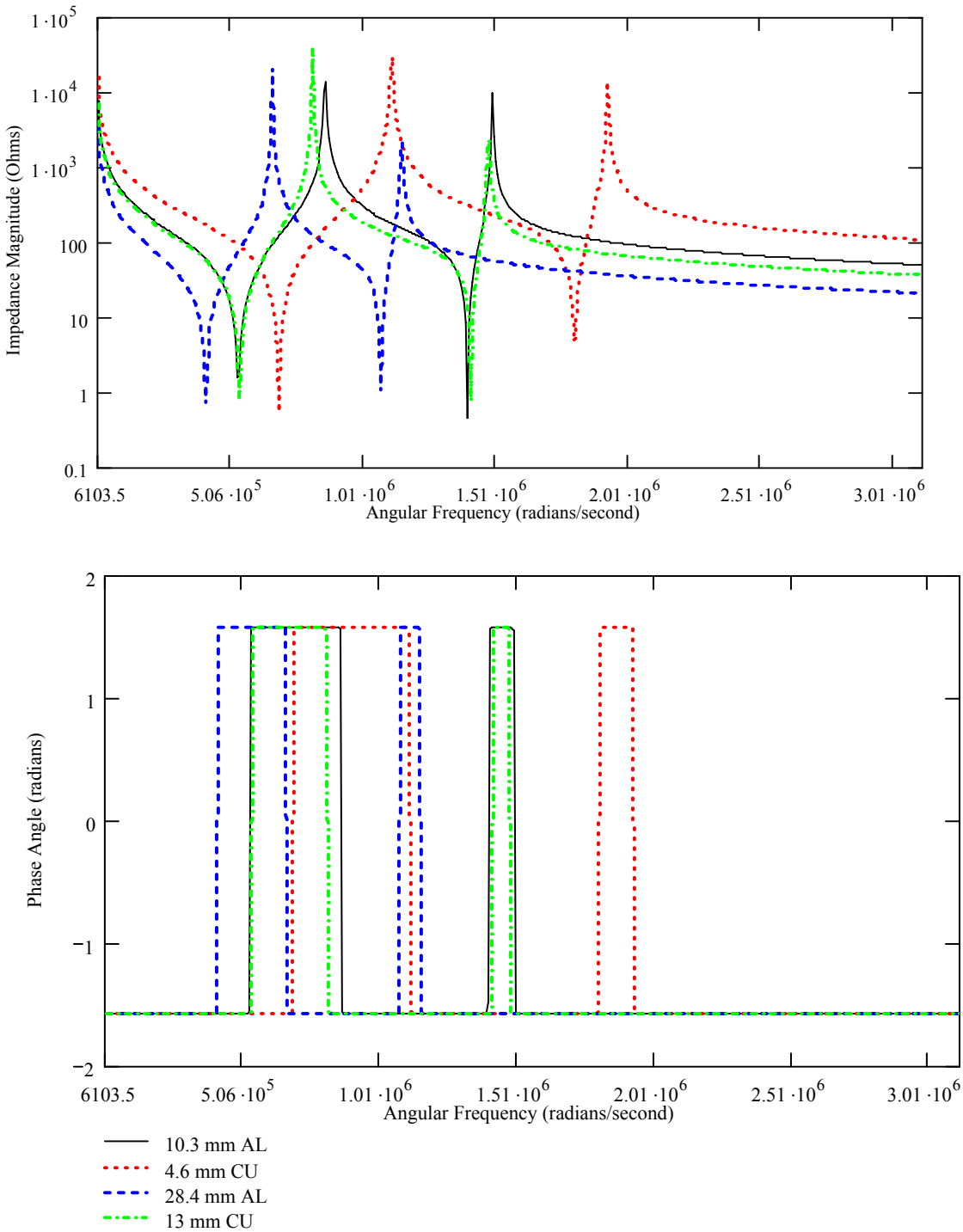

Figure 4.15 Calculated Impedance Magnitude and Phase Angle vs Frequency
22 Impedance Element Model, L=100 m, D=10.3 & 28.4 mm AL,
4.45 mm XLPE, D=4.6 & 13 mm CU, 5.59 mm HMWPE

Effects of Simulated Water Trees

The next group of calculations with the theoretical model focused on the effect of simulated water trees. This is an important issue since premature cable failure typically appears to be tied to water trees. This section looks at water tree location, the severity of water trees; both length and number and the effect on different cable lengths and cable section models.

Z1, Z2, Z3 and Z4 in Figure 4.6 are the group of insulation impedances between the conductor and concentric neutral nearest the voltage source. Figure 4.16 compares the impedance magnitude, in ohms, and phase angle, in radians, over the frequency range of interest of a XLPE cable with a 10.3 mm OD aluminum conductor, an insulation thickness of 4.45 mm and a cable length of 100 m for the cases without versus with a water tree in the Z1 location. Compared to the calculation without a water tree, the associated impedance magnitude maxima peaks are shifted to lower frequencies while the minima peaks remain at the same frequency. The water tree cable impedance magnitudes are also of a higher and lower magnitude for the 1^{st} and 2^{nd} maxima respectively while the minima peaks remain unchanged. Additionally, the water tree cable phase angle step changes have been shifted commensurate with the impedance magnitude peaks. However, there is no change in the phase angle values which remains at $\pm\Pi/2$.

Figure 4.17 and Figures E.7 and E.8 (Appendix E) demonstrate that there is also no change in impedance magnitude and phase angle spectra with the position of the water tree in this insulation group; that is it does not matter which impedance, Z1 to Z4, is modified, the results are the same. If additional water trees are added into insulation; for

example both Z1 and Z2 are modified as shown in Figure 4.18; further reduction in both maxima magnitude and further shifting of the maxima peaks location to a lower frequency occurs. The negative minima continue to remain unaffected. The water tree cable phase angle step changes continue to shift commensurate with the impedance magnitude peaks without changing the phase angle values which remain at ±Π/2.

As the water trees grow in the insulation, Figure 4.19, the impedance magnitude maxima peaks continue to decrease and shift to a lower frequency and once the entire insulation is bridged, Figure 4.20, the resonance pairs have almost disappeared with the impedance magnitude decaying exponentially with increasing frequency. Additionally, the water tree cable phase angle step changes have almost vanished commensurate with the impedance magnitude modifications. The phase angle values remain primarily at -Π/2 with a very short excursion to + Π/2.

Figure 4.21 summarizes the calculated results of Figures 4.16, 4.18 to 4.20. This figure provides a visual summary of how water trees and their length impacts the impedance magnitude and phase angle for a fixed conductor size, cable length and insulation thickness for the insulation group closest to the voltage source.

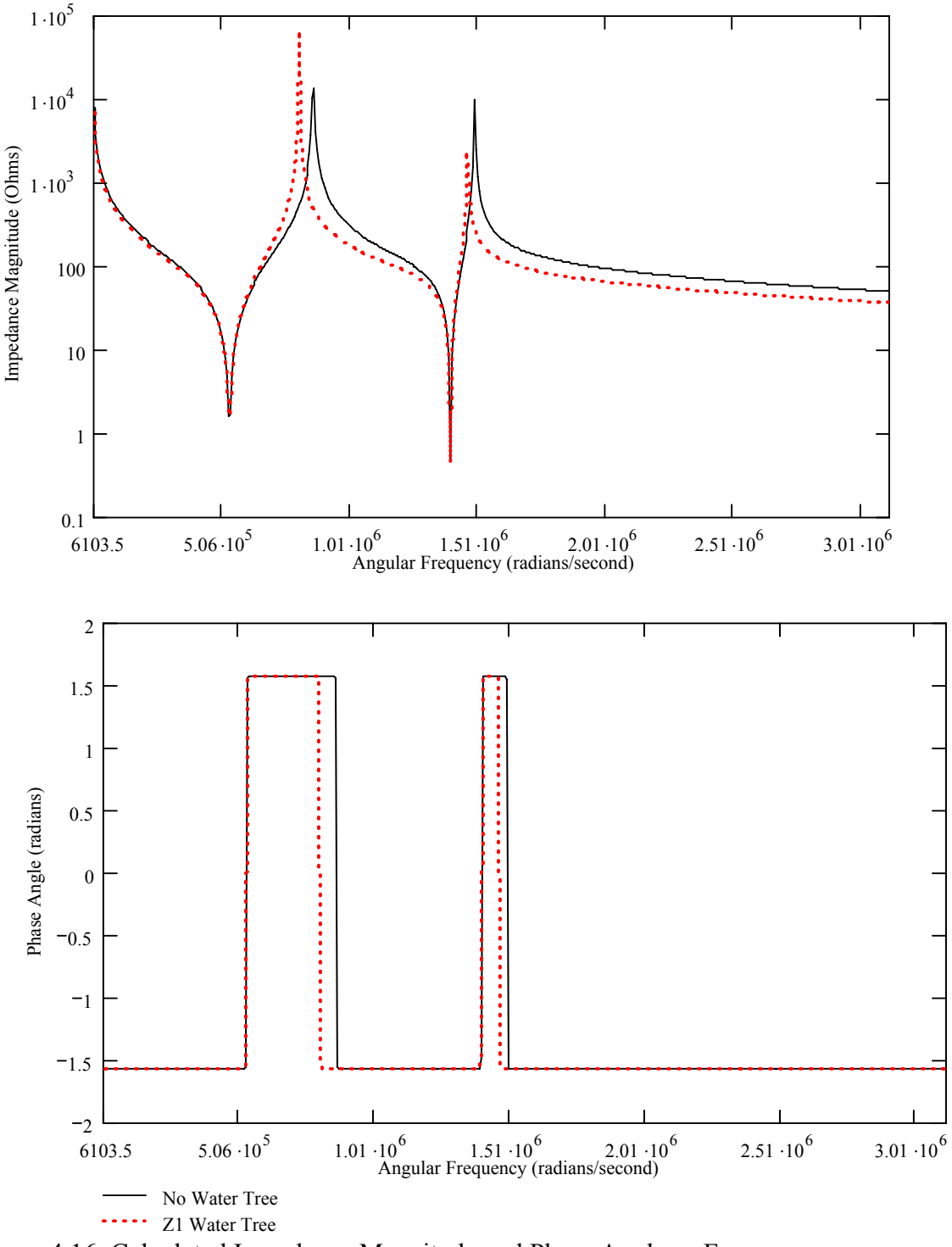

Figure 4.16 Calculated Impedance Magnitude and Phase Angle vs Frequency
22 Impedance Element Model, L=100 m, D=10.3 mm AL, 4.45 mm XLPE,
Without vs With Z1 Water Tree

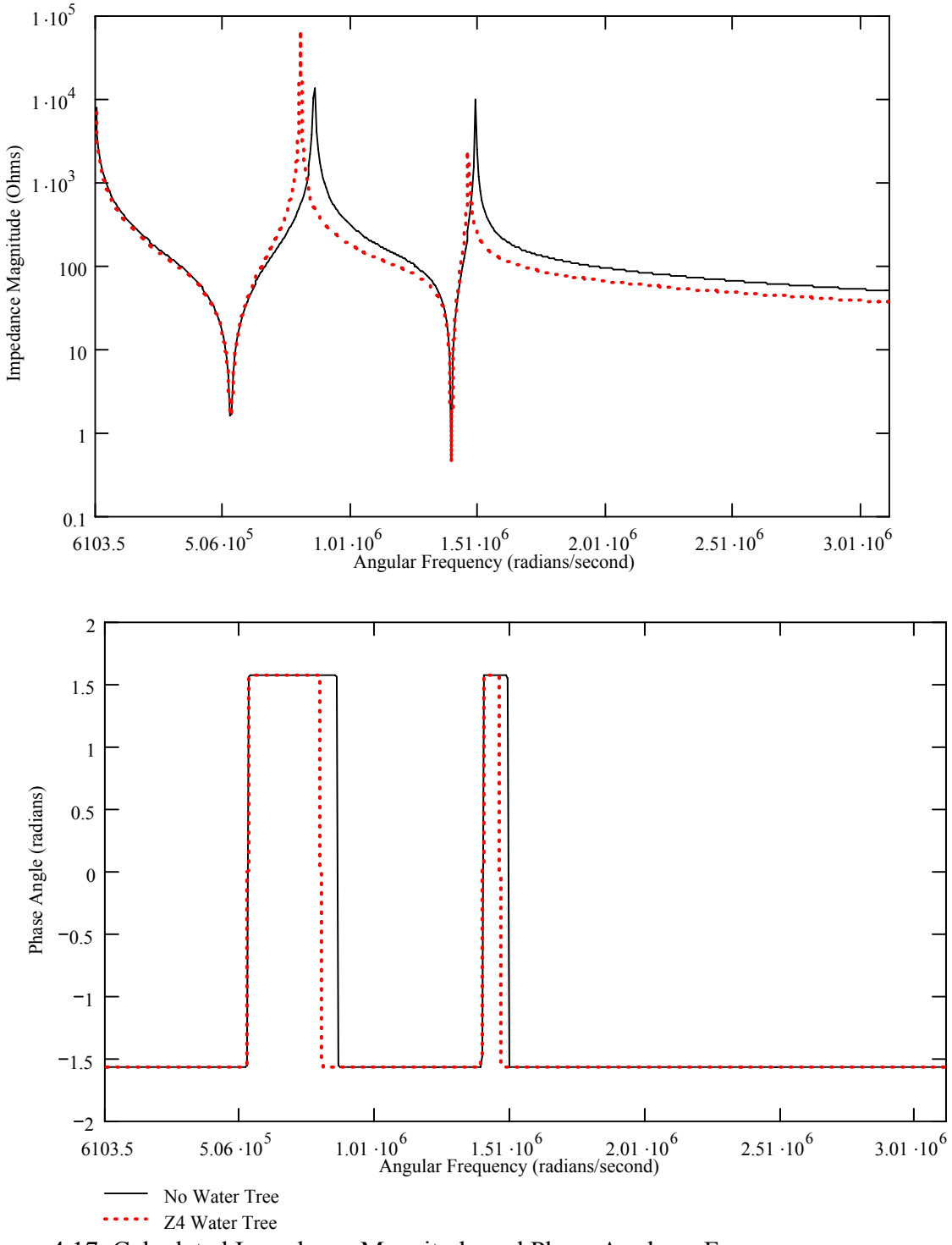

Figure 4.17 Calculated Impedance Magnitude and Phase Angle vs Frequency
22 Impedance Element Model, L=100 m, D=10.3 mm AL, 4.45 mm XLPE,
Without vs With Z4 Water Tree

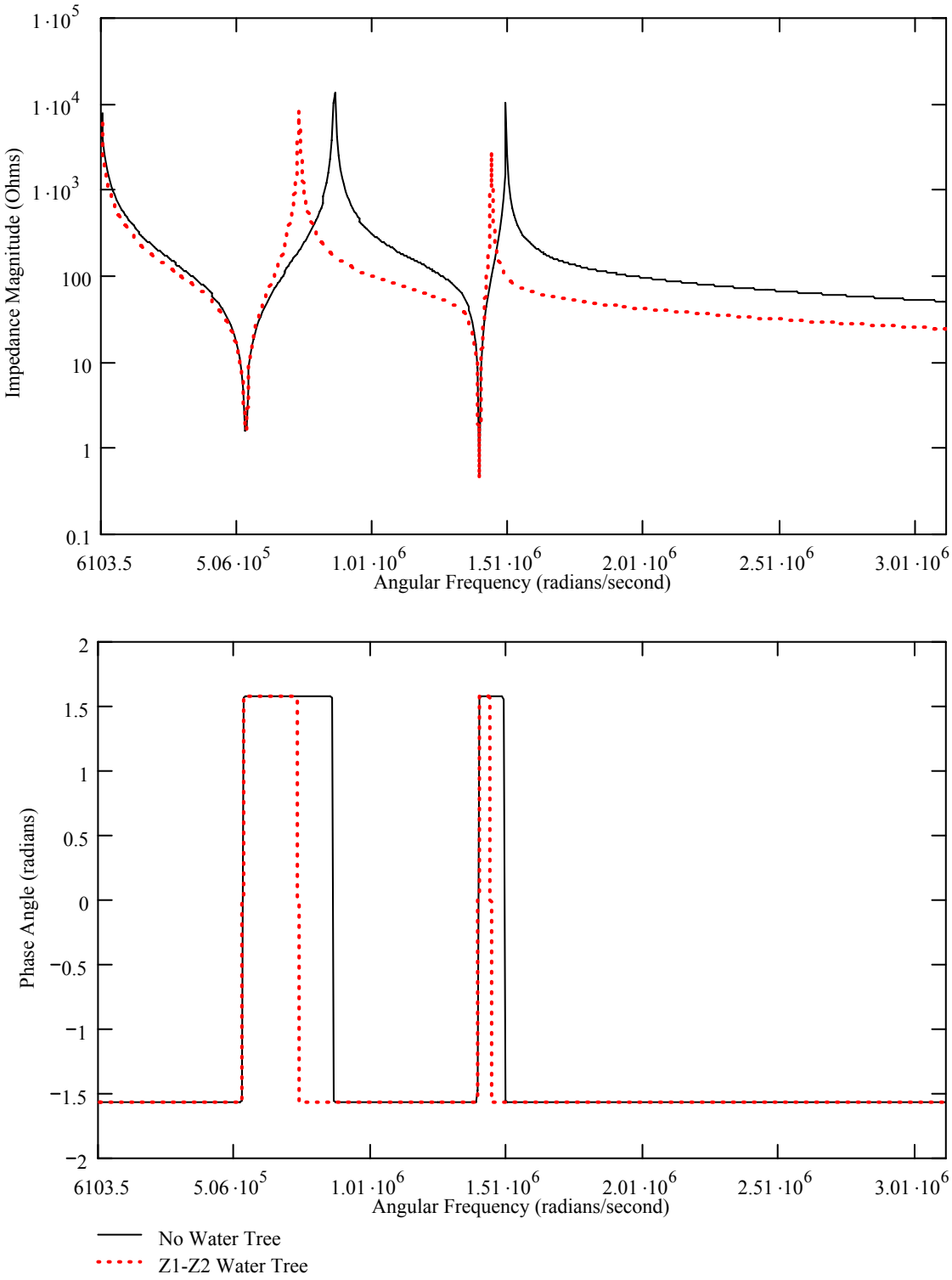

Figure 4.18 Calculated Impedance Magnitude and Phase Angle vs Frequency
22 Impedance Element Model, L=100 m, D=10.3 mm AL, 4.45 mm XLPE,
Without vs With Z1-Z2 Water Tree

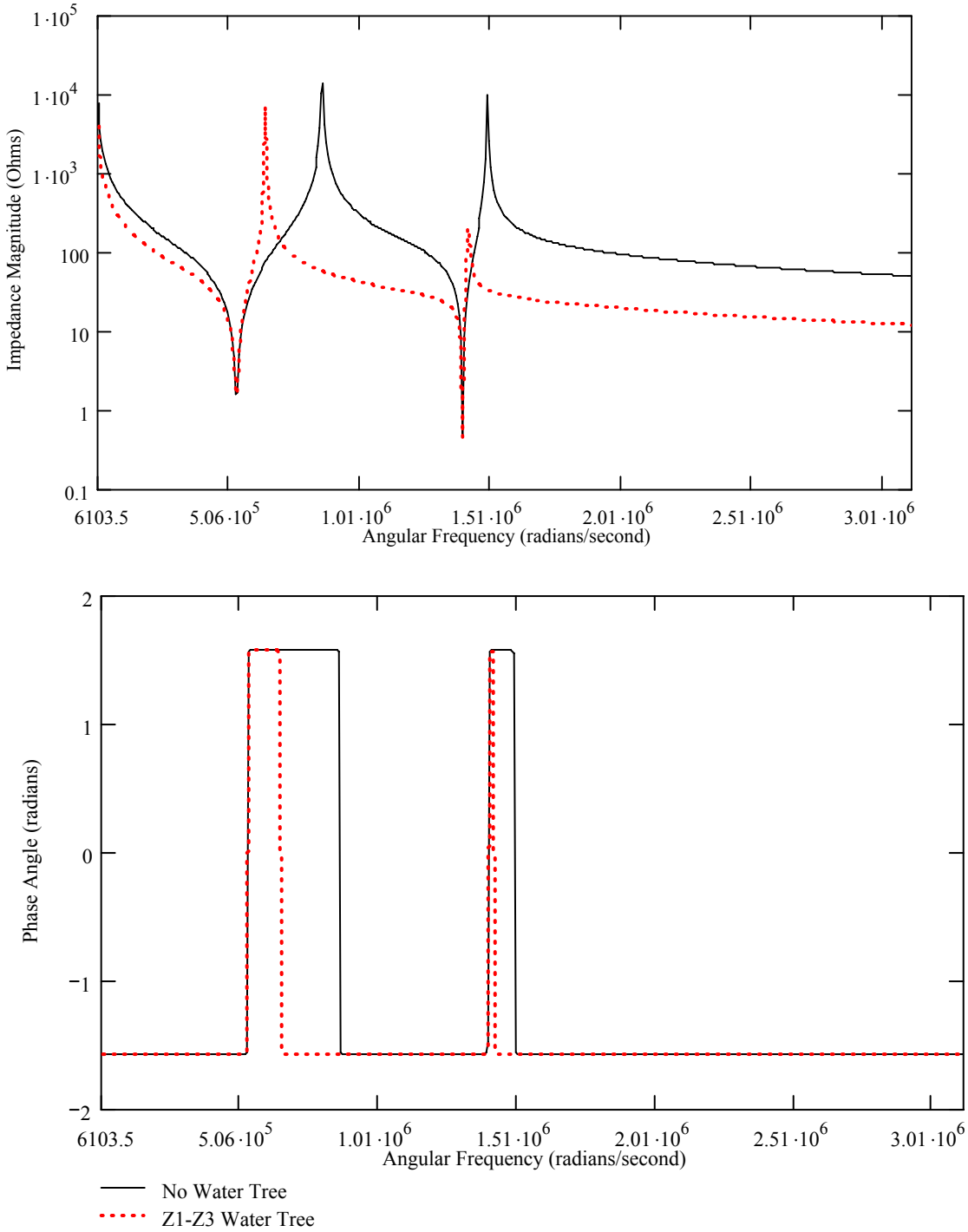

Figure 4.19 Calculated Impedance Magnitude and Phase Angle vs Frequency
22 Impedance Element Model, L=100 m, D=10.3 mm AL, 4.45 mm XLPE,
Without vs With Z1-Z3 Water Tree

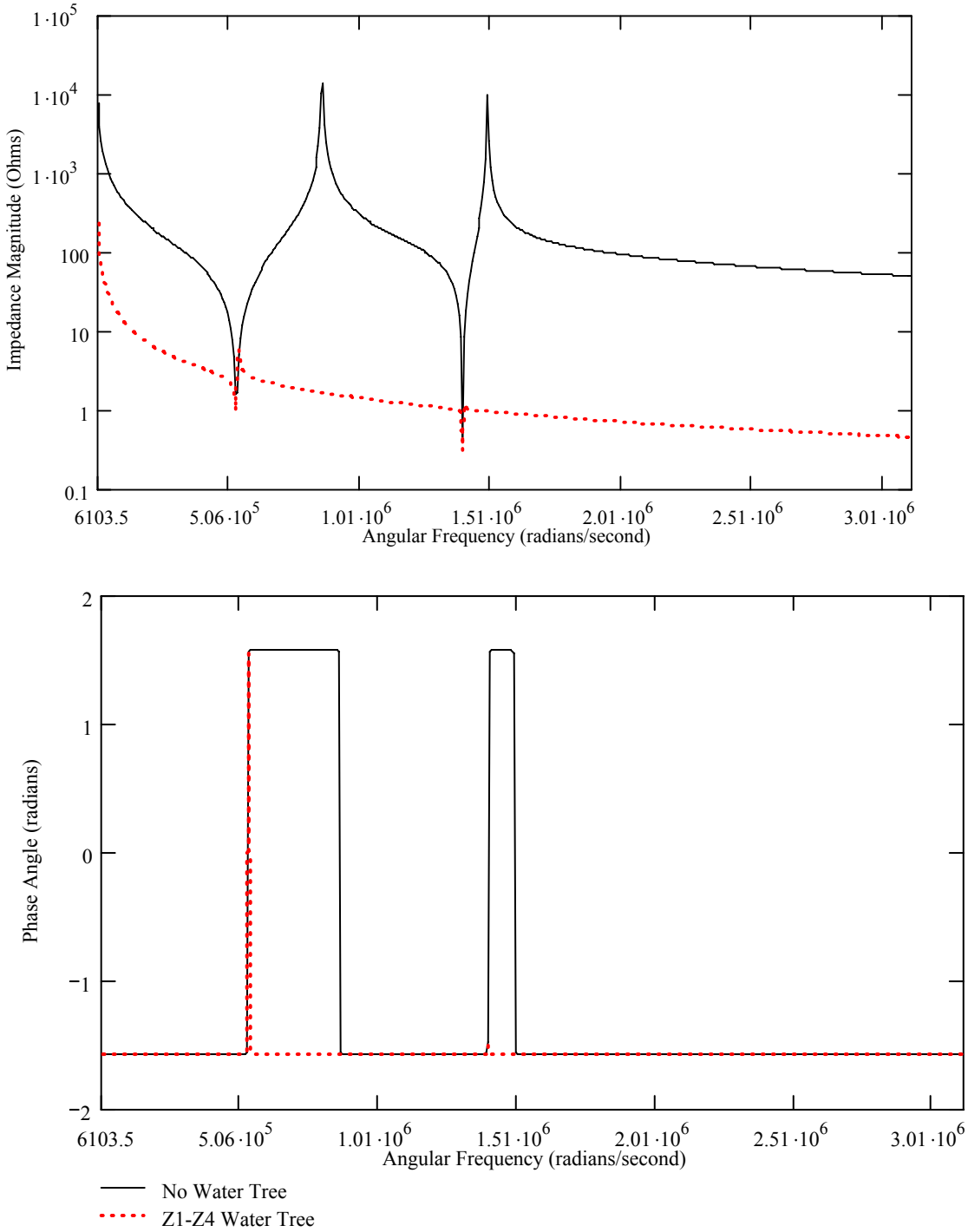

Figure 4.20 Calculated Impedance Magnitude and Phase Angle vs Frequency
22 Impedance Element Model, L=100 m, D=10.3 mm AL, 4.45 mm XLPE,
Without vs With Z1-Z4 Water Tree

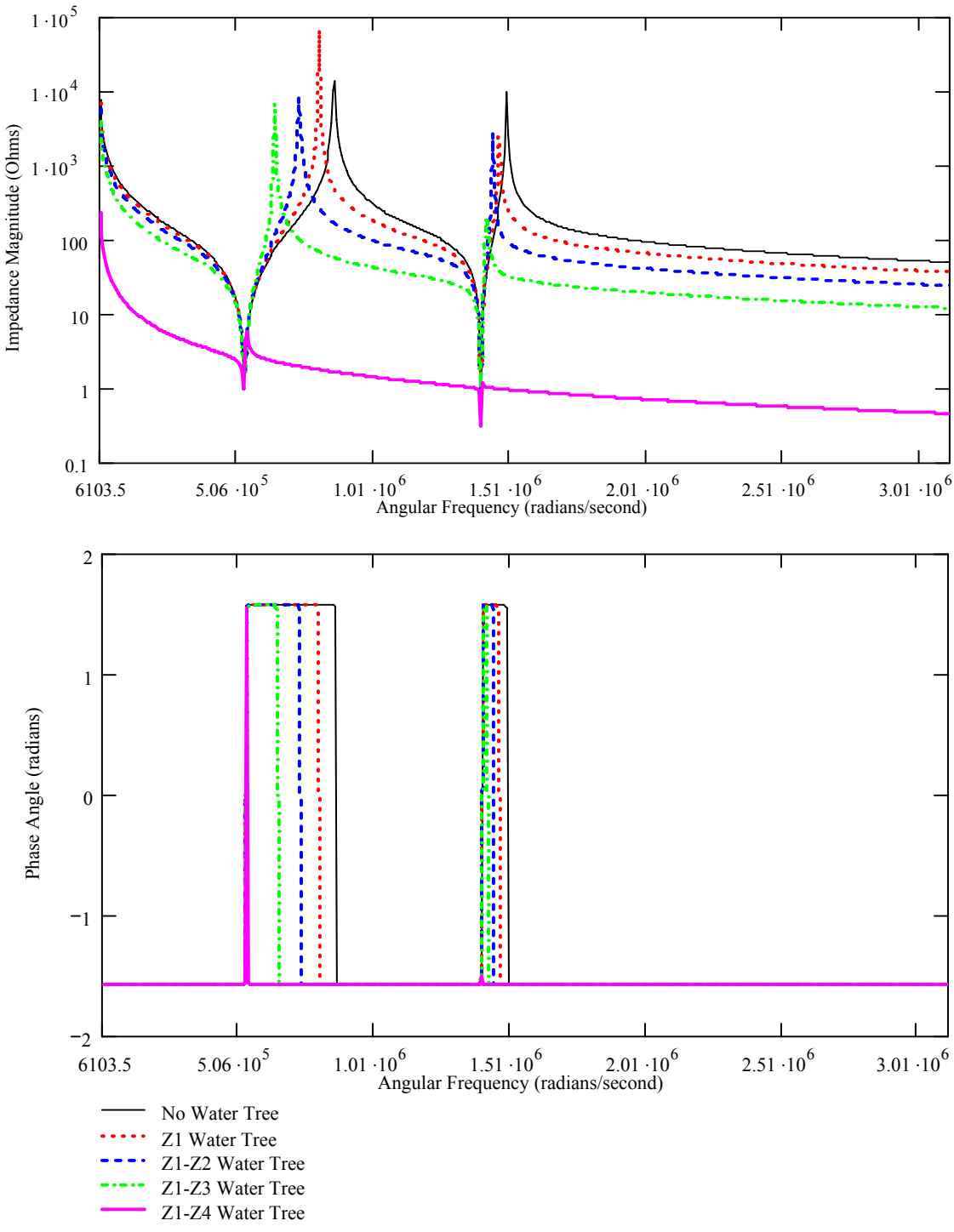

Figure 4.21 Calculated Impedance Magnitude and Phase Angle vs Frequency
22 Impedance Element Model, L=100 m, D=10.3 mm AL, 4.45 mm XLPE,
Without vs With Z1, Z1-Z2,Z1-Z3 & Z1-Z4 Water Trees

The middle insulation group of Figure 4.6 consists of Z10, Z11, Z12 and Z19 impedances. Figure 4.22 compares the impedance magnitude, in ohms, and phase angle, in radians, over the frequency range of interest of a XLPE cable identical to the cable described in the previous section. In this case the calculations are performed without versus with a water tree in the Z10 location. Compared to the calculation without a water tree, the associated impedance magnitude 2nd maxima and minima peaks are shifted to lower frequencies while the 1st maxima peak remains at the same frequency. The water tree cable impedance magnitudes are also of a higher magnitude for the 2nd maxima and minima and of a lower magnitude for the 1st minima respectively while the 1st maxima peak remain unchanged. Additionally, the water tree cable phase angle step changes have been shifted commensurate with the impedance magnitude modifications. However, there is no change in the phase angle values which remains at $\pm\Pi/2$.

Figures E.14, E.15 and E.16 (Appendix E) demonstrate that there is also no change with the position of the water tree in the insulation group; that is it does not matter which impedance, Z10 to Z13, is modified, the results are the same. If additional water trees are added into insulation; for example both Z10 and Z11 are modified as shown in Figure 4.23; the associated impedance magnitude 2nd maxima and minima are continue to be shifted to lower frequencies while the 1st maxima remains at the same frequency. The water tree cable impedance magnitudes are now of a lower magnitude for the 1st and 2nd minima and maxima and of a higher magnitude for the 2nd minima respectively while the 1st maxima remain unchanged. The water tree cable phase angle

step changes continue to shift commensurate with the impedance magnitude modifications without changing the phase angle values which remain at ±Π/2.

As the water trees grow in the insulation, Figure 4.24, the impedance magnitude 2nd maxima and both minima continue to minimally change and shift to a lower frequency and once the entire insulation is bridged, Figure 4.25, the second resonance pair has disappeared with the impedance magnitude maxima and minima and increased and decreased respectively. The water tree cable phase angle step changes have decreased to a single resonance pair commensurate with the impedance magnitude changes and the phase angle values remain at ±Π/2.

Figure 4.26 summarizes the calculated results of Figures 4.22 to 4.25. This figure provides a visual summary of how water trees and their length impacts the impedance magnitude and phase angle for a fixed conductor size, cable length and insulation thickness for the insulation group in the middle of the cable.

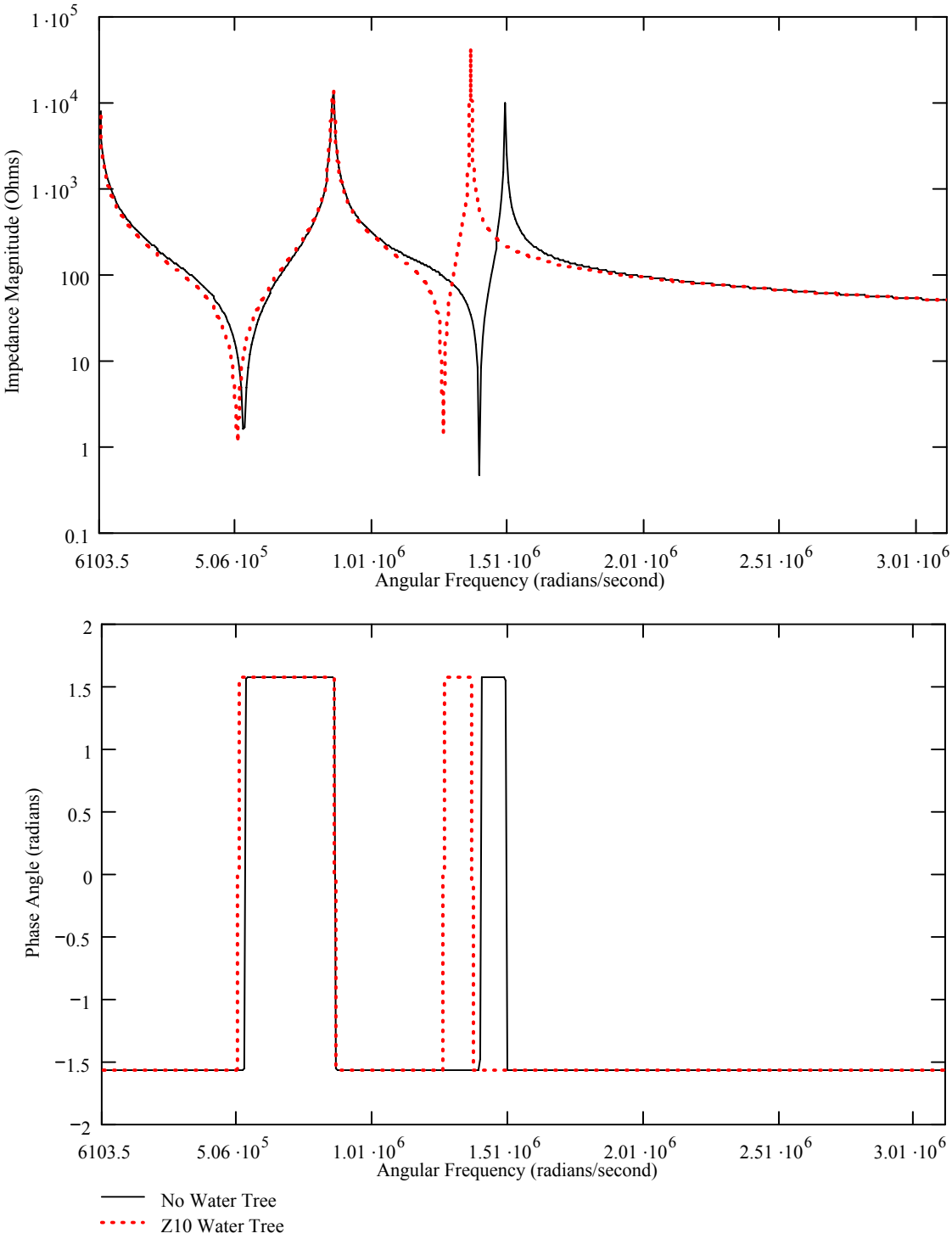

Figure 4.22 Calculated Impedance Magnitude and Phase Angle vs Frequency
22 Impedance Element Model, L=100 m, D=10.3 mm AL, 4.45 mm XLPE,
Without vs With Z10 Water Tree

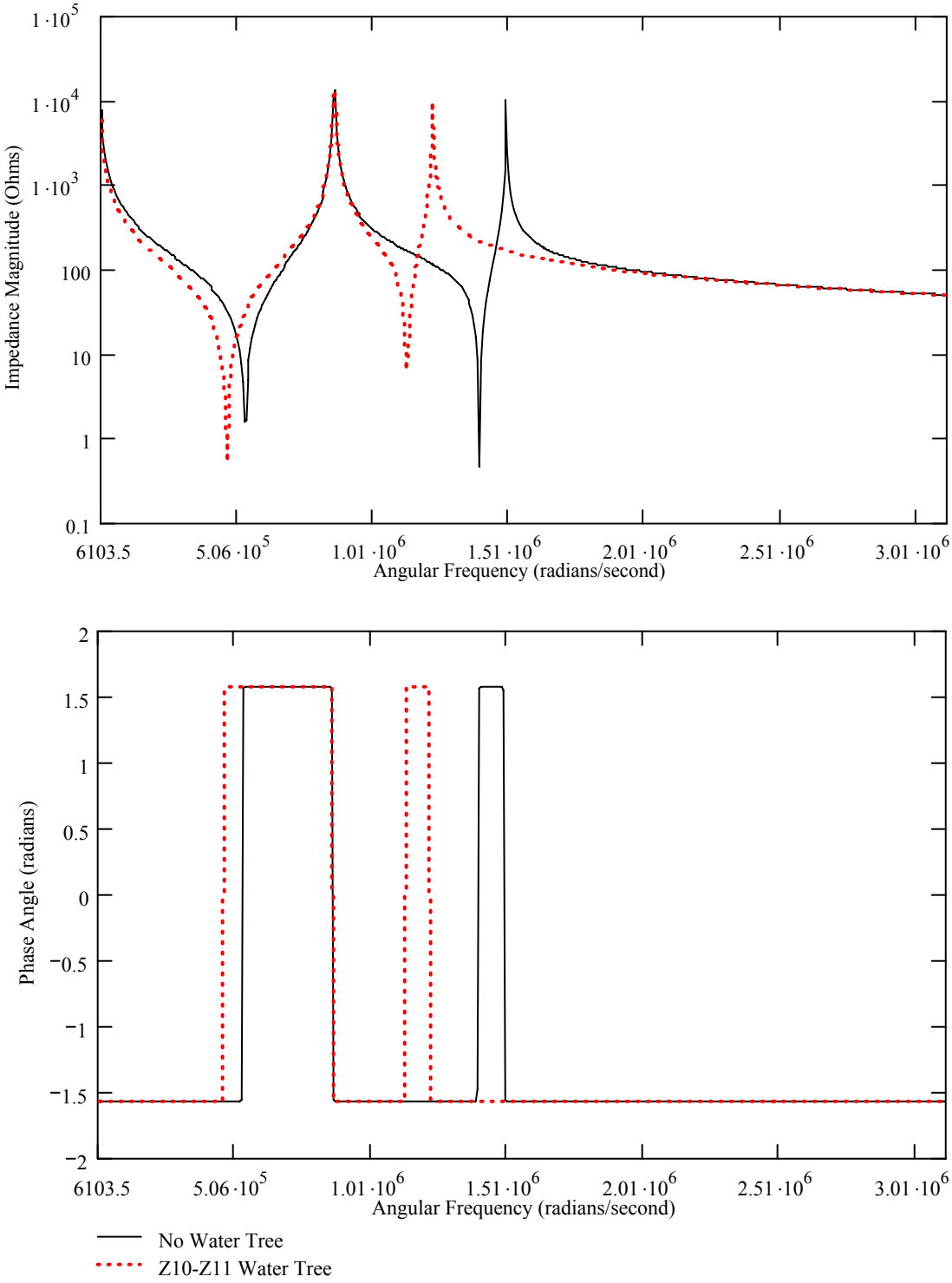

Figure 4.23 Calculated Impedance Magnitude and Phase Angle vs Frequency
22 Impedance Element Model, L=100 m, D=10.3 mm AL, 4.45 mm XLPE,
Without vs With Z10-Z11 Water Tree

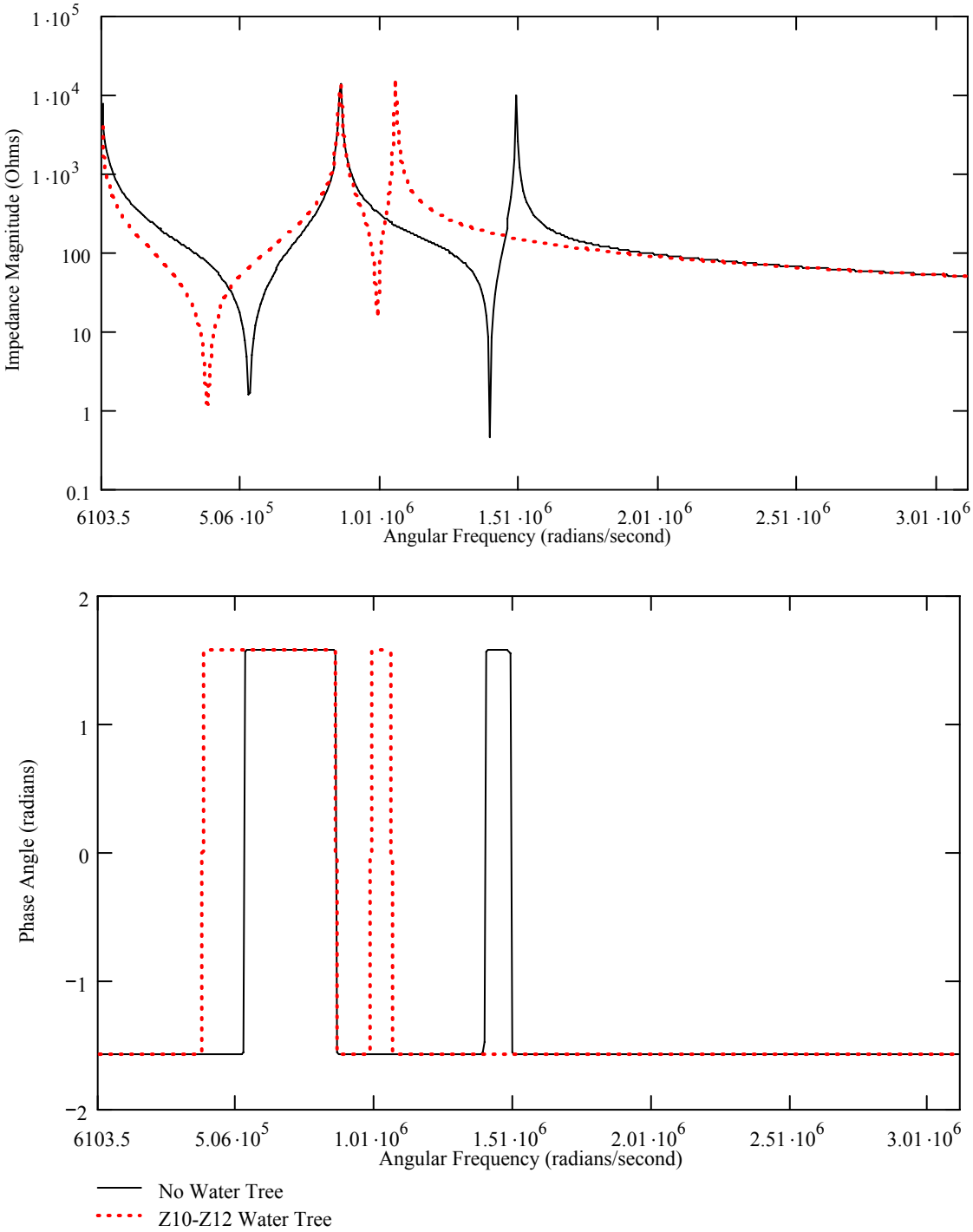

Figure 4.24 Calculated Impedance Magnitude and Phase Angle vs Frequency
22 Impedance Element Model, L=100 m, D=10.3 mm AL, 4.45 mm XLPE,
Without vs With Z10-Z12 Water Tree

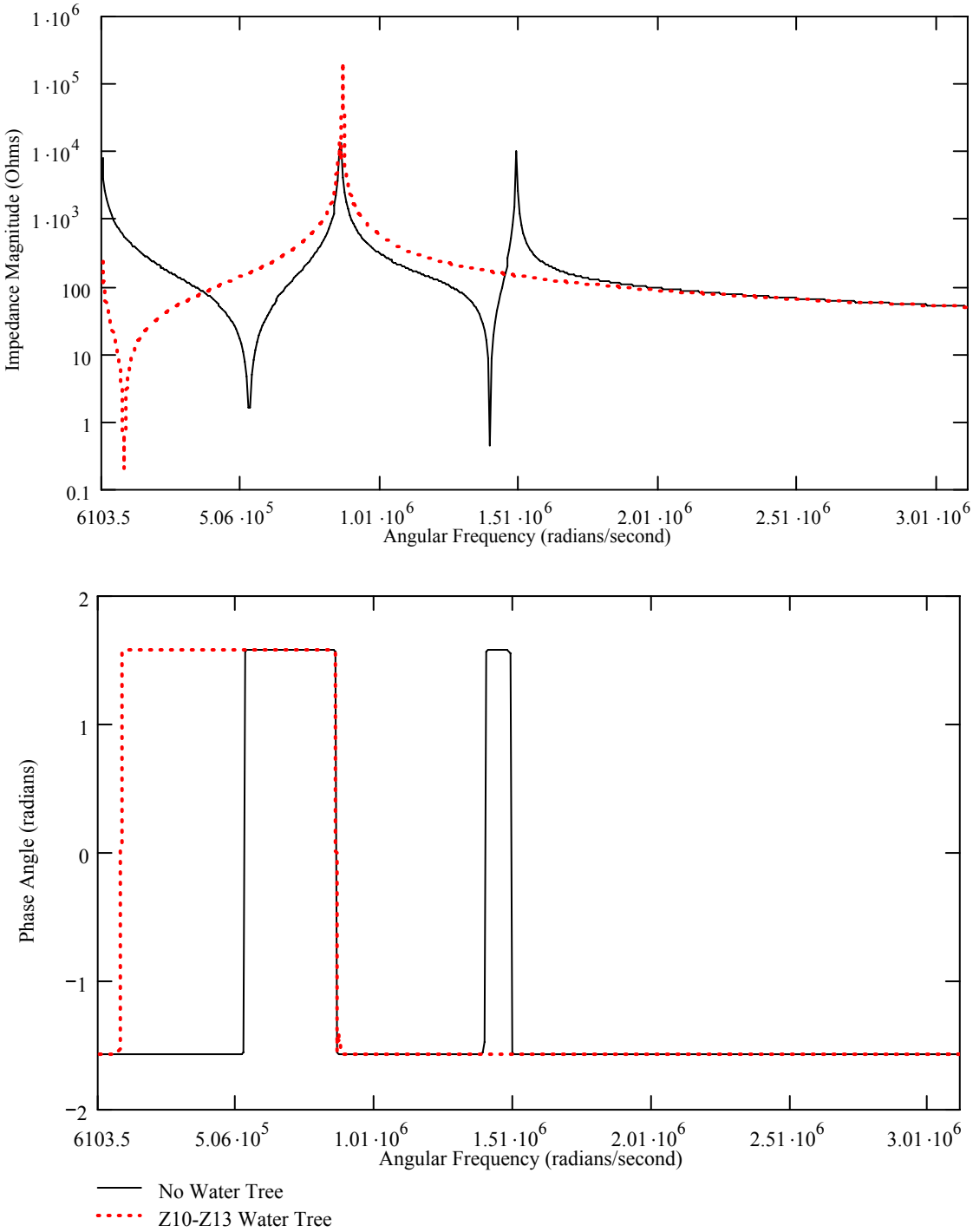

Figure 4.25 Calculated Impedance Magnitude and Phase Angle vs Frequency
22 Impedance Element Model, L=100 m, D=10.3 mm AL, 4.45 mm XLPE,
Without vs With Z10-Z13 Water Tree

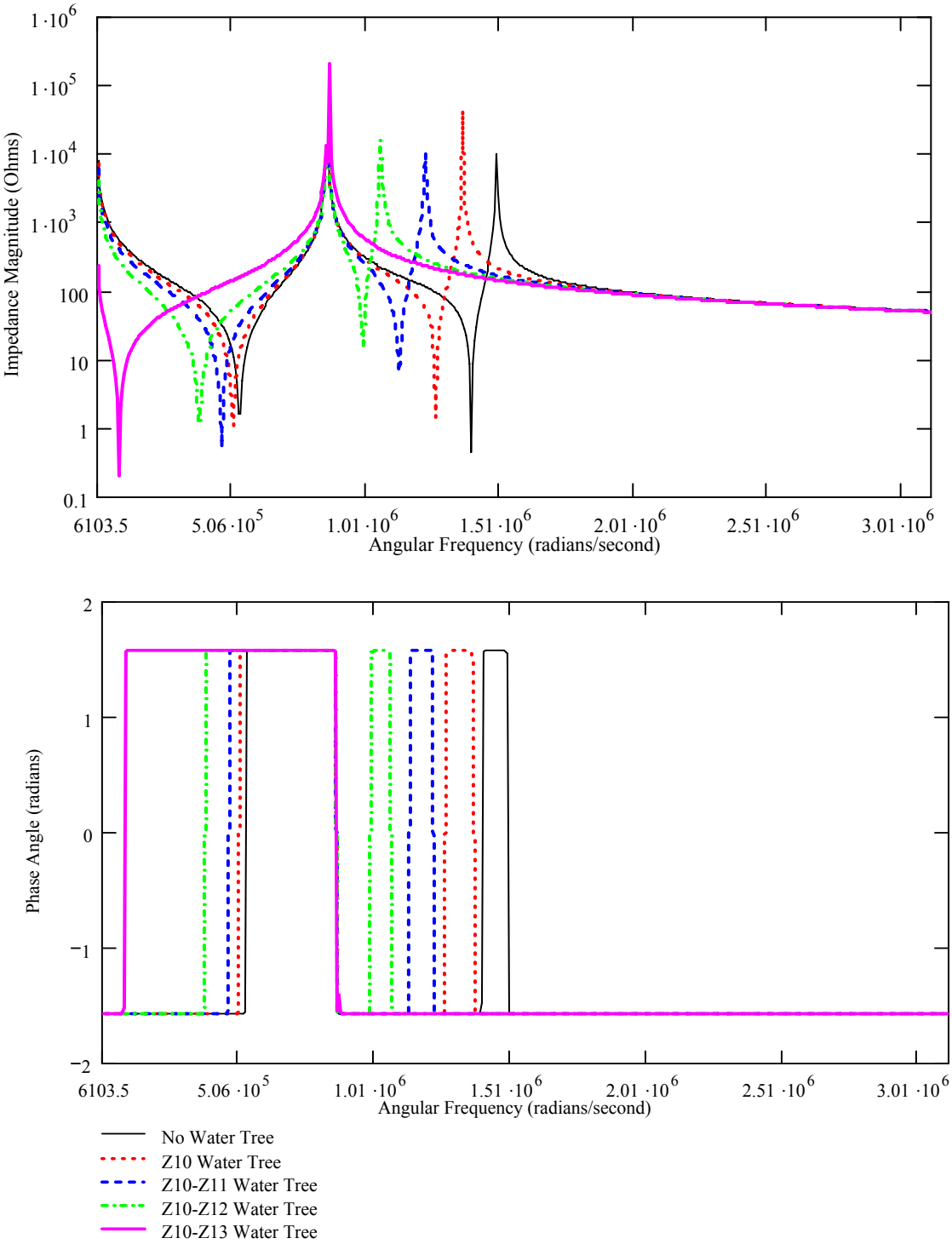

Figure 4.26 Calculated Impedance Magnitude and Phase Angle vs Frequency
22 Impedance Element Model, L=100 m, D=10.3 mm AL, 4.45 mm XLPE,
Without vs With Z10, Z10-Z11, Z10-Z12 & Z10-Z13 Water Trees

As for the final group of impedances furthest from voltage source, Z19, Z20, Z21 and Z22., Figure 4.27 compares the impedance magnitude, in ohms, and phase angle, in radians, over the frequency range of interest of a XLPE cable identical to the cable described in the previous section. In this case the calculations are performed without versus with a water tree in the Z19 location. Compared to the calculation without a water tree, the associated impedance magnitude of all maxima and minima are shifted to lower frequencies. The water tree cable impedance magnitudes are also of a higher magnitude for the 1st maxima and 2nd minima and of a lower magnitude for the 2nd maxima respectively while the 1st minima peak remains unchanged. As seen previously, the water tree cable phase angle step changes have been shifted commensurate with the impedance magnitude modifications. However, there is no change in the phase angle values which remains at $\pm\Pi/2$.

Figures E.21, E.22 and E.23 (Appendix E) again demonstrate that there is also no change with the position of the water tree in the insulation group; that is it does not matter which impedance Z19 to Z23 is modified, the results are the same. If additional water trees are added into insulation; for example both Z19 and Z20 are modified as shown in Figure 4.28; all associated impedance magnitude maxima and minima continue to be shifted to lower frequencies. The water tree cable impedance magnitudes are now of a lower magnitude for the 1st and 2nd maxima and minima and of a higher magnitude for the 2nd maxima respectively while the 1st minima continues to remain unchanged. The water tree cable phase angle step changes continue to shift commensurate with the

modification of the impedance magnitude without changing the phase angle values which remain at ±Π/2.

With increasing water trees growth in the insulation, Figure 4.29, all impedance magnitude maxima and minima peaks continue to change and shift to a lower frequency and once the entire insulation is bridged, Figure 4.30, the resonance pairs complete moving to a lower frequency with the most significant impedance magnitude change a lower 1st minima. The water tree cable phase angle step changes have decreased to a single resonance pair commensurate with the impedance magnitude changes. The phase angle values remain at ±Π/2.

Figure 4.31 summarizes the calculated results of Figures 4.27 to 4.30. This figure provides a visual summary of how water trees and their length impacts the impedance magnitude and phase angle for a fixed conductor size, cable length and insulation thickness for the insulation group at the open end of the cable.

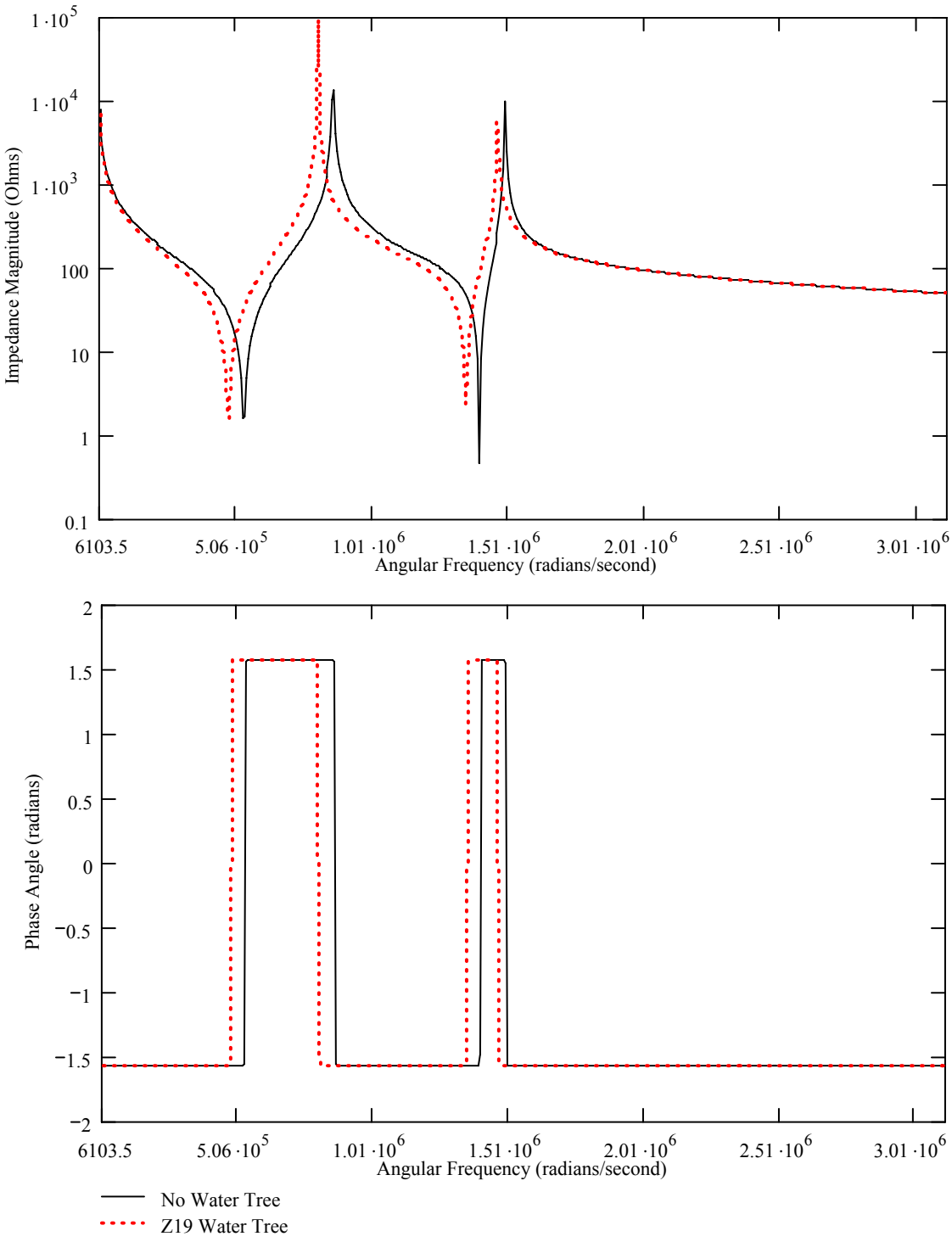

Figure 4.27 Calculated Impedance Magnitude and Phase Angle vs Frequency
22 Impedance Element Model, L=100 m, D=10.3 mm AL, 4.45 mm XLPE,
Without vs With Z19 Water Tree

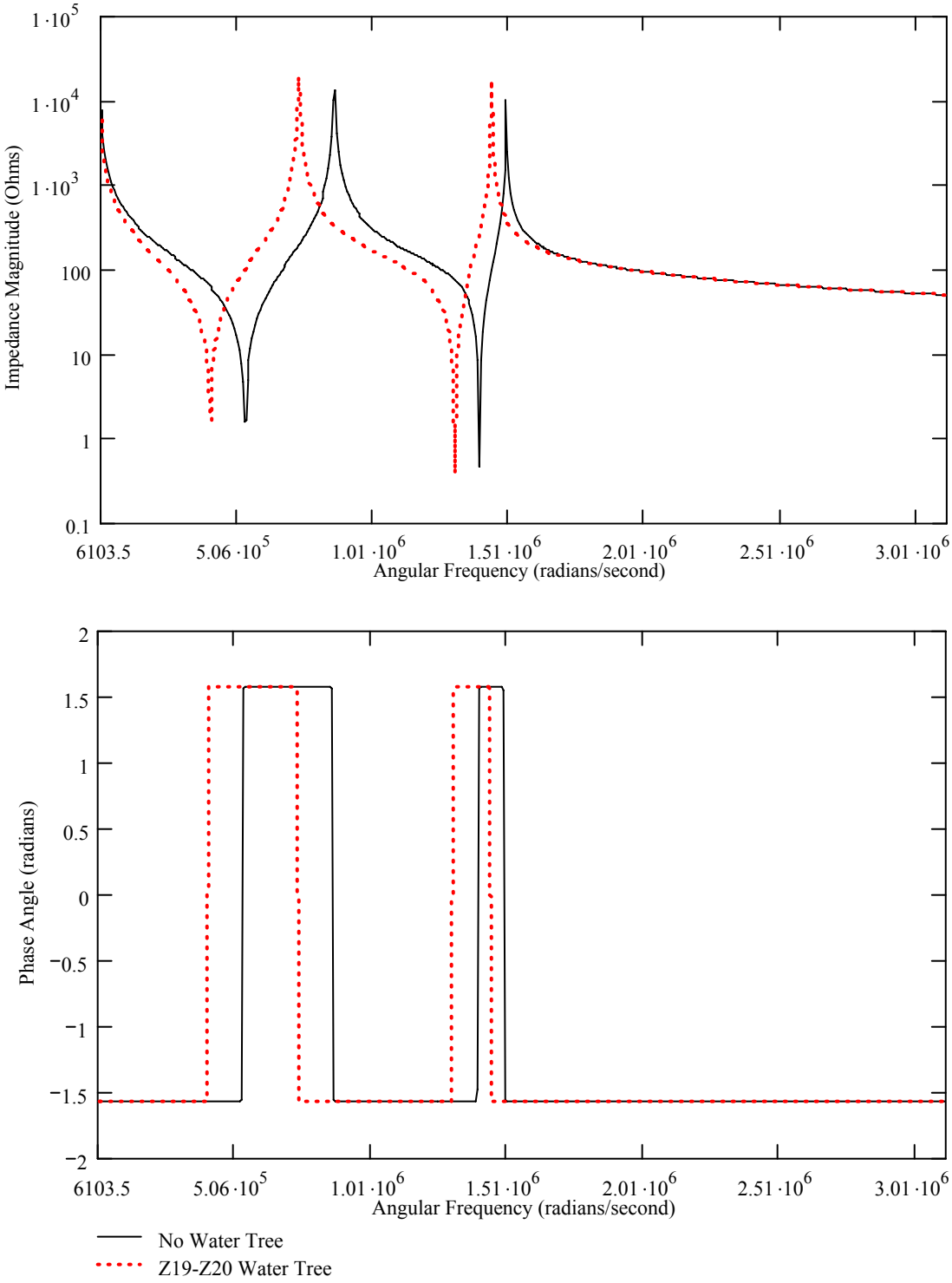

Figure 4.28 Calculated Impedance Magnitude and Phase Angle vs Frequency
22 Impedance Element Model, L=100 m, D=10.3 mm AL, 4.45 mm XLPE,
Without vs With Z19-Z20 Water Tree

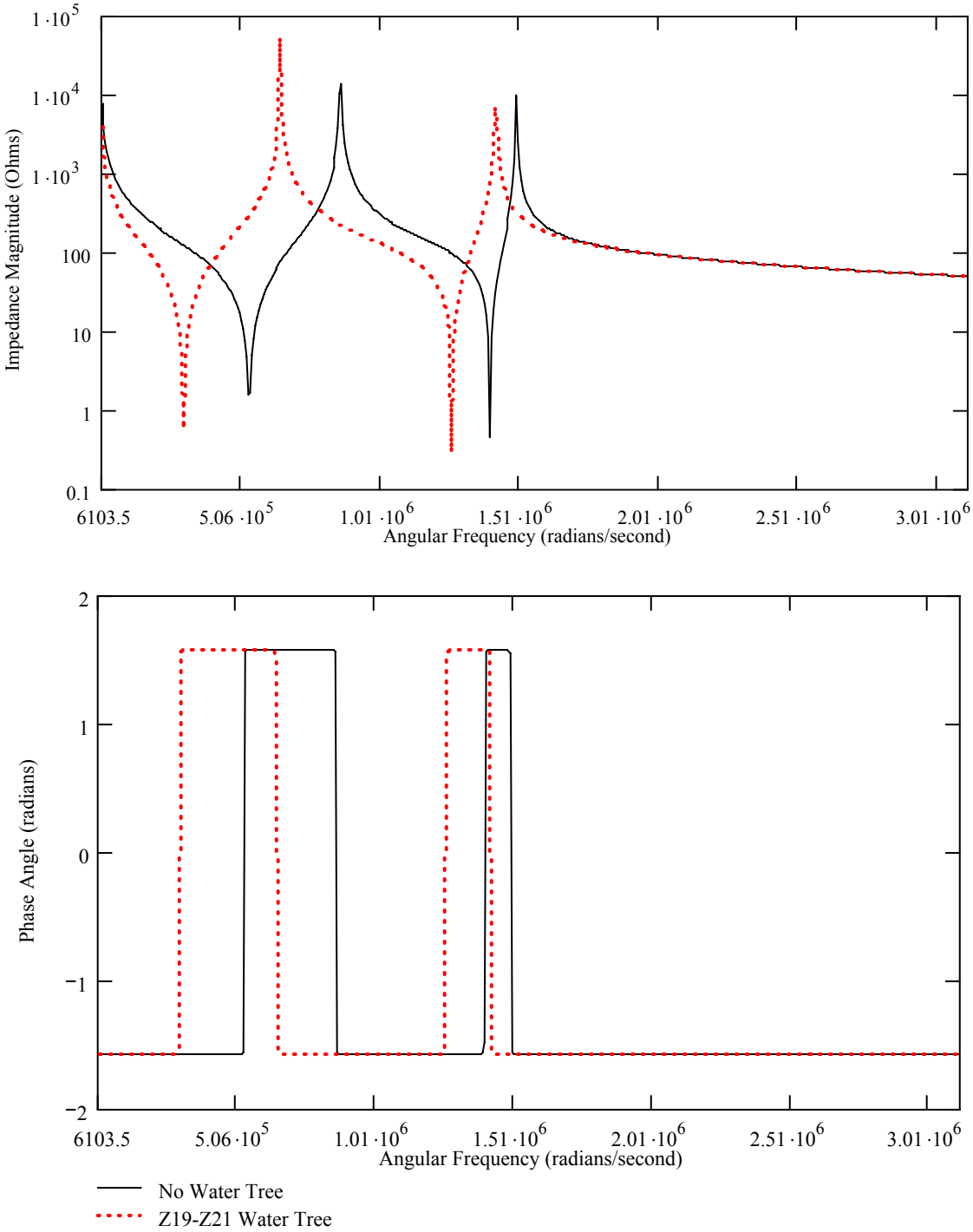

Figure 4.29 Calculated Impedance Magnitude and Phase Angle vs Frequency
22 Impedance Element Model, L=100 m, D=10.3 mm AL, 4.45 mm XLPE,
Without vs With Z19-Z21 Water Tree

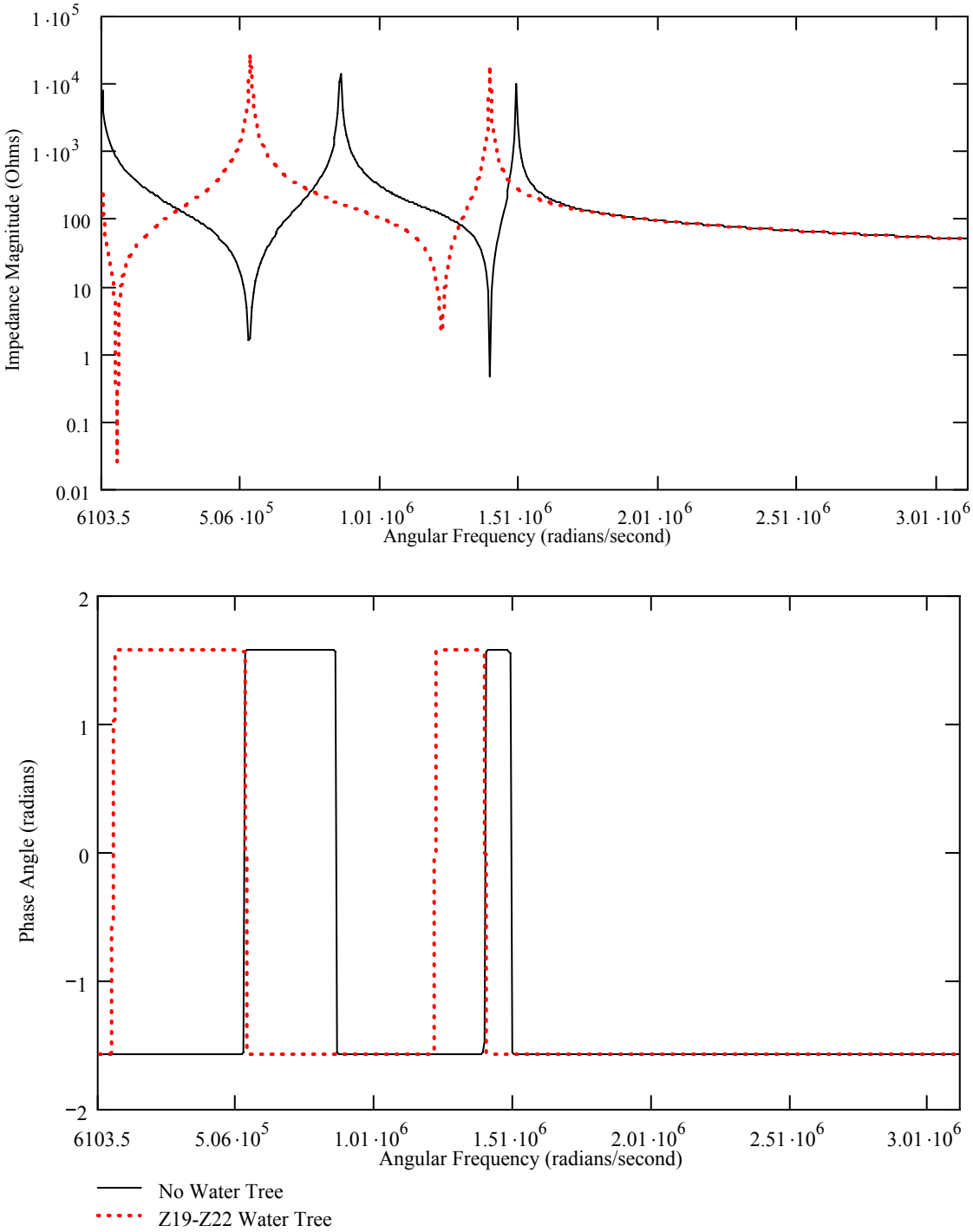

Figure 4.30 Calculated Impedance Magnitude and Phase Angle vs Frequency
22 Impedance Element Model, L=100 m, D=10.3 mm AL, 4.45 mm XLPE,
Without vs With Z19-Z22 Water Tree

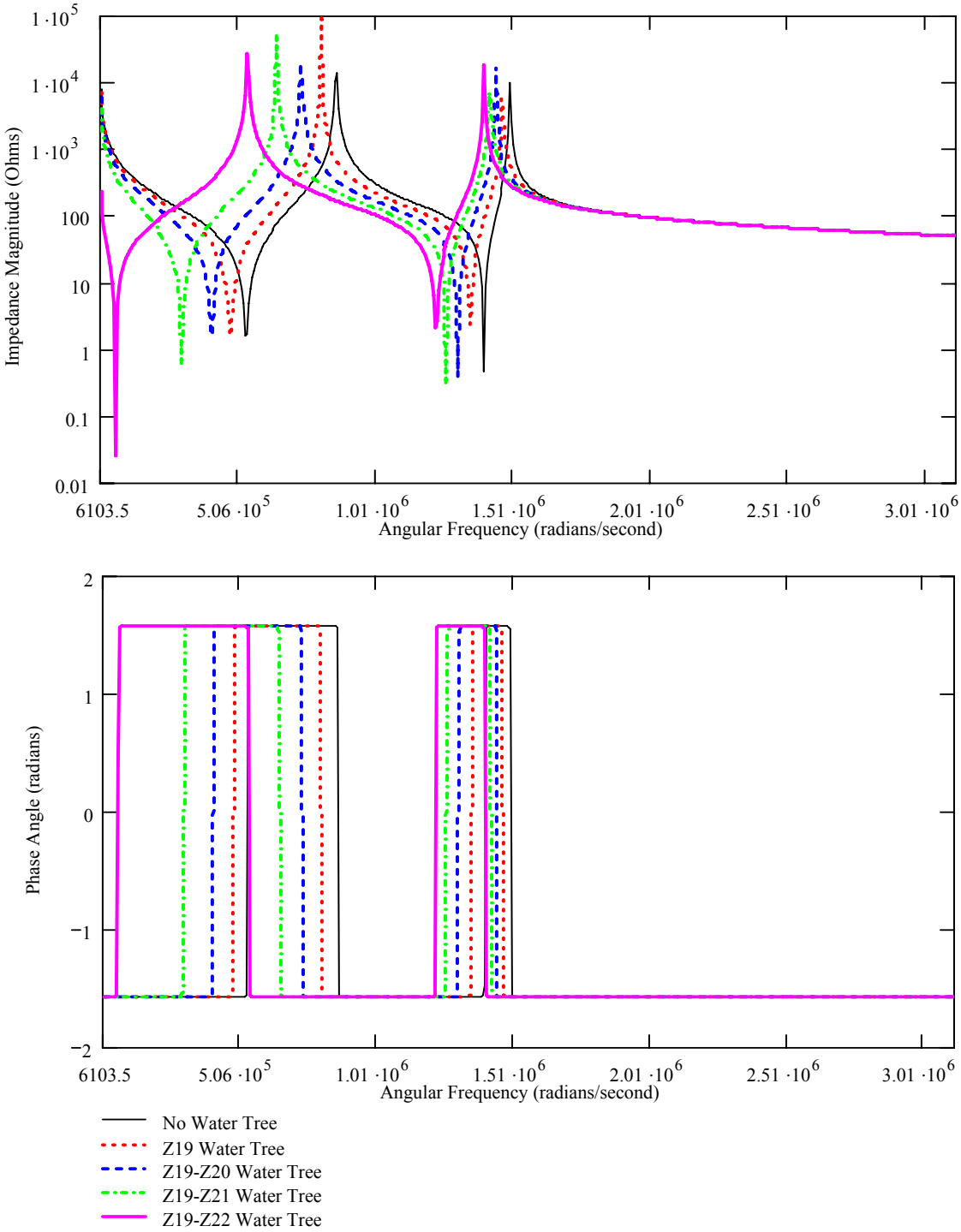

Figure 4.31 Calculated Impedance Magnitude and Phase Angle vs Frequency
22 Impedance Element Model, L=100 m, D=10.3 mm AL, 4.45 mm XLPE,
Without vs With Z19, Z19-Z20, Z19-Z21 & Z19-Z22 Water Trees

Calculations were also performed on the equivalent circuit model with uniform degradation across all insulation sections, comparing the impedance magnitude, in ohms, and phase angle, in radians, of a XLPE cable with a 10.3 mm OD aluminum conductor, an insulation thickness of 4.45 mm and a cable length of 100 m for the cases without versus with a water tree in the Z1, Z10 and Z19 locations. This simulates uniform water tree penetration over the entire length of the cable section. As shown in Figure 4.32, the most significant change with a simulated uniform water tree depth of one impedance is the increased shifting to a lower frequency of both resonance pairs, particularly the 2^{nd} resonance pair, and changing impedance maxima and minima magnitudes. Figure 4.33 has the water trees placed at the Z4, Z13 and Z22 location which simulates water tree initiated at the insulation shield and the result is identical to Figure 4.32 which simulates water trees initiated at the conductor shield. Figures 4.34, 4.35 and 4.36 show the water trees progressing toward a complete bridging of the insulation. Ultimately, all resonance pairs are shifted to lower frequencies with the largest shift occurring for the 2^{nd} maxima, the second largest shift for the 2^{nd} minima peak, and the third largest shift for the 1^{st} maxima and the smallest shift for the 1^{st} minima peak. All impedance maxima and minima magnitudes have also been reduced significantly. There is also a commensurate change in phase angle location but not magnitude, which remains at $\pm\Pi/2$.

Figure 4.37 shows the calculated results of Figures 4.32, 4.34 to 4.36. This figure summarizes how uniform water trees and their length impacts the impedance magnitude and phase angle for a fixed conductor size, cable length and insulation thickness for the insulation group closest to the voltage source.

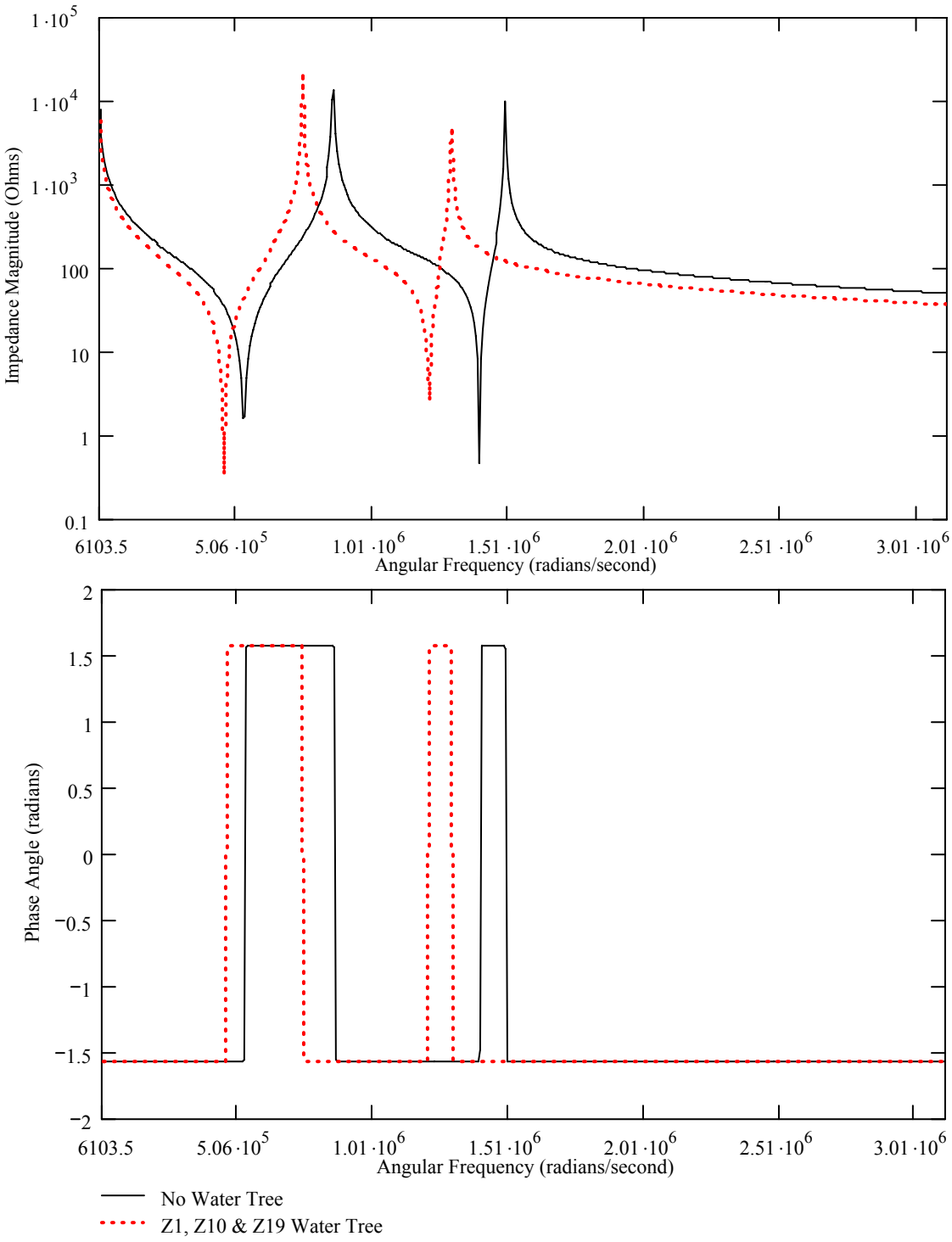

Figure 4.32 Calculated Impedance Magnitude and Phase Angle vs Frequency
22 Impedance Element Model, L=100 m, D=10.3 mm AL, 4.45 mm XLPE,
Without vs With Z1, Z10 & Z19 Water Trees

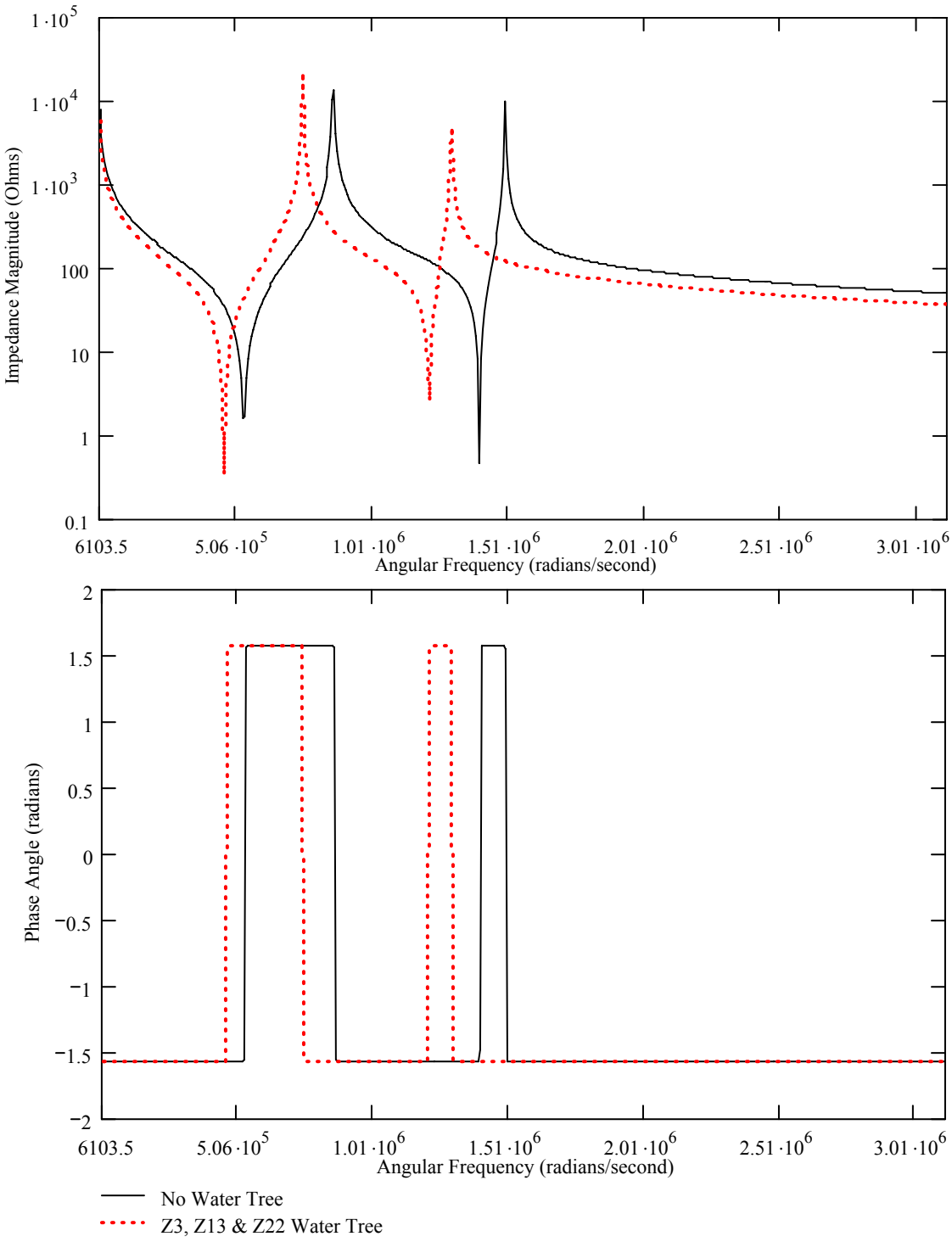

Figure 4.33 Calculated Impedance Magnitude and Phase Angle vs Frequency
22 Impedance Element Model, L=100 m, D=10.3 mm AL, 4.45 mm XLPE,
Without vs With Z4, Z13 & Z22 Water Trees

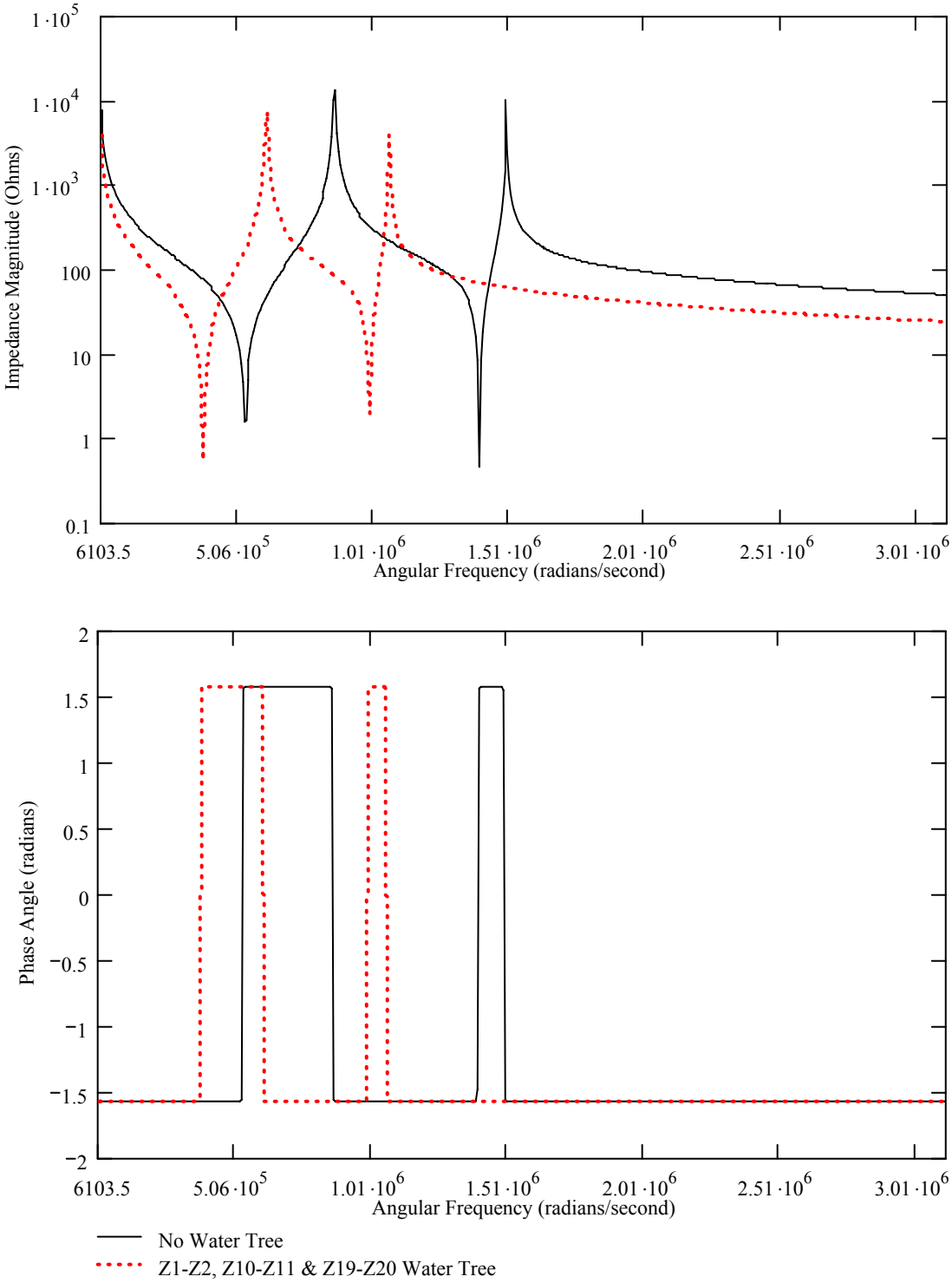

Figure 4.34 Calculated Impedance Magnitude and Phase Angle vs Frequency
22 Impedance Element Model, L=100 m, D=10.3 mm AL, 4.45 mm XLPE,
Without vs With Z1-Z2, Z10-Z11 & Z19-Z20 Water Trees

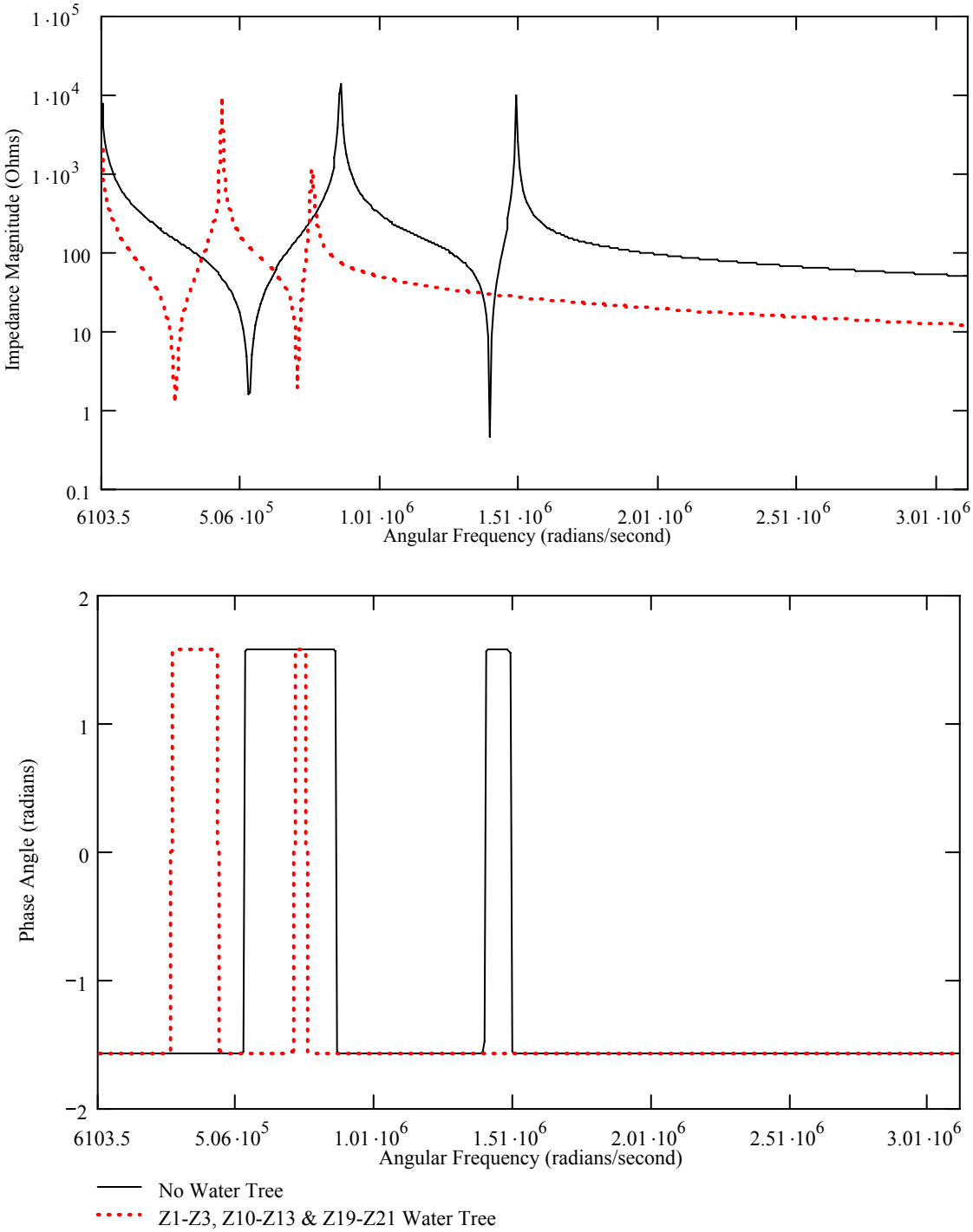

Figure 4.35 Calculated Impedance Magnitude and Phase Angle vs Frequency
22 Impedance Element Model, L=100 m, D=10.3 mm AL, 4.45 mm XLPE,
Without vs With Z1-Z3, Z10-Z12 & Z19-Z21 Water Trees

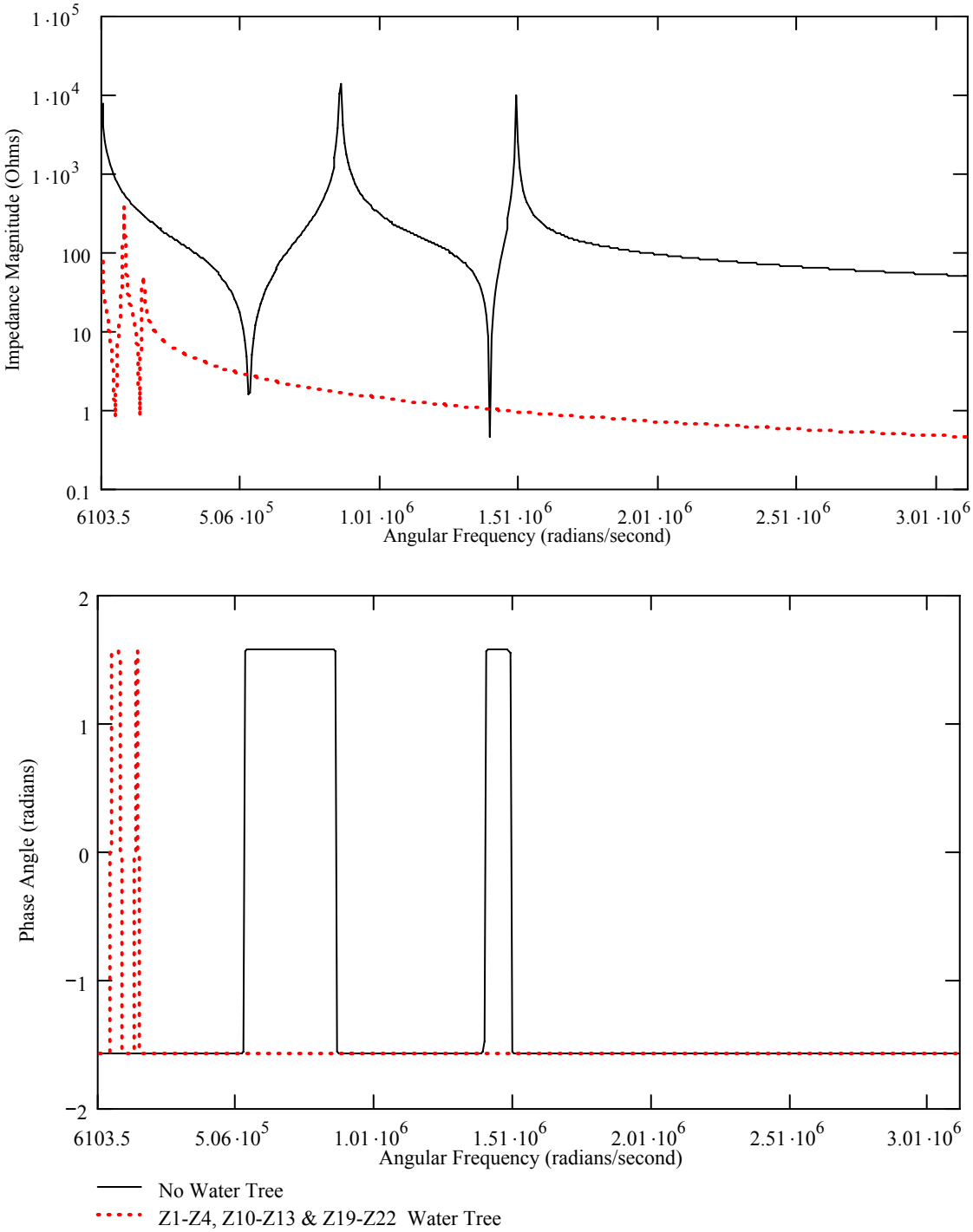

Figure 4.36 Calculated Impedance Magnitude and Phase Angle vs Frequency
22 Impedance Element Model, L=100 m, D=10.3 mm AL, 4.45 mm XLPE,
Without vs With Z1-Z4, Z10-Z13 & Z19-Z22 Water Trees

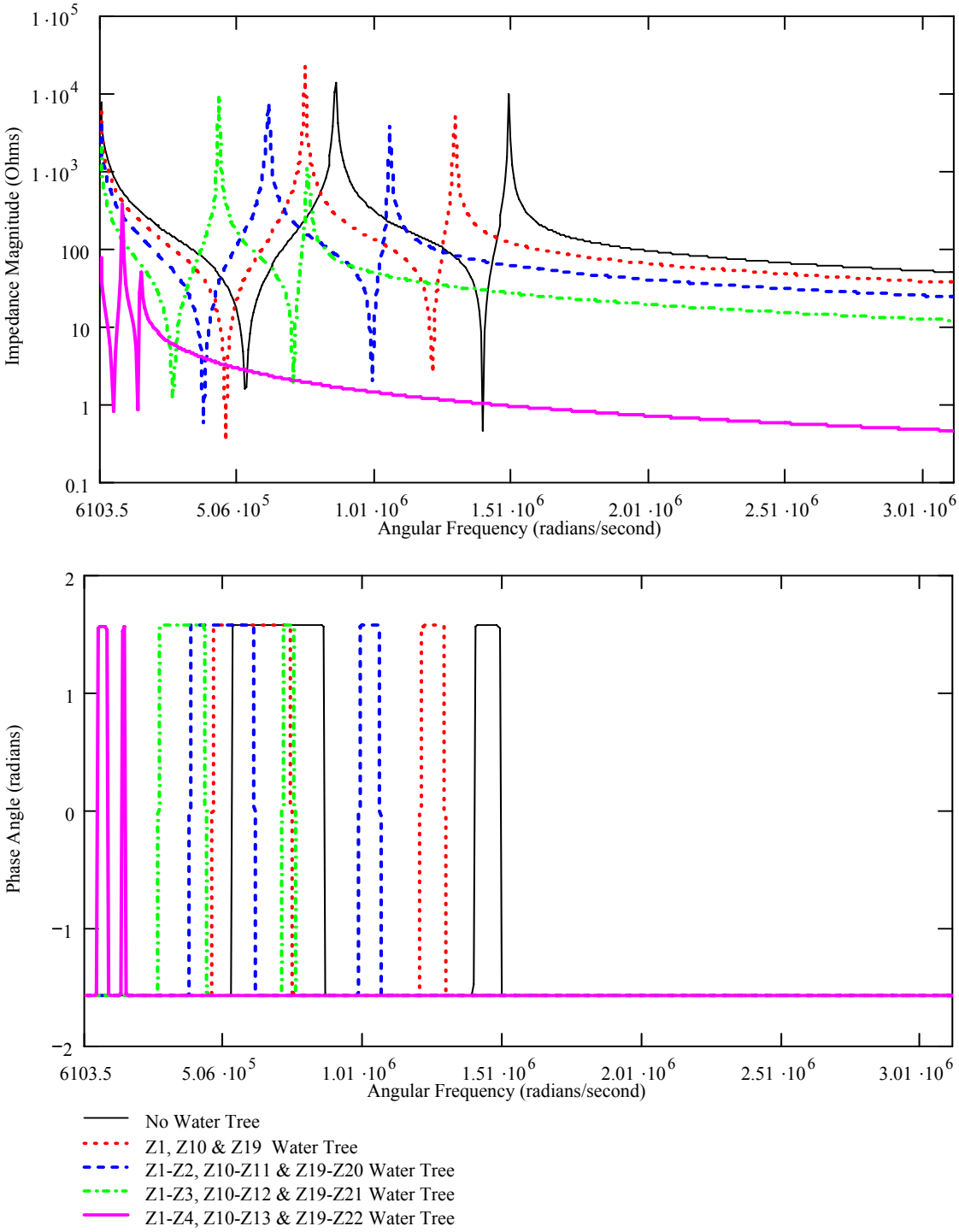

Figure 4.37 Calculated Impedance Magnitude and Phase Angle vs Frequency
22 Impedance Element Model, L=100 m, D=10.3 mm AL, 4.45 mm XLPE,
Without vs With Z1, Z10 & Z19 Branch Water Trees

Equivalent Circuit Model Impact on Water Tree Effect

Water tree effect calculations were also performed utilizing the three conductor equivalent circuit model of Figure 4.8. These additional calculations were performed to determine the effect of model choice on the theoretical observations since this model creates a third resonance pair. Z1, Z2 and Z3 in Figure 4.8 are the group of insulation impedances between the conductor and concentric neutral nearest the voltage source. Figure 4.38 compares the impedance magnitude, in ohms, and phase angle, in radians, over the frequency range of interest of a XLPE cable with a 10.3 mm OD aluminum conductor, an insulation thickness of 4.45 mm and a cable length of 100 m for the cases without versus with a water tree in the Z1 location. Compared to the calculation without a water tree, the associated impedance magnitude maxima are shifted to lower frequencies while the minima remain at the same frequency. The water tree cable impedance magnitudes are also of a lower magnitude for the 1^{st} , 2^{nd} and 3^{rd} maxima respectively while the minima remain unchanged. Additionally, the water tree cable phase angle step changes have been shifted commensurate with the impedance magnitude modifications. However, there is no change in the phase angle values which remains at $\pm\Pi/2$.

Z8, Z9 and Z10 in Figure 4.8 are the 2^{nd} group of insulation impedances between the conductor and concentric neutral nearest the voltage source. Figure 4.39 compares the impedance magnitude, in ohms, and phase angle, in radians, over the frequency range of interest of an identical XLPE cable as described in the previous paragraph for the cases without versus with a water tree in the Z8 location. Compared to the calculation without

a water tree, the numbers of resonance pairs are reduced to two. The associated impedance magnitude maxima peaks are shifted to lower frequencies while the 1st and 2nd minima are shifted to a higher and lower frequency respectively. The water tree cable impedance magnitudes are also of a lower and higher magnitude for the 1st and 2nd maxima and minima respectively. The water tree cable phase angle step changes have been shifted commensurate with the impedance magnitude changes once again. However, there is still no change in the phase angle values which remains at ±Π/2.

Figure 4.40 evaluates the water tree effect for the group of insulation impedances between the conductor and concentric neutral third closest to the voltage source Z15, Z16 and Z17 in Figure 4.8. Again the impedance magnitude, in ohms, and phase angle, in radians, over the frequency range of interest of an identical XLPE cable as described in the previous paragraphs is compared for the cases without versus with a water tree in the Z15 location. Compared to the calculation without a water tree, the associated impedance magnitude 2nd maxima and 3rd maxima and minima are shifted to lower frequencies while the remaining maxima and minima appear to shift a barely discernable amount to a lower frequency. The water tree cable impedance magnitudes are also of a higher magnitude for all maxima while the 2nd and 3rd minima are of higher magnitude. The water tree cable phase angle step changes have been shifted commensurate with the impedance magnitude modifications. However, there is no change in the phase angle values which remains at ±Π/2.

Z22, Z23 and Z24 in Figure 4.8 are the group of insulation impedances between the conductor and concentric neutral furthest from the voltage source. Figure 4.41

compares the impedance magnitude, in ohms, and phase angle, in radians, over the frequency range of interest of an identical XLPE cable as described in the previous paragraphs for the cases without versus with a water tree in the Z22 location. Compared to the calculation without a water tree, all the associated impedance magnitude peaks are shifted to a lower frequency. The water tree cable impedance magnitudes are of a lower magnitude for the 1st maxima and minima and 2nd minima while 2nd maxima and 3rd maxima and minima are of a higher value. Additionally, the water tree cable phase angle step changes have been shifted commensurate with the impedance magnitude movement. However, the phase angle values still remains at ±Π/2.

For this equivalent circuit model the effect of a single simulated water tree, whether a three or two section conductor impedance model is utilized, produces similar behavior for groups nearest and furthest away from voltage source. There is hybrid behavior for the 3 middle sections versus 2 middle sections due to the bigger impact of water trees as they now cover 33% vs 25% of the radial distance between the conductor and the concentric neutral. Additionally, in either model there are commensurate changes in phase angle location with the impedance magnitude modifications but not magnitude.

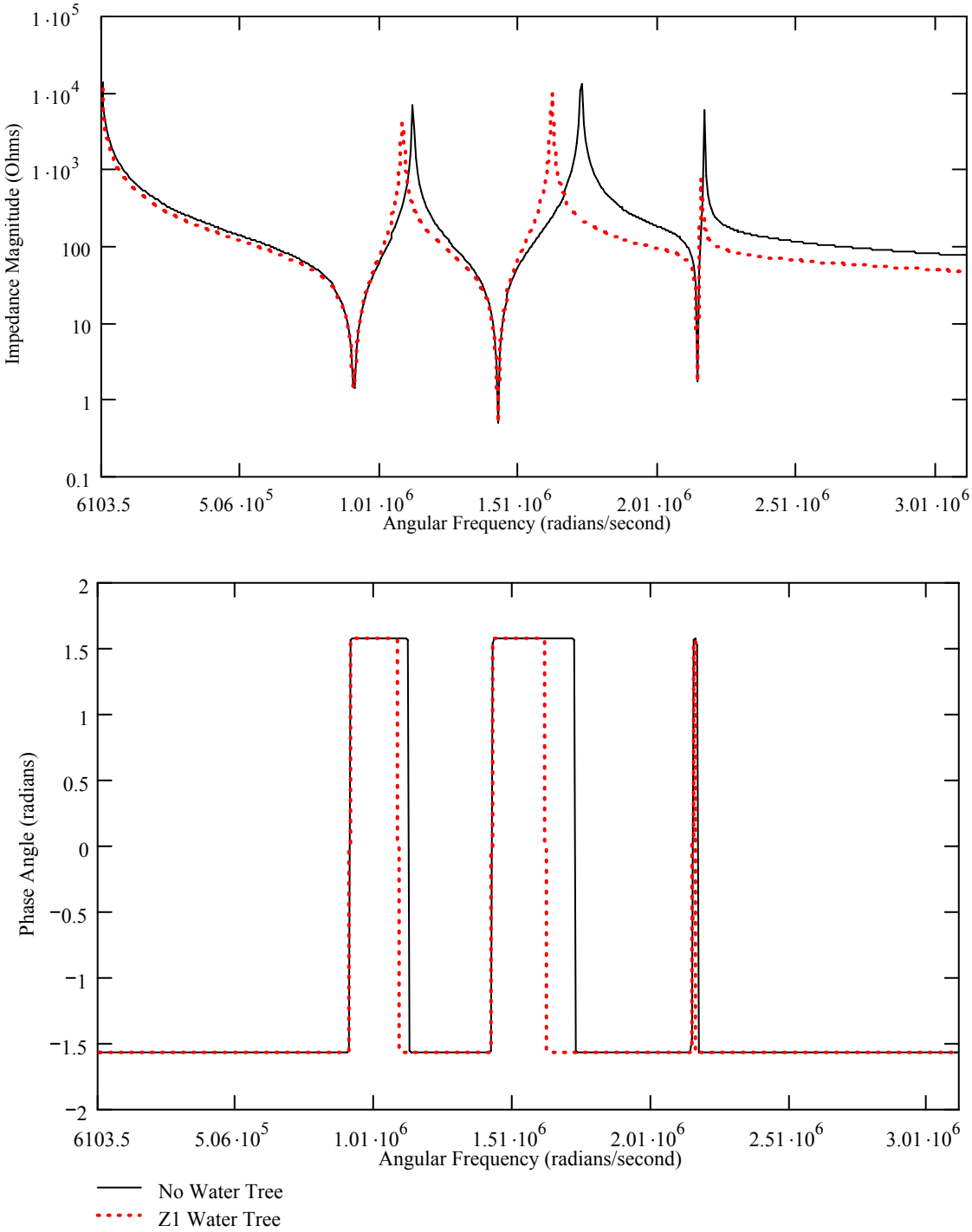

Figure 4.38 Calculated Impedance Magnitude and Phase Angle vs Frequency
24 Impedance Element Model, L=100 m, D=10.3 mm AL, 4.45 mm XLPE,
Without vs With Z1 Water Tree

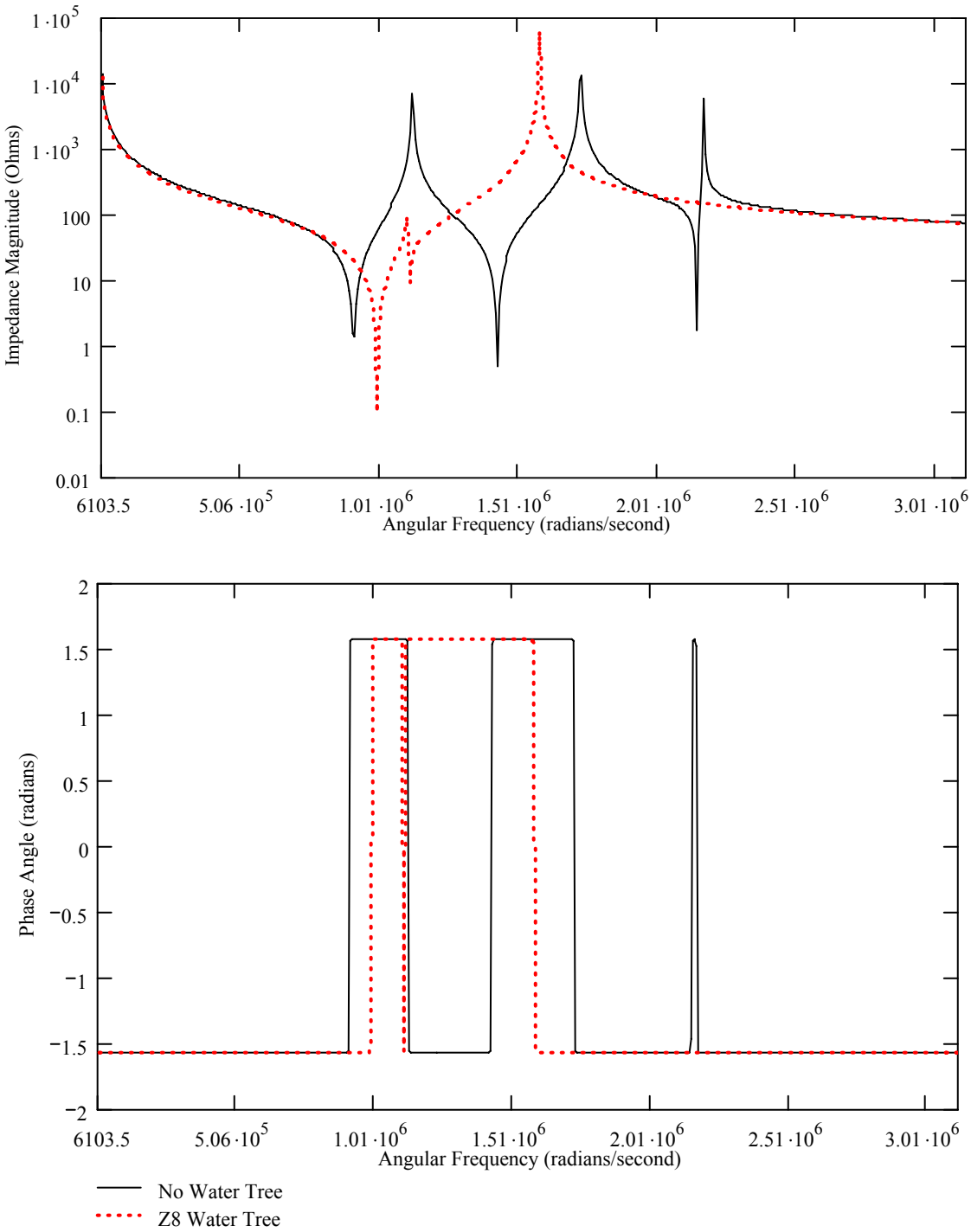

Figure 4.39 Calculated Impedance Magnitude and Phase Angle vs Frequency
24 Impedance Element Model, L=100 m, D=10.3 mm AL, 4.45 mm XLPE,
Without vs With Z8 Water Tree

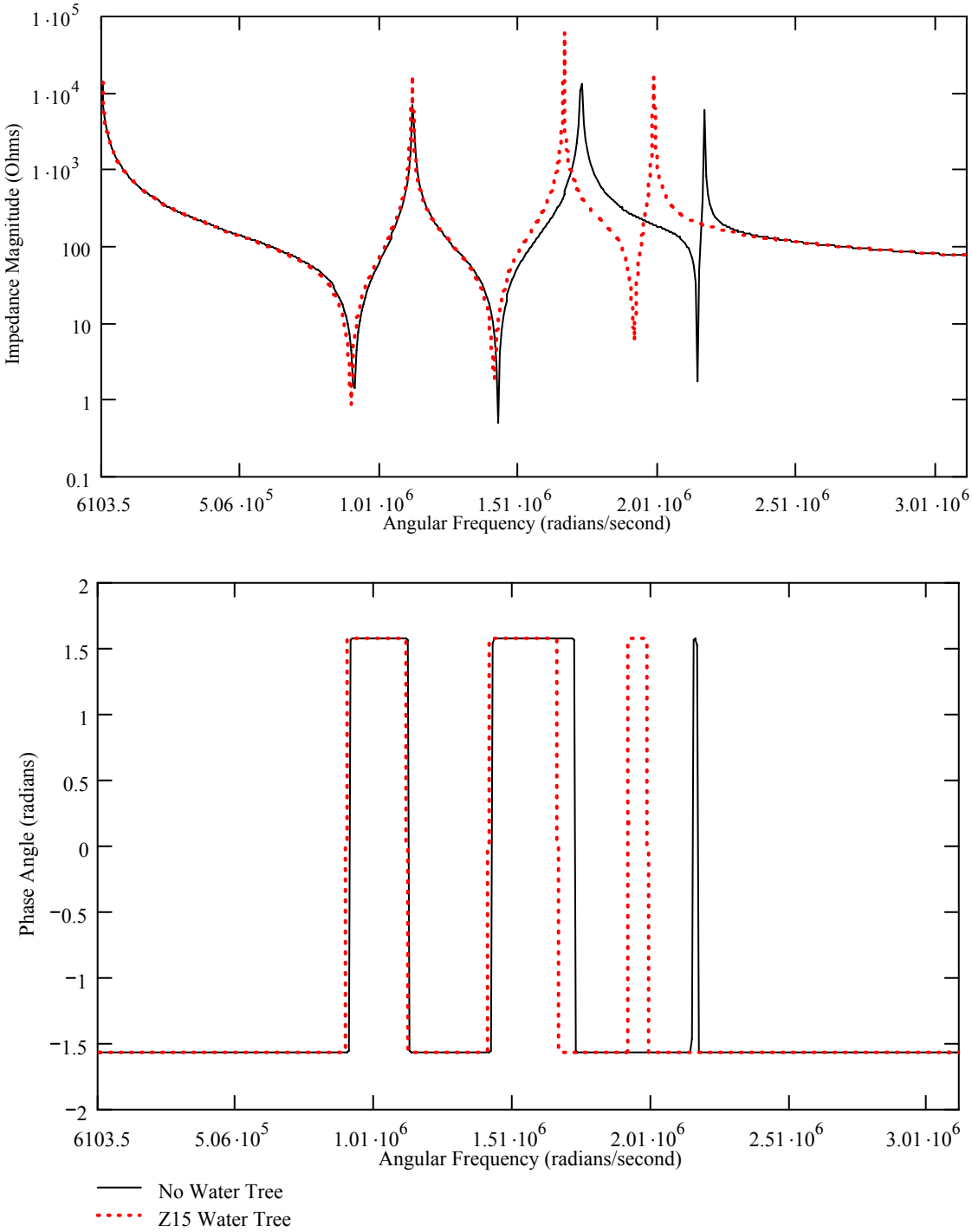

Figure 4.40 Calculated Impedance Magnitude and Phase Angle vs Frequency
24 Impedance Element Model, L=100 m, D=10.3 mm AL, 4.45 mm XLPE,
Without vs With Z15 Water Tree

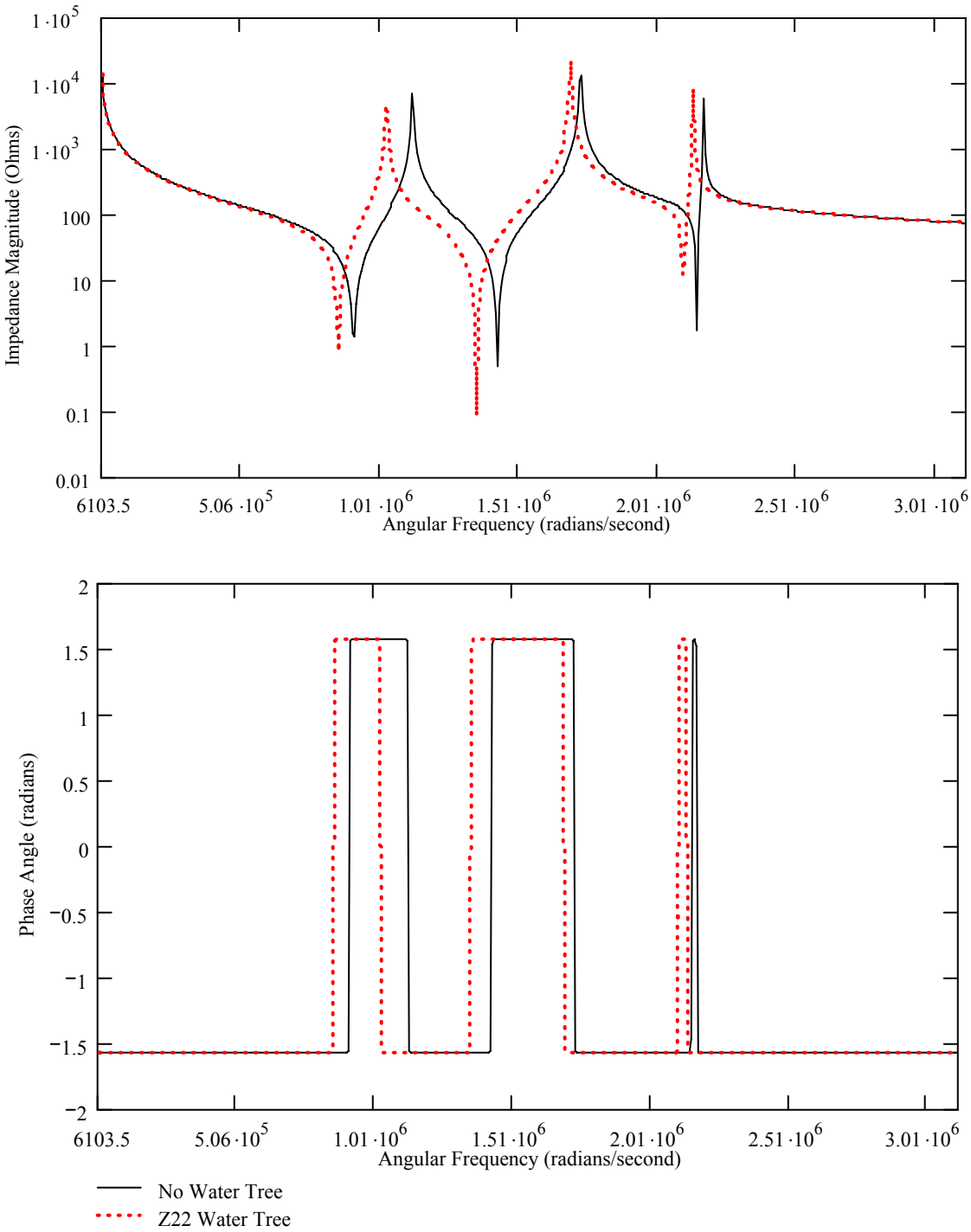

Figure 4.41 Calculated Impedance Magnitude and Phase Angle vs Frequency
24 Impedance Element Model, L=100 m, D=10.3 mm AL, 4.45 mm XLPE,
Without vs With Z22 Water Tree

Cable Length Impact on Water Tree Effect

As was discussed earlier, the length of the cable utilized in the equivalent circuit model of Figure 4.6 had the effect of shifting the resonance pairs to a lower and higher frequency for longer and shorter cable lengths respectively. It is also important to determine whether or not the effect of a water tree would be impacted by the cable length. Figures 4.42, 4.43 and 4.44 present the effect of a water tree on the impedance magnitude, in ohms, and phase angle, in radians, over the frequency range of interest of a XLPE cable with a 10.3 mm OD aluminum conductor, an insulation thickness of 4.45 mm and a cable length of 1000 m. The water tree location for the three figures is impedance Z1, Z10 and Z19 of Figure 4.6 respectively. The only difference between the calculations associated with Figures 4.42, 4.43 and 4.44 and Figures 4.16, 4.22 and 4.27 is the difference in cable lengths, 1000 m versus 100 m which results in increased capacitance, resistance and inductance values for the longer cable. The observed behavior of the impedance magnitude maxima and minima shifting to lower frequencies is identical to regardless of the cable length. However, the impact on the impedance magnitude maxima and minima is changed for the first water tree. Phase angle changes are identical regardless of the cable length.

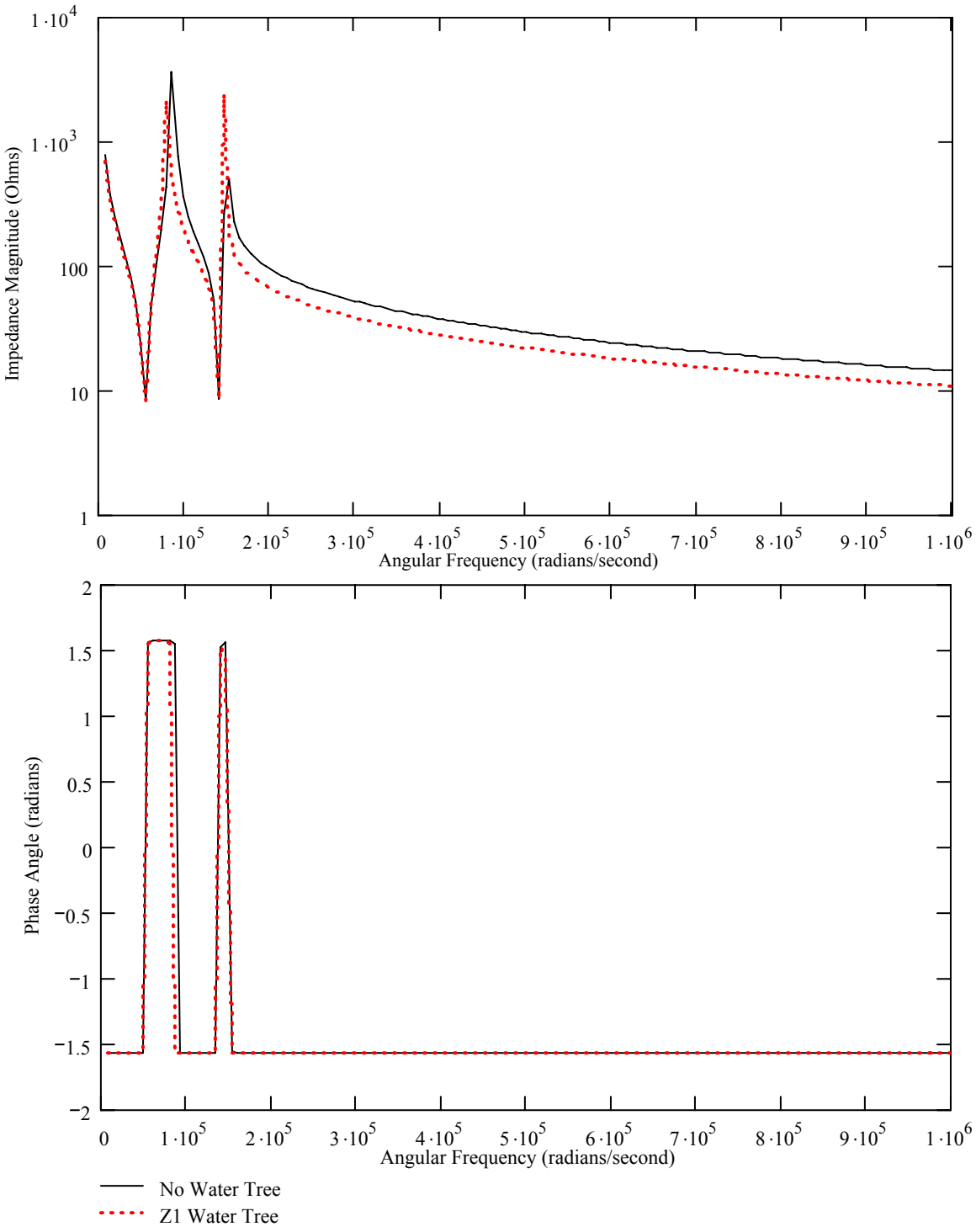

Figure 4.42 Calculated Impedance Magnitude and Phase Angle vs Frequency 22 Impedance Element Model, L=1000 m, D=10.3 mm AL, 4.45 mm XLPE, Without vs With Z1 Water Tree

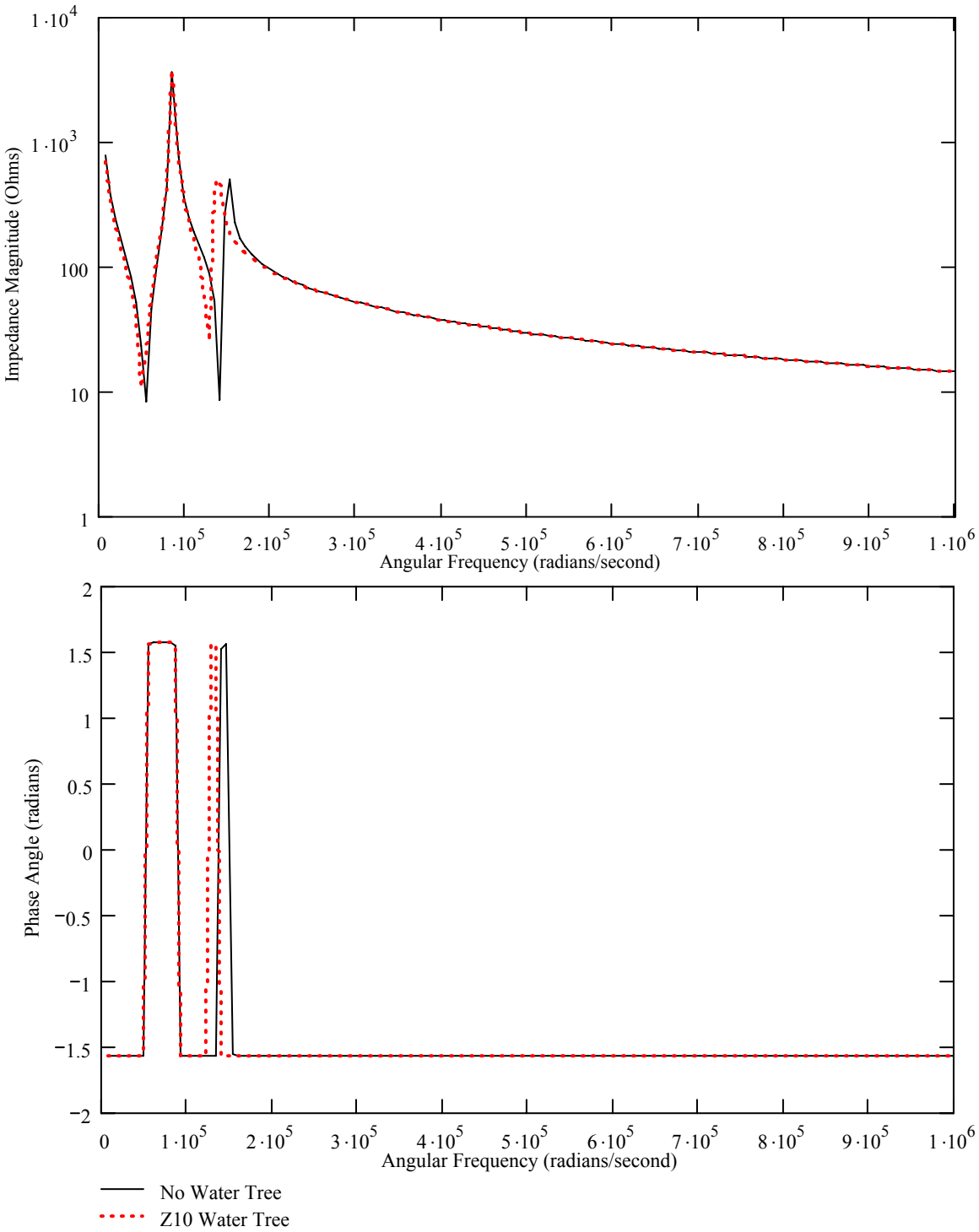

Figure 4.43 Calculated Impedance Magnitude and Phase Angle vs Frequency 22 Impedance Element Model, L=1000 m, D=10.3 mm AL, 4.45 mm XLPE, Without vs With Z10 Water Tree

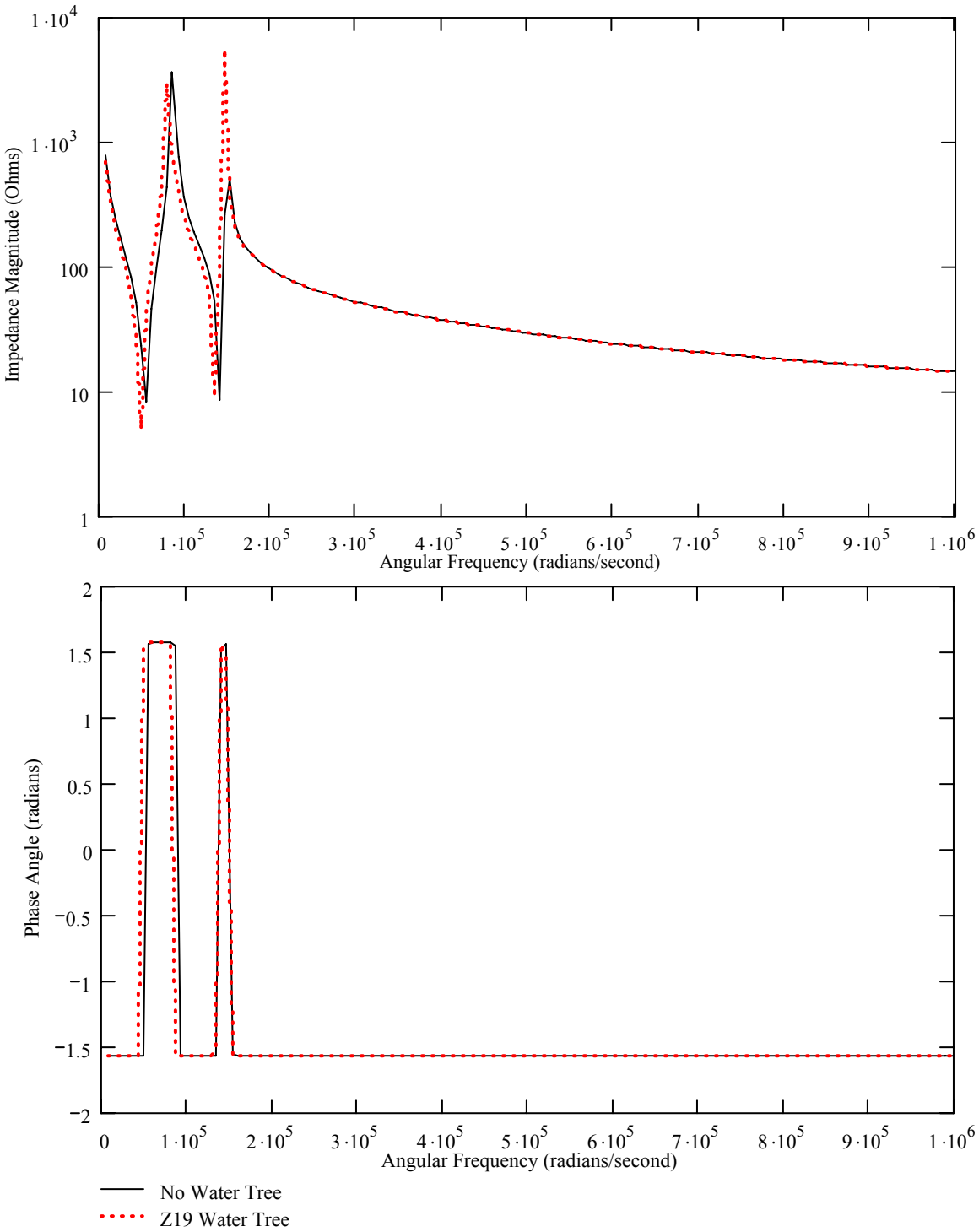

Figure 4.44 Calculated Impedance Magnitude and Phase Angle vs Frequency 22 Impedance Element Model, L=1000 m, D=10.3 mm AL, 4.45 mm XLPE, Without vs With Z19 Water Tree

Effects of Simulated Neutral Corrosion

The last groups of calculations conducted on the theoretical equivalent circuit model, Figure 4.6, are to investigate the effect of concentric neutral corrosion. Cables installed in the field are buried in the ground, typically in duct packages for San Diego Gas & Electric, and these duct packages can get filled with water from either rainfall or irrigation sprinklers. The effect of the water and associated chemicals is to corrode the copper neutrals. This corrosion results in cables with varying levels of intact concentric neutrals. Since the proposed measurement methodology measures the current flowing from the conductor, through the insulation and returning through the concentric neutrals it is important to determine what effect, if any, this will have on the impedance magnitude and phase angle.

The calculation results shown in Figures 4.45 and 4.46 demonstrate that there is no observable change in the impedance magnitude and phase angle versus frequency until the concentric neutrals open at some location and only a high impedance path back to the impulse voltage source remains. The responses of both the impedance magnitude, in ohms, and phase angle, in radians, are dependant upon return path impedance that is utilized. With an open concentric neutral impedance of 200 ohms spaced equally along the cable model, shown in Figure 4.46, the impedance magnitude of the resonance pairs maxima and minima has been significantly damped, rounded and almost flattened. As this impedance rises above 200 ohms, the impedance magnitude maxima and minima disappear and the magnitude exponentially decays with increasing frequency. The impedance phase angle now increases slowly to its peak value at approximately 700

kradians/sec and then also exponentially decays with a second maximum at 1.3 Mradians/sec.

It was also observed that the impedance magnitude and phase angle response is dependant upon the location of the open neutrals, shown in Figures 4.47 and 4.48, but in either instance there is significant damping of the two resonance pairs. When the cable was modeled with the neutrals open in the 1st half of the cable, Figure 4.47, the distinction between the two impedance magnitude and two phase angle peaks is more pronounced. For the cable with the neutrals open in the 2nd half of the cable, Figure 4.48, the impedance magnitude now only shows a 1st minima followed by a maxima and an exponential decay to approximately 70 ohms. The two phase angle peaks have blurred into a single peak curve with a small protrusion correlated to the new impedance magnitude maxima. Overall the step changes in phase angle due to resonance peaks have been greatly impacted and the phase angle changes over a larger frequency range. The initial and final phase angle values are -Π/2; however, the phase angle is only slightly positive for a short frequency range.

Figure 4.49 summarizes the calculated results of Figures 4.46 to 4.48. This figure provides a visual summary of how neutral corrosion and its location impacts the impedance magnitude and phase angle for a fixed conductor size, cable length and insulation thickness.

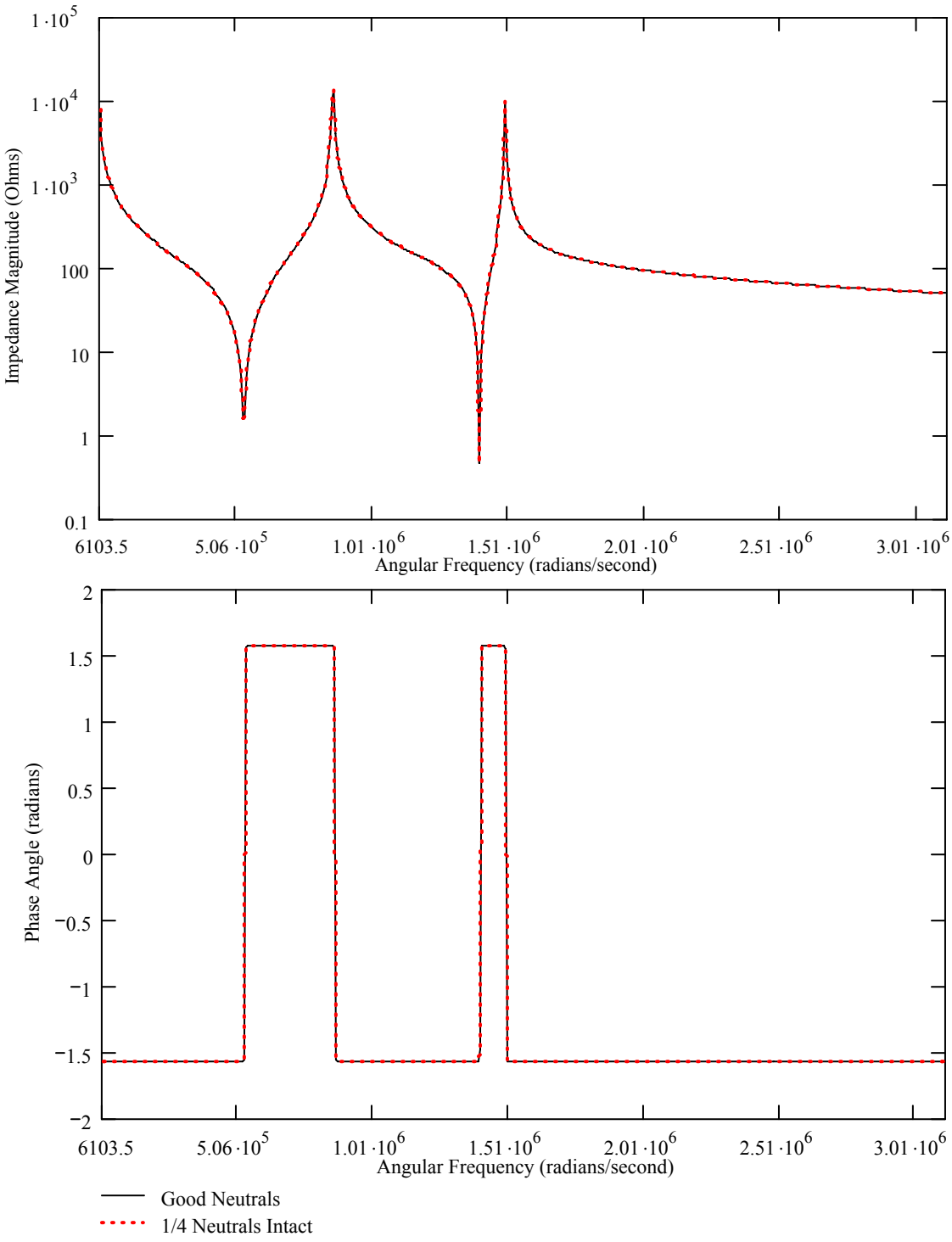

Figure 4.45 Calculated Impedance Magnitude and Phase Angle vs Frequency
22 Impedance Element Model, L=100 m, D=10.3 mm AL, 4.45 mm XLPE,
Good Neutrals vs ¼ of Neutrals Intact

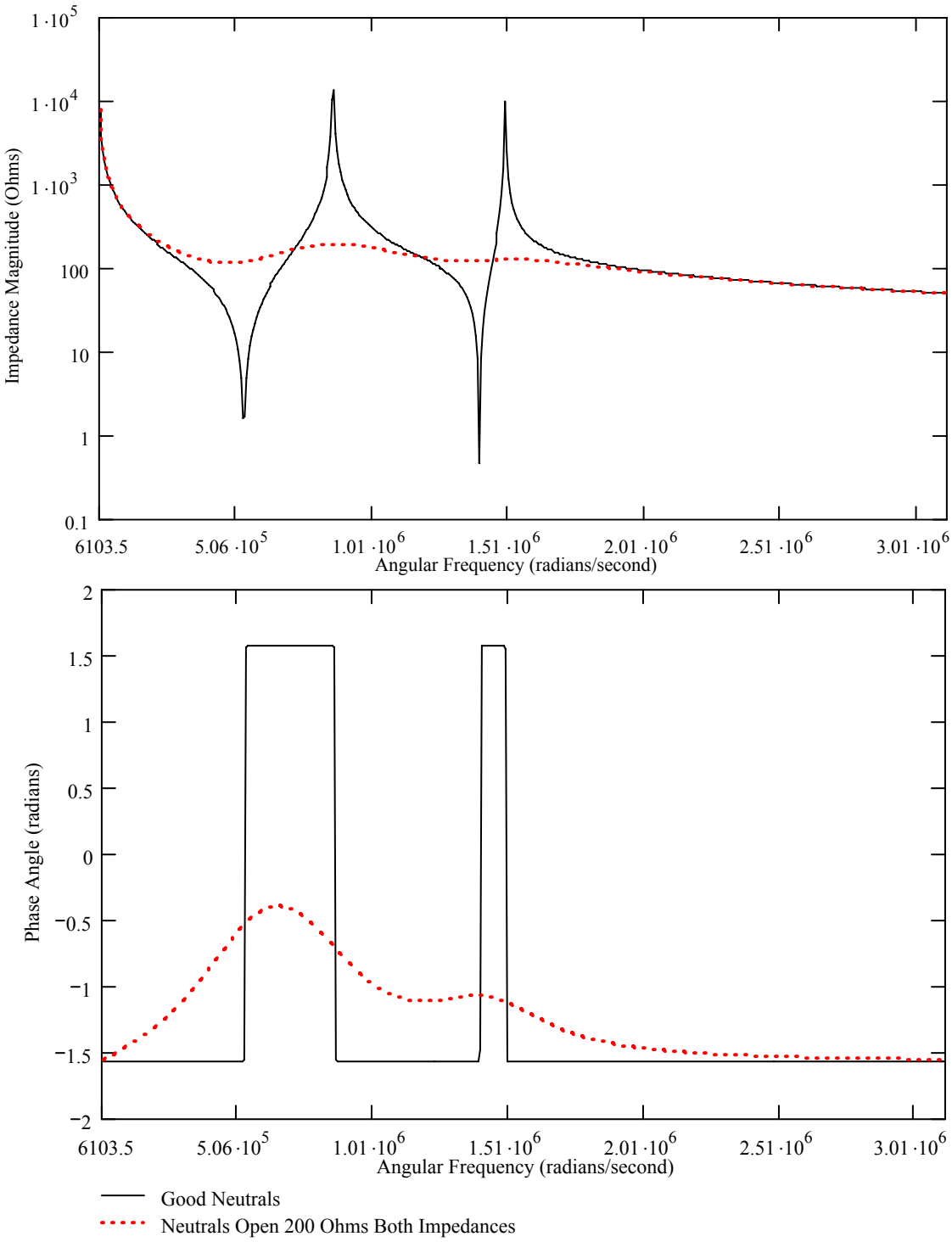

Figure 4.46 Calculated Impedance Magnitude and Phase Angle vs Frequency
22 Impedance Element Model, L=100 m, D=10.3 mm AL, 4.45 mm XLPE,
Good Neutrals vs Neutrals Open, 200 Ω Both Impedances

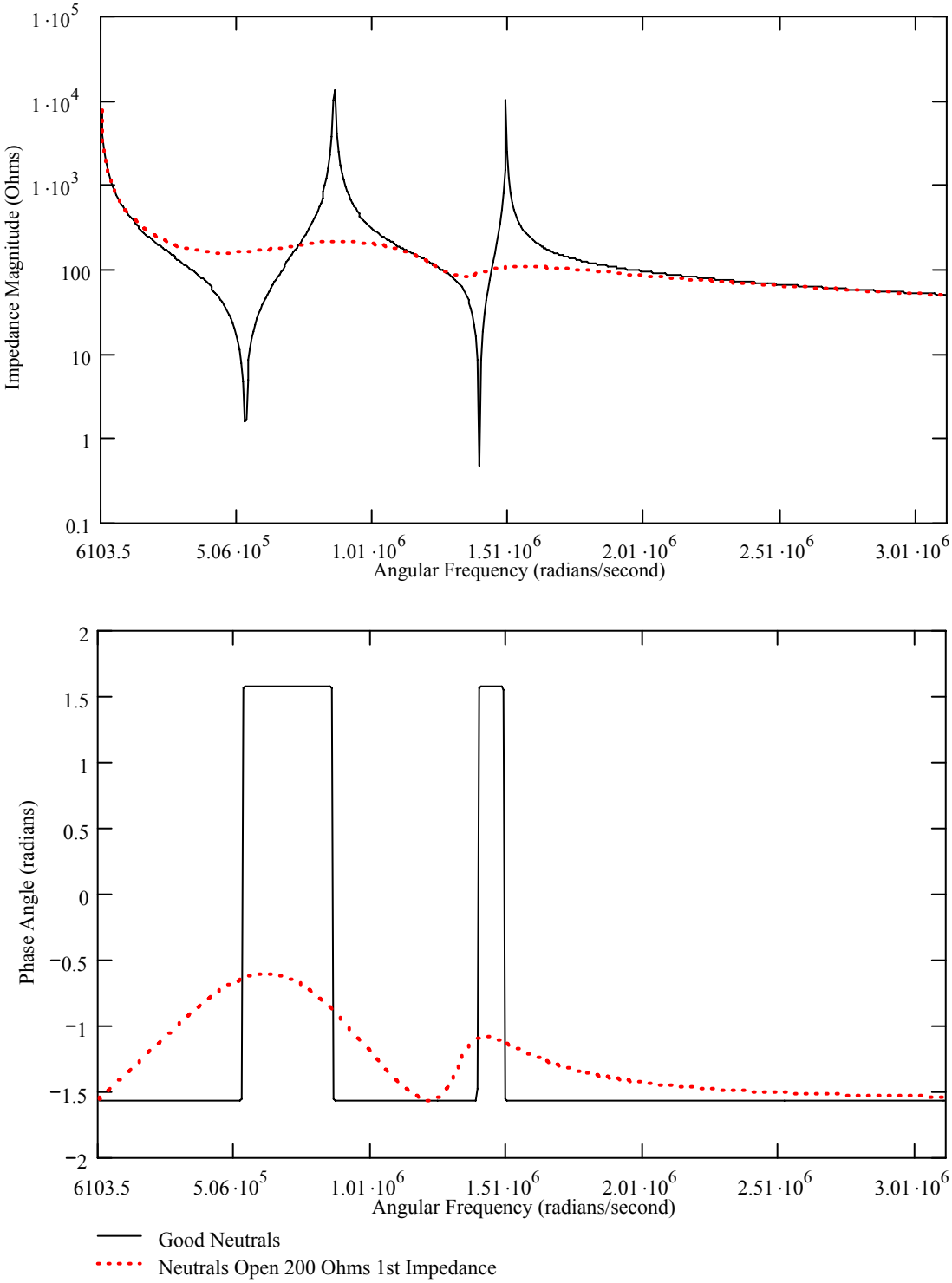

Figure 4.47 Calculated Impedance Magnitude and Phase Angle vs Frequency
22 Impedance Element Model, L=100 m, D=10.3 mm AL, 4.45 mm XLPE,
Good Neutrals vs Neutrals Open, 200 Ω 1st Impedance

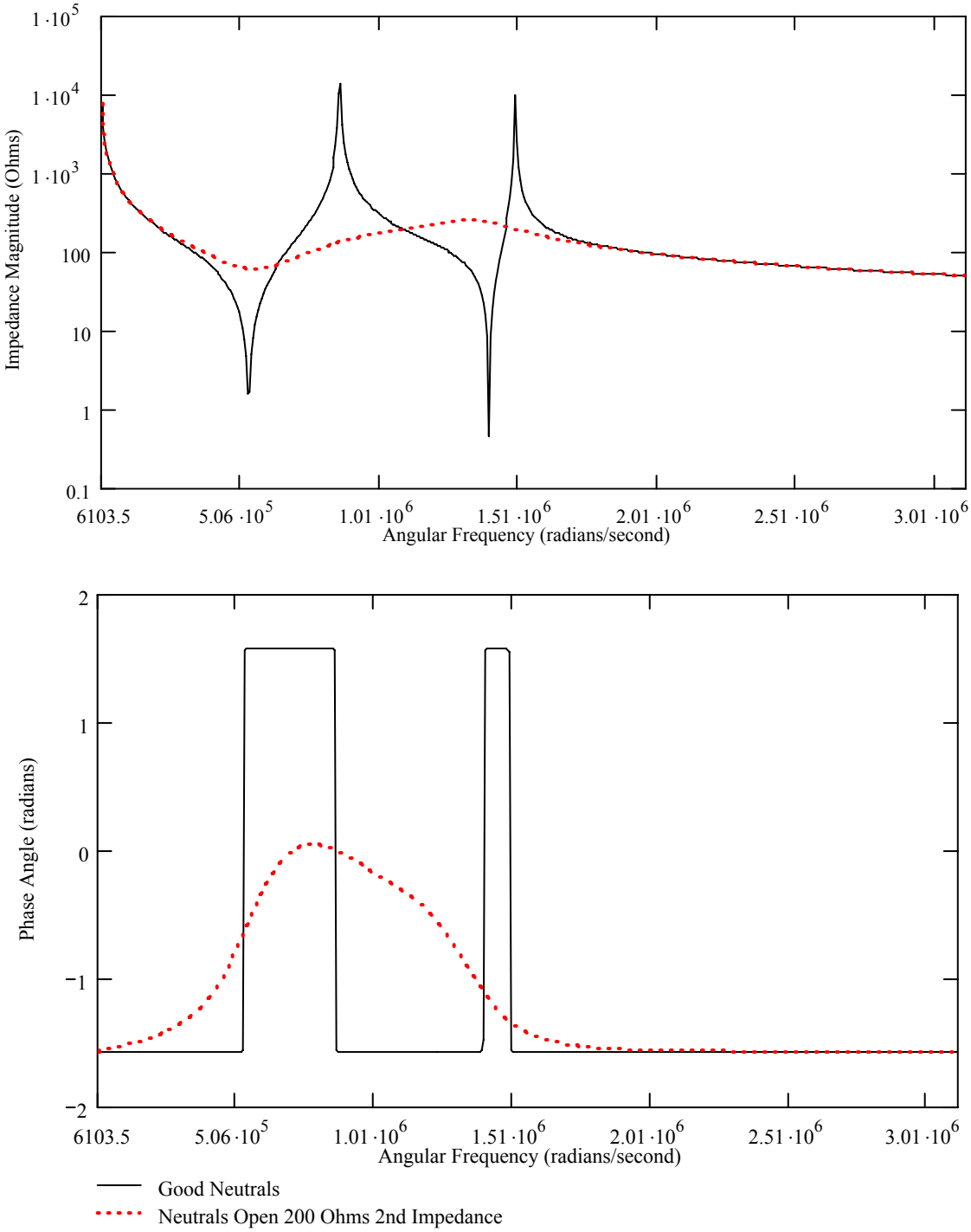

Figure 4.48 Calculated Impedance Magnitude and Phase Angle vs Frequency
22 Impedance Element Model, L=100 m, D=10.3 mm AL, 4.45 mm XLPE,
Good Neutrals vs Neutrals Open, 200 Ω 2nd Impedance

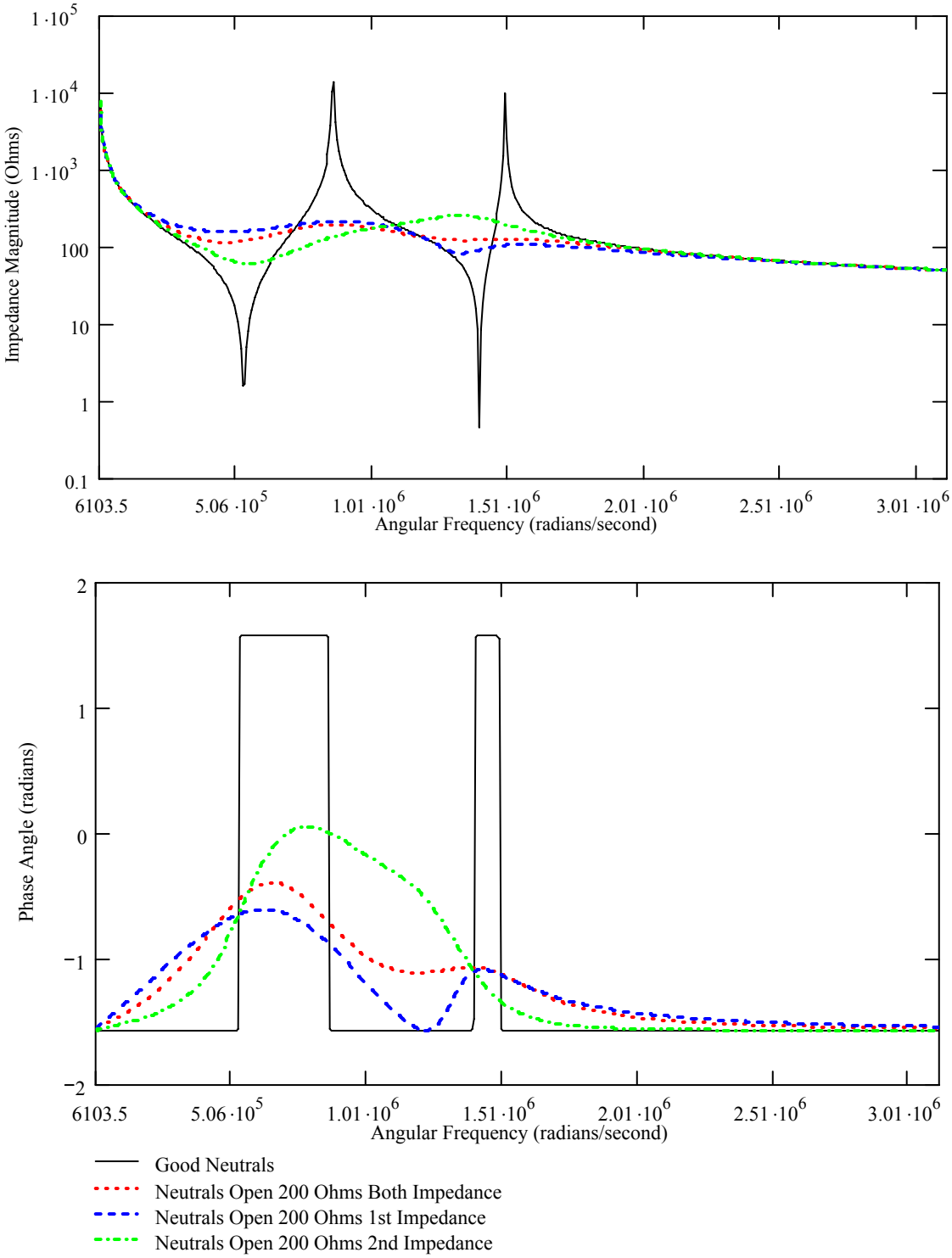

Figure 4.49 Calculated Impedance Magnitude and Phase Angle vs Frequency
22 Impedance Element Model, L=100 m, D=10.3 mm AL, 4.45 mm XLPE,
Good Neutrals vs Neutrals Open, 200 Ω Both, 1st & 2nd Impedance

The final calculations on the theoretical equivalent circuit model of Figure 4.6 were to observe how water trees impact the resonance peaks for a cable without concentric neutrals. It was previously observed that the effect of neutral corrosion is to significantly impact the resonance peak pairs and this impact is first dependant upon the open neutral location and then second dependant upon the water tree location. The effect was also found to continue to increase with length of water trees within the insulation.

For the specific case of no intact concentric neutrals spread along the length of the cable it is observed in Figure 4.50 that a water tree in the insulation group closest to voltage source, Z1, resulted in reduced impedance magnitude after the 1st minima. When the water tree was located in middle group, Z10, it is observed in Figure 4.51 that there is higher and shifted 2nd maxima but otherwise there was little change in the impedance magnitude. For the case of a water tree in the insulation group furthest from the voltage source, Z19, Figure 4.52 shows there is no discernable change in the impedance magnitude other that the shifting of all peaks to a lower frequency. The commensurate changes in phase angle are much larger than those observed for the impedance magnitude.

When the condition no intact neutrals exists in either the 1st or 2nd half of the cable and the water tree belonged to the insulation group closest to the voltage source, Z1, it is observed in Figures 4.53 and 4.54 that after the 1st impedance magnitude minima the remaining maxima and minima were damped and of lower magnitude. If the water tree was in the insulation group furthest from the voltage source, Z19, the 1st maxima and minima and 2nd minima impedance magnitudes are observed in Figures 4.55 and 4.56 to

be shifted to a lower frequency. The commensurate changes in phase angle are again much larger than those observed for the impedance magnitude.

The application of a voltage over a range of frequencies applied to the theoretical cable, modeled as an impedance matrix, has demonstrated that it is theoretically possible to discern changes within a cable system due to water trees. The next step is to perform actual measurements to demonstrate the feasibility of the proposed method.

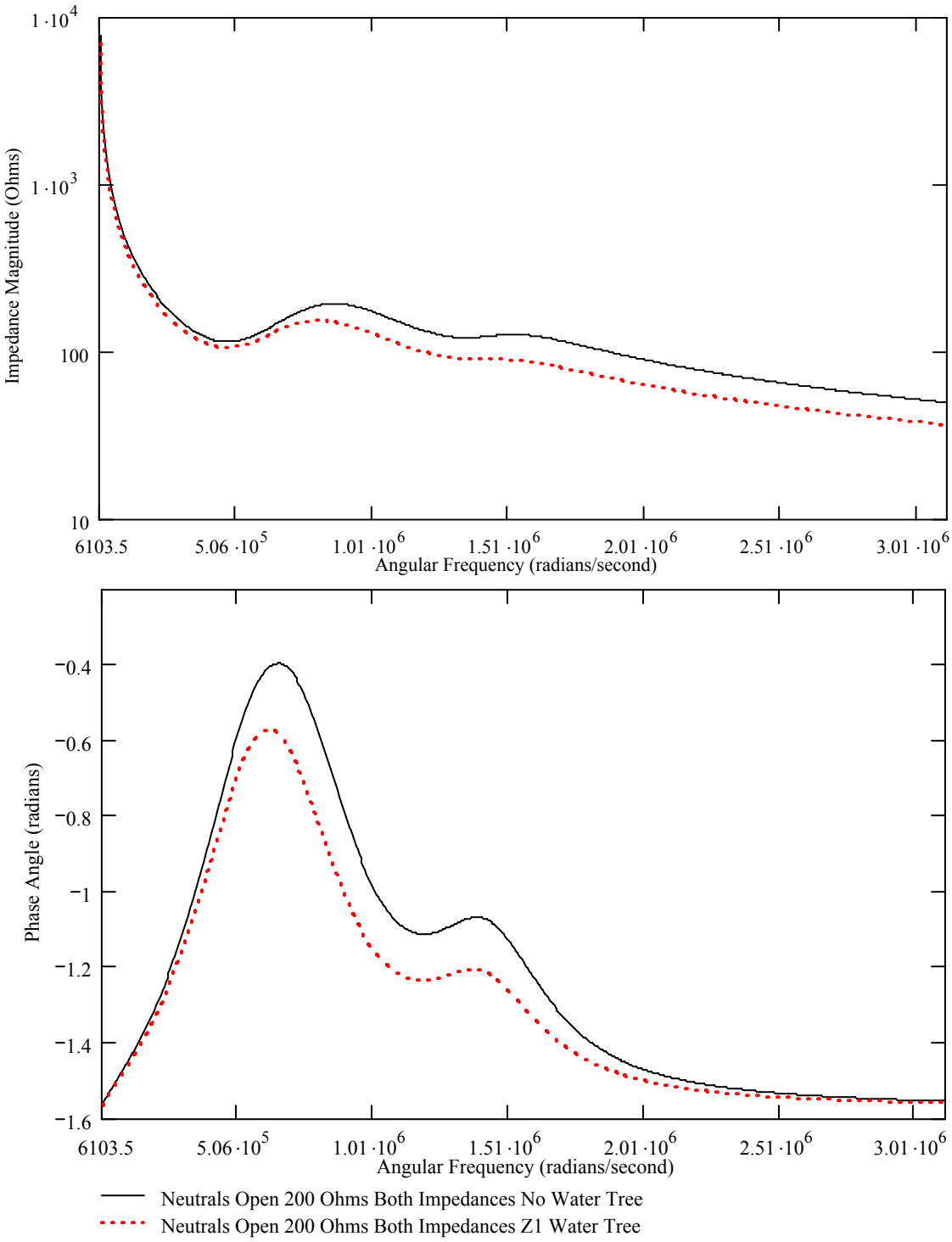

Figure 4.50 Calculated Impedance Magnitude and Phase Angle vs Frequency
22 Impedance Element Model, L=100 m, D=10.3 mm AL, 4.45 mm XLPE,
Neutrals Open, 200 Ω Both Impedances, No Water Tree vs Z1 Water Tree

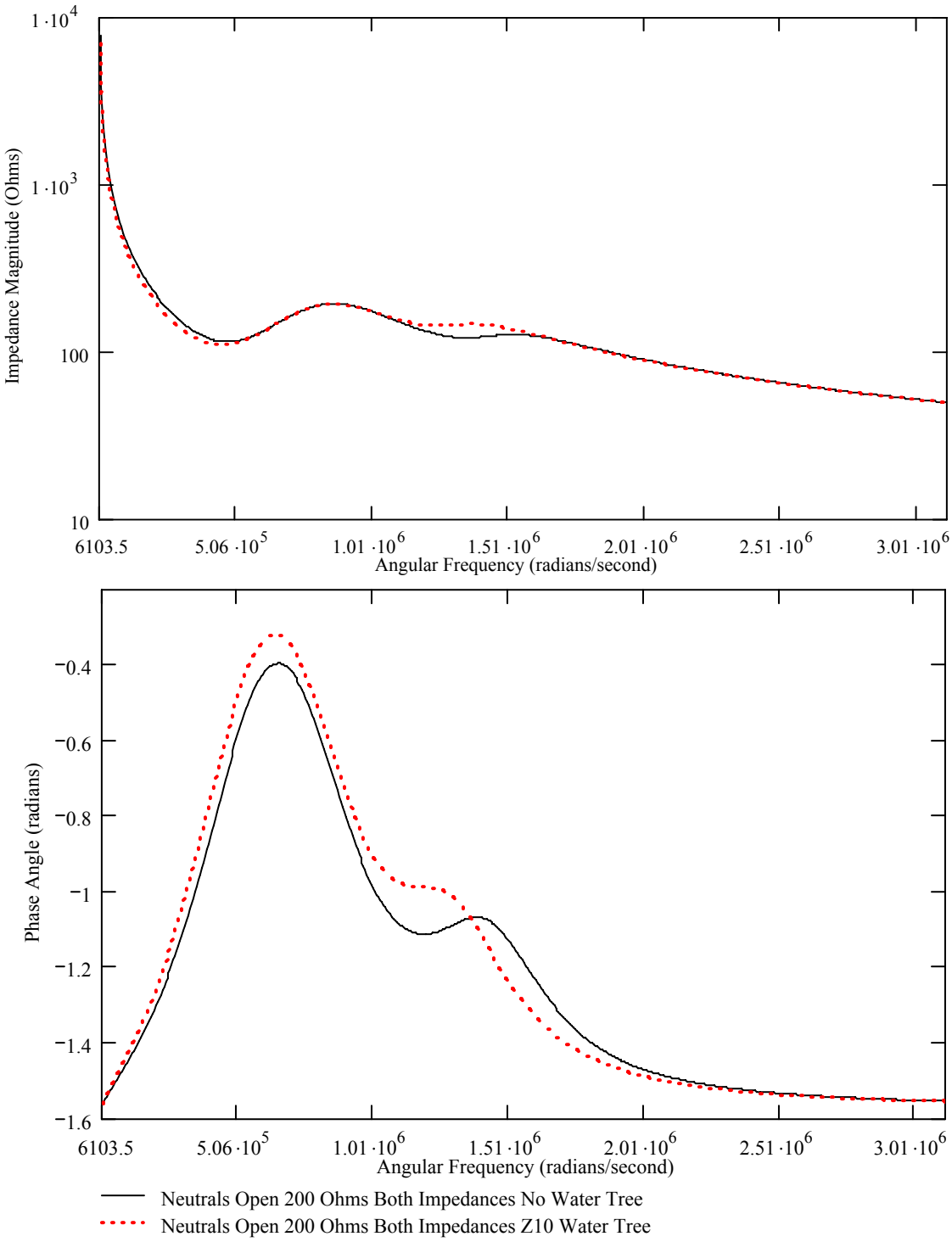

Figure 4.51 Calculated Impedance Magnitude and Phase Angle vs Frequency
22 Impedance Element Model, L=100 m, D=10.3 mm AL, 4.45 mm XLPE,
Neutrals Open, 200 Ω Both Impedances, No Water Tree vs Z10 Water Tree

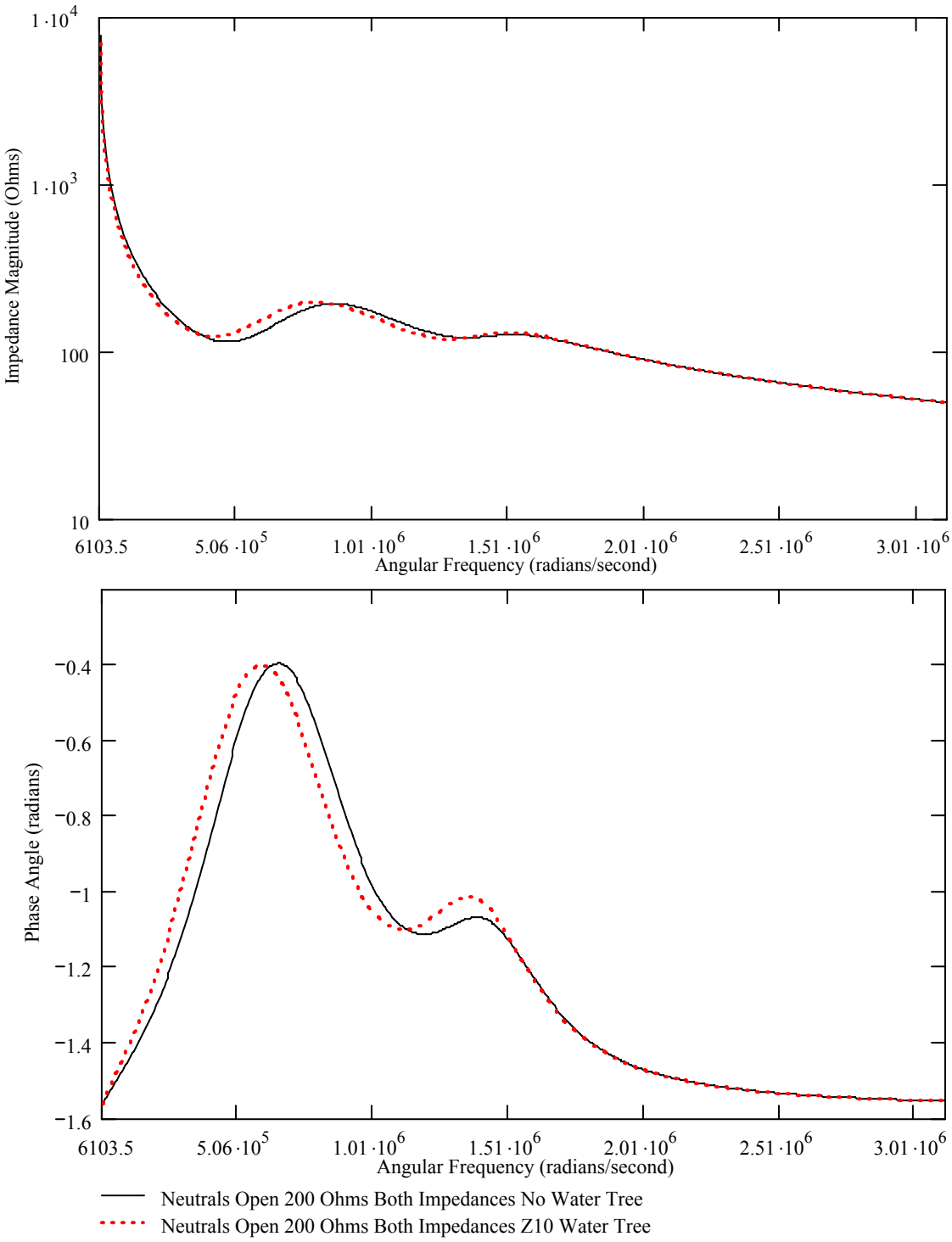

Figure 4.52 Calculated Impedance Magnitude and Phase Angle vs Frequency
22 Impedance Element Model, L=100 m, D=10.3 mm AL, 4.45 mm XLPE,
Neutrals Open, 200 Ω Both Impedances, No Water Tree vs Z19 Water Tree

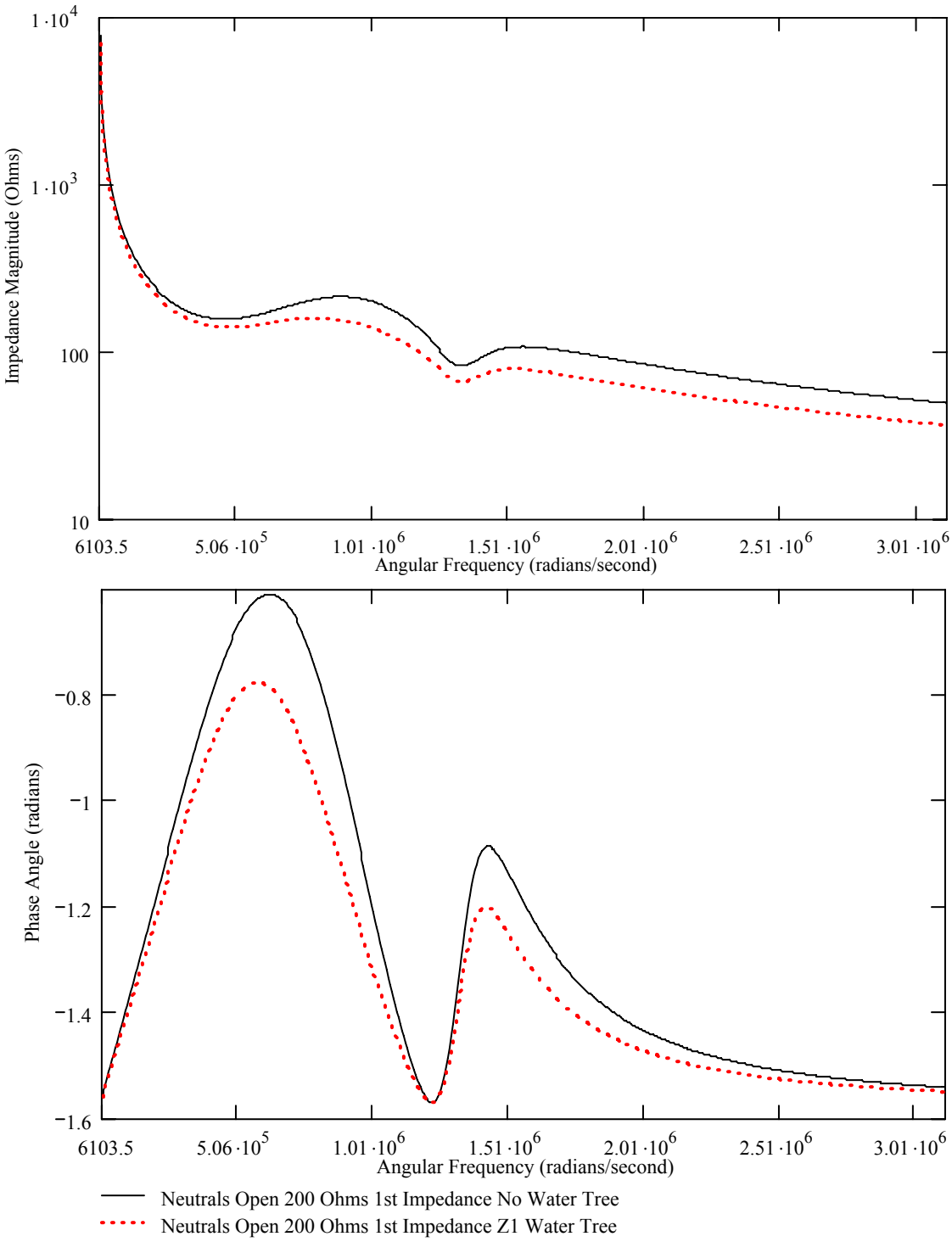

Figure 4.53 Calculated Impedance Magnitude and Phase Angle vs Frequency
22 Impedance Element Model, L=100 m, D=10.3 mm AL, 4.45 mm XLPE,
Neutrals Open, 200 Ω 1st Impedances, No Water Tree vs Z1 Water Tree

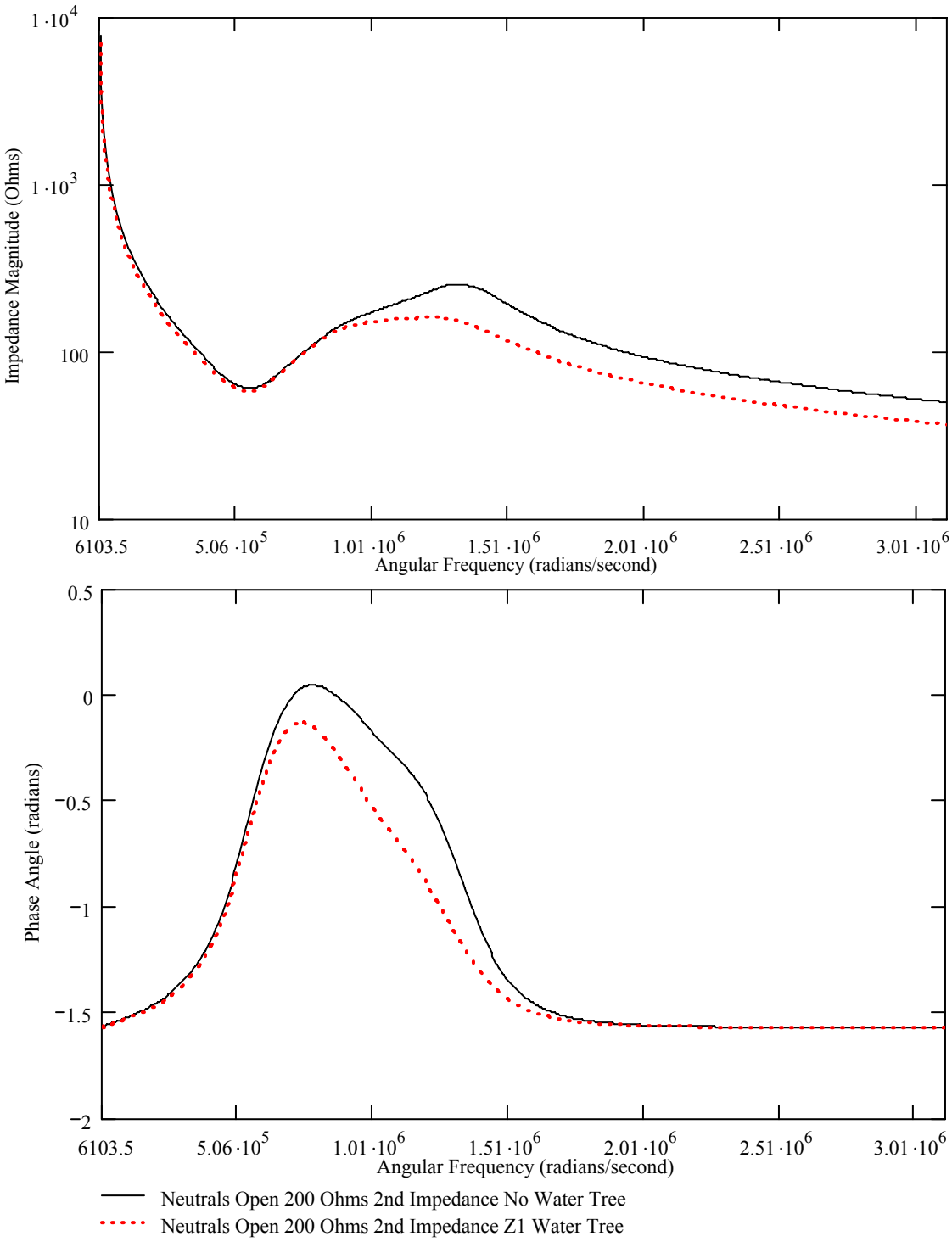

Figure 4.54 Calculated Impedance Magnitude and Phase Angle vs Frequency
22 Impedance Element Model, L=100 m, D=10.3 mm AL, 4.45 mm XLPE,
Neutral Open, 200 Ω 2nd Impedance, No Water Tree vs Z1 Water Tree

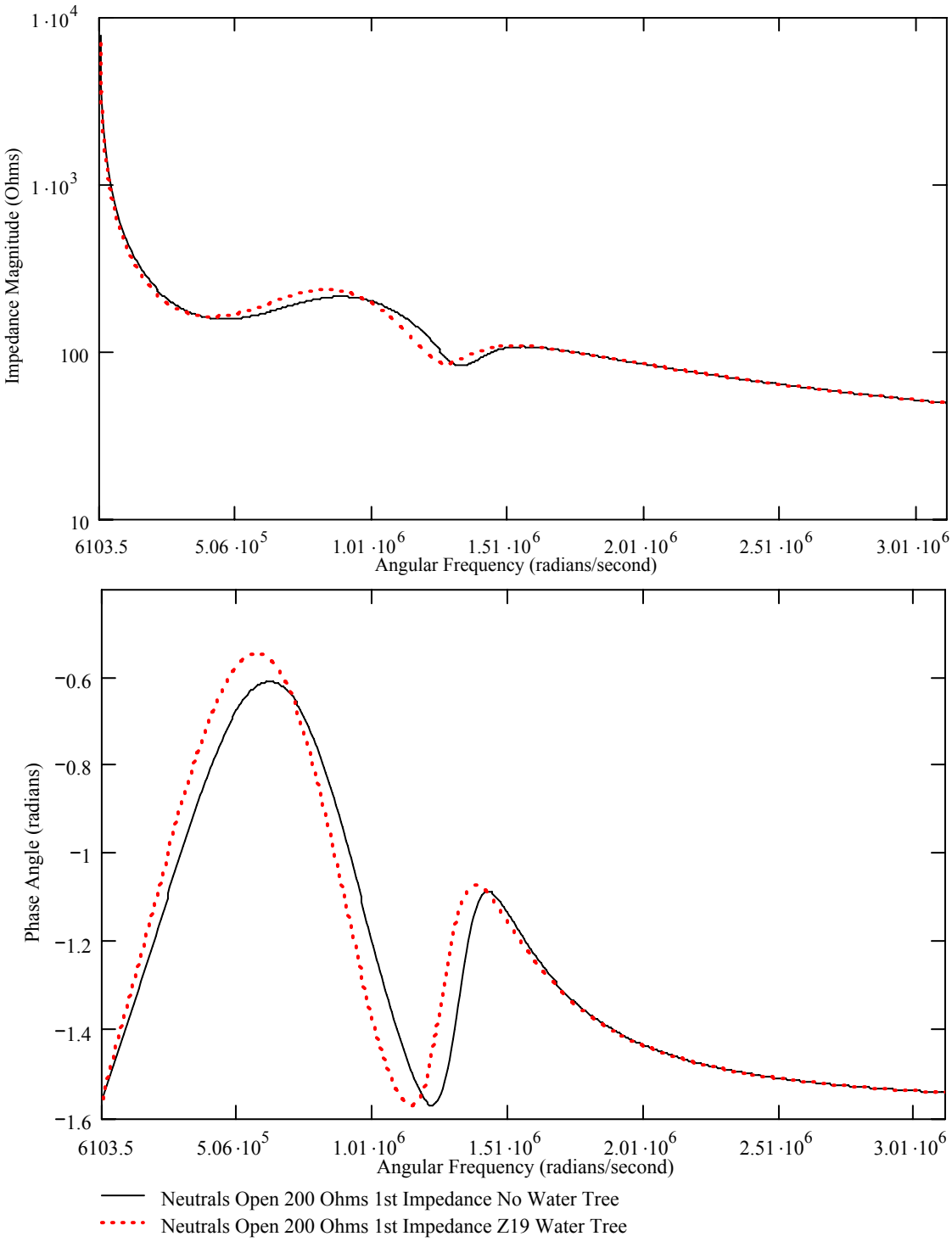

Figure 4.55 Calculated Impedance Magnitude and Phase Angle vs Frequency
22 Impedance Element Model, L=100 m, D=10.3 mm AL, 4.45 mm XLPE,
Neutral Open, 200 Ω 1st Impedance, No Water Tree vs Z19 Water Tree

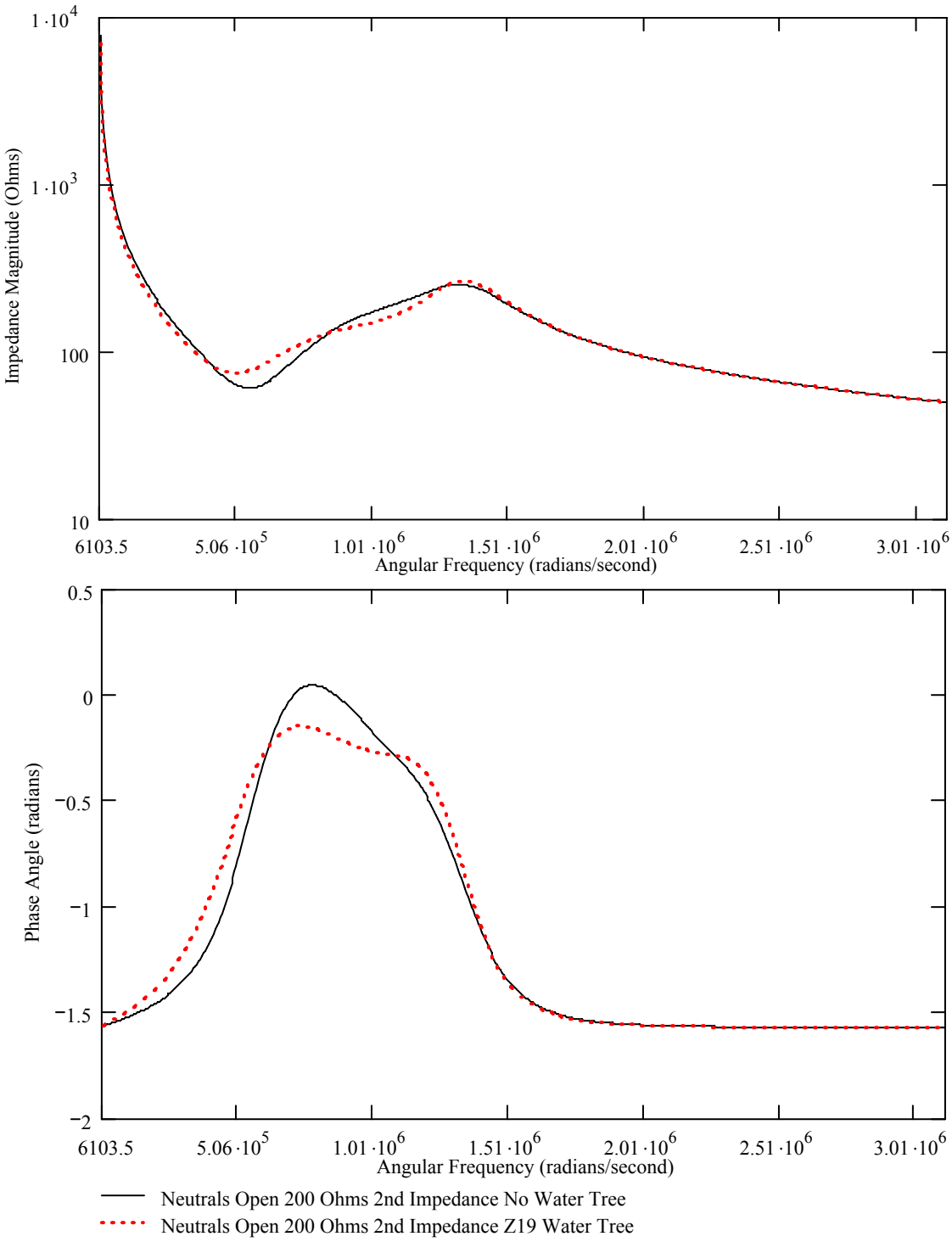

Figure 4.56 Calculated Impedance Magnitude and Phase Angle vs Frequency
22 Impedance Element Model, L=100 m, D=10.3 mm AL, 4.45 mm XLPE, Neutral Open, 200 Ω 2nd Impedance, No Water Tree vs Z19 Water Tree

CHAPTER V

FEASIBILITY, LABORATORY MEASUREMENTS

Test Setup

As shown in Figure 5.1 and discussed previously, this dissertation proposes to measure high-voltage impulses, created by switching a charged capacitor into a de-energized cable system, with voltage dividers and a Rogowski coil which provide analog signals to a digital storage oscilloscope. These waveform forms are digitized and the data is transferred to a personal computer where Fast Fourier Transforms, FFTs, are performed to transform the time domain voltage and current waveforms into the frequency domain. The Fast Fourier Transform, FFT, of a digitized time domain signal produces both the signal amplitude and phase angle versus frequency in the frequency domain with a continuum of frequency components (magnitude and phase angle spectra). Dividing the transformed current by the transformed voltage will allow derivation of the transfer function. Dividing the transformed voltage by the transformed current will produce the impedance magnitude and phase angle as function of frequency.

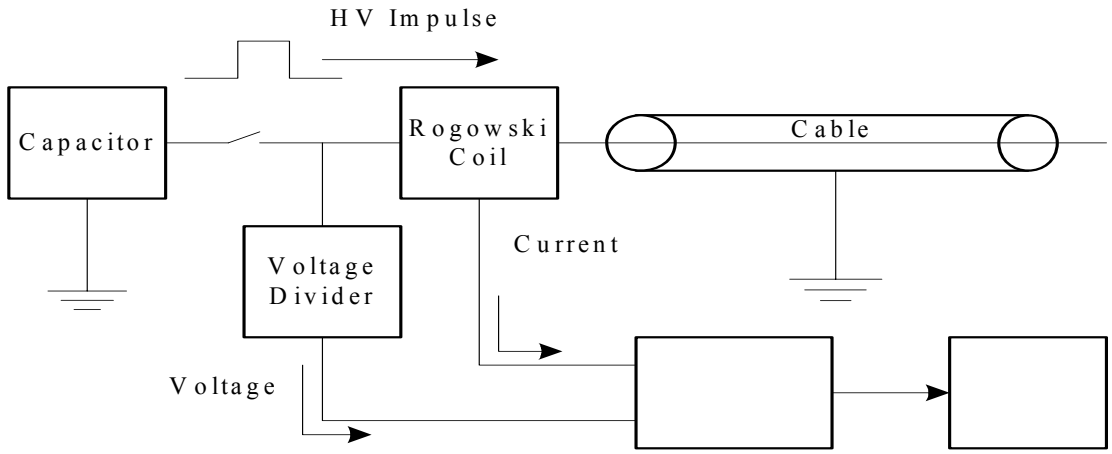

Figure 5.1 Test Setup Block Diagram

Oscilloscope Choice and Setup

A Nicolet Accura 100HV, 100 Msample/sec, 12 bit vertical resolution oscilloscope was purchased to measure the voltage and current. The oscilloscope also has a 16 bit vertical, 25 Ms/sec transient capture capability. To optimize the test method various tests were performed to determine the performance tradeoffs designed into the oscilloscope. It was determined that choosing the oscilloscope's record size and full trace window dictates the sampling rate at levels up to and including the maximum sampling rate. Next choosing a record length sized above the level required to maximize the sampling rate causes the full trace window to increase in length. Once the sampling rate is chosen, the minimum and incremental frequency values in the frequency domain are dictated for FFT calculations. Additionally, the record length and minimum frequency values chosen dictate the maximum frequency in the frequency domain. In performing the FFT calculation dividing the FFT length by factors of 2 in order to average the calculation doubles the minimum and incremental frequency but leaves the maximum frequency unchanged. However, utilizing a reduction formula and sampling

the record by factors of 2, results in halving the maximum frequency while maintaining the minimum and incremental frequency. Measurements of capacitive discharge waveforms for 30 and 10 m cables produced signals of approximately 50 and 25 microseconds length respectively, provides an indication of the necessary oscilloscope sweep time. Lastly, it is necessary to average the measured signals over a number of shots to reduce the measured noise.

Incorporating the above information into the development of the measurement methodology resulted in the following choices. A 16 bit vertical, 25 Ms/s, 4096 record length setup was chosen for the Nicolet oscilloscope. For the measured signals this choice would prevent aliasing as the sampling rate would exceed the Nyquist criteria for the upper range of measured waveforms, 3 MHz [61]. The choice of 16 bits would reduce the oscilloscope noise threshold such the least significant bit error would be reduced to –95 dB. Using a record length of 4096 points results in utilizing an integral of 2^n which maximizes the point usage [56]. For example if a record length of 5000 points was utilized it would be truncated to 4096 points in order to perform the FFT calculation which operates only on integrals of 2^n. Additionally, a 4096 record is of sufficient length to ensure distinct frequency components for the FFT calculation and results in a lowest frequency of 6.1 kHz, an increment of 6.1 kHz and an upper frequency of 12.5 MHz.

Measured Trace Modifications

The voltage and current traces that are ultimately recorded by the Nicolet oscilloscope must be modified to account for voltage divider and current transformer

ratios. Additionally, it is important to apply an exponential window to the traces to ensure that the waveforms are forced to zero by end of trace. Otherwise the FFT algorithm, which assumes periodicity will see a discontinuity and include the frequency components of a unit step function which will add errors to the final FFT calculated values [59, 60, 62]. Next the waveforms will be reduced by sampling the waveforms 4 times and then averaging these new waveforms. The effect of the reduction formula will be to limit the FFT calculation to an upper frequency of 3.1 MHz without changing the lowest and incremental frequencies that the FFT calculation will be performed at. This upper frequency limit is appropriate as it coincides with the upper cutoff frequency response of the dividers and the observed waveforms. All trace modifications are performed in a commercially available signal processing software package, Nicolet Impression 6.0.

Impedance Magnitude and Phase Angle as a Function of Frequency

Once the trace modifications have occurred the Impression 6.0 is utilized to perform the FFT calculations. There is no need to apply an additional window to reduce problems associated with periodicity issues. The FFT calculation is applied to the 5 voltage and current impulses measured for each test scenario. The voltage magnitude FFT is divided the current magnitude FFT to obtain the impedance magnitude FFT while the current phase FFT is subtracted from the voltage phase FFT to obtain the impedance phase FFT. Next the five impedance magnitude and five impedance phase angle FFTs are averaged to reduce noise.

The comparisons between the various cables that will be tested will be performed utilizing the average of the five FFTs; consequently, it is necessary to compute the standard deviation associated the average values to produce upper and lower 95% confidence bounds on the average values. Changes between the different cable samples are not significant at 95% level unless bounds do not overlap. All the algorithms just discussed were programmed into the Nicolet Impression 6.0 software.

Preliminary Measurements

Measurements Test Configuration

Tests were conducted on new 30 m long XLPE cable , 28.4 mm OD aluminum conductor with an insulation thickness of 4.45 mm and concentric neutral to demonstrate that the proposed methodology can discern between new and failed cable. The test setup is shown in Figure 5.2. An HDW cable thumper is used as the pulse generator. This cable thumper, shown as a DC power supply and capacitor in Figure 5.2, charges an internal capacitor to a selected voltage, 7 kV, and then the charged capacitor is connected to the de-energized test cable through the closure of the second switch creating a high-voltage impulse. Next the switch is opened and the cable conductor is shorted to neutral and grounded for safety. The voltage waveforms are measured at both ends of the test cable with Ross damped capacitive voltage dividers, nominal ratio 1000:1, which are shown as the parallel RC circuits. The current waveform is measured with a Pearson split-core Rogowski current transformer, 0.1 V/A, which is shown as the inductor before

the cable section. The voltage and current signal outputs are connected to a Nicolet Accura 100HV, 12 bit, 100 Ms/sec digital storage oscilloscope.

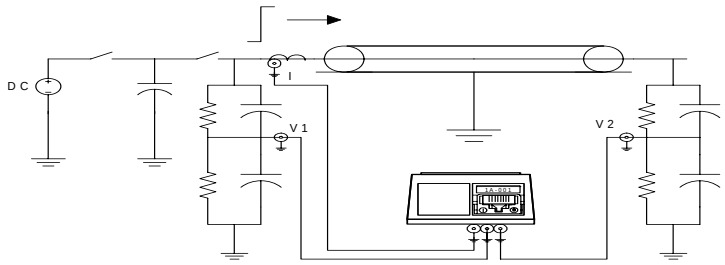

Figure 5.2 Test Setup

Test Plan and Results

Three sets of tests were conducted on this cable: 1) cable in good condition, 2) cable with a hole drilled from the insulation shield to the conductor at the cable midpoint and finally 3) the same cable as in 2) but with a copper wire inserted into the hole, shorting the conductor to the concentric neutral. The two voltage and single current waveforms were recorded for each test condition. These waveforms were then transferred to a computer where signal processing utilized the Nicolet Impression 6.0 software. This commercially available software performs both basic mathematical manipulations in order to calculate differential voltages and impedance as well as more complex signal processing including FFT and filtering.

Figures 5.3 and 5.4 are the time domain and impedance magnitude in the frequency domain results for test condition 1). It can be seen in the time domain that there is considerable high frequency oscillations on the voltage and current waveforms

for the first 100 μsec of the traces. After this period of time the fundamental oscillation with a frequency of approximately 210 kHz remains. As the voltage on the cable sample approaches its final DC value, approximately –4 kV, additional high frequency oscillations are again present. It should be noted that the voltage at the open end of the cable, V2, is approximately double the sending end voltage, V1, as would be expected from traveling wave theory. The impedance magnitude as a function of frequency, Figure 5.4, was calculated by taking the voltage, V1 FFT and dividing by the current FFT. The display is terminated at 3 MHz since the voltage and current waveform both display negligible values at higher frequencies. This impedance magnitude spectra is the baseline spectra to compare the remaining test results against.

Figures 5.5 and 5.6 are the time domain and impedance magnitude in the frequency domain results for test condition 2). It should be noted that in the time domain there are only subtle difference between the base case and the damaged but not failed test sample. However, when the impedance magnitude spectra of Figures 5.4 and 5.6 are compared there are obvious differences in the impedance magnitude. The differences are especially obvious at certain frequencies, perhaps indicative of partial discharges.

Figures 5.7 and 5.8 are the time domain and impedance magnitude in the frequency domain results for test condition 3). It is obvious from both the time and frequency domain that there has been a dramatic change in the cable properties due to shorting the conductor to ground.

Figure 5.9 takes the original test data and performs the final recommended methodology. As can be seen from the figure, there are clear statistical differences between the three test results since the curves for each test incorporate the upper and lower confidence bounds. For example at approximately 800 kHz there is a clear drop in the impedance magnitude between the good cable and the cable with a hole to the conductor, potentially indicating partial discharge. The phase angle spectra are also included; however, the interpretation of the results is extremely problematic compared to the theoretical discussions. This issue will be discussed further in the presentation of the final tests on good and field aged cable.

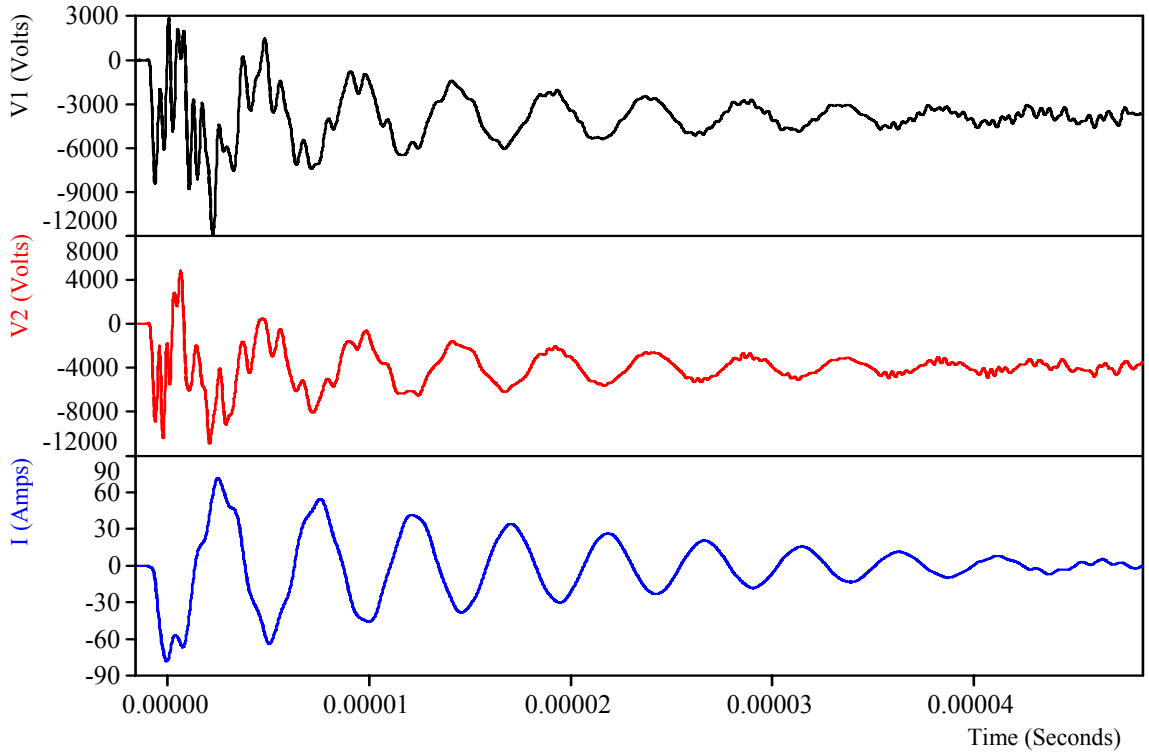

Figure 5.3 Test 1, Good Cable, Measured Voltages at Source, V1, and Open End, V2, and Current vs Time, L=30 m, D=28.4 mm AL, 4.45 mm XLPE

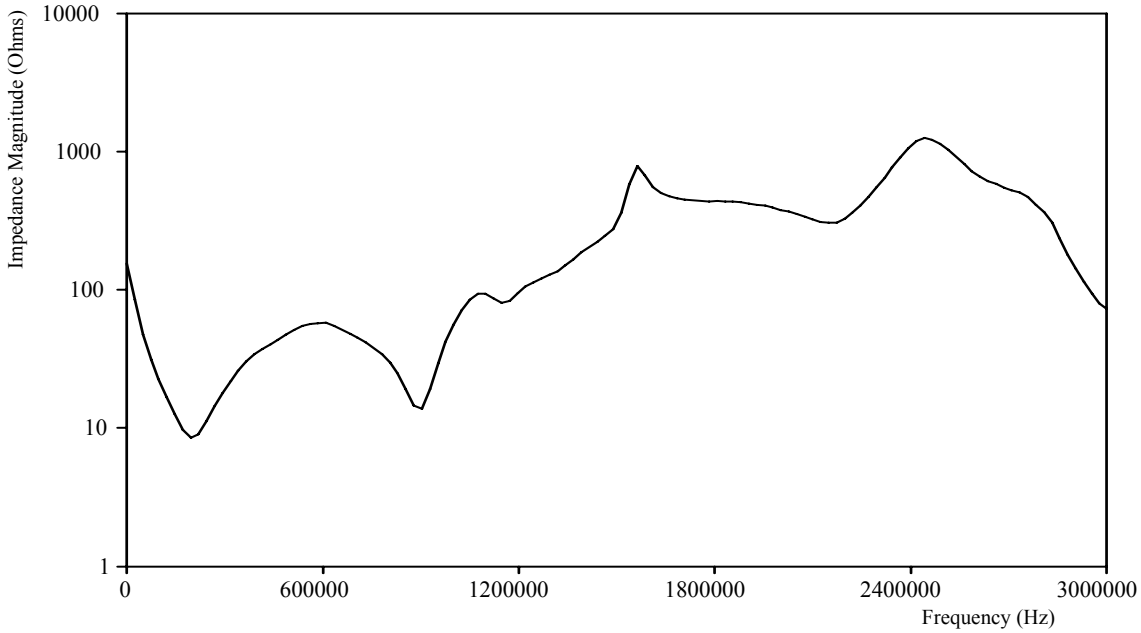

Figure 5.4 Test 1, Good Cable, Measured Impedance Magnitude vs Frequency, L=30 m, D=28.4 mm AL, 4.45 mm XLPE

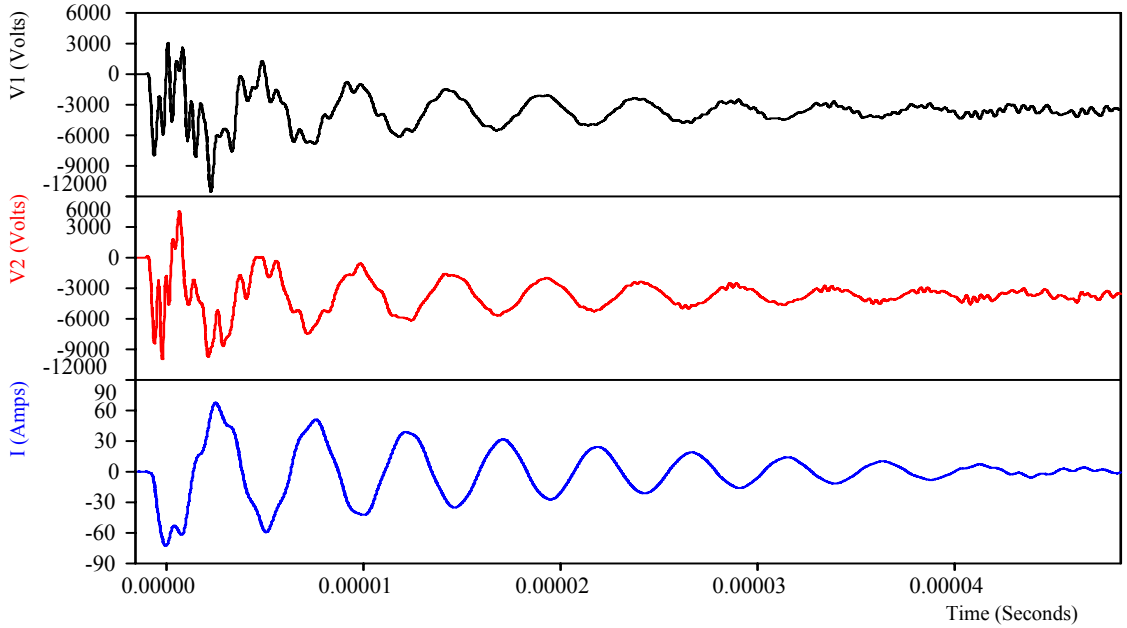

Figure 5.5 Test 2, Cable with Hole to Conductor at 15 m, Measured Voltages at Source, V1, and Open End, V2, and Current vs Time, L=30 m, D=28.4 mm AL, 4.45 mm XLPE

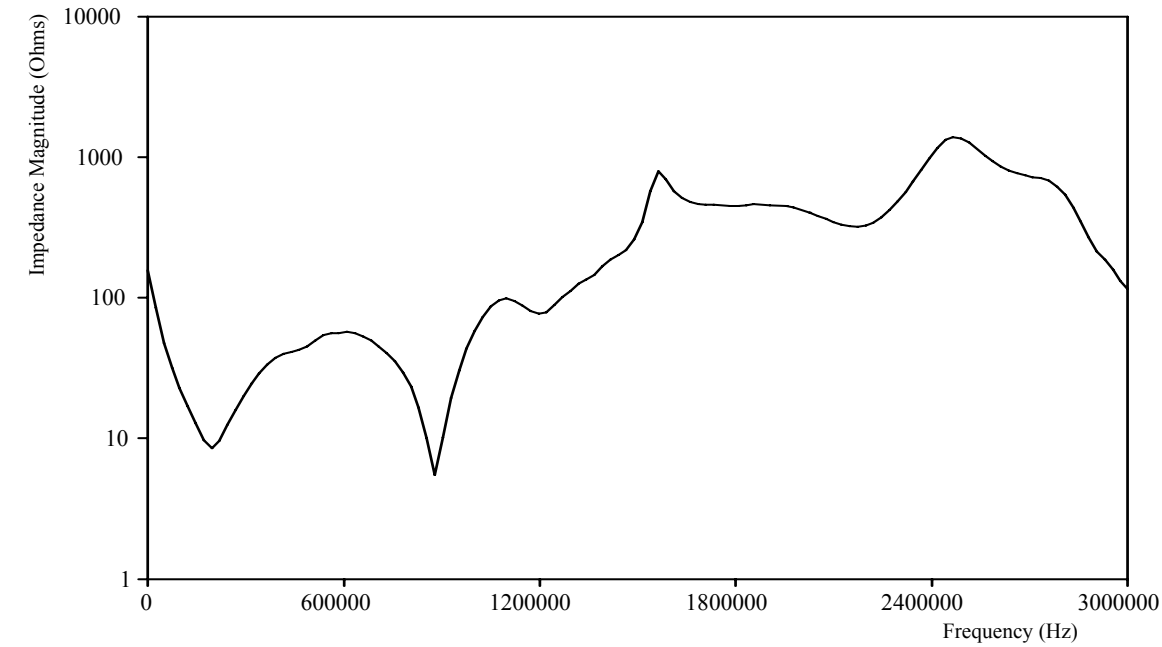

Figure 5.6 Test 2, Cable with Hole to Conductor at 15 m, Measured Impedance Magnitude vs Frequency, L=30 m, D=28.4 mm AL, 4.45 mm XLPE

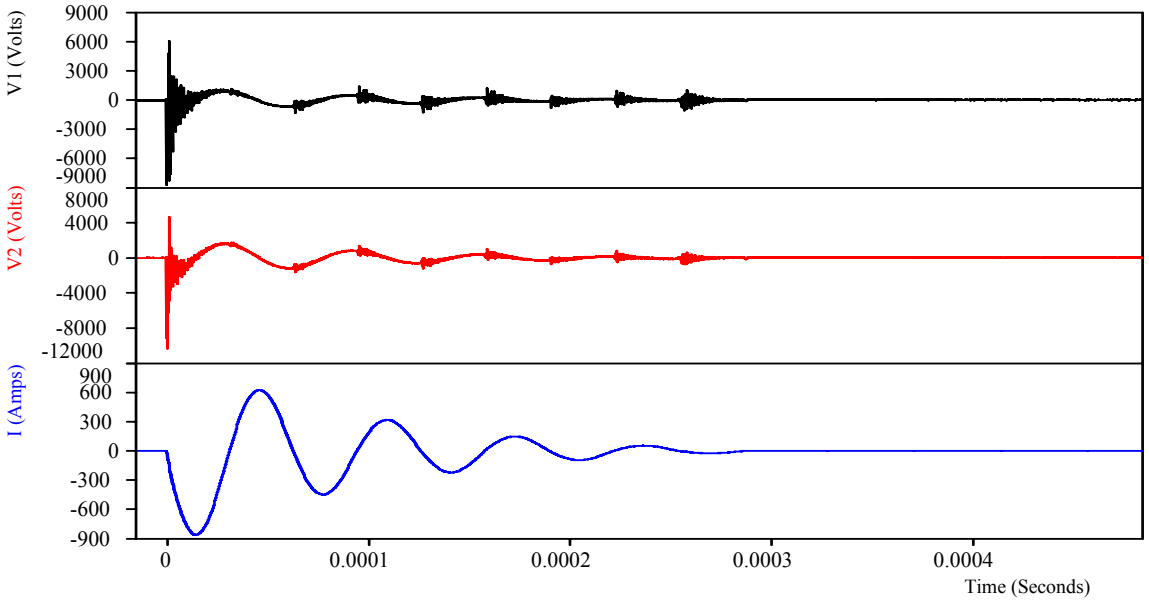

Figure 5.7 Test 1, Shorted Cable, Measured Voltages at Source, V1, and Open End, V2, and Current vs Time, L=30 m, D=28.4 mm AL, 4.45 mm XLPE

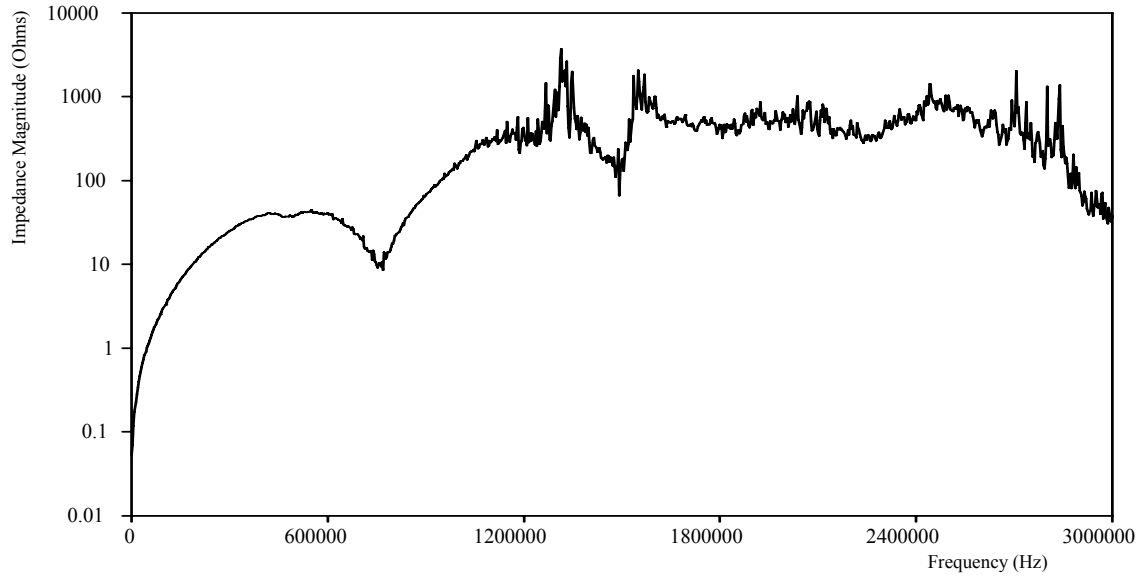

Figure 5.8 Test 1, Shorted Cable, Measured Impedance Magnitude vs Frequency, L=30 m, D=28.4 mm AL, 4.45 mm XLPE

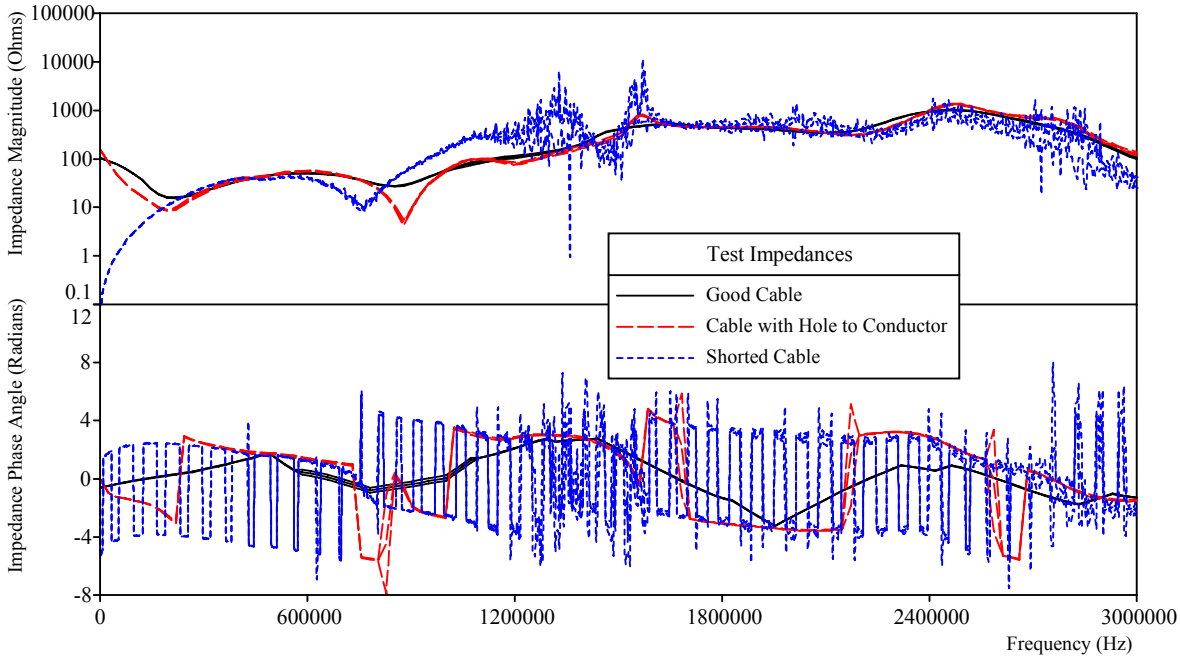

Figure 5.9 Measured Impedance Magnitude and Phase Angle vs Frequency Inter-Test Comparison, 95% Confidence Bounds, L=30 m, D=28.4 mm AL, 4.45 mm XLPE

Assessment

The proposed measurement methodology clearly demonstrates superior sensitivity to changes in the cable insulation properties than what can be determined by examination of the time domain waveforms. It would appear that not only is it possible to detect failure but certainly other properties changes, such as partial discharge, as well. The refined test and signal processing methodology offers much clearer, easier to interpret results which will be discussed with relationship to the previous theoretical results in the next section. Phase angle information appears to be problematic to interpret and therefore not as useful as the impedance magnitude spectra.

Test Samples and Measurement Results

Table 5.1 provides a summary description of the test samples that were utilized as part of the dissertation program. A more detailed description of the samples, condition assessments and tests performed can be found in Appendix G. The total number of cables tested were 42 good and 34 field aged. The entire collection of impedance magnitude and phase angle spectra is included in Appendix F. The 1997 vintage cables had never been installed underground but had been stored at an San Diego Gas & Electric operating center yard and subject to the environment only. The age of field aged cables varied from 25 to 33 years of age and had been removed from operation prior to tests being performed.

As can be observed in Table 5.1, conductors of different outside diameter, OD, different types of insulation materials, insulation thickness and length of conductors were tested. The variety of samples tested re-emphasizes the need for a good theoretical model to provide the means of extrapolating performance results.

Table 5.1

Final Test Samples

Vintage	Conductor Size OD	Conductor Type	Insulation Type	Insulation Thickness	Length	Number of Samples
1997	28.4 mm	Aluminum	XLPE	4.45 mm	100 m	27
1997	10.3 mm	Aluminum	XLPE	4.45 mm	60 m	3
1997	10.3 mm	Aluminum	XLPE	4.45 mm	100 m	12
1971	13 mm	Copper	HMWPE	5.59 mm	30 m	6
1978	10.3 mm	Aluminum	XLPE	4.45 mm	30 m	15
1974	4.6 mm	Copper	HMWPE	5.59 mm	30 m	6
1974	4.6 mm	Copper	HMWPE	5.59 mm	23 m	3
1974	4.6 mm	Copper	HMWPE	5.59 mm	15 m	4

Good Cable Samples Test Measurements

The 42 good samples were subjected to a number of tests as detailed in Appendix G, Table G1 for each individual test. Each sample was given a unique identifier, SRA to SRZ and CWA to CWP. There were two sets of test sequences: 1) to

provide a baseline followed by the creation of defects and 2) to provide a baseline followed by the removal of concentric neutrals and then the creation of defects. After all tests had been completed a section of cable was cut and taken to San Diego Gas & Electric's Materials Laboratory for dimensional checks as well voids and contaminant counts and measurements. All good samples utilized XLPE, 4.45 mm thick as the insulation between the conductor and the concentric neutral. Two distinct conductor sizes were tested, 28.4 mm OD and 10.3 mm OD, which typify cables currently installed in San Diego Gas & Electric's underground distribution system.

First the 28.4 mm OD, 100 m good cable test results of cable samples in Table 5.1 will be examined. Figure 5.10 shows the 5 shot average impedance magnitude versus frequency results for 27 cable sections. The impedance magnitude and phase angle versus frequency or impedance spectra information for the individual samples can be found in Appendix F. The phase angle versus frequency information while valuable in the theoretical evaluation is extremely problematic in the test measurement making its interpretation questionable; therefore, the discussion focuses on the impedance magnitude spectra. As indicated in Figure 5.10, the impedance magnitude versus frequency graphs of all 27 cable sections are overlapped, indicating slight resonance peak shifts due to small impedance variances resulting from inexact cable section lengths. There appears to be five resonance pairs in the test results impedance magnitude spectra and each pair has significantly different minimum and maximum ranges. After the initial decrease there is an overall exponential increase up to 2.8 MHz. Values beyond 2.8 MHz diverge greatly suggesting noise issues in this region of the spectra which further supports the 3 MHz

cutoff for the FFT calculation. Compared to the theoretical results there are clear differences in impedance magnitude; however, as we continue to examine the measured behavior, the theoretical model is still shown to be a useful tool in determining test performance.

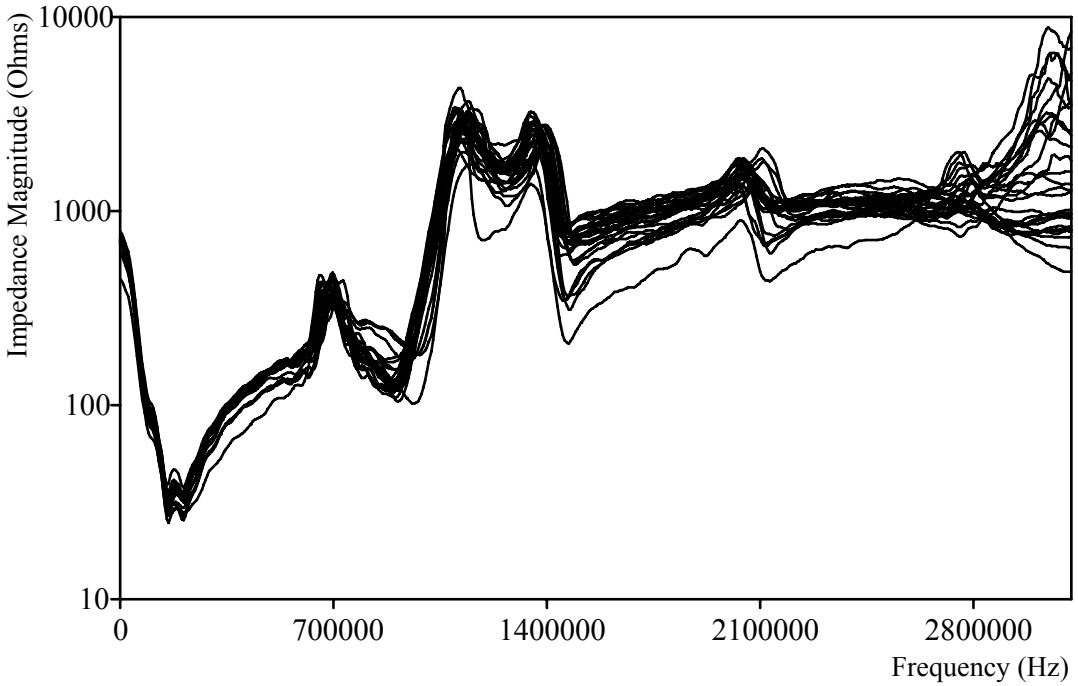

Figure 5.10 Measured Average Impedance Magnitude vs Frequency, L=100 m, D=28.4 mm AL, 4.45 mm XLPE, 27 New Cables

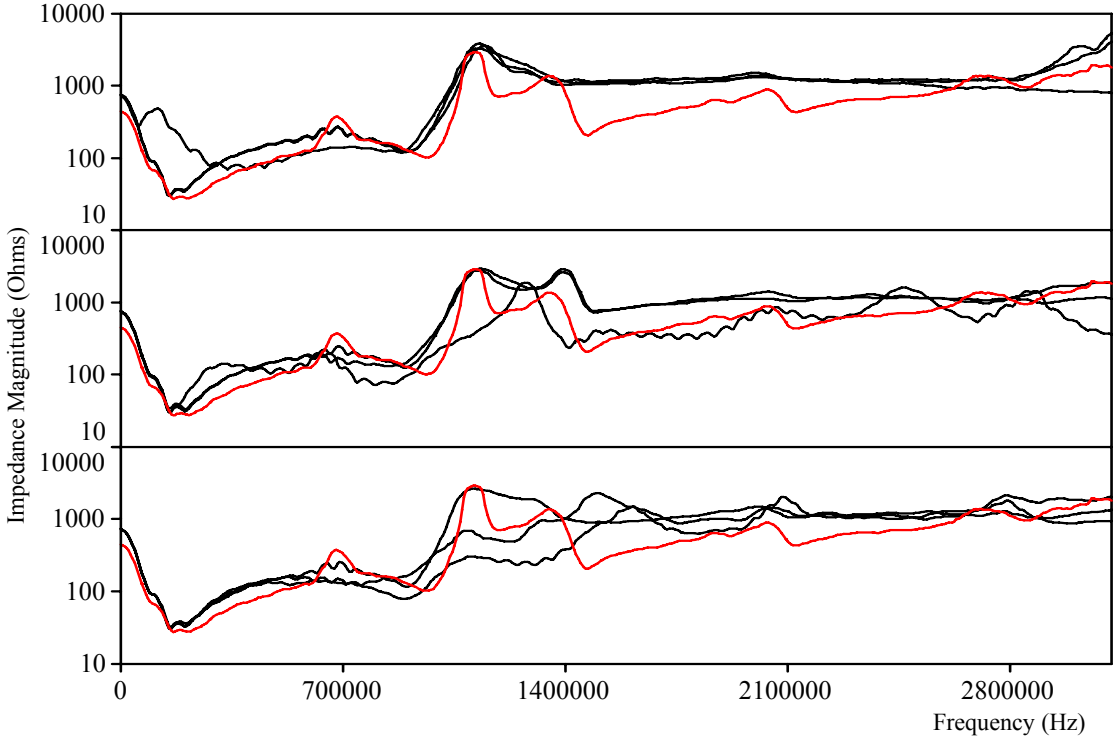

Figure 5.11 Measured Average Impedance Magnitude vs Frequency for Simulated Neutral Corrosion, L=100 m, D=28.4 mm AL, 4.45 mm XLPE, Red Trace Good Neutrals, Top Trace Neutrals Open at 25 m, Middle Trace Neutrals Open at 50 m, Bottom Trace Neutrals Open at 75 m

Figure 5.11 shows measurement results of cables without concentric neutrals that were previously tested with intact concentric neutrals and whose measured results were shown in Figure 5.10 The effect of no concentric neutral conductors on some of the cable is pronounced and dependant upon location. The three different impedance magnitude spectra groupings in Figure 5.11 are for no neutrals located at 25, 50 and 75 meters respectively from the voltage source end. The five impedance resonance pairs in Figure 5.10 have been damped and reduced in number to two or three. In all three different impedance magnitude spectra groupings the impedance magnitude value beyond 1.4 MHz becomes an approximate constant value, the maxima at 700 kHz is significantly

damped and the two higher frequency resonance pairs are no longer observed. Consistent with the theoretical results discussed previously, the impedance magnitude maxima at approximately 1.2 MHz is increased while the 1.4 MHz maxima is reduced when the neutrals are open nearest the voltage source, the top group of curves. When the neutrals are open in the middle, the middle groups of curves, the results are somewhat consistent with theory showing an overall damping. For the last case, the bottom curves, when the open neutrals are located in the second half of the cable furthest from the voltage source, the impedance magnitude maxima at approximately 1.2 MHz is reduced while the 1.4 MHz maxima is increased; again consistent with the theoretical results.

The next good cables to be tested were the 10.3 mm OD, XLPE , 60 and 100 m sections. The complete individual impedance spectra can again be found in Appendix F. Figure 5.12 show the impedance magnitude versus frequency of the 12, 100 m samples on top and the 3, 60 m sections on the bottom of the graph. As can be seen for both cable lengths there is similar overlapping shapes of graphs for all sections which differ slightly in impedance magnitude only with a small amount of resonance peak shift. There appears to four impedance resonance pairs in the test results impedance magnitude spectra for the 100 m sections and four pairs for the 60 m sections. As with the 28.4 mm OD samples in Figure 5.10, each pair has significantly different maxima and minima values. Compared to the 28.4 mm OD samples the 100 m resonance pairs are shifted towards a higher frequency and the 60 m resonance pairs shifted higher still. The 28.4 mm OD maxima at 1.2 MHz appears to be significantly attenuated in both 10.3 mm OD cases. These measured results are again consistent with the theoretical results which

predict a shifting of maxima and minima frequencies to a higher value for both a smaller conductor with a fixed length and a reduced length with the same conductor.

Figure 5.13 shows the effect of no concentric neutral on the 10.3 mm OD cable sections and the effect is again pronounced and dependant upon location. The three different impedance magnitude spectra groupings in Figure 5.13 are for no neutrals located at 25, 50, 30 and 75 meters respectively from the voltage source end. In all three instances of the 100 m cable lengths, the impedance magnitude beyond 1.8 MHz becomes approximately constant, the positive peaks at 800 kHz and 1.6 MHz are significantly damped and the two higher frequency resonance pairs are difficult to observe. While the observed results appear consistent with the theoretical results, the 10.3 mm OD sample size tested is too small to confirm the correlation exists.

When comparing new cable test results to physical measurements, as shown in Appendix G, Table G2, there are no obvious correlations other than that of cable length or conductor and insulation thickness variability.

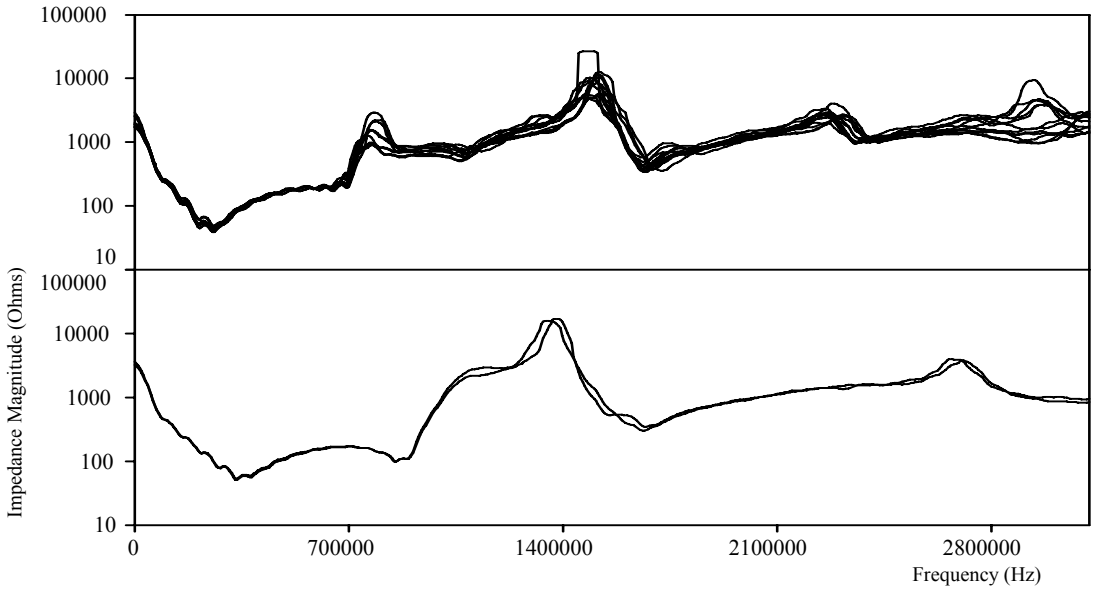

Figure 5.12 Measured Average Impedance Magnitude vs Frequency, D=10.3 mm AL, 4.45 mm XLPE, Top Trace L=100 m 12 Cables, Bottom Trace L=60 m 3 Cables

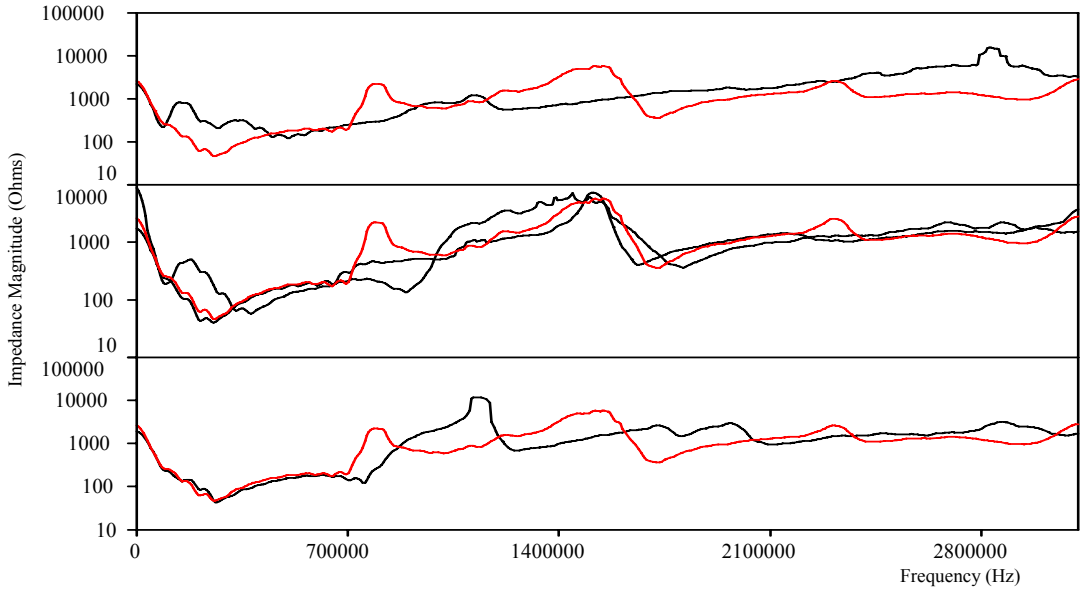

Figure 5.13 Measured Average Impedance Magnitude vs Frequency for Simulated Neutral Corrosion, L=100 m, D=10.3 mm AL, 4.45 mm XLPE, Red Trace Good Neutrals, Top Trace Neutrals Open at 25 m, Middle Trace Neutrals Open at 50 m, Bottom Trace Neutrals Open at 75 m

Field Aged Cable Samples Test Measurements

The 34 field aged samples were also subjected to a number of tests as detailed in Appendix G, Table G1 for each individual test. Each sample was given a unique identifier CIRA to CIRZ and RUNA to RUNJ. There was only one test sequence: 5 impulse applications at approximately 7 kVp followed by an additional 5 impulse applications at approximately 14 kVp. After all tests had been completed a segment from each cable section was cut and taken to San Diego Gas & Electric's Materials Laboratory for dimensional checks, voids, contaminant counts and measurements, as well as water tree counts.

The field aged samples utilized either XLPE, 4.45 mm thick or HMWPE, 5.59 mm thick as the insulation between the conductor and the concentric neutral. Three different conductors sizes; 13 mm OD, 10.3 mm OD and 4.6 mm OD; and two different; materials copper and aluminum; were the cable sections tested. The maximum cable section length tested was 30 m since only a limited sample of field aged cable was available.

The significance of the two test voltages was to investigate the feasibility of determining if the cable had partial discharge sites or if impedance spectra were stable as a function of applied voltage. Cable test samples which exhibit a reduction in impedance magnitude at a fixed frequency are expected to have partial discharge sites. Whereas cable test samples which exhibit a shift in impedance magnitude maxima versus frequency exhibit an impedance change. While both of these performance characteristics suggest the cable sample is in distress, a change in impedance magnitude maxima versus

frequency is more significant. In an on-line test protocol the two voltages can be obtained by controlling the point-on-wave switching of the high-voltage impulse.

The 10.3 mm OD aluminum field aged cables were all 30 m in length. As shown in Figure 5.14 there are three distinct sets of average value curves, applied voltage 7 kV, for neutrals okay; CIRO, P, Q; neutrals corroded; CIRG, H, J, U, V, W, X, Y, Z; and neutrals open; CIRR, S, T. There is also a significant shift of the resonance pairs to a higher frequency and there has been a loss of additional resonance; now only two resonance pairs. As the neutrals corrode and finally open the resonance pairs above 1.4 MHz disappear. When displayed with confidence bounds and plotted against good cable, as shown in Figure 5.15, the curves indicate significant deviations from each other. It is possible to apply theoretical observations to determine degradation effects by combining the independent effects of loss of concentric neutral and water tree degradation. Curves with sharp, well defined resonance peak pairs show cables that are in good condition with concentric neutral intact. Modification of peak magnitude and shifting of the peak to a lower frequency is likely the result of water degradation. The physical measurements, Appendix G, Table G2, show evidence of numerous small water trees. Significant changes in the peak magnitudes alone are the result of corroded neutrals or open neutrals.

In Figure 5.16 the 13 mm OD copper field aged 7 kVp, average value test results are shown. For these particular samples; CIRA, B, C, D, E, F; all neutrals were intact and the impedance magnitude spectra reveals distinct resonance pairs with some shifting of the maxima at 2 MHz and magnitude reduction; this is likely due to minor insulation

deterioration from water trees. When one curve is plotted with confidence bounds against the 100 m, 10.3 mm OD aluminum good cable, as shown in Figure5.17, it shows a high degree of correlation with the good cable and is shifted as would be expected for a shorter piece of cable. Therefore, it appears that this 33 year old cable is in relatively good condition. The complete results in Appendix F also demonstrate no voltage induced changes.

The last group of field aged cable tested was 4.6 mm OD copper of varying lengths. The results shown in Figure 5.18 include the four different impedance magnitude spectra groupings for 30 m neutrals intact; CIRM, N; and corroded; CIRK, L, RUND, E; 23 m neutrals corroded; RUNA, B, C; and 15 m neutrals corroded; RUNF, G, H, J. Most of the 30 m cable sections, even some of the cables with corroded neutrals, look in reasonable condition and show a shift of peaks to higher frequencies commensurate with the smaller conductor size. For the cables with significant neutral corrosion there is a loss of the resonance pair at approximately 2.1 MHz. Figure 5.19 displays one of each cable category with confidence bounds plotted against good cable. The curves now show significant deviations from each other. Once again it is possible to apply the theoretical observations to determine degradation effects and the measured values continue to show consistency with theoretical model results. For example the 4.6 mm OD copper cable is only 30 m long; therefore, it has a lower capacitance, inductance and resistance value and this results in the shift of resonance pairs to a higher frequency. Additionally, as the 4.6 mm OD copper conductor sample length decreases the resonance pairs continue to shift to a higher frequency, with insulation degradation the impedance

magnitude maxima and minima are affected and shifted to a lower frequency and neutral corrosion results in the elimination of higher frequency resonance pairs and modification of the remaining impedance maxima and minima magnitudes.

Comparing the field aged cable tests to the physical measurements in Appendix G, Table G2, there are no obvious correlations between water trees, whether lengths or magnitudes, and cable section lengths. However, the effect of neutral corrosion is pronounced.

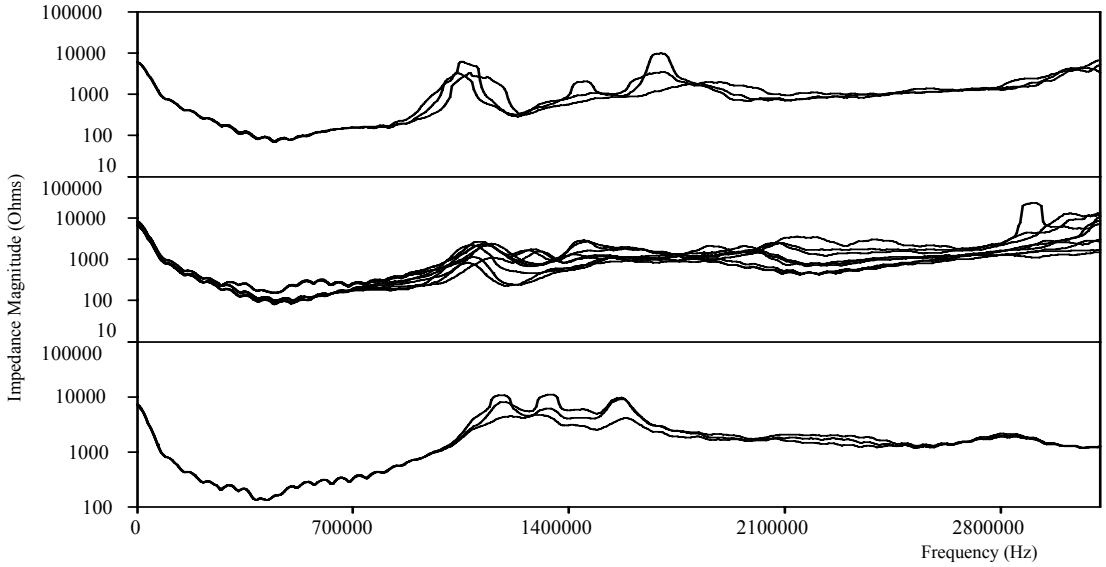

Figure 5.14 Measured Average Impedance Magnitude vs Frequency,
27 Years Field Aged D=10.3 mm AL, 4.45 mm XLPE,
Top Trace L=30 m Good Neutrals,
Middle Trace L=30 m Neutrals Corroded,
Bottom Trace L=30 m Neutrals Open

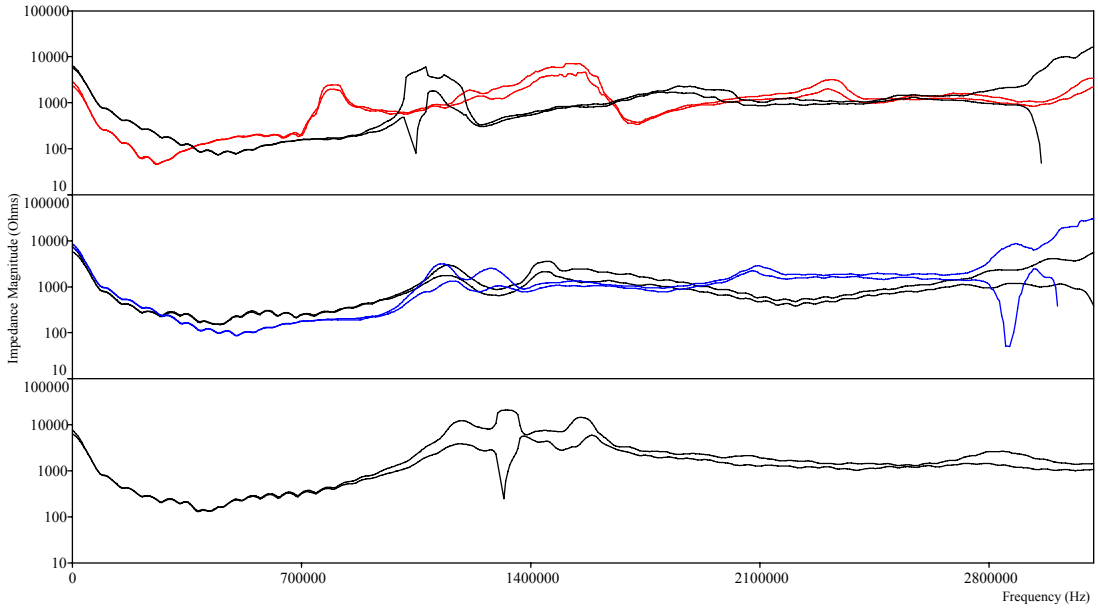

Figure 5.15 Measured Impedance Magnitude vs Frequency, 95% Confidence Bounds,
27 Years Field Aged, D=10.3 mm AL, 4.45 mm XLPE,
Top Trace Red L=100 m New Cable, L=30 m Good Neutrals,
Middle Trace L=30 m Neutrals Corroded,
Bottom Trace L=30 m Neutrals Open

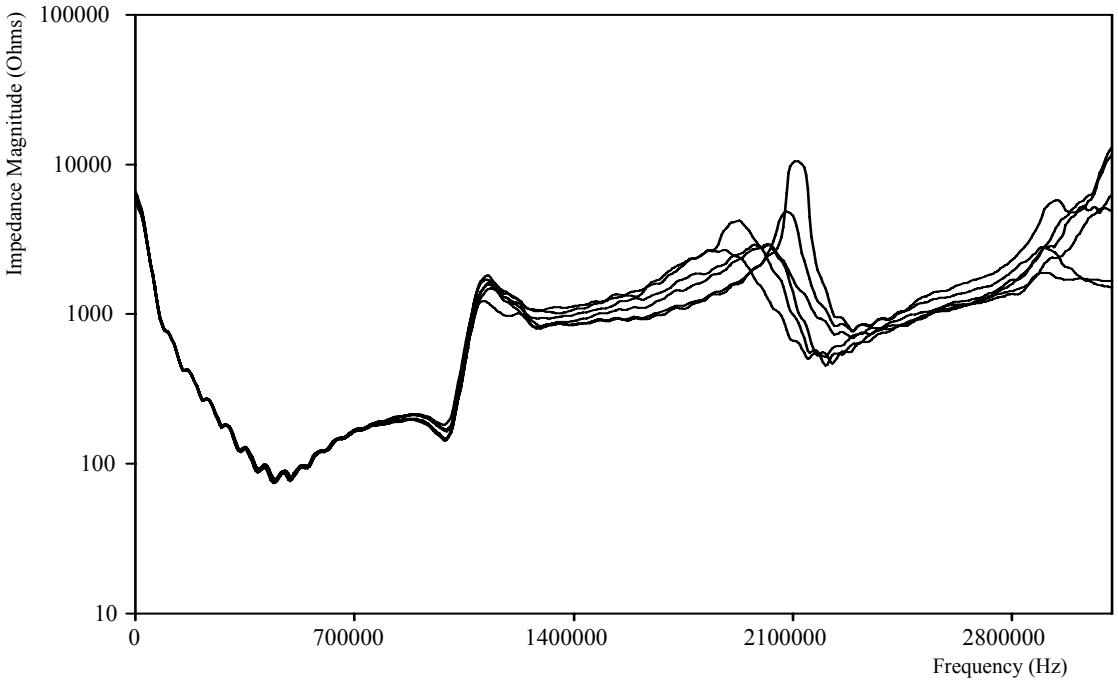

Figure 5.16 Measured Average Impedance Magnitude vs Frequency,
34 Years Field Aged L=30 m, D=13 mm CU, 5.59 mm HMWPE

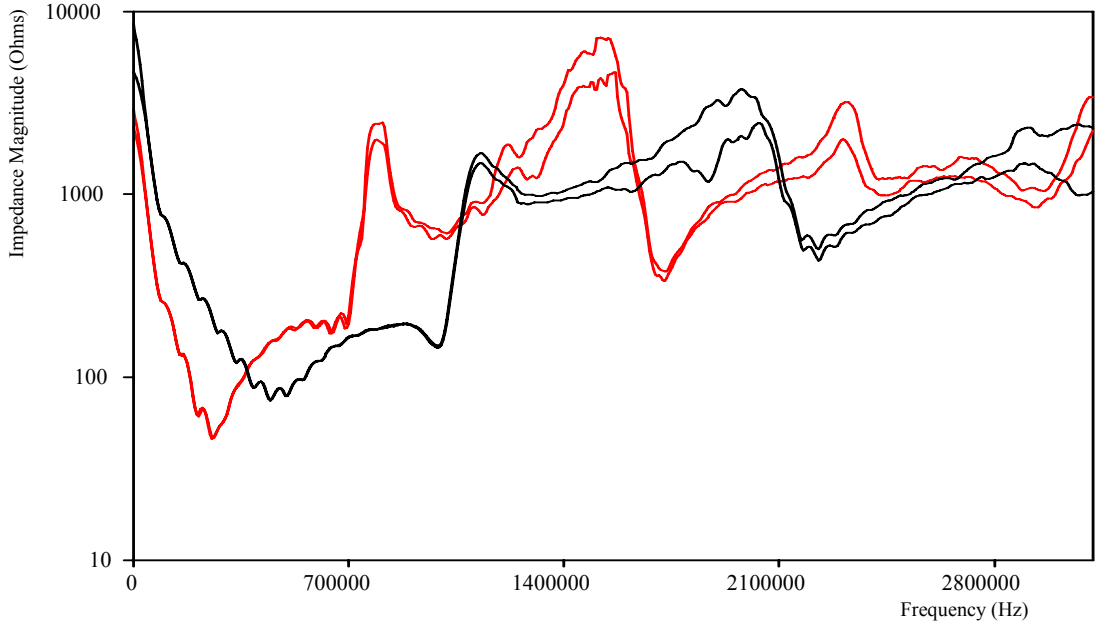

Figure 5.17 Measured Impedance Magnitude vs Frequency, 95% Confidence Bounds,
34 Years Field Aged, L=30 m, D=13 mm CU, 5.59 mm HMWPE vs Red
L=100 m, D=10.3 mm AL, 4.45 mm XLPE, Good Cable

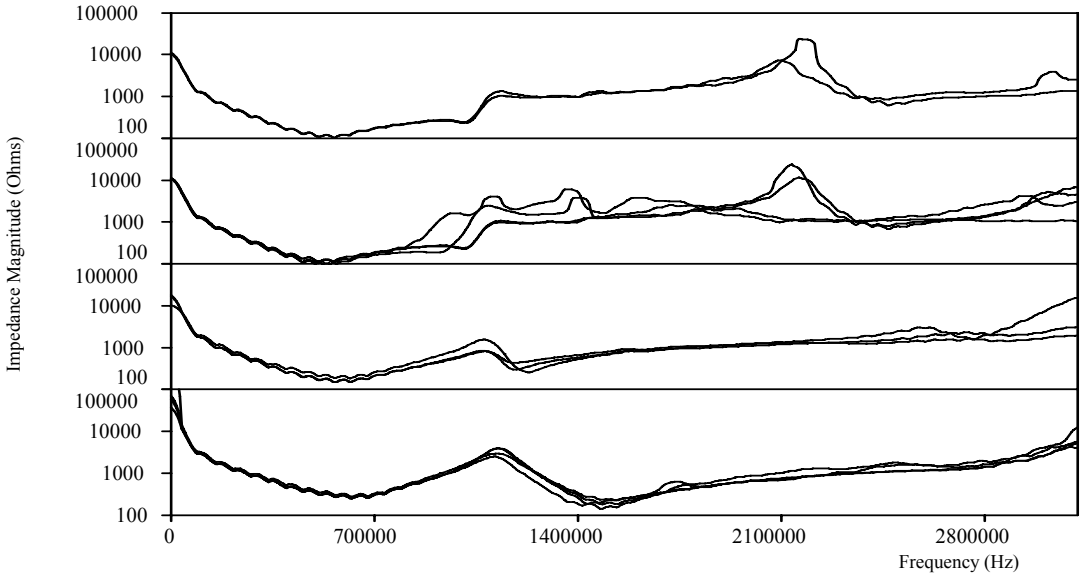

Figure 5.18 Measured Average Impedance Magnitude vs Frequency,
30 Years Field Aged D=4.6 mm CU, 5.59 mm HMWPE,
Top Trace L=30 m Good Neutrals,
2nd Trace L=30 m Neutrals Corroded,
3rd Trace L=23 m Neutrals Corroded,
Bottom Trace L=30 m Neutrals Open

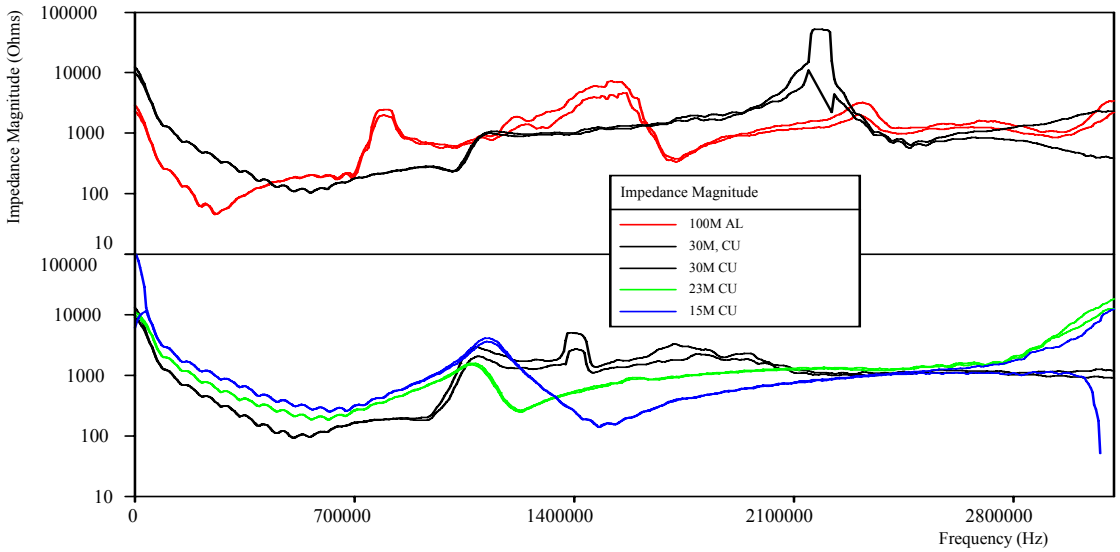

Figure 5.19 Measured Impedance Magnitude vs Frequency, 95% Confidence Bounds,
30 Years Field Aged, L=30 m, D=4.6 mm CU, 5.59 mm HMWPE vs
L=100 m, D=10.3 mm AL, 4.45 mm XLPE, Good Cable,
Top Trace Good Neutrals, Bottom Trace Corroded Neutrals

CHAPTER VI

CONCLUSION AND FUTURE WORK

Conclusion

Failure of underground cables on San Diego Gas & Electric's distribution system is a problem which is increasing in magnitude every year. Existing diagnostic test methods may not produce the voltage distribution within the cable insulation that occurs in service and most test methods which have been developed to date are off-line tests. It appears that a test which provides overall information regarding the cable condition as well as more location specific results will provide the results necessary to discriminate against which cables to replace. If this test can be conducted on-line then the acceptance by utility personnel would be greater as outages can be avoided.

This dissertation proposed development of a diagnostic measurement methodology based upon measuring transients that normally occur in the field during capacitor switching events, but are simulated with high voltage impulses, and converting the voltage and current time signals into the frequency domain through the use of Fast Fourier Transforms. The voltage is then divided by current to obtain the cable section impedance magnitude and phase angle as a function of frequency. It was demonstrated that these transients have adequate frequency spectra to provide for an upper frequency limit in the 3 MHz range.

A theoretical equivalent circuit model of the cable system was also developed. This model was utilized to test assumptions regarding the effect of water trees in a cable as well as the loss of the concentric neutral conductors. The current model was limited to a 10 by 10 impedance matrix due to limitations with MathCAD's matrices capabilities without invoking more complicated functions as well as a desire to limit computation times to several minutes. Most theoretical evaluations occurred with a 9 by 9 matrix which resulted in the occurrence of two resonance pairs. Water trees were simulated by increasing the impedance section dielectric constant to 100 and decreasing the resistance to 1 ohm. Concentric neutral corrosion was modeled by increasing the neutral resistance.

Various lengths of cable and conductor outside diameters were modeled. For a fixed conductor size and insulation thickness, a longer cable section resulted in shifting of the resonance pairs to a lower frequency. For a fixed cable section length and insulation thickness, a smaller conductor resulted in shifting the resonance pairs to a higher frequency. Consequently, the most significant usefulness of this model is that results from a tested cable size of particular length can be extrapolated for differing cable sizes and lengths.

The effect of water trees was shown to be location specific and resulted in shifting of some of the maxima and minima to lower frequencies and a change in the maxima and minima magnitude. As the severity of the water tree increased, simulated by modification of additional series connected impedance elements, the maxima and minima continued to shift to lower frequencies and their magnitudes continued to change. In the limiting case, the impedance magnitude spectra started from a peak value and then

exponentially decayed without any resonance pairs. Longer and shorter cable sections for a fixed insulation thickness were modeled and the water tree behavior was similar to what was previously discussed; however, the resonance pairs were shifted.

The impedance phase angle spectra experienced commensurate changes with the impedance magnitude maxima and minima modifications; however, the value was either approximately –1.5 or 1.5 radians,±Π/2. It is the range of frequencies over which the phase angle magnitude is constant that changes corresponding resonance pairs frequency shifting for the impedance magnitudes. Similar observations were noted for longer and shorter runs of cable of the same insulation thickness except the change in the resonance pairs occurred at lower and higher frequencies respectively.

When concentric neutral corrosion was modeled there was no observable change in either the impedance magnitude or phase angle until there was no concentric neutral, i.e. the neutral impedance was large. It was observed that the model for both magnitude and phase angle was sensitive to the concentric neutral open location.. Additionally, the impedance phase angle was no longer oscillating between ±Π/2 but rather took on discrete values that were primarily negative.

When the cable section was modeled to have both water trees and concentric neutral corrosion, it was observed that the two separate effects were combined. The neutral corrosion effect took priority with the water tree effects occurring next.
The equivalent circuit model is not perfect and does not match the measured results exactly. However, the insights obtained from the simulations are very constructive to understanding what is occurring with the field test results.

Substantial time and effort was spent developing the test and analytical methodologies. The sampling rate and record length needed to be chosen to prevent signal aliasing at higher frequencies while maximizing the efficiency of the Fast Fourier Transform for the frequencies of interest. Exponential windowing was utilized to force the signal to zero prior to the end of the record to minimize insertion of white noise. Signal reduction occurred to limit the upper frequency of the FFT calculation to 3 MHz. Five different transients were recorded at each test configuration to allow for signal averaging and reduction of noise. Lastly statistical analysis of the results was developed to ensure that any observed deviations between different configurations could be interpreted as statistically significant.

Preliminary tests were performed on short 10 m runs of 28.4 mm OD, 4.55 mm insulated, XLPE cables. These cable sections were from a reel that had never been installed in the field but had been stored outdoors at one of San Diego Gas & Electric's construction and operations centers. The good cable had defects of various size inserted into the cable and a series of five transients were applied and measured at each level. The impedance magnitude and phase angle results demonstrated that the measurement methodology could discern between a good cable, a damaged cable and a failed cable.

The measurement methodology allows one to conclude with a 95% confidence level that these changes between degrees of degradation are distinct. In fact the analysis shows that not only does the measurement methodology distinguish between changes in cable impedance but it also appears to indicate that partial discharges are occurring in the cable. The impedance phase angle spectra while showing differences was not as simple to interpret as the theoretical results.

Next longer runs of good cable were tested as well as samples retrieved from the field. The good cable tests while not producing identical impedance magnitude and phase angle spectra to the equivalent circuit model, displayed similar behavior as was observed through the theoretical simulations. This included both changes due to defects as well as the loss of the concentric neutral. There was some variability due to the difference in the cable physical dimensions and manufacturing. The impedance phase angle spectra while showing differences was not as simple to interpret as the theoretical results and appears to be of limited value at this point in time.

The field aged cable tests were conducted at two distinct voltage levels, 7 and 14 kV. This provides the opportunity to determine if any significant impedance changes due to voltage are observed. Cables with sharp distinct resonance pairs appear to be cable in relatively good condition. Some cable sections had significant neutral corrosion. As the resonance pairs become more rounded and shift towards lower frequency this appears to be due to neutral corrosion, if it exists, and water trees. Cable tests results at two different voltage levels, demonstrate voltage dependant behavior as well as what

appears to be partial discharge. Cable sections which exhibit this behavior are expected to be degraded.

Physical examination of the cable occurred after the tests were completed. The difference in good cable performance appears to be a function of dimensional changes. The difference in field aged cable performance is primarily due to water trees and neutral corrosion; however, correlation to physical measurements is questionable.

This new approach to performing cable diagnostic measurements offers the convenience to test and diagnose underground cables as current methods without the key limitations of current on-line and off-line methods. This methodology as currently developed provides a measure of the overall average condition of the cable one of the key measures of cable insulation deterioration. The combination of these techniques and theoretical modeling applied to high-voltage impulse measurements for cables and the statistical analysis is unique provides the foundation for a new cable diagnostic measurement has not been developed by any other researcher and will assist in the evaluation of the condition of cable insulation systems.

The results of this dissertation have shown this measurement methodology to be a promising and capable of discerning between the level of degradation of field aged cable. The theoretical model results allow the measurements to be extrapolated for different cable types and lengths.

Future Work

As discussed in the conclusion, this measurement methodology is promising; however, to become of practical use additional work needs to be performed in four main areas: Fourier Transforms, on-line test development, analysis methodology and statistical correlation to remaining life times.

The current FFT algorithm produces measured impedance phase angle versus frequency results which are problematic. As shown in the theoretical evaluation section, there is information in the phase angle measurements which aid in the interpretation of the cable condition. Therefore, more advance FFT algorithms should be investigated.

All measurements for this dissertation were conducted on sections of cable removed from SDG&E's underground distribution system. This measurement methodology needs to transistion to an on-line methodology to reach its full potential. This work would include the development of operating and test procedures and tools and equipment to work with an energized electric distribution system.

The analysis of the measurements is currently performed in an office environment by personnel intimately familiar with the theoretical aspects. However, for this methodology to be truly successful there needs to be simple pass/fail criteria so that suitably trained technicians can perform the work.

Lastly, statistical correlation to remaining life needs to be developed by testing additional samples, analyzing the measurements and allowing the cables to remain in-service. This will provide the confidence that "bad" cables are indeed about to fail.

BIBLIOGRAPHY

[1] B.S. Bernstein et al, "High Voltage VLF Testing of Power Cables", IEEE Transactions on Power Delivery, Vol. 12, No. 2, April 1997, pg. 565-570

[2] B. Holmgren et al, "Correlation Between AC Breakdown Strength and Low Frequency Dielectric Loss of Water Tree Aged XLPE Cables", IEEE Transactions on Power Delivery, Vol. 13, No. 1, January 1998, pg. 40-45

[3] J. Densley, "Ageing Mechanisms and Diagnostics for Power Cables – An Overview", IEEE Electrical Insulation Magazine, Vol. 17, No. 1, January/February 2001, pg. 14-22

[4] W.A. Thue, "Let's Put Field Testing of Cable in Perspective", IEEE Electrical Insulation Magazine, Vol. 12, No. 5, September/October 1996, pg. 31-32

[5] R. Reid, "High Voltage VLF Test Equipment With Sinusoidal Waveform", IEEE Transactions on Power Delivery, Vol. 12, No. 2, April 1997, pg. 565-570

[6] R. Bartnikas et al, "In-Service Location of Partial Discharge Sites in Polymeric Distribution Cables using Capacitive and Inductive Probes", IEEE Transactions on Power Delivery, Vol. 12, No. 2, April 1997, pg. 565-570

[7] E. Gulski et al, "Recognition of Defects in High Voltage Cables Using Statistical Tools", Proceedings of the 4th International Conference on Conduction and Breakdown in Solid Dielectrics, Sestri Levante, Italy, June 1992, pg. 139-144

[8] T. Nakayama, "On-Line Cable Monitor Developed in Japan", IEEE Transactions on Power Delivery, Vol. 6, No. 4, October 1991, pg. 1359-1365

[9] M. Aihara et al, "Application of GPT to Tanδ Measuring Apparatus for Distribution Cable in Hot Line", IEEE/PES 1991 Winter Meeting, New York, New York, February 1991, 91 WM 251-9 PWRD

[10] Y. Akutsu et al, "Insulation Deterioration Monitoring System for Ungrounded Power Distribution Systems", IEEE/PES 1993 Summer Meeting, Vancouver, Canada, July 1993, SM 406-9 PWRD

[11] K. Hirotsu et al, "Study On Detection For the Defects of XLPE Cable Lines", IEEE Transactions on Power Delivery, Vol. 11, No. 2, April 1996, pg 663-668

[12] N. Ahmed and N. Srinivas, "Partial Discharge Measurements in Distribution Class Extruded Cables", IEEE/PES 1991 Winter Meeting, New York, New York, February 1991, 91 WM 255-0 PWRD

[13] S. Grzybowski and R.L. McMellon, "Electrical Strength of XLPE Cables Under Combined AC-DC Voltage", 9th International Symposium on High Voltage Engineering, Graz, Austria, August 28 – September 1, 1995, pg. 1086-1 to 1086

[14] M. Kosaki et al, "New Approach to Diagnostic Method of Water Trees", IEEE International Symposium on Electrical Insulation, Toronto, Canada, June 3-6, 1990, pg. 296-299

[15] G.S. Eager Jr. et al, "Effect of DC Testing Water Tree Deteriorated Cable and a Preliminary Evalution of VLF as Alternative", IEEE Transactions on Power Delivery, Vol. 7, No. 3, 1992, pg. 1582-1591

[16] O. Fukuda et al, "Development of a Hot-Line Diagnostic Method for XLPE Cables and Measurement Results", IEEE Transactions on Power Delivery, Vol. 4, No. 2, April 1989

[17] B.H. Ward and J.P. Steiner, "An Alternative to DC Testing of Installed Polymeric Power Cables", 7th International Symposium on High Voltage Engineering, Dresden, Germany, August 26-30, 1991, pg. 177-180

[18] C.J. Doman and S.J. Heyer, "AC Testing Without Cable Degradation", Transmission and Distribution World, July 1999

[19] C.M. Cooke, "Space Charge Measurement in XLPE", 1999 IEEE PES T&D Conference, New Orleans, Louisiana, April 1999, Panel Session #9

[20] V. Buchholz and S. Cherukupalli, "Review of Emerging Cable Test Methods for Condition Assessment of Underground Distribution Cable Assets", 1999 IEEE PES T&D Conference, New Orleans, Louisiana, April 1999, Panel Session #9

[21] M. Wendell and M. Walton, "Application of Partial Discharge Test Methodology with ACLT Aging to Estimate Performance of Installed XLPE-Insulated Cables", 1999 IEEE PES T&D Conference, New Orleans, Louisiana, April 1999, Panel Session on Cable Partial Discharge Location as a Diagnostic Tool

[22] D. Flaten and W. Reder, "Partial Discharge Testing, Non-Destructive 60 Hz", 1999 IEEE PES T&D Conference, New Orleans, Louisiana, April 1999, Panel Session on Cable Partial Discharge Location as a Diagnostic Tool

[23] W. Boone, "Predictive Maintenance for Distribution Cable Circuits Based on Partial Discharge Detection", 1999 IEEE PES T&D Conference, New Orleans, Louisiana, April 1999, Session on Cable Partial Discharge Location as a Diagnostic Tool

[24] G. Hoff and H.-G. Krantz, "Isothermal Relaxation Current Analysis: A New Non-Destructive Diagnostic Tool for Polymeric Power Distribution Cables", 1999 IEEE PES T&D Conference, New Orleans, Louisiana, April 1999, Panel Session on Diagnostic Measurement Techniques For Power Cables

[25] P. Werelius, "Power Cable Diagnostics by Dielectric Spectroscopy", 1999 IEEE PES T&D Conference, New Orleans, Louisiana, April 1999, Panel Session on Diagnostic Measurement Techniques For Power Cables

[26] A. Bulinski, E. So and S. Bamji, "Measurement of the Harmonic Distortion of Insulation Loss Current as a Diagnostic Tool for Cable Insulation", 1999 IEEE PES T&D Conference, New Orleans, Louisiana, April 1999, Panel Session on Diagnostic Measurement Techniques For Power Cables

[27] E. Gockenbach and W. Hauschild, "The Selection of the Frequency Range for High-Voltage On-Site Testing of Extruded Insulation Cable Systems", IEEE Electrical Insulation Magazine, Vol. 16, No. 6, November/December 2000, pg. 11-16

[28] P. Tharning and P. Werelius, "High Voltage Dielectric Response Analyzer for Cable Diagnostics", IEEE Conference on Electrical Insulation and Dielectric Phenomena, Pocono Manor, Pennsylvania, October 1993, pg. 745-750

[29] J.M. Braun et al, "A New Low Frequency High Voltage Analyzer Using Transient Methods", IEEE Conference on Electrical Insulation and Dielectric Phenomena, Victoria, Canada, October 1992, pg. 328-333

[30] A. van Roggen and H. Zhou, "Data Analysis in Dielectric Time-domain Spectroscopy", IEEE Conference on Electrical Insulation and Dielectric Phenomena, Victoria, Canada, October 1992, pg. 322-327

[31] M. Beigert and H.-G. Kranz, "Destruction Free Ageing Diagnosis of Power Cable Insulation Using Isothermal Relaxation Current Analysis", IEEE International Symposium on Electrical Insulation, Pittsburgh, Pennsylvania, June 1994, pg 17-21

[32] U. Gafvert et al, "Relation Between Return Voltage and Other Methods for Measurement of Dielectric Response", IEEE International Symposium on Electrical Insulation, Pittsburgh, Pennsylvania, June 1994, pg 25-28

[33] A. Bulinski et al, "Diagnostic Measurements of High Voltage Insulation Using Current Comparator Technology", IEEE International Symposium on Electrical Insulation, Pittsburgh, Pennsylvania, June 1994, pg 115-118

[34] T. Leibfried and K. Feser, "On-Line Monitoring of Transformers by Means of the Transfer Function Method", IEEE International Symposium on Electrical Insulation, Pittsburgh, Pennsylvania, June 1994, pg 111-114

[35] T. Leibfried and K. Feser, "Monitoring of Power Transformers Using the Transfer Function Method", IEEE Transactions on Power Delivery, Vol. 14, No. 4, October 1999, pg. 1333-1341

[36] G.D. Allen et al, "Transient Overvoltages and Overcurrents on 12.47 kV Distribution Lines: Field Test Results", IEEE PES 1991 Winter Meeting, New York, New York, February 1991, 91 WM 097-6 PWRD

[37] J. Bak-Jensen et al, "Detection of Faults and Ageing Phenomena in Transformers by Transfer Functions", IEEE PES 1994 Summer Meeting, San Francisco, California, July 1994, 94 SM 412-7 PWRD

[38] H.G. Tempelaar and C.G.A. Koreman, "The Use of Digital Techniques for High Voltage Measurements", 4th International Symposium on High Voltage Engineering, Athens, Greece, September 5-9, 1983, paper 65-07

[39] R. Malewski and B. Poulin, "Impulse Testing of Power Transformers Using the Transfer Function Method", IEEE Transactions on Power Delivery, Vol. 3, No. 2, April 1988, pg. 476-489

[40] R. Malewski and B. Poulin, "Digital Monitoring Technique for HV Impulse Tests", IEEE Transactions on Power Apparatus and Systems, Vol. PAS-104, No. 11, November 1985, pg. 3108-3114

[41] E. Hanique, "A Transfer Function is a Reliable Tool for Comparison of Full and Chopped Lightning Impulse Tests", IEEE PES 1994 Winter Meeting, New York, New York, January 30 – February 4, 1994, 94 WM 149-5 PWRD

[42] E. Hanique, "Practical Implementation of a Digital Recording System for Lightning Impulse Tests", International Symposium on Digital Techniques in High-Voltage Measurements, Toronto, Canada, October 28-30, 1991, pg. 3.18-3.22

[43] T. Leibfried and K. Feser, "Some Aspects using the Transfer Function Concept in High Voltage Impulse Testing of Transformers", International Symposium on Digital Techniques in High-Voltage Measurements, Toronto, Canada, October 28-30, 1991, pg. 5.3-5.7

[44] D.J. Tschudi and A.J. Germond, "Transformer Impulse Test Failure Location Using DSP Techniques", International Symposium on Digital Techniques in High-Voltage Measurements, Toronto, Canada, October 28-30, 1991, pg. 5.8-5.12

[45] J. Douville et al, "Measurement of Switching Transients in 735 kV Substations and Assessment of Their Severity for Transformer Insulation", IEEE Transactions on Power Delivery, Vol. PWRD-3, No. 4, 1989, pg. 1380-1387

[46] W. Janischewskyj et al, "Application of Spectrum Analysis in Lightning Impulse Testing", International Symposium on Digital Techniques in High-Voltage Measurements, Toronto, Canada, October 28-30, 1991, pg. 5.24-5.28

[47] H.M. Banford et al, "Diagnostic Dielectric Spectroscopy Methods Applied to Water-treed Cable", IEEE Transactions on Dielectrics and Electrical Insulation, Vol. 8, No. 6, December 2001, pg. 917-920

[48] J. Hallstrom and L. Satish, "Some Effects of Data Preprocessing on Transfer Function Calculation", CIGRE WG33-03 Meeting, September 1998, paper 25

[49] B.I. Gururaj and L. Satish, "Some Thoughts on Transfer Function and Coherence in Lightning Impulse Testing of Transformers", CIGRE WG33-03 Meeting, September 1998, paper 32

[50] W.H. Hayt and J.E. Kemmerly, *Engineering Circuit Analysis*, McGraw-Hill Book Company, 1978, ISBN 0-07-027393-6

[51] D.E. Johnson et al, *Basic Electric Circuit Analysis*, Prentice-Hall Inc., Englewood Cliffs, NJ 07632, 1978, ISBN 0-13-060137-3

[52] A. Greenwood, *Electrical Transients in Power Systems*, John Wiley & Sons Inc., 1991, ISBN 0-471-62058-0

[53] T.O. Bialek and S. Grzybowski, "Investigation of the Performance of New XLPE and EPR Cables", IEEE 1999 Conference on Electrical Insulation and Dielectric Phenomena , Oct. 17-20, 1999, Austin, Texas

[54] T.O. Bialek and S. Grzybowski, "Investigation of the Performance of Field Aged HMWPE and XLPE Cables", IEEE 2000 Conference on Electrical Insulation and Dielectric Phenomena , Oct. 15-18, 2000, Victoria, British Columbia, Canada

[55] E. Gulski et al, "PD Diagnosis and Condition Assessment of Distribution Power Cables using Damped AC Voltages", XIII International Symposium on High Voltage Engineering, Netherlands 2003

[56] xxxx, The Scientist and Engineer's Guide to Digital Signal Processing

[57] Bruel & Kjaer, Dual Channel FFT Analysis (Part I), Technical Review No. 1 – 1984

[58] Bruel & Kjaer, Dual Channel FFT Analysis (Part II), Technical Review No. 2 – 1984

[59] Bruel & Kjaer, Windows to FFT Analysis (Part I), Technical Review No. 3 – 1987

[60] Hewlett-Packard, A Refresher Course on Windowing and Measurements, Realtime Update, Fall1995/Winter1996

[61] National Instruments, The Fundamentals of FFT-Based Signal Analysis and Measurement, Application Note 041, July 2000

[62] Nicolet, Windowing for Dynamic Measurements, Technical Note

APPENDIX A

VOLTAGE DISTRIBUTION CALCULATION OF A CABLE WITH A CIRCUMFERENTIAL GAS BUBBLE

For a coaxial, three layer system which simulates a cable insulation with a gas bubble located uniformly throughout the insulation one can calculate the electric field and voltage distribution as follows.

For layer one

$$\vec{Y}_1 = G_1 + j\cdot\omega\cdot C_1 \qquad \text{(A-1)}$$

For layer two

$$\vec{Y}_2 = G_2 + j\cdot\omega\cdot C_2 \qquad \text{(A-2)}$$

For layer three

$$\vec{Y}_3 = G_3 + j\cdot\omega\cdot C_3 \qquad \text{(A-3)}$$

Now

$$G = \frac{\gamma\cdot 2\cdot\pi\cdot L}{\ln\left(\frac{r_b}{r_a}\right)} \qquad \text{(A-4)} \qquad \text{and} \qquad C = \frac{2\cdot\pi\cdot\varepsilon_o\cdot\varepsilon_r\cdot L}{\ln\left(\frac{r_b}{r_a}\right)} \qquad \text{(A-5)}$$

Assuming γ and ε_r are constant throughout the material we can solve in terms of per unit length G/L and C/L

Therefore

$$G_1 = \frac{\gamma_{1}\cdot 2\cdot\pi}{\ln\left(\frac{r_2}{r_1}\right)} \qquad \text{(A-6)} \qquad G_2 = \frac{\gamma_{2}\cdot 2\cdot\pi}{\ln\left(\frac{r_3}{r_2}\right)} \qquad \text{(A-7)} \qquad G_3 = \frac{\gamma_{3}\cdot 2\cdot\pi}{\ln\left(\frac{r_4}{r_3}\right)} \qquad \text{(A-8)}$$

$$C_1 = \frac{2\cdot\pi\cdot\varepsilon_o\cdot\varepsilon_1}{\ln\left(\frac{r_2}{r_1}\right)} \qquad \text{(A-9)} \qquad C_2 = \frac{2\cdot\pi\cdot\varepsilon_o\cdot\varepsilon_2}{\ln\left(\frac{r_3}{r_2}\right)} \qquad \text{(A-10)} \qquad C_3 = \frac{2\cdot\pi\cdot\varepsilon_o\cdot\varepsilon_3}{\ln\left(\frac{r_4}{r_3}\right)} \qquad \text{(A-11)}$$

Now

$$\vec{I} = \vec{V}_1\cdot\vec{Y}_1 \qquad \text{(A-12)} \qquad \vec{I} = \vec{V}_2\cdot\vec{Y}_2 \qquad \text{(A-13)} \qquad \vec{I} = \vec{V}_3\cdot\vec{Y}_3 \qquad \text{(A-14)}$$

Substituting for Y_1, Y_2 and Y_3

$$\vec{I} = \vec{V}_1\cdot\left(\frac{\gamma_{1}\cdot 2\cdot\pi}{\ln\left(\frac{r_2}{r_1}\right)} + \frac{j\cdot\omega\cdot 2\cdot\pi\cdot\varepsilon_o\cdot\varepsilon_1}{\ln\left(\frac{r_2}{r_1}\right)}\right) \qquad \text{(A-15)}$$

$$\dot{I} = \vec{V_2}\cdot\left(\frac{\gamma_{2}\cdot 2\cdot\pi}{\ln\left(\frac{r_3}{r_2}\right)} + \frac{j\cdot\omega\cdot 2\cdot\pi\cdot\varepsilon_o\cdot\varepsilon_2}{\ln\left(\frac{r_3}{r_2}\right)}\right) \qquad \text{(A-16)}$$

$$\dot{I} = \vec{V_3}\cdot\left(\frac{\gamma_{3}\cdot 2\cdot\pi}{\ln\left(\frac{r_4}{r_3}\right)} + \frac{j\cdot\omega\cdot 2\cdot\pi\cdot\varepsilon_o\cdot\varepsilon_3}{\ln\left(\frac{r_4}{r_3}\right)}\right) \qquad \text{(A-17)}$$

Now pulling out the common terms

$$\dot{I} = \frac{\vec{V_1}\cdot 2\cdot\pi}{\ln\left(\frac{r_2}{r_1}\right)}\cdot\left(\gamma_1 + j\cdot\omega\cdot\varepsilon_o\cdot\varepsilon_1\right) \qquad \text{(A-18)}$$

$$\dot{I} = \frac{\vec{V_2}\cdot 2\cdot\pi}{\ln\left(\frac{r_3}{r_2}\right)}\cdot\left(\gamma_2 + j\cdot\omega\cdot\varepsilon_o\cdot\varepsilon_2\right) \qquad \text{(A-19)}$$

$$\dot{I} = \frac{\vec{V_3}\cdot 2\cdot\pi}{\ln\left(\frac{r_4}{r_3}\right)}\cdot\left(\gamma_3 + j\cdot\omega\cdot\varepsilon_o\cdot\varepsilon_3\right) \qquad \text{(A-20)}$$

Now $\left|\dot{I}\right| = I$

Therefore

$$\left|\vec{\dot{I}}\right| = \frac{\vec{V_1}\cdot 2\cdot\pi}{\ln\left(\frac{r_2}{r_1}\right)}\cdot\sqrt{\left(\gamma_1\right)^2 + \left(\omega\cdot\varepsilon_o\cdot\varepsilon_1\right)^2} \qquad \text{(A-21)}$$

$$\left|\vec{\dot{I}}\right| = \frac{\vec{V_2}\cdot 2\cdot\pi}{\ln\left(\frac{r_3}{r_2}\right)}\cdot\sqrt{\left(\gamma_2\right)^2 + \left(\omega\cdot\varepsilon_o\cdot\varepsilon_2\right)^2} \qquad \text{(A-22)}$$

$$\left|\vec{\dot{I}}\right| = \frac{\vec{V_3}\cdot 2\cdot\pi}{\ln\left(\frac{r_4}{r_3}\right)}\cdot\sqrt{\left(\gamma_3\right)^2 + \left(\omega\cdot\varepsilon_o\cdot\varepsilon_3\right)^2} \qquad \text{(A-23)}$$

But we know that

$$E_{1max} = \frac{V_1}{r_1 \cdot \ln\left(\frac{r_2}{r_1}\right)} \qquad \text{(A-24)} \qquad E_{2max} = \frac{V_2}{r_2 \cdot \ln\left(\frac{r_3}{r_2}\right)} \qquad \text{(A-25)}$$

$$E_{3max} = \frac{V_3}{r_3 \cdot \ln\left(\frac{r_4}{r_3}\right)} \qquad \text{(A-26)}$$

Therefore, substituting (A-24) into (A-21), (A-25) into (A-22) and (A-26) into (A-23) and equating the magnitudes of current we obtain

$$E_{1max} \cdot r_1 \cdot 2 \cdot \pi \cdot \sqrt{(\gamma_1)^2 + (\omega \cdot \varepsilon_o \cdot \varepsilon_1)^2} = E_{2max} \cdot r_2 \cdot 2 \cdot \pi \cdot \sqrt{(\gamma_2)^2 + (\omega \cdot \varepsilon_o \cdot \varepsilon_2)^2} \qquad \text{(A-27)}$$

$$E_{1max} \cdot r_1 \cdot 2 \cdot \pi \cdot \sqrt{(\gamma_1)^2 + (\omega \cdot \varepsilon_o \cdot \varepsilon_1)^2} = E_{3max} \cdot r_3 \cdot 2 \cdot \pi \cdot \sqrt{(\gamma_3)^2 + (\omega \cdot \varepsilon_o \cdot \varepsilon_3)^2} \qquad \text{(A-28)}$$

Solving for E_{2max} and E_{3max} in terms of E_{1max}

$$E_{2max} = E_{1max} \cdot \frac{r_1}{r_2} \cdot \frac{\sqrt{(\gamma_1)^2 + (\omega \cdot \varepsilon_o \cdot \varepsilon_1)^2}}{\sqrt{(\gamma_2)^2 + (\omega \cdot \varepsilon_o \cdot \varepsilon_2)^2}} \qquad \text{(A-29)}$$

$$E_{3max} = E_{1max} \cdot \frac{r_1}{r_3} \cdot \frac{\sqrt{(\gamma_1)^2 + (\omega \cdot \varepsilon_o \cdot \varepsilon_1)^2}}{\sqrt{(\gamma_3)^2 + (\omega \cdot \varepsilon_o \cdot \varepsilon_3)^2}} \qquad \text{(A-30)}$$

But

$V = V_1 + V_2 + V_3$

Therefore

$$V = E_{1max} \cdot r_1 \cdot \ln\left(\frac{r_2}{r_1}\right) + E_{1max} \cdot \frac{r_1}{r_2} \cdot \frac{\sqrt{(\gamma_1)^2 + (\omega \cdot \varepsilon_o \cdot \varepsilon_1)^2}}{\sqrt{(\gamma_2)^2 + (\omega \cdot \varepsilon_o \cdot \varepsilon_2)^2}} \cdot r_2 \cdot \ln\left(\frac{r_3}{r_2}\right) \ldots$$

$$+ E_{1max} \cdot \frac{r_1}{r_3} \cdot \frac{\sqrt{(\gamma_1)^2 + (\omega \cdot \varepsilon_o \cdot \varepsilon_1)^2}}{\sqrt{(\gamma_3)^2 + (\omega \cdot \varepsilon_o \cdot \varepsilon_3)^2}} \cdot r_3 \cdot \ln\left(\frac{r_4}{r_3}\right) \qquad \text{(A-31)}$$

Combining like terms

$$V = E_{1max} \cdot r_1 \cdot \left[\ln\left(\frac{r_2}{r_1}\right) + \ln\left(\frac{r_3}{r_2}\right) \cdot \frac{\sqrt{(\gamma_1)^2 + (\omega \cdot \varepsilon_o \cdot \varepsilon_1)^2}}{\sqrt{(\gamma_2)^2 + (\omega \cdot \varepsilon_o \cdot \varepsilon_2)^2}} + \ln\left(\frac{r_4}{r_3}\right) \cdot \frac{\sqrt{(\gamma_1)^2 + (\omega \cdot \varepsilon_o \cdot \varepsilon_1)^2}}{\sqrt{(\gamma_3)^2 + (\omega \cdot \varepsilon_o \cdot \varepsilon_3)^2}} \right]$$

(A-32)

Solving for E_{1max}

$$E_{1max} = \frac{V}{\left[r_1 \cdot \left[\ln\left(\frac{r_2}{r_1}\right) + \ln\left(\frac{r_3}{r_2}\right) \cdot \frac{\sqrt{(\gamma_1)^2 + (\omega \cdot \varepsilon_o \cdot \varepsilon_1)^2}}{\sqrt{(\gamma_2)^2 + (\omega \cdot \varepsilon_o \cdot \varepsilon_2)^2}} + \ln\left(\frac{r_4}{r_3}\right) \cdot \frac{\sqrt{(\gamma_1)^2 + (\omega \cdot \varepsilon_o \cdot \varepsilon_1)^2}}{\sqrt{(\gamma_3)^2 + (\omega \cdot \varepsilon_o \cdot \varepsilon_3)^2}} \right] \right]}$$

(A-33)

Following identical calculations for E_{2max} and E_{3max}

$$E_{2max} = \frac{V}{\left[r_2 \cdot \left[\ln\left(\frac{r_2}{r_1}\right) \cdot \frac{\sqrt{(\gamma_2)^2 + (\omega \cdot \varepsilon_o \cdot \varepsilon_2)^2}}{\sqrt{(\gamma_1)^2 + (\omega \cdot \varepsilon_o \cdot \varepsilon_1)^2}} + \ln\left(\frac{r_3}{r_2}\right) + \ln\left(\frac{r_4}{r_3}\right) \cdot \frac{\sqrt{(\gamma_2)^2 + (\omega \cdot \varepsilon_o \cdot \varepsilon_2)^2}}{\sqrt{(\gamma_3)^2 + (\omega \cdot \varepsilon_o \cdot \varepsilon_3)^2}} \right] \right]}$$

(A-34)

$$E_{3max} = \frac{V}{\left[r_3 \cdot \left[\ln\left(\frac{r_2}{r_1}\right) \cdot \frac{\sqrt{(\gamma_3)^2 + (\omega \cdot \varepsilon_o \cdot \varepsilon_3)^2}}{\sqrt{(\gamma_1)^2 + (\omega \cdot \varepsilon_o \cdot \varepsilon_1)^2}} + \ln\left(\frac{r_3}{r_2}\right) \cdot \frac{\sqrt{(\gamma_3)^2 + (\omega \cdot \varepsilon_o \cdot \varepsilon_3)^2}}{\sqrt{(\gamma_2)^2 + (\omega \cdot \varepsilon_o \cdot \varepsilon_2)^2}} + \ln\left(\frac{r_4}{r_3}\right) \right] \right]}$$

(A-35)

For DC conditions $\omega=0$

Therefore,

$$E_{1max} = \frac{V}{r_1 \cdot \left(\ln\left(\frac{r_2}{r_1}\right) + \ln\left(\frac{r_3}{r_2}\right) \cdot \frac{\gamma_1}{\gamma_2} + \ln\left(\frac{r_4}{r_3}\right) \cdot \frac{\gamma_1}{\gamma_3} \right)} \quad \text{(A-36)}$$

$$E_{2max} = \frac{V}{r_2 \cdot \left(\ln\left(\frac{r_2}{r_1}\right) \cdot \frac{\gamma_2}{\gamma_1} + \ln\left(\frac{r_3}{r_2}\right) + \ln\left(\frac{r_4}{r_3}\right) \cdot \frac{\gamma_2}{\gamma_3} \right)} \quad \text{(A-37)}$$

$$E_{3max} = \frac{V}{r_3 \cdot \left(\ln\left(\frac{r_2}{r_1}\right) \cdot \frac{\gamma_3}{\gamma_1} + \ln\left(\frac{r_3}{r_2}\right) \cdot \frac{\gamma_3}{\gamma_2} + \ln\left(\frac{r_4}{r_3}\right) \right)} \quad \text{(A-38)}$$

For AC conditions $\omega\varepsilon_o\varepsilon_r >> \gamma$

$$E_{1max} = \frac{V}{r_1 \cdot \left(\ln\left(\frac{r_2}{r_1}\right) + \ln\left(\frac{r_3}{r_2}\right) \cdot \frac{\varepsilon_1}{\varepsilon_2} + \ln\left(\frac{r_4}{r_3}\right) \cdot \frac{\varepsilon_1}{\varepsilon_3} \right)} \quad \text{(A-39)}$$

$$E_{2max} = \frac{V}{r_2 \cdot \left(\ln\left(\frac{r_2}{r_1}\right) \cdot \frac{\varepsilon_2}{\varepsilon_1} + \ln\left(\frac{r_3}{r_2}\right) + \ln\left(\frac{r_4}{r_3}\right) \cdot \frac{\varepsilon_2}{\varepsilon_3} \right)} \quad \text{(A-40)}$$

$$E_{3max} = \frac{V}{r_3 \cdot \left(\ln\left(\frac{r_2}{r_1}\right) \cdot \frac{\varepsilon_3}{\varepsilon_1} + \ln\left(\frac{r_3}{r_2}\right) \cdot \frac{\varepsilon_3}{\varepsilon_2} + \ln\left(\frac{r_4}{r_3}\right) \right)} \quad \text{(A-41)}$$

APPENDIX B

RLC STEP RESPONSE DERIVATION FOR A LUMPED PARAMETER CABLE EQUIVALENT CIRCUIT

Solving for the parallel RLC case

$$-C\cdot\frac{d}{dt}V_C = I_L + \frac{V_C}{R} \tag{B-1}$$

But

$$V_C = L\cdot\frac{d}{dt}I_L \tag{B-2}$$

Substituting Equation B-2 into B-1

$$-C\cdot L\cdot\frac{d^2}{dt^2}I_L = I_L + \frac{L}{R}\cdot\frac{d}{dt}I_L$$

Rearranging

$$\frac{d^2}{dt^2}I_L + \frac{1}{R\cdot C}\cdot\frac{d}{dt}I_L + \frac{I_L}{LC} = 0$$

let τ_p=RC and T^2=LC

$$\frac{d^2}{dt^2}I_L + \frac{1}{\tau_p}\cdot\frac{d}{dt}I_L + \frac{I_L}{T^2} = 0 \tag{B-3}$$

Now converting A2-3 into its Laplace Transform

$$\left(s^2 + \frac{s}{\tau_p} + \frac{1}{T^2}\right)\cdot i_L\cdot(s) = \left[\left(s + \frac{1}{\tau_p}\right)\cdot I_L\cdot(0)\right] + \frac{d}{dt}I_L(0) \tag{B-4}$$

But $I_L(0)=0$ and $I'_L(0)=V_C(0)/L$

Therefore

$$i_L(s) = \frac{V_C(0)}{L}\cdot\frac{1}{s^2 + \frac{s}{\tau_p} + \frac{1}{T^2}} \tag{B-5}$$

This equals

$$i_L(s) = \frac{V_C(0)}{L}\cdot\frac{1}{(s-a)\cdot(s-b)} \tag{B-6}$$

Where

$$a = \frac{-1}{2\cdot\tau_p} + \frac{1}{2}\cdot\sqrt{\frac{1}{(\tau_p)^2} - \frac{4}{T^2}}$$

$$b = \frac{-1}{2\cdot\tau_p} - \frac{1}{2}\cdot\sqrt{\frac{1}{(\tau_p)^2} - \frac{4}{T^2}}$$

Now taking the inverse Laplace Transform

$$I_L(t) = \frac{V_C(0)}{L\cdot\sqrt{\frac{1}{(\tau_p)^2} - \frac{4}{T^2}}}\cdot\left(e^{a\cdot t} - e^{b\cdot t}\right) \tag{B-7}$$

Now let η=R/Zo where Zo=(L/C)$^{1/2}$ and rewrite a and b in terms of η for > ½

$$a = \frac{-1}{2\cdot\tau_p}\cdot\left(1 - i\cdot\sqrt{4\cdot\eta^2 - 1}\right) \tag{B-8}$$

$$b = \frac{-1}{2\cdot\tau_p}\cdot\left(1 + i\cdot\sqrt{4\cdot\eta^2 - 1}\right)$$

$$I_L(t) = \frac{V_C(0)\cdot\tau_p\cdot e^{\frac{-t}{2\cdot\tau_p}}}{L\cdot i\cdot\sqrt{4\cdot\eta^2 - 1}}\cdot\left[e^{\frac{\left(i\cdot\sqrt{4\cdot\eta^2-1}\right)\cdot t}{2\cdot\tau_p}} - e^{\frac{-\left[\left(i\cdot\sqrt{4\cdot\eta^2-1}\right)\cdot t\right]}{2\cdot\tau_p}}\right]$$

or rewriting utilizing Euler's identity

$$I_L(t) = \frac{V_C(0)\cdot 2\cdot\tau_p\cdot e^{\frac{-t}{2\cdot\tau_p}}}{L\cdot\sqrt{4\cdot\eta^2 - 1}}\cdot\sin\left(\sqrt{4\cdot\eta^2 - 1}\cdot\frac{t}{2\cdot\tau_p}\right) \tag{B-9}$$

Now for η <1/2

$$a = \frac{-1}{2\cdot\tau_p}\cdot\left(1 - \sqrt{4\cdot\eta^2 - 1}\right) \tag{B-10}$$

$$b = \frac{-1}{2\cdot\tau_p}\cdot\left(1 + \sqrt{4\cdot\eta^2 - 1}\right)$$

$$I_L(t) = \frac{V_C(0)\cdot\tau_p\cdot e^{\frac{-t}{2\cdot\tau_p}}}{L\cdot\sqrt{\left(1 - 4\cdot\eta^2\right)}}\cdot\left[e^{\frac{\left(\sqrt{1-4\cdot\eta^2}\right)\cdot t}{2\cdot\tau_p}} - e^{\frac{-\left(\sqrt{1-4\cdot\eta^2}\right)\cdot t}{2\cdot\tau_p}}\right]$$

Or rewriting utilizing Euler's identity

$$I_L(t) = \frac{V_C\cdot(0)\cdot 2\cdot\tau_p\cdot e^{\frac{-t}{2\cdot\tau_p}}}{L\cdot\sqrt{\left(1-4\cdot\eta^2\right)}}\cdot\sinh\left(\sqrt{1-4\cdot\eta^2}\cdot\frac{t}{2\cdot\tau_p}\right) \qquad \text{(B-11)}$$

Now for the case when $\eta=1/2$

$$a = b$$

$$a = \frac{-1}{2\cdot\tau_p}$$

$$i_L(s) = \frac{V_C(0)}{L}\cdot\frac{1}{(s+a)^2}$$

and taking the inverse Laplace Transform

$$I_L(t) = \frac{V_C(0)}{L}\cdot t\cdot e^{\frac{-t}{2\cdot\tau_p}} \qquad \text{(B-12)}$$

Therefore the solutions for the three cases are as follows

$I_L(t)$ roots complex, $1/\tau_p{}^2<4/T^2$ $\eta>1/2$ under damped

$$I_L(t) = \frac{V_C\cdot(0)\cdot 2\cdot\tau_p\cdot e^{\frac{-t}{2\cdot\tau_p}}}{L\cdot\sqrt{4\cdot\eta^2-1}}\cdot\sin\left(\sqrt{4\cdot\eta^2-1}\cdot\frac{t}{2\cdot\tau_p}\right) \qquad \text{(B-13)}$$

$I_L(t)$ roots real, $1/\tau_p{}^2>4/T^2$ $\eta<1/2$ over damped

$$I_L(t) = \frac{V_C\cdot(0)\cdot 2\cdot\tau_p\cdot e^{\frac{-t}{2\cdot\tau_p}}}{L\cdot\sqrt{\left(1-4\cdot\eta^2\right)}}\cdot\sinh\left(\sqrt{1-4\cdot\eta^2}\cdot\frac{t}{2\cdot\tau_p}\right) \qquad \text{(B-14)}$$

$I_L(t)$ roots equal, $1/\tau_p^2=4/T^2$ $\eta=1/2$ critically damped

$$I_L(t) = \frac{V_C(0)}{L}\cdot t\cdot e^{\frac{-t}{2\cdot\tau_p}} \tag{B-15}$$

Similarly expression for the series RLC connection can be derived and the solutions are shown below for $\lambda=Zo/R$ and $\tau_S=L/R$ and $T^2=LC$

I(t) roots complex, $1/\tau_S^2<4/T^2$ $\lambda>1/2$ under damped

$$I(t) = \frac{V\cdot 2\cdot\tau_S\cdot e^{\frac{-t}{2\cdot\tau_S}}}{L\cdot\sqrt{4\cdot\lambda^2-1}}\cdot\sin\left(\sqrt{4\cdot\lambda^2-1}\cdot\frac{t}{2\cdot\tau_S}\right) \tag{B-16}$$

I(t) roots real, $1/\tau_S^2>4/T^2$ $\lambda<1/2$ over damped

$$I(t) = \frac{V\cdot 2\cdot\tau_S\cdot e^{\frac{-t}{2\cdot\tau_S}}}{L\cdot\sqrt{\left(1-4\cdot\lambda^2\right)}}\cdot\sinh\left(\sqrt{1-4\cdot\lambda^2}\cdot\frac{t}{2\cdot\tau_S}\right) \tag{B-17}$$

I(t) roots equal, $1/\tau_S^2=4/T^2$ $\lambda=1/2$ critically damped

$$I(t) = \frac{V}{L}\cdot t\cdot e^{\frac{-t}{2\cdot\tau_S}} \tag{B-18}$$

APPENDIX C

RLC STEP RESPONSE FOURIER TRANSFORM DERIVATION FOR A LUMPED PARAMETER CABLE EQUIVALENT CIRCUIT

The Fourier Transform of a function, f(t), is given by the following expression.

$$F(j\omega) = \int_{-\infty}^{\infty} f(t)\cdot e^{-j\cdot\omega\cdot t}\,dt \qquad \text{(C-1)}$$

and for two functions $f_1(t)$ and $f_2(t)$

$F(f_1(t)+f_2(t)) = F(f_1(t)) + F(f_2(t))$

Now let's look at the three possible solutions for a step response of a RLC circuit as calculated in Appendix B. The step is applied at time t=0.

I(t) roots complex, $1/\tau_S^2<4/T^2$ $\lambda>1/2$ under damped

$$I(t) = \frac{V\cdot 2\cdot\tau_S\cdot e^{\frac{-t}{2\cdot\tau_s}}}{L\cdot\sqrt{4\cdot\lambda^2-1}}\cdot\sin\left(\sqrt{4\cdot\lambda^2-1}\cdot\frac{t}{2\cdot\tau_s}\right) \qquad \text{(C-2)}$$

I(t) roots real, $1/\tau_S^2>4/T^2$ $\lambda<1/2$ over damped

$$I(t) = \frac{V\cdot 2\cdot\tau_S\cdot e^{\frac{-t}{2\cdot\tau_s}}}{L\cdot\sqrt{\left(1-4\cdot\lambda^2\right)}}\cdot\sinh\left(\sqrt{1-4\cdot\lambda^2}\cdot\frac{t}{2\cdot\tau_s}\right) \qquad \text{(C-3)}$$

I(t) roots equal, $1/\tau_S^2=4/T^2$ $\lambda=1/2$ critically damped

$$I(t) = \frac{V}{L}\cdot t\cdot e^{\frac{-t}{2\cdot\tau_s}} \qquad \text{(C-4)}$$

Solution Case $\lambda<1/2$

$$I(j\omega) = \int_{-\infty}^{\infty} \frac{V\cdot 2\cdot\tau_S\cdot e^{\frac{-t}{2\cdot\tau_s}}}{L\cdot\sqrt{\left(1-4\cdot\lambda^2\right)}}\cdot\sinh\left(\sqrt{1-4\cdot\lambda^2}\cdot\frac{t}{2\cdot\tau_s}\right)\cdot e^{-j\cdot\omega\cdot t}\,dt \qquad \text{(C-5)}$$

But $\sinh(u) = (e^u - e^{-u})/2$

$$I(j\omega) = \int_{-\infty}^{\infty} \frac{V\cdot 2\cdot\tau_s\cdot e^{\frac{-t}{2\cdot\tau_s}}}{L\cdot\sqrt{\left(1-4\cdot\lambda^2\right)}}\cdot\left[e^{\left(\sqrt{1-4\cdot\lambda^2}\cdot\frac{t}{2\cdot\tau_s}\right)} - e^{-\left(\sqrt{1-4\cdot\lambda^2}\cdot\frac{t}{2\cdot\tau_s}\right)}\right]\cdot e^{-j\cdot\omega\cdot t}\,dt \qquad \text{(C-6)}$$

$$I(j\omega) = \int_{-\infty}^{\infty} \frac{V\cdot 2\cdot\tau_s}{L\cdot\sqrt{\left(1-4\cdot\lambda^2\right)}}\cdot e^{\left[\frac{-\left(1-\sqrt{1-4\cdot\lambda^2}\right)}{2\cdot\tau_s}-j\cdot\omega\right]\cdot t}\,dt \ldots \qquad \text{(C-7)}$$

$$+\int_{-\infty}^{\infty} \frac{-V\cdot 2\cdot\tau_s}{L\cdot\sqrt{\left(1-4\cdot\lambda^2\right)}}\cdot e^{-\left[\frac{-\left(1+\sqrt{1-4\cdot\lambda^2}\right)}{2\cdot\tau_s}-j\cdot\omega\right]\cdot t}\,dt$$

From CRC Tables

$$I(j\omega) = \frac{V\cdot 2\cdot\tau_s}{L\cdot\sqrt{\left(1-4\cdot\lambda^2\right)}}\cdot\left[\left[\frac{e^{\left[\frac{-\left(1-\sqrt{1-4\cdot\lambda^2}\right)}{2\cdot\tau_s}-j\cdot\omega\right]\cdot t}}{\left[\frac{-\left(1-\sqrt{1-4\cdot\lambda^2}\right)}{2\cdot\tau_s}-j\cdot\omega\right]}\cdot\right|_0^{\infty} - \frac{e^{-\left[\frac{-\left(1+\sqrt{1-4\cdot\lambda^2}\right)}{2\cdot\tau_s}-j\cdot\omega\right]\cdot t}}{-\left[\frac{-\left(1+\sqrt{1-4\cdot\lambda^2}\right)}{2\cdot\tau_s}-j\cdot\omega\right]}\cdot\right|_0^{\infty}\Bigg]$$

But at t = infinity $e^{\left[\frac{-\left(1-\sqrt{1-4\cdot\lambda^2}\right)}{2\cdot\tau_s}-j\cdot\omega\right]\cdot t}$ and $e^{-\left[\frac{-\left(1+\sqrt{1-4\cdot\lambda^2}\right)}{2\cdot\tau_s}-j\cdot\omega\right]\cdot t}$ equal 0

and at t=0 $e^{\left[\frac{-\left(1-\sqrt{1-4\cdot\lambda^2}\right)}{2\cdot\tau_s}-j\cdot\omega\right]\cdot t}$ and $e^{-\left[\frac{-\left(1+\sqrt{1-4\cdot\lambda^2}\right)}{2\cdot\tau_s}-j\cdot\omega\right]\cdot t}$ equal 1

Therefore,

$$I(j\omega) = \frac{V\cdot 2\cdot\tau_s}{L\cdot\sqrt{\left(1-4\cdot\lambda^2\right)}}\cdot\left[\frac{-1}{\left[\frac{-\left(1-\sqrt{1-4\cdot\lambda^2}\right)}{2\cdot\tau_s}-j\cdot\omega\right]} - \frac{-1}{-\left[\frac{-\left(1+\sqrt{1-4\cdot\lambda^2}\right)}{2\cdot\tau_s}-j\cdot\omega\right]}\right] \qquad \text{(C-8)}$$

Rationalizing the function

$$I(j\omega) = \frac{V\cdot\tau_s}{L\sqrt{\left(1-4\cdot\lambda^2\right)}}\cdot\left[\frac{1}{\frac{\left(1-\sqrt{1-4\cdot\lambda^2}\right)}{2\cdot\tau_s}+j\cdot\omega}-\frac{1}{\frac{\left(1+\sqrt{1-4\cdot\lambda^2}\right)}{2\cdot\tau_s}+j\cdot\omega}\right] \tag{C-9}$$

Solution Case $\lambda > 1/2$

$$I(j\omega) = \int_{-\infty}^{\infty}\frac{V\cdot 2\cdot\tau_s\cdot e^{\frac{-t}{2\cdot\tau_s}}}{L\sqrt{\left(1-4\cdot\lambda^2\right)}}\cdot\sin\left(\sqrt{1-4\cdot\lambda^2}\cdot\frac{t}{2\cdot\tau_s}\right)\cdot e^{-j\cdot\omega\cdot t}\,dt \tag{C-10}$$

Rearranging terms and combining the exponentials

$$I(j\omega) = \int_{-\infty}^{\infty}\frac{V\cdot 2\cdot\tau_s}{L\sqrt{\left(1-4\cdot\lambda^2\right)}}\cdot\sin\left(\frac{\sqrt{1-4\cdot\lambda^2}}{2\cdot\tau_s}\cdot t\right)\cdot e^{-\left(\frac{1}{2\cdot\tau_s}+j\cdot\omega\right)\cdot t}\,dt \tag{C-11}$$

From the CRC Tables

$$I(j\omega) = \frac{V\cdot 2\cdot\tau_s}{L\sqrt{\left(1-4\cdot\lambda^2\right)}}\cdot\frac{e^{-\left(\frac{1}{2\cdot\tau_s}+j\cdot\omega\right)\cdot t}}{\left(\frac{1}{2\cdot\tau_s}+j\cdot\omega\right)^2+\left(\frac{\sqrt{1-4\cdot\lambda^2}}{2\cdot\tau_s}\cdot t\right)^2}\cdot\blacksquare\ \ldots$$
$$+\left[-\left(\frac{1}{2\cdot\tau_s}+j\cdot\omega\right)\cdot\sin\left(\frac{\sqrt{1-4\cdot\lambda^2}}{2\cdot\tau_s}\cdot t\right)-\frac{\sqrt{1-4\cdot\lambda^2}}{2\cdot\tau_s}\cdot\cos\left(\frac{\sqrt{1-4\cdot\lambda^2}}{2\cdot\tau_s}\cdot t\right)\right]$$

Evaluated at infinity and zero

But at t = infinity $e^{-\left(\frac{1}{2\cdot\tau_s}+j\cdot\omega\right)\cdot t}$ equals 0

and at t=0 $e^{-\left(\frac{1}{2\cdot\tau_s}+j\cdot\omega\right)\cdot t}$ equals 1 and sin(0) equals 0 and cos(0) equals 1

Therefore,

$$I(j\omega) = \frac{V \cdot 2 \cdot \tau_s}{L \cdot \sqrt{\left(1 - 4 \cdot \lambda^2\right)}} \cdot \frac{-1}{\left[\left(\frac{1}{2 \cdot \tau_s} + j \cdot \omega\right)^2 + \left(\frac{\sqrt{1 - 4 \cdot \lambda^2}}{2 \cdot \tau_s}\right)^2\right]} \cdot \left(0 - \frac{\sqrt{1 - 4 \cdot \lambda^2}}{2 \cdot \tau_s}\right)$$

Carrying through the multiplication

$$I(j\omega) = \frac{V}{L} \cdot \frac{1}{\left[\left(\frac{1}{2 \cdot \tau_s} + j \cdot \omega\right)^2 + \left(\frac{\sqrt{1 - 4 \cdot \lambda^2}}{2 \cdot \tau_s}\right)^2\right]} \tag{C-12}$$

Solution Case $\lambda = 1/2$

$$I(j\omega) = \int_{-\infty}^{\infty} \frac{V}{L} \cdot t \cdot e^{\frac{-t}{2 \cdot \tau_s}} \cdot e^{-j \cdot \omega \cdot t} \, dt \tag{C-13}$$

Combining the exponential terms

$$I(j\omega) = \int_{-\infty}^{\infty} \frac{V}{L} \cdot t \cdot e^{-\left(\frac{1}{2 \cdot \tau_s} + j \cdot \omega\right) \cdot t} \, dt \tag{C-14}$$

Now from CRC tables

$$I(j\omega) = \frac{V}{L} \cdot \frac{e^{-\left(\frac{1}{2 \cdot \tau_s} + j \cdot \omega\right) \cdot t}}{\left(\frac{1}{2 \cdot \tau_s} + j \cdot \omega\right)^2} \cdot \left[-\left(\frac{1}{2 \cdot \tau_s} + j \cdot \omega\right) \cdot t - 1\right] \cdot \Big|_0^{\infty}$$

But at t = infinity $e^{-\left(\frac{1}{2 \cdot \tau_s} + j \cdot \omega\right) \cdot t}$ equals 0

and at t=0 $e^{-\left(\frac{1}{2 \cdot \tau_s} + j \cdot \omega\right) \cdot t}$ equals 1 and t equals 0

Therefore,

$$I(j\omega) = \frac{V}{L}\cdot\frac{-1}{\left(\frac{1}{2\cdot\tau_s} + j\cdot\omega\right)^2}\cdot -1$$

$$I(j\omega) = \frac{V}{L}\cdot\frac{1}{\left(\frac{1}{2\cdot\tau_s} + j\cdot\omega\right)^2} \qquad \text{(C-15)}$$

Summarizing for the three cases in the Frequency domain

$\lambda<1/2$

$$I(j\omega) = \frac{V\cdot\tau_s}{L\cdot\sqrt{\left(1-4\cdot\lambda^2\right)}}\cdot\left[\frac{1}{\frac{\left(1-\sqrt{1-4\cdot\lambda^2}\right)}{2\cdot\tau_s} + j\cdot\omega} - \frac{1}{\frac{\left(1+\sqrt{1-4\cdot\lambda^2}\right)}{2\cdot\tau_s} + j\cdot\omega}\right] \qquad \text{(C-16)}$$

$\lambda > 1/2$

$$I(j\omega) = \frac{V}{L}\cdot\frac{1}{\left[\left(\frac{1}{2\cdot\tau_s} + j\cdot\omega\right)^2 + \left(\frac{\sqrt{1-4\cdot\lambda^2}}{2\cdot\tau_s}\right)^2\right]} \qquad \text{(C-17)}$$

$\lambda = 1/2$

$$I(j\omega) = \frac{V}{L}\cdot\frac{1}{\left(\frac{1}{2\cdot\tau_s} + j\cdot\omega\right)^2} \qquad \text{(C-18)}$$

APPENDIX D

IMPEDANCE MATRIX SOLUTION OF A GENERIC CABLE THEORETICAL EQUIVALENT CIRCUIT

For the network one can write the mesh equations as follows.

$$(Z_1+Z_2+Z_3+Z_4)I_1-Z_1I_2-Z_2I_3-Z_3I_4-Z_4I_5=V_1 \quad \text{(D-1)}$$
$$-Z_1I_1+(Z_1+Z_5+Z_6+Z_{10})I_2-Z_6I_3-Z_{10}I_6=V_2 \quad \text{(D-2)}$$
$$-Z_2I_1-Z_6I_2+(Z_2+Z_6+Z_7+Z_{11})I_3-Z_7I_4-Z_{11}I_7=V_3 \quad \text{(D-3)}$$
$$-Z_3I_1-Z_7I_3+(Z_3+Z_7+Z_8+Z_{12})I_4-Z_8I_5-Z_{12}I_8=V_4 \quad \text{(D-4)}$$
$$-Z_4I_1-Z_8I_4+(Z_4+Z_8+Z_9+Z_{13})I_5-Z_{13}I_9=V_5 \quad \text{(D-5)}$$
$$-Z_{10}I_2+(Z_{10}+Z_{14}+Z_{15}+Z_{19})I_6-Z_{15}I_7=V_6 \quad \text{(D-6)}$$
$$-Z_{11}I_3-Z_{15}I_6+(Z_{11}+Z_{15}+Z_{16}+Z_{20})I_7-Z_{16}I_8=V_7 \quad \text{(D-7)}$$
$$-Z_{12}I_4-Z_{16}I_7+(Z_{12}+Z_{16}+Z_{17}+Z_{21})I_8-Z_{17}I_9=V_8 \quad \text{(D-8)}$$
$$-Z_{13}I_5-Z_{17}I_8+(Z_{13}+Z_{17}+Z_{18}+Z_{22})I_9=V_9 \quad \text{(D-9)}$$

The 9 equations in 9 unknowns can be solved utilizing Cramer's rule.
Where the per section parallel capacitor and resistor is converted to its series equivalent and the solution is obtained for ω=0.001 to 0.1.

$V1 = 1\cdot10^{4}$
$V2 = 0$
$V3 = 0$
$V4 = 0$
$V5 = 0$
$V6 = 0$
$V7 = 0$
$V8 = 0$
$V9 = 0$
$\omega = 0.001, 0.0011.. 0.1$
$Rp = 1\cdot10^{9}$
$Cp = 32\cdot10^{-9}$
$$Rs(\omega) = \frac{Rp}{1+\omega^{2}\cdot Rp^{2}\cdot Cp^{2}}$$
$$Cs(\omega) = Cp + \frac{1}{\omega^{2}\cdot Rp^{2}\cdot Cp}$$
$L = 7.5\cdot10^{-5}$
$R1(\omega) = Rs(\omega)$
$$X1(\omega) = \frac{-1}{\omega\cdot Cs(\omega)}$$
$$Rt(\omega) = \frac{R1(\omega)}{1\cdot10^{9}}$$
$X2(\omega) = 0$
$R2 = 1\cdot10^{20}$

$R3 = 0.007$

$X3(\omega) = \omega \cdot L$

$Z1(\omega) = R1(\omega) + i \cdot X1(\omega)$

$Z2(\omega) = R1(\omega) + i \cdot X1(\omega)$

$Z3(\omega) = R1(\omega) + i \cdot X1(\omega)$

$Z4(\omega) = R1(\omega) + i \cdot X1(\omega)$

$Z5(\omega) = R3 + i \cdot X3(\omega)$

$Z6(\omega) = R2 + i \cdot X2(\omega)$

$Z7(\omega) = R2 + i \cdot X2(\omega)$

$Z8(\omega) = R2 + i \cdot X2(\omega)$

$Z9(\omega) = R3 + i \cdot X3(\omega)$

$Z10(\omega) = R1(\omega) + i \cdot X1(\omega)$

$Z11(\omega) = R1(\omega) + i \cdot X1(\omega)$

$Z12(\omega) = R1(\omega) + i \cdot X1(\omega)$

$Z13(\omega) = R1(\omega) + i \cdot X1(\omega)$

$Z14(\omega) = R3 + i \cdot X3(\omega)$

$Z15(\omega) = R2 + i \cdot X2(\omega)$

$Z16(\omega) = R2 + i \cdot X2(\omega)$

$Z17(\omega) = R2 + i \cdot X2(\omega)$

$Z18(\omega) = R3 + i \cdot X3(\omega)$

$Z19(\omega) = R1(\omega) + i \cdot X1(\omega)$

$Z20(\omega) = R1(\omega) + i \cdot X1(\omega)$

$Z21(\omega) = R1(\omega) + i \cdot X1(\omega)$

$Z22(\omega) = R1(\omega) + i \cdot X1(\omega)$

Defining the impedance around each loop and substituting into equations D-1 through D-9 one obtains equations D-10 to D-18.

$$ZL1(\omega) = Z1(\omega) + Z2(\omega) + Z3(\omega) + Z4(\omega) \quad \text{(D-10)}$$

$$ZL2(\omega) = Z1(\omega) + Z5(\omega) + Z6(\omega) + Z10(\omega) \quad \text{(D-11)}$$

$$ZL3(\omega) = Z2(\omega) + Z6(\omega) + Z7(\omega) + Z11(\omega) \quad \text{(D-12)}$$

$$ZL4(\omega) = Z3(\omega) + Z7(\omega) + Z8(\omega) + Z12(\omega) \quad \text{(D-13)}$$

$$ZL5(\omega) = Z4(\omega) + Z8(\omega) + Z9(\omega) + Z13(\omega) \quad \text{(D-14)}$$

$$ZL6(\omega) = Z10(\omega) + Z14(\omega) + Z15(\omega) + Z19(\omega) \quad \text{(D-15)}$$

$$ZL7(\omega) = Z11(\omega) + Z15(\omega) + Z16(\omega) + Z20(\omega) \quad \text{(D-16)}$$

$$ZL8(\omega) = Z12(\omega) + Z16(\omega) + Z17(\omega) + Z21(\omega) \quad \text{(D-17)}$$

$$ZL9(\omega) = Z13(\omega) + Z17(\omega) + Z18(\omega) + Z22(\omega) \quad \text{(D-18)}$$

Then the nine equations in nine unknowns can be put into the appropriate matrices.

$$\Delta(\omega) = \begin{pmatrix} ZL1(\omega) & -Z1(\omega) & -Z2(\omega) & -Z3(\omega) & -Z4(\omega) & 0 & 0 & 0 & 0 \\ -Z1(\omega) & ZL2(\omega) & -Z6(\omega) & 0 & 0 & -Z10(\omega) & 0 & 0 & 0 \\ -Z2(\omega) & -Z6(\omega) & ZL3(\omega) & -Z7(\omega) & 0 & 0 & -Z11(\omega) & 0 & 0 \\ -Z3(\omega) & 0 & -Z7(\omega) & ZL4(\omega) & -Z8(\omega) & 0 & 0 & -Z12(\omega) & 0 \\ -Z4(\omega) & 0 & 0 & -Z8(\omega) & ZL5(\omega) & 0 & 0 & 0 & -Z13(\omega) \\ 0 & -Z10(\omega) & 0 & 0 & 0 & ZL6(\omega) & -Z15(\omega) & 0 & 0 \\ 0 & 0 & -Z11(\omega) & 0 & 0 & -Z15(\omega) & ZL7(\omega) & -Z16(\omega) & 0 \\ 0 & 0 & 0 & -Z12(\omega) & 0 & 0 & -Z16(\omega) & ZL8(\omega) & -Z17(\omega) \\ 0 & 0 & 0 & 0 & -Z13(\omega) & 0 & 0 & -Z17(\omega) & ZL9(\omega) \end{pmatrix} \quad \text{(D-19)}$$

$$\Delta 1(\omega) = \begin{pmatrix} V1 & -Z1(\omega) & -Z2(\omega) & -Z3(\omega) & -Z4(\omega) & 0 & 0 & 0 & 0 \\ V2 & ZL2(\omega) & -Z6(\omega) & 0 & 0 & -Z10(\omega) & 0 & 0 & 0 \\ V3 & -Z6(\omega) & ZL3(\omega) & -Z7(\omega) & 0 & 0 & -Z11(\omega) & 0 & 0 \\ V4 & 0 & -Z7(\omega) & ZL4(\omega) & -Z8(\omega) & 0 & 0 & -Z12(\omega) & 0 \\ V5 & 0 & 0 & -Z8(\omega) & ZL5(\omega) & 0 & 0 & 0 & -Z13(\omega) \\ V6 & -Z10(\omega) & 0 & 0 & 0 & ZL6(\omega) & -Z15(\omega) & 0 & 0 \\ V7 & 0 & -Z11(\omega) & 0 & 0 & -Z15(\omega) & ZL7(\omega) & -Z16(\omega) & 0 \\ V8 & 0 & 0 & -Z12(\omega) & 0 & 0 & -Z16(\omega) & ZL8(\omega) & -Z17(\omega) \\ V9 & 0 & 0 & 0 & -Z13(\omega) & 0 & 0 & -Z17(\omega) & ZL9(\omega) \end{pmatrix} \quad \text{(D-20)}$$

$$\Delta 2(\omega) = \begin{pmatrix} ZL1(\omega) & V1 & -Z2(\omega) & -Z3(\omega) & -Z4(\omega) & 0 & 0 & 0 & 0 \\ -Z1(\omega) & V2 & -Z6(\omega) & 0 & 0 & -Z10(\omega) & 0 & 0 & 0 \\ -Z2(\omega) & V3 & ZL3(\omega) & -Z7(\omega) & 0 & 0 & -Z11(\omega) & 0 & 0 \\ -Z3(\omega) & V4 & -Z7(\omega) & ZL4(\omega) & -Z8(\omega) & 0 & 0 & -Z12(\omega) & 0 \\ -Z4(\omega) & V5 & 0 & -Z8(\omega) & ZL5(\omega) & 0 & 0 & 0 & -Z13(\omega) \\ 0 & V6 & 0 & 0 & 0 & ZL6(\omega) & -Z15(\omega) & 0 & 0 \\ 0 & V7 & -Z11(\omega) & 0 & 0 & -Z15(\omega) & ZL7(\omega) & -Z16(\omega) & 0 \\ 0 & V8 & 0 & -Z12(\omega) & 0 & 0 & -Z16(\omega) & ZL8(\omega) & -Z17(\omega) \\ 0 & V9 & 0 & 0 & -Z13(\omega) & 0 & 0 & -Z17(\omega) & ZL9(\omega) \end{pmatrix} \quad \text{(D-21)}$$

$$\Delta 3(\omega) = \begin{pmatrix} ZL1(\omega) & -Z1(\omega) & V1 & -Z3(\omega) & -Z4(\omega) & 0 & 0 & 0 & 0 \\ -Z1(\omega) & ZL2(\omega) & V2 & 0 & 0 & -Z10(\omega) & 0 & 0 & 0 \\ -Z2(\omega) & -Z6(\omega) & V3 & -Z7(\omega) & 0 & 0 & -Z11(\omega) & 0 & 0 \\ -Z3(\omega) & 0 & V4 & ZL4(\omega) & -Z8(\omega) & 0 & 0 & -Z12(\omega) & 0 \\ -Z4(\omega) & 0 & V5 & -Z8(\omega) & ZL5(\omega) & 0 & 0 & 0 & -Z13(\omega) \\ 0 & -Z10(\omega) & V6 & 0 & 0 & ZL6(\omega) & -Z15(\omega) & 0 & 0 \\ 0 & 0 & V7 & 0 & 0 & -Z15(\omega) & ZL7(\omega) & -Z16(\omega) & 0 \\ 0 & 0 & V8 & -Z12(\omega) & 0 & 0 & -Z16(\omega) & ZL8(\omega) & -Z17(\omega) \\ 0 & 0 & V9 & 0 & -Z13(\omega) & 0 & 0 & -Z17(\omega) & ZL9(\omega) \end{pmatrix} \quad \text{(D-22)}$$

$$\Delta 4(\omega) = \begin{pmatrix} ZL1(\omega) & -Z1(\omega) & -Z2(\omega) & V1 & -Z4(\omega) & 0 & 0 & 0 & 0 \\ -Z1(\omega) & ZL2(\omega) & -Z6(\omega) & V2 & 0 & -Z10(\omega) & 0 & 0 & 0 \\ -Z2(\omega) & -Z6(\omega) & ZL3(\omega) & V3 & 0 & 0 & -Z11(\omega) & 0 & 0 \\ -Z3(\omega) & 0 & -Z7(\omega) & V4 & -Z8(\omega) & 0 & 0 & -Z12(\omega) & 0 \\ -Z4(\omega) & 0 & 0 & V5 & ZL5(\omega) & 0 & 0 & 0 & -Z13(\omega) \\ 0 & -Z10(\omega) & 0 & V6 & 0 & ZL6(\omega) & -Z15(\omega) & 0 & 0 \\ 0 & 0 & -Z11(\omega) & V7 & 0 & -Z15(\omega) & ZL7(\omega) & -Z16(\omega) & 0 \\ 0 & 0 & 0 & V8 & 0 & 0 & -Z16(\omega) & ZL8(\omega) & -Z17(\omega) \\ 0 & 0 & 0 & V9 & -Z13(\omega) & 0 & 0 & -Z17(\omega) & ZL9(\omega) \end{pmatrix} \quad \text{(D-23)}$$

$$\Delta 5(\omega) = \begin{pmatrix} ZL1(\omega) & -Z1(\omega) & -Z2(\omega) & -Z3(\omega) & V1 & 0 & 0 & 0 & 0 \\ -Z1(\omega) & ZL2(\omega) & -Z6(\omega) & 0 & V2 & -Z10(\omega) & 0 & 0 & 0 \\ -Z2(\omega) & -Z6(\omega) & ZL3(\omega) & -Z7(\omega) & V3 & 0 & -Z11(\omega) & 0 & 0 \\ -Z3(\omega) & 0 & -Z7(\omega) & ZL4(\omega) & V4 & 0 & 0 & -Z12(\omega) & 0 \\ -Z4(\omega) & 0 & 0 & -Z8(\omega) & V5 & 0 & 0 & 0 & -Z13(\omega) \\ 0 & -Z10(\omega) & 0 & 0 & V6 & ZL6(\omega) & -Z15(\omega) & 0 & 0 \\ 0 & 0 & -Z11(\omega) & 0 & V7 & -Z15(\omega) & ZL7(\omega) & -Z16(\omega) & 0 \\ 0 & 0 & 0 & -Z12(\omega) & V8 & 0 & -Z16(\omega) & ZL8(\omega) & -Z17(\omega) \\ 0 & 0 & 0 & 0 & V9 & 0 & 0 & -Z17(\omega) & ZL9(\omega) \end{pmatrix} \quad \text{(D-24)}$$

$$\Delta 6(\omega) = \begin{pmatrix} ZL1(\omega) & -Z1(\omega) & -Z2(\omega) & -Z3(\omega) & -Z4(\omega) & V1 & 0 & 0 & 0 \\ -Z1(\omega) & ZL2(\omega) & -Z6(\omega) & 0 & 0 & V2 & 0 & 0 & 0 \\ -Z2(\omega) & -Z6(\omega) & ZL3(\omega) & -Z7(\omega) & 0 & V3 & -Z11(\omega) & 0 & 0 \\ -Z3(\omega) & 0 & -Z7(\omega) & ZL4(\omega) & -Z8(\omega) & V4 & 0 & -Z12(\omega) & 0 \\ -Z4(\omega) & 0 & 0 & -Z8(\omega) & ZL5(\omega) & V5 & 0 & 0 & -Z13(\omega) \\ 0 & -Z10(\omega) & 0 & 0 & 0 & V6 & -Z15(\omega) & 0 & 0 \\ 0 & 0 & -Z11(\omega) & 0 & 0 & V7 & ZL7(\omega) & -Z16(\omega) & 0 \\ 0 & 0 & 0 & -Z12(\omega) & 0 & V8 & -Z16(\omega) & ZL8(\omega) & -Z17(\omega) \\ 0 & 0 & 0 & 0 & -Z13(\omega) & V9 & 0 & -Z17(\omega) & ZL9(\omega) \end{pmatrix} \quad \text{(D-25)}$$

$$\Delta 7(\omega) = \begin{pmatrix} ZL1(\omega) & -Z1(\omega) & -Z2(\omega) & -Z3(\omega) & -Z4(\omega) & 0 & V1 & 0 & 0 \\ -Z1(\omega) & ZL2(\omega) & -Z6(\omega) & 0 & 0 & -Z10(\omega) & V2 & 0 & 0 \\ -Z2(\omega) & -Z6(\omega) & ZL3(\omega) & -Z7(\omega) & 0 & 0 & V3 & 0 & 0 \\ -Z3(\omega) & 0 & -Z7(\omega) & ZL4(\omega) & -Z8(\omega) & 0 & V4 & -Z12(\omega) & 0 \\ -Z4(\omega) & 0 & 0 & -Z8(\omega) & ZL5(\omega) & 0 & V5 & 0 & -Z13(\omega) \\ 0 & -Z10(\omega) & 0 & 0 & 0 & ZL6(\omega) & V6 & 0 & 0 \\ 0 & 0 & -Z11(\omega) & 0 & 0 & -Z15(\omega) & V7 & -Z16(\omega) & 0 \\ 0 & 0 & 0 & -Z12(\omega) & 0 & 0 & V8 & ZL8(\omega) & -Z17(\omega) \\ 0 & 0 & 0 & 0 & -Z13(\omega) & 0 & V9 & -Z17(\omega) & ZL9(\omega) \end{pmatrix} \quad \text{(D-26)}$$

$$\Delta 8(\omega) = \begin{pmatrix} ZL1(\omega) & -Z1(\omega) & -Z2(\omega) & -Z3(\omega) & -Z4(\omega) & 0 & 0 & V1 & 0 \\ -Z1(\omega) & ZL2(\omega) & -Z6(\omega) & 0 & 0 & -Z10(\omega) & 0 & V2 & 0 \\ -Z2(\omega) & -Z6(\omega) & ZL3(\omega) & -Z7(\omega) & 0 & 0 & -Z11(\omega) & V3 & 0 \\ -Z3(\omega) & 0 & -Z7(\omega) & ZL4(\omega) & -Z8(\omega) & 0 & 0 & V4 & 0 \\ -Z4(\omega) & 0 & 0 & -Z8(\omega) & ZL5(\omega) & 0 & 0 & V5 & -Z13(\omega) \\ 0 & -Z10(\omega) & 0 & 0 & 0 & ZL6(\omega) & -Z15(\omega) & V6 & 0 \\ 0 & 0 & -Z11(\omega) & 0 & 0 & -Z15(\omega) & ZL7(\omega) & V7 & 0 \\ 0 & 0 & 0 & -Z12(\omega) & 0 & 0 & -Z16(\omega) & V8 & -Z17(\omega) \\ 0 & 0 & 0 & 0 & -Z13(\omega) & 0 & 0 & V9 & ZL9(\omega) \end{pmatrix} \quad \text{(D-27)}$$

$$\Delta 9(\omega) = \begin{pmatrix} ZL1(\omega) & -Z1(\omega) & -Z2(\omega) & -Z3(\omega) & -Z4(\omega) & 0 & 0 & 0 & V1 \\ -Z1(\omega) & ZL2(\omega) & -Z6(\omega) & 0 & 0 & -Z10(\omega) & 0 & 0 & V2 \\ -Z2(\omega) & -Z6(\omega) & ZL3(\omega) & -Z7(\omega) & 0 & 0 & -Z11(\omega) & 0 & V3 \\ -Z3(\omega) & 0 & -Z7(\omega) & ZL4(\omega) & -Z8(\omega) & 0 & 0 & -Z12(\omega) & V4 \\ -Z4(\omega) & 0 & 0 & -Z8(\omega) & ZL5(\omega) & 0 & 0 & 0 & V5 \\ 0 & -Z10(\omega) & 0 & 0 & 0 & ZL6(\omega) & -Z15(\omega) & 0 & V6 \\ 0 & 0 & -Z11(\omega) & 0 & 0 & -Z15(\omega) & ZL7(\omega) & -Z16(\omega) & V7 \\ 0 & 0 & 0 & -Z12(\omega) & 0 & 0 & -Z16(\omega) & ZL8(\omega) & V8 \\ 0 & 0 & 0 & 0 & -Z13(\omega) & 0 & 0 & -Z17(\omega) & V9 \end{pmatrix} \quad \text{(D-28)}$$

The current of each loop is 9x9 determinant with the appropriate column replaced by the voltages divided by the determinant.

$$I1(\omega) = \frac{|\Delta 1(\omega)|}{|\Delta(\omega)|} \quad \text{(D-29)}$$

$$I2(\omega) = \frac{|\Delta 2(\omega)|}{|\Delta(\omega)|} \quad \text{(D-30)}$$

$$I3(\omega) = \frac{|\Delta 3(\omega)|}{|\Delta(\omega)|} \quad \text{(D-31)}$$

$$I4(\omega) = \frac{|\Delta 4(\omega)|}{|\Delta(\omega)|} \quad \text{(D-32)}$$

$$I5(\omega) = \frac{|\Delta 5(\omega)|}{|\Delta(\omega)|} \quad \text{(D-33)}$$

$$I6(\omega) = \frac{|\Delta 6(\omega)|}{|\Delta(\omega)|} \quad \text{(D-34)}$$

$$I7(\omega) = \frac{|\Delta 7(\omega)|}{|\Delta(\omega)|} \quad \text{(D-35)}$$

$$I8(\omega) = \frac{|\Delta 8(\omega)|}{|\Delta(\omega)|} \quad \text{(D-36)}$$

$$I9(\omega) = \frac{|\Delta 9(\omega)|}{|\Delta(\omega)|} \tag{D-37}$$

The magnitude and phase angle of the transfer function are given by equations D-38 and D-39 respectively.

$$H(\omega) = \frac{I1(\omega)}{V1} \tag{D-38}$$

$$H\theta(\omega) = \operatorname{atan}\left(\frac{Im(H(\omega))}{Re(H(\omega))}\right) \tag{D-39}$$

The equivalent impedance, capacitance and tangent delta as a function of frequency are given by equations D-40, D-41 and D-42 respectively.

$$Zeq(\omega) = \frac{V1}{I1(\omega)} \tag{D-40}$$

$$C(\omega) = \frac{-1}{\omega \cdot Im(Zeq(\omega))} \tag{D-41}$$

$$t\sigma(\omega) = \frac{Re(I1(\omega))}{Im(I1(\omega))} \tag{D-42}$$

Now to repeat the calculations for Z12 modified to represent a water tree. The resistance is lowered and the capacitance is increase by a factor of 100 to account for the presence of water. All calculations are now repeated with the modified values.

$$Z12(\omega) = Rt(\omega) + i \cdot X1(\omega) \cdot 10($$
$$ZL1(\omega) = Z1(\omega) + Z2(\omega) + Z3(\omega) + Z4(\omega)$$
$$ZL2(\omega) = Z1(\omega) + Z5(\omega) + Z6(\omega) + Z10(\omega)$$
$$ZL3(\omega) = Z2(\omega) + Z6(\omega) + Z7(\omega) + Z11(\omega)$$
$$ZL4(\omega) = Z3(\omega) + Z7(\omega) + Z8(\omega) + Z12(\omega)$$
$$ZL5(\omega) = Z4(\omega) + Z8(\omega) + Z9(\omega) + Z13(\omega)$$
$$ZL6(\omega) = Z10(\omega) + Z14(\omega) + Z15(\omega) + Z19(\omega)$$
$$ZL7(\omega) = Z11(\omega) + Z15(\omega) + Z16(\omega) + Z20(\omega)$$
$$ZL8(\omega) = Z12(\omega) + Z16(\omega) + Z17(\omega) + Z21(\omega)$$
$$ZL9(\omega) = Z13(\omega) + Z17(\omega) + Z18(\omega) + Z22(\omega)$$

$$\Delta m(\omega) = \begin{pmatrix} ZL1(\omega) & -Z1(\omega) & -Z2(\omega) & -Z3(\omega) & -Z4(\omega) & 0 & 0 & 0 & 0 \\ -Z1(\omega) & ZL2(\omega) & -Z6(\omega) & 0 & 0 & -Z10(\omega) & 0 & 0 & 0 \\ -Z2(\omega) & -Z6(\omega) & ZL3(\omega) & -Z7(\omega) & 0 & 0 & -Z11(\omega) & 0 & 0 \\ -Z3(\omega) & 0 & -Z7(\omega) & ZL4(\omega) & -Z8(\omega) & 0 & 0 & -Z12(\omega) & 0 \\ -Z4(\omega) & 0 & 0 & -Z8(\omega) & ZL5(\omega) & 0 & 0 & 0 & -Z13(\omega) \\ 0 & -Z10(\omega) & 0 & 0 & 0 & ZL6(\omega) & -Z15(\omega) & 0 & 0 \\ 0 & 0 & -Z11(\omega) & 0 & 0 & -Z15(\omega) & ZL7(\omega) & -Z16(\omega) & 0 \\ 0 & 0 & 0 & -Z12(\omega) & 0 & 0 & -Z16(\omega) & ZL8(\omega) & -Z17(\omega) \\ 0 & 0 & 0 & 0 & -Z13(\omega) & 0 & 0 & -Z17(\omega) & ZL9(\omega) \end{pmatrix}$$

$$\Delta 1m(\omega) = \begin{pmatrix} V1 & -Z1(\omega) & -Z2(\omega) & -Z3(\omega) & -Z4(\omega) & 0 & 0 & 0 & 0 \\ V2 & ZL2(\omega) & -Z6(\omega) & 0 & 0 & -Z10(\omega) & 0 & 0 & 0 \\ V3 & -Z6(\omega) & ZL3(\omega) & -Z7(\omega) & 0 & 0 & -Z11(\omega) & 0 & 0 \\ V4 & 0 & -Z7(\omega) & ZL4(\omega) & -Z8(\omega) & 0 & 0 & -Z12(\omega) & 0 \\ V5 & 0 & 0 & -Z8(\omega) & ZL5(\omega) & 0 & 0 & 0 & -Z13(\omega) \\ V6 & -Z10(\omega) & 0 & 0 & 0 & ZL6(\omega) & -Z15(\omega) & 0 & 0 \\ V7 & 0 & -Z11(\omega) & 0 & 0 & -Z15(\omega) & ZL7(\omega) & -Z16(\omega) & 0 \\ V8 & 0 & 0 & -Z12(\omega) & 0 & 0 & -Z16(\omega) & ZL8(\omega) & -Z17(\omega) \\ V9 & 0 & 0 & 0 & -Z13(\omega) & 0 & 0 & -Z17(\omega) & ZL9(\omega) \end{pmatrix}$$

$$\Delta 2m(\omega) = \begin{pmatrix} ZL1(\omega) & V1 & -Z2(\omega) & -Z3(\omega) & -Z4(\omega) & 0 & 0 & 0 & 0 \\ -Z1(\omega) & V2 & -Z6(\omega) & 0 & 0 & -Z10(\omega) & 0 & 0 & 0 \\ -Z2(\omega) & V3 & ZL3(\omega) & -Z7(\omega) & 0 & 0 & -Z11(\omega) & 0 & 0 \\ -Z3(\omega) & V4 & -Z7(\omega) & ZL4(\omega) & -Z8(\omega) & 0 & 0 & -Z12(\omega) & 0 \\ -Z4(\omega) & V5 & 0 & -Z8(\omega) & ZL5(\omega) & 0 & 0 & 0 & -Z13(\omega) \\ 0 & V6 & 0 & 0 & 0 & ZL6(\omega) & -Z15(\omega) & 0 & 0 \\ 0 & V7 & -Z11(\omega) & 0 & 0 & -Z15(\omega) & ZL7(\omega) & -Z16(\omega) & 0 \\ 0 & V8 & 0 & -Z12(\omega) & 0 & 0 & -Z16(\omega) & ZL8(\omega) & -Z17(\omega) \\ 0 & V9 & 0 & 0 & -Z13(\omega) & 0 & 0 & -Z17(\omega) & ZL9(\omega) \end{pmatrix}$$

$$\Delta 3m(\omega) = \begin{pmatrix} ZL1(\omega) & -Z1(\omega) & V1 & -Z3(\omega) & -Z4(\omega) & 0 & 0 & 0 & 0 \\ -Z1(\omega) & ZL2(\omega) & V2 & 0 & 0 & -Z10(\omega) & 0 & 0 & 0 \\ -Z2(\omega) & -Z6(\omega) & V3 & -Z7(\omega) & 0 & 0 & -Z11(\omega) & 0 & 0 \\ -Z3(\omega) & 0 & V4 & ZL4(\omega) & -Z8(\omega) & 0 & 0 & -Z12(\omega) & 0 \\ -Z4(\omega) & 0 & V5 & -Z8(\omega) & ZL5(\omega) & 0 & 0 & 0 & -Z13(\omega) \\ 0 & -Z10(\omega) & V6 & 0 & 0 & ZL6(\omega) & -Z15(\omega) & 0 & 0 \\ 0 & 0 & V7 & 0 & 0 & -Z15(\omega) & ZL7(\omega) & -Z16(\omega) & 0 \\ 0 & 0 & V8 & -Z12(\omega) & 0 & 0 & -Z16(\omega) & ZL8(\omega) & -Z17(\omega) \\ 0 & 0 & V9 & 0 & -Z13(\omega) & 0 & 0 & -Z17(\omega) & ZL9(\omega) \end{pmatrix}$$

$$\Delta 4m(\omega) = \begin{pmatrix} ZL1(\omega) & -Z1(\omega) & -Z2(\omega) & V1 & -Z4(\omega) & 0 & 0 & 0 & 0 \\ -Z1(\omega) & ZL2(\omega) & -Z6(\omega) & V2 & 0 & -Z10(\omega) & 0 & 0 & 0 \\ -Z2(\omega) & -Z6(\omega) & ZL3(\omega) & V3 & 0 & 0 & -Z11(\omega) & 0 & 0 \\ -Z3(\omega) & 0 & -Z7(\omega) & V4 & -Z8(\omega) & 0 & 0 & -Z12(\omega) & 0 \\ -Z4(\omega) & 0 & 0 & V5 & ZL5(\omega) & 0 & 0 & 0 & -Z13(\omega) \\ 0 & -Z10(\omega) & 0 & V6 & 0 & ZL6(\omega) & -Z15(\omega) & 0 & 0 \\ 0 & 0 & -Z11(\omega) & V7 & 0 & -Z15(\omega) & ZL7(\omega) & -Z16(\omega) & 0 \\ 0 & 0 & 0 & V8 & 0 & 0 & -Z16(\omega) & ZL8(\omega) & -Z17(\omega) \\ 0 & 0 & 0 & V9 & -Z13(\omega) & 0 & 0 & -Z17(\omega) & ZL9(\omega) \end{pmatrix}$$

$$\Delta 5m(\omega) = \begin{pmatrix} ZL1(\omega) & -Z1(\omega) & -Z2(\omega) & -Z3(\omega) & V1 & 0 & 0 & 0 & 0 \\ -Z1(\omega) & ZL2(\omega) & -Z6(\omega) & 0 & V2 & -Z10(\omega) & 0 & 0 & 0 \\ -Z2(\omega) & -Z6(\omega) & ZL3(\omega) & -Z7(\omega) & V3 & 0 & -Z11(\omega) & 0 & 0 \\ -Z3(\omega) & 0 & -Z7(\omega) & ZL4(\omega) & V4 & 0 & 0 & -Z12(\omega) & 0 \\ -Z4(\omega) & 0 & 0 & -Z8(\omega) & V5 & 0 & 0 & 0 & -Z13(\omega) \\ 0 & -Z10(\omega) & 0 & 0 & V6 & ZL6(\omega) & -Z15(\omega) & 0 & 0 \\ 0 & 0 & -Z11(\omega) & 0 & V7 & -Z15(\omega) & ZL7(\omega) & -Z16(\omega) & 0 \\ 0 & 0 & 0 & -Z12(\omega) & V8 & 0 & -Z16(\omega) & ZL8(\omega) & -Z17(\omega) \\ 0 & 0 & 0 & 0 & V9 & 0 & 0 & -Z17(\omega) & ZL9(\omega) \end{pmatrix}$$

$$\Delta 6m(\omega) = \begin{pmatrix} ZL1(\omega) & -Z1(\omega) & -Z2(\omega) & -Z3(\omega) & -Z4(\omega) & V1 & 0 & 0 & 0 \\ -Z1(\omega) & ZL2(\omega) & -Z6(\omega) & 0 & 0 & V2 & 0 & 0 & 0 \\ -Z2(\omega) & -Z6(\omega) & ZL3(\omega) & -Z7(\omega) & 0 & V3 & -Z11(\omega) & 0 & 0 \\ -Z3(\omega) & 0 & -Z7(\omega) & ZL4(\omega) & -Z8(\omega) & V4 & 0 & -Z12(\omega) & 0 \\ -Z4(\omega) & 0 & 0 & -Z8(\omega) & ZL5(\omega) & V5 & 0 & 0 & -Z13(\omega) \\ 0 & -Z10(\omega) & 0 & 0 & 0 & V6 & -Z15(\omega) & 0 & 0 \\ 0 & 0 & -Z11(\omega) & 0 & 0 & V7 & ZL7(\omega) & -Z16(\omega) & 0 \\ 0 & 0 & 0 & -Z12(\omega) & 0 & V8 & -Z16(\omega) & ZL8(\omega) & -Z17(\omega) \\ 0 & 0 & 0 & 0 & -Z13(\omega) & V9 & 0 & -Z17(\omega) & ZL9(\omega) \end{pmatrix}$$

$$\Delta 7m(\omega) = \begin{pmatrix} ZL1(\omega) & -Z1(\omega) & -Z2(\omega) & -Z3(\omega) & -Z4(\omega) & 0 & V1 & 0 & 0 \\ -Z1(\omega) & ZL2(\omega) & -Z6(\omega) & 0 & 0 & -Z10(\omega) & V2 & 0 & 0 \\ -Z2(\omega) & -Z6(\omega) & ZL3(\omega) & -Z7(\omega) & 0 & 0 & V3 & 0 & 0 \\ -Z3(\omega) & 0 & -Z7(\omega) & ZL4(\omega) & -Z8(\omega) & 0 & V4 & -Z12(\omega) & 0 \\ -Z4(\omega) & 0 & 0 & -Z8(\omega) & ZL5(\omega) & 0 & V5 & 0 & -Z13(\omega) \\ 0 & -Z10(\omega) & 0 & 0 & 0 & ZL6(\omega) & V6 & 0 & 0 \\ 0 & 0 & -Z11(\omega) & 0 & 0 & -Z15(\omega) & V7 & -Z16(\omega) & 0 \\ 0 & 0 & 0 & -Z12(\omega) & 0 & 0 & V8 & ZL8(\omega) & -Z17(\omega) \\ 0 & 0 & 0 & 0 & -Z13(\omega) & 0 & V9 & -Z17(\omega) & ZL9(\omega) \end{pmatrix}$$

$$\Delta 8m(\omega) = \begin{pmatrix} ZL1(\omega) & -Z1(\omega) & -Z2(\omega) & -Z3(\omega) & -Z4(\omega) & 0 & 0 & V1 & 0 \\ -Z1(\omega) & ZL2(\omega) & -Z6(\omega) & 0 & 0 & -Z10(\omega) & 0 & V2 & 0 \\ -Z2(\omega) & -Z6(\omega) & ZL3(\omega) & -Z7(\omega) & 0 & 0 & -Z11(\omega) & V3 & 0 \\ -Z3(\omega) & 0 & -Z7(\omega) & ZL4(\omega) & -Z8(\omega) & 0 & 0 & V4 & 0 \\ -Z4(\omega) & 0 & 0 & -Z8(\omega) & ZL5(\omega) & 0 & 0 & V5 & -Z13(\omega) \\ 0 & -Z10(\omega) & 0 & 0 & 0 & ZL6(\omega) & -Z15(\omega) & V6 & 0 \\ 0 & 0 & -Z11(\omega) & 0 & 0 & -Z15(\omega) & ZL7(\omega) & V7 & 0 \\ 0 & 0 & 0 & -Z12(\omega) & 0 & 0 & -Z16(\omega) & V8 & -Z17(\omega) \\ 0 & 0 & 0 & 0 & -Z13(\omega) & 0 & 0 & V9 & ZL9(\omega) \end{pmatrix}$$

$$\Delta 9m(\omega) = \begin{pmatrix} ZL1(\omega) & -Z1(\omega) & -Z2(\omega) & -Z3(\omega) & -Z4(\omega) & 0 & 0 & 0 & V1 \\ -Z1(\omega) & ZL2(\omega) & -Z6(\omega) & 0 & 0 & -Z10(\omega) & 0 & 0 & V2 \\ -Z2(\omega) & -Z6(\omega) & ZL3(\omega) & -Z7(\omega) & 0 & 0 & -Z11(\omega) & 0 & V3 \\ -Z3(\omega) & 0 & -Z7(\omega) & ZL4(\omega) & -Z8(\omega) & 0 & 0 & -Z12(\omega) & V4 \\ -Z4(\omega) & 0 & 0 & -Z8(\omega) & ZL5(\omega) & 0 & 0 & 0 & V5 \\ 0 & -Z10(\omega) & 0 & 0 & 0 & ZL6(\omega) & -Z15(\omega) & 0 & V6 \\ 0 & 0 & -Z11(\omega) & 0 & 0 & -Z15(\omega) & ZL7(\omega) & -Z16(\omega) & V7 \\ 0 & 0 & 0 & -Z12(\omega) & 0 & 0 & -Z16(\omega) & ZL8(\omega) & V8 \\ 0 & 0 & 0 & 0 & -Z13(\omega) & 0 & 0 & -Z17(\omega) & V9 \end{pmatrix}$$

$$I1m(\omega) = \frac{|\Delta 1m(\omega)|}{|\Delta m(\omega)|}$$

$$I2m(\omega) = \frac{|\Delta 2m(\omega)|}{|\Delta m(\omega)|}$$

$$I3m(\omega) = \frac{|\Delta 3m(\omega)|}{|\Delta m(\omega)|}$$

$$I4m(\omega) = \frac{|\Delta 4m(\omega)|}{|\Delta m(\omega)|}$$

$$I5m(\omega) = \frac{|\Delta 5m(\omega)|}{|\Delta m(\omega)|}$$

$$I6m(\omega) = \frac{|\Delta 6m(\omega)|}{|\Delta m(\omega)|}$$

$$I7m(\omega) = \frac{|\Delta 7m(\omega)|}{|\Delta m(\omega)|}$$

$$I8m(\omega) = \frac{|\Delta 8m(\omega)|}{|\Delta m(\omega)|}$$

$$I9m(\omega) = \frac{|\Delta 9m(\omega)|}{|\Delta m(\omega)|}$$

$$Hm(\omega) = \frac{I1m(\omega)}{V1}$$

$$H\theta m(\omega) = \operatorname{atan}\left(\frac{Im(Hm(\omega))}{Re(Hm(\omega))}\right)$$

$$Zeqm(\omega) = \frac{V1}{I1m(\omega)}$$

$$Cm(\omega) = \frac{-1}{\omega \cdot Im(Zeqm(\omega))}$$

$$t\sigma m(\omega) = \frac{Re(I1m(\omega))}{Im(I1m(\omega))}$$

APPENDIX E

THEORETICAL EQUIVALENT CIRCUIT MODEL CALCULATIONS FOR VARIOUS CABLE CONDITIONS

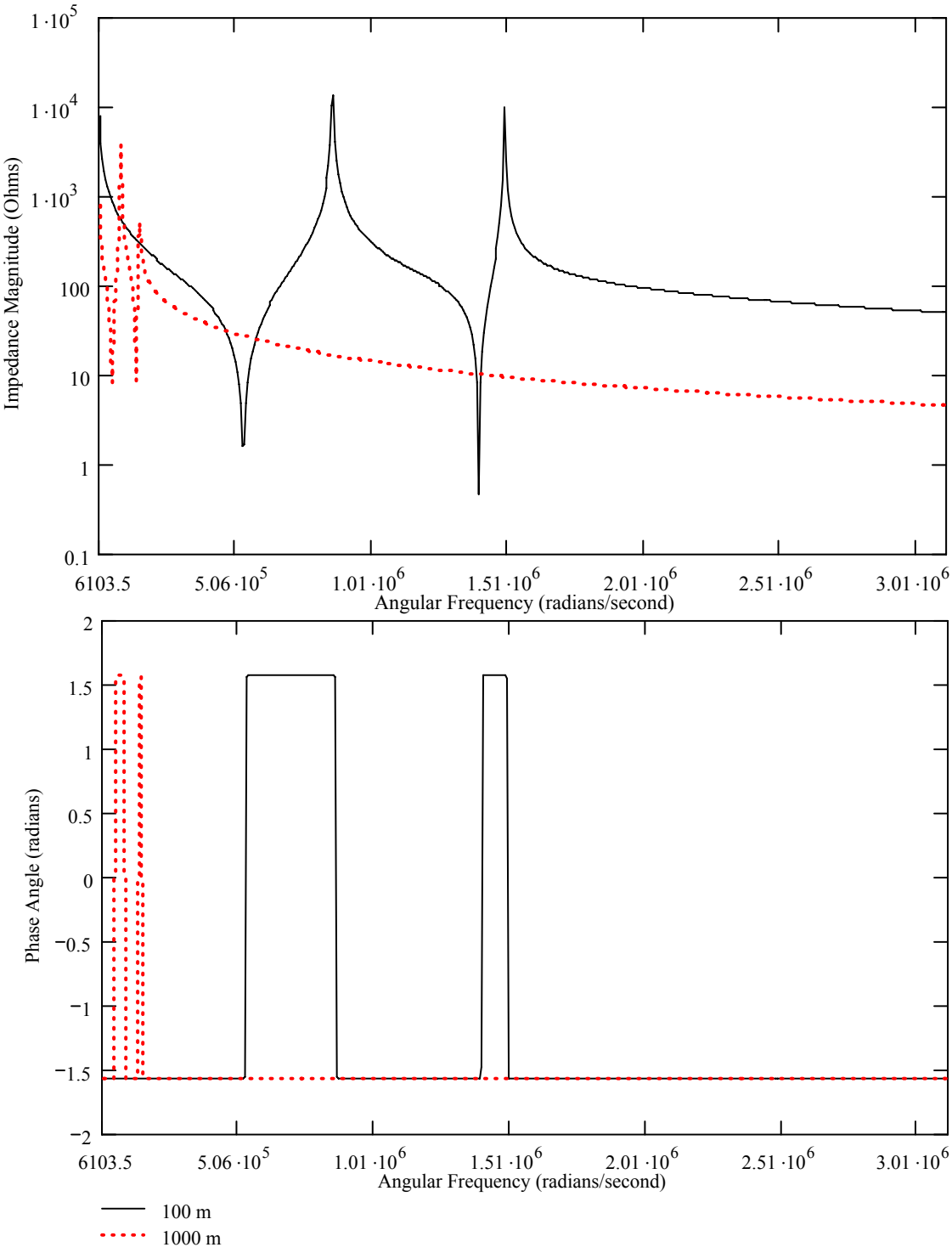

Figure E.1 Calculated Impedance Magnitude and Phase Angle vs Frequency
22 Impedance Element Model, L=100 vs 1000 m, D=10.3 mm AL,
4.45 mm XLPE

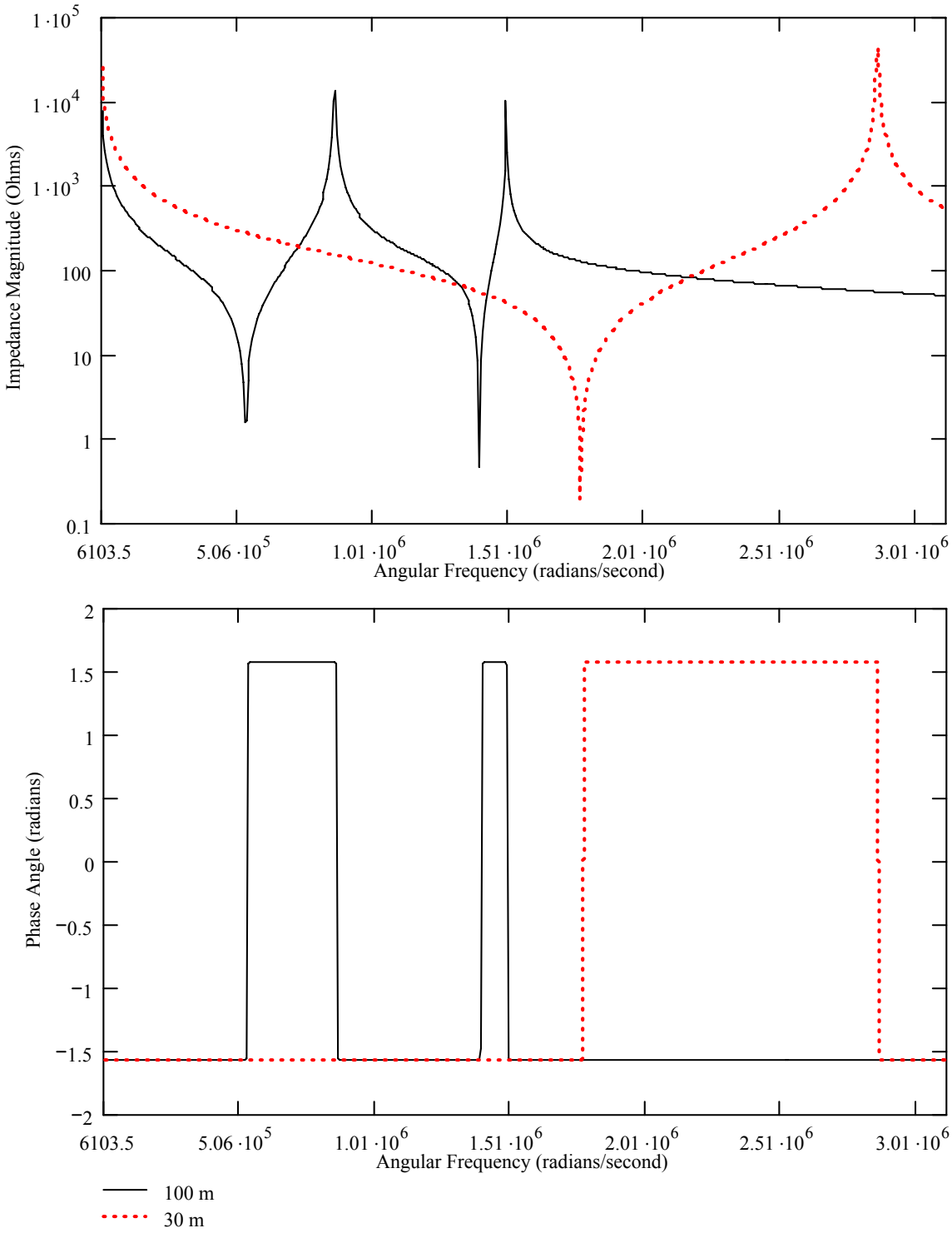

Figure E.2 Calculated Impedance Magnitude and Phase Angle vs Frequency
22 Impedance Element Model, L=100 vs 30 m, D=10.3 mm AL,
4.45 mm XLPE

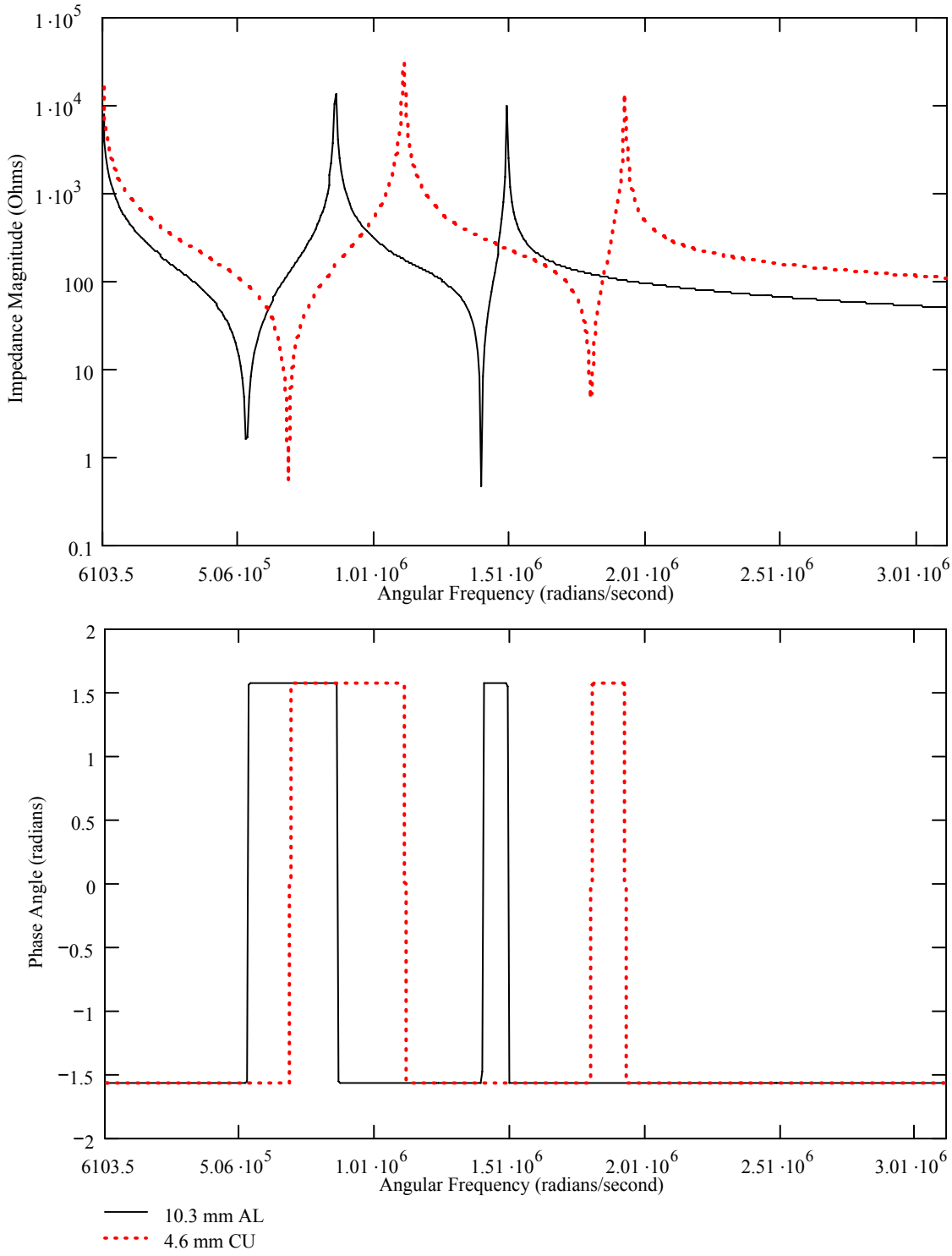

Figure E.3 Calculated Impedance Magnitude and Phase Angle vs Frequency
22 Impedance Element Model, L=100 m, D=10.3 mm AL, 4.45 mm XLPE
vs D=4.6 mm CU, 5.59 mm HMWPE

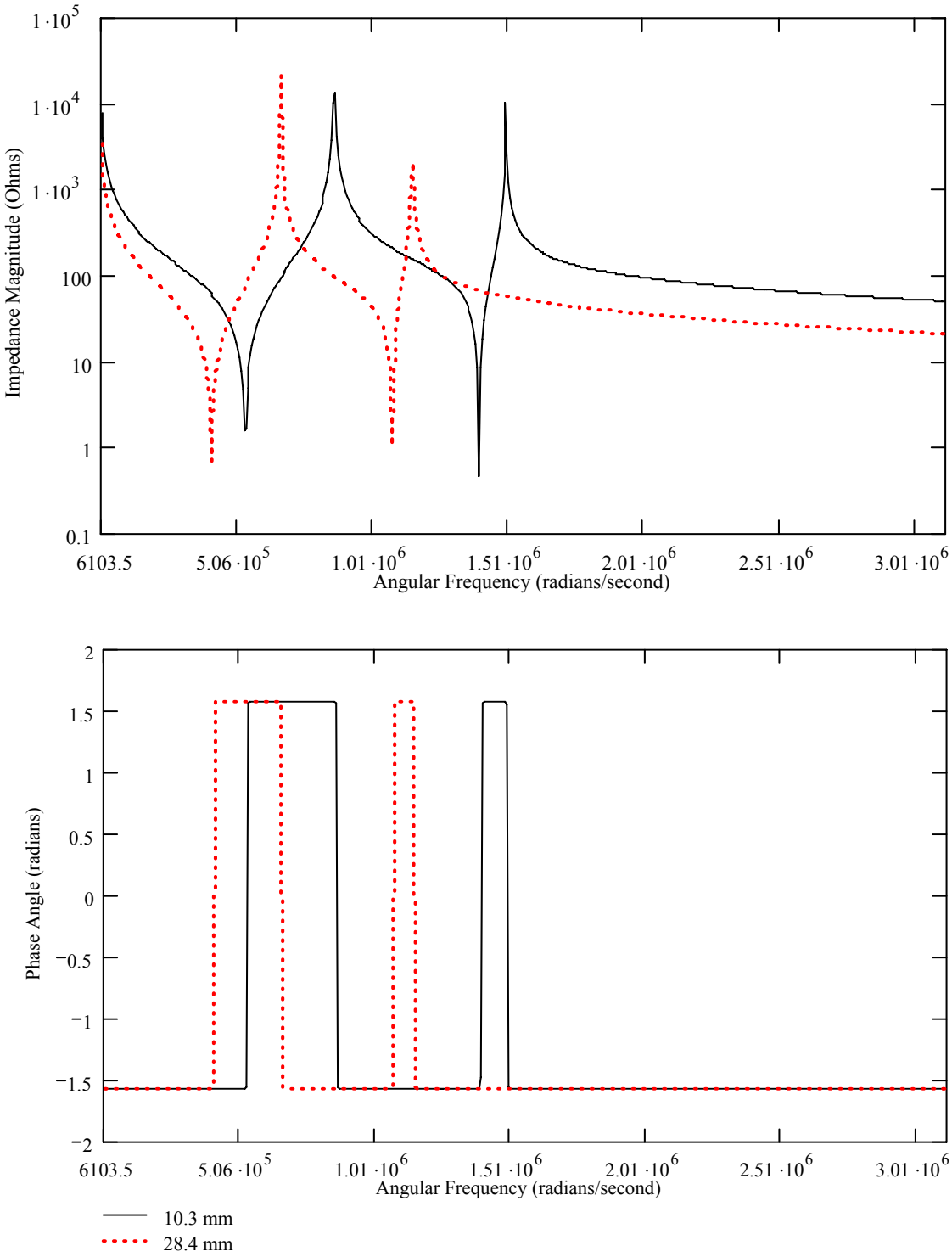

Figure E.4 Calculated Impedance Magnitude and Phase Angle vs Frequency
22 Impedance Element Model, L=100 m, D=10.3 vs 28.4 mm AL,
4.45 mm XLPE

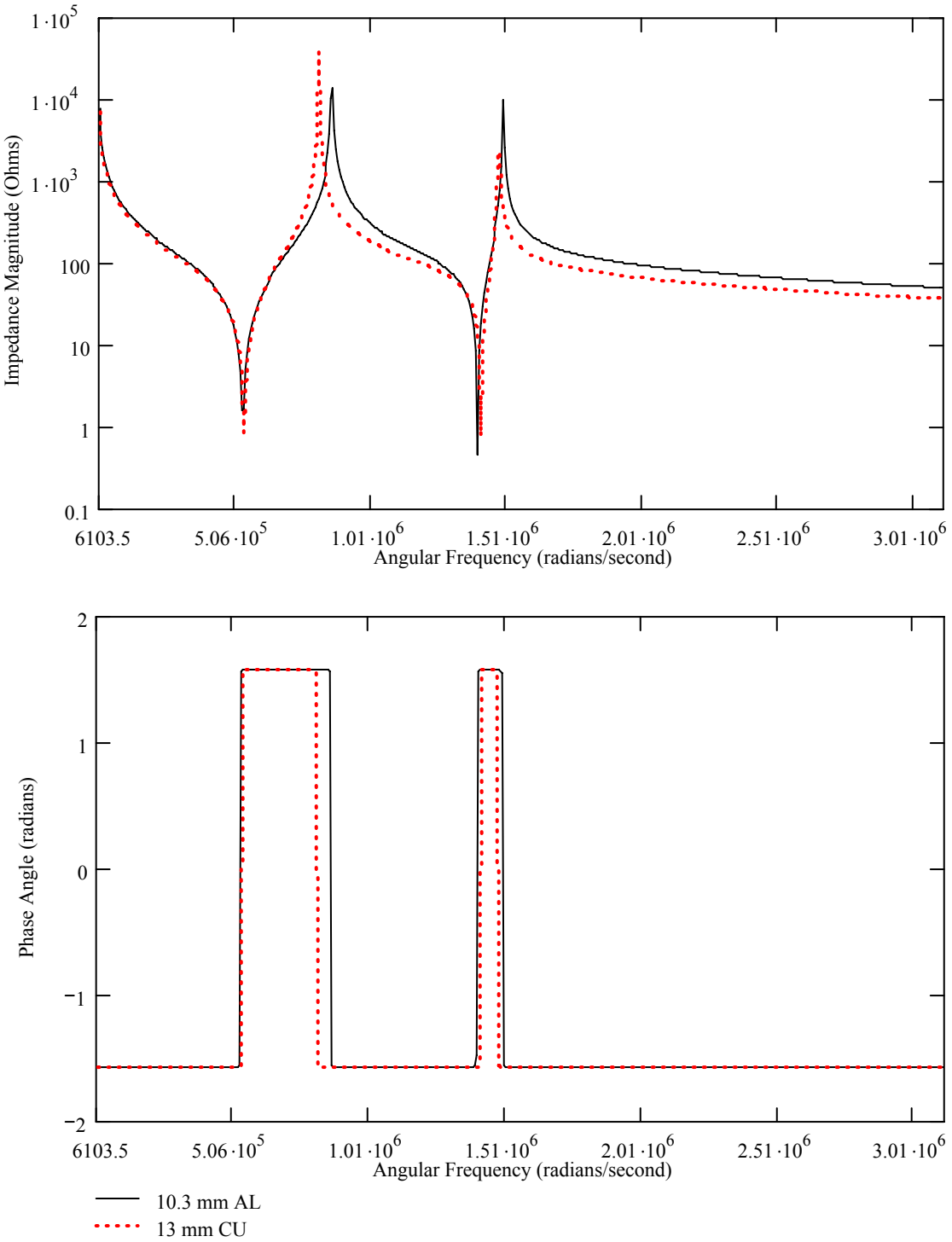

Figure E.5 Calculated Impedance Magnitude and Phase Angle vs Frequency
22 Impedance Element Model, L=100 m, D=10.3 mm AL, 4.45 mm XLPE vs D=13 mm CU, 5.59 mm HMWPE

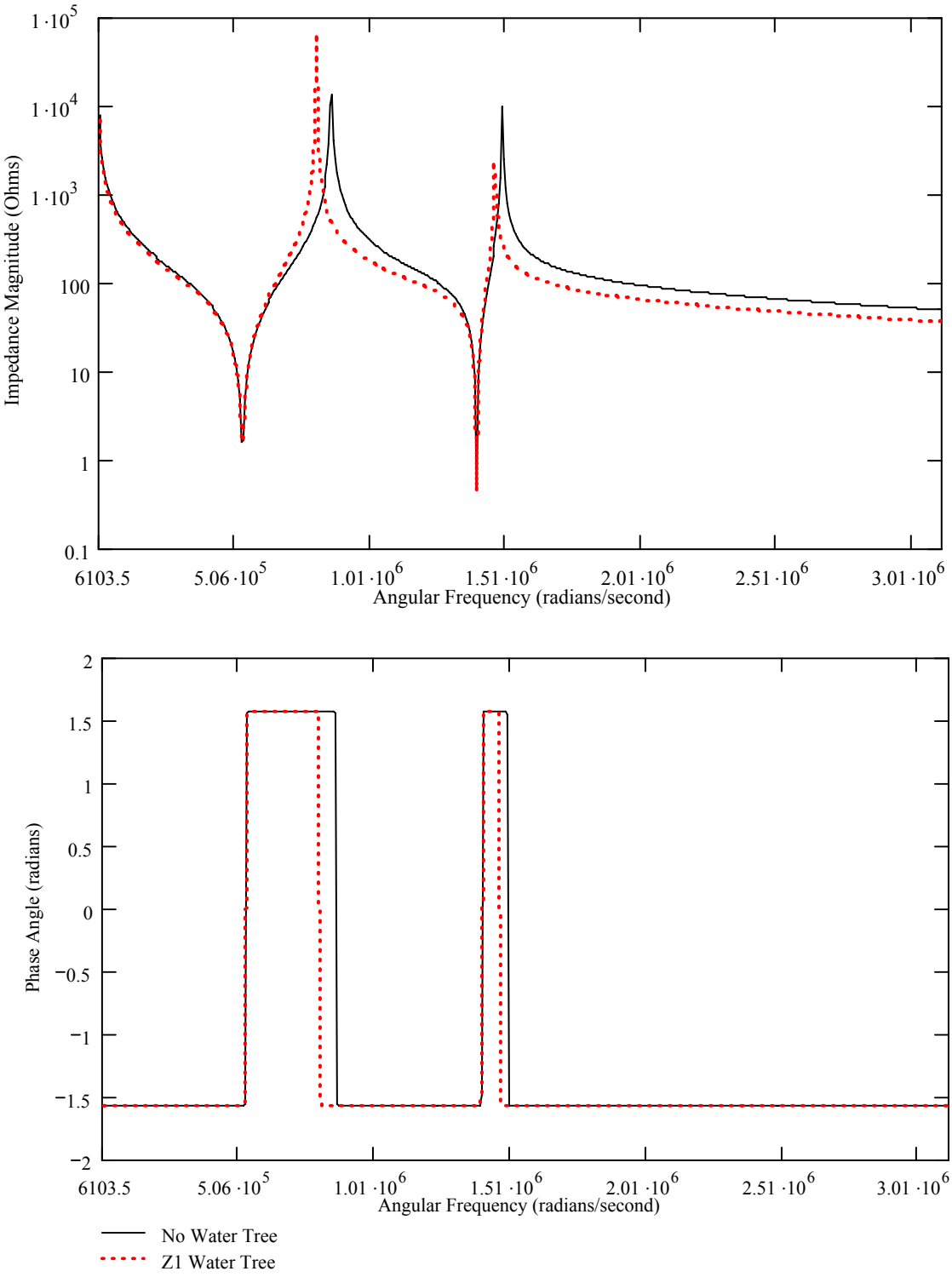

Figure E.6 Calculated Impedance Magnitude and Phase Angle vs Frequency
22 Impedance Element Model, L=100 m, D=10.3 mm AL, 4.45 mm XLPE,
Without vs With Z1 Water Tree

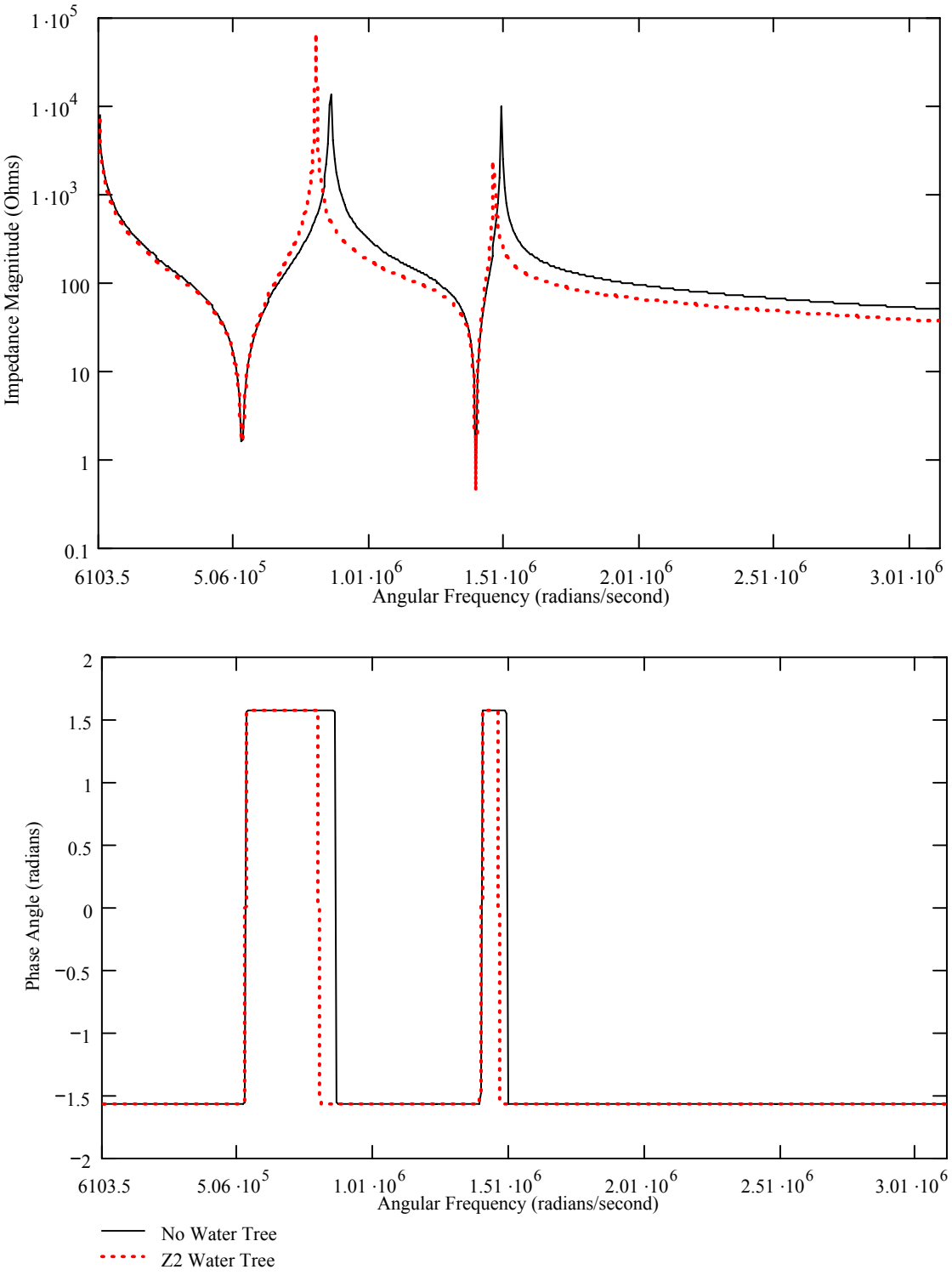

Figure E.7 Calculated Impedance Magnitude and Phase Angle vs Frequency
22 Impedance Element Model, L=100 m, D=10.3 mm AL, 4.45 mm XLPE,
Without vs With Z2 Water Tree

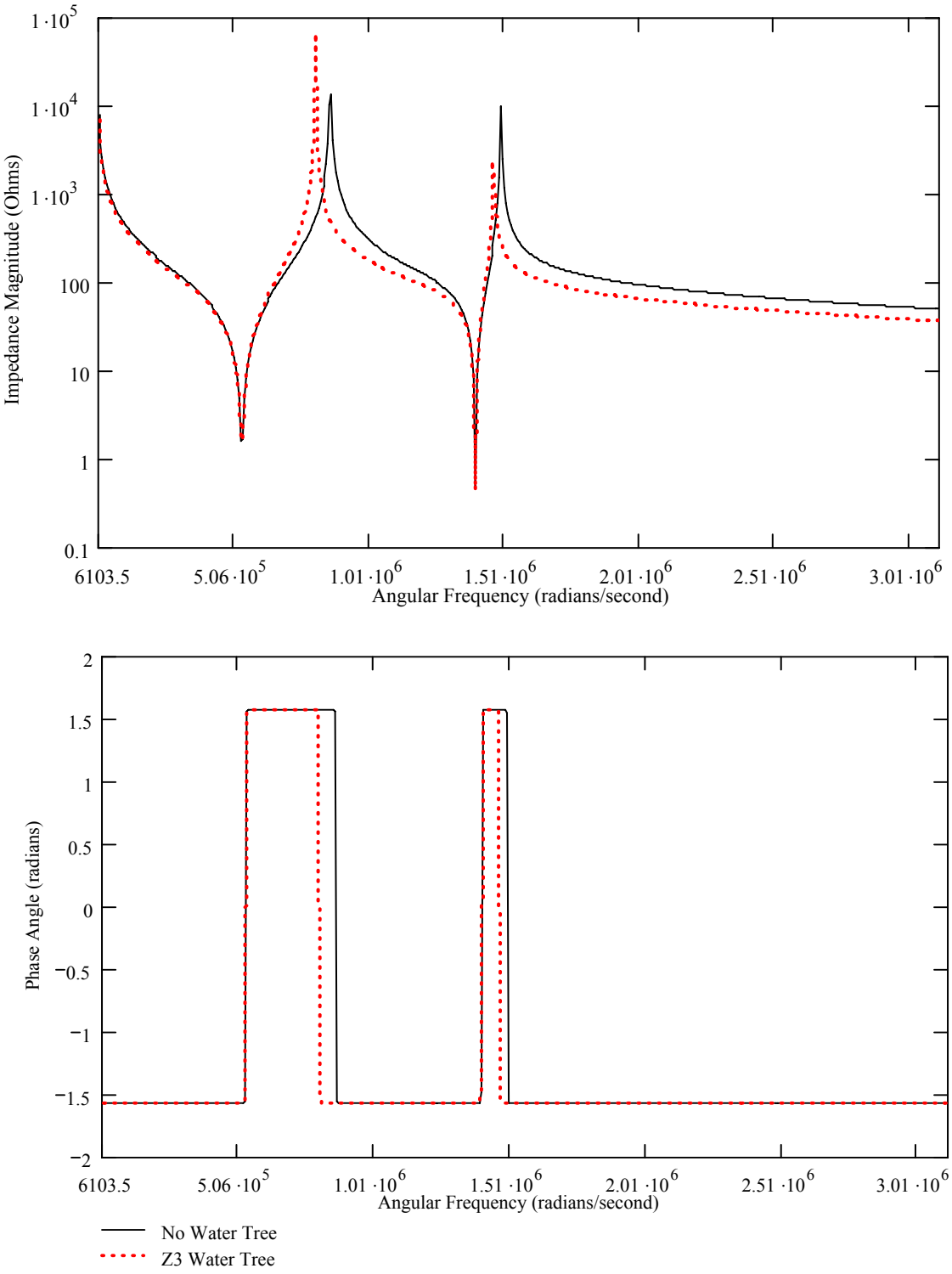

Figure E.8 Calculated Impedance Magnitude and Phase Angle vs Frequency
22 Impedance Element Model, L=100 m, D=10.3 mm AL, 4.45 mm XLPE,
Without vs With Z3 Water Tree

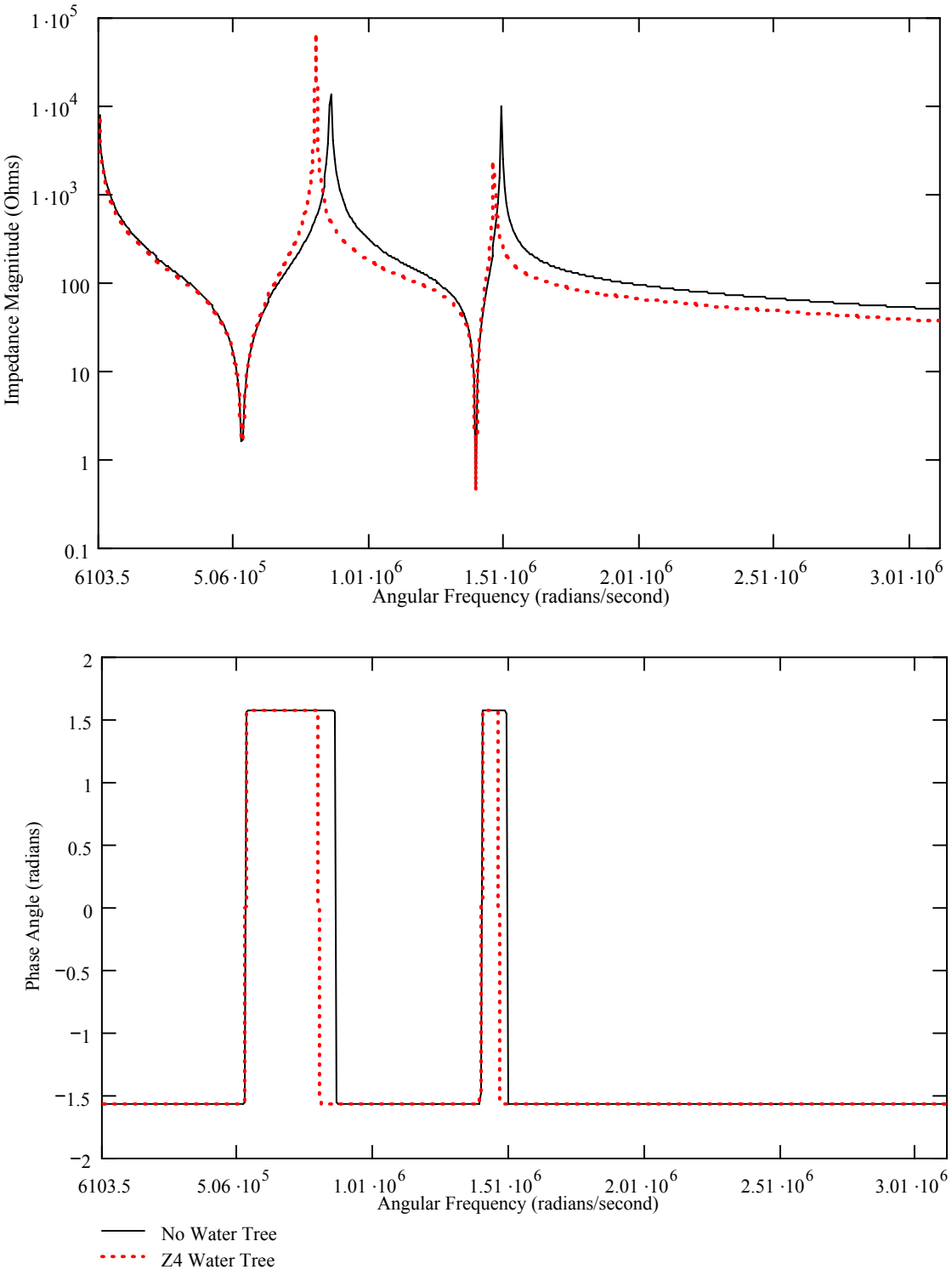

Figure E.9 Calculated Impedance Magnitude and Phase Angle vs Frequency
22 Impedance Element Model, L=100 m, D=10.3 mm AL, 4.45 mm XLPE,
Without vs With Z4 Water Tree

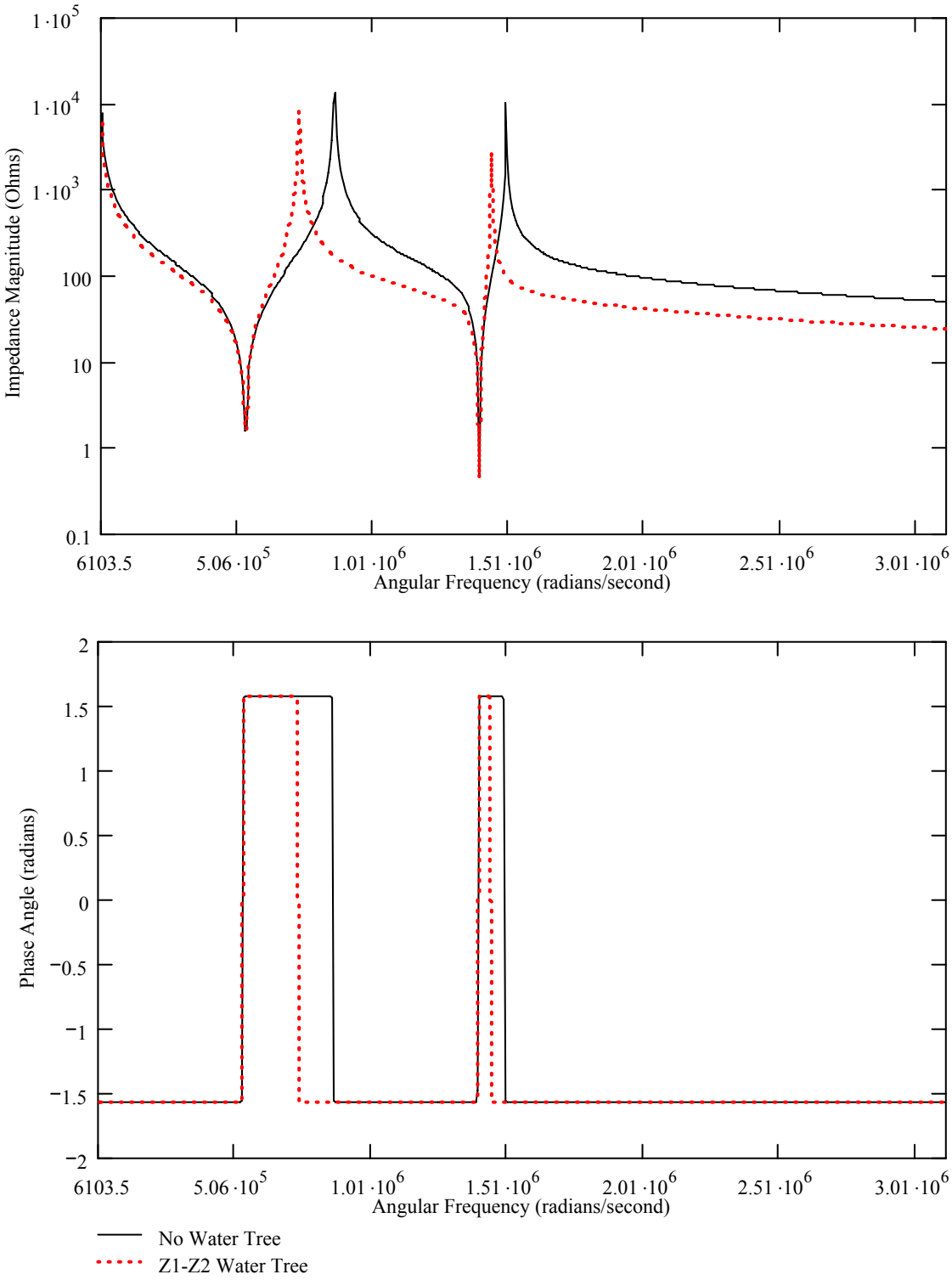

Figure E.10 Calculated Impedance Magnitude and Phase Angle vs Frequency
22 Impedance Element Model, L=100 m, D=10.3 mm AL, 4.45 mm XLPE,
Without vs With Z1-Z2 Water Tree

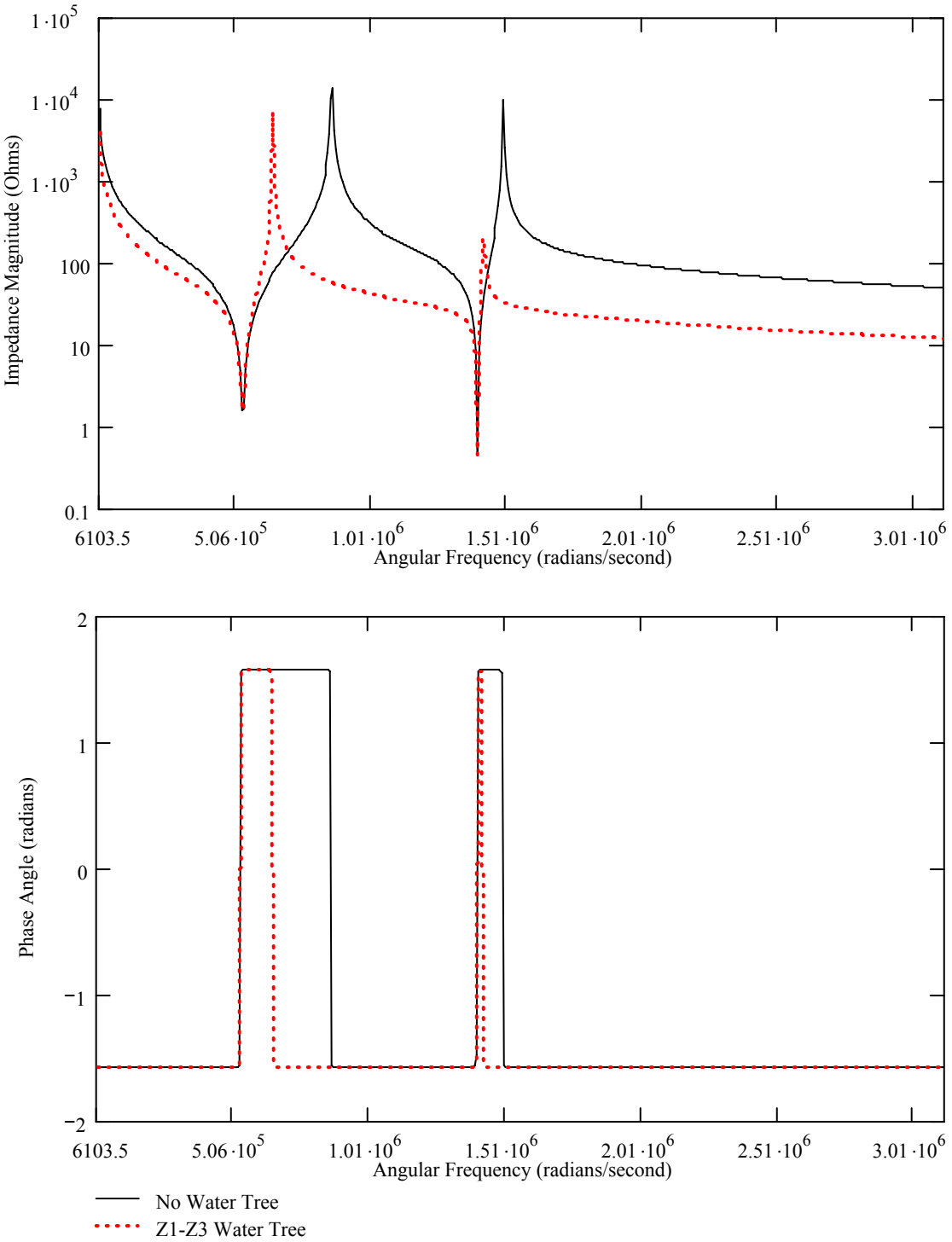

Figure E.11 Calculated Impedance Magnitude and Phase Angle vs Frequency
22 Impedance Element Model, L=100 m, D=10.3 mm AL, 4.45 mm XLPE,
Without vs With Z1-Z3 Water Tree

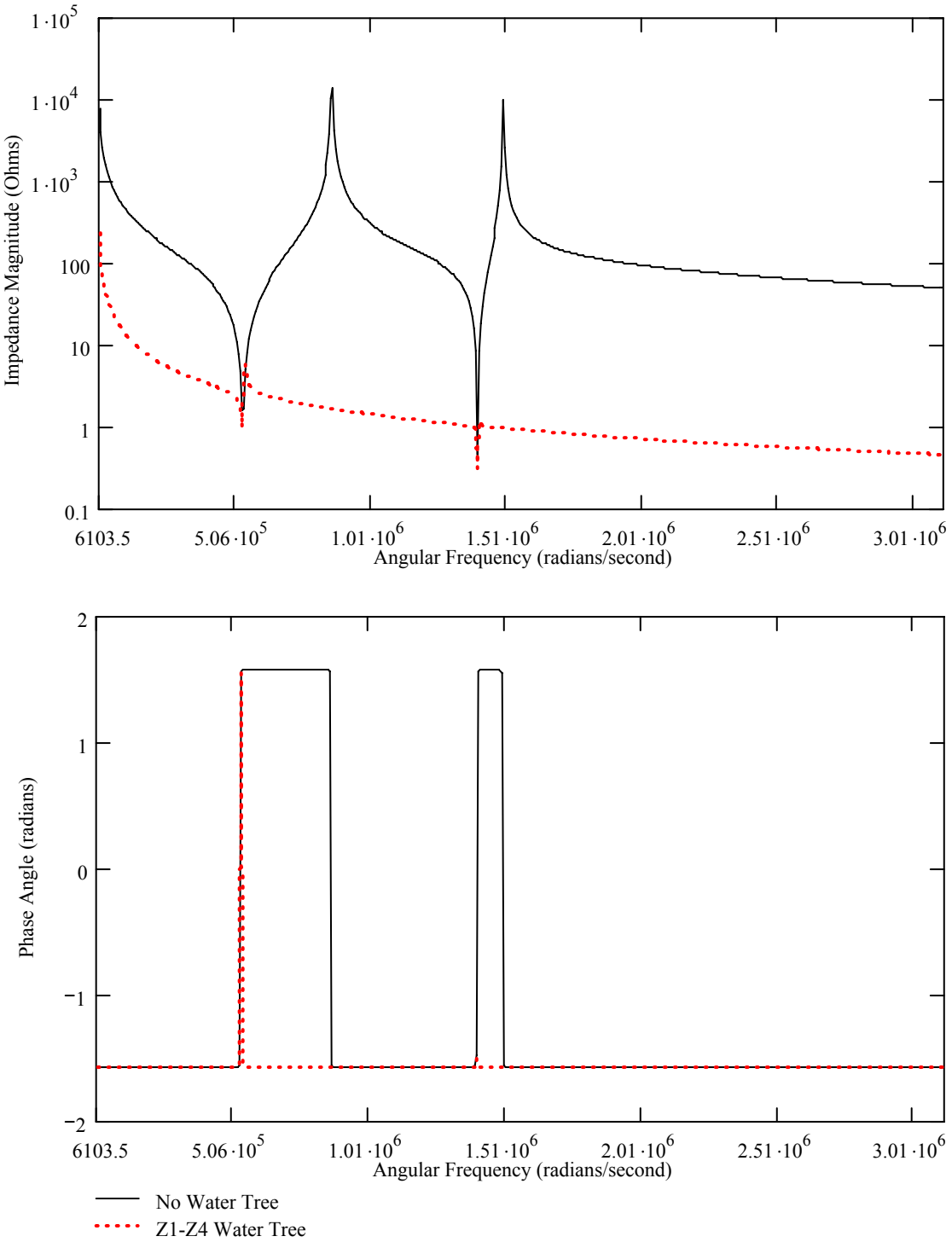

Figure E.12 Calculated Impedance Magnitude and Phase Angle vs Frequency
22 Impedance Element Model, L=100 m, D=10.3 mm AL, 4.45 mm XLPE,
Without vs With Z1-Z4 Water Tree

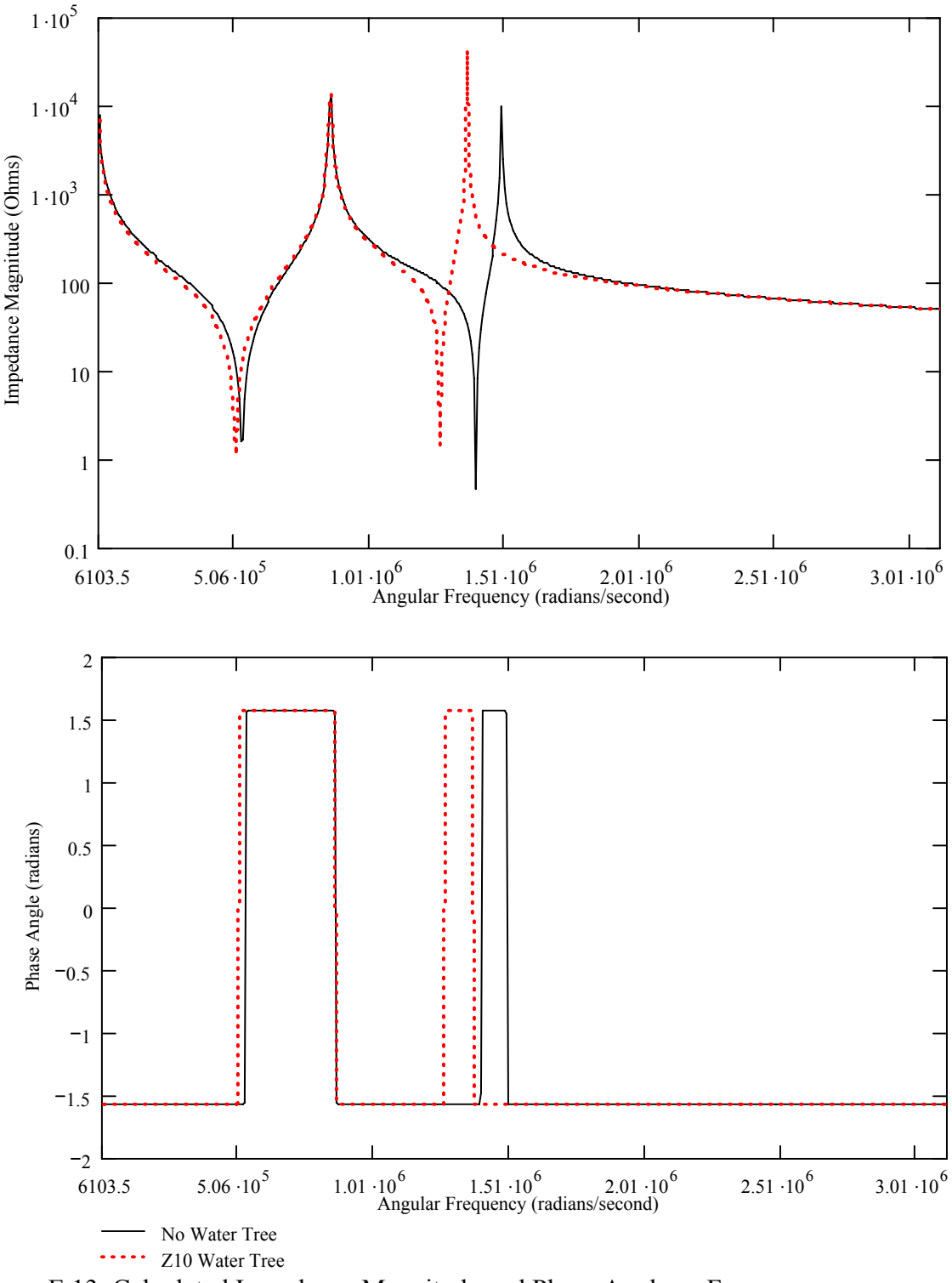

Figure E.13 Calculated Impedance Magnitude and Phase Angle vs Frequency
22 Impedance Element Model, L=100 m, D=10.3 mm AL, 4.45 mm XLPE,
Without vs With Z10 Water Tree

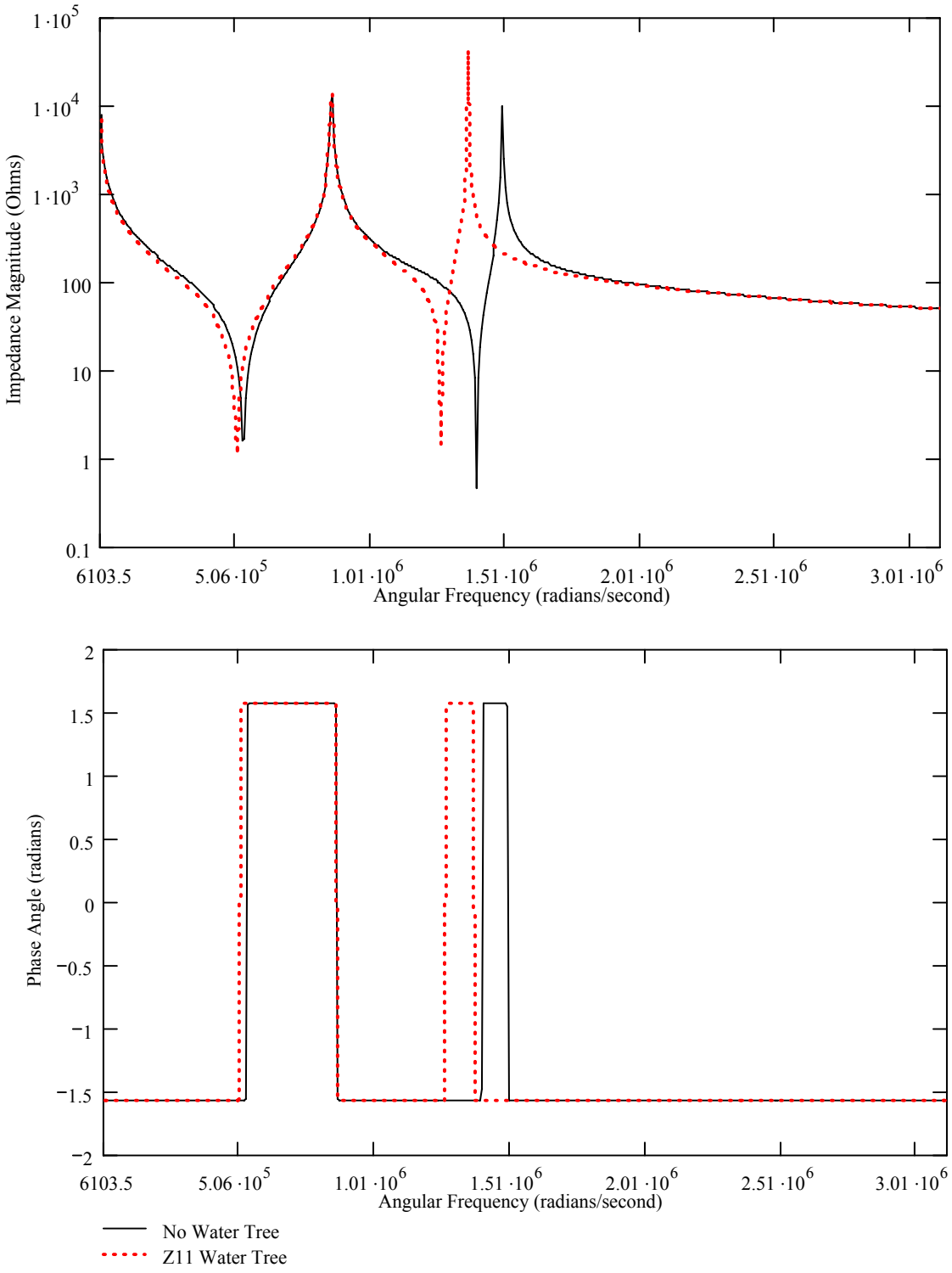

Figure E.14 Calculated Impedance Magnitude and Phase Angle vs Frequency
22 Impedance Element Model, L=100 m, D=10.3 mm AL, 4.45 mm XLPE,
Without vs With Z11 Water Tree

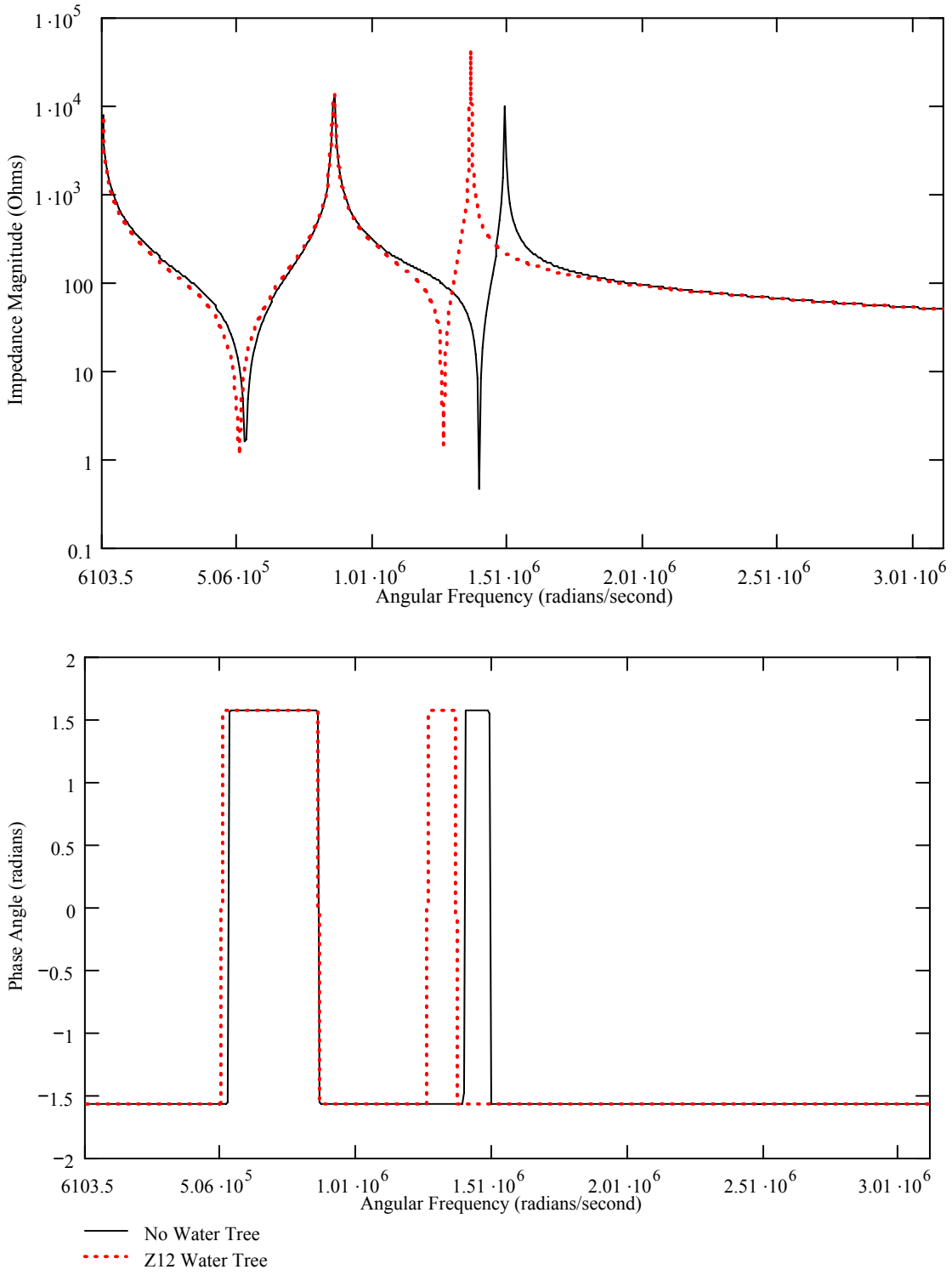

Figure E.15 Calculated Impedance Magnitude and Phase Angle vs Frequency
22 Impedance Element Model, L=100 m, D=10.3 mm AL, 4.45 mm XLPE,
Without vs With Z12 Water Tree

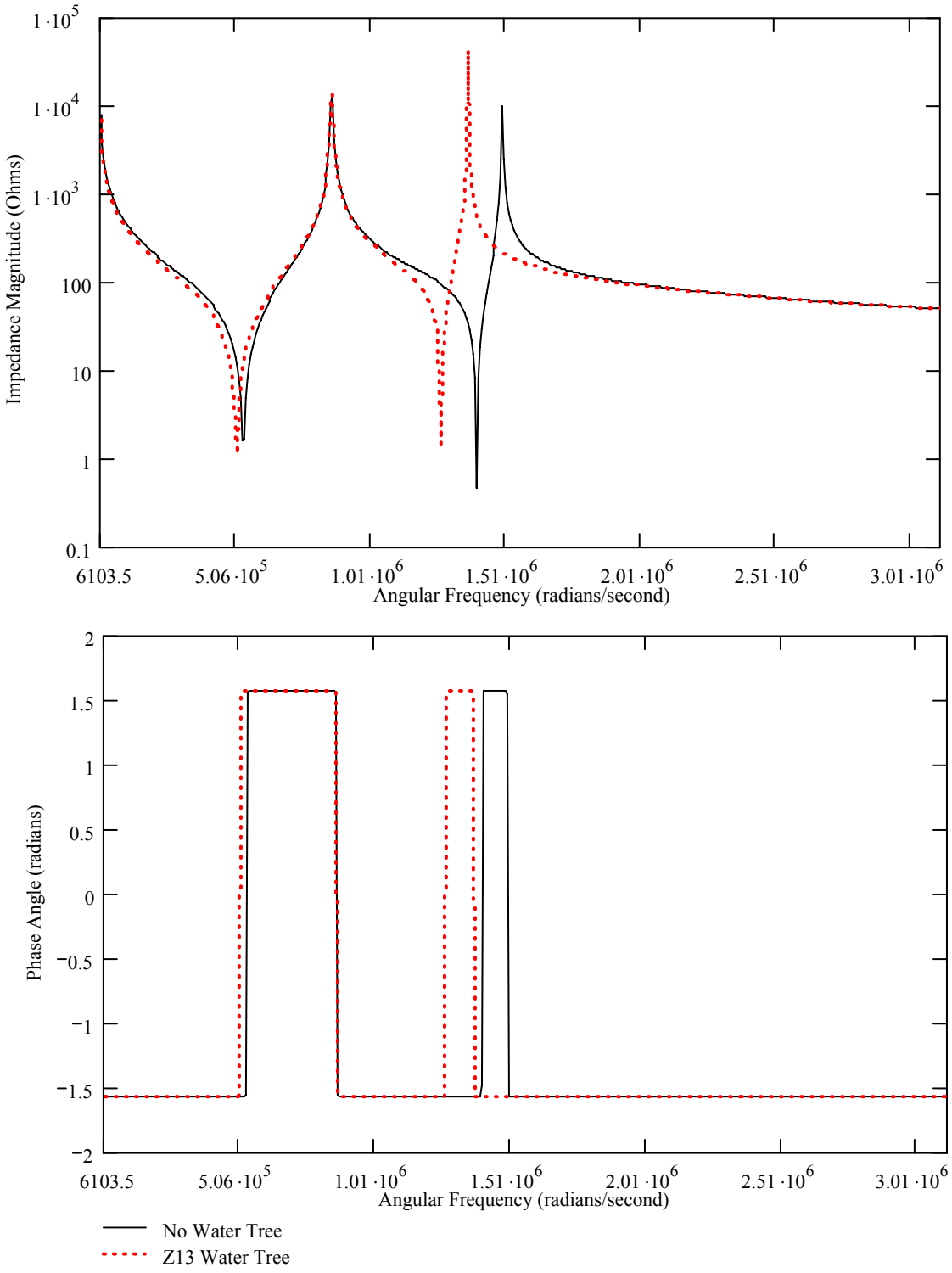

Figure E.16 Calculated Impedance Magnitude and Phase Angle vs Frequency
22 Impedance Element Model, L=100 m, D=10.3 mm AL, 4.45 mm XLPE,
Without vs With Z13 Water Tree

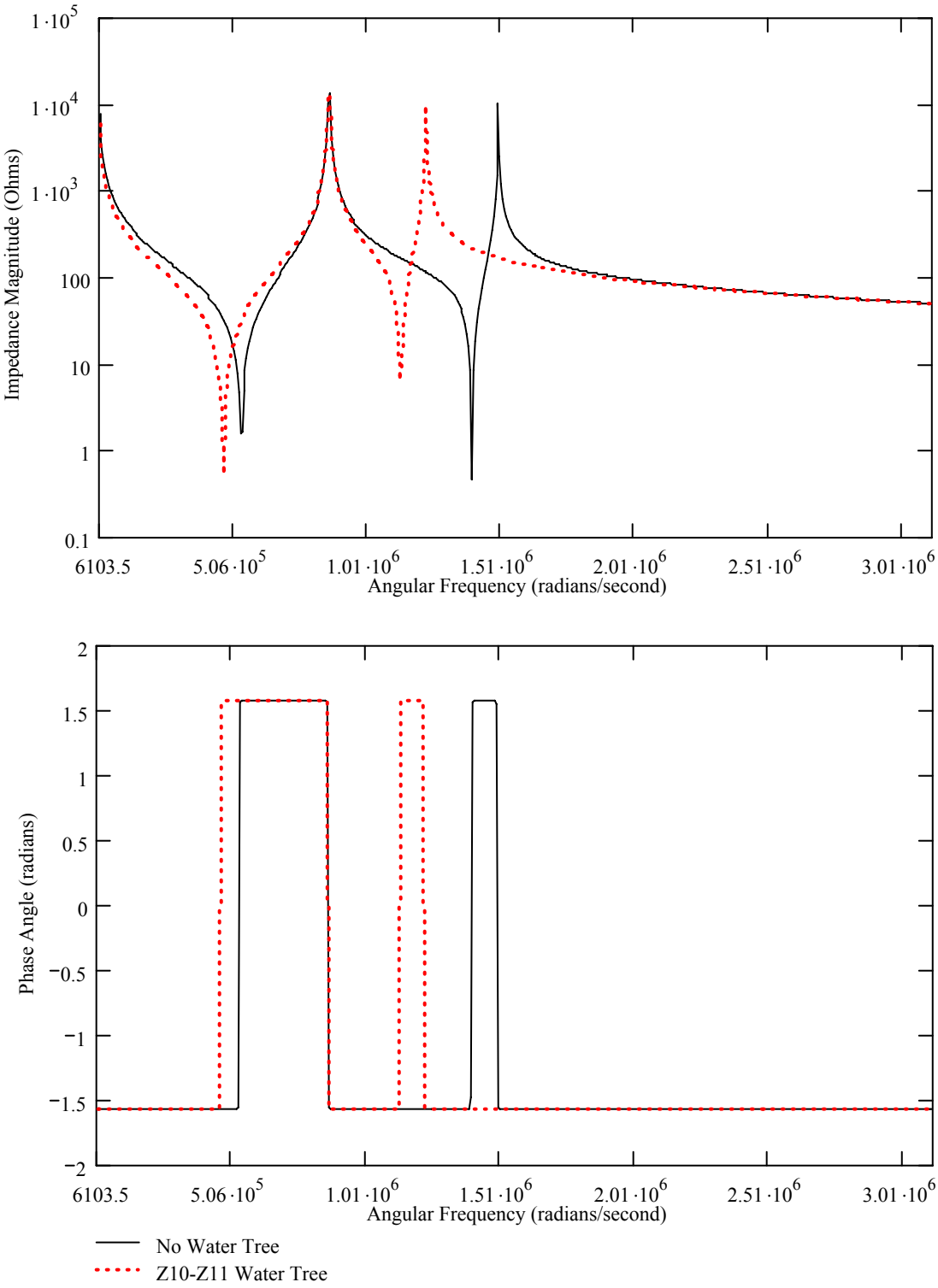

Figure E.17 Calculated Impedance Magnitude and Phase Angle vs Frequency
22 Impedance Element Model, L=100 m, D=10.3 mm AL, 4.45 mm XLPE,
Without vs With Z10-Z11 Water Tree

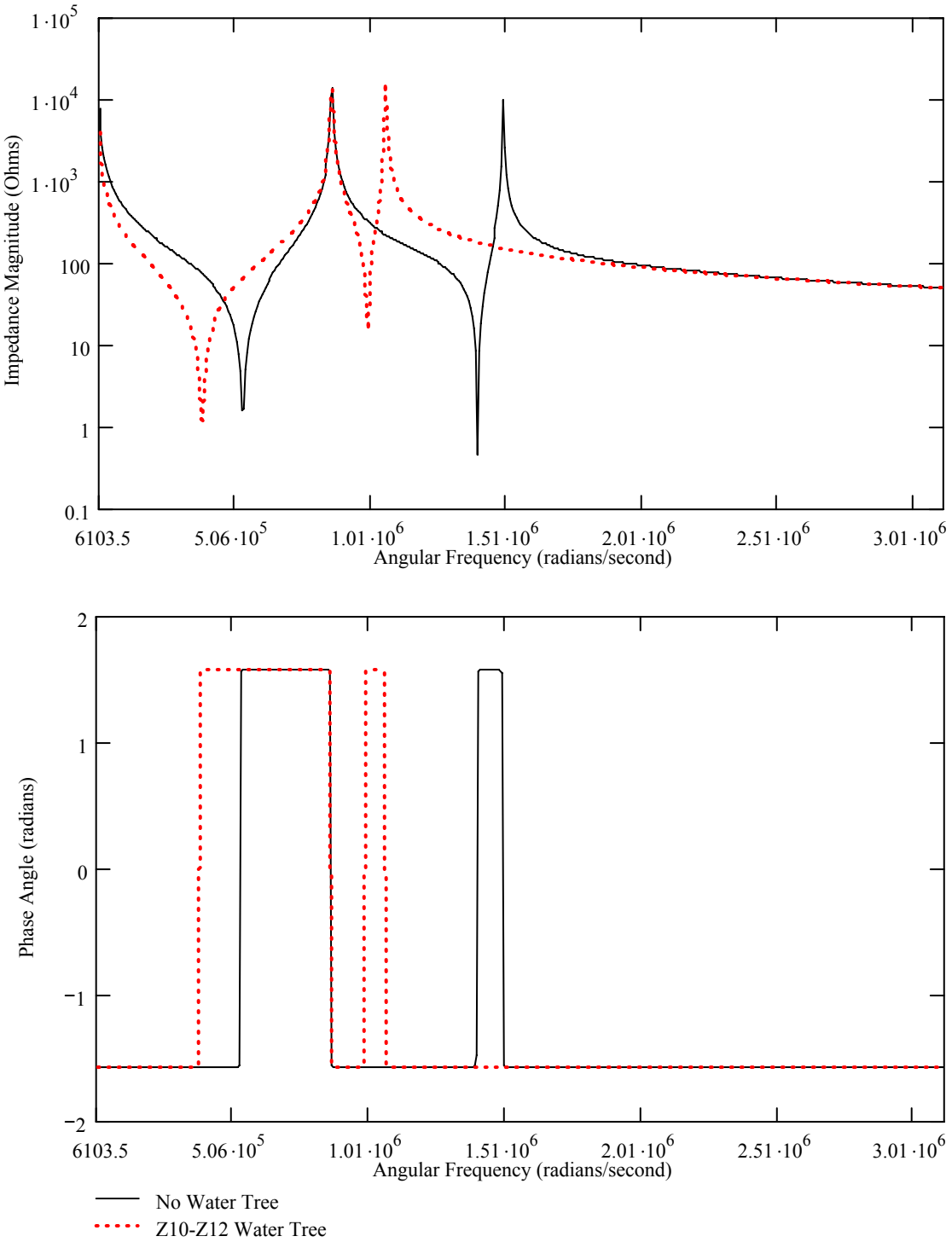

Figure E.18 Calculated Impedance Magnitude and Phase Angle vs Frequency
22 Impedance Element Model, L=100 m, D=10.3 mm AL, 4.45 mm XLPE,
Without vs With Z10-Z12 Water Tree

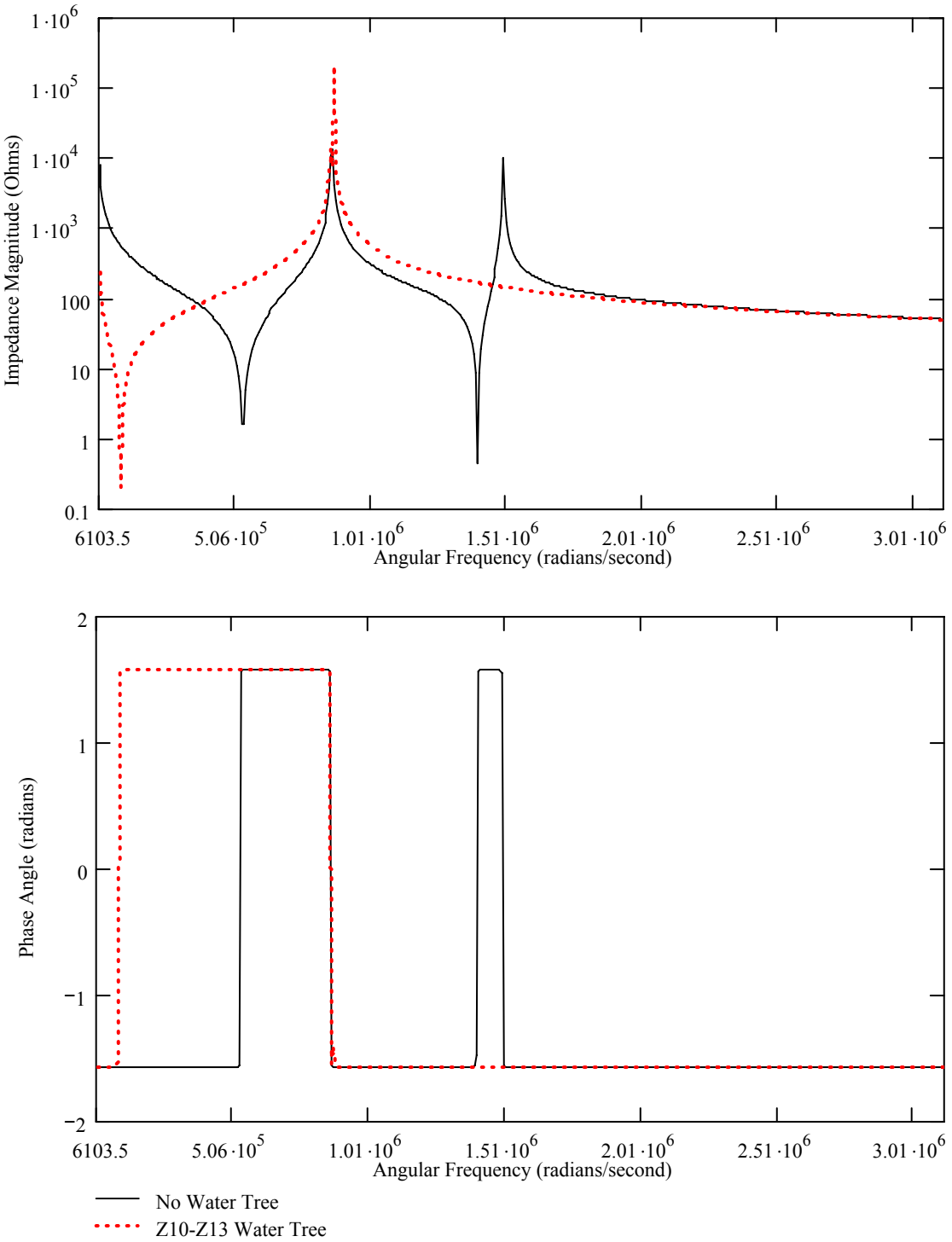

Figure E.19 Calculated Impedance Magnitude and Phase Angle vs Frequency
22 Impedance Element Model, L=100 m, D=10.3 mm AL, 4.45 mm XLPE,
Without vs With Z10-Z13 Water Tree

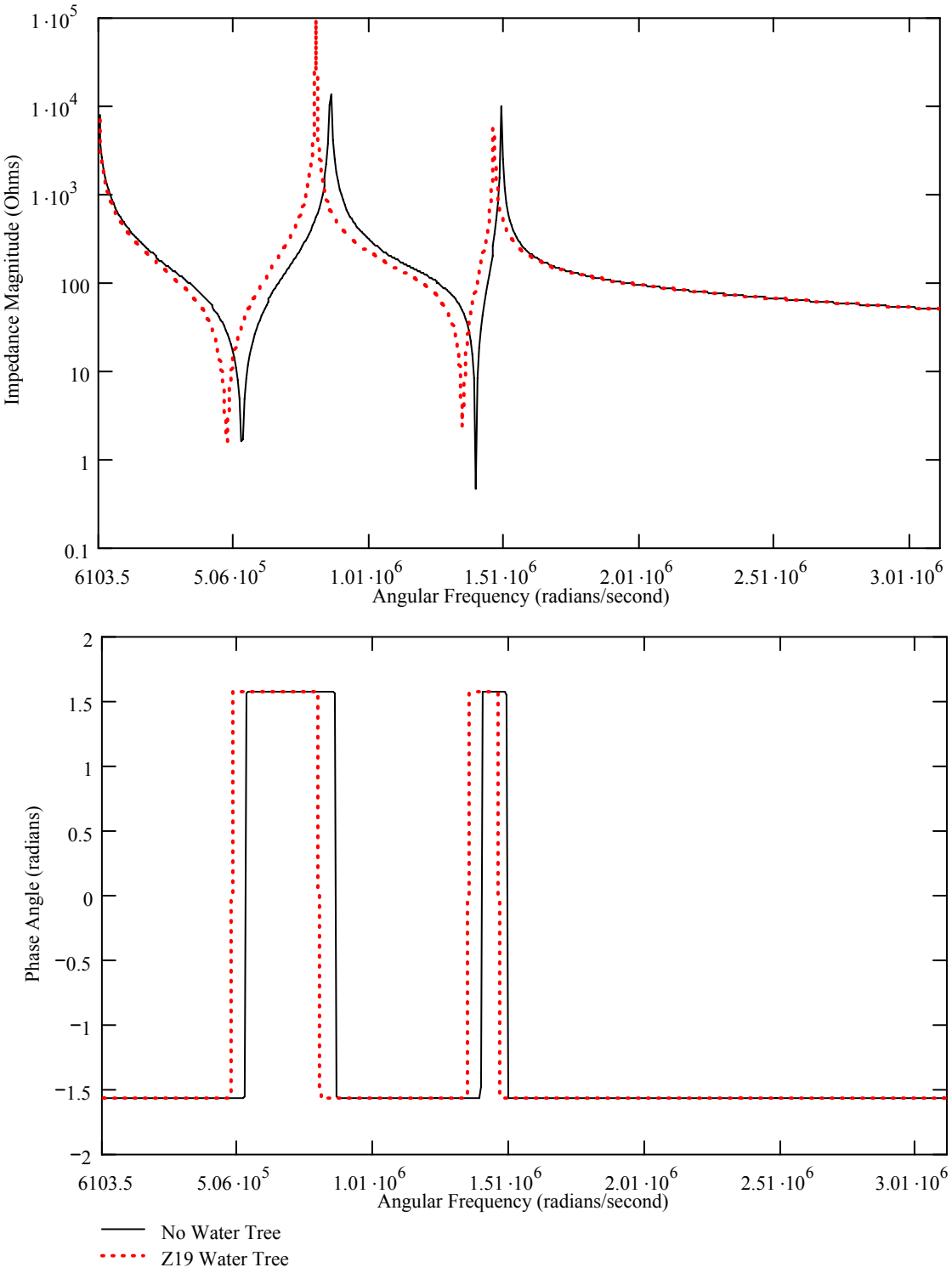

Figure E.20 Calculated Impedance Magnitude and Phase Angle vs Frequency
22 Impedance Element Model, L=100 m, D=10.3 mm AL, 4.45 mm XLPE,
Without vs With Z19 Water Tree

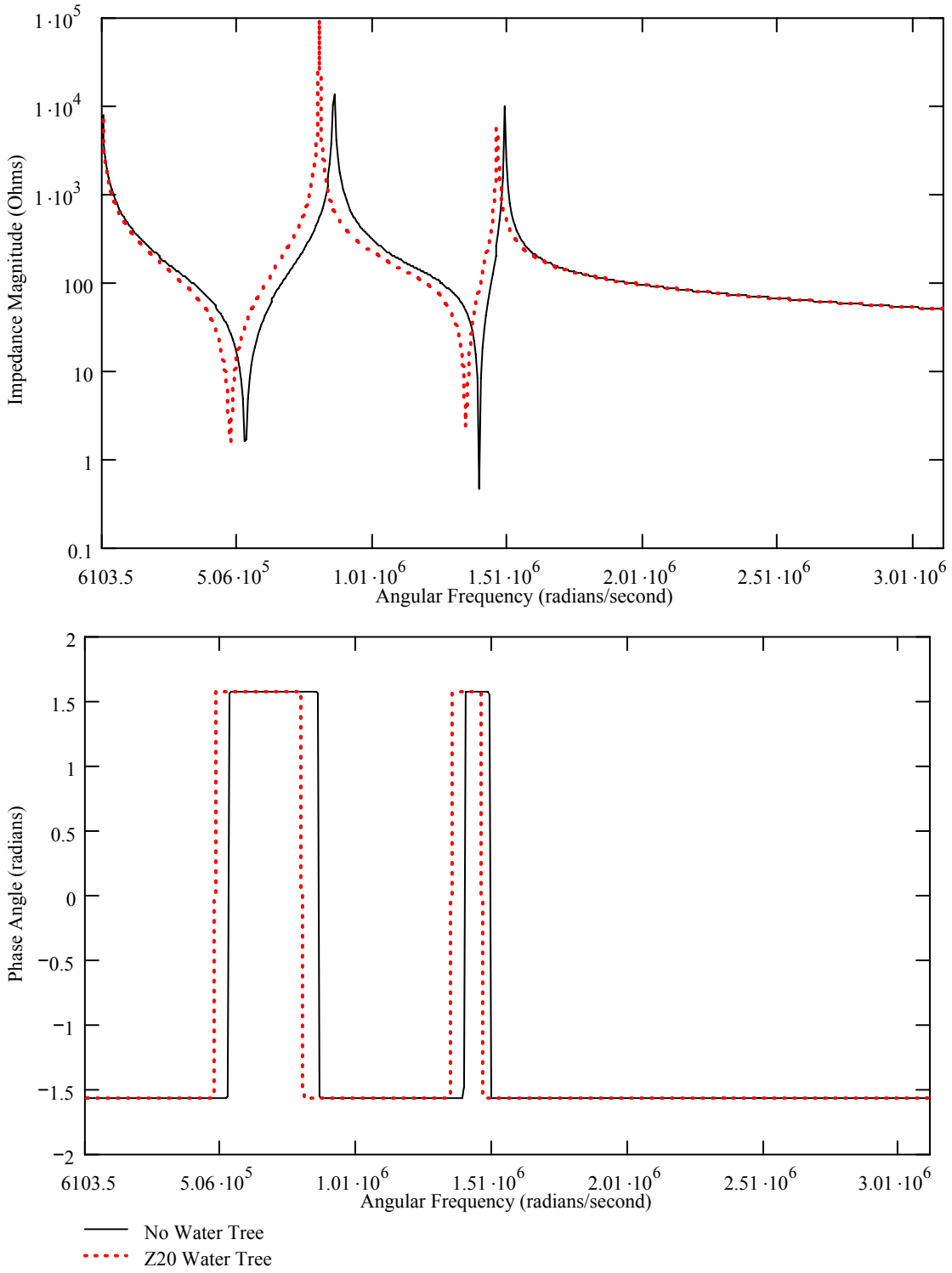

Figure E.21 Calculated Impedance Magnitude and Phase Angle vs Frequency
22 Impedance Element Model, L=100 m, D=10.3 mm AL, 4.45 mm XLPE,
Without vs With Z20 Water Tree

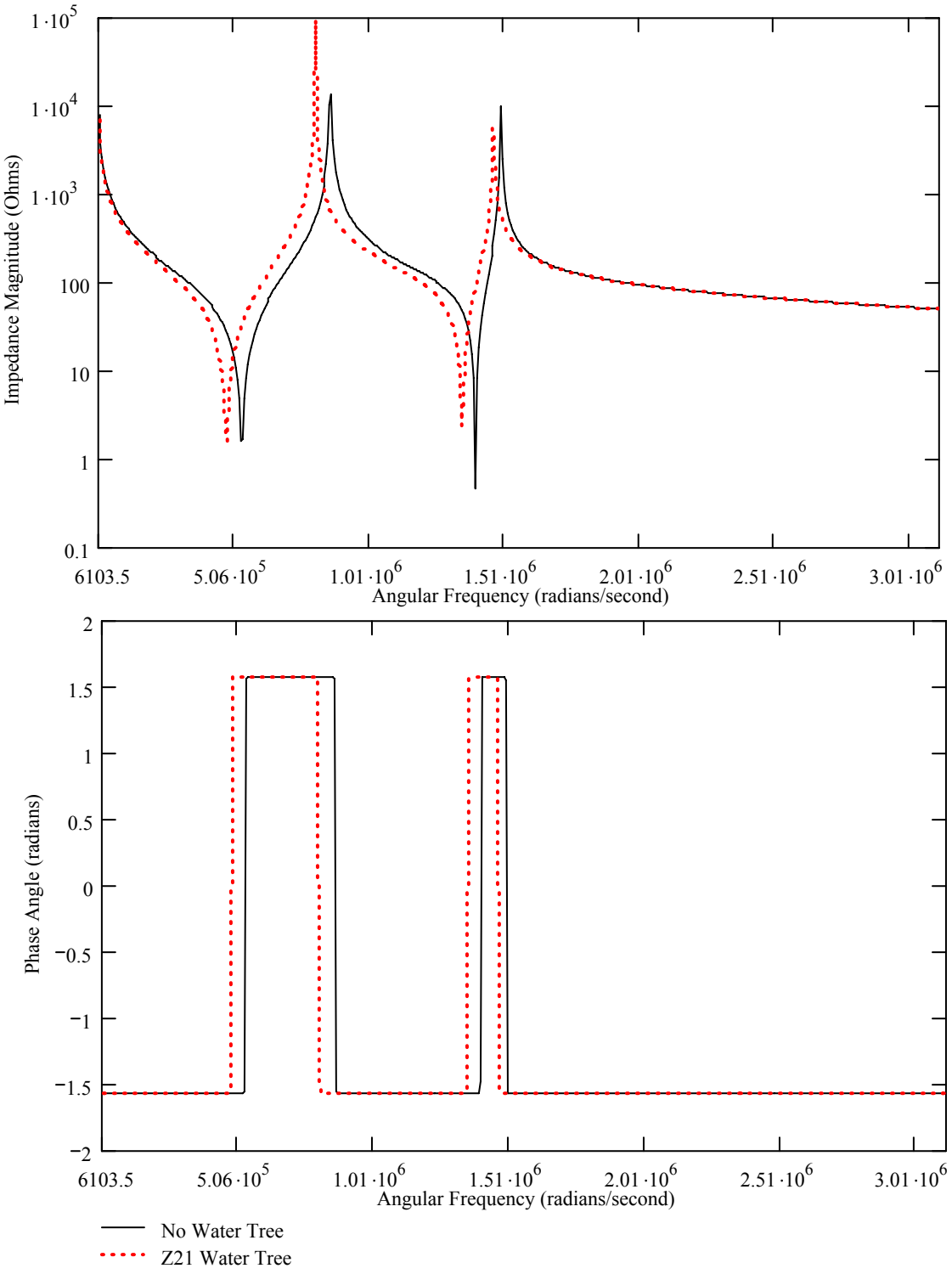

Figure E.22 Calculated Impedance Magnitude and Phase Angle vs Frequency
22 Impedance Element Model, L=100 m, D=10.3 mm AL, 4.45 mm XLPE,
Without vs With Z21 Water Tree

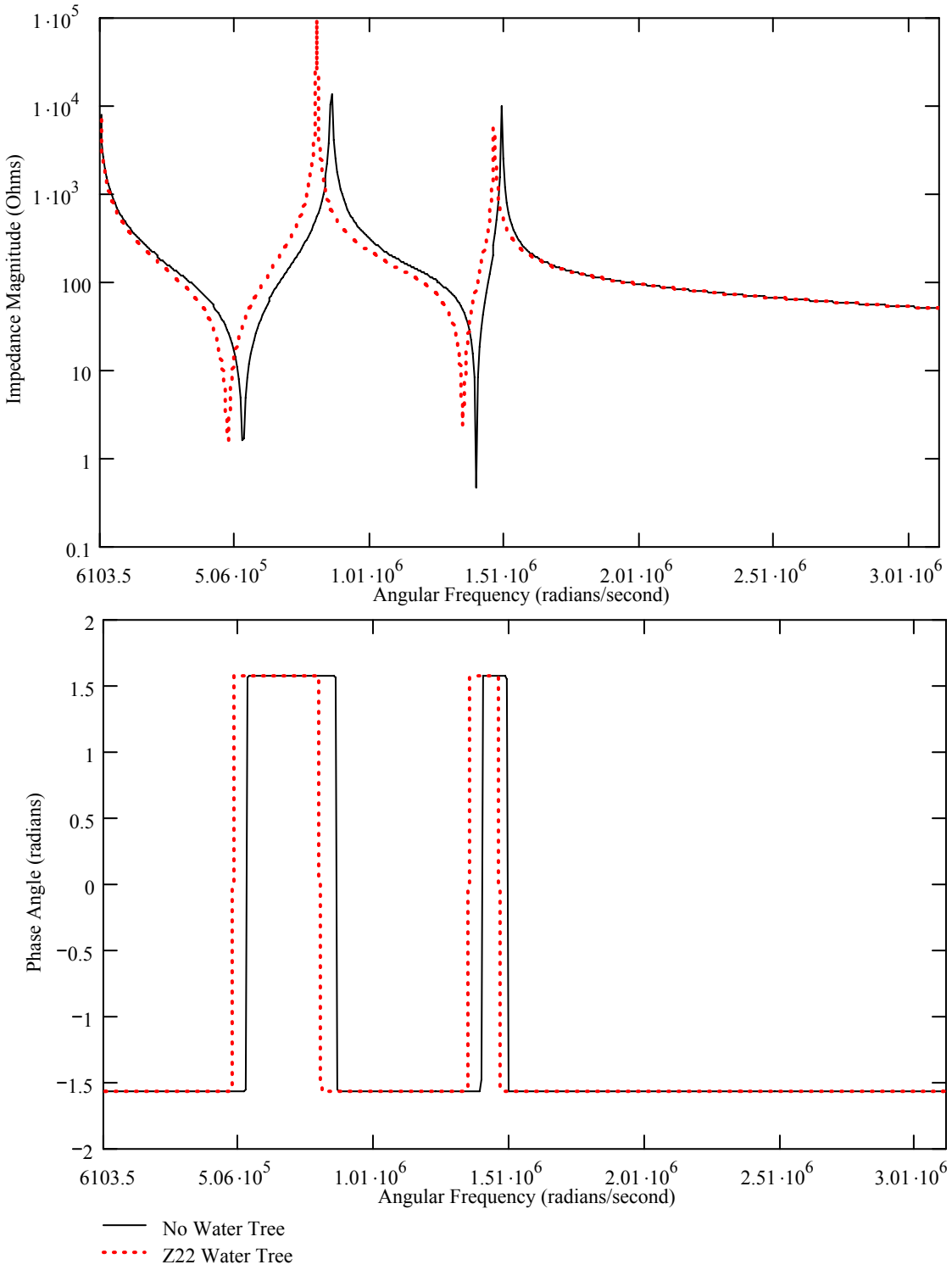

Figure E.23 Calculated Impedance Magnitude and Phase Angle vs Frequency
22 Impedance Element Model, L=100 m, D=10.3 mm AL, 4.45 mm XLPE,
Without vs With Z22 Water Tree

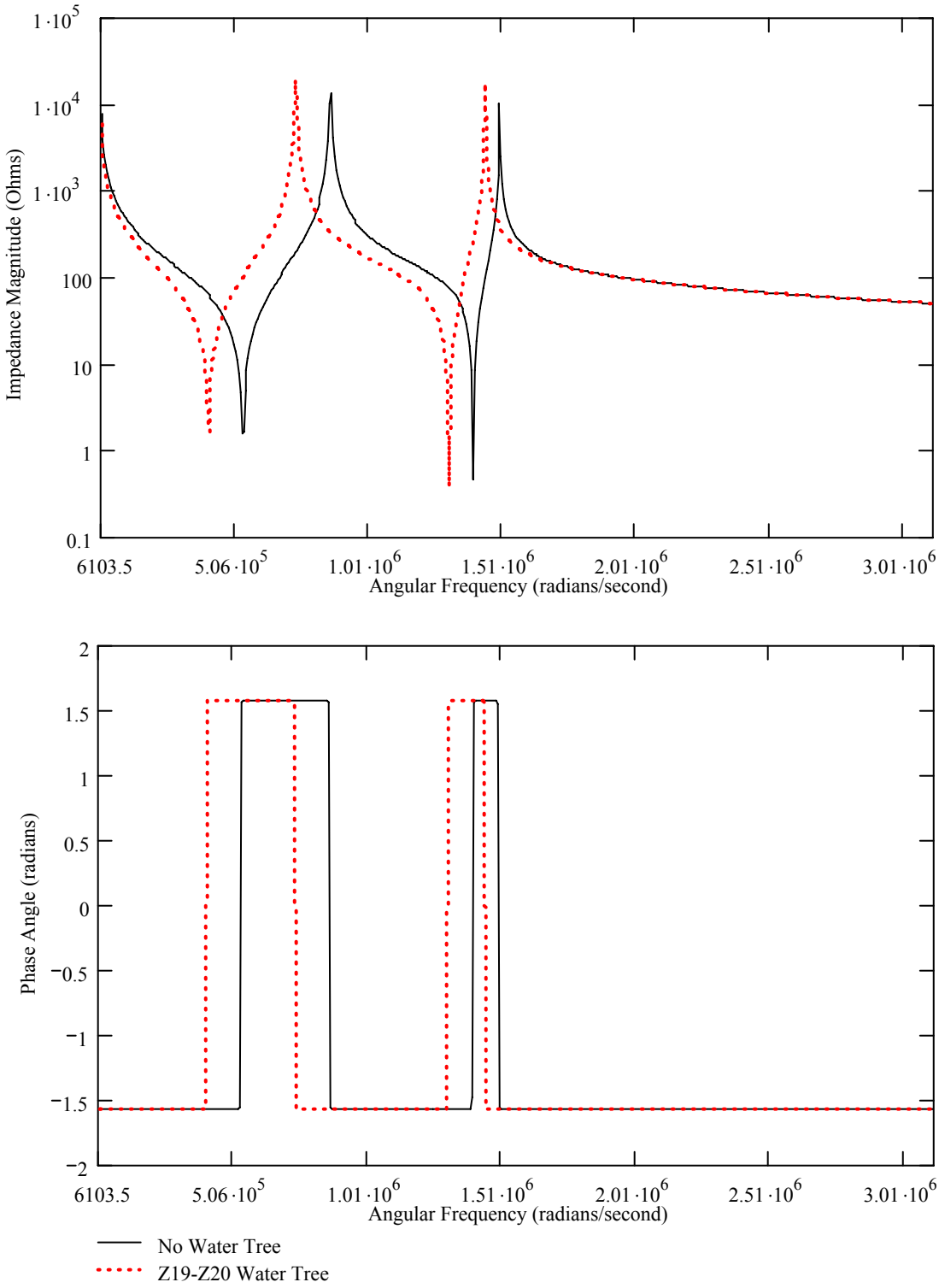

Figure E.24 Calculated Impedance Magnitude and Phase Angle vs Frequency
22 Impedance Element Model, L=100 m, D=10.3 mm AL, 4.45 mm XLPE,
Without vs With Z19-Z20 Water Tree

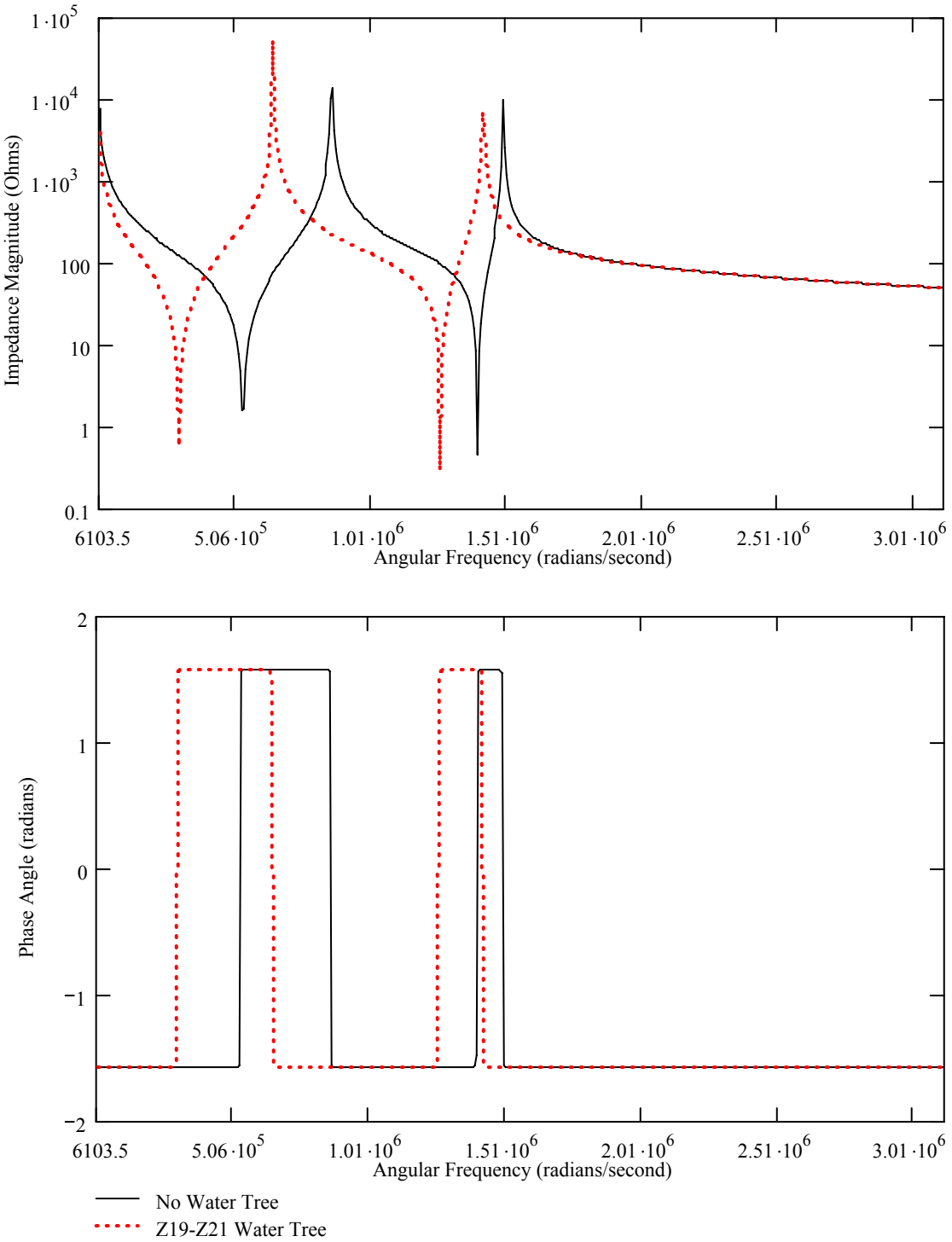

Figure E.25 Calculated Impedance Magnitude and Phase Angle vs Frequency
22 Impedance Element Model, L=100 m, D=10.3 mm AL, 4.45 mm XLPE,
Without vs With Z19-Z21 Water Tree

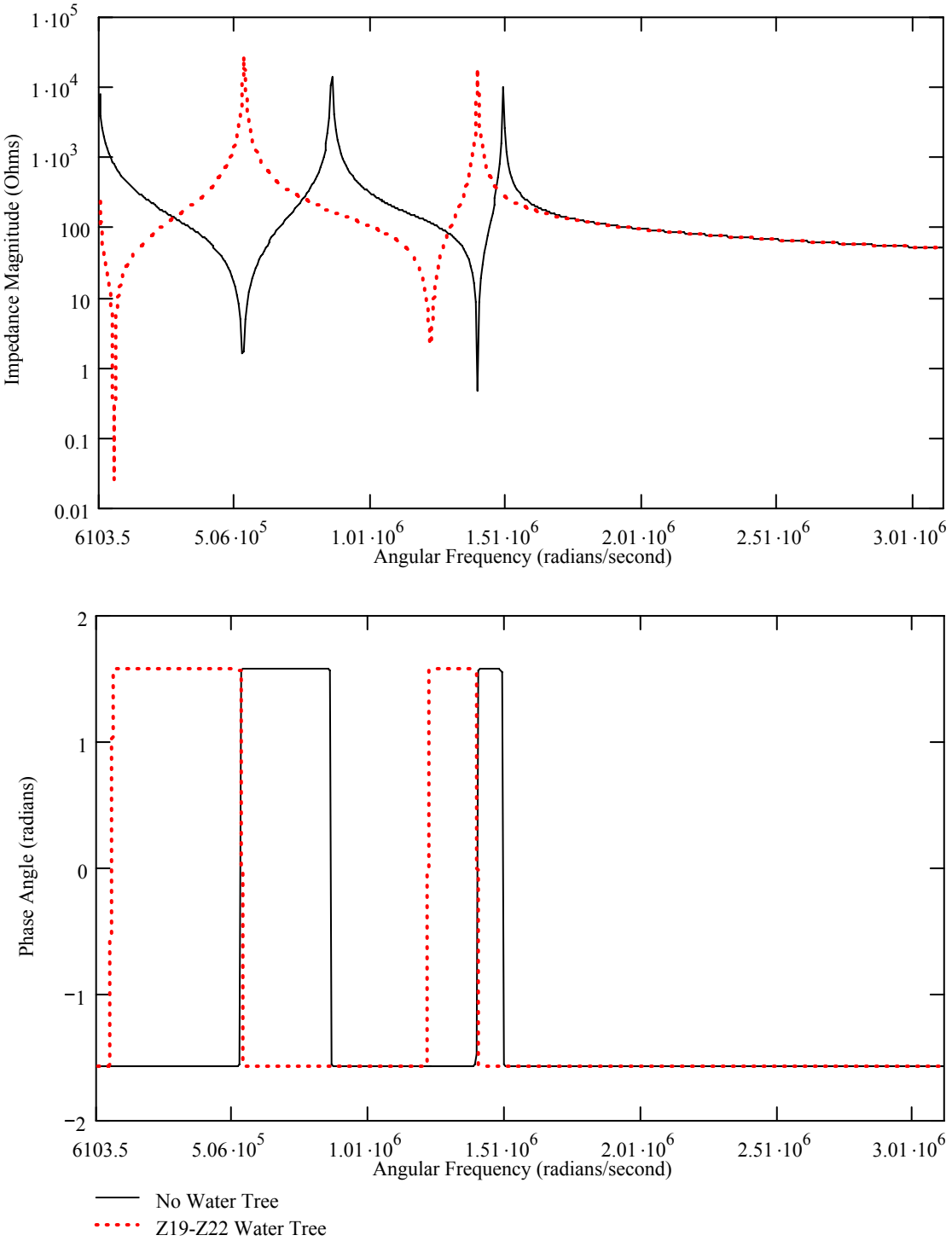

Figure E.26 Calculated Impedance Magnitude and Phase Angle vs Frequency
22 Impedance Element Model, L=100 m, D=10.3 mm AL, 4.45 mm XLPE,
Without vs With Z19-Z22 Water Tree

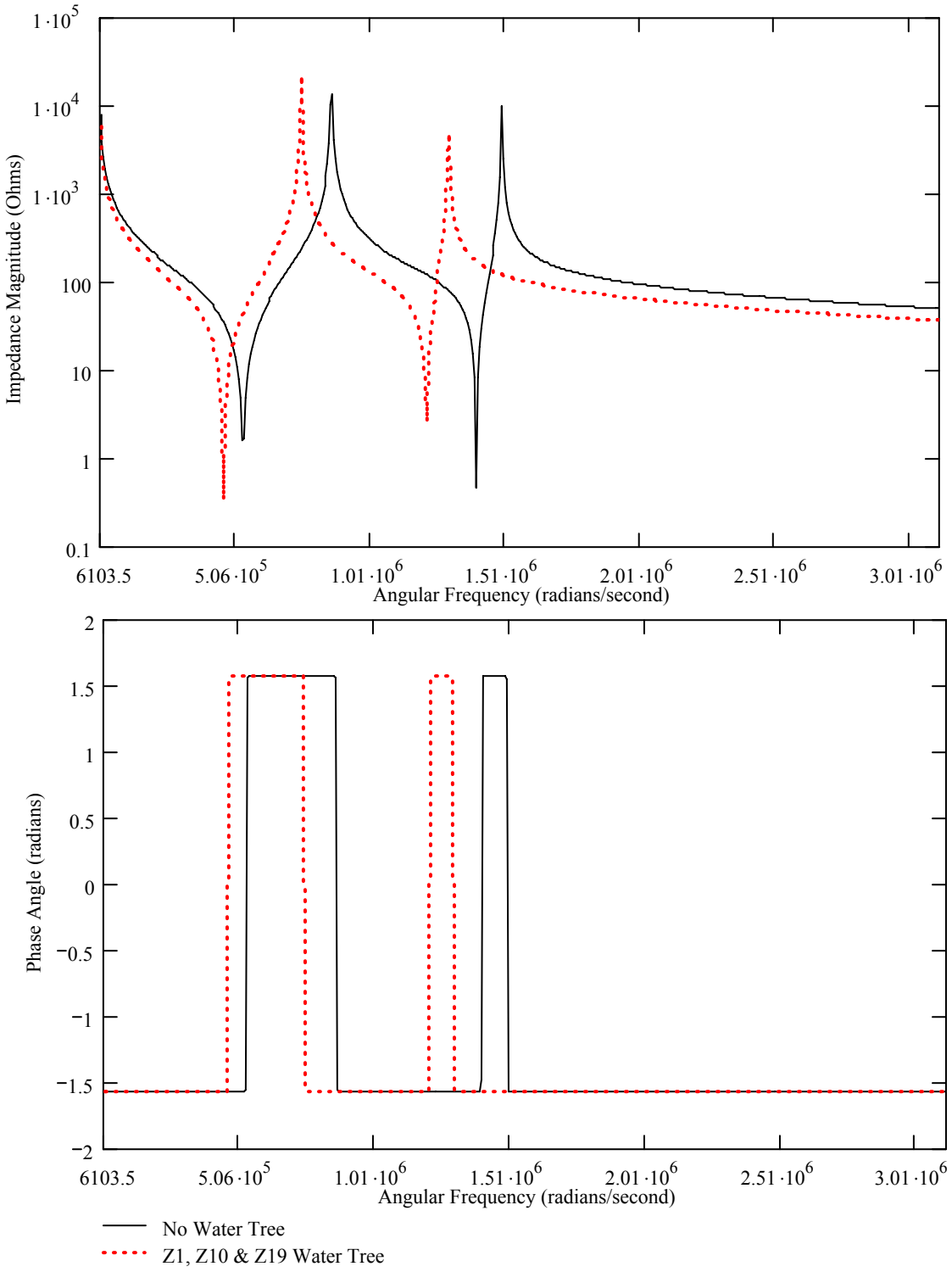

Figure E.27 Calculated Impedance Magnitude and Phase Angle vs Frequency
22 Impedance Element Model, L=100 m, D=10.3 mm AL, 4.45 mm XLPE,
Without vs With Z1, Z10 & Z19 Water Trees

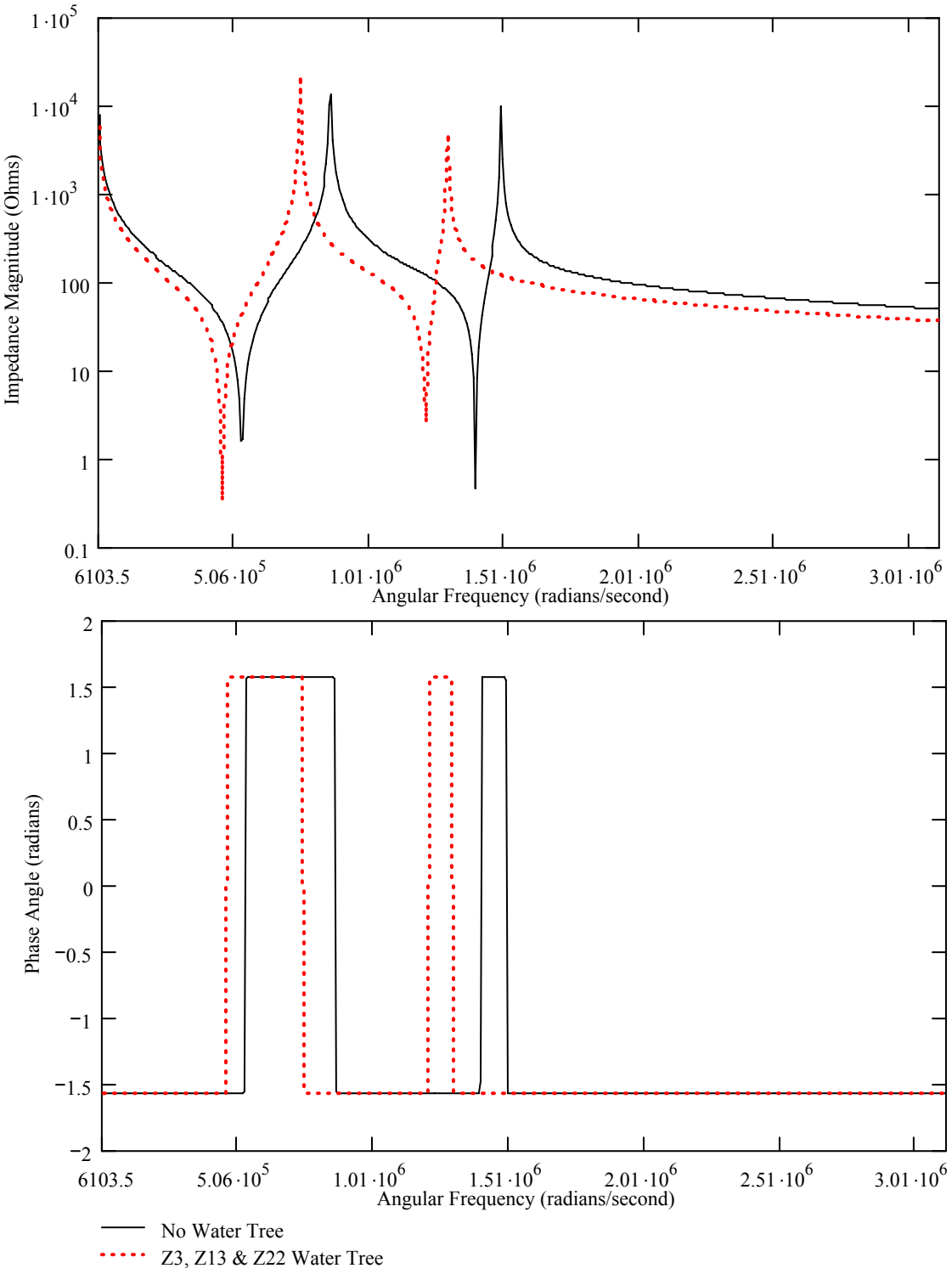

Figure E.28 Calculated Impedance Magnitude and Phase Angle vs Frequency
22 Impedance Element Model, L=100 m, D=10.3 mm AL, 4.45 mm XLPE,
Without vs With Z4, Z13 & Z22 Water Trees

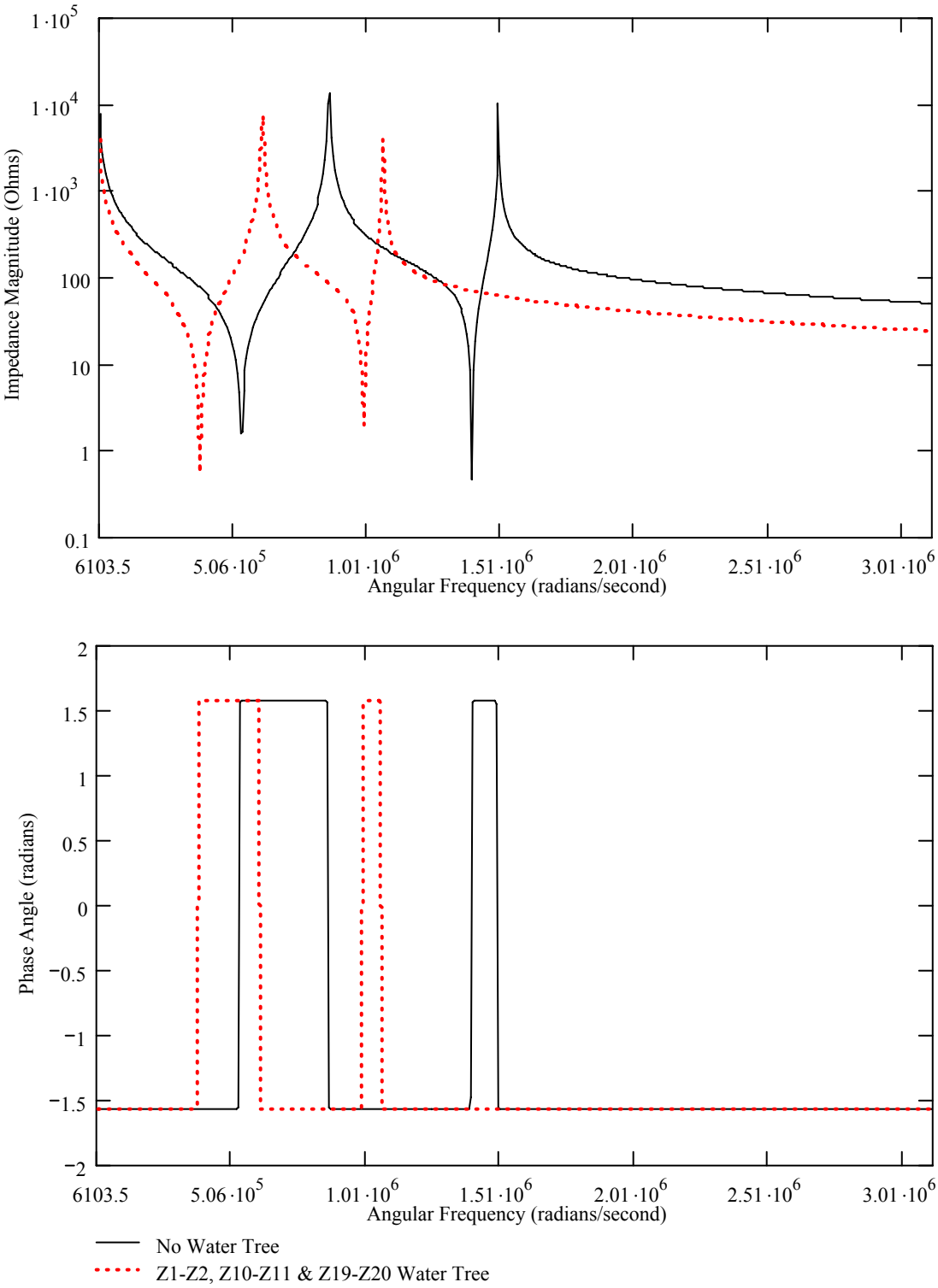

Figure E. 29 Calculated Impedance Magnitude and Phase Angle vs Frequency
22 Impedance Element Model, L=100 m, D=10.3 mm AL, 4.45 mm XLPE,
Without vs With Z1-Z2, Z10-Z11 & Z19-Z20 Water Trees

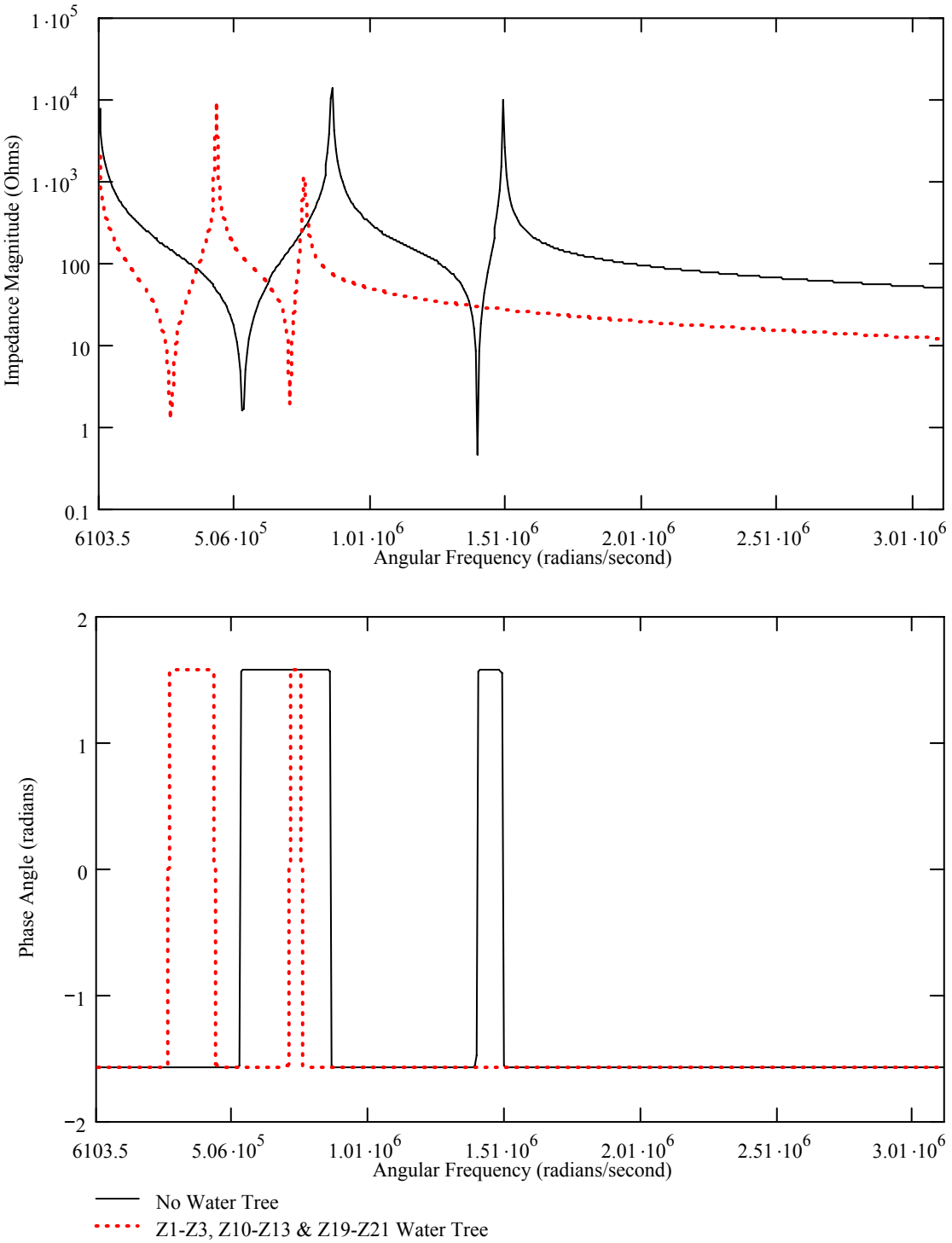

Figure E.30 Calculated Impedance Magnitude and Phase Angle vs Frequency
22 Impedance Element Model, L=100 m, D=10.3 mm AL, 4.45 mm XLPE,
Without vs With Z1-Z3, Z10-Z12 & Z19-Z21 Water Trees

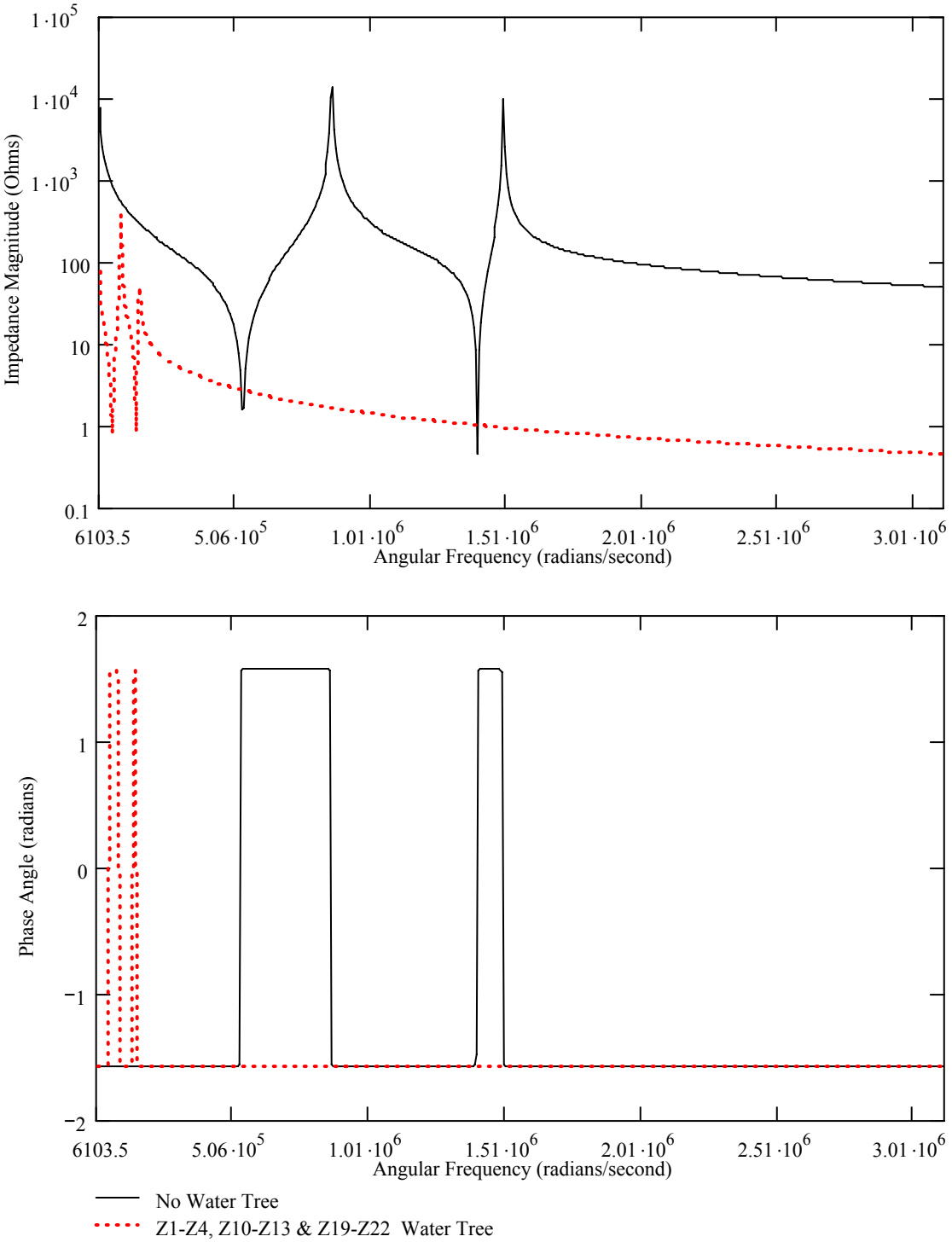

Figure E.31 Calculated Impedance Magnitude and Phase Angle vs Frequency
22 Impedance Element Model, L=100 m, D=10.3 mm AL, 4.45 mm XLPE,
Without vs With Z1-Z4, Z10-Z13 & Z19-Z22 Water Trees

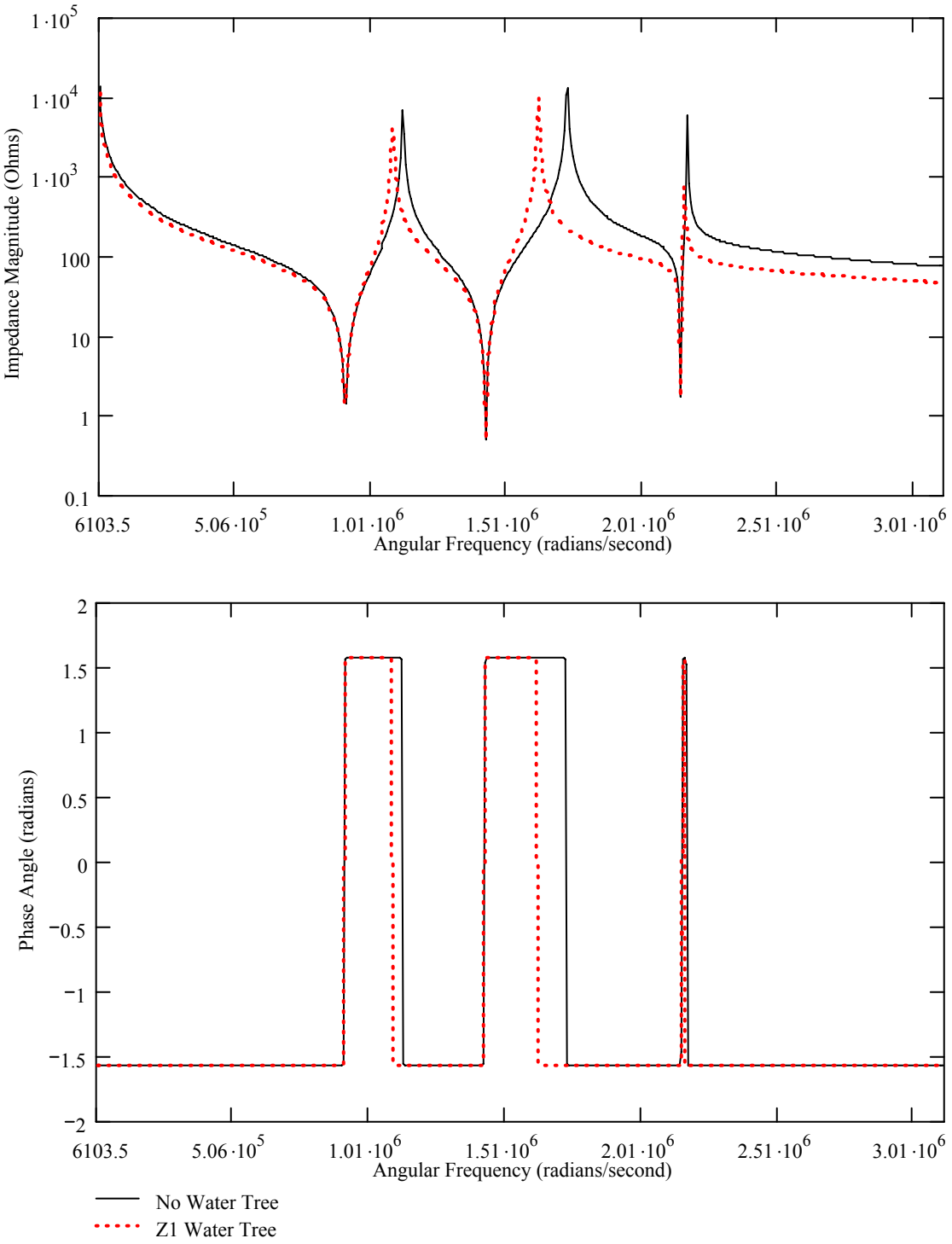

Figure E.32 Calculated Impedance Magnitude and Phase Angle vs Frequency
24 Impedance Element Model, L=100 m, D=10.3 mm AL, 4.45 mm XLPE,
Without vs With Z1 Water Tree

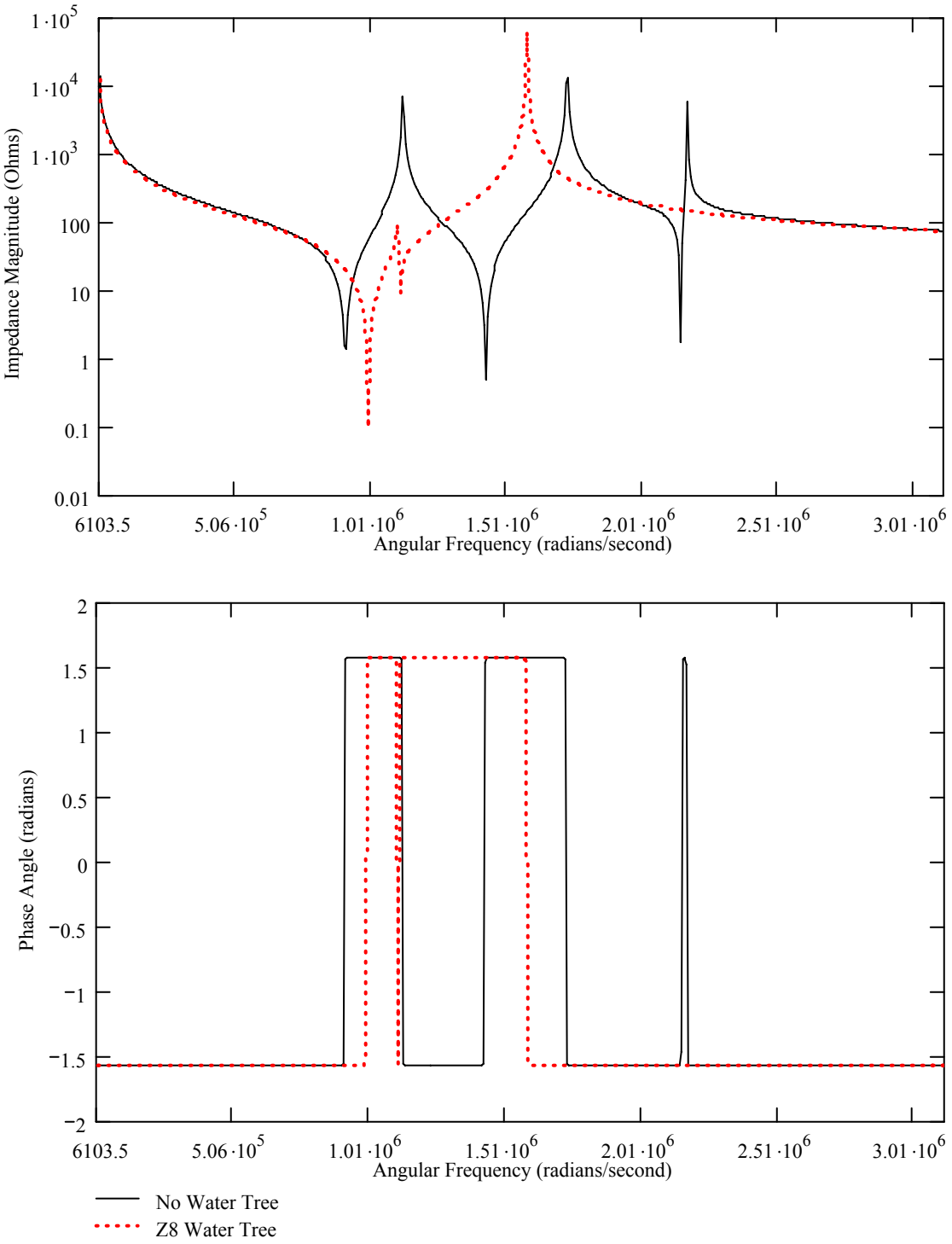

Figure E.33 Calculated Impedance Magnitude and Phase Angle vs Frequency
24 Impedance Element Model, L=100 m, D=10.3 mm AL, 4.45 mm XLPE,
Without vs With Z8 Water Tree

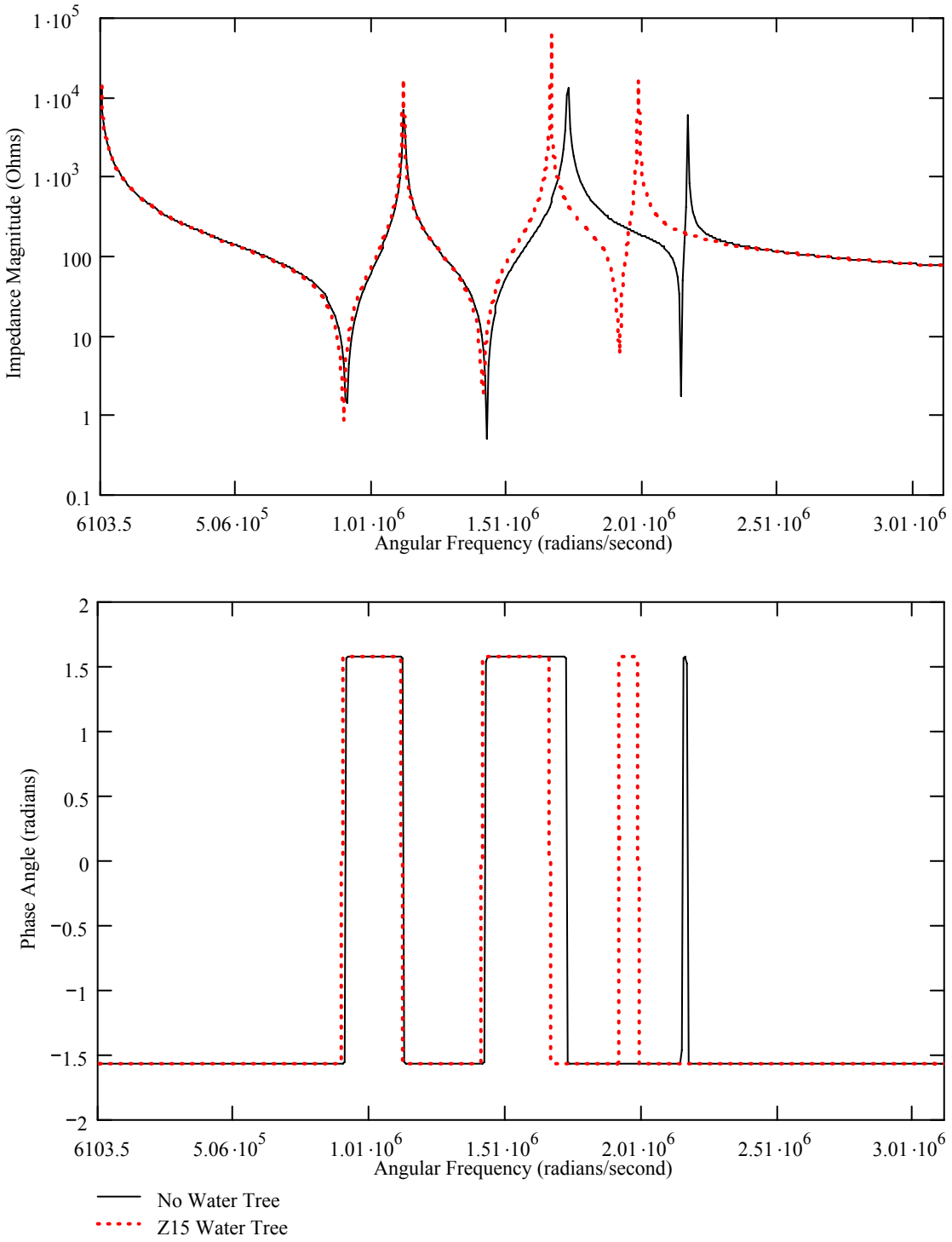

Figure E.34 Calculated Impedance Magnitude and Phase Angle vs Frequency
24 Impedance Element Model, L=100 m, D=10.3 mm AL, 4.45 mm XLPE,
Without vs With Z15 Water Tree

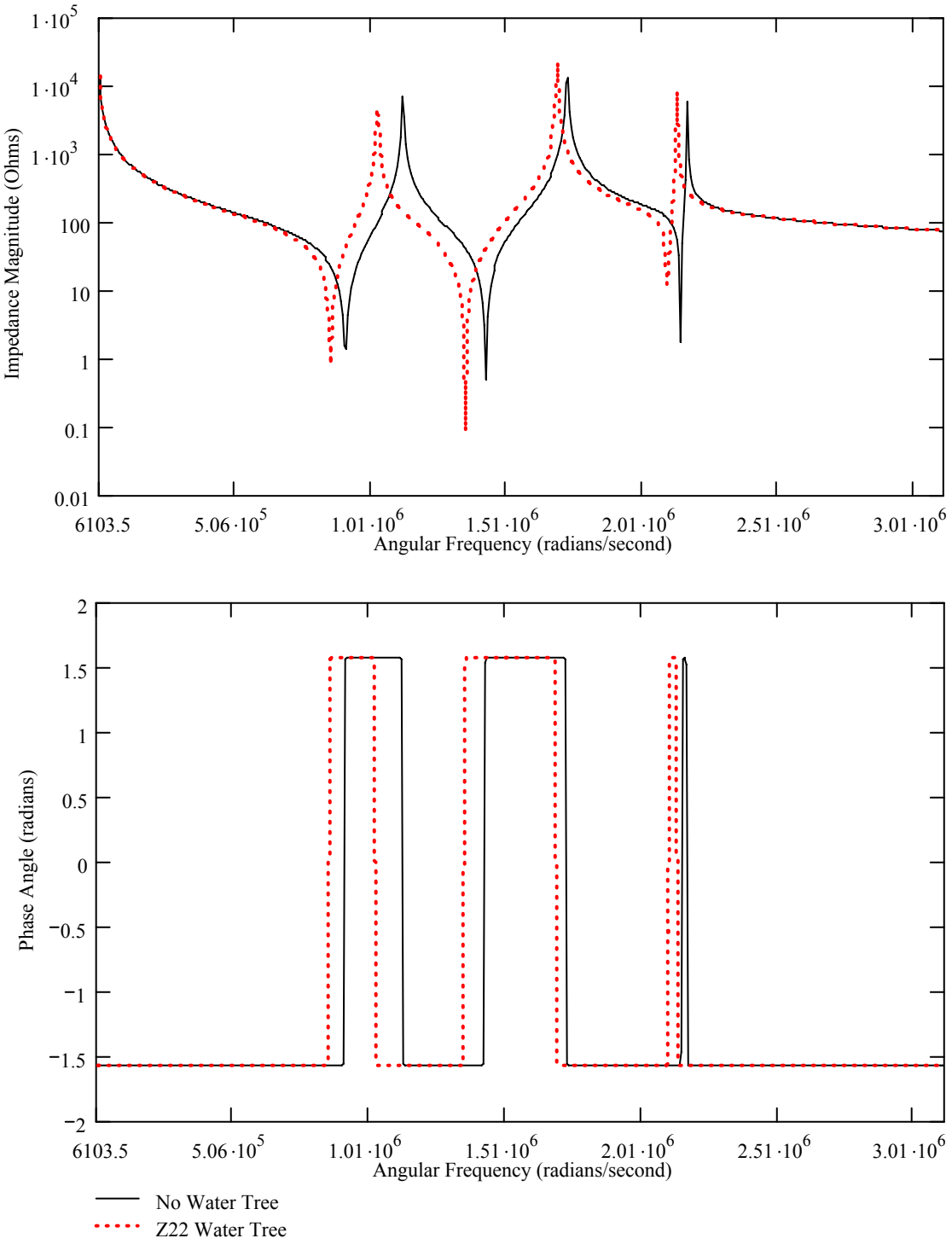

Figure E.35 Calculated Impedance Magnitude and Phase Angle vs Frequency
24 Impedance Element Model, L=100 m, D=10.3 mm AL, 4.45 mm XLPE,
Without vs With Z22 Water Tree

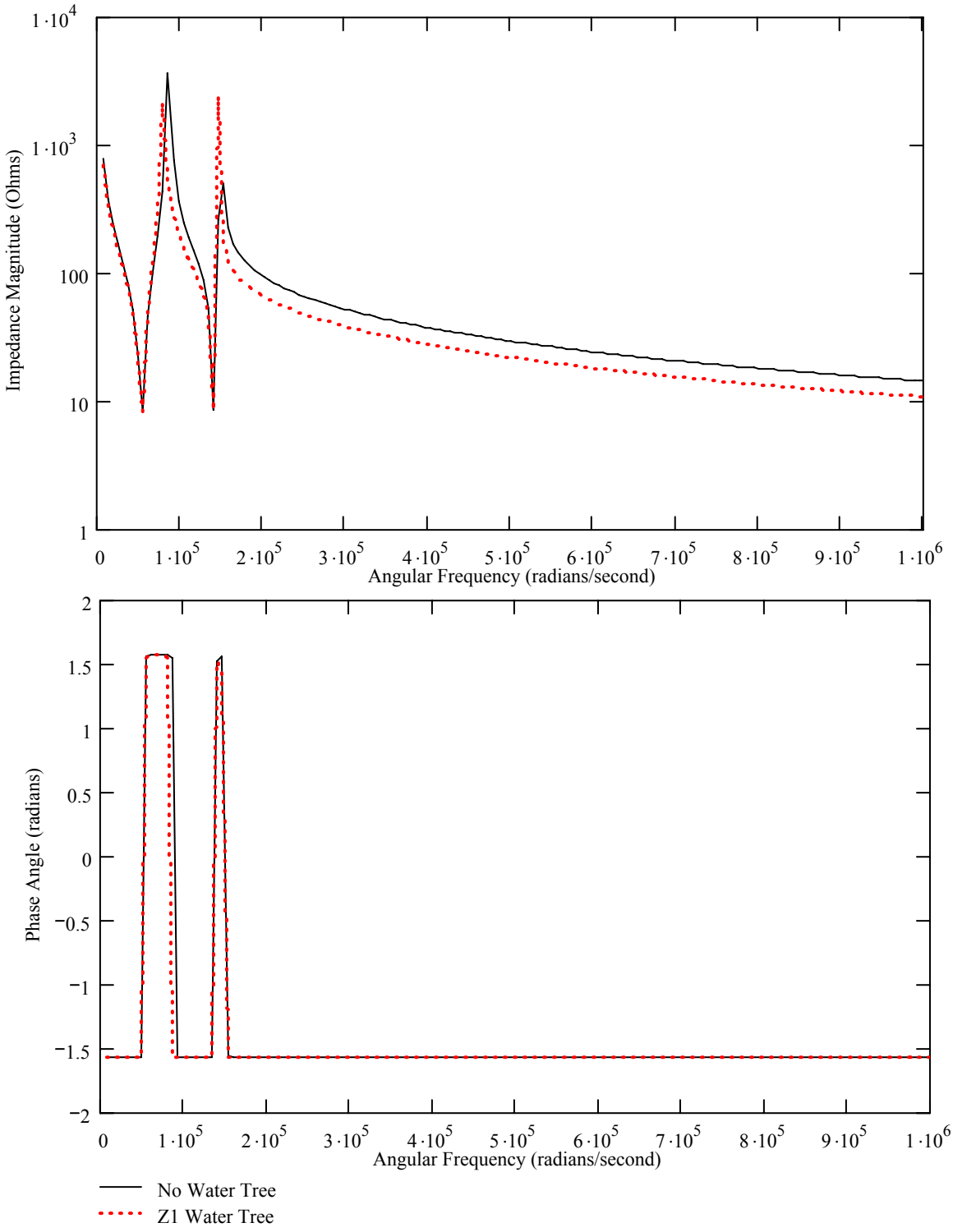

Figure E.36 Calculated Impedance Magnitude and Phase Angle vs Frequency 22 Impedance Element Model, L=1000 m, D=10.3 mm AL, 4.45 mm XLPE, Without vs With Z1 Water Tree

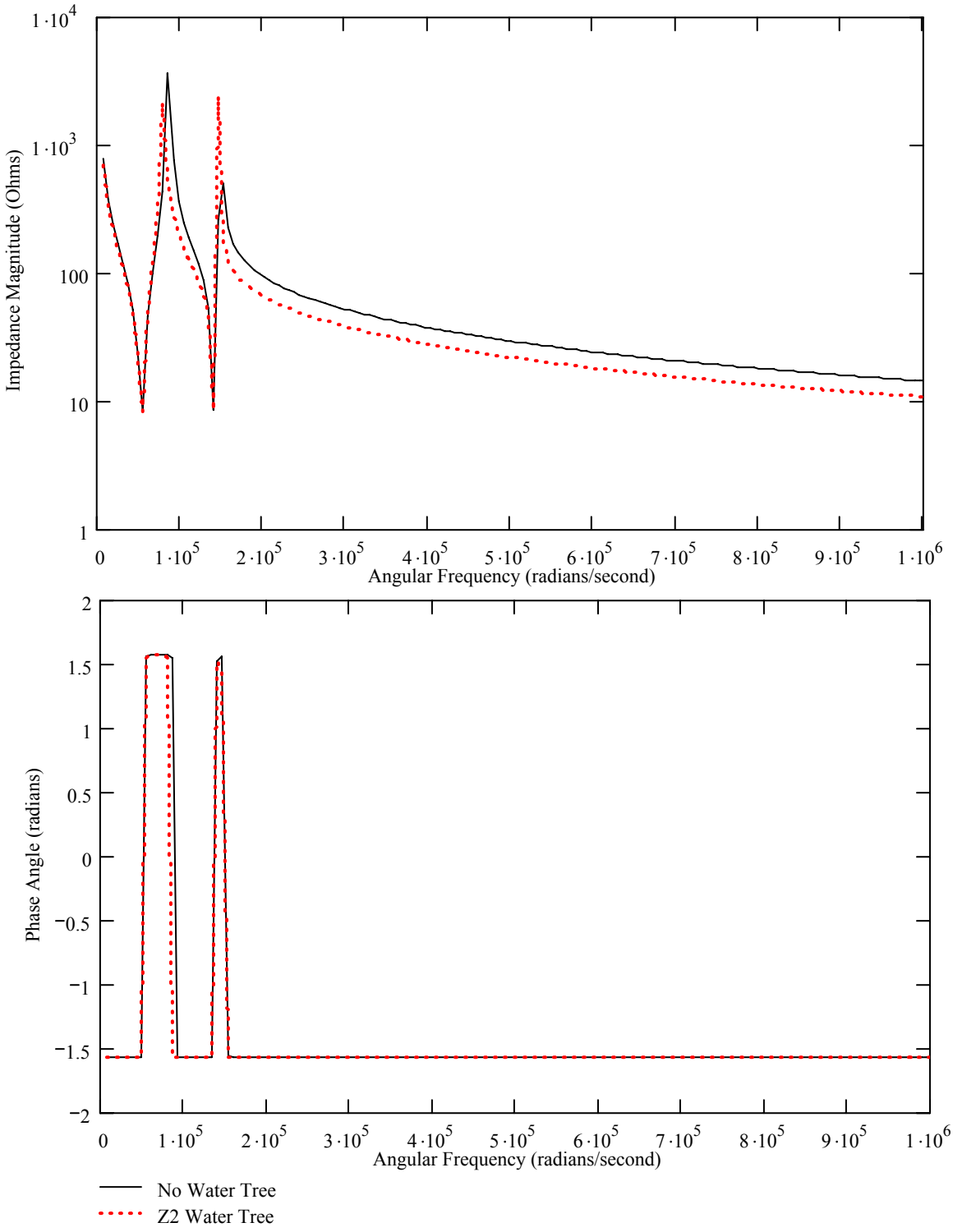

Figure E.37 Calculated Impedance Magnitude and Phase Angle vs Frequency 22 Impedance Element Model, L=1000 m, D=10.3 mm AL, 4.45 mm XLPE, Without vs With Z2 Water Tree

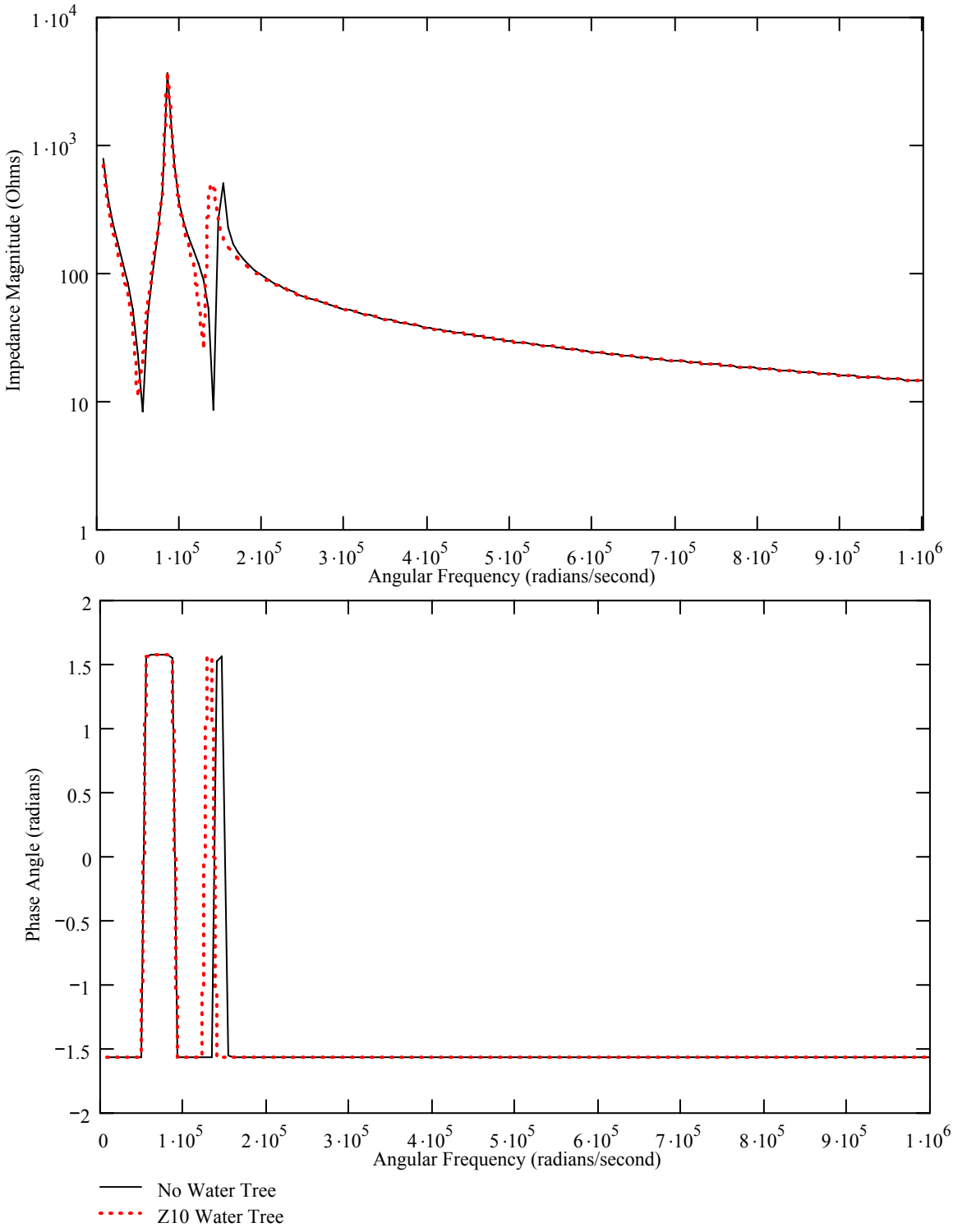

Figure E.38 Calculated Impedance Magnitude and Phase Angle vs Frequency 22 Impedance Element Model, L=1000 m, D=10.3 mm AL, 4.45 mm XLPE, Without vs With Z10 Water Tree

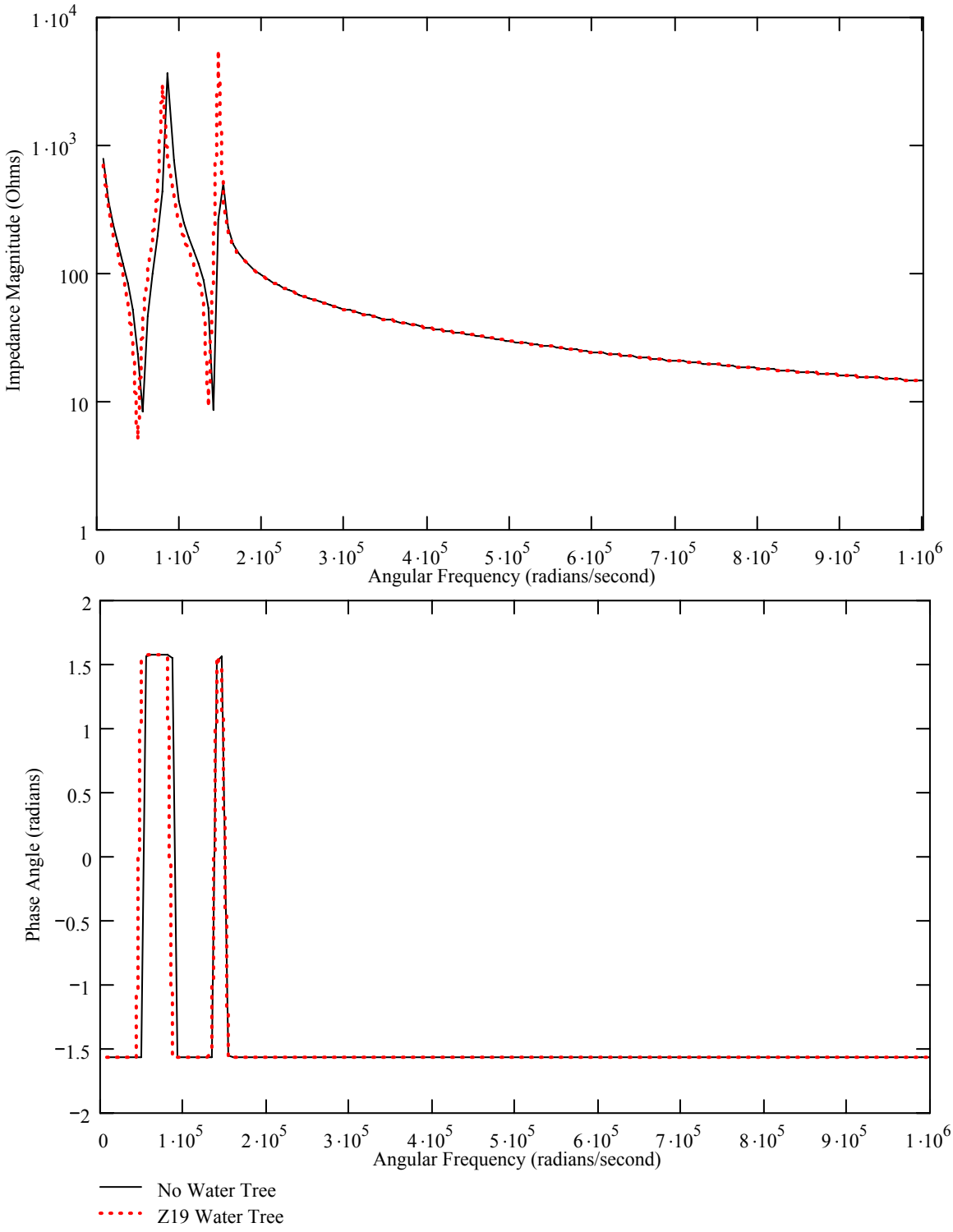

Figure E.39 Calculated Impedance Magnitude and Phase Angle vs Frequency 22 Impedance Element Model, L=1000 m, D=10.3 mm AL, 4.45 mm XLPE, Without vs With Z19 Water Tree

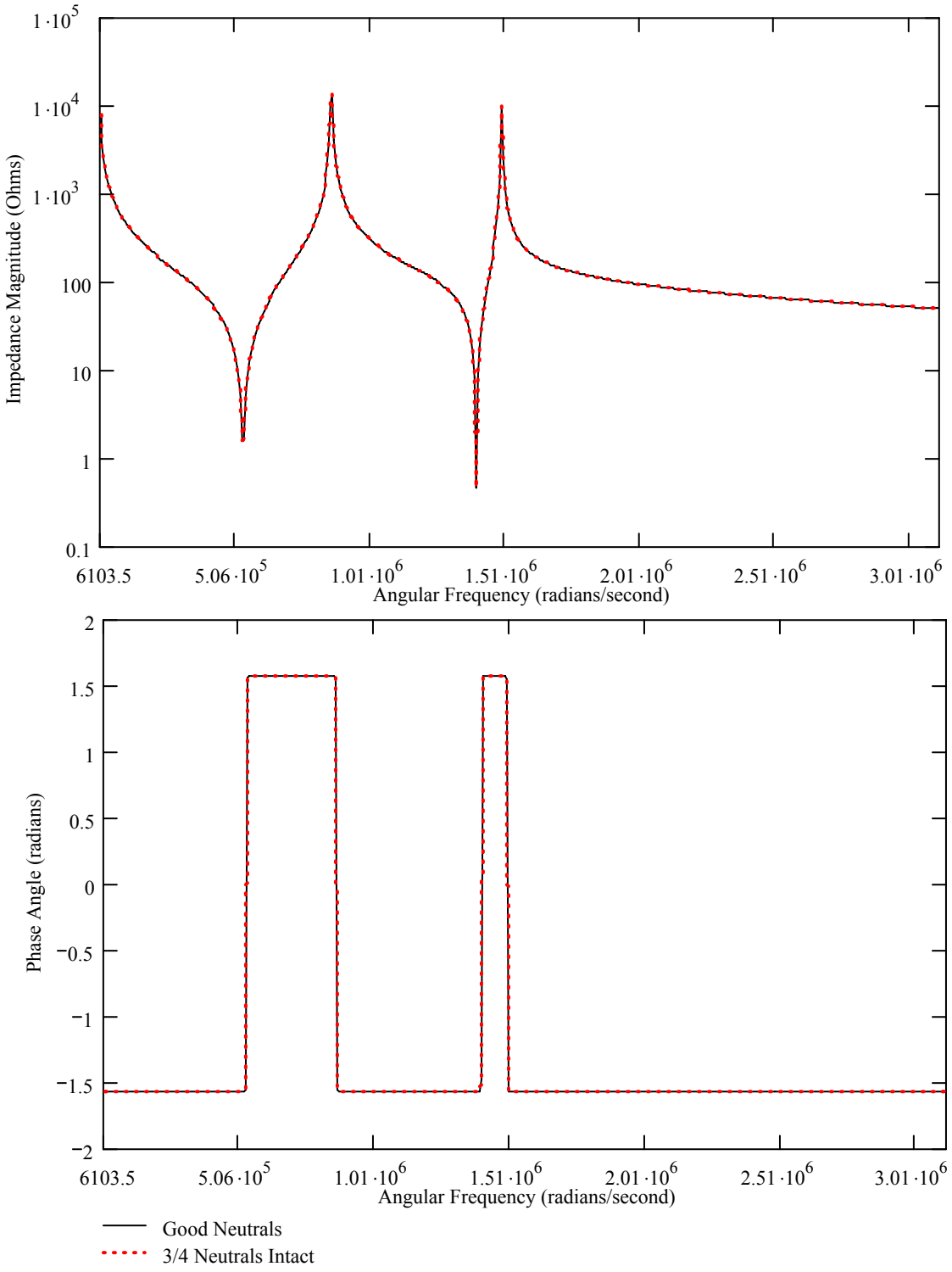

Figure E.40 Calculated Impedance Magnitude and Phase Angle vs Frequency
22 Impedance Element Model, L=100 m, D=10.3 mm AL, 4.45 mm XLPE,
Good Neutrals vs ¾ of Neutrals Intact

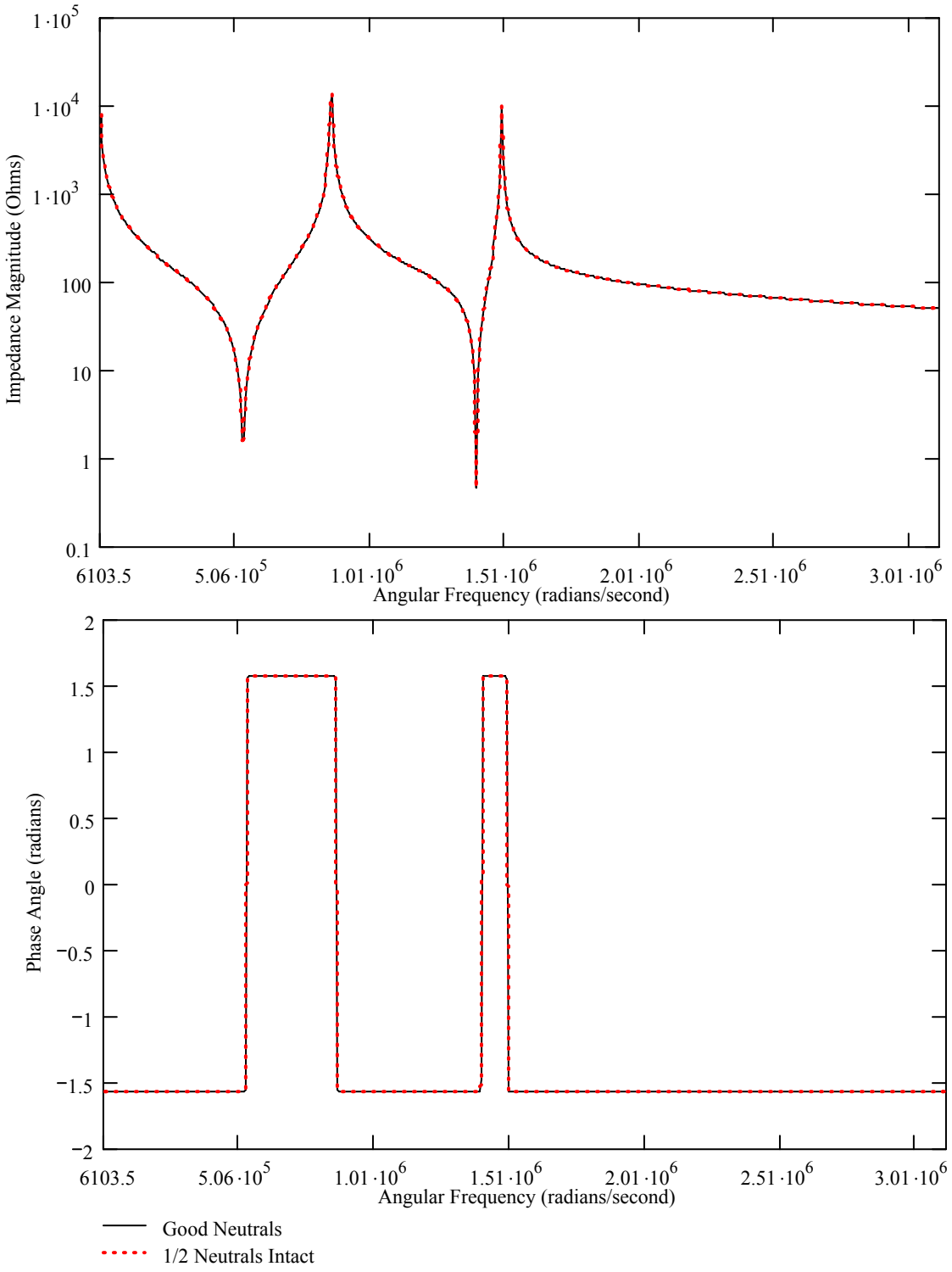

Figure E.41 Calculated Impedance Magnitude and Phase Angle vs Frequency
22 Impedance Element Model, L=100 m, D=10.3 mm AL, 4.45 mm XLPE,
Good Neutrals vs ½ of Neutrals Intact

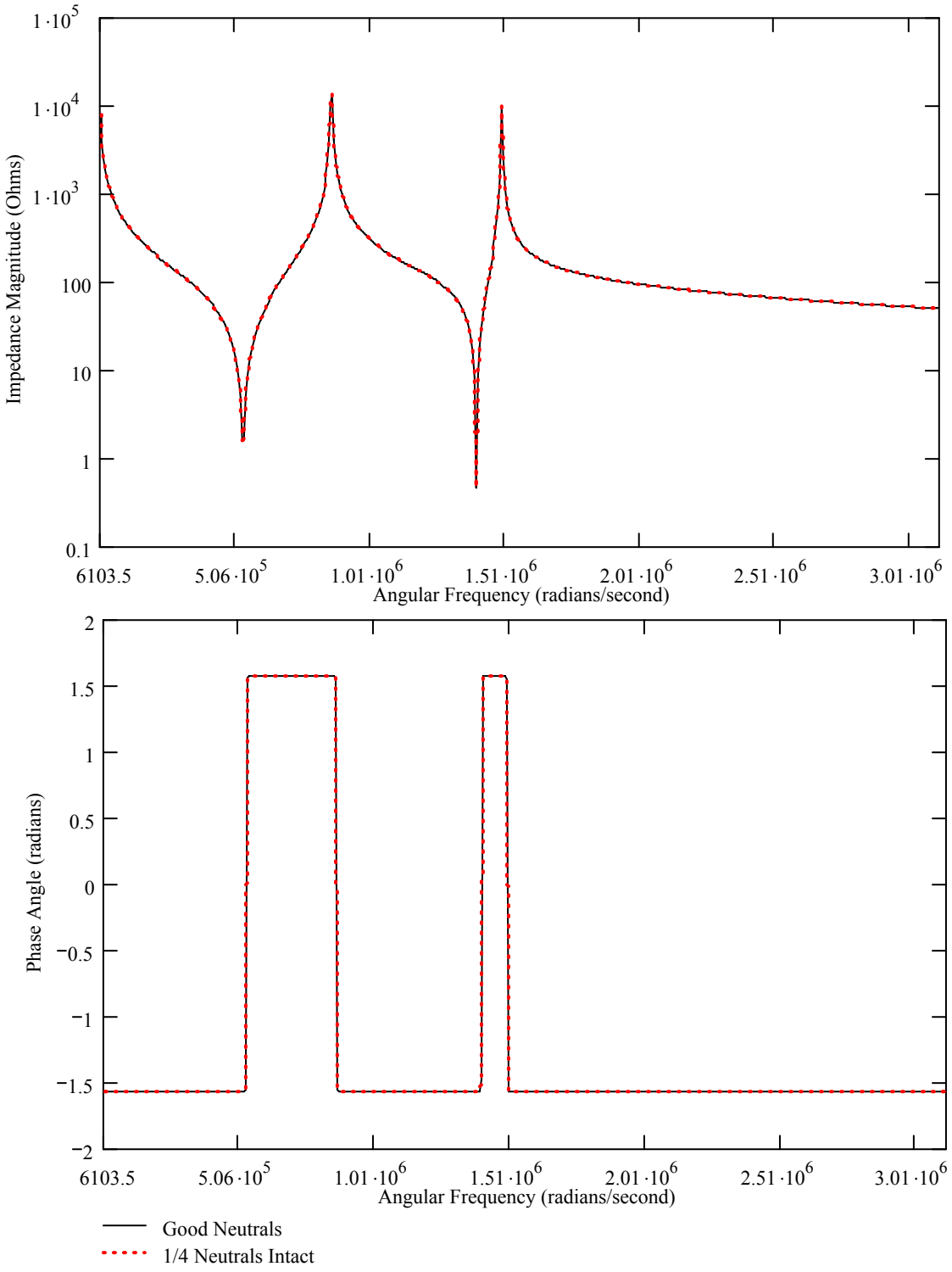

Figure E.42 Calculated Impedance Magnitude and Phase Angle vs Frequency
22 Impedance Element Model, L=100 m, D=10.3 mm AL, 4.45 mm XLPE,
Good Neutrals vs ¼ of Neutrals Intact

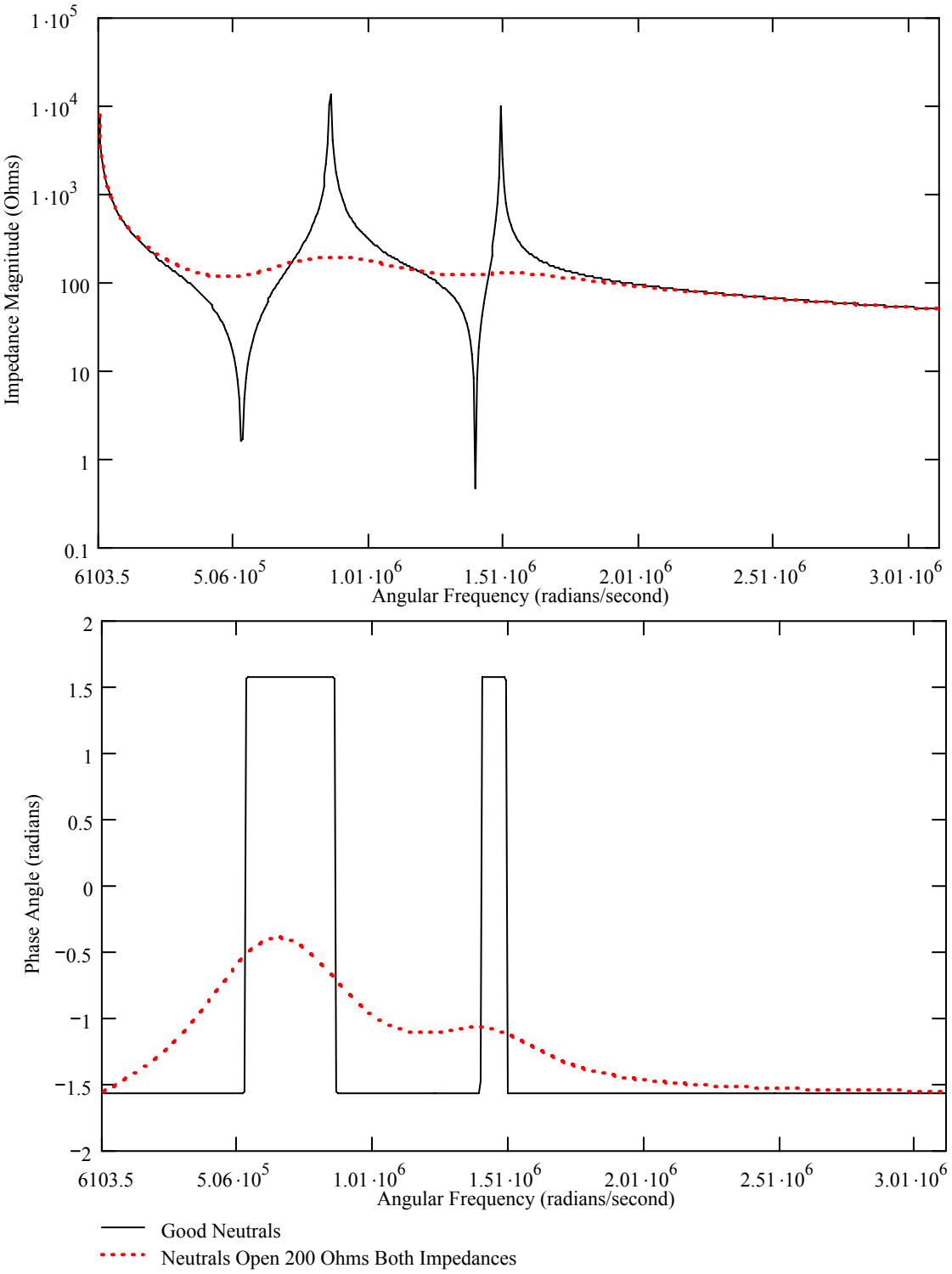

Figure E.43 Calculated Impedance Magnitude and Phase Angle vs Frequency
22 Impedance Element Model, L=100 m, D=10.3 mm AL, 4.45 mm XLPE,
Good Neutrals vs Neutrals Open, 200 Ω Both Impedances

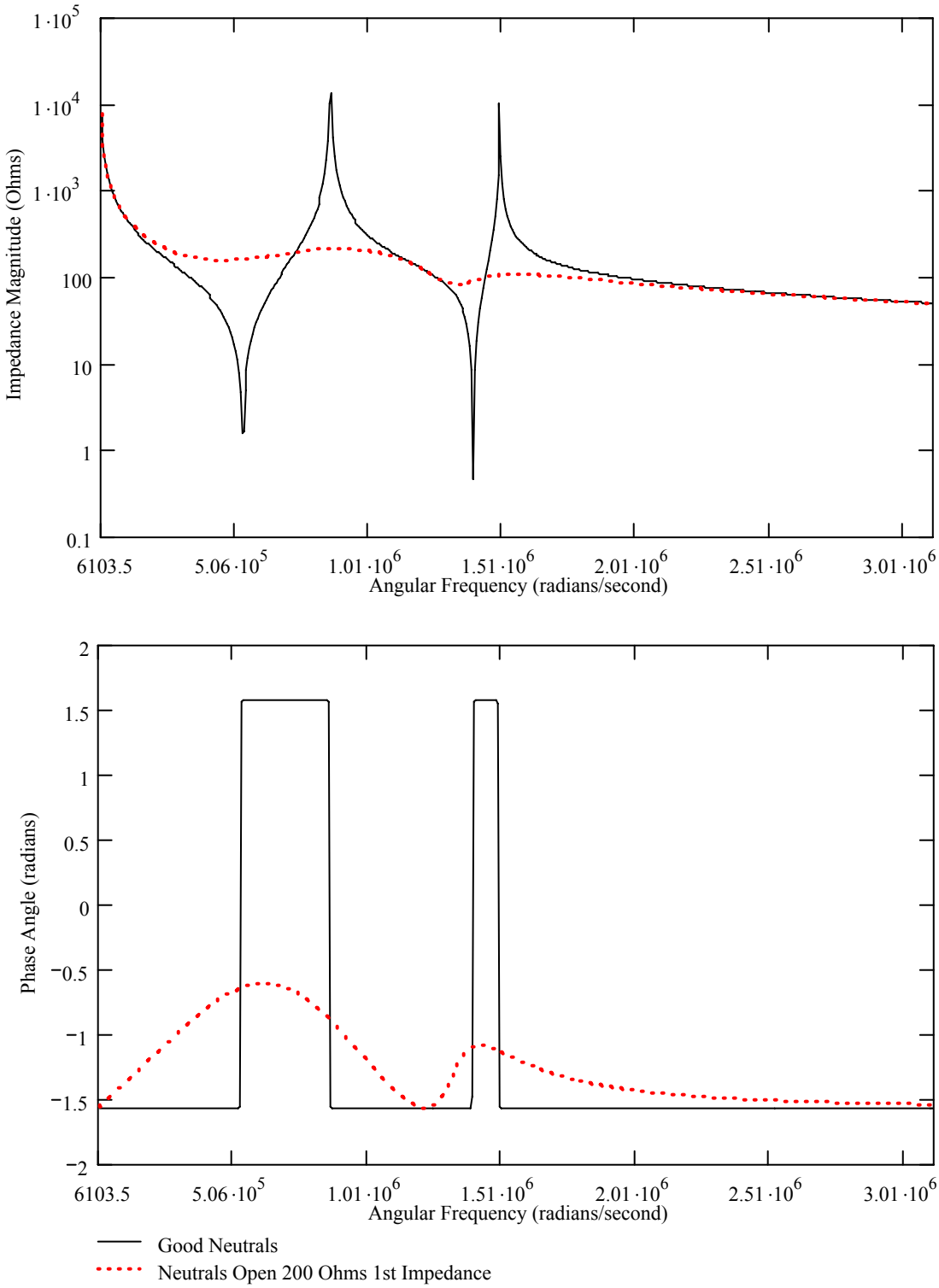

Figure E.44 Calculated Impedance Magnitude and Phase Angle vs Frequency
22 Impedance Element Model, L=100 m, D=10.3 mm AL, 4.45 mm XLPE,
Good Neutrals vs Neutrals Open, 200 Ω 1st Impedance

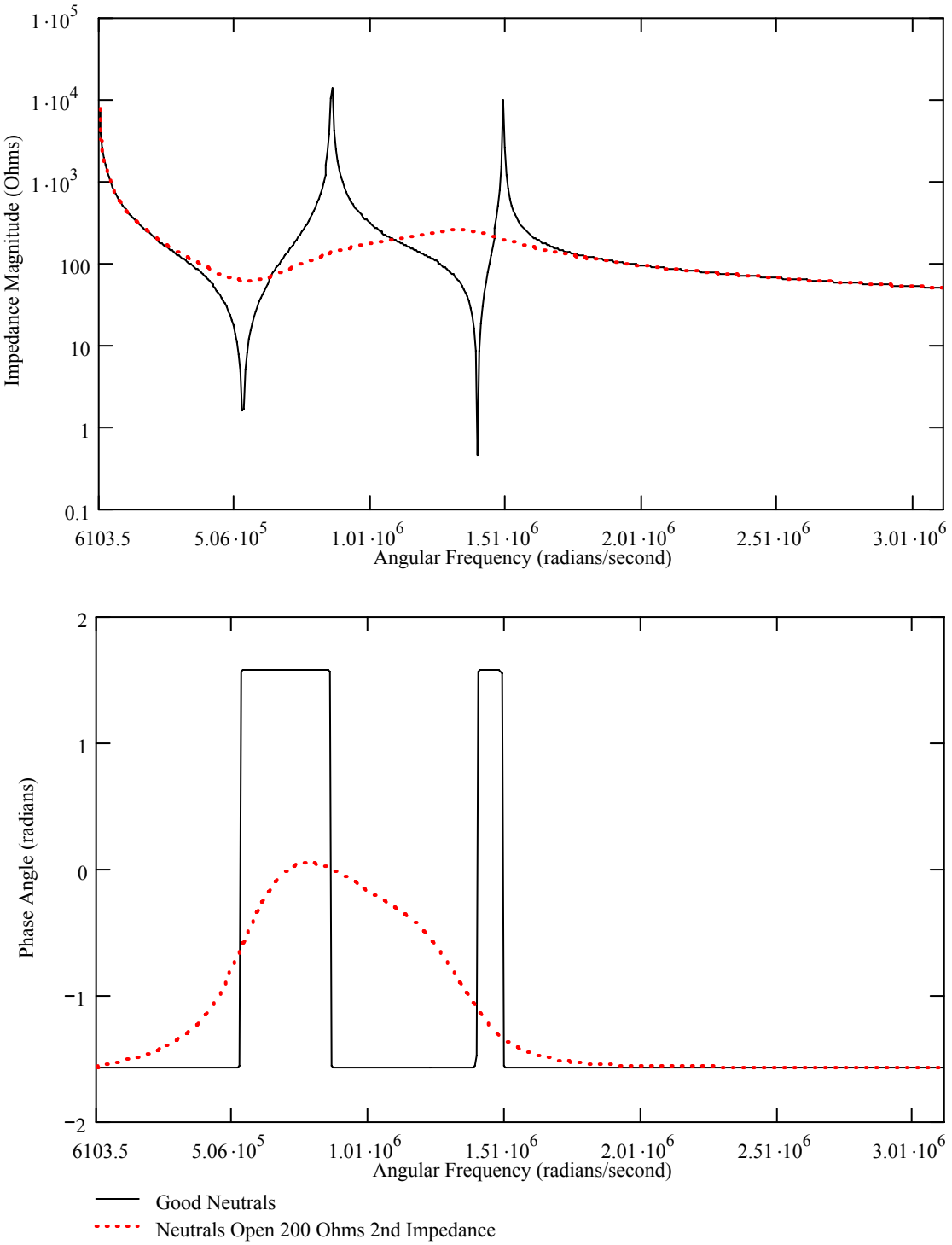

Figure E.45 Calculated Impedance Magnitude and Phase Angle vs Frequency
22 Impedance Element Model, L=100 m, D=10.3 mm AL, 4.45 mm XLPE,
Good Neutrals vs Neutrals Open, 200 Ω 2nd Impedance

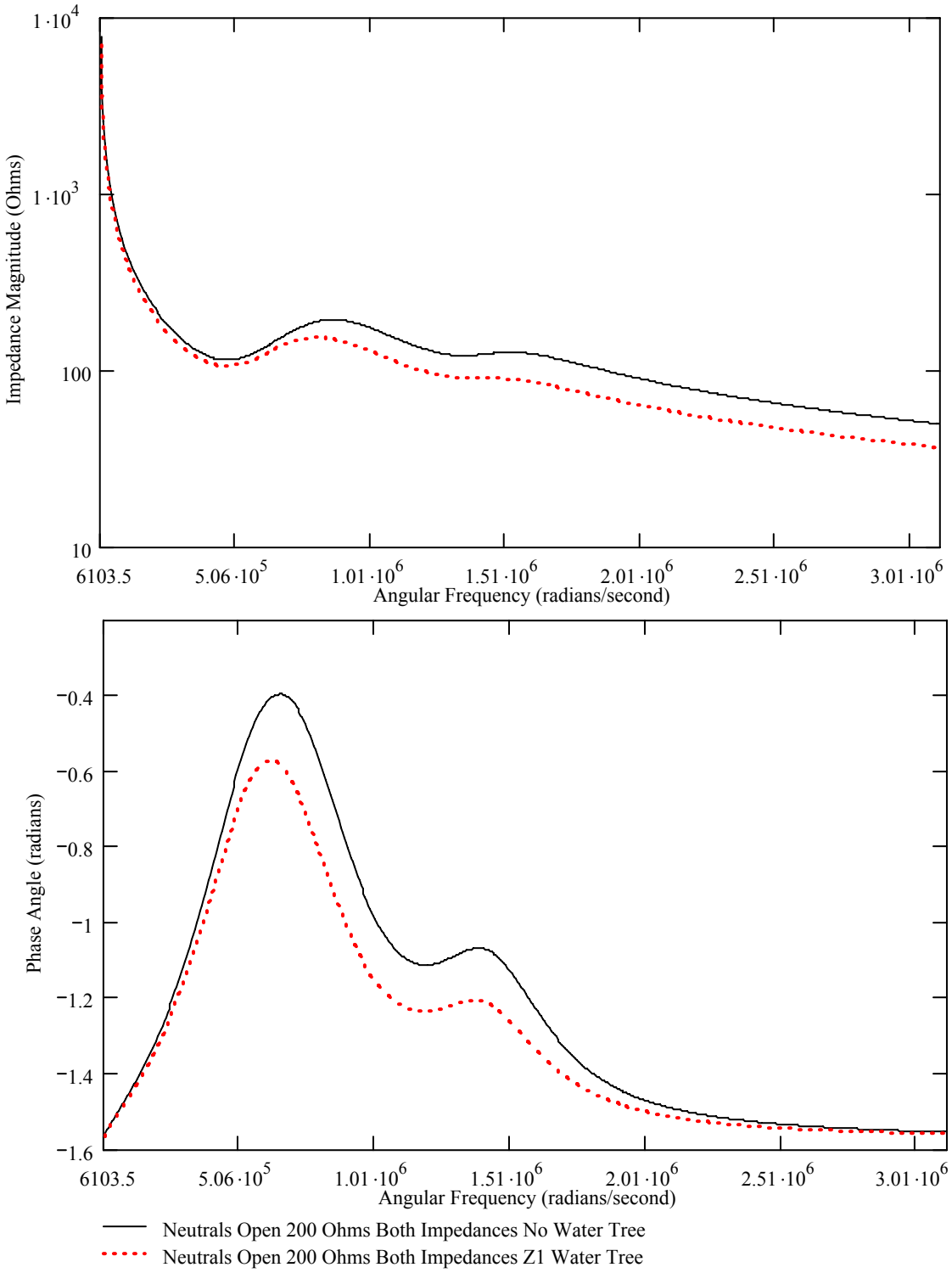

Figure E.46 Calculated Impedance Magnitude and Phase Angle vs Frequency
22 Impedance Element Model, L=100 m, D=10.3 mm AL, 4.45 mm XLPE,
Neutrals Open, 200 Ω Both Impedances, No Water Tree vs Z1 Water Tree

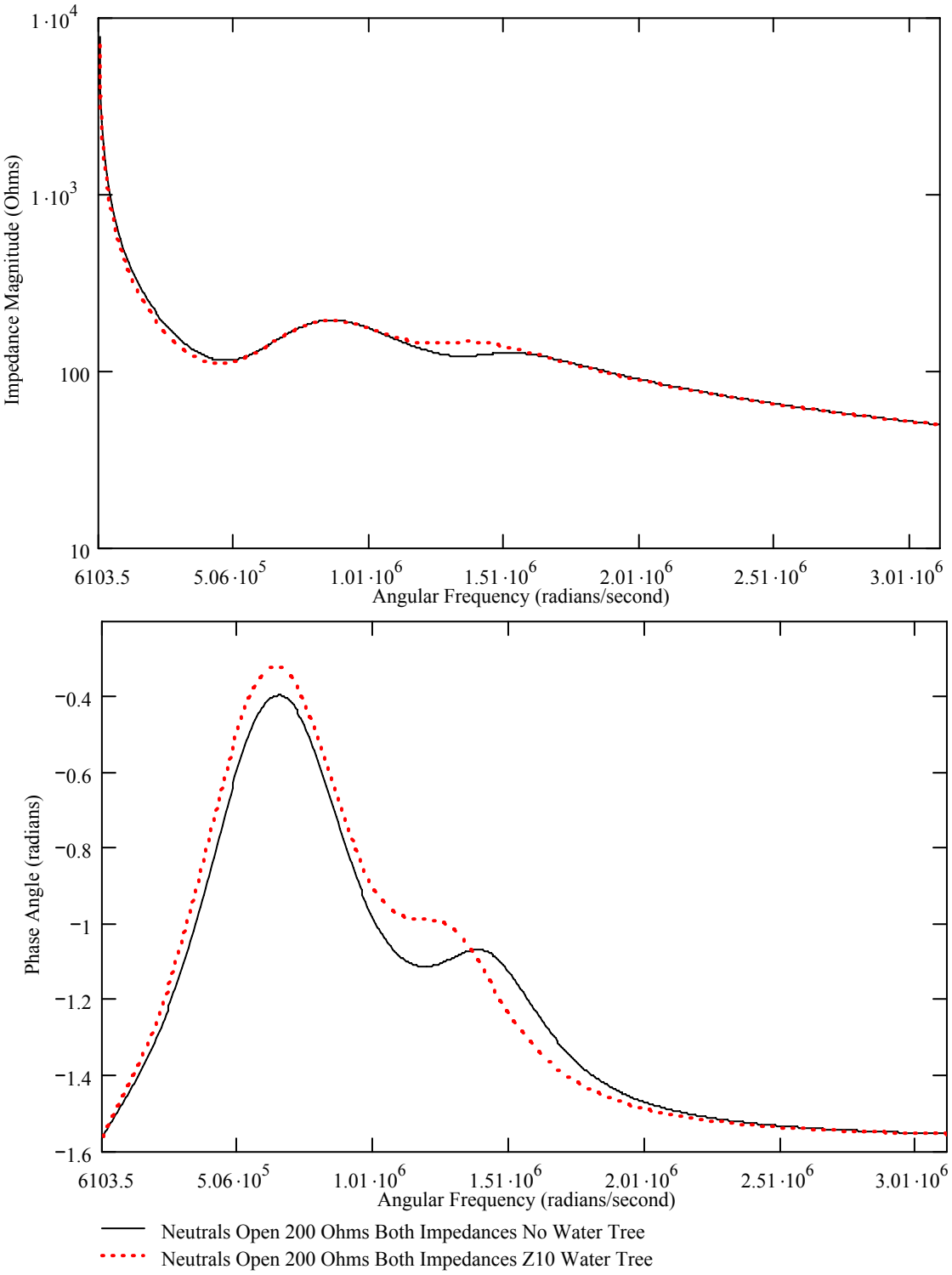

Figure E.47 Calculated Impedance Magnitude and Phase Angle vs Frequency
22 Impedance Element Model, L=100 m, D=10.3 mm AL, 4.45 mm XLPE,
Neutrals Open, 200 Ω Both Impedances, No Water Tree vs Z10 Water Tree

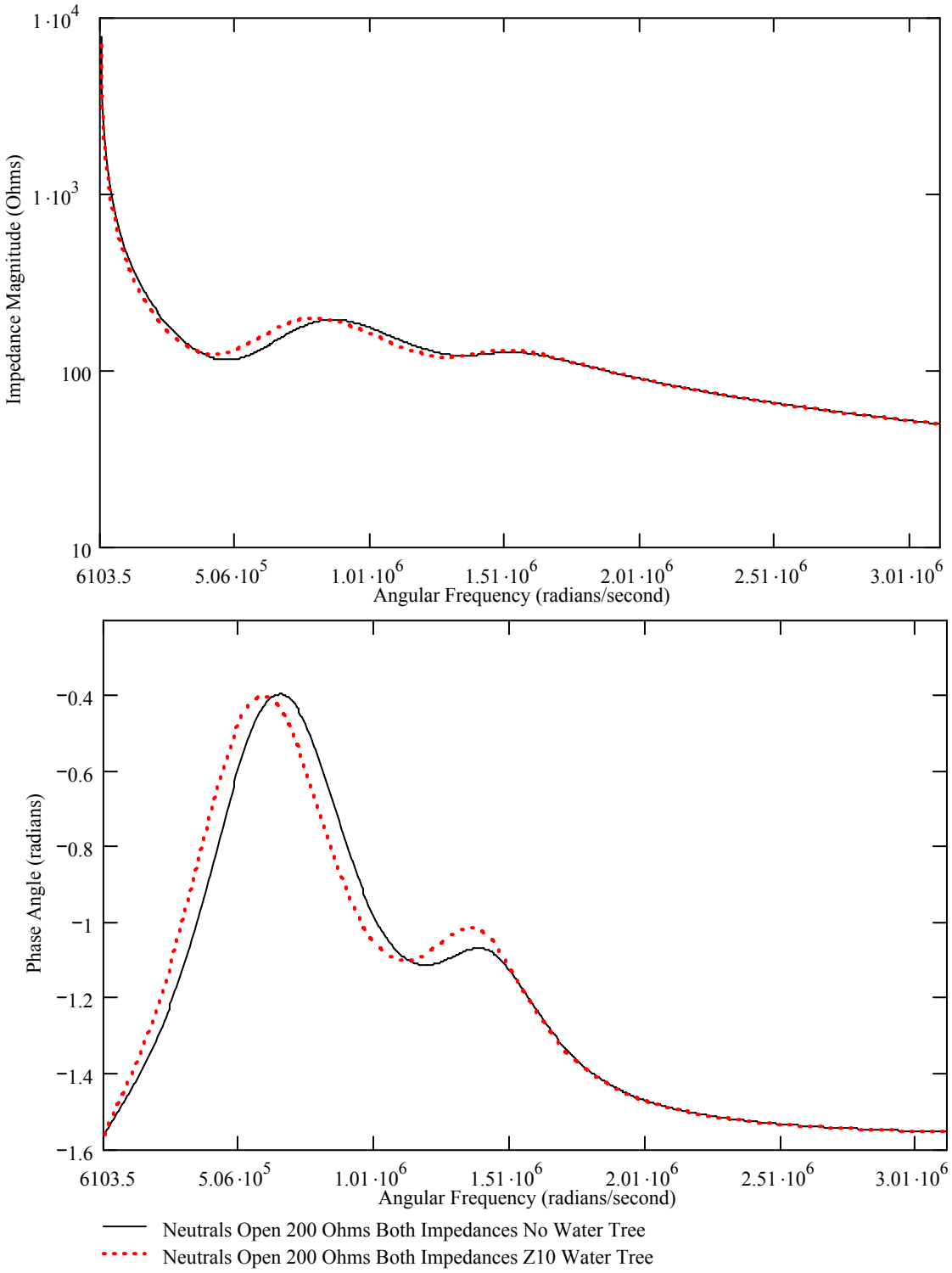

Figure E.48 Calculated Impedance Magnitude and Phase Angle vs Frequency
22 Impedance Element Model, L=100 m, D=10.3 mm AL, 4.45 mm XLPE,
Neutrals Open, 200 Ω Both Impedances, No Water Tree vs Z19 Water Tree

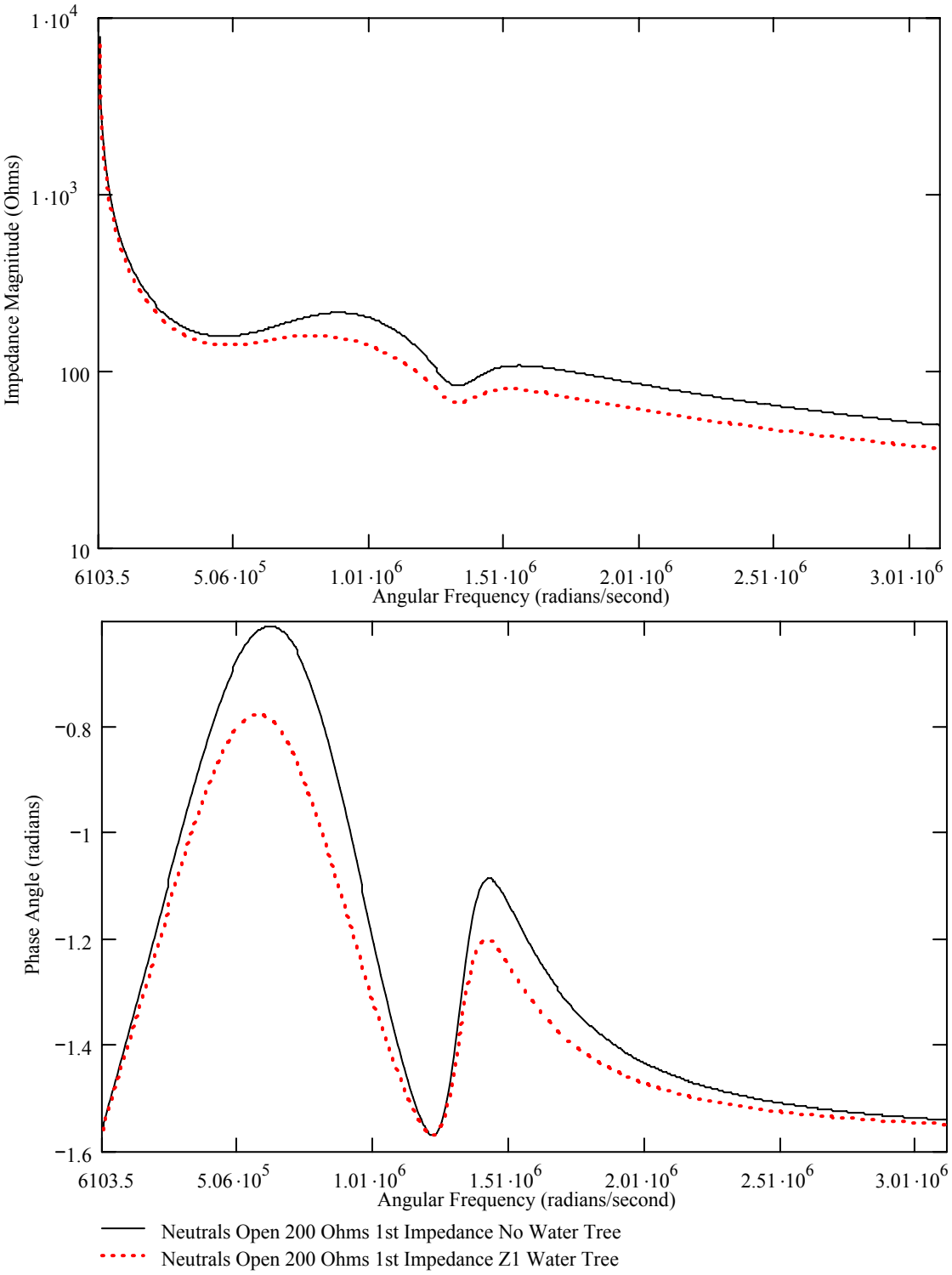

Figure E.49 Calculated Impedance Magnitude and Phase Angle vs Frequency
22 Impedance Element Model, L=100 m, D=10.3 mm AL, 4.45 mm XLPE,
Neutrals Open, 200 Ω 1st Impedances, No Water Tree vs Z1 Water Tree

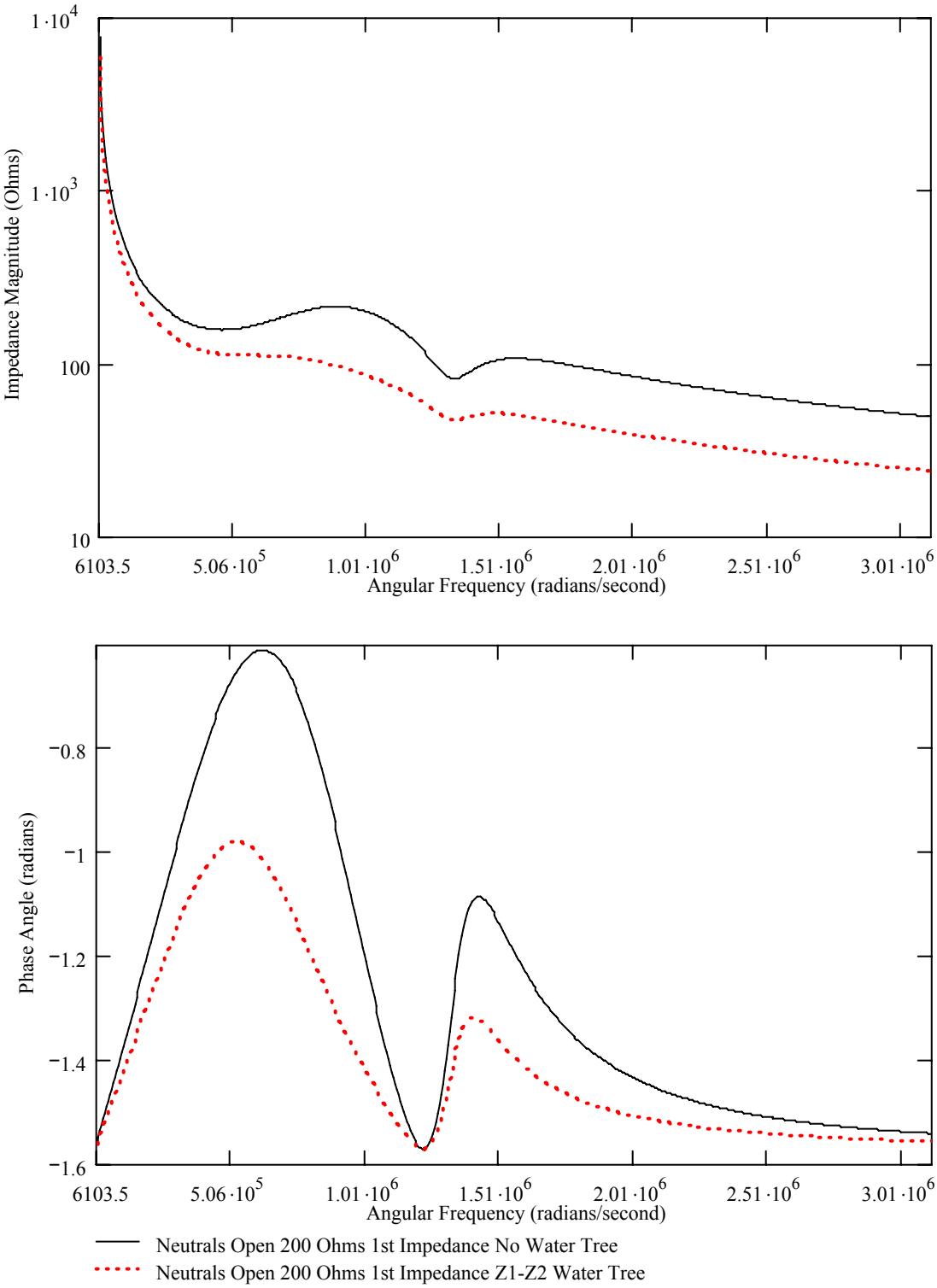

Figure E.50 Calculated Impedance Magnitude and Phase Angle vs Frequency
22 Impedance Element Model, L=100 m, D=10.3 mm AL, 4.45 mm XLPE,
Neutrals Open, 200 Ω 1st Impedances, No Water Tree vs Z1-Z2 Water Tree

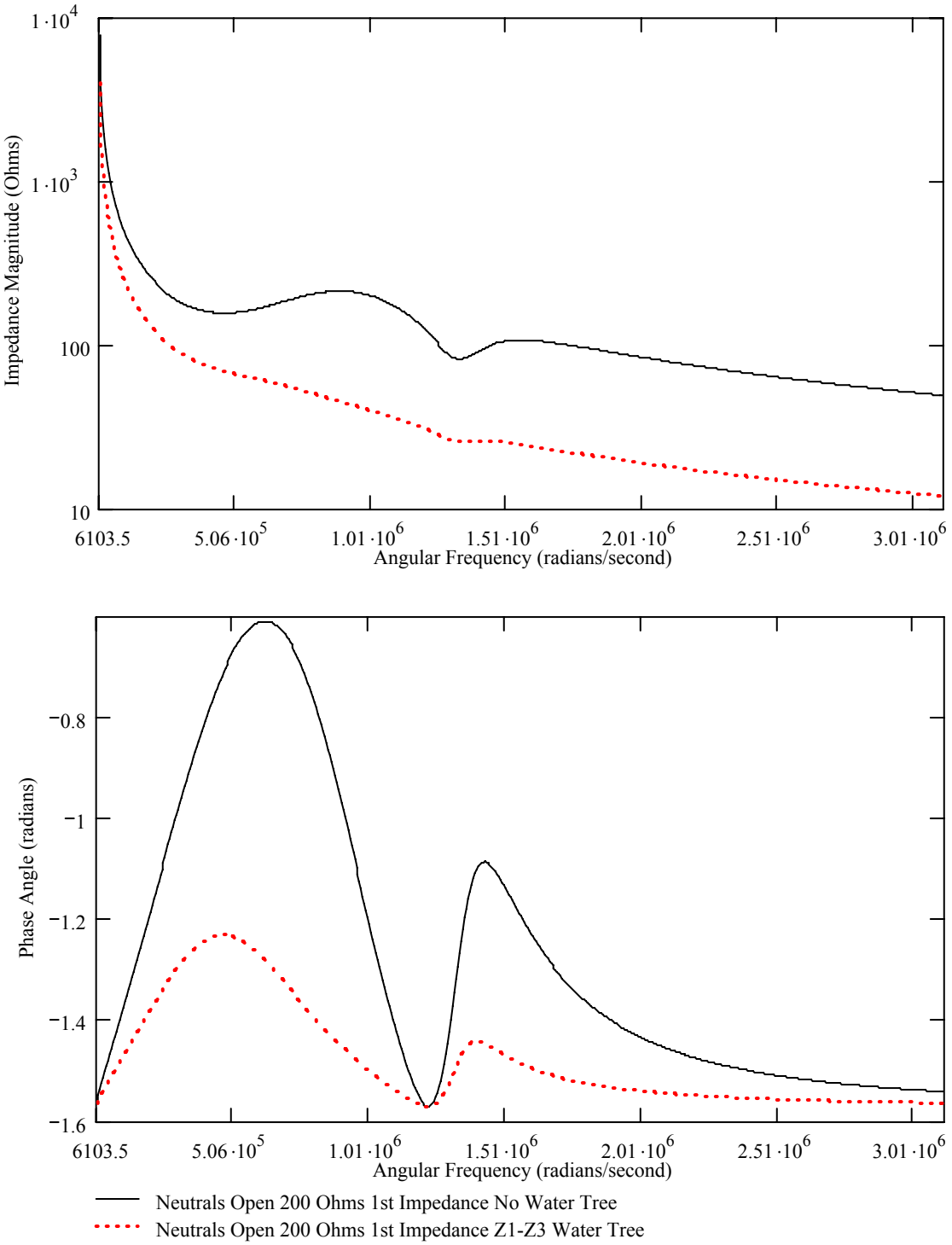

Figure E.51 Calculated Impedance Magnitude and Phase Angle vs Frequency
22 Impedance Element Model, L=100 m, D=10.3 mm AL, 4.45 mm XLPE,
Neutrals Open, 200 Ω 1st Impedances, No Water Tree vs Z1-Z3 Water Tree

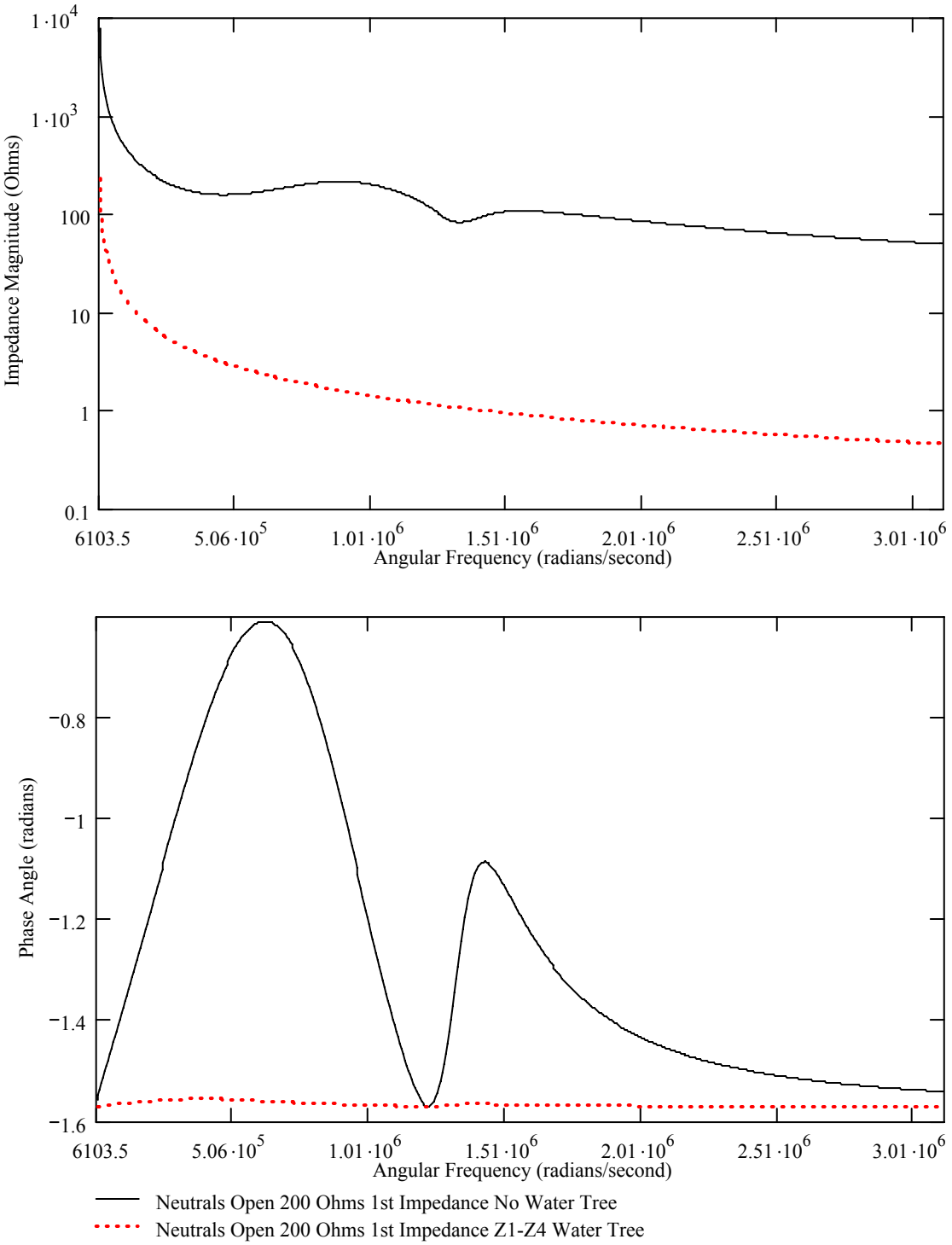

Figure E.52 Calculated Impedance Magnitude and Phase Angle vs Frequency
22 Impedance Element Model, L=100 m, D=10.3 mm AL, 4.45 mm XLPE,
Neutrals Open, 200 Ω 1st Impedances, No Water Tree vs Z1-Z4 Water Tree

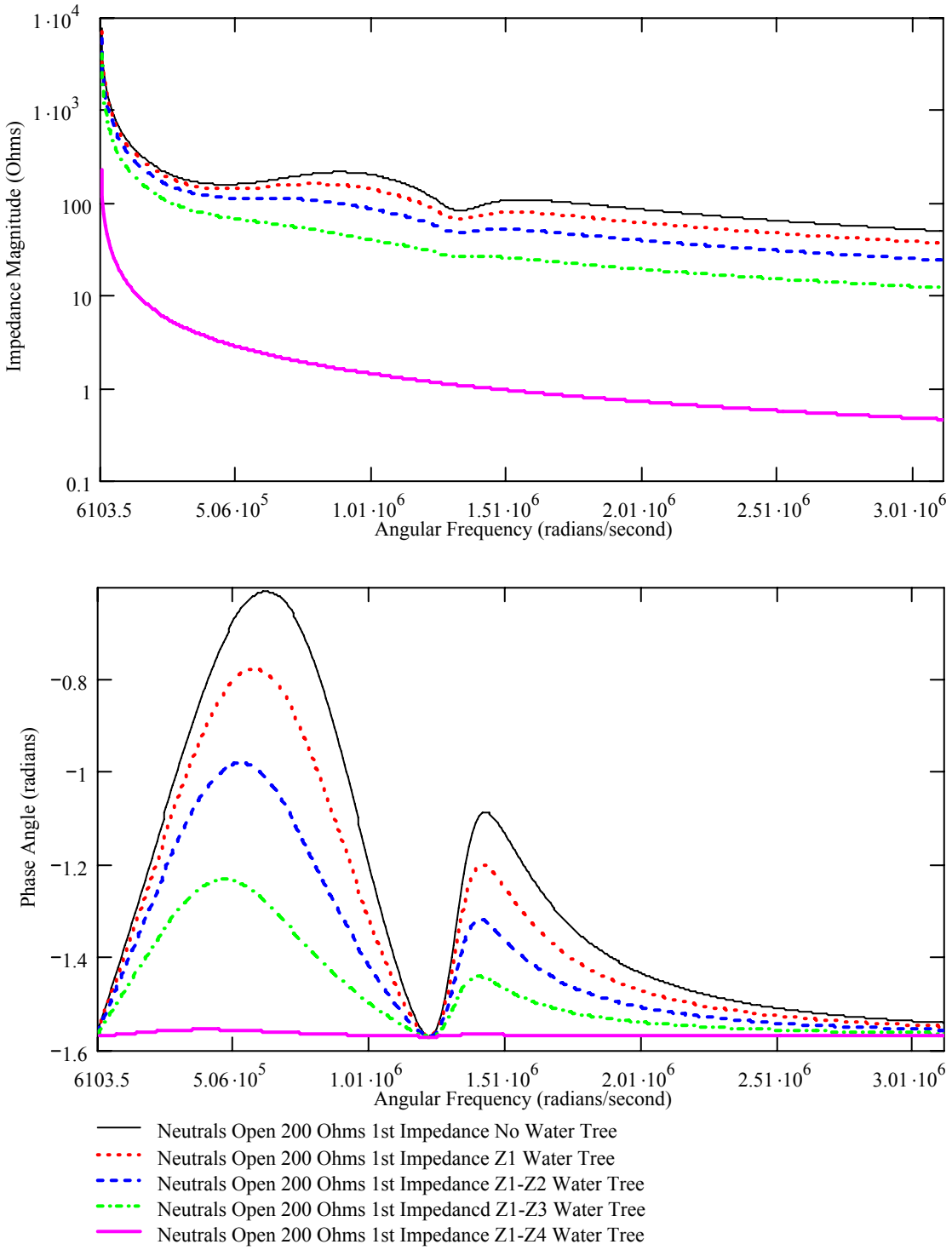

Figure E.53 Calculated Impedance Magnitude and Phase Angle vs Frequency
22 Impedance Element Model, L=100 m, D=10.3 mm AL, 4.45 mm XLPE,
Neutrals Open, 200 Ω 1st Impedances, No Water Tree vs Water Trees

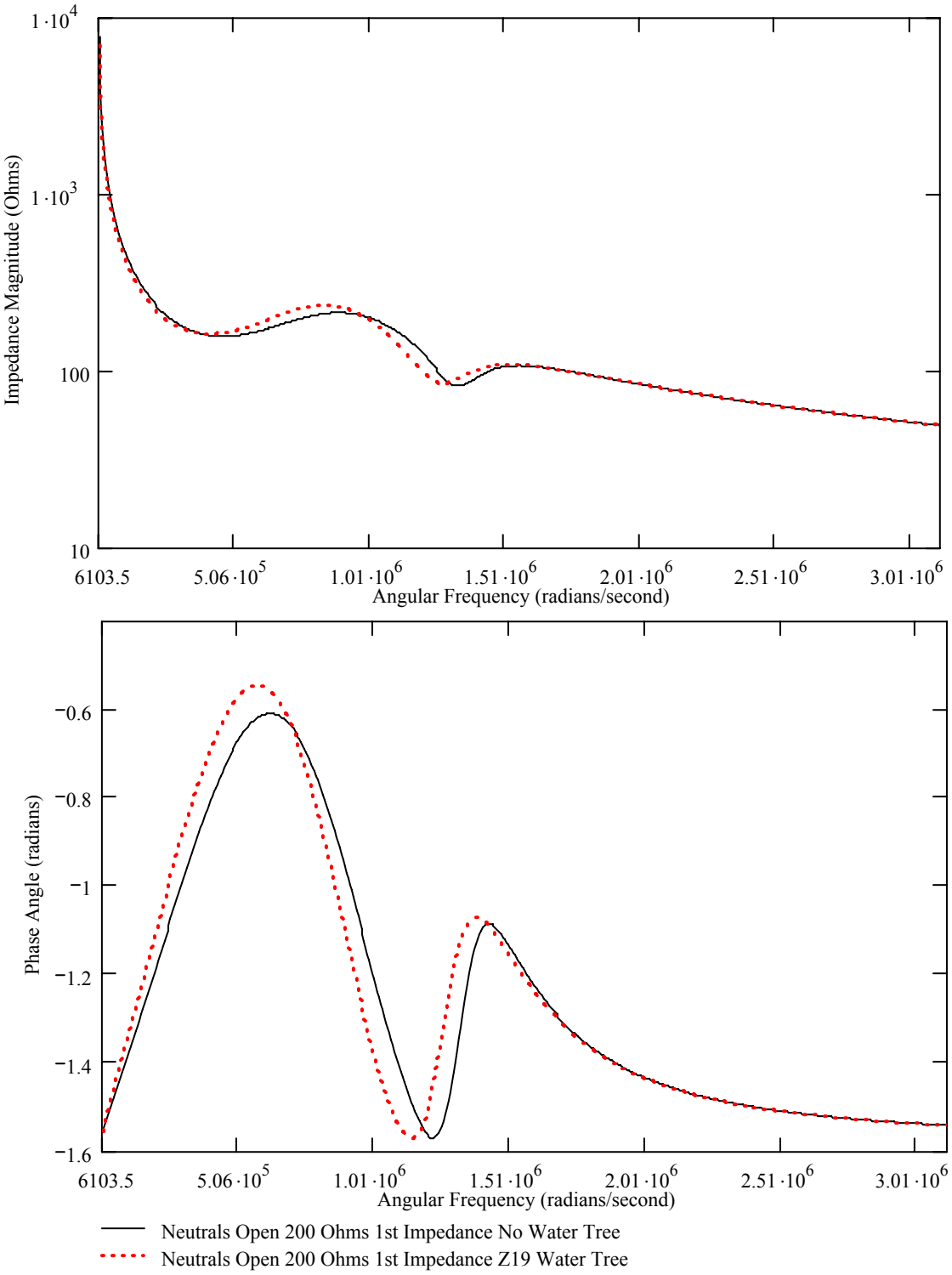

Figure E.54 Calculated Impedance Magnitude and Phase Angle vs Frequency
22 Impedance Element Model, L=100 m, D=10.3 mm AL, 4.45 mm XLPE,
Neutral Open, 200 Ω 1st Impedance, No Water Tree vs Z19 Water Tree

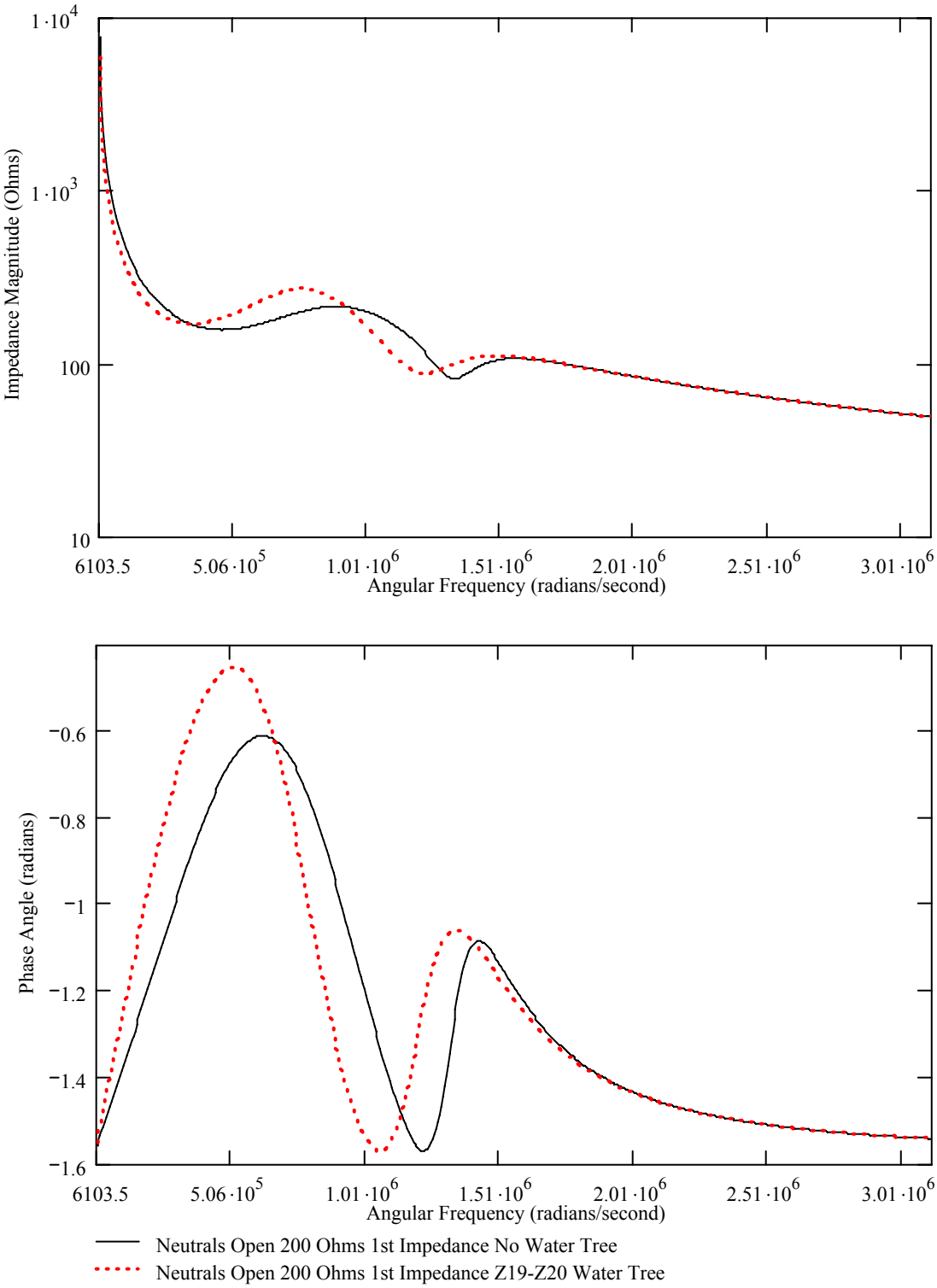

Figure E.55 Calculated Impedance Magnitude and Phase Angle vs Frequency
22 Impedance Element Model, L=100 m, D=10.3 mm AL, 4.45 mm XLPE,
Neutral Open, 200 Ω 1st Impedance, No Water Tree vs Z19-Z20 Water Tree

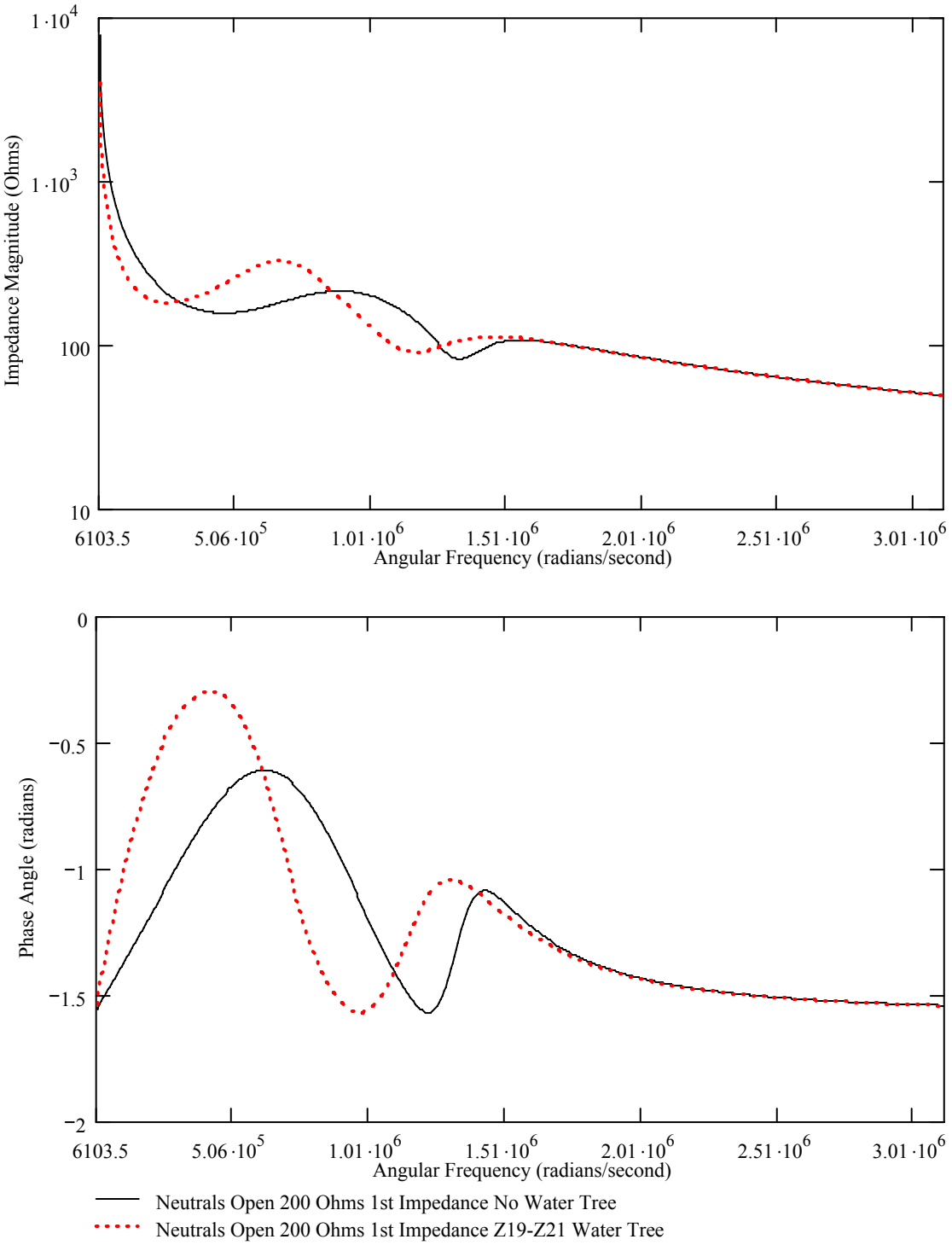

Figure E.56 Calculated Impedance Magnitude and Phase Angle vs Frequency
22 Impedance Element Model, L=100 m, D=10.3 mm AL, 4.45 mm XLPE,
Neutral Open, 200 Ω 1st Impedance, No Water Tree vs Z19-Z21 Water Tree

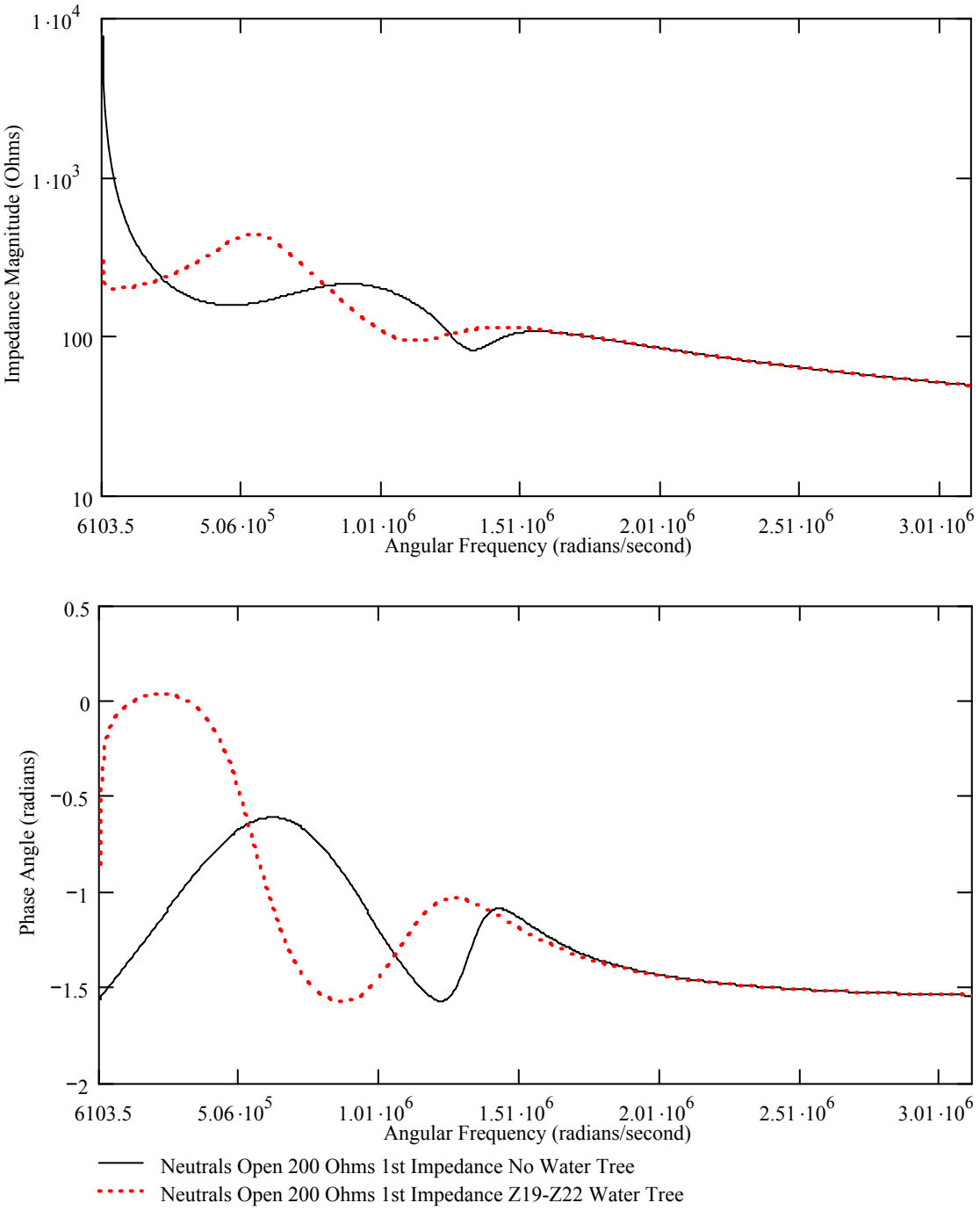

Figure E.57 Calculated Impedance Magnitude and Phase Angle vs Frequency
22 Impedance Element Model, L=100 m, D=10.3 mm AL, 4.45 mm XLPE,
Neutral Open, 200 Ω 1st Impedance, No Water Tree vs Z19-Z22 Water Tree

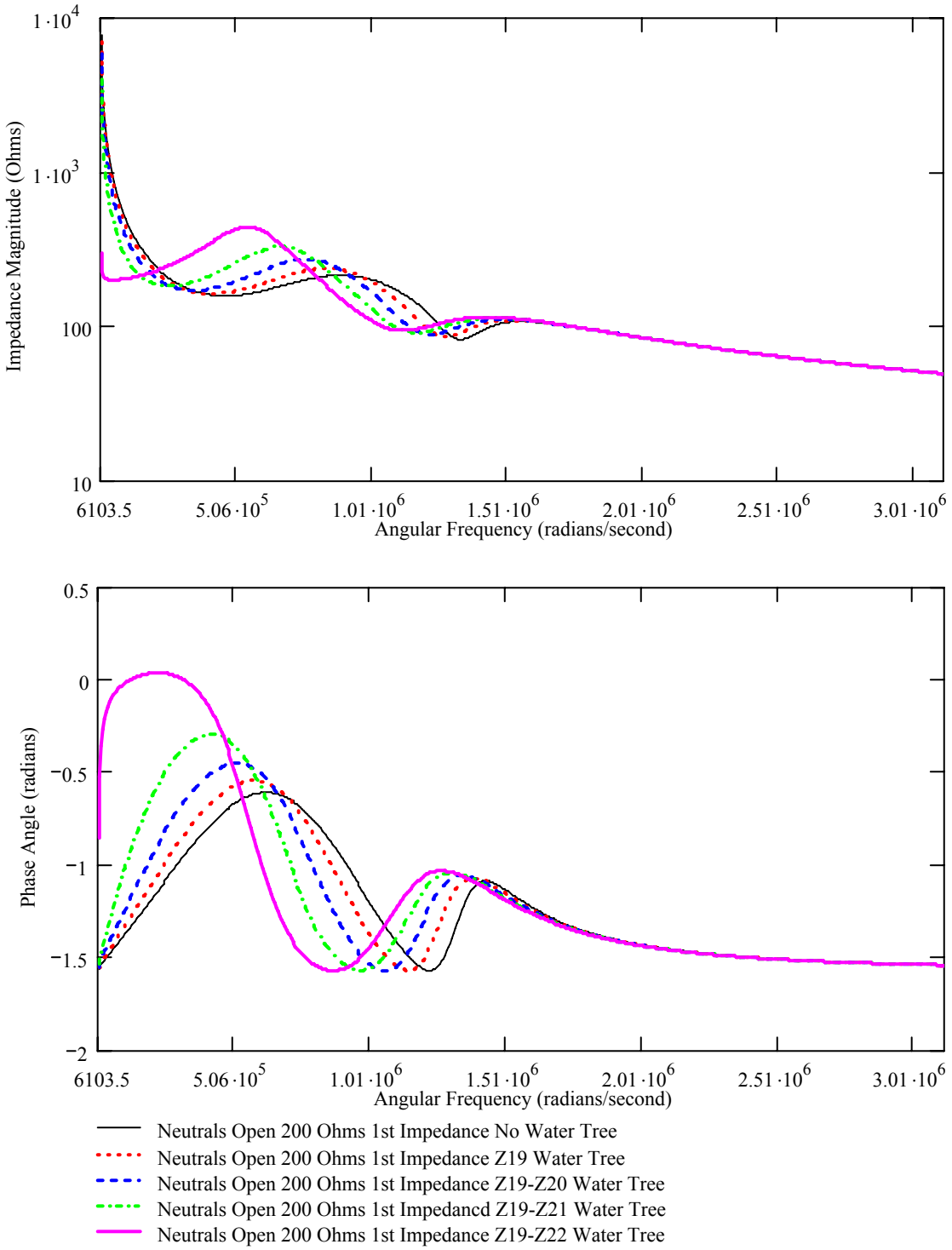

Figure E.58 Calculated Impedance Magnitude and Phase Angle vs Frequency 22 Impedance Element Model, L=100 m, D=10.3 mm AL, 4.45 mm XLPE, Neutral Open, 200 Ω 1st Impedance, No Water Tree vs Water Trees

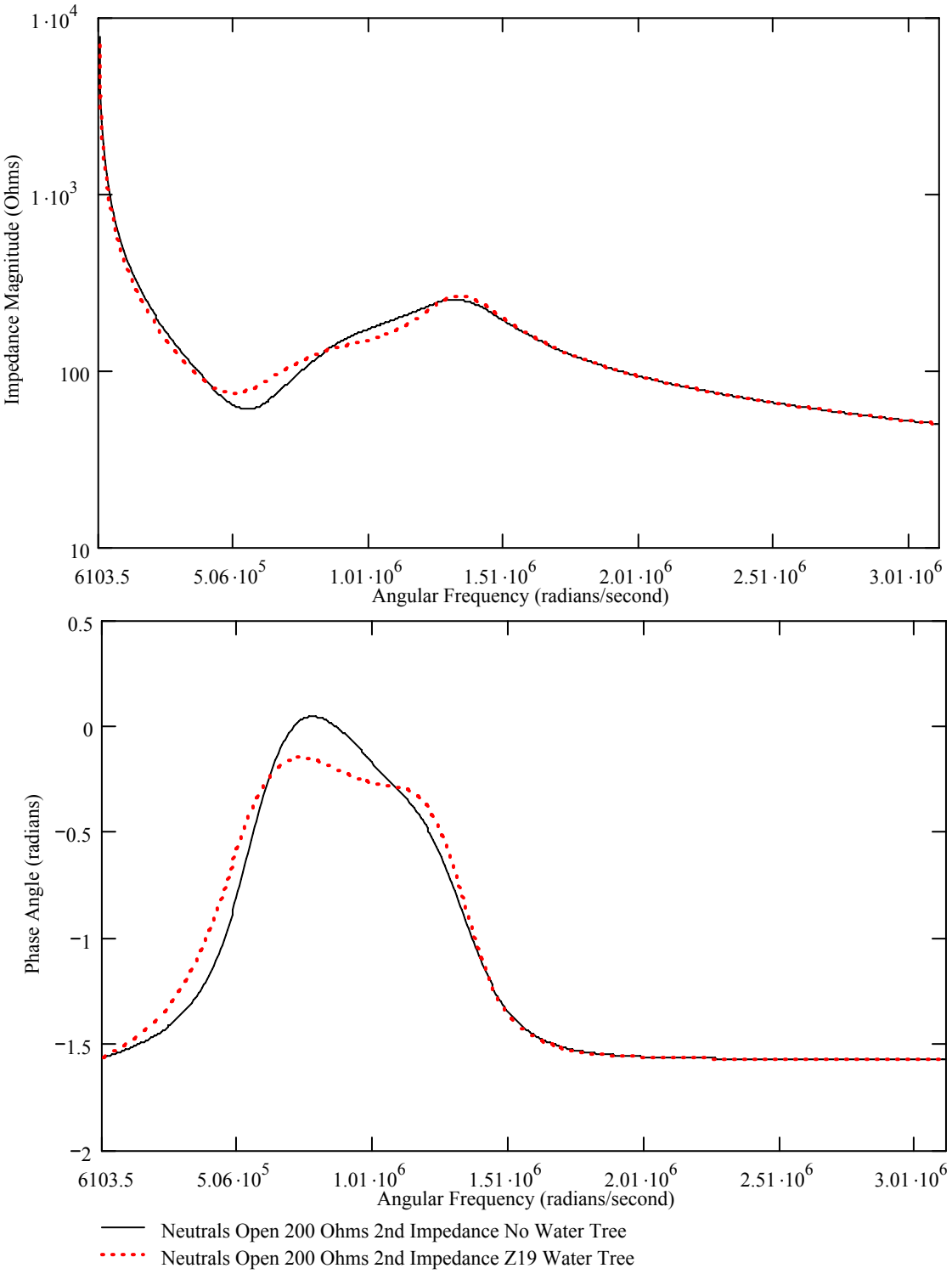

Figure E.59 Calculated Impedance Magnitude and Phase Angle vs Frequency
22 Impedance Element Model, L=100 m, D=10.3 mm AL, 4.45 mm XLPE,
Neutral Open, 200 Ω 2nd Impedance, No Water Tree vs Z19 Water Tree

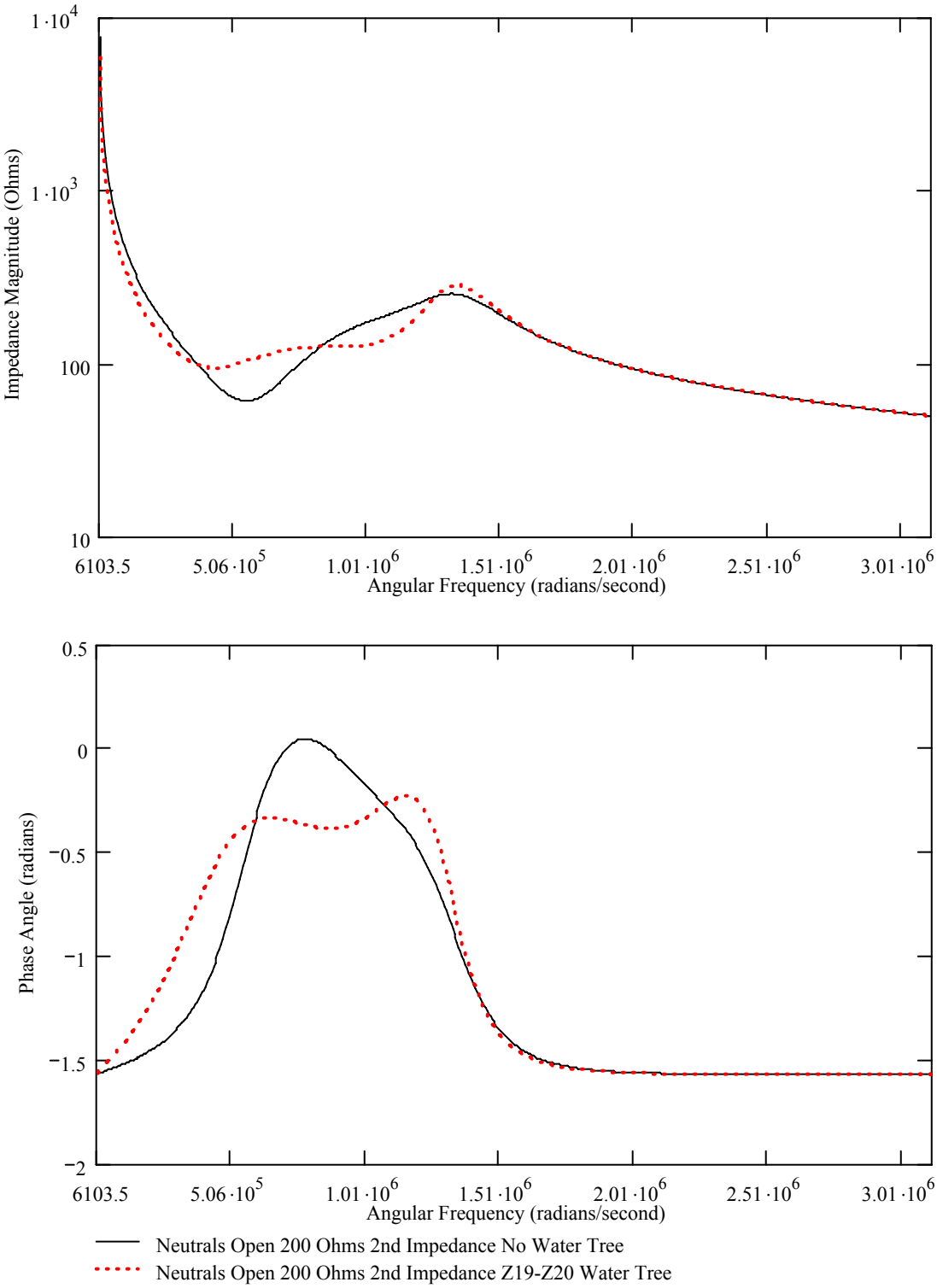

Figure E.60 Calculated Impedance Magnitude and Phase Angle vs Frequency
22 Impedance Element Model, L=100 m, D=10.3 mm AL, 4.45 mm XLPE,
Neutral Open, 200 Ω 2nd Impedance, No Water Tree vs Z19-Z20 Water Tree

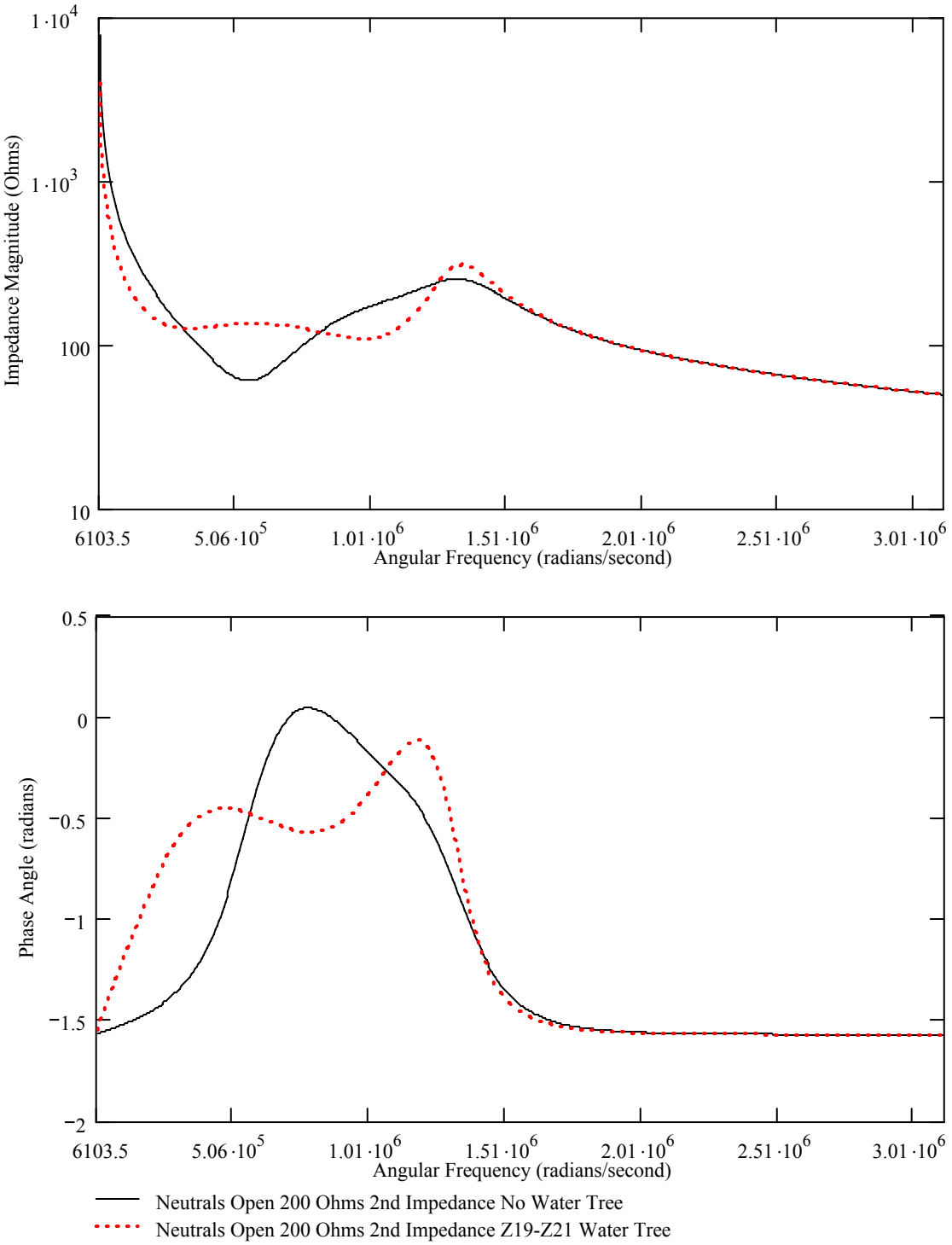

Figure E.61 Calculated Impedance Magnitude and Phase Angle vs Frequency
22 Impedance Element Model, L=100 m, D=10.3 mm AL, 4.45 mm XLPE,
Neutral Open, 200 Ω 2nd Impedance, No Water Tree vs Z19-Z21 Water Tree

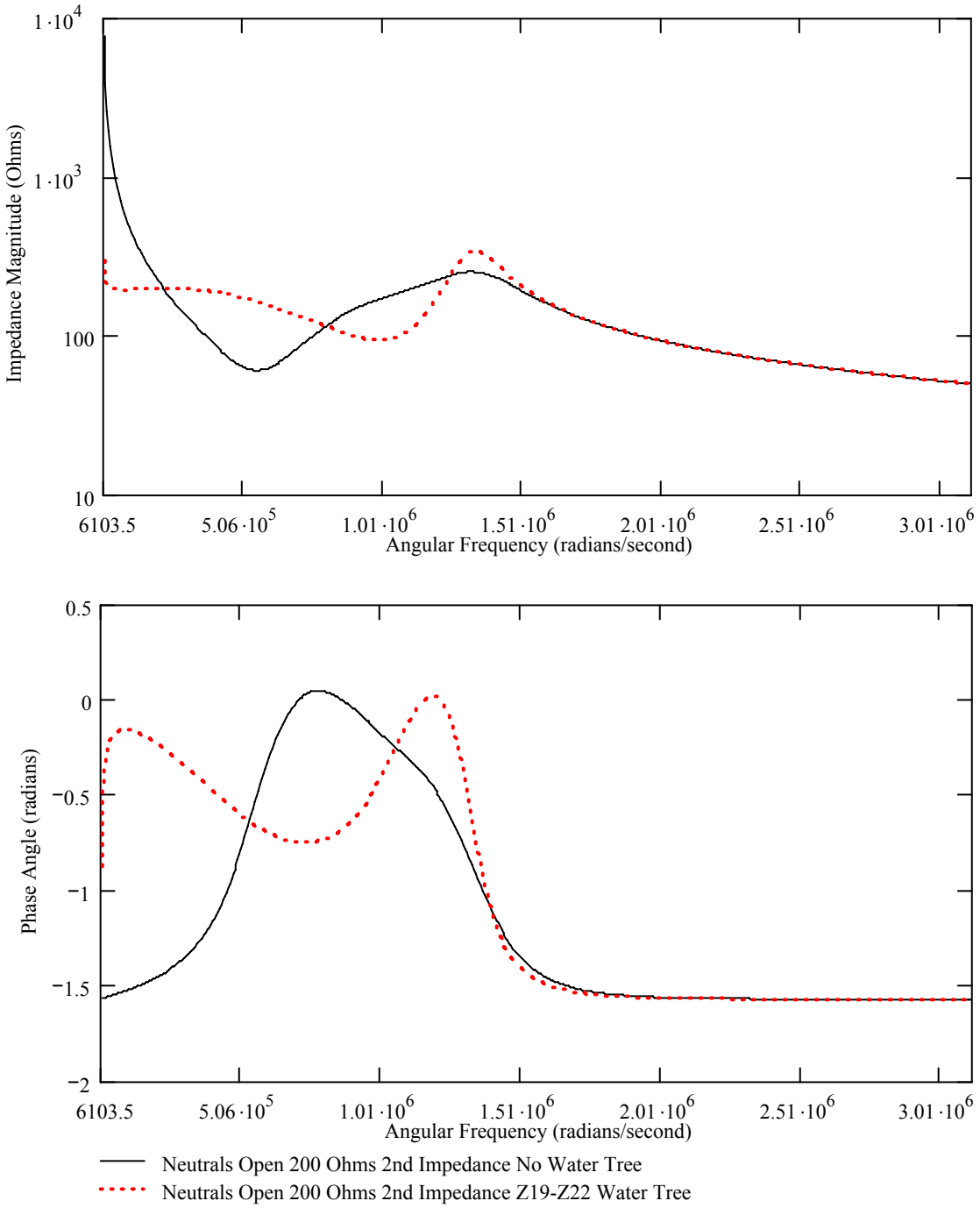

Figure E.62 Calculated Impedance Magnitude and Phase Angle vs Frequency
22 Impedance Element Model, L=100 m, D=10.3 mm AL, 4.45 mm XLPE,
Neutral Open, 200 Ω 2nd Impedance, No Water Tree vs Z19-Z22 Water Tree

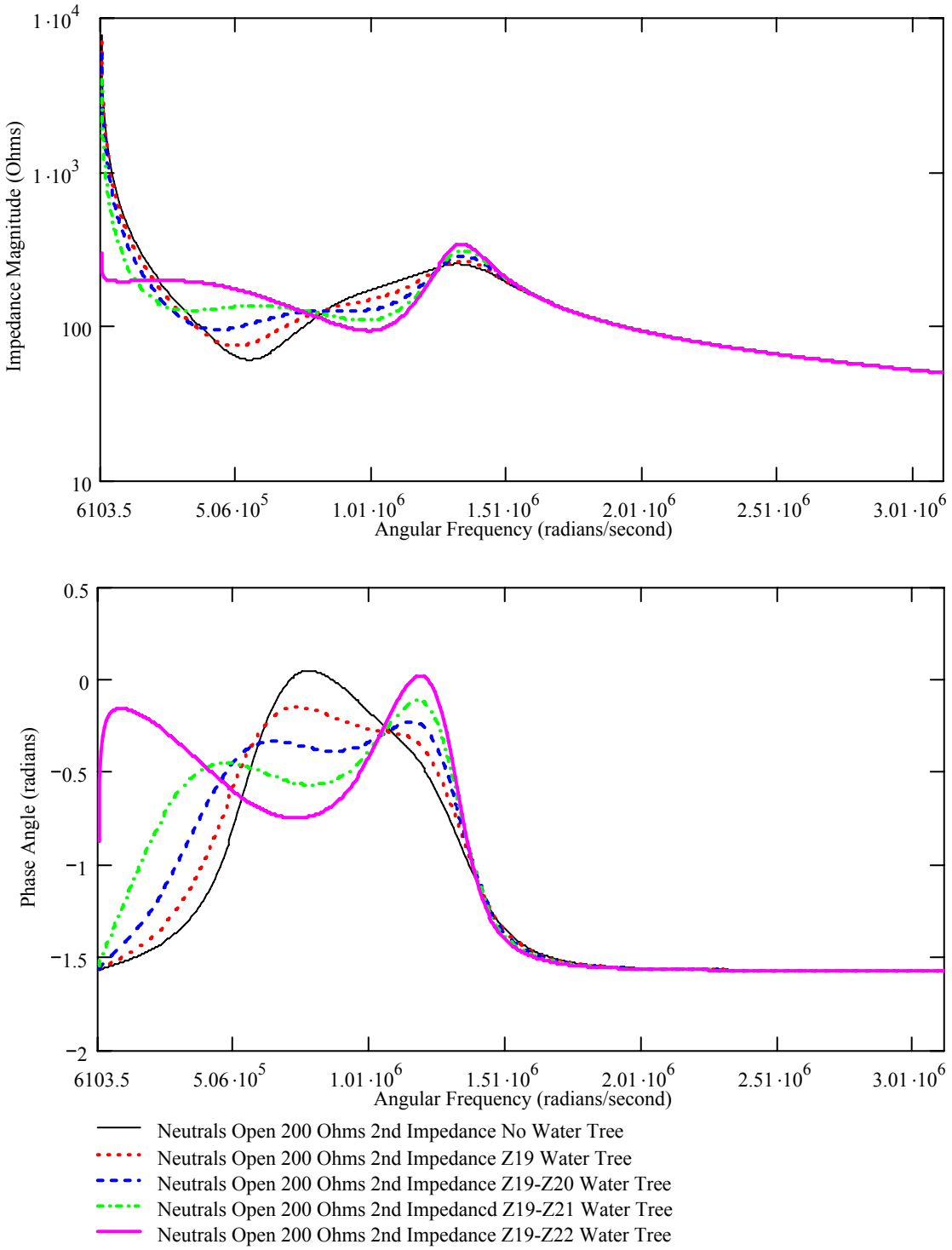

Figure E.63 Calculated Impedance Magnitude and Phase Angle vs Frequency
22 Impedance Element Model, L=100 m, D=10.3 mm AL, 4.45 mm XLPE,
Neutral Open, 200 Ω 2nd Impedance, No Water Tree vs Water Trees

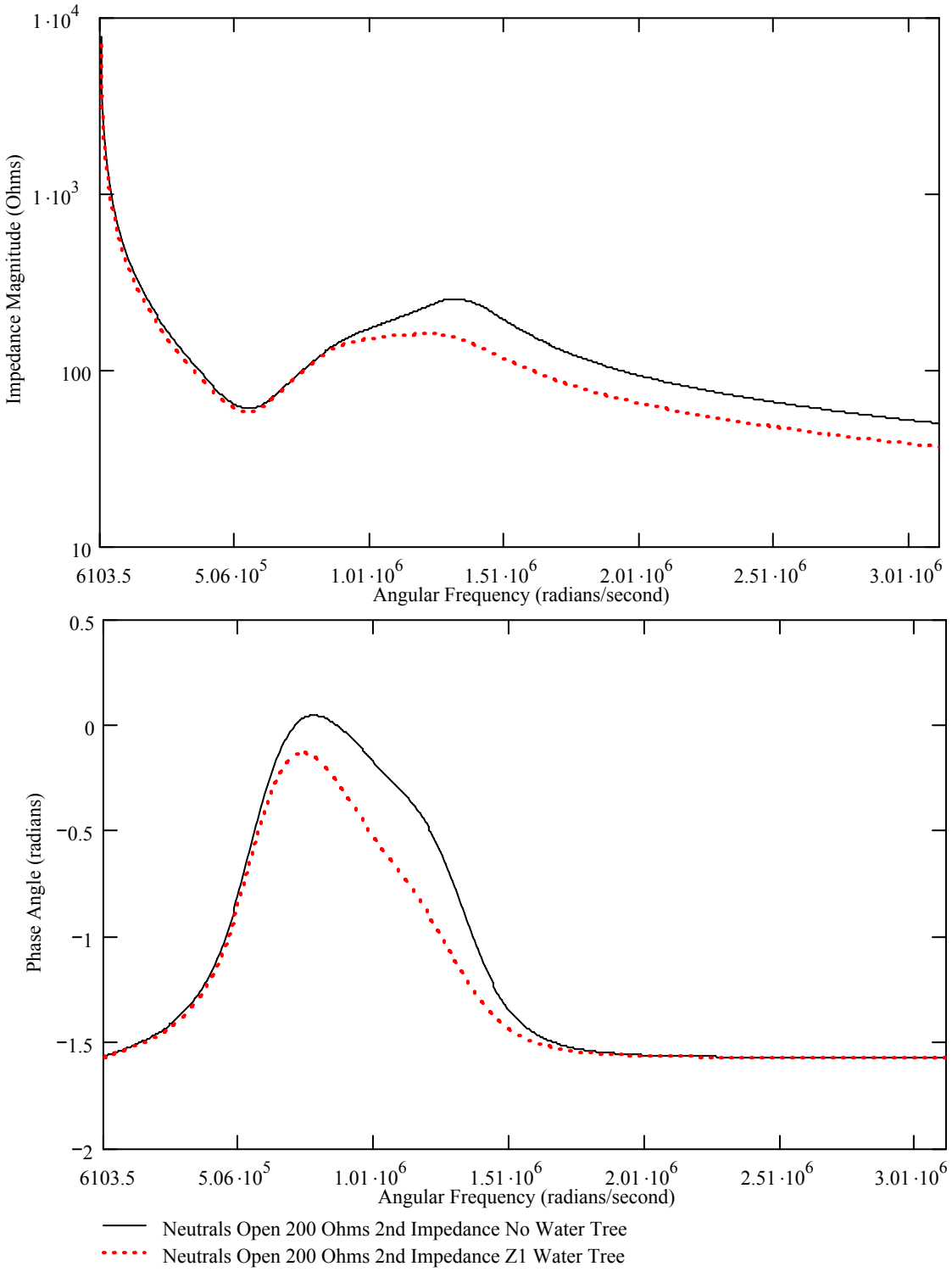

Figure E.64 Calculated Impedance Magnitude and Phase Angle vs Frequency
22 Impedance Element Model, L=100 m, D=10.3 mm AL, 4.45 mm XLPE,
Neutral Open, 200 Ω 2nd Impedance, No Water Tree vs Z1 Water Tree

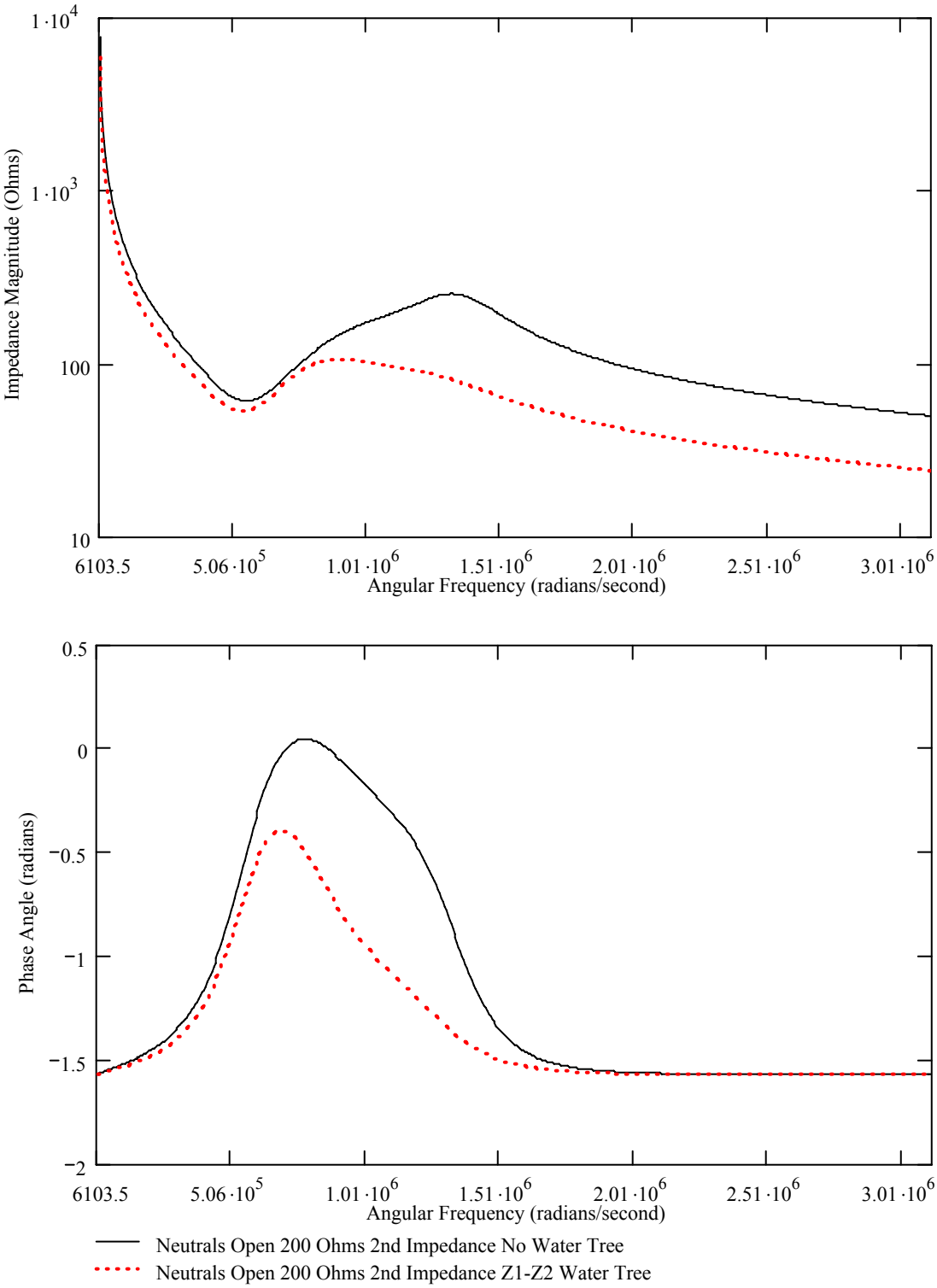

Figure E.65 Calculated Impedance Magnitude and Phase Angle vs Frequency
22 Impedance Element Model, L=100 m, D=10.3 mm AL, 4.45 mm XLPE,
Neutral Open, 200 Ω 2nd Impedance, No Water Tree vs Z1-Z2 Water Tree

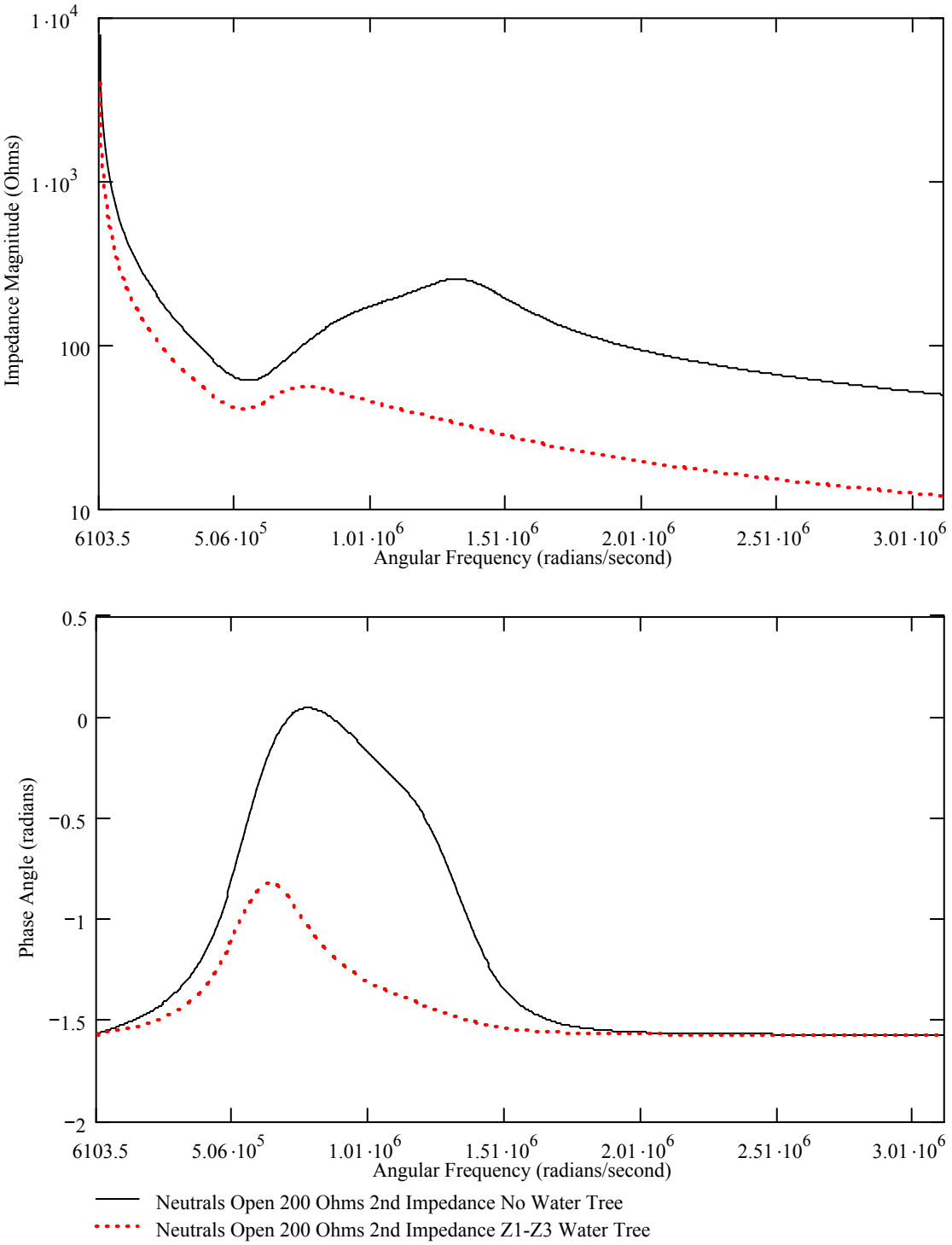

Figure E.66 Calculated Impedance Magnitude and Phase Angle vs Frequency
22 Impedance Element Model, L=100 m, D=10.3 mm AL, 4.45 mm XLPE,
Neutral Open, 200 Ω 2nd Impedance, No Water Tree vs Z1-Z3 Water Tree

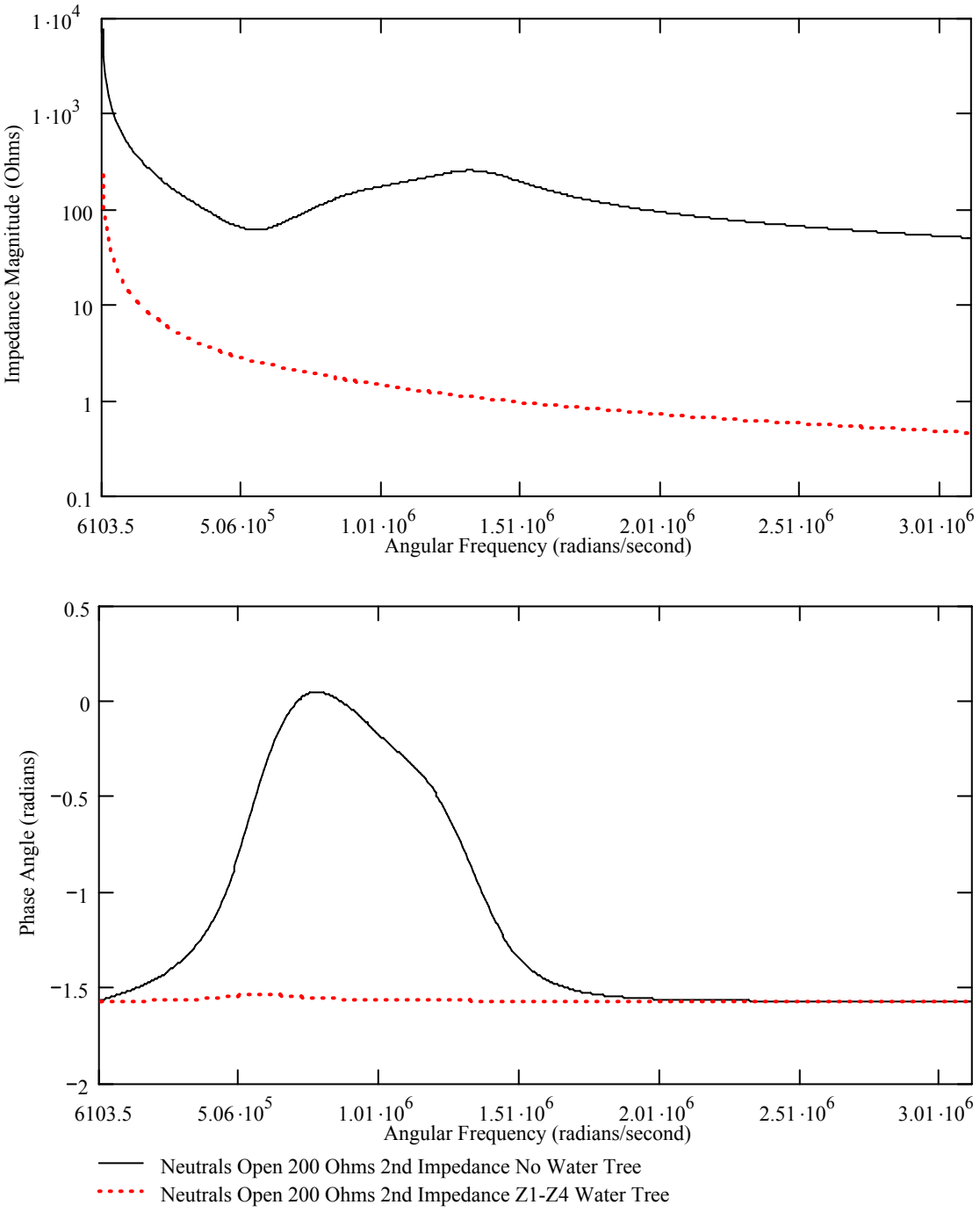

Figure E.67 Calculated Impedance Magnitude and Phase Angle vs Frequency
22 Impedance Element Model, L=100 m, D=10.3 mm AL, 4.45 mm XLPE,
Neutral Open, 200 Ω 2nd Impedance, No Water Tree vs Z1-Z4 Water Tree

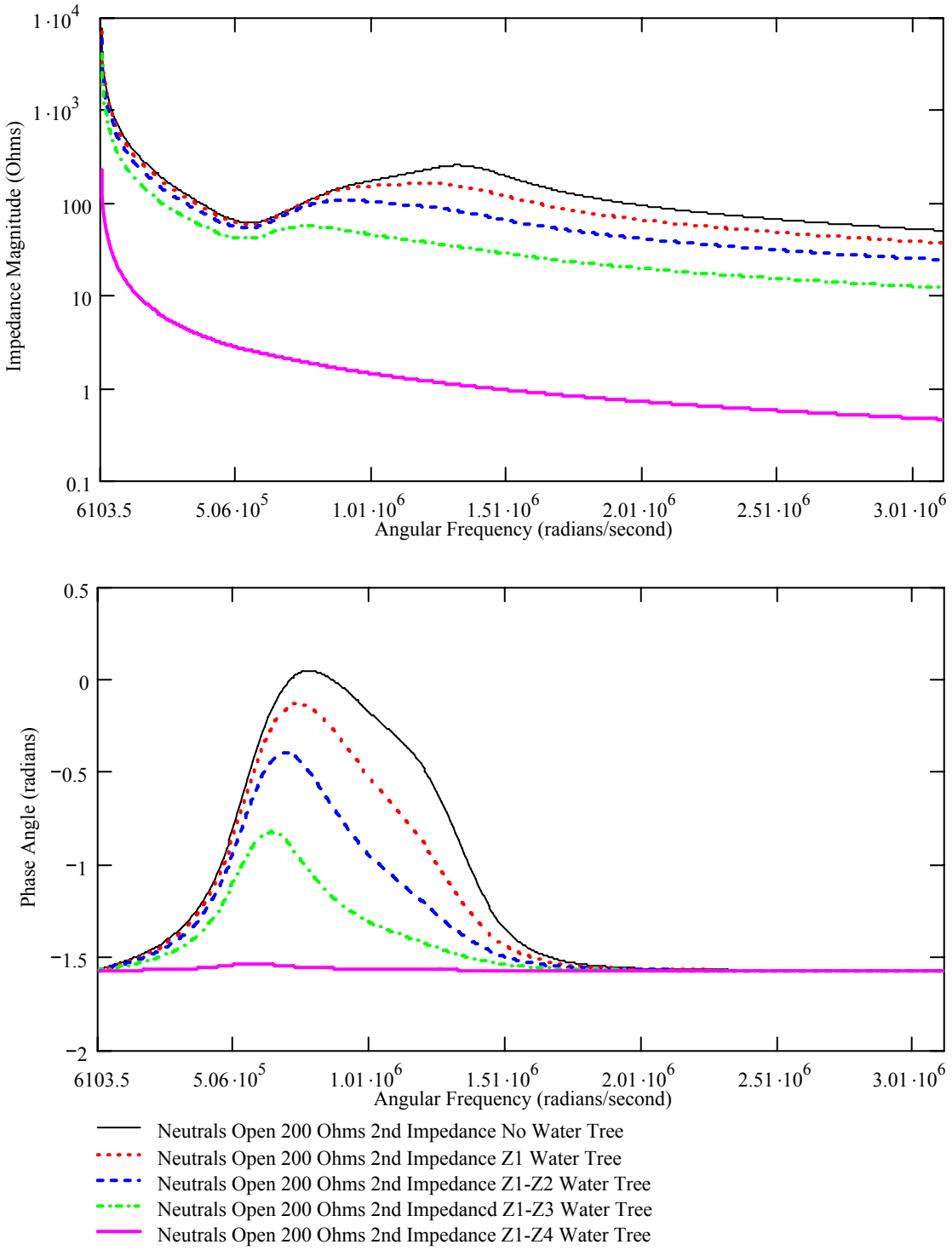

Figure E.68 Calculated Impedance Magnitude and Phase Angle vs Frequency
22 Impedance Element Model, L=100 m, D=10.3 mm AL, 4.45 mm XLPE,
Neutral Open, 200 Ω 2nd Impedance, No Water Tree vs Water Trees

APPENDIX F

FIELD AGED CABLE DIAGNOSTIC TEST MEASUREMENT RESULTS

All figures in this appendix show the impedance magnitude, in ohms versus frequency, impedance magnitude spectra, as the upper traces in the figure. The phase angle, in radians, versus frequency, impedance phase angle spectra, is shown as the lower traces. The impedance magnitude and phase angle versus frequency measurements are also denoted by the term impedance spectra. The values for the curves are the average of five consecutive high-voltage impulses results. The terms G1 to G9 refer to the test conditions under which the five consecutive high-voltage impulses results were measured. The descriptor SRA to SRZ, CWA to CWP, CIRA to CIRZ and RUNA to RUNJ associated with each figure provides a unique identifier for each cable sample that was tested. This can be compared to Appendix G, Table 1 information regarding all the cable and test information that was noted.

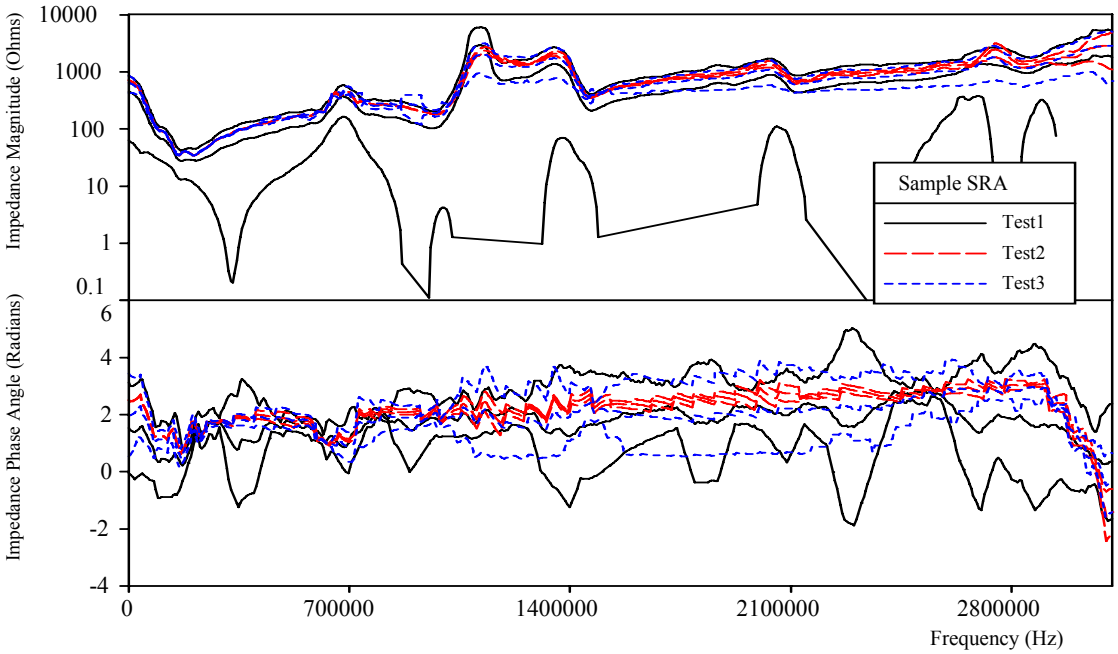

Figure F.1 New Cable Sample SRA, L=100 m, D=28.4 mm AL, 4.45 mm XLPE, Measured Impedance Magnitude and Phase Angle vs Frequency, Average and 95% Confidence Bounds

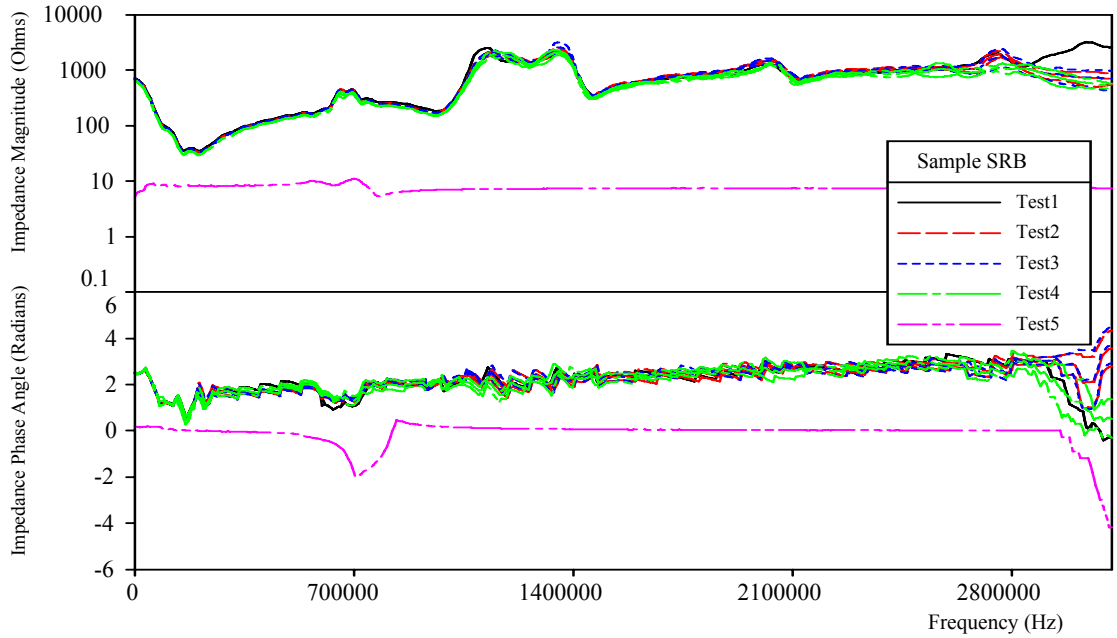

Figure F.2 New Cable Sample SRB, L=100 m, D=28.4 mm AL, 4.45 mm XLPE, Measured Impedance Magnitude and Phase Angle vs Frequency, Average and 95% Confidence Bounds

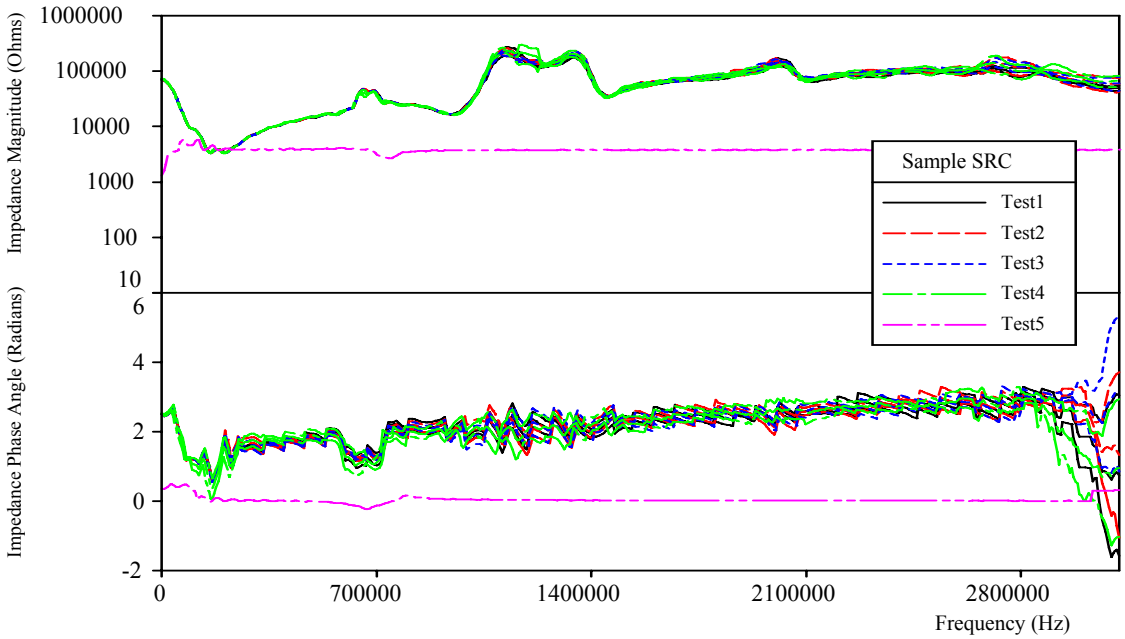

Figure F.3 New Cable Sample SRC, L=100 m, D=28.4 mm AL, 4.45 mm XLPE, Measured Impedance Magnitude and Phase Angle vs Frequency, Average and 95% Confidence Bounds

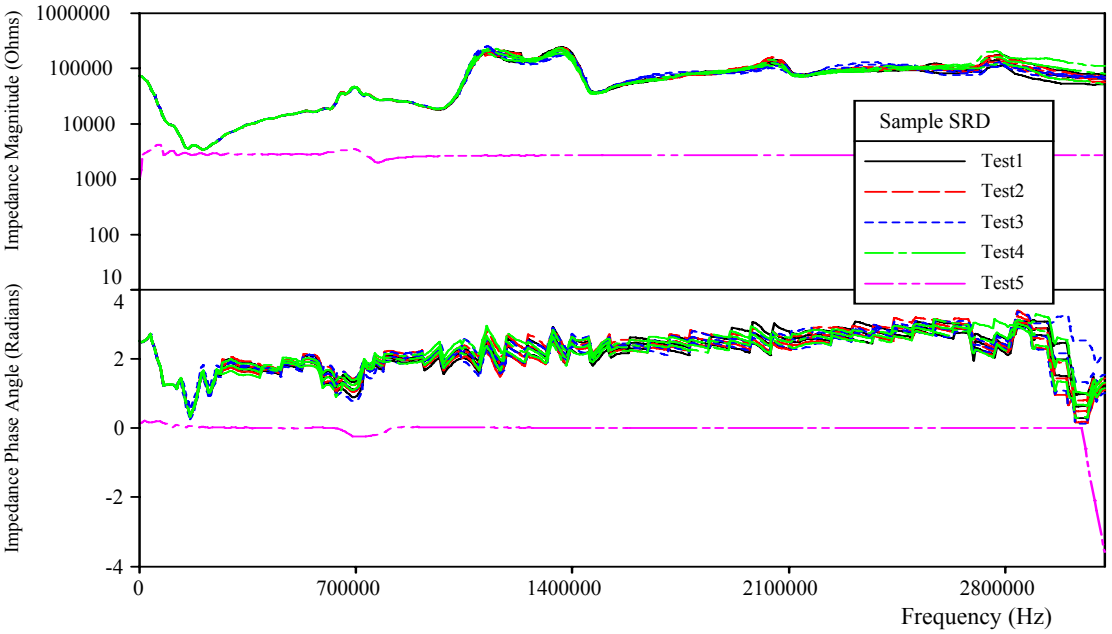

Figure F.4 New Cable Sample SRD, L=100 m, D=28.4 mm AL, 4.45 mm XLPE, Measured Impedance Magnitude and Phase Angle vs Frequency, Average and 95% Confidence Bounds

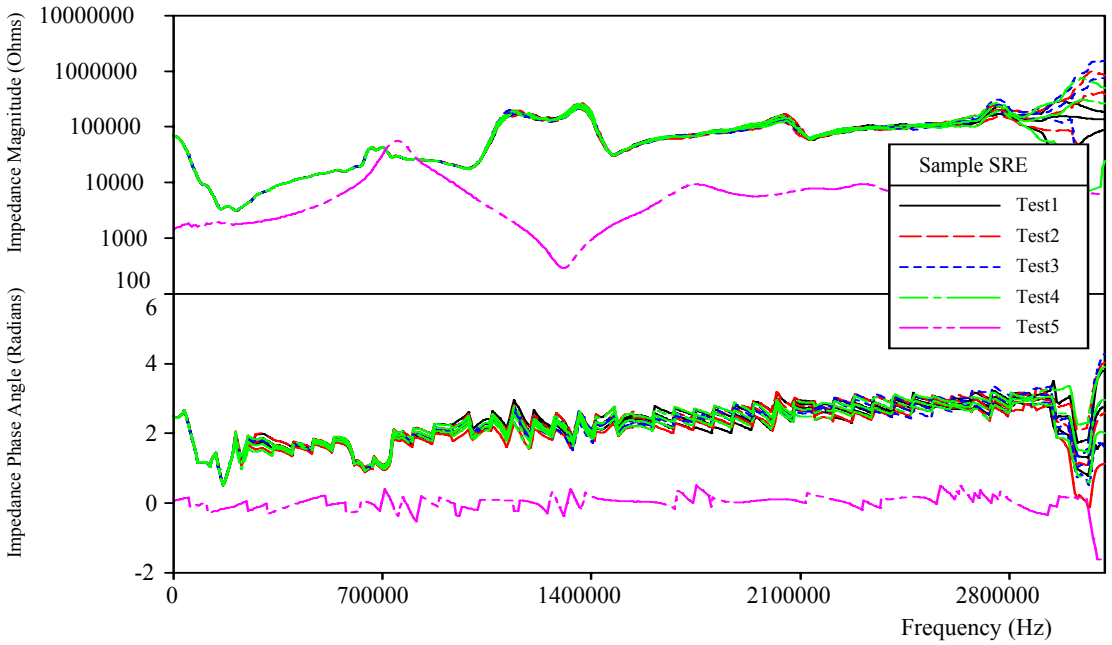

Figure F.5 New Cable Sample SRE, L=100 m, D=28.4 mm AL, 4.45 mm XLPE, Measured Impedance Magnitude and Phase Angle vs Frequency, Average and 95% Confidence Bounds

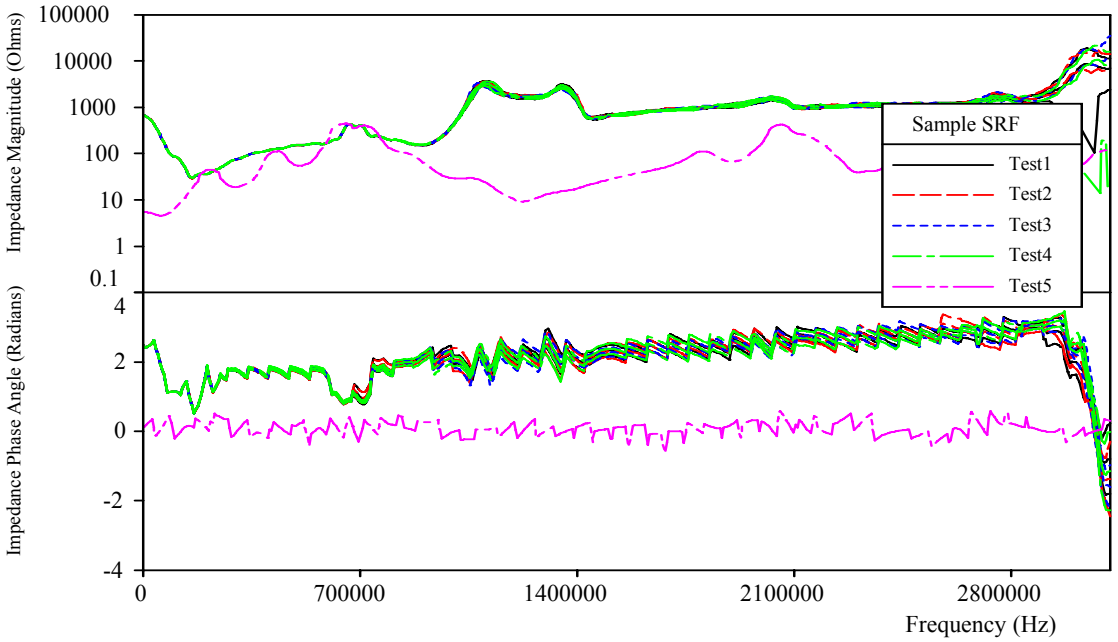

Figure F.6 New Cable Sample SRF, L=100 m, D=28.4 mm AL, 4.45 mm XLPE, Measured Impedance Magnitude and Phase Angle vs Frequency, Average and 95% Confidence Bounds

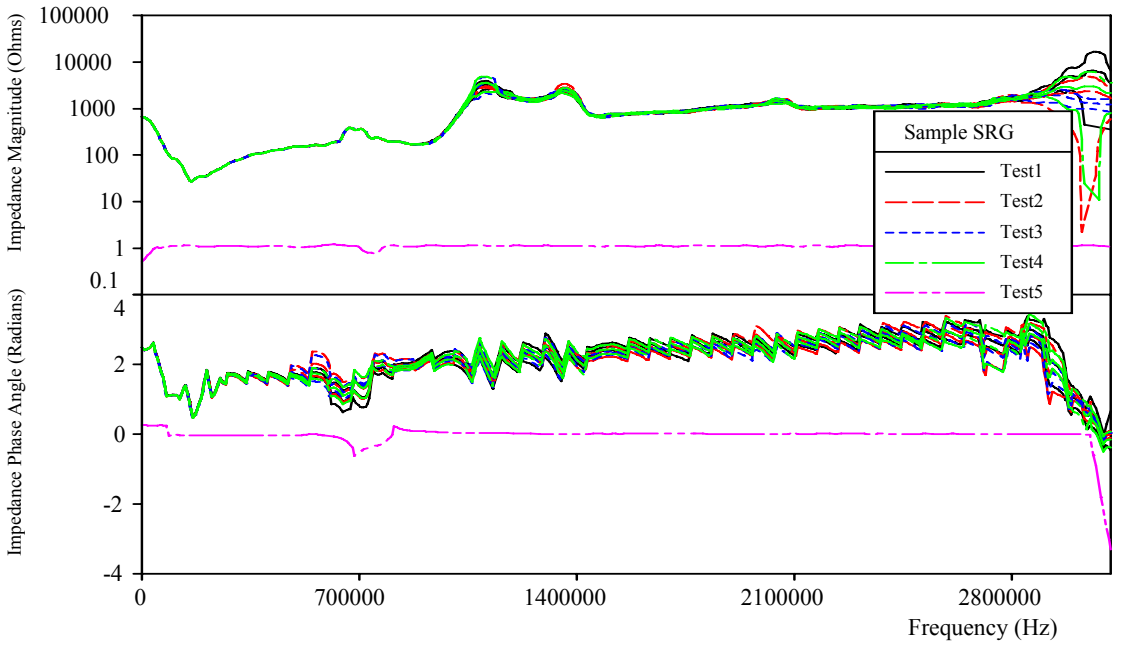

Figure F.7 New Cable Sample SRG, L=100 m, D=28.4 mm AL, 4.45 mm XLPE, Measured Impedance Magnitude and Phase Angle vs Frequency, Average and 95% Confidence Bounds

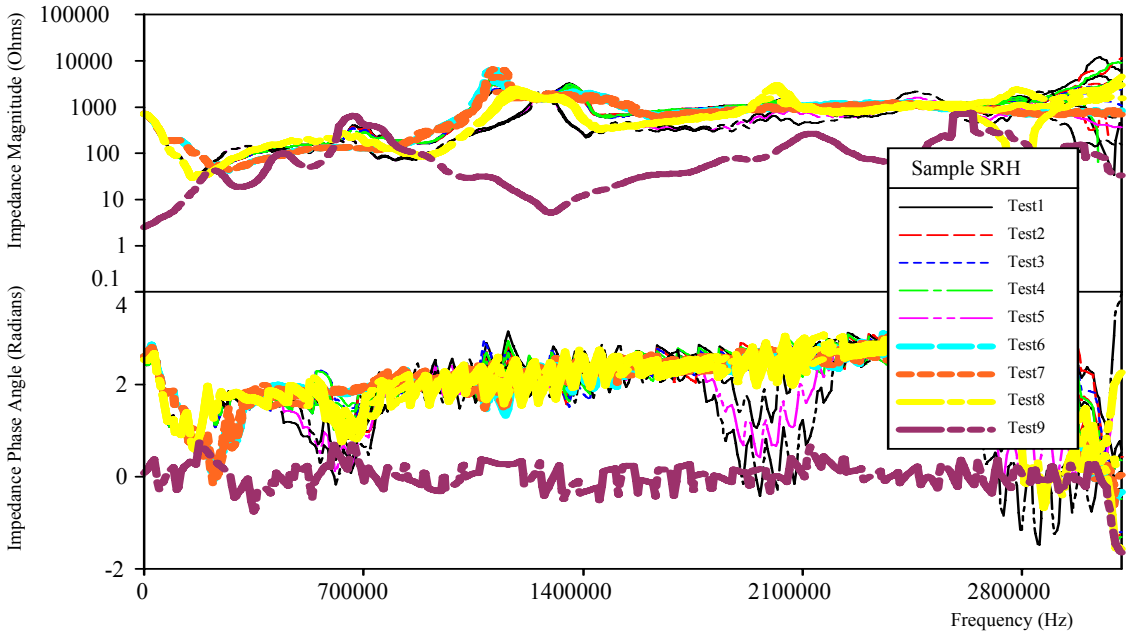

Figure F.8 New Cable Sample SRH, L=100 m, D=28.4 mm AL, 4.45 mm XLPE, Measured Impedance Magnitude and Phase Angle vs Frequency, Average and 95% Confidence Bounds

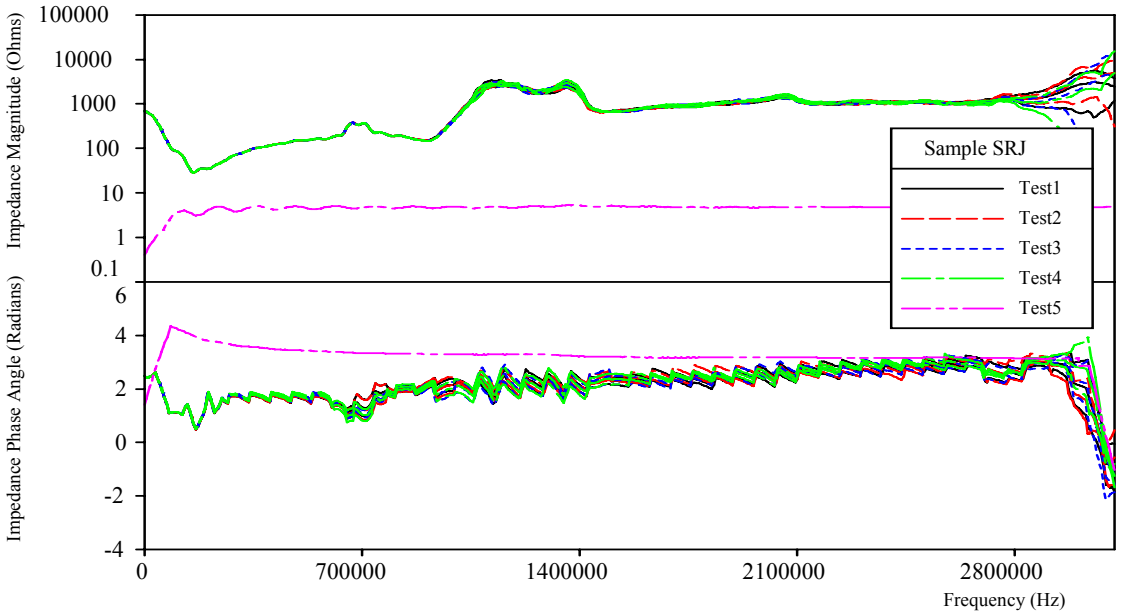

Figure F.9 New Cable Sample SRJ, L=100 m, D=28.4 mm AL, 4.45 mm XLPE, Measured Impedance Magnitude and Phase Angle vs Frequency, Average and 95% Confidence Bounds

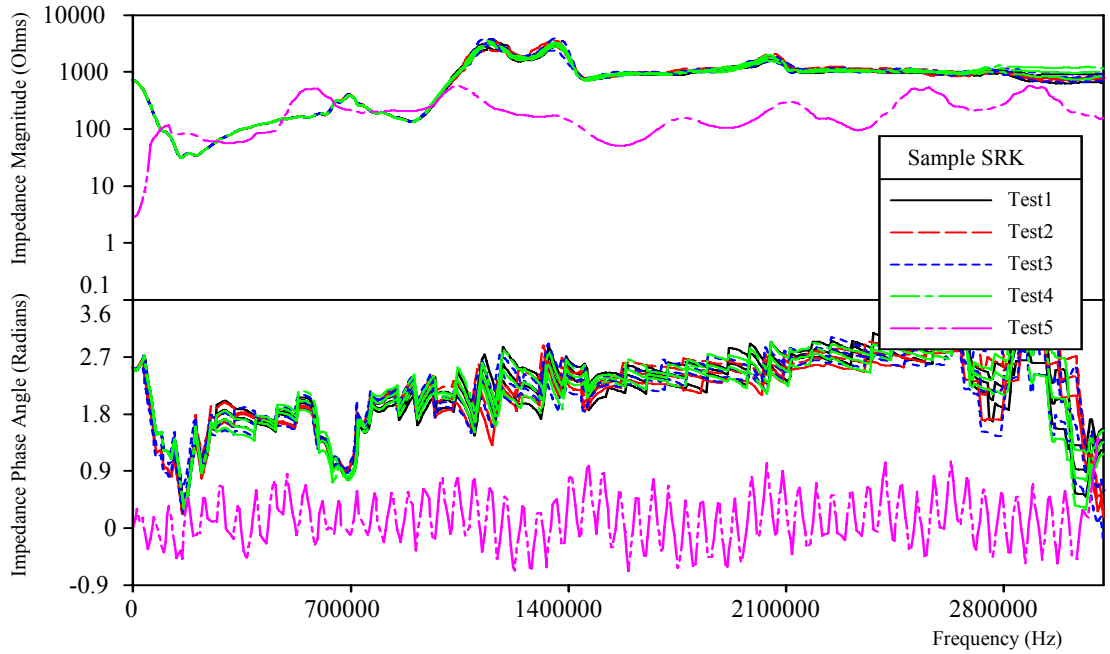

Figure F.10 New Cable Sample SRK, L=100 m, D=28.4 mm AL, 4.45 mm XLPE, Measured Impedance Magnitude and Phase Angle vs Frequency, Average and 95% Confidence Bounds

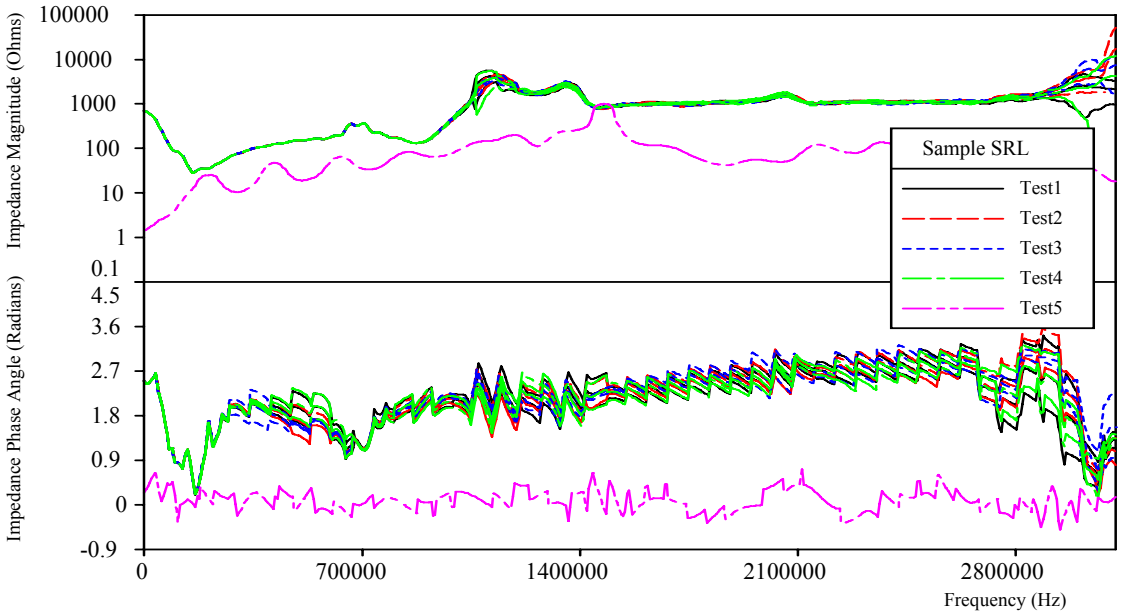

Figure F.11 New Cable Sample SRL, L=100 m, D=28.4 mm AL, 4.45 mm XLPE, Measured Impedance Magnitude and Phase Angle vs Frequency, Average and 95% Confidence Bounds

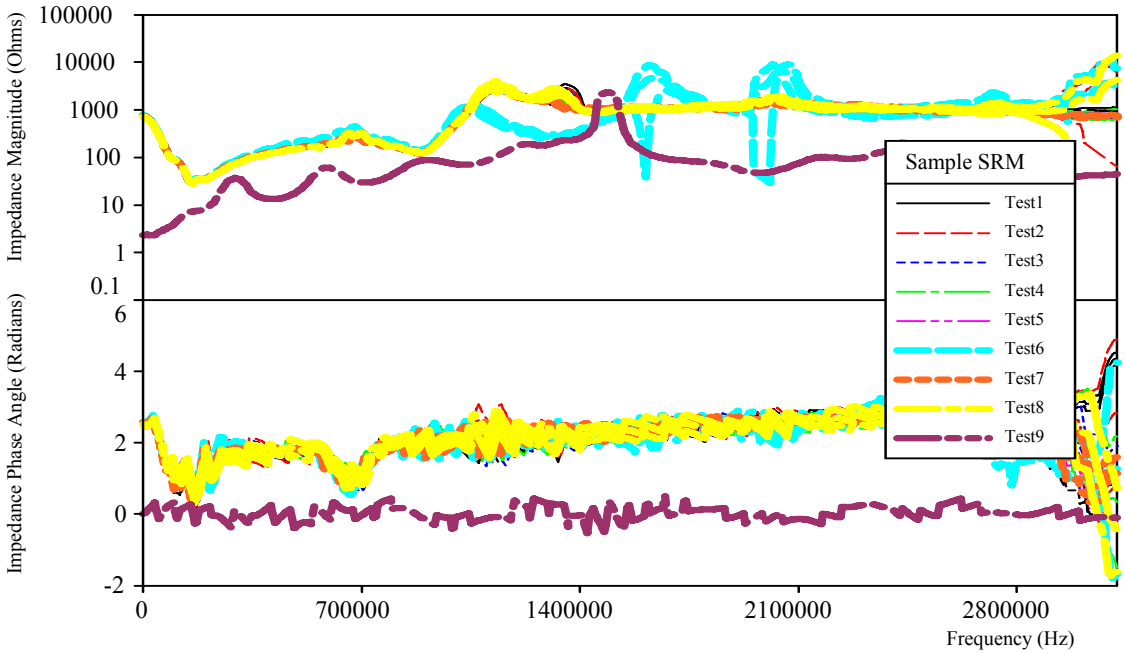

Figure F.12 New Cable Sample SRM, L=100 m, D=28.4 mm AL, 4.45 mm XLPE, Measured Impedance Magnitude and Phase Angle vs Frequency, Average and 95% Confidence Bounds

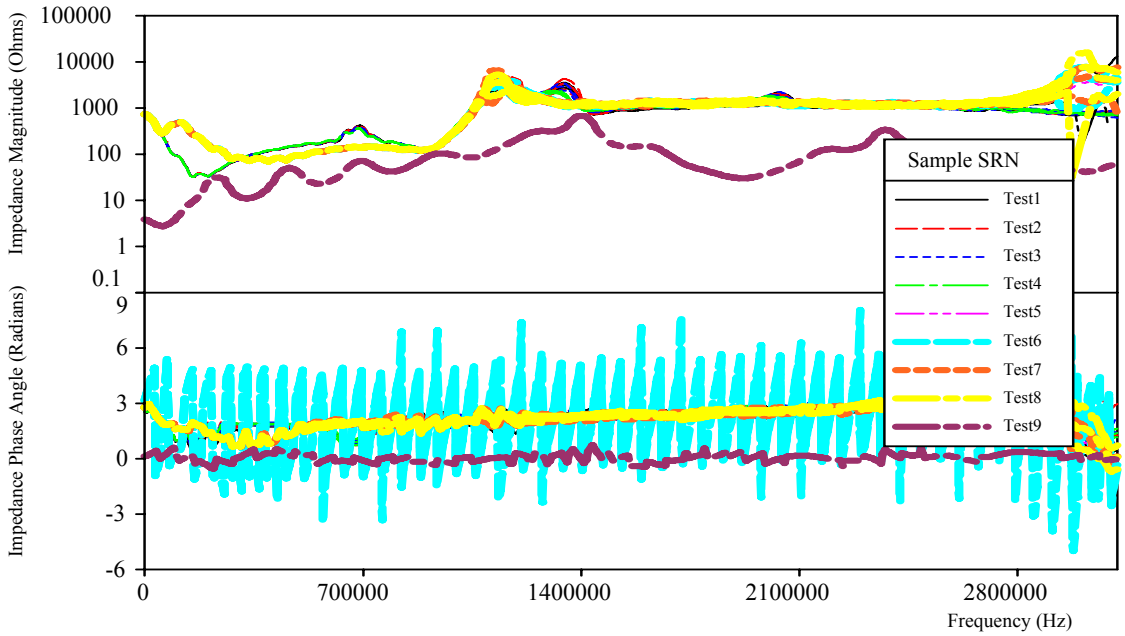

Figure F.13 New Cable Sample SRN, L=100 m, D=28.4 mm AL, 4.45 mm XLPE, Measured Impedance Magnitude and Phase Angle vs Frequency, Average and 95% Confidence Bounds

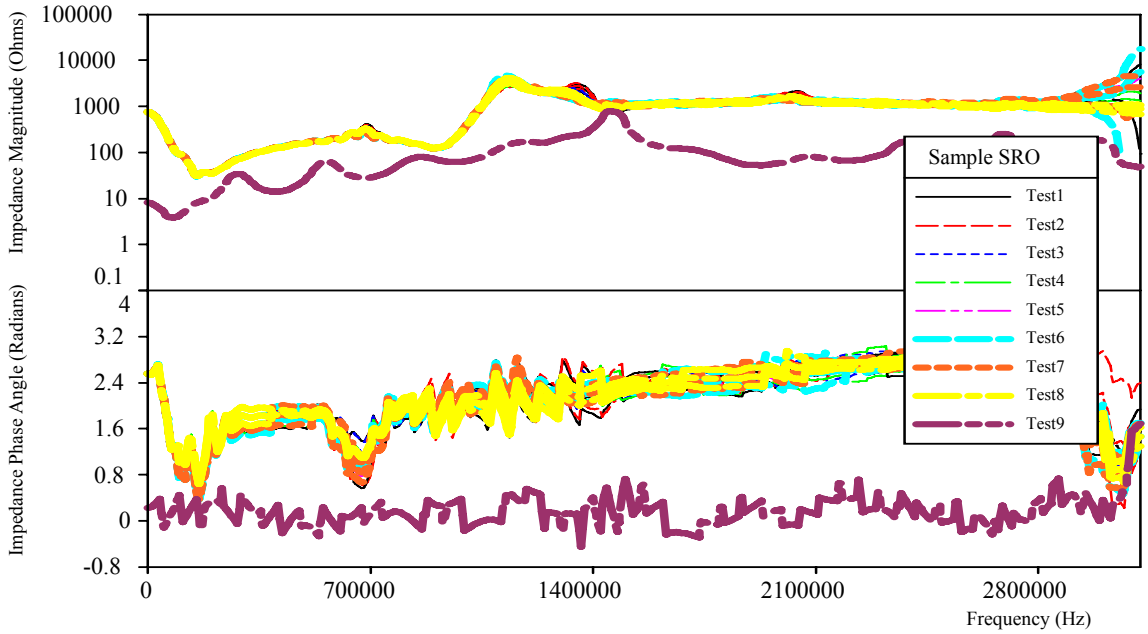

Figure F.14 New Cable Sample SRO, L=100 m, D=28.4 mm AL, 4.45 mm XLPE, Measured Impedance Magnitude and Phase Angle vs Frequency, Average and 95% Confidence Bounds

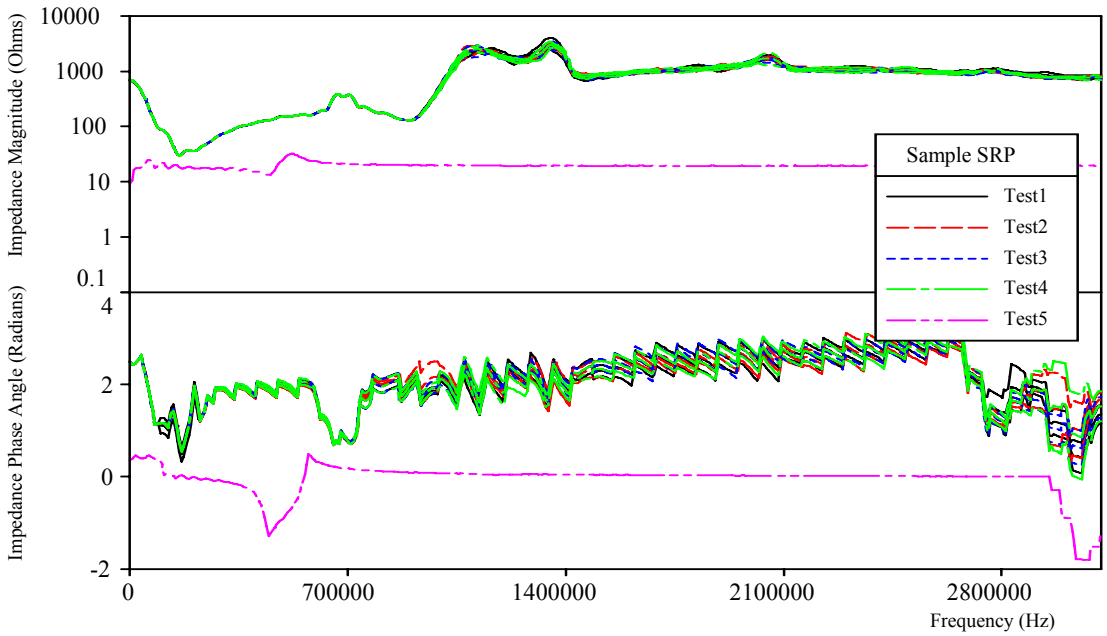

Figure F.15 New Cable Sample SRP, L=100 m, D=28.4 mm AL, 4.45 mm XLPE, Measured Impedance Magnitude and Phase Angle vs Frequency, Average and 95% Confidence Bounds

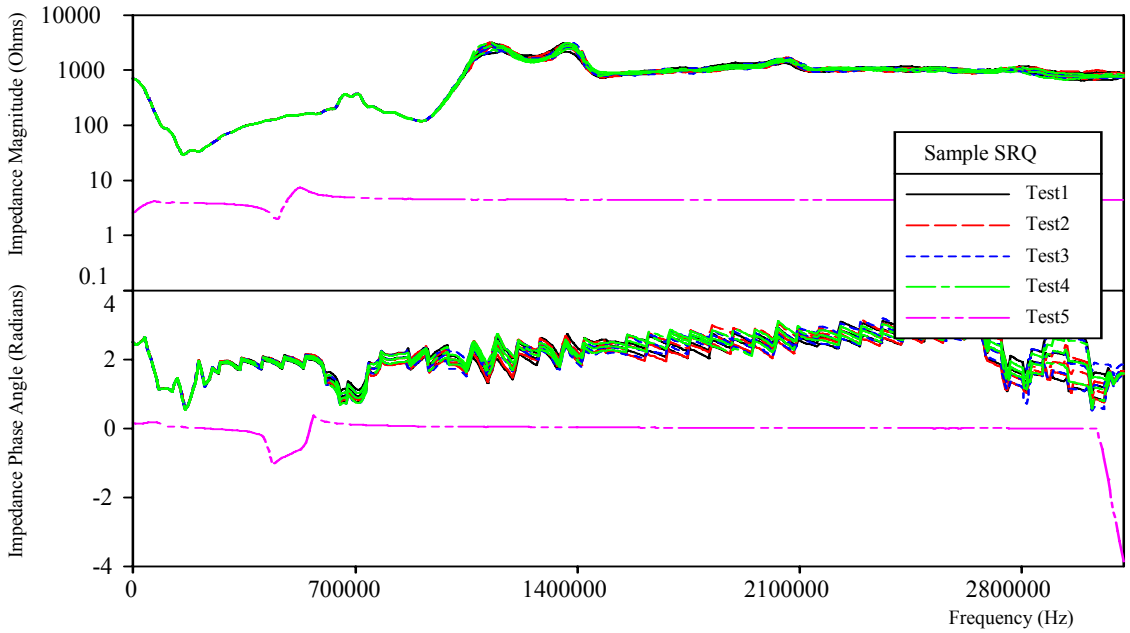

Figure F.16 New Cable Sample SRQ, L=100 m, D=28.4 mm AL, 4.45 mm XLPE, Measured Impedance Magnitude and Phase Angle vs Frequency, Average and 95% Confidence Bounds

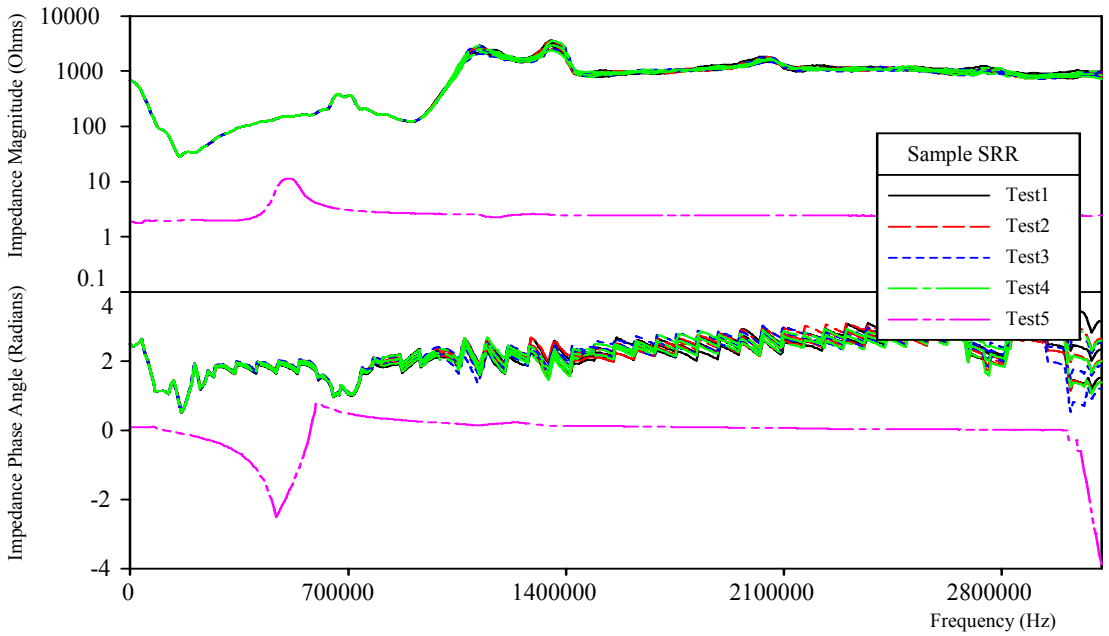

Figure F.17 New Cable Sample SRR, L=100 m, D=28.4 mm AL, 4.45 mm XLPE, Measured Impedance Magnitude and Phase Angle vs Frequency, Average and 95% Confidence Bounds

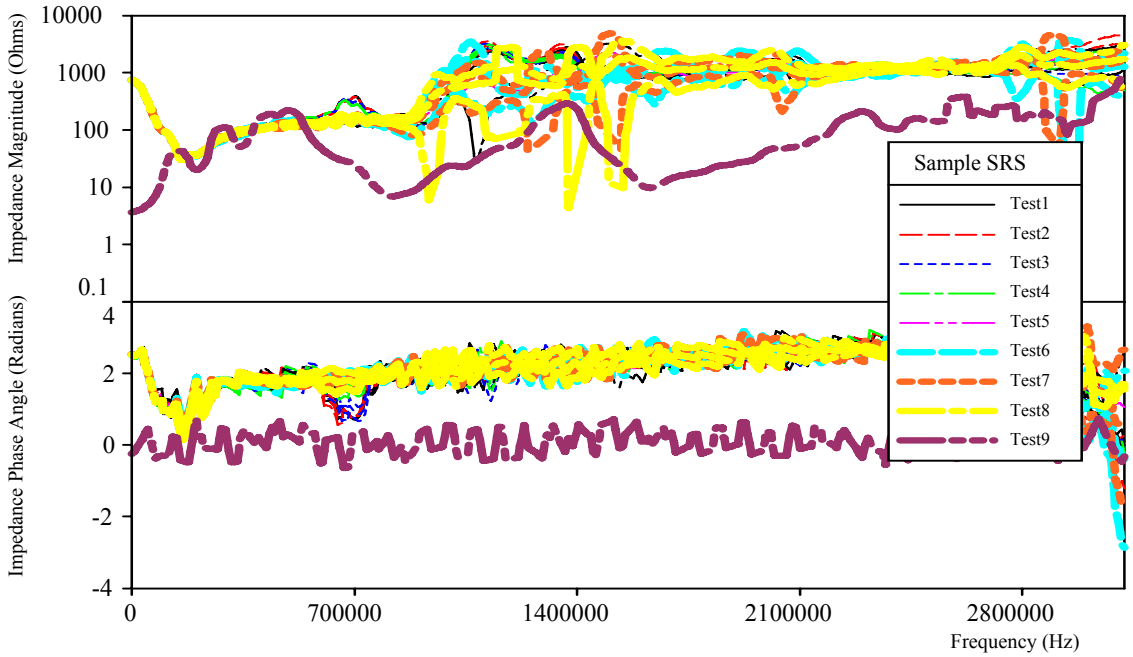

Figure F.18 New Cable Sample SRS, L=100 m, D=28.4 mm AL, 4.45 mm XLPE, Measured Impedance Magnitude and Phase Angle vs Frequency, Average and 95% Confidence Bounds

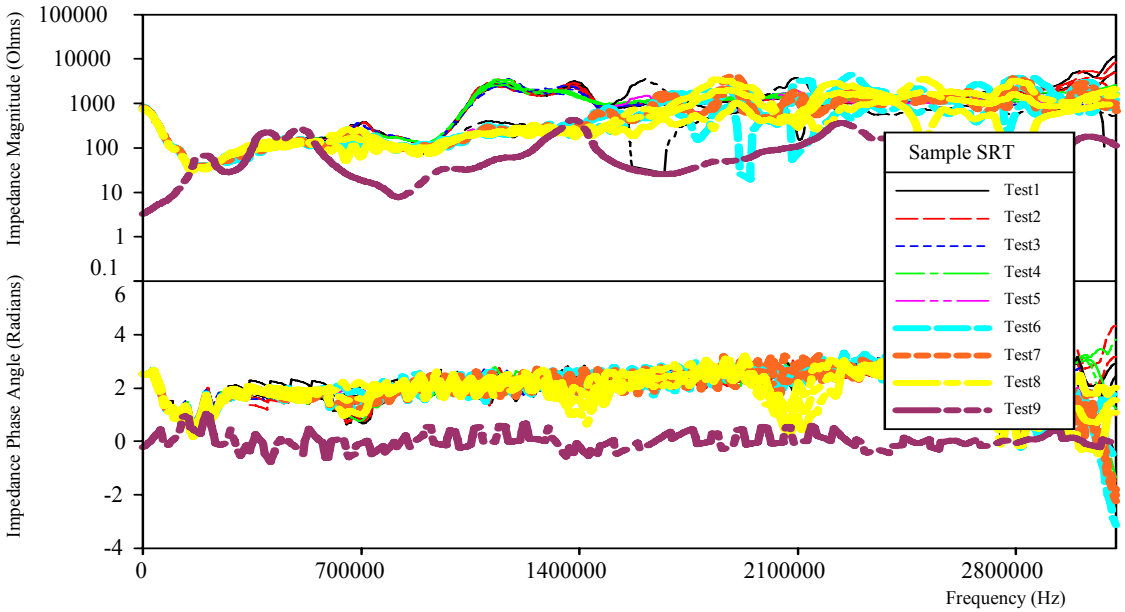

Figure F.19 New Cable Sample SRT, L=100 m, D=28.4 mm AL, 4.45 mm XLPE, Measured Impedance Magnitude and Phase Angle vs Frequency, Average and 95% Confidence Bounds

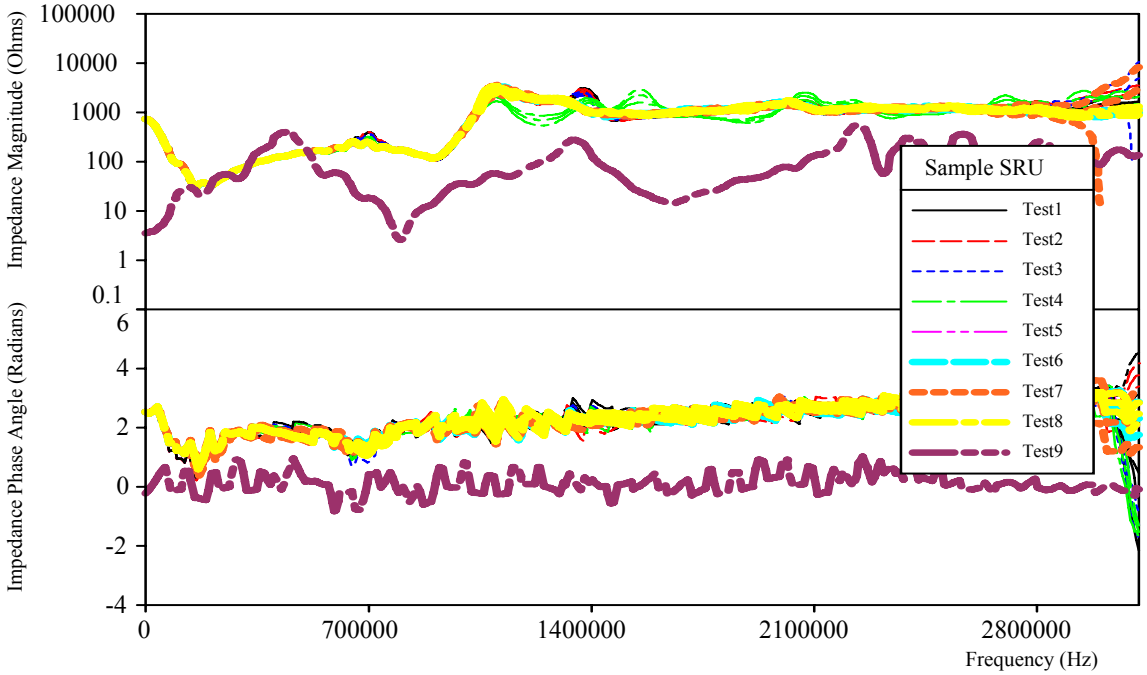

Figure F.20 New Cable Sample SRU, L=100 m, D=28.4 mm AL, 4.45 mm XLPE, Measured Impedance Magnitude and Phase Angle vs Frequency, Average and 95% Confidence Bounds

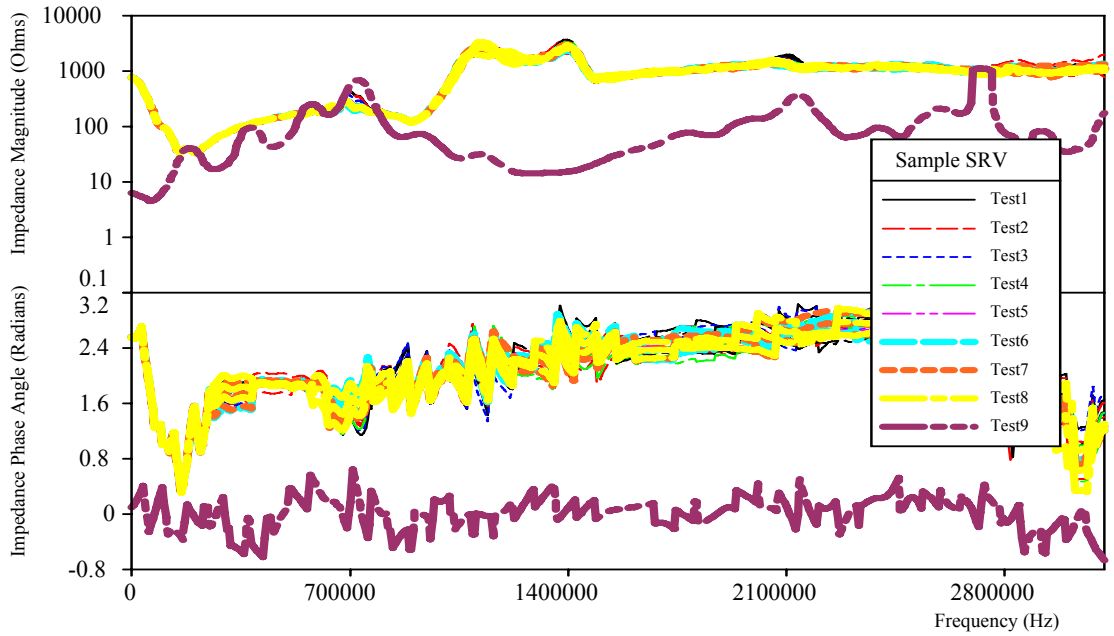

Figure F.21 New Cable Sample SRV, L=100 m, D=28.4 mm AL, 4.45 mm XLPE, Measured Impedance Magnitude and Phase Angle vs Frequency, Average and 95% Confidence Bounds

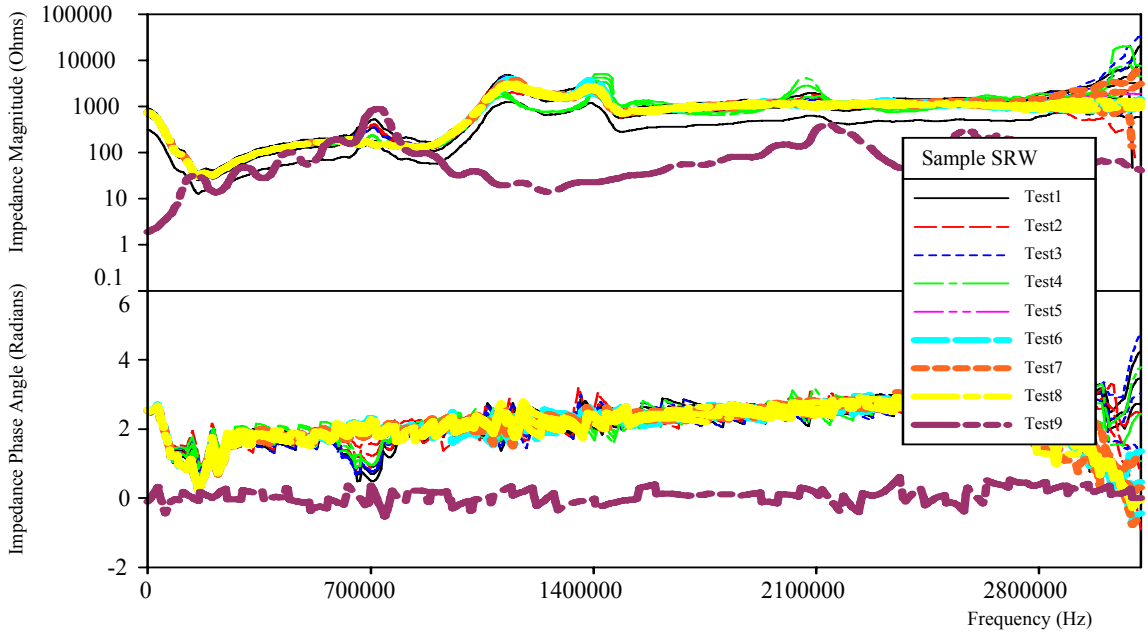

Figure F.22 New Cable Sample SRW, L=100 m, D=28.4 mm AL, 4.45 mm XLPE, Measured Impedance Magnitude and Phase Angle vs Frequency, Average and 95% Confidence Bounds

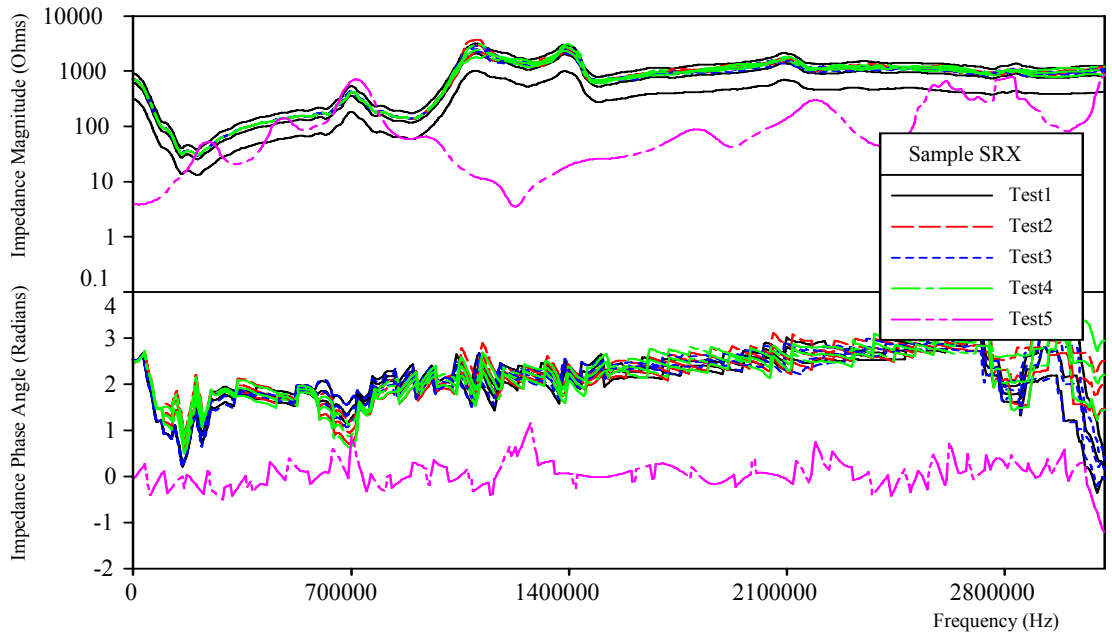

Figure F.23 New Cable Sample SRX, L=100 m, D=28.4 mm AL, 4.45 mm XLPE, Measured Impedance Magnitude and Phase Angle vs Frequency, Average and 95% Confidence Bounds

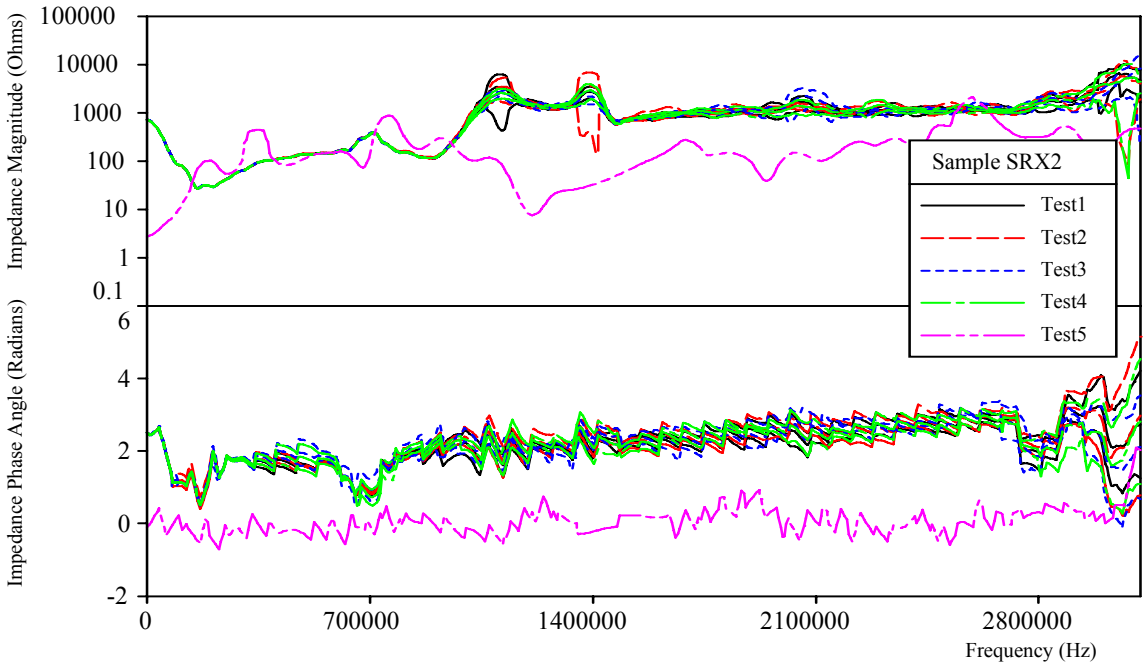

Figure F.24 New Cable Sample SRX2, L=100 m, D=28.4 mm AL, 4.45 mm XLPE, Measured Impedance Magnitude and Phase Angle vs Frequency, Average and 95% Confidence Bounds

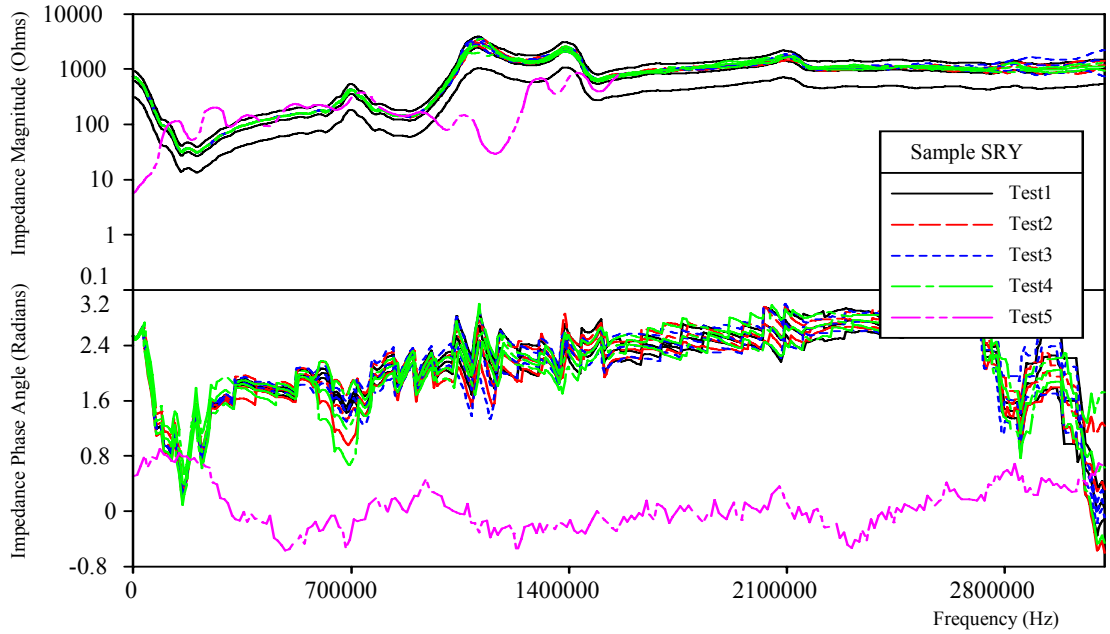

Figure F.25 New Cable Sample SRY, L=100 m, D=28.4 mm AL, 4.45 mm XLPE, Measured Impedance Magnitude and Phase Angle vs Frequency, Average and 95% Confidence Bounds

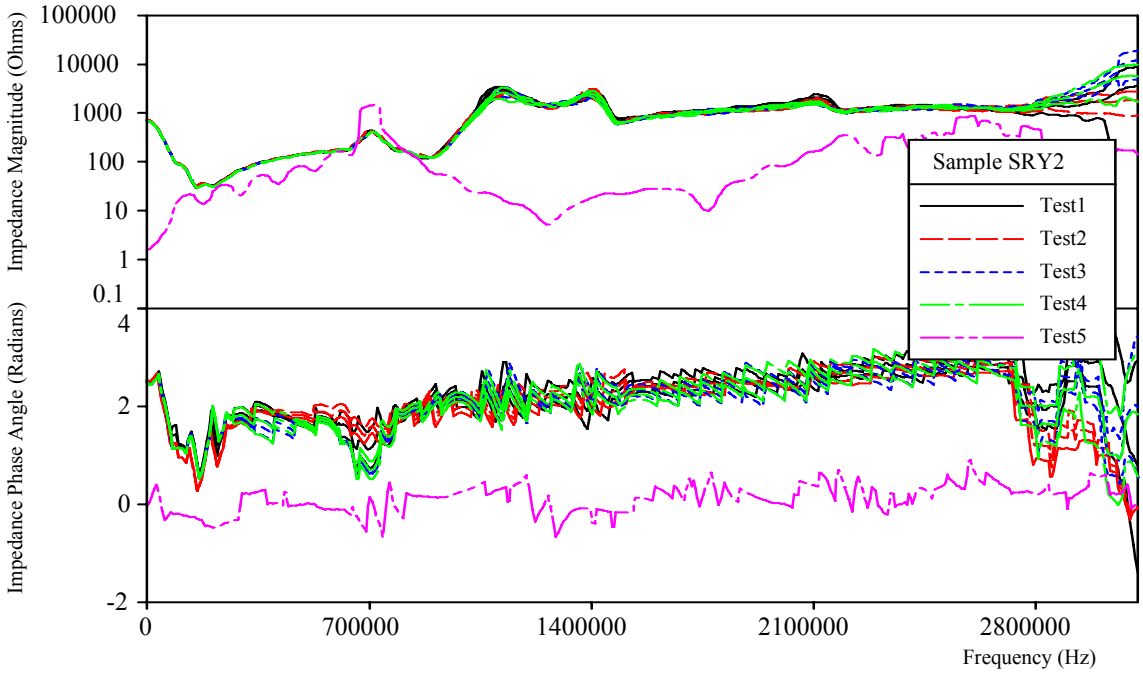

Figure F.26 New Cable Sample SRY2, L=100 m, D=28.4 mm AL, 4.45 mm XLPE, Measured Impedance Magnitude and Phase Angle vs Frequency, Average and 95% Confidence Bounds

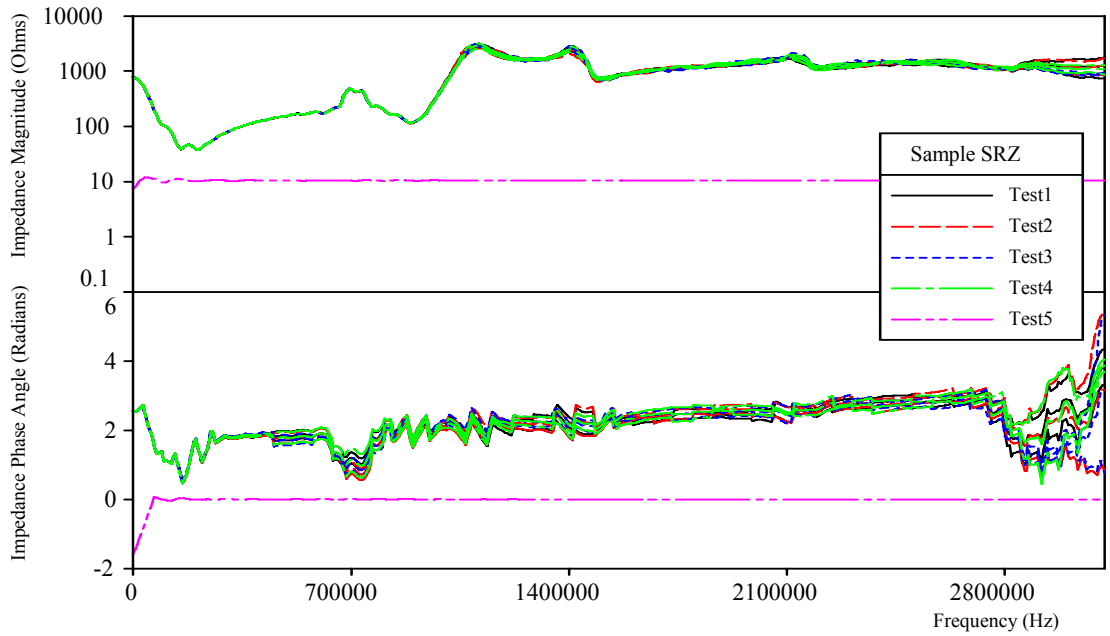

Figure F.27 New Cable Sample SRZ, L=100 m, D=28.4 mm AL, 4.45 mm XLPE, Measured Impedance Magnitude and Phase Angle vs Frequency, Average and 95% Confidence Bounds

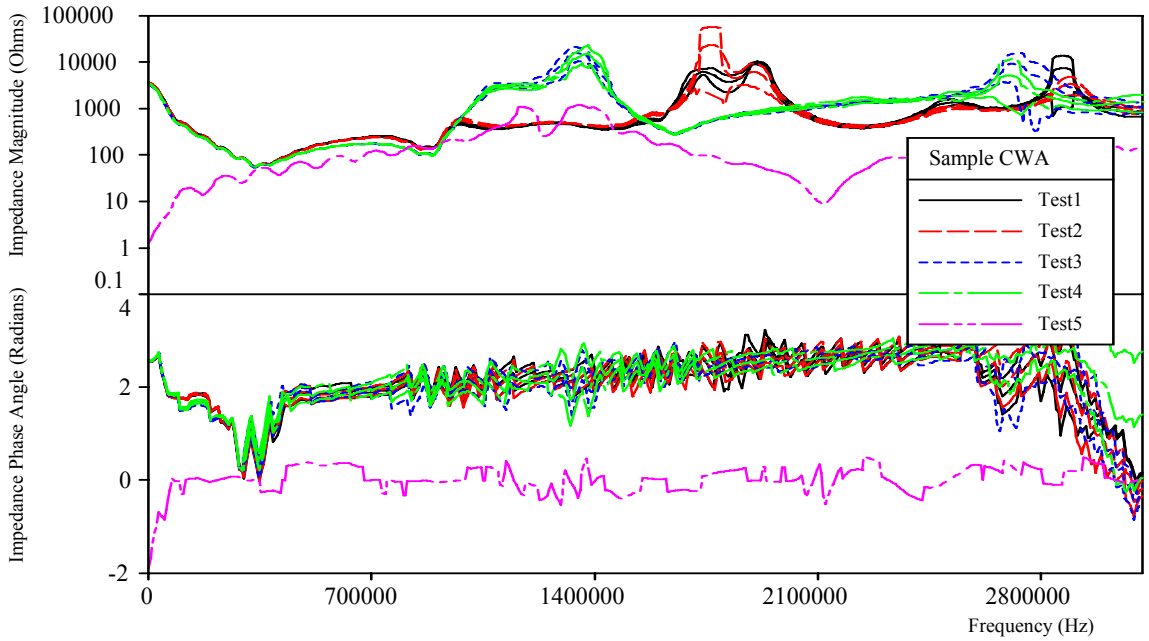

Figure F.28 New Cable Sample CWA, L=60 m, D=10.3 mm AL, 4.45 mm XLPE, Measured Impedance Magnitude and Phase Angle vs Frequency, Average and 95% Confidence Bounds

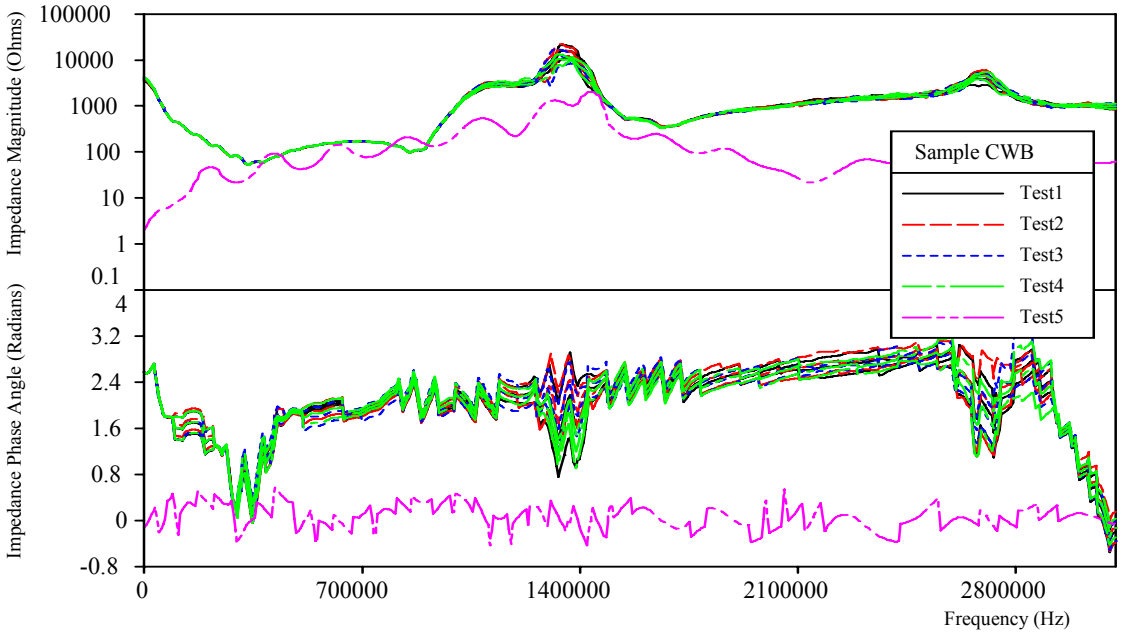

Figure F.29 New Cable Sample CWB, L=60 m, D=10.3 mm AL, 4.45 mm XLPE, Measured Impedance Magnitude and Phase Angle vs Frequency, Average and 95% Confidence Bounds

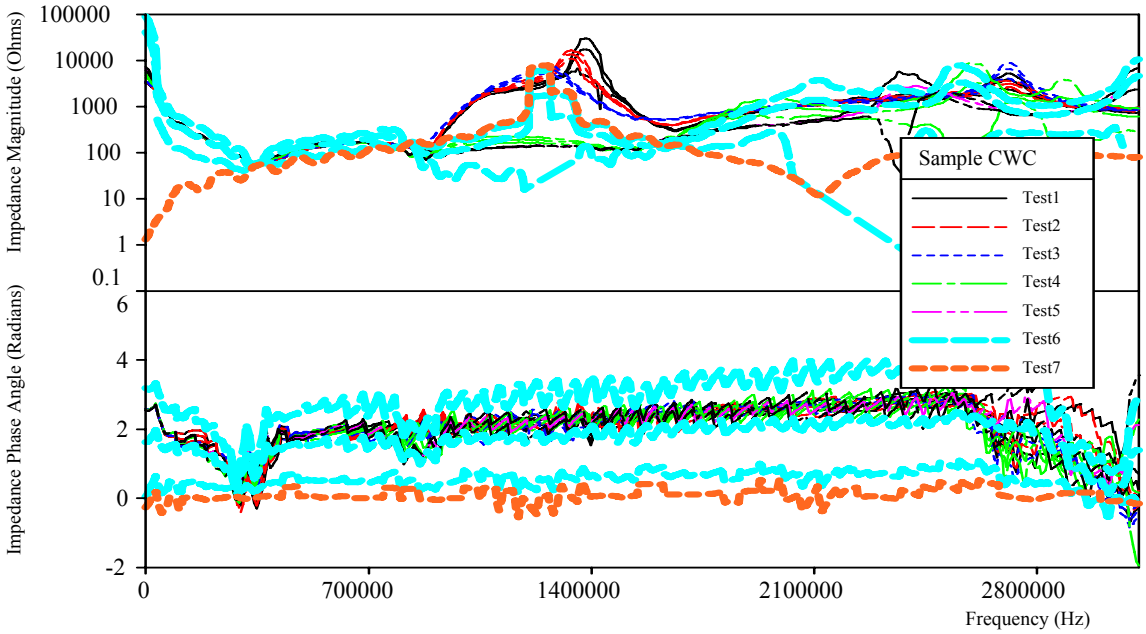

Figure F.30 New Cable Sample CWC, L=60 m, D=10.3 mm AL, 4.45 mm XLPE, Measured Impedance Magnitude and Phase Angle vs Frequency, Average and 95% Confidence Bounds

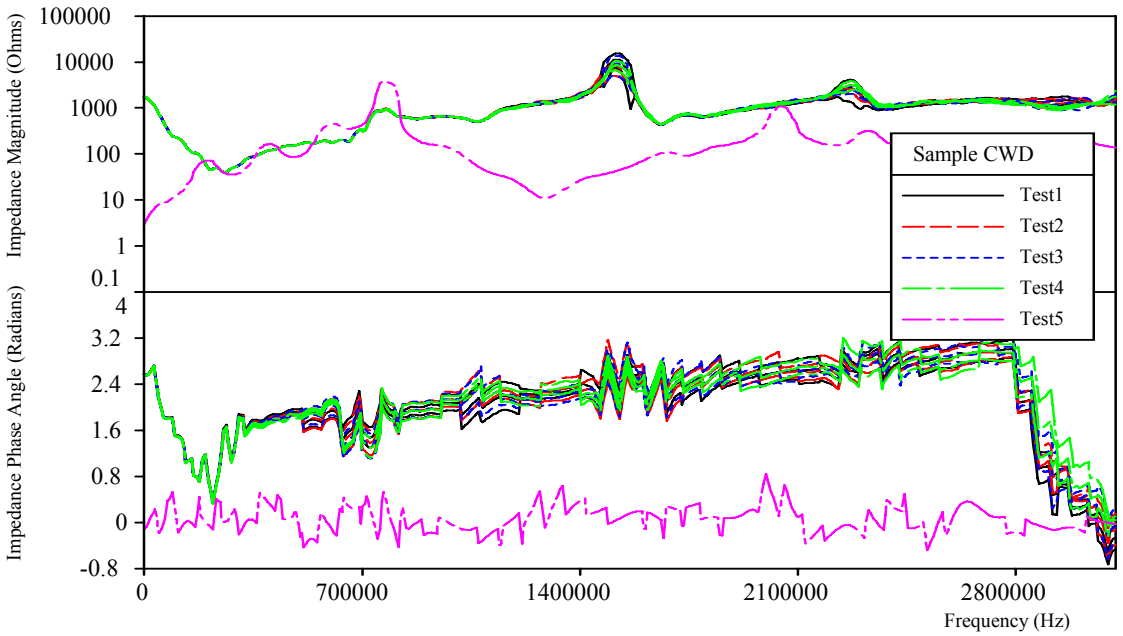

Figure F.31 New Cable Sample CWD, L=100 m, D=10.3 mm AL, 4.45 mm XLPE, Measured Impedance Magnitude and Phase Angle vs Frequency, Average and 95% Confidence Bounds

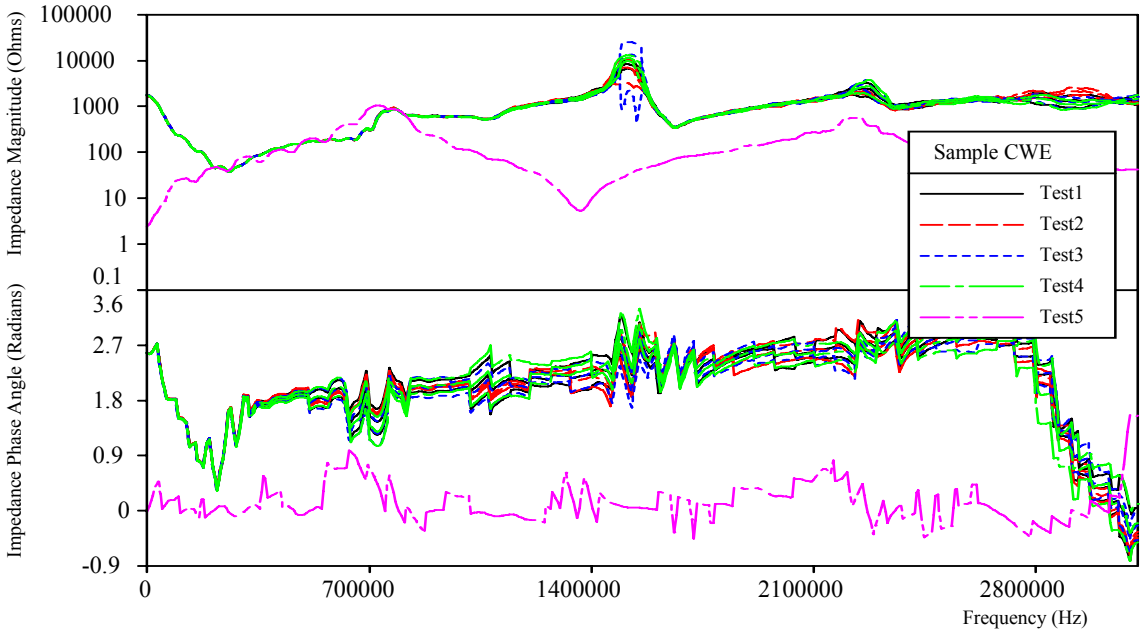

Figure F.32 New Cable Sample CWE, L=100 m, D=10.3 mm AL, 4.45 mm XLPE, Measured Impedance Magnitude and Phase Angle vs Frequency, Average and 95% Confidence Bounds

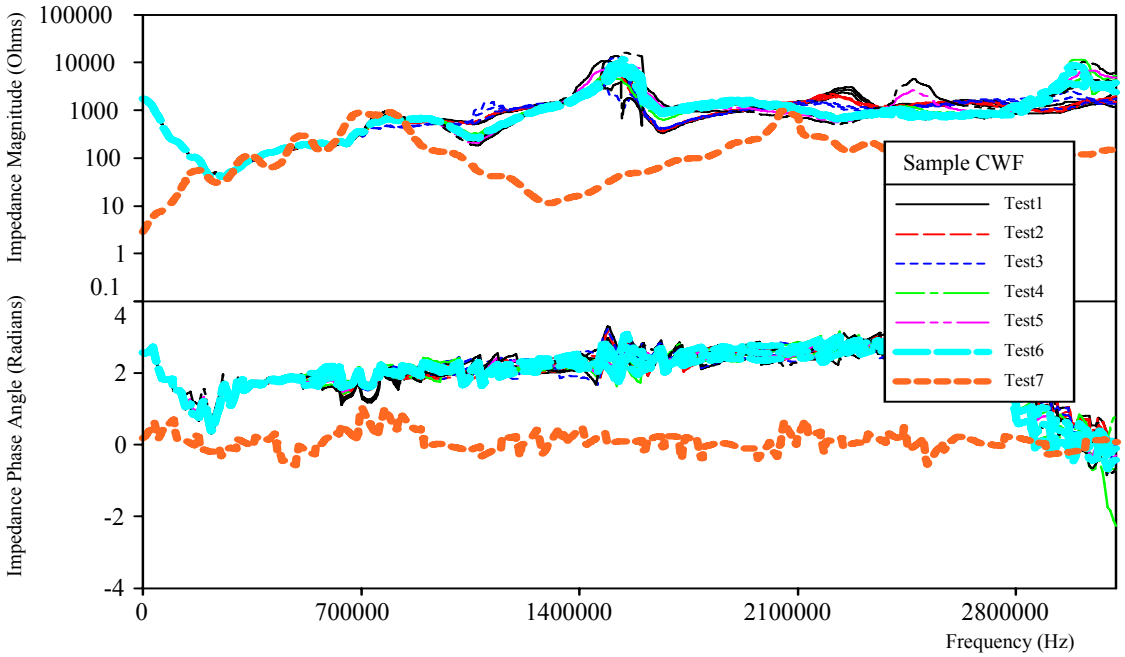

Figure F.33 New Cable Sample CWF, L=100 m, D=10.3 mm AL, 4.45 mm XLPE, Measured Impedance Magnitude and Phase Angle vs Frequency, Average and 95% Confidence Bounds

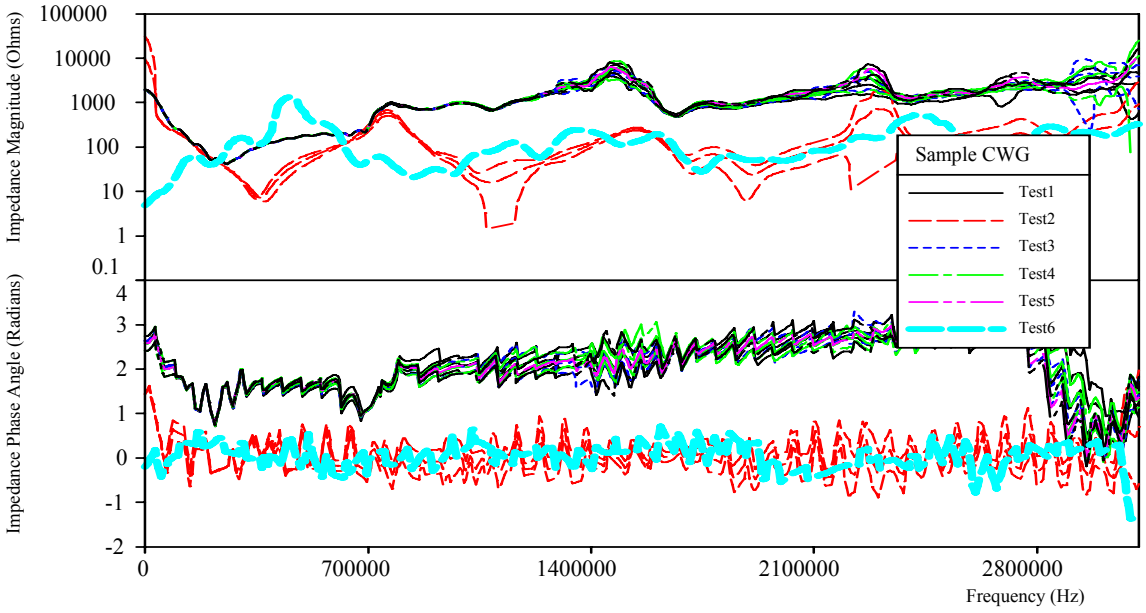

Figure F.34 New Cable Sample CWG, L=100 m, D=10.3 mm AL, 4.45 mm XLPE, Measured Impedance Magnitude and Phase Angle vs Frequency, Average and 95% Confidence Bounds

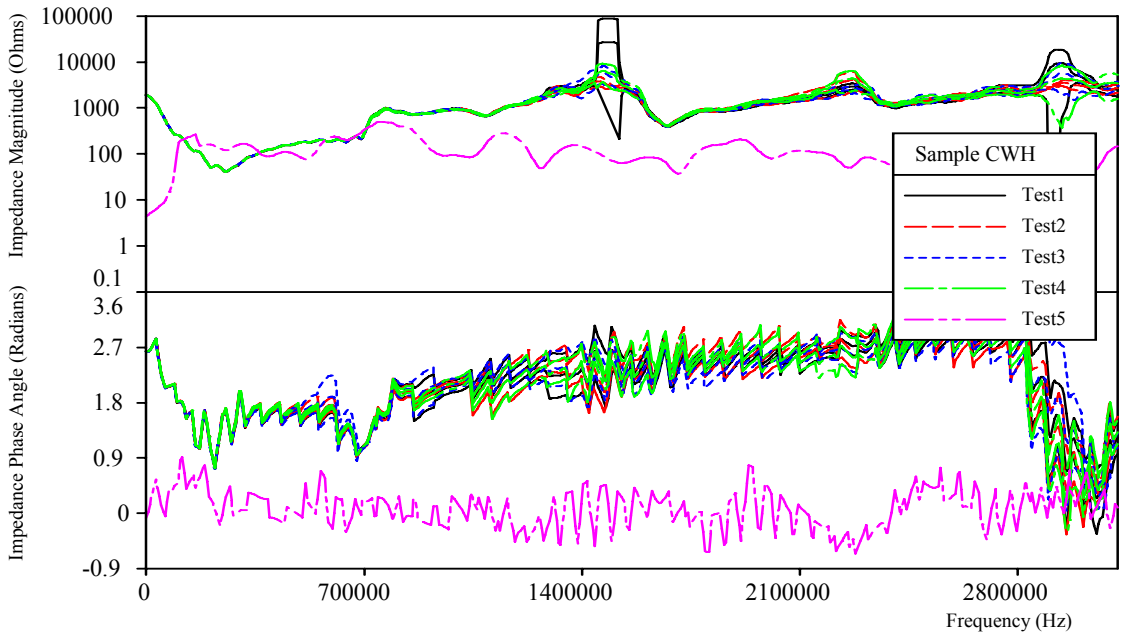

Figure F.35 New Cable Sample CWH, L=100 m, D=10.3 mm AL, 4.45 mm XLPE, Measured Impedance Magnitude and Phase Angle vs Frequency, Average and 95% Confidence Bounds

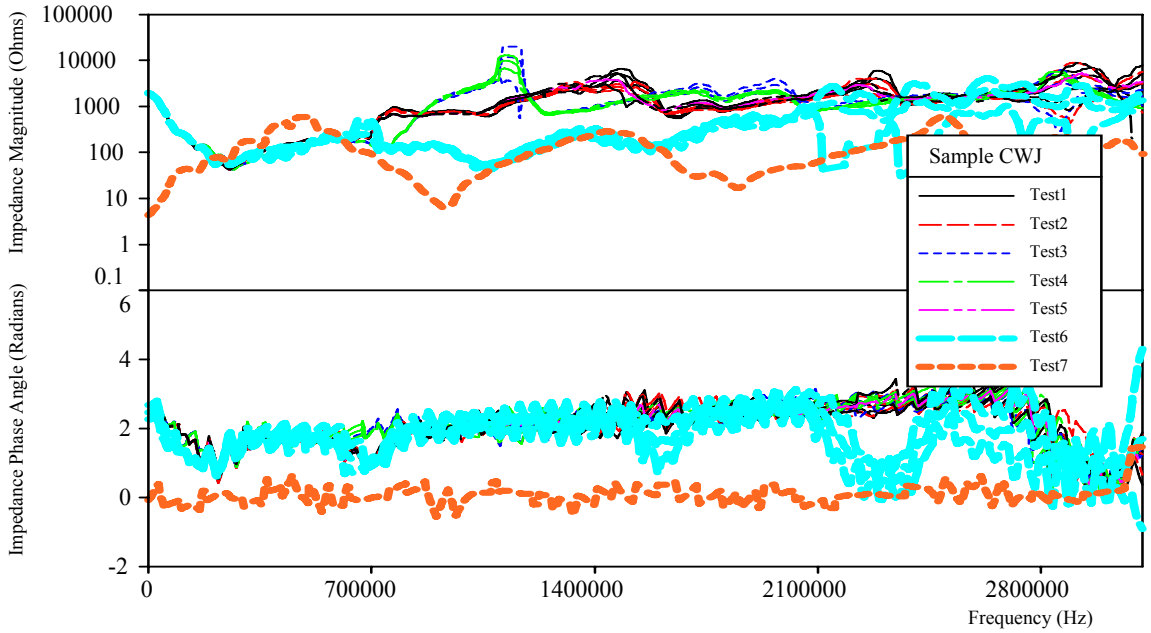

Figure F.36 New Cable Sample CWJ, L=100 m, D=10.3 mm AL, 4.45 mm XLPE, Measured Impedance Magnitude and Phase Angle vs Frequency, Average and 95% Confidence Bounds

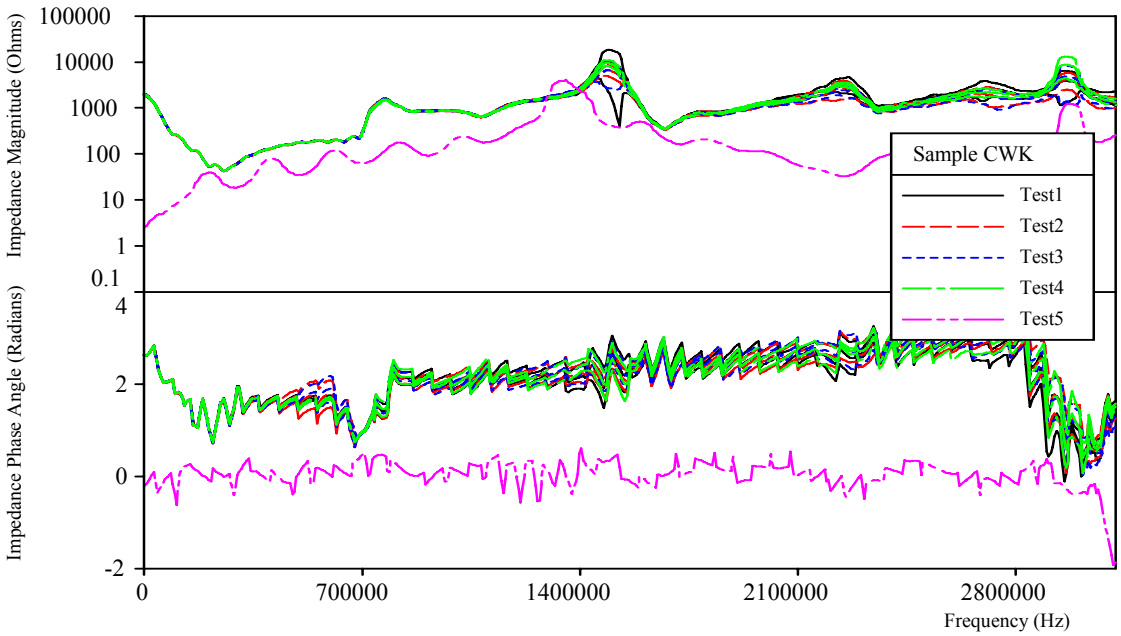

Figure F.37 New Cable Sample CWK, L=100 m, D=10.3 mm AL, 4.45 mm XLPE, Measured Impedance Magnitude and Phase Angle vs Frequency, Average and 95% Confidence Bounds

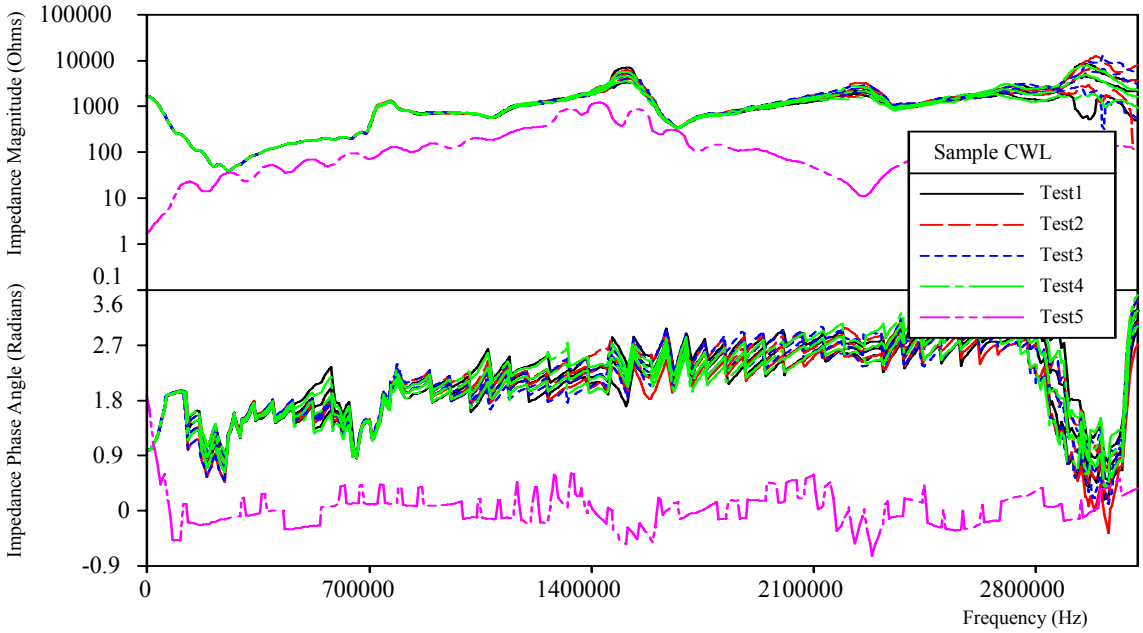

Figure F.38 New Cable Sample CWL, L=100 m, D=10.3 mm AL, 4.45 mm XLPE, Measured Impedance Magnitude and Phase Angle vs Frequency, Average and 95% Confidence Bounds

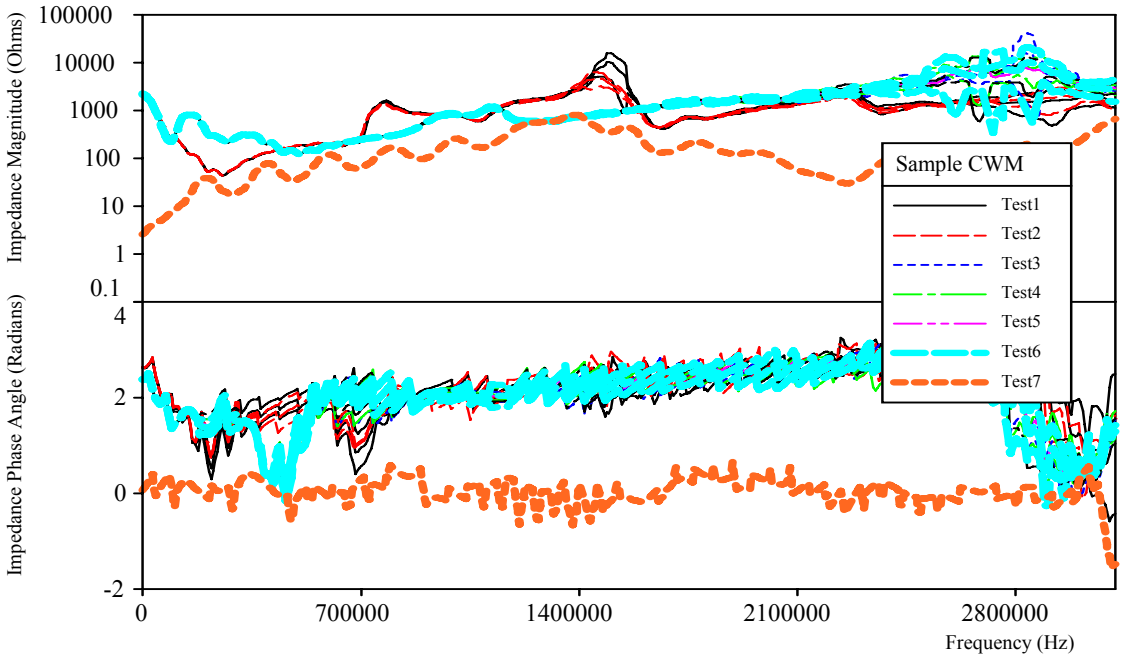

Figure F.39 New Cable Sample CWM, L=100 m, D=10.3 mm AL, 4.45 mm XLPE, Measured Impedance Magnitude and Phase Angle vs Frequency, Average and 95% Confidence Bounds

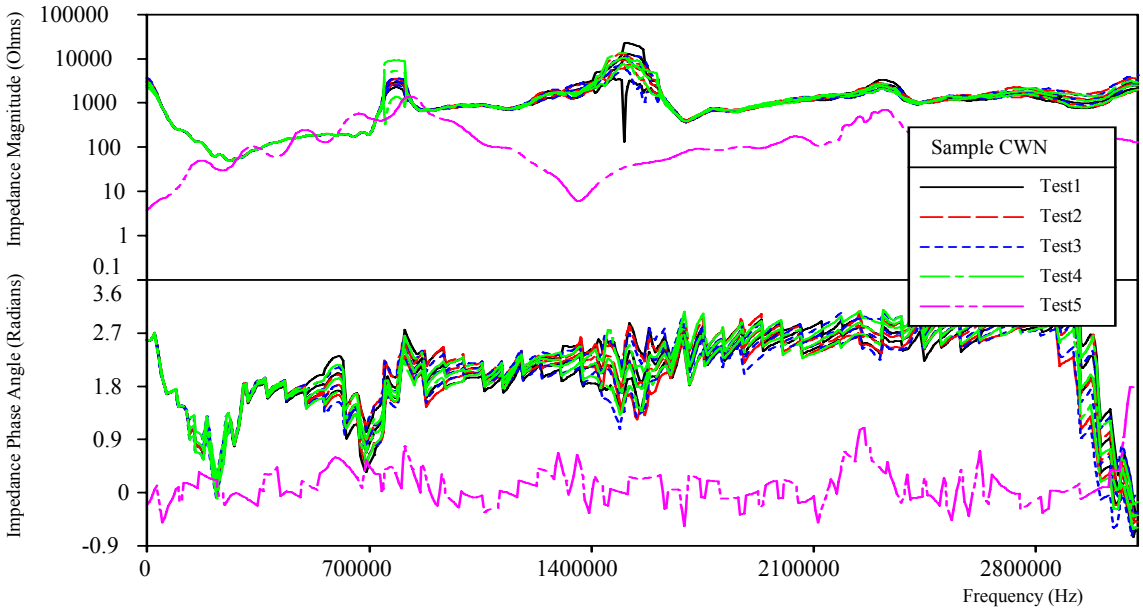

Figure F.40 New Cable Sample CWN, L=100 m, D=10.3 mm AL, 4.45 mm XLPE, Measured Impedance Magnitude and Phase Angle vs Frequency, Average and 95% Confidence Bounds

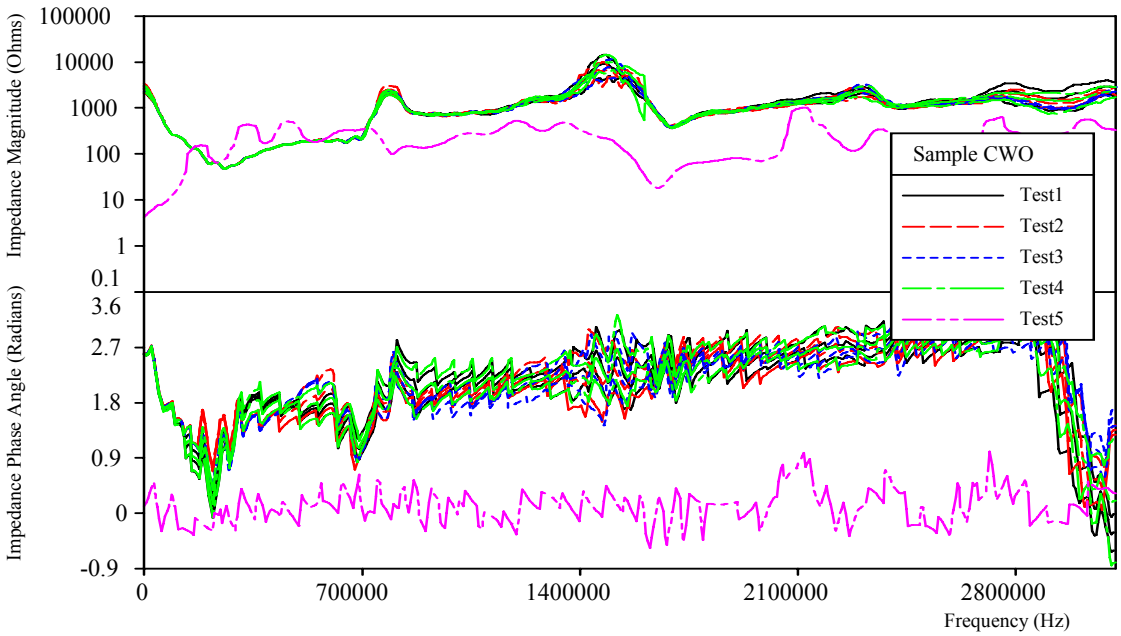

Figure F.41 New Cable Sample CWO, L=100 m, D=10.3 mm AL, 4.45 mm XLPE, Measured Impedance Magnitude and Phase Angle vs Frequency, Average and 95% Confidence Bounds

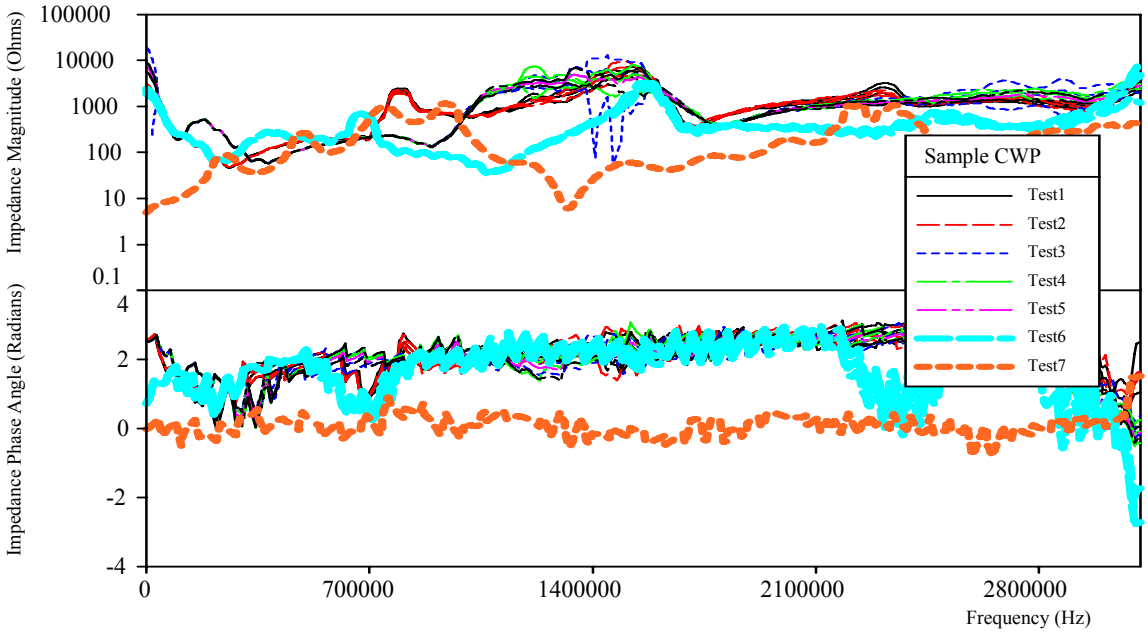

Figure F.42 New Cable Sample CWP, L=100 m, D=10.3 mm AL, 4.45 mm XLPE, Measured Impedance Magnitude and Phase Angle vs Frequency, Average and 95% Confidence Bounds

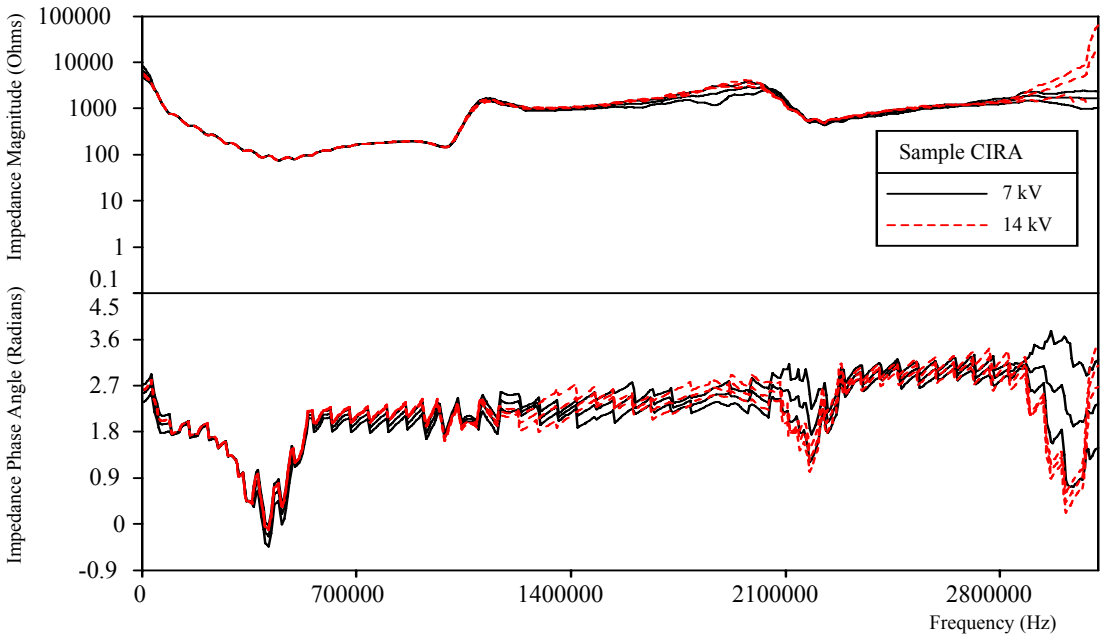

Figure F.43 Aged Cable Sample CIRA, L=30 m, D=13 mm CU, 5.59 mm HMWPE, Measured Impedance Magnitude and Phase Angle vs Frequency, Average and 95% Confidence Bounds

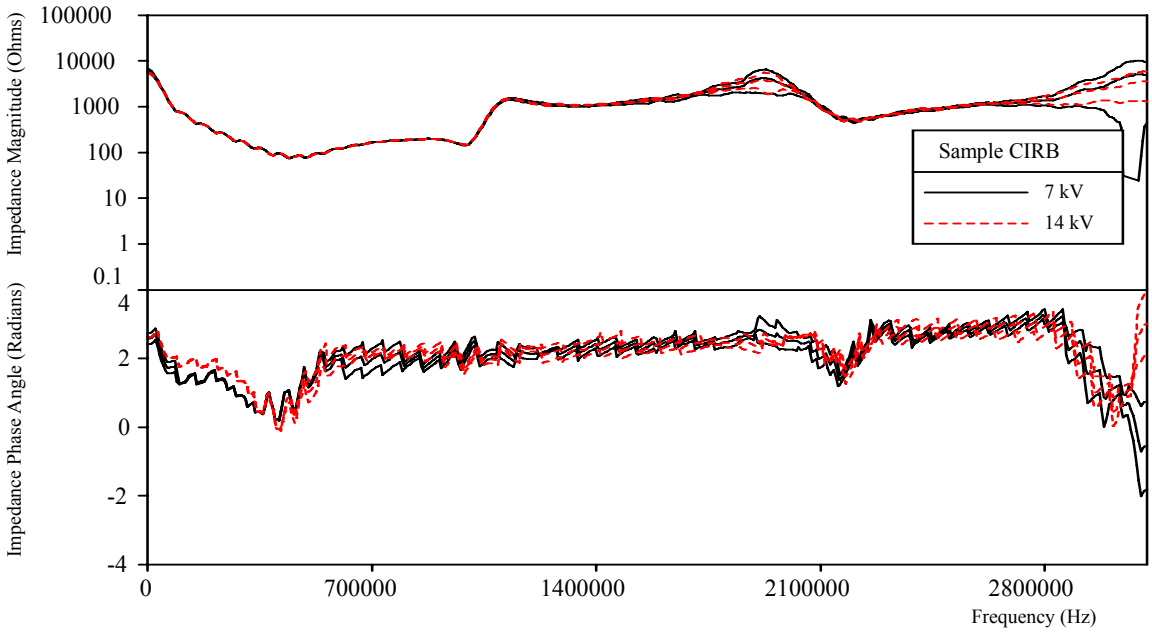

Figure F.44 Aged Cable Sample CIRB, L=30 m, D=13 mm CU, 5.59 mm HMWPE, Measured Impedance Magnitude and Phase Angle vs Frequency, Average and 95% Confidence Bounds

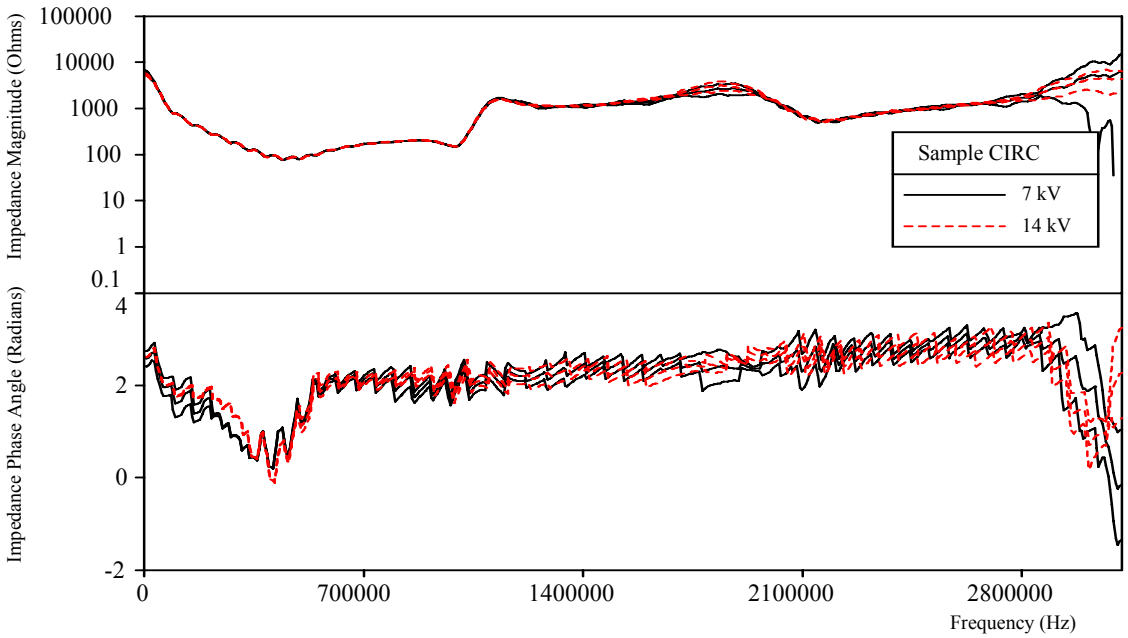

Figure F.45 Aged Cable Sample CIRC, L=30 m, D=13 mm CU, 5.59 mm HMWPE, Measured Impedance Magnitude and Phase Angle vs Frequency, Average and 95% Confidence Bounds

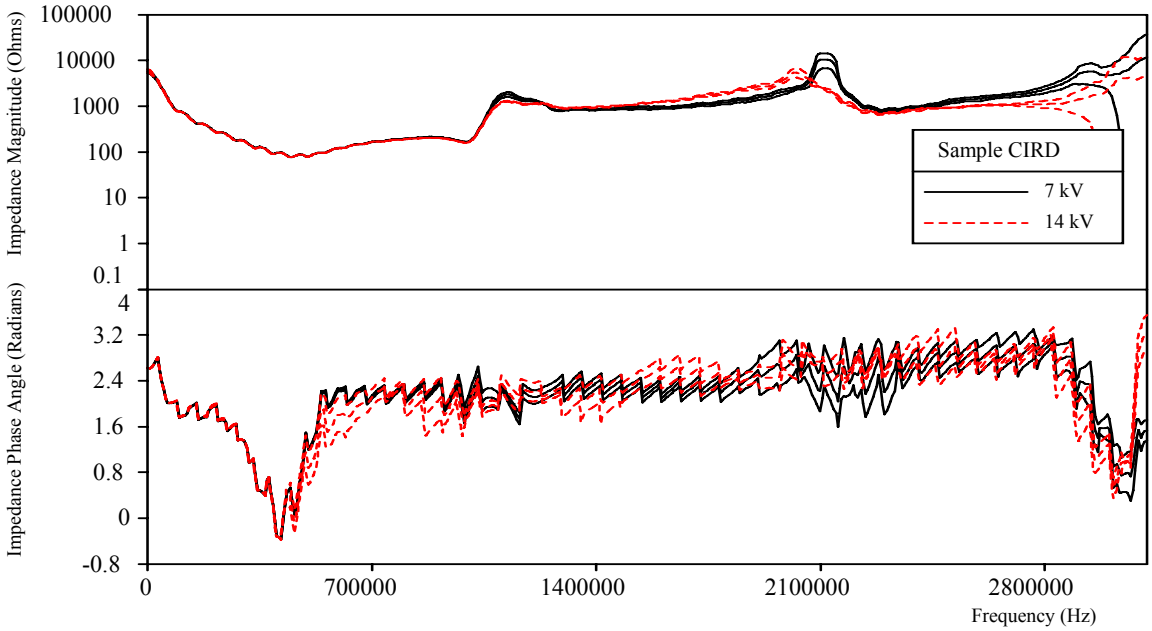

Figure F.46 Aged Cable Sample CIRD, L=30 m, D=13 mm CU, 5.59 mm HMWPE, Measured Impedance Magnitude and Phase Angle vs Frequency, Average and 95% Confidence Bounds

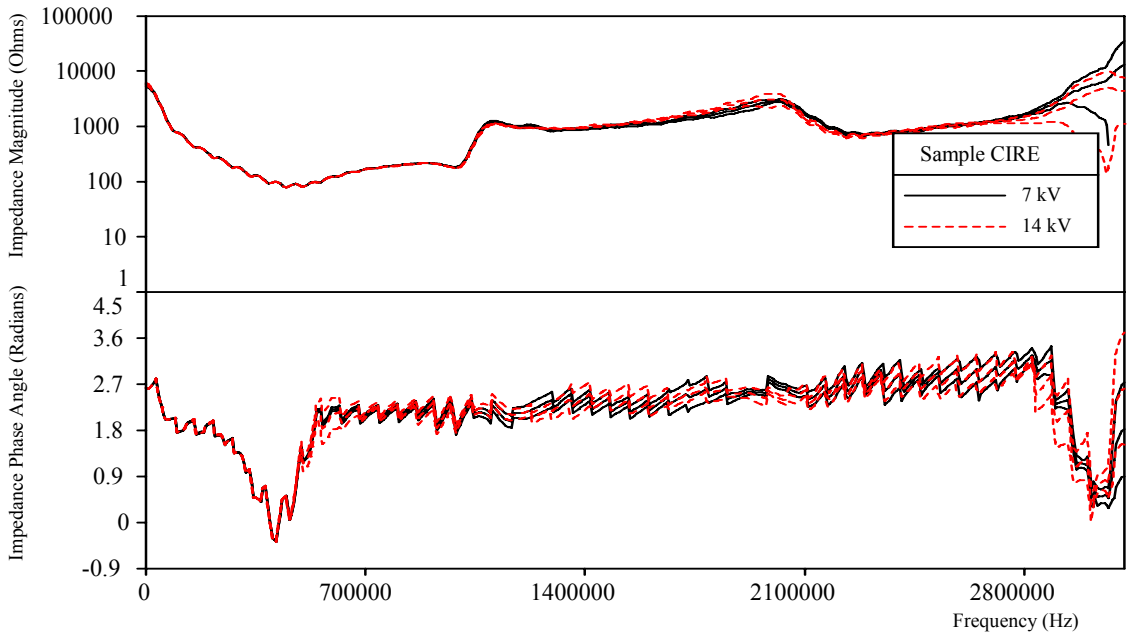

Figure F.47 Aged Cable Sample CIRE, L=30 m, D=13 mm CU, 5.59 mm HMWPE, Measured Impedance Magnitude and Phase Angle vs Frequency, Average and 95% Confidence Bounds

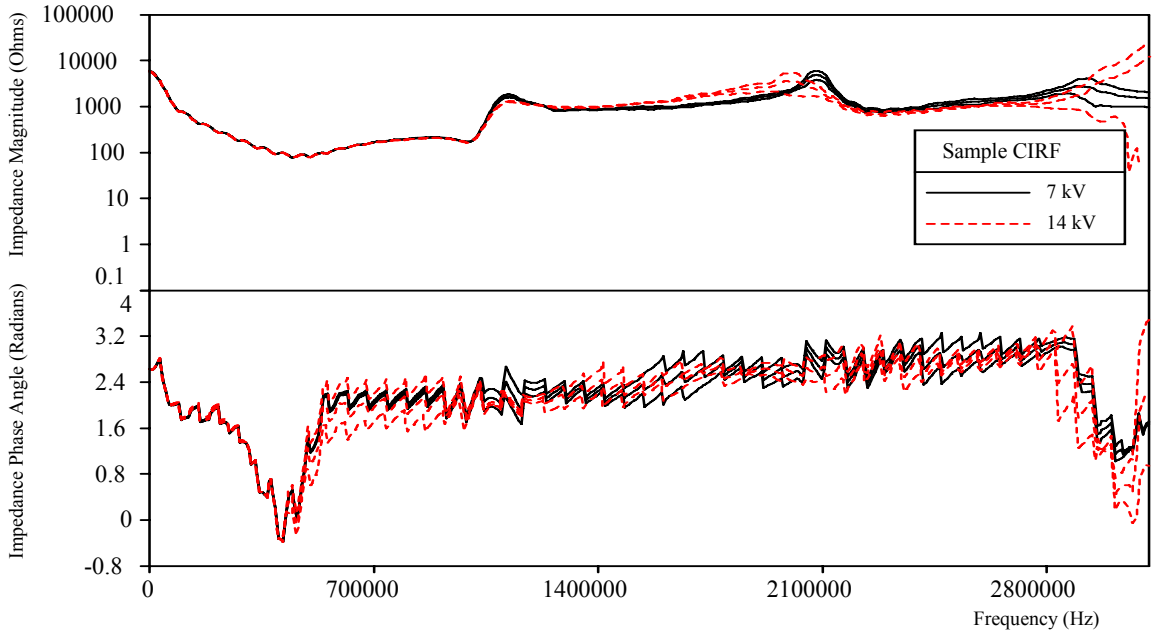

Figure F.48 Aged Cable Sample CIRF, L=30 m, D=13 mm CU, 5.59 mm HMWPE, Measured Impedance Magnitude and Phase Angle vs Frequency, Average and 95% Confidence Bounds

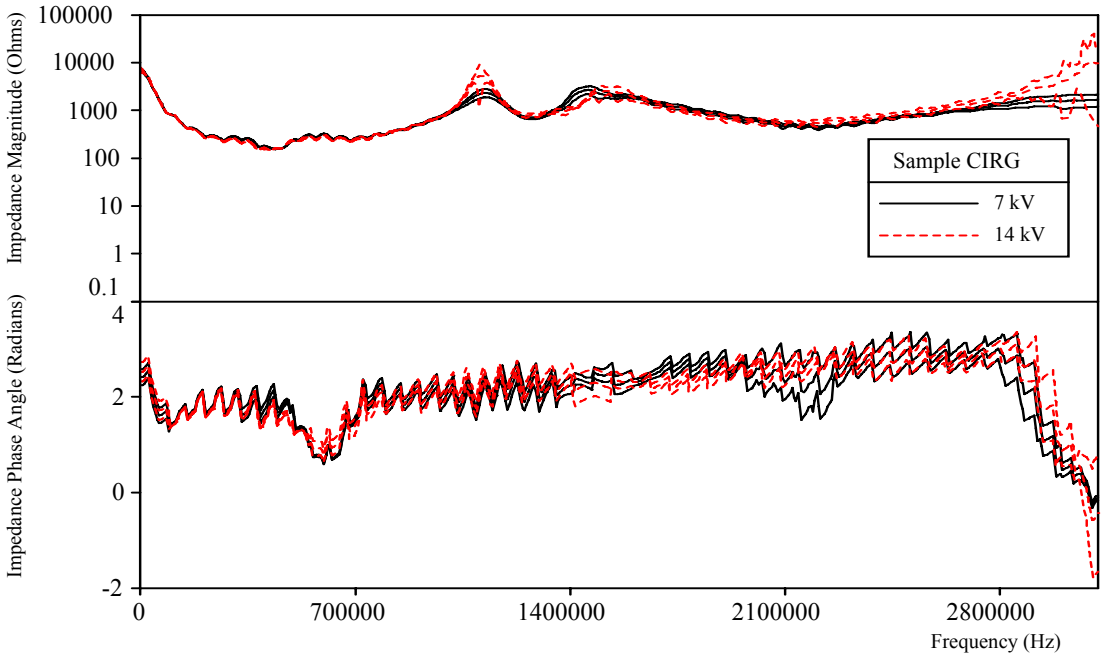

Figure F.49 Aged Cable Sample CIRG, L=30 m, D=10.3 mm AL, 4.45 mm XLPE, Measured Impedance Magnitude and Phase Angle vs Frequency, Average and 95% Confidence Bounds

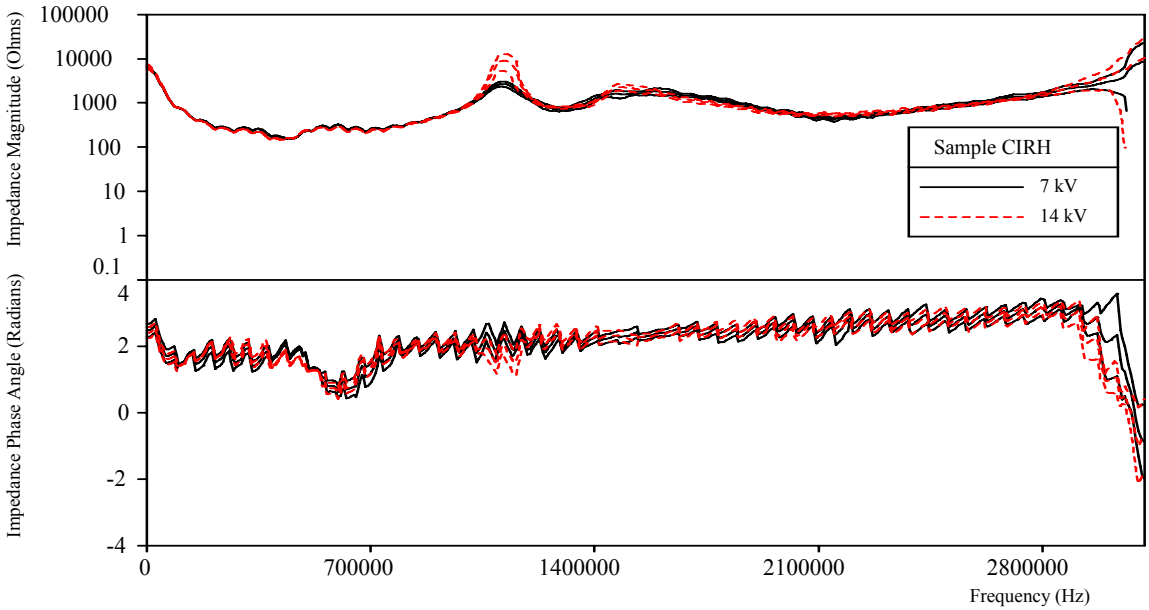

Figure F.50 Aged Cable Sample CIRH, L=30 m, D=10.3 mm AL, 4.45 mm XLPE, Measured Impedance Magnitude and Phase Angle vs Frequency, Average and 95% Confidence Bounds

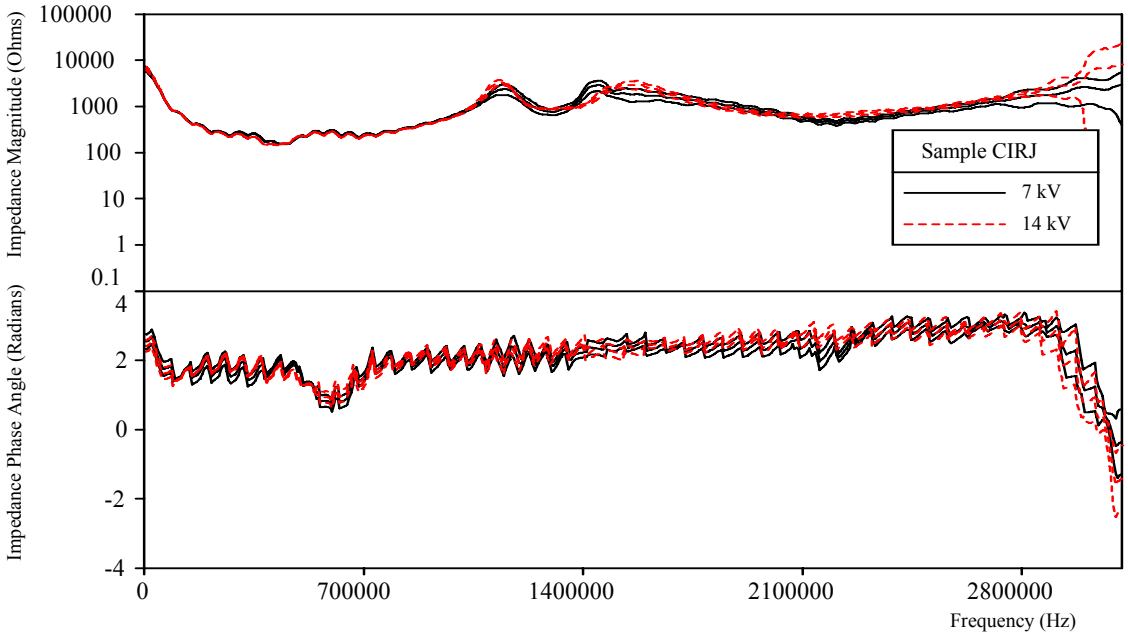

Figure F.51 Aged Cable Sample CIRJ, L=30 m, D=10.3 mm AL, 4.45 mm XLPE, Measured Impedance Magnitude and Phase Angle vs Frequency, Average and 95% Confidence Bounds

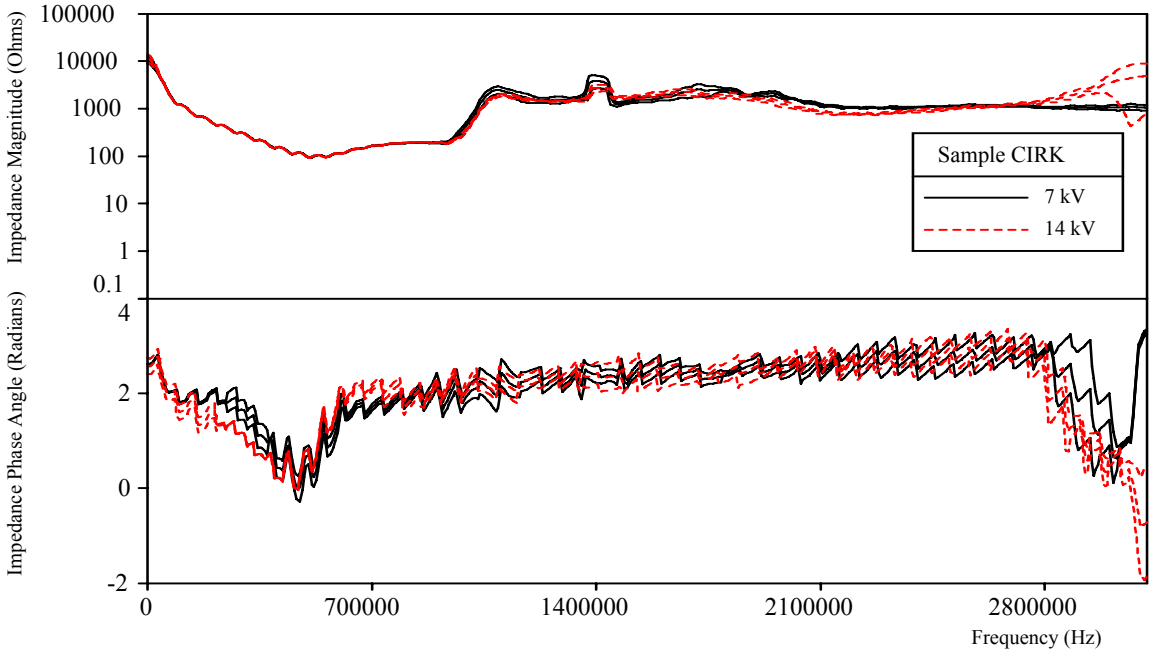

Figure F.52 Aged Cable Sample CIRK, L=30 m, D=4.6 mm CU, 5.59 mm HMWPE, Measured Impedance Magnitude and Phase Angle vs Frequency, Average and 95% Confidence Bounds

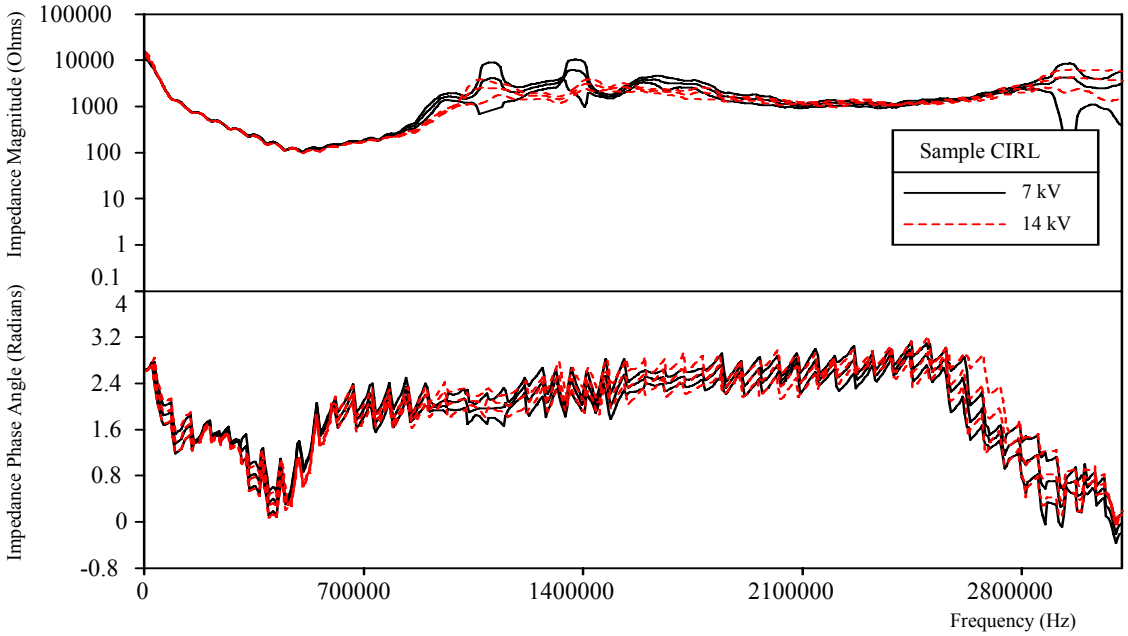

Figure F.53 Aged Cable Sample CIRL, L=30 m, D=4.6 mm CU, 5.59 mm HMWPE, Measured Impedance Magnitude and Phase Angle vs Frequency, Average and 95% Confidence Bounds

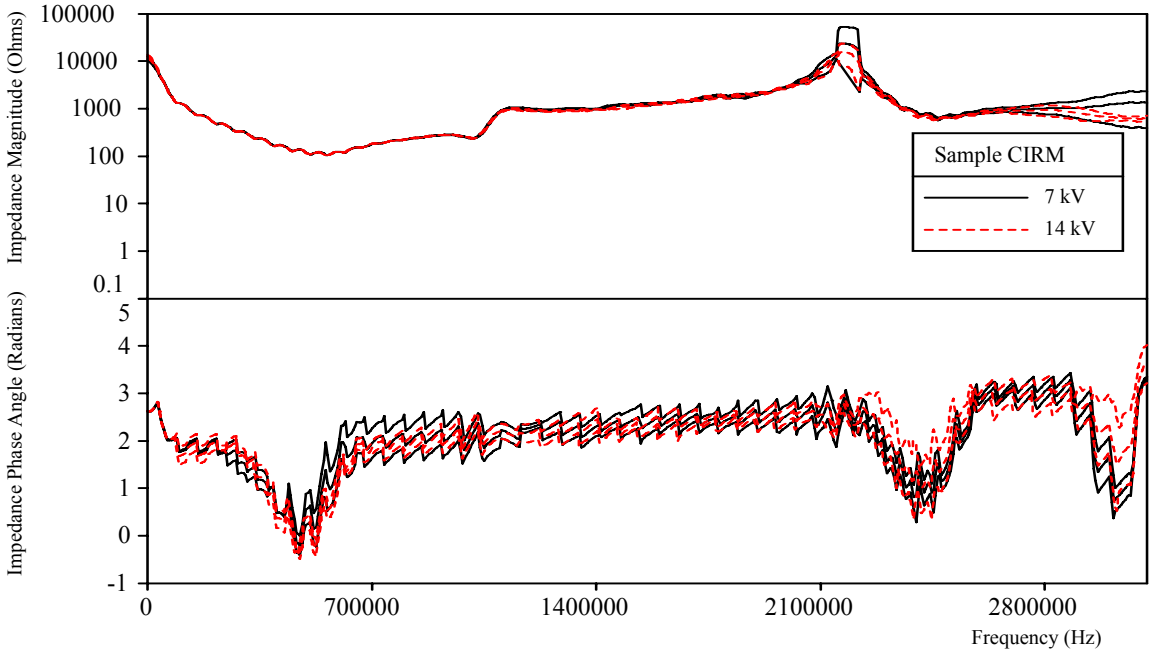

Figure F.54 Aged Cable Sample CIRM, L=30 m, D=4.6 mm CU, 5.59 mm HMWPE, Measured Impedance Magnitude and Phase Angle vs Frequency, Average and 95% Confidence Bounds

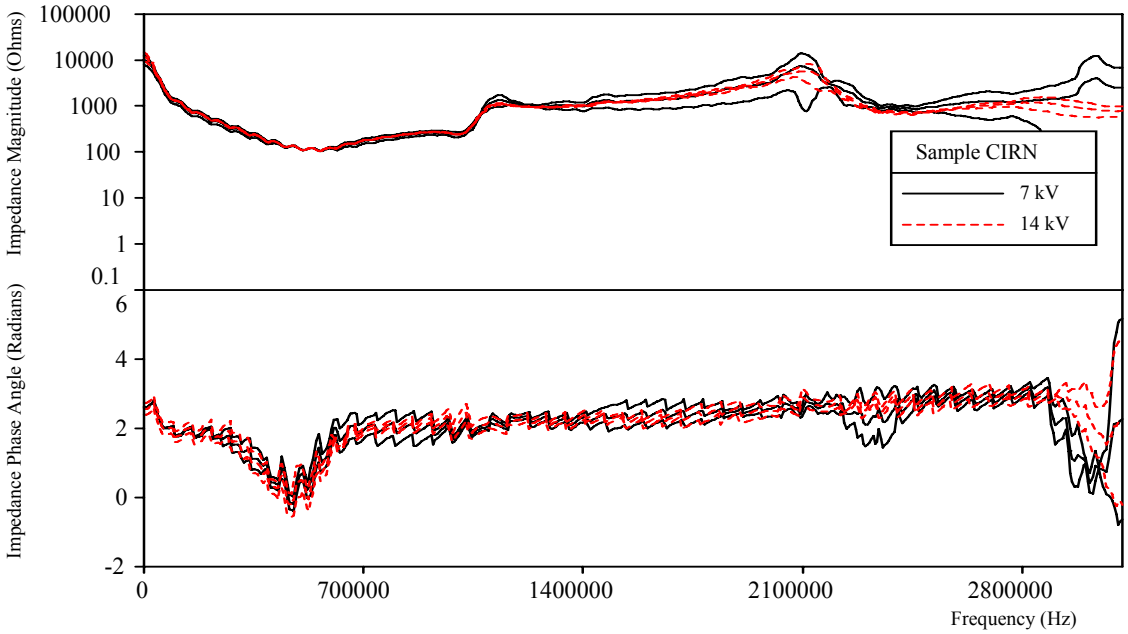

Figure F.55 Aged Cable Sample CIRN, L=30 m, D=4.6 mm CU, 5.59 mm HMWPE, Measured Impedance Magnitude and Phase Angle vs Frequency, Average and 95% Confidence Bounds

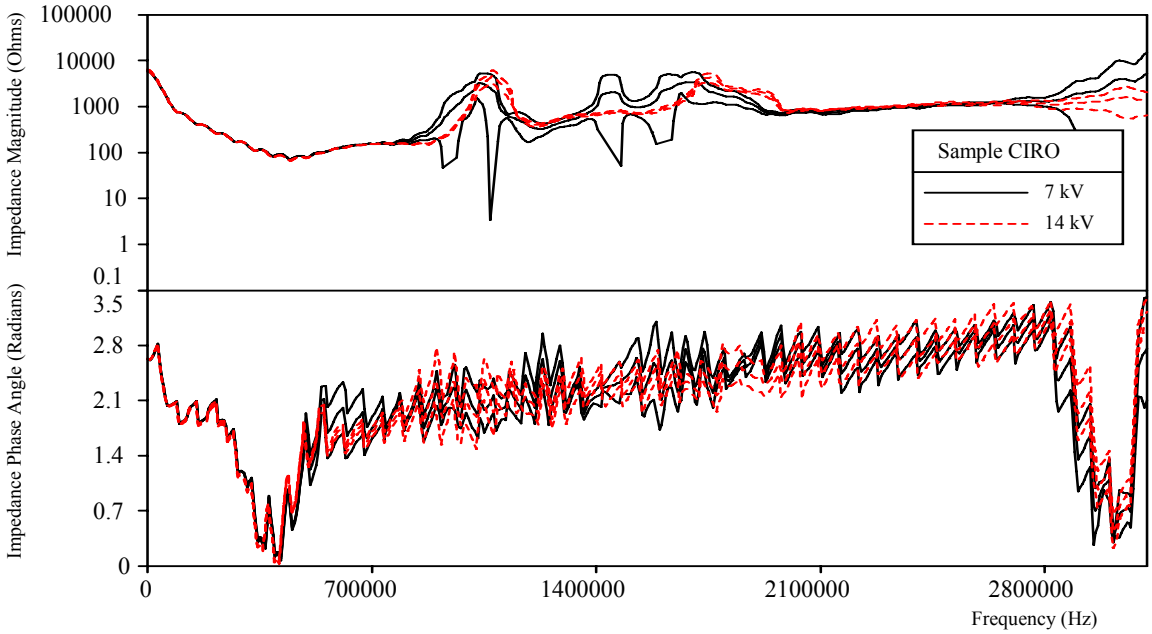

Figure F.56 Aged Cable Sample CIRO, L=30 m, D=10.3 mm AL, 4.45 mm XLPE, Measured Impedance Magnitude and Phase Angle vs Frequency, Average and 95% Confidence Bounds

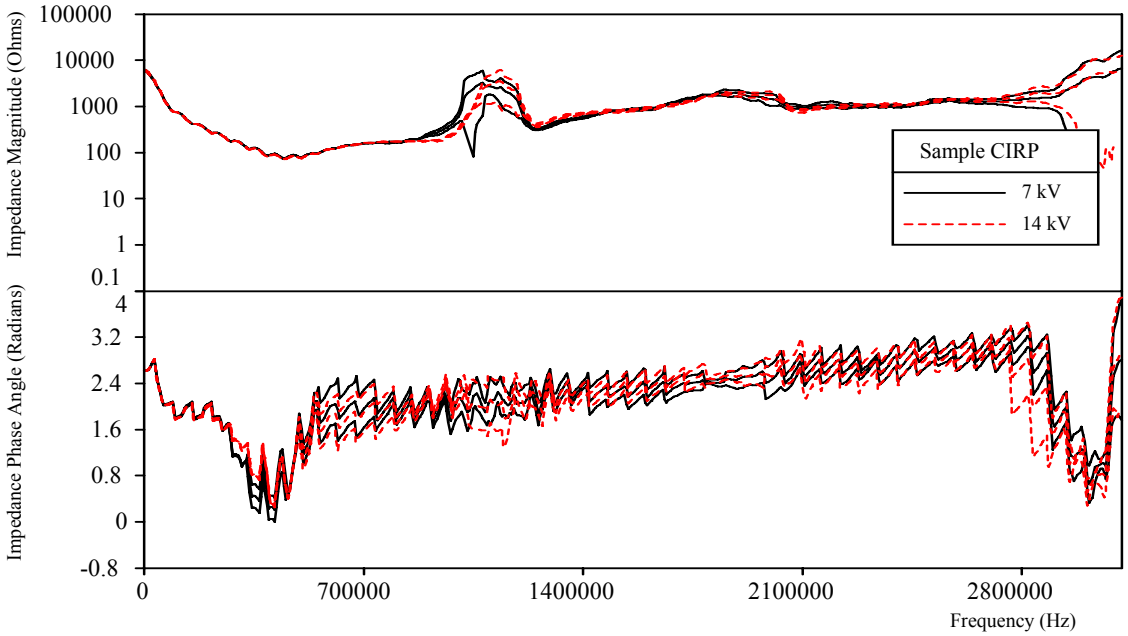

Figure F.57 Aged Cable Sample CIRP, L=30 m, D=10.3 mm AL, 4.45 mm XLPE, Measured Impedance Magnitude and Phase Angle vs Frequency, Average and 95% Confidence Bounds

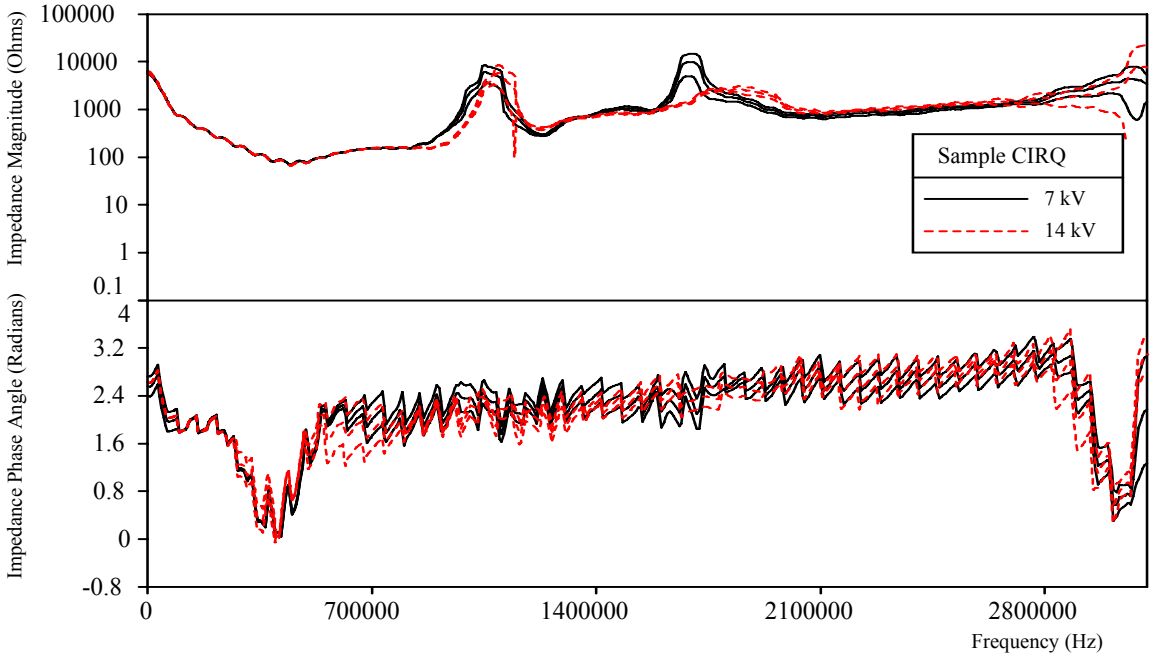

Figure F.58 Aged Cable Sample CIRQ, L=30 m, D=10.3 mm AL, 4.45 mm XLPE, Measured Impedance Magnitude and Phase Angle vs Frequency, Average and 95% Confidence Bounds

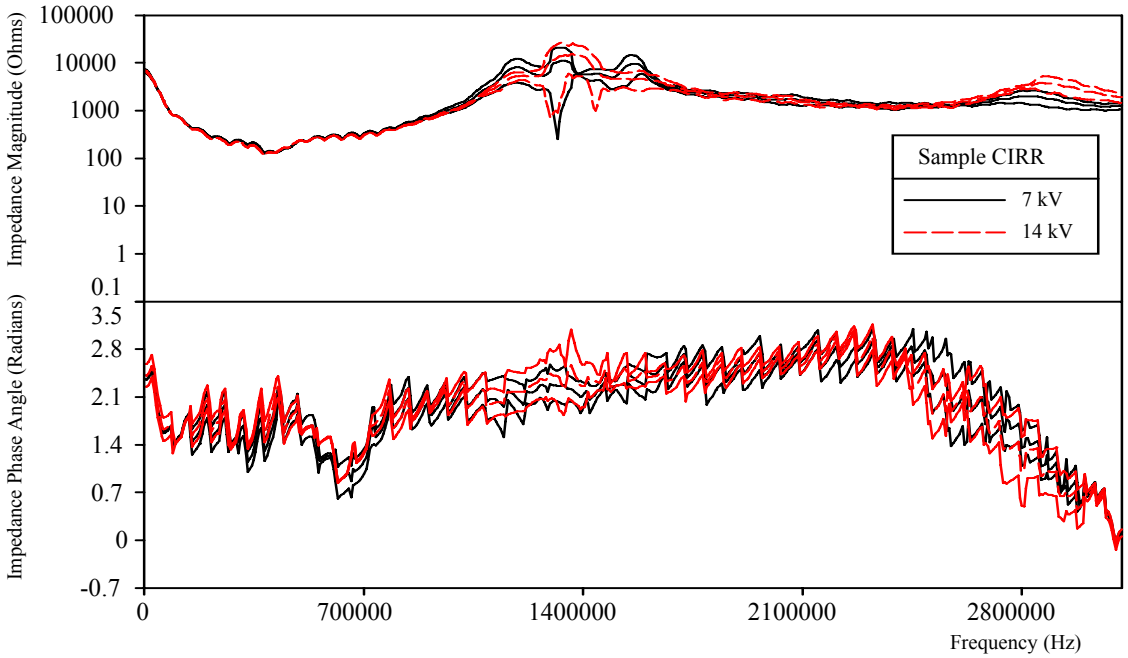

Figure F.59 Aged Cable Sample CIRR, L=30 m, D=10.3 mm AL, 4.45 mm XLPE, Measured Impedance Magnitude and Phase Angle vs Frequency, Average and 95% Confidence Bounds

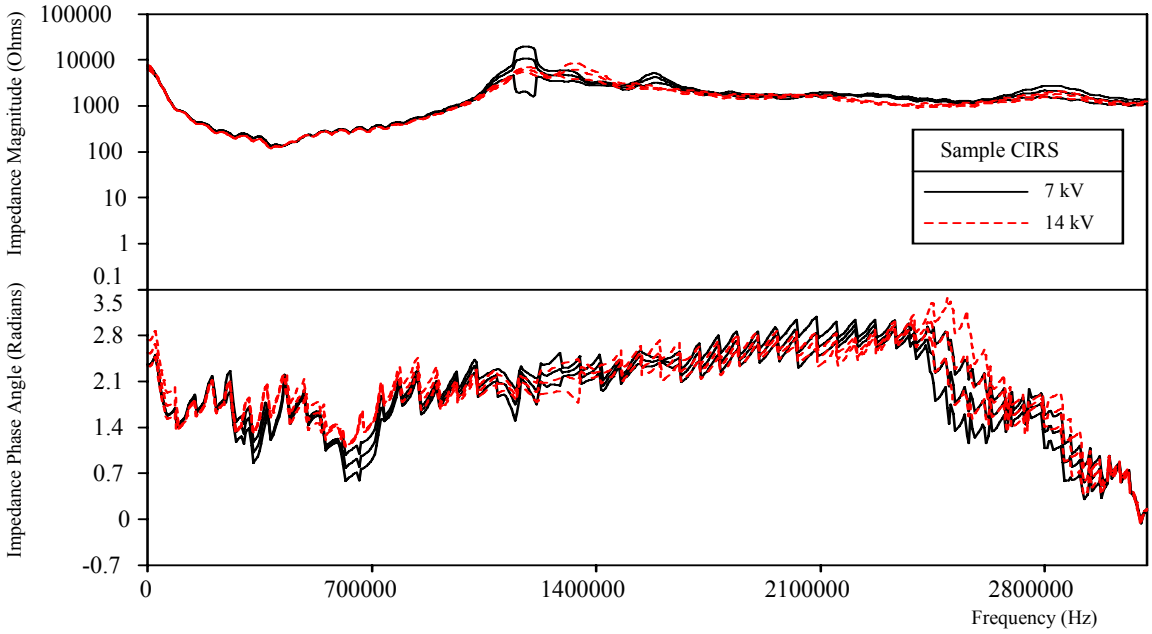

Figure F.60 Aged Cable Sample CIRS, L=30 m, D=10.3 mm AL, 4.45 mm XLPE, Measured Impedance Magnitude and Phase Angle vs Frequency, Average and 95% Confidence Bounds

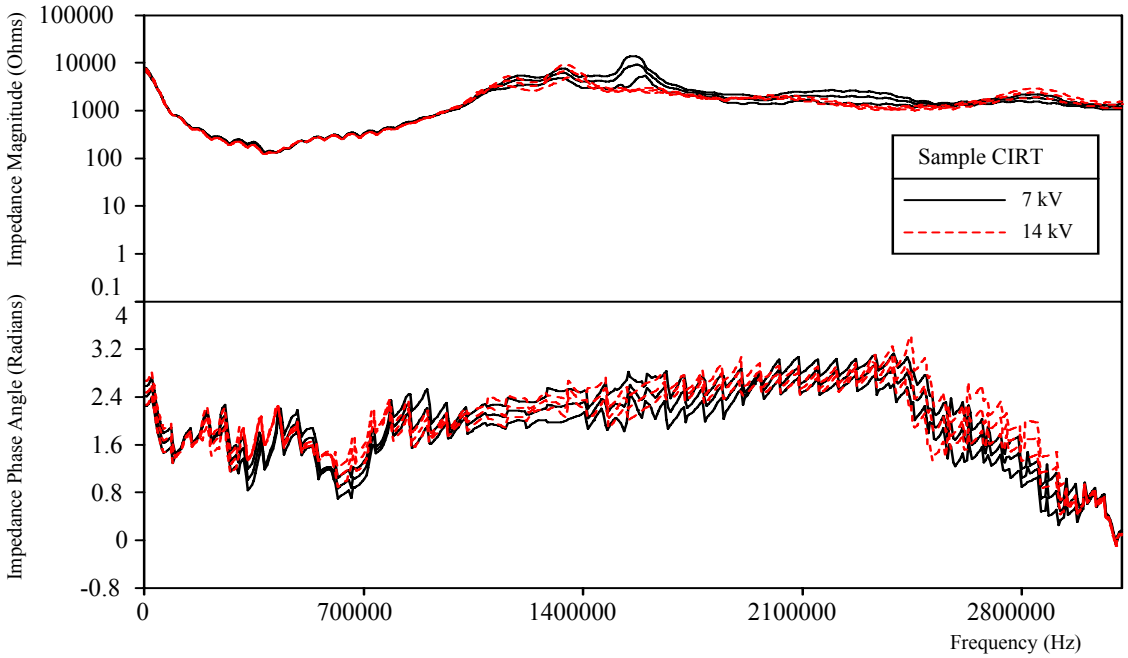

Figure F.61 Aged Cable Sample CIRT, L=30 m, D=10.3 mm AL, 4.45 mm XLPE, Measured Impedance Magnitude and Phase Angle vs Frequency, Average and 95% Confidence Bounds

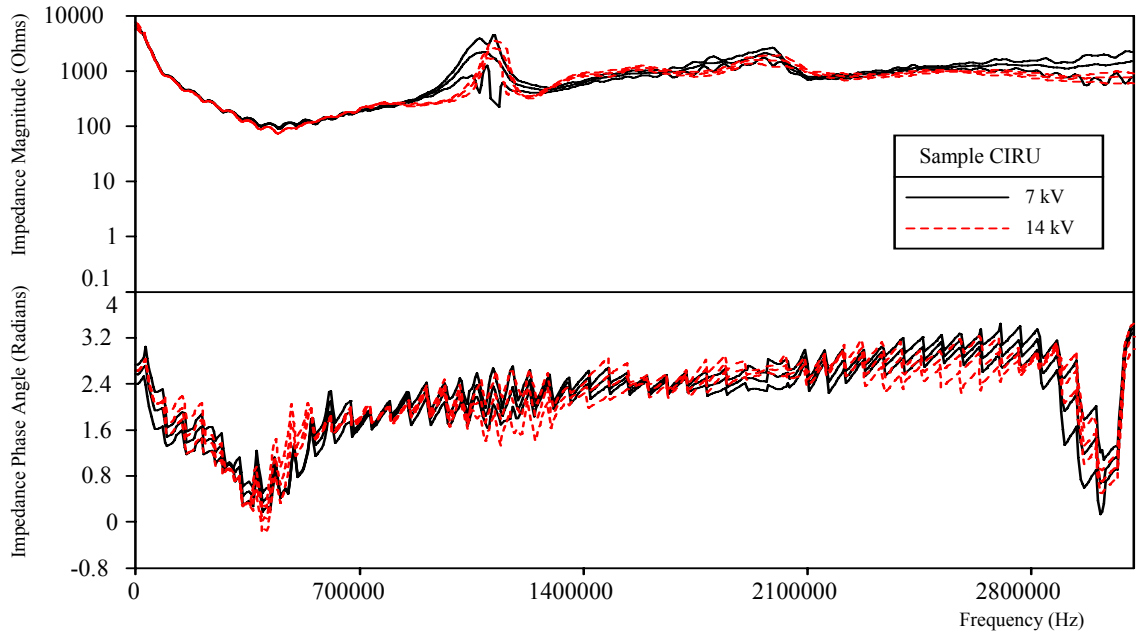

Figure F.62 Aged Cable Sample CIRU, L=30 m, D=10.3 mm AL, 4.45 mm XLPE, Measured Impedance Magnitude and Phase Angle vs Frequency, Average and 95% Confidence Bounds

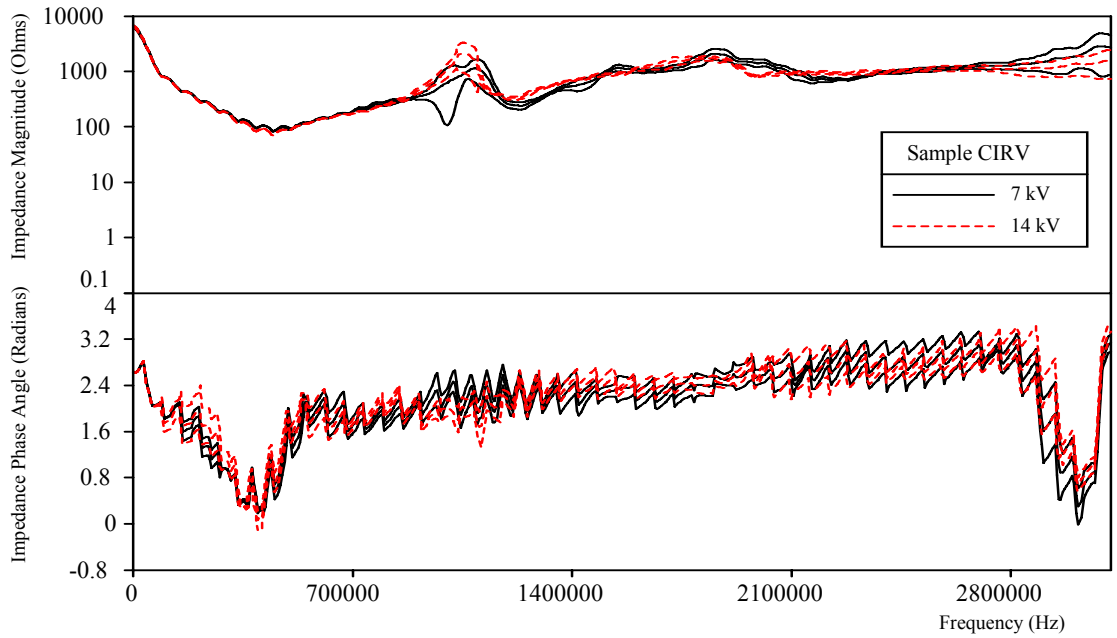

Figure F.63 Aged Cable Sample CIRV, L=30 m, D=10.3 mm AL, 4.45 mm XLPE, Measured Impedance Magnitude and Phase Angle vs Frequency, Average and 95% Confidence Bounds

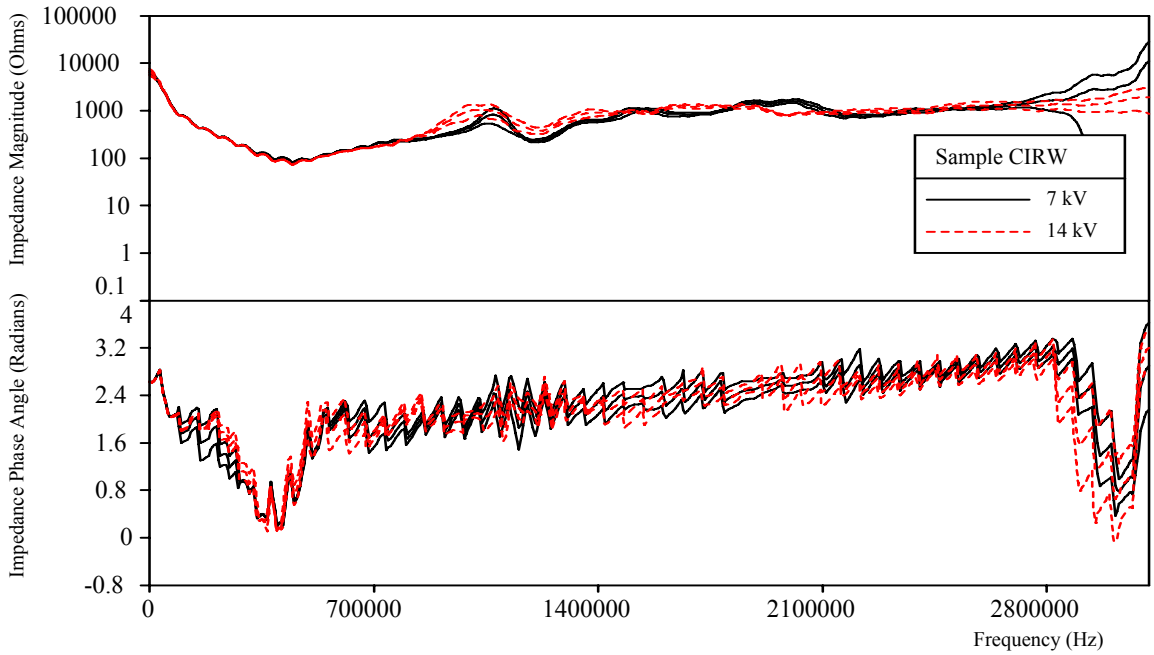

Figure F.64 Aged Cable Sample CIRW, L=30 m, D=10.3 mm AL, 4.45 mm XLPE, Measured Impedance Magnitude and Phase Angle vs Frequency, Average and 95% Confidence Bounds

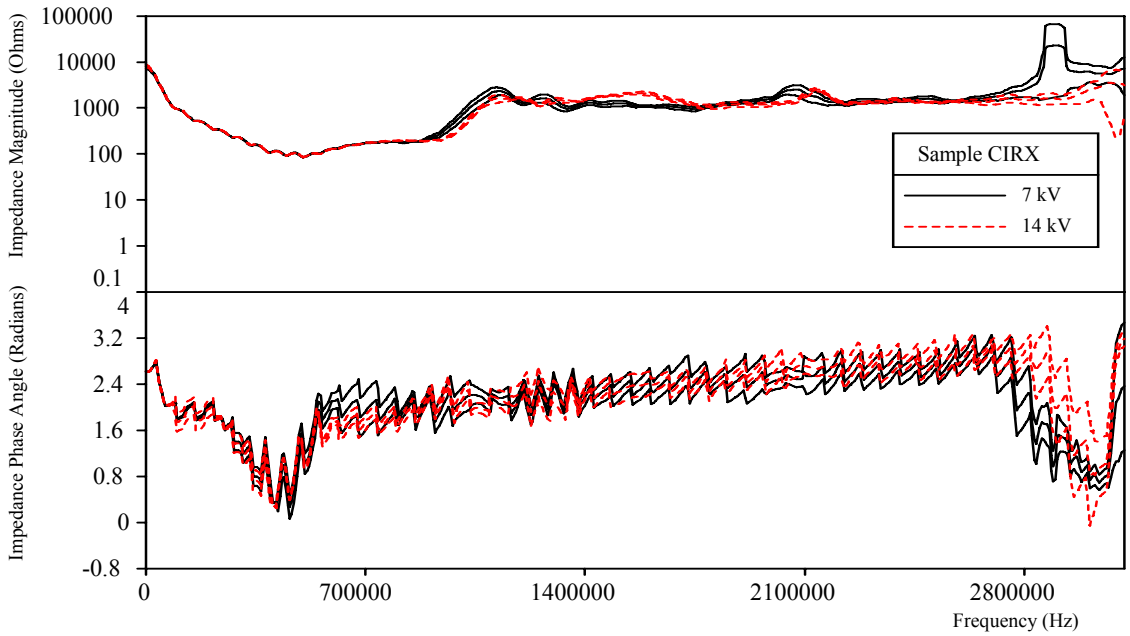

Figure F.65 Aged Cable Sample CIRX, L=30 m, D=10.3 mm AL, 4.45 mm XLPE, Measured Impedance Magnitude and Phase Angle vs Frequency, Average and 95% Confidence Bounds

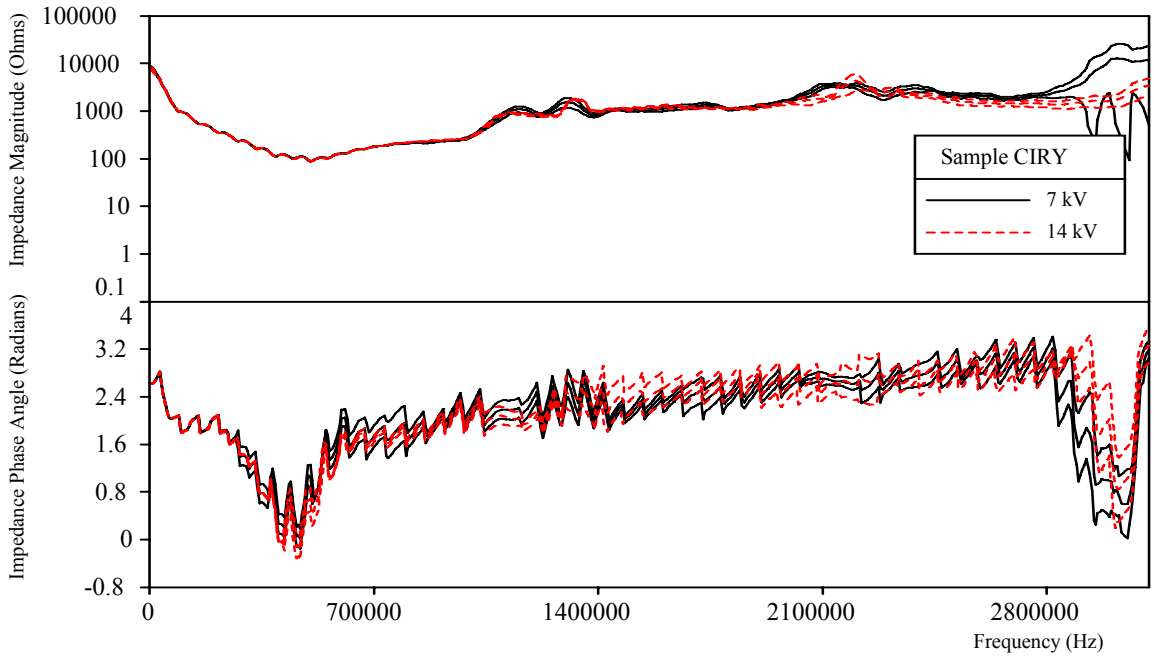

Figure F.66 Aged Cable Sample CIRY, L=30 m, D=10.3 mm AL, 4.45 mm XLPE, Measured Impedance Magnitude and Phase Angle vs Frequency, Average and 95% Confidence Bounds

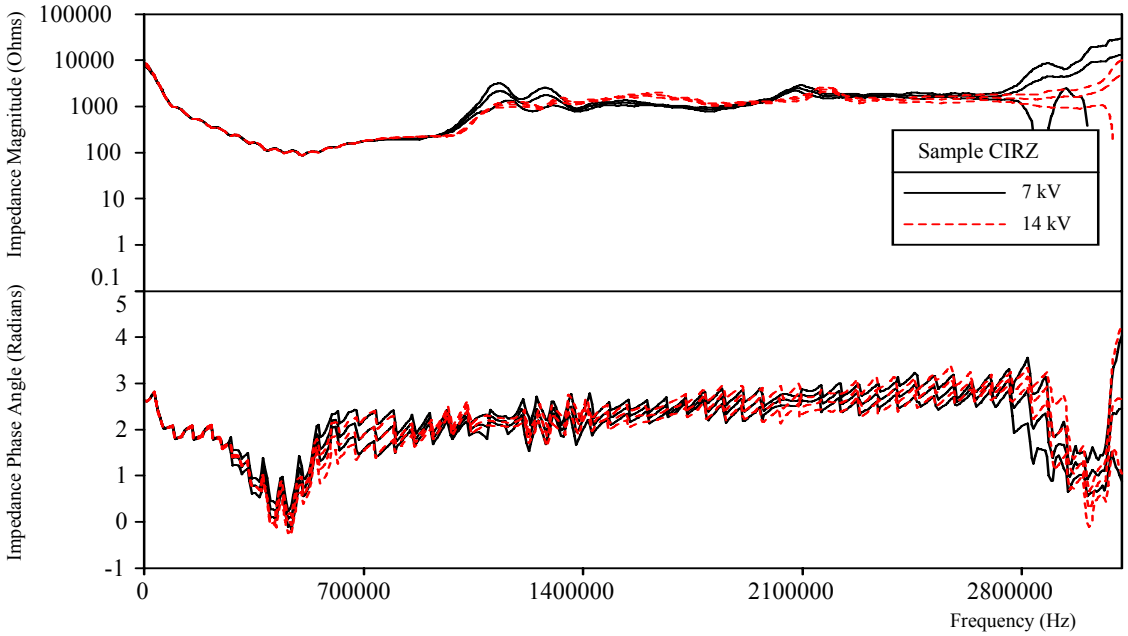

Figure F.67 Aged Cable Sample CIRZ, L=30 m, D=10.3 mm AL, 4.45 mm XLPE, Measured Impedance Magnitude and Phase Angle vs Frequency, Average and 95% Confidence Bounds

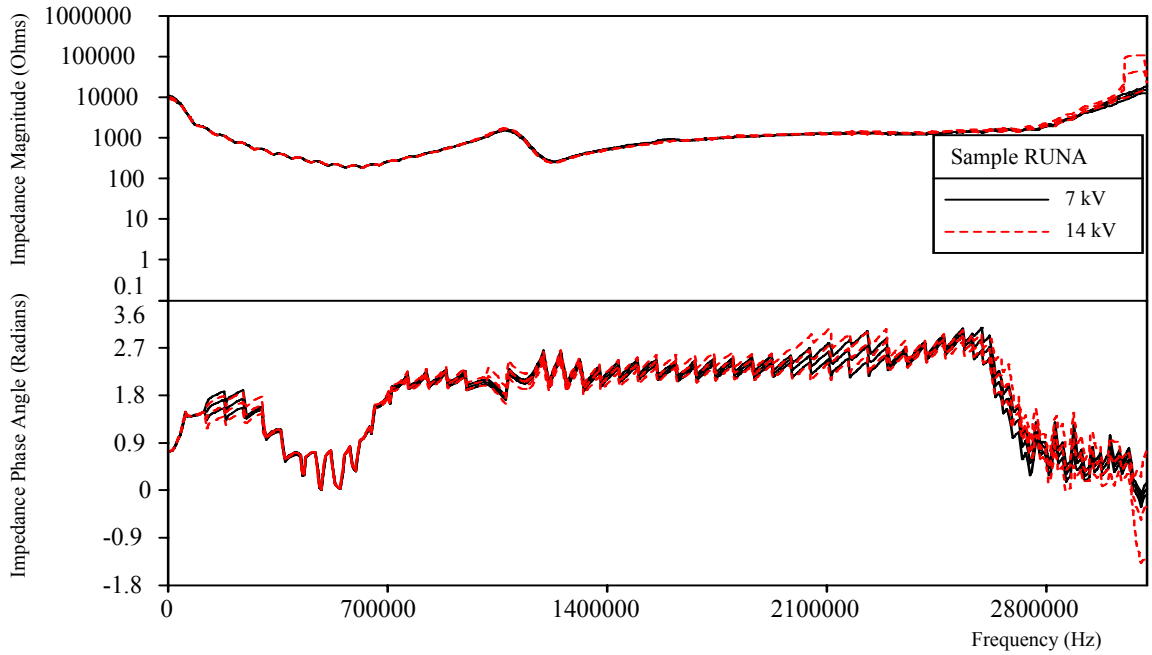

Figure F.68 Aged Cable Sample RUNA, L=23 m, D=4.6 mm CU, 5.59 mm HMWPE, Measured Impedance Magnitude and Phase Angle vs Frequency, Average and 95% Confidence Bounds

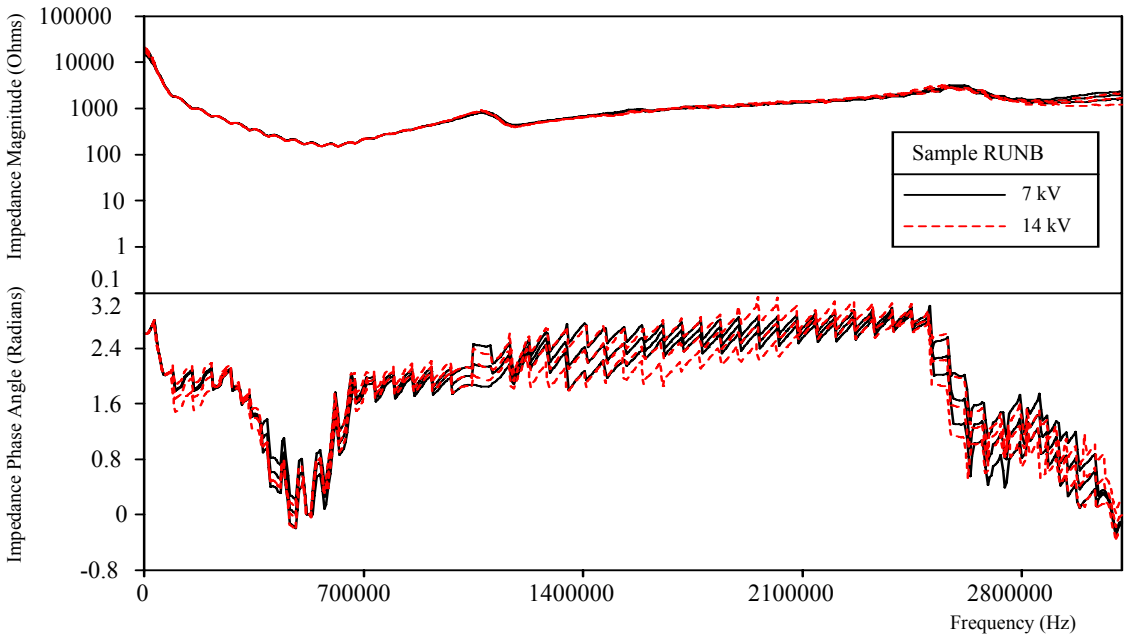

Figure F.69 Aged Cable Sample RUNB, L=23 m, D=4.6 mm CU, 5.59 mm HMWPE, Measured Impedance Magnitude and Phase Angle vs Frequency, Average and 95% Confidence Bounds

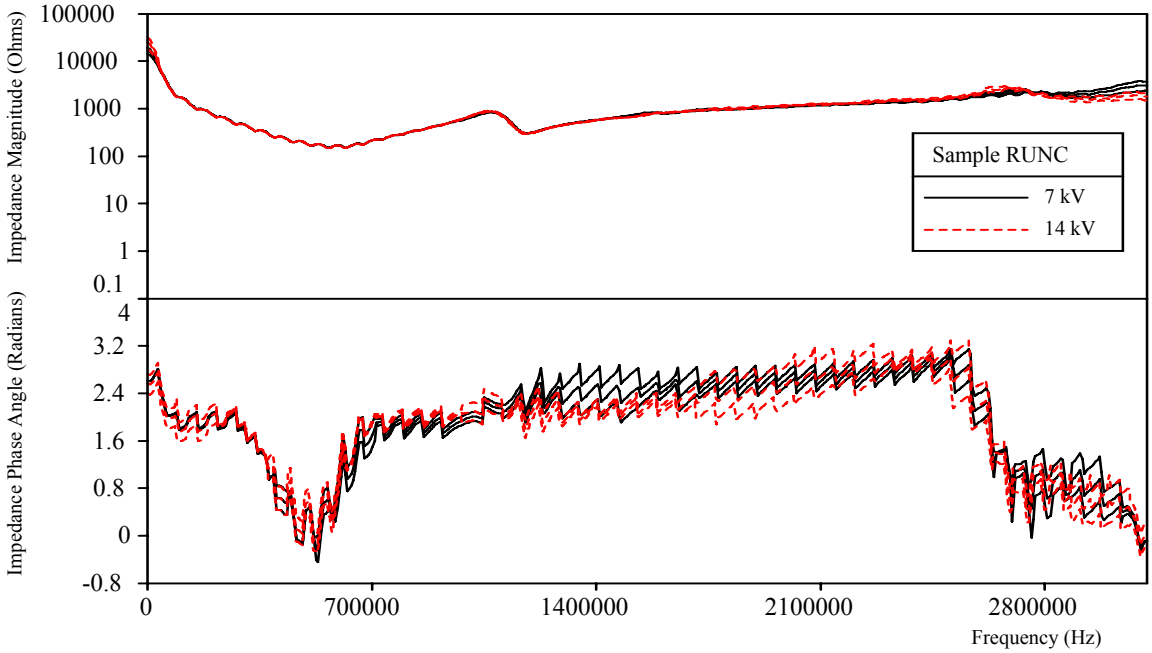

Figure F.70 Aged Cable Sample RUNC, L=23 m, D=4.6 mm CU, 5.59 mm HMWPE, Measured Impedance Magnitude and Phase Angle vs Frequency, Average and 95% Confidence Bounds

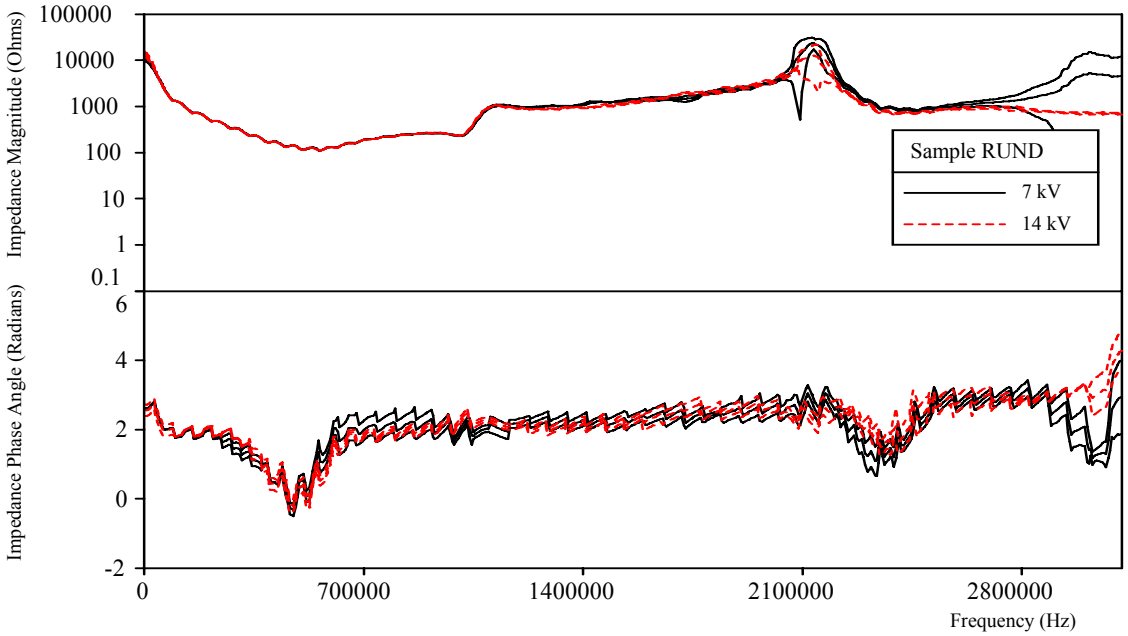

Figure F.71 Aged Cable Sample RUND, L=30 m, D=4.6 mm CU, 5.59 mm HMWPE, Measured Impedance Magnitude and Phase Angle vs Frequency, Average and 95% Confidence Bounds

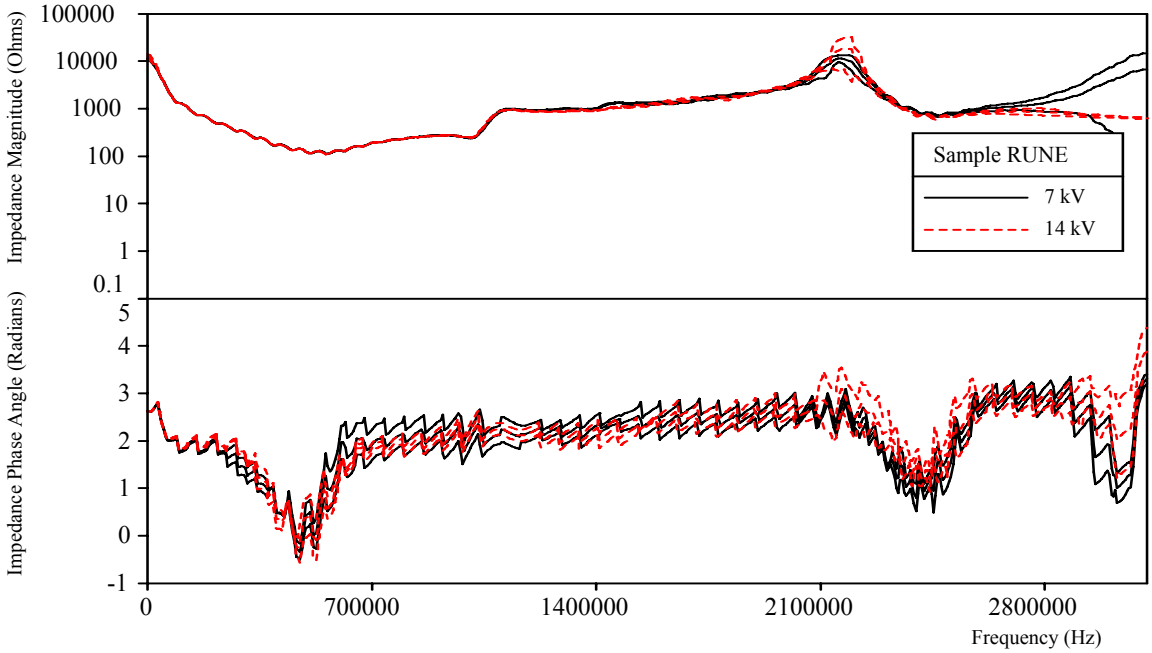

Figure F.72 Aged Cable Sample RUNE, L=30 m, D=4.6 mm CU, 5.59 mm HMWPE, Measured Impedance Magnitude and Phase Angle vs Frequency, Average and 95% Confidence Bounds

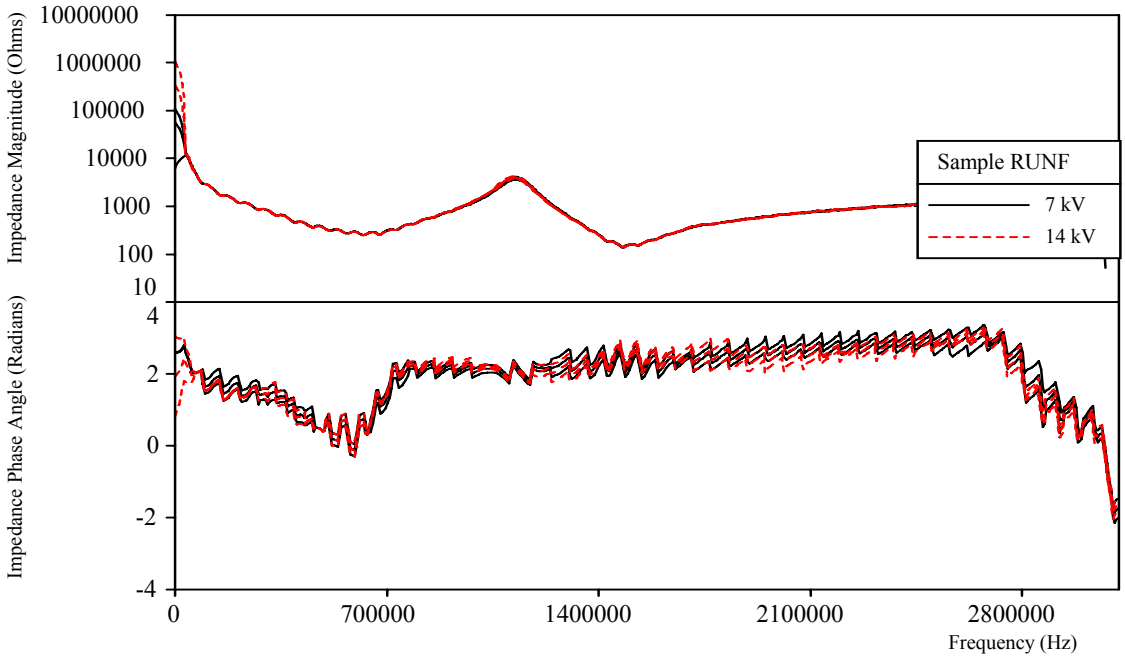

Figure F.73 Aged Cable Sample RUNF, L=15 m, D=4.6 mm CU, 5.59 mm HMWPE, Measured Impedance Magnitude and Phase Angle vs Frequency, Average and 95% Confidence Bounds

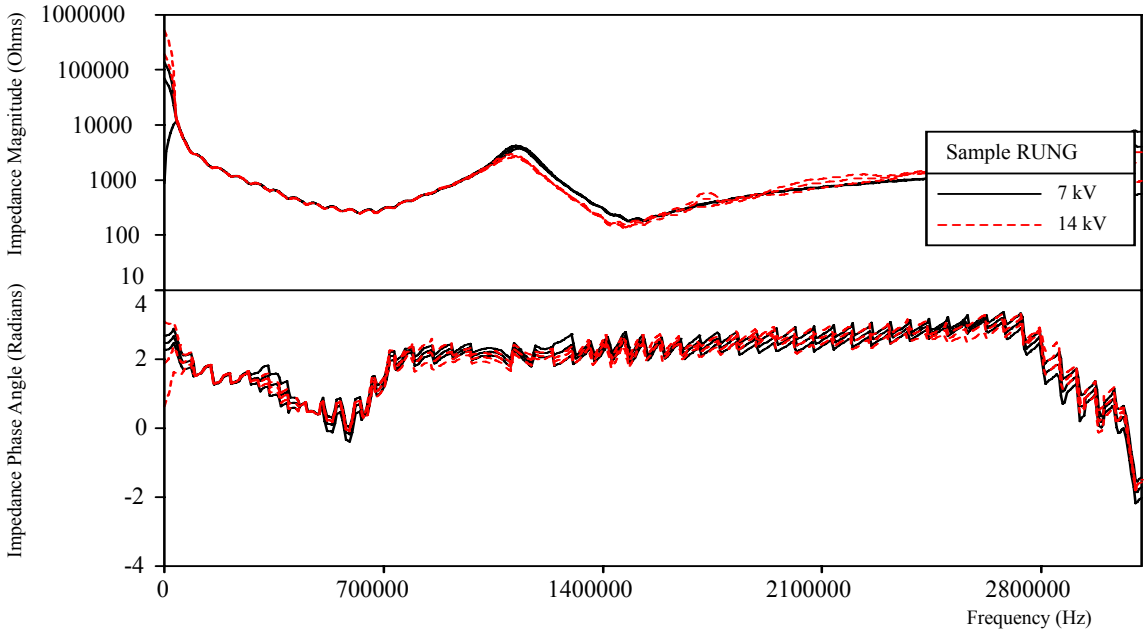

Figure F.74 Aged Cable Sample RUNG, L=15 m, D=4.6 mm CU, 5.59 mm HMWPE, Measured Impedance Magnitude and Phase Angle vs Frequency, Average and 95% Confidence Bounds

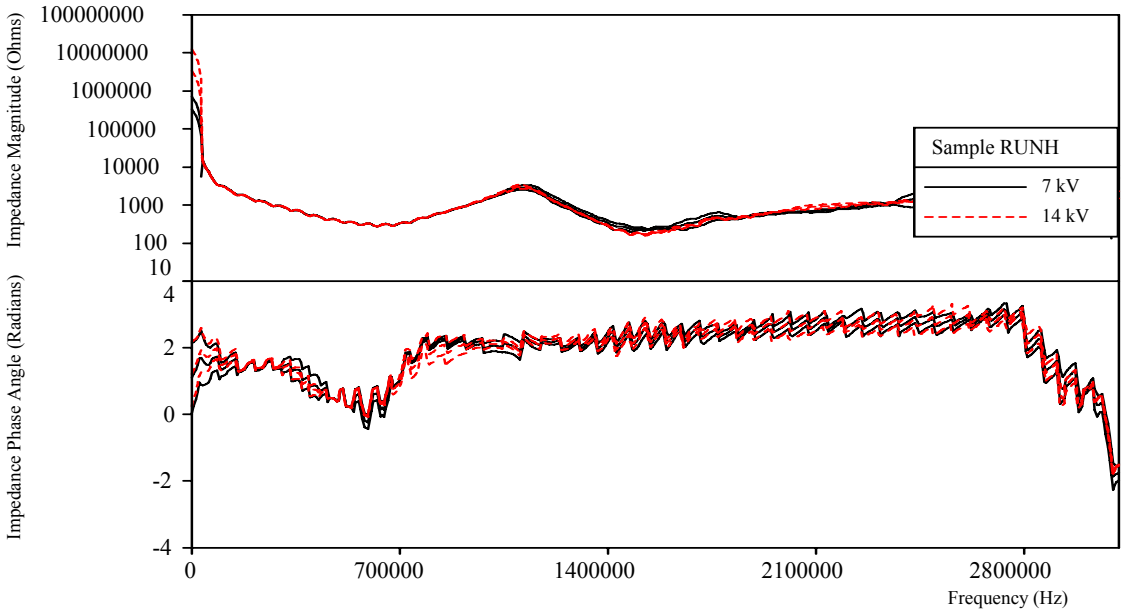

Figure F.75 Aged Cable Sample RUNH, L=15 m, D=4.6 mm CU, 5.59 mm HMWPE, Measured Impedance Magnitude and Phase Angle vs Frequency, Average and 95% Confidence Bounds

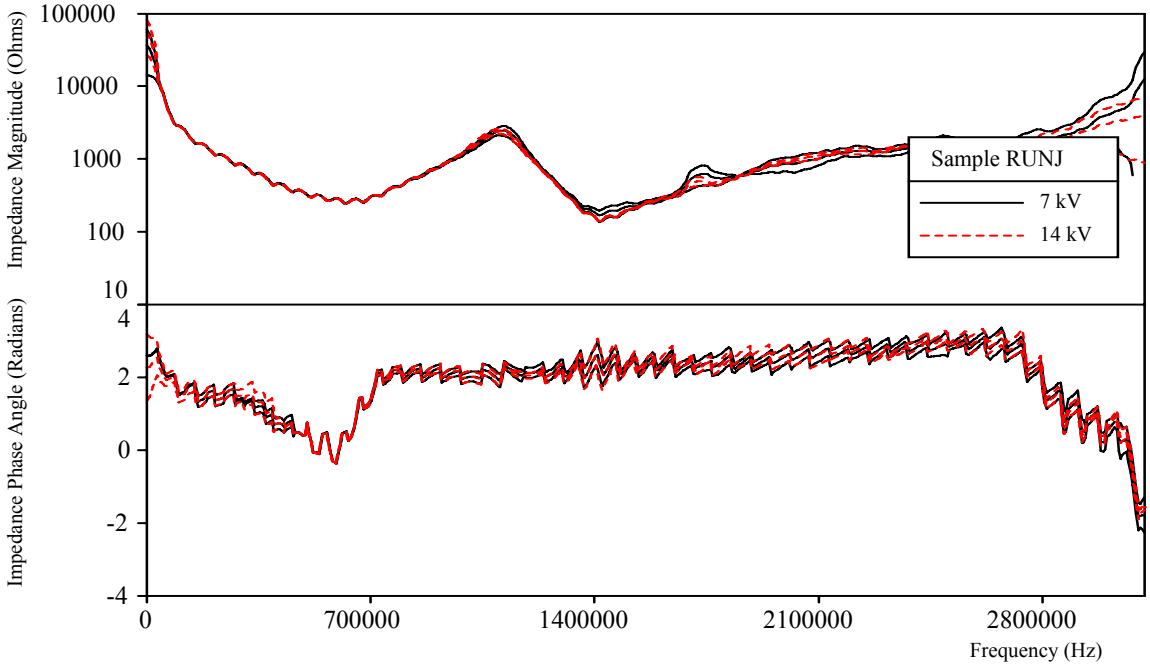

Figure F.76 Aged Cable Sample RUNJ, L=15 m, D=4.6 mm CU, 5.59 mm HMWPE, Measured Impedance Magnitude and Phase Angle vs Frequency, Average and 95% Confidence Bounds

APPENDIX G

SUMMARY OF CABLE IDENTIFICATION INFORMATION AND DIAGNOSTIC TEST MEASUREMENTS AND RESULTS OF CABLE PHYSICAL MEASUREMENTS

Table G. 1

Cable Identification Information and Diagnostic Test Measurements

State	Vintage	Mfg	Length	Size OD	Conductor	Insulation	Thickness	Defect Site	Neutrals	ID	Date	Time Started	Comments
New	1997	Pirelli	100 m	28.4 mm	Al	XLPE	4.45 mm	1/2	New	SRA	4/6/2004	11:42	Good, Drill 1/2, 3/4, Wire, shorted to conductor
New	1997	Pirelli	100 m	28.4 mm	Al	XLPE	4.45 mm	1/2	New	SRB	4/6/2004	13:51	Good, Drill 1/2, 3/4, Wire, shorted to conductor
New	1997	Pirelli	100 m	28.4 mm	Al	XLPE	4.45 mm	1/2	New	SRC	4/6/2004	14:18	Good, Drill 1/2, 3/4, Wire, shorted to conductor
New	1997	Pirelli	100 m	28.4 mm	Al	XLPE	4.45 mm	1/2	New	SRD	4/6/2004	14:39	Good, Drill 1/2, 3/4, Wire, shorted to conductor
New	1997	Pirelli	100 m	28.4 mm	Al	XLPE	4.45 mm	1/2	New	SRE	4/6/2004	14:56	Good, Drill 1/2, 3/4, Wire, shorted to conductor
New	1997	Pirelli	100 m	28.4 mm	Al	XLPE	4.45 mm	1/2	New	SRF	4/7/2004	10:17	Good, Drill 1/2, 3/4, Wire, shorted to conductor
New	1997	Pirelli	100 m	28.4 mm	Al	XLPE	4.45 mm	1/2	New	SRG	4/7/2004	10:40	Good, Drill 1/2, 3/4, Wire, shorted to conductor
New	1997	Pirelli	100 m	28.4 mm	Al	XLPE	4.45 mm	1/2	New	SRX	4/8/2004	13:59	Good, Drill 1/2, 3/4, Wire, shorted to conductor
New	1997	Pirelli	100 m	28.4 mm	Al	XLPE	4.45 mm	1/2	New	SRY	4/8/2004	14:14	Good, Drill 1/2, 3/4, Wire, shorted to conductor
New	1997	Pirelli	100 m	28.4 mm	Al	XLPE	4.45 mm	1/2	New	SRX	4/12/2004	9:41	Good, Drill 1/2, 3/4, Wire, shorted to conductor
New	1997	Pirelli	100 m	28.4 mm	Al	XLPE	4.45 mm	1/2	New	SRY	4/12/2004	10:05	Good, Drill 1/2, 3/4, Wire, shorted to conductor
New	1997	Pirelli	100 m	28.4 mm	Al	XLPE	4.45 mm	1/2	New	SRZ	4/12/2004	10:25	Good, Drill 1/2, 3/4, Wire, shorted to conductor
New	1997	Pirelli	100 m	28.4 mm	Al	XLPE	4.45 mm	1/2	New	SRH	4/7/2004	10:59	Good, Neutrals 3/4, 1/2, 1/4, none, Drill 1/2, 3/4, Wire, shorted to conductor

Table G. 1 Continued

State	Vintage	Mfg	Length	Size OD	Conductor	Insulation	Thickness	Defect Site	Neutrals	ID	Date	Time Started	Comments
New	1997	Pirelli	100 m	28.4 mm	Al	XLPE	4.45 mm	1/2	New	SRV	4/8/2004	13:01	Good, Neutrals 3/4, 1/2, 1/4, none, Drill 1/2, 3/4, Wire, shorted to conductor
New	1997	Pirelli	100 m	28.4 mm	Al	XLPE	4.45 mm	1/2	New	SRW	4/8/2004	13:29	Good, Neutrals 3/4, 1/2, 1/4, none, Drill 1/2, 3/4, Wire, shorted to conductor
New	1997	Pirelli	100 m	28.4 mm	Al	XLPE	4.45 mm	1/4	New	SRJ	4/7/2004	12:59	Good, Drill 1/2, 3/4, Wire, shorted to conductor
New	1997	Pirelli	100 m	28.4 mm	Al	XLPE	4.45 mm	1/4	New	SRK	4/7/2004	13:16	Good, Drill 1/2, 3/4, Wire, shorted to conductor
New	1997	Pirelli	100 m	28.4 mm	Al	XLPE	4.45 mm	1/4	New	SRL	4/7/2004	13:31	Good, Drill 1/2, 3/4, Wire, shorted to conductor
New	1997	Pirelli	100 m	28.4 mm	Al	XLPE	4.45 mm	1/4	New	SRM	4/7/2004	13:57	Good, Neutrals 3/4, 1/2, 1/4, none, Drill 1/2, 3/4, Wire, shorted to conductor
New	1997	Pirelli	100 m	28.4 mm	Al	XLPE	4.45 mm	1/4	New	SRN	4/7/2004	14:20	Good, Neutrals 3/4, 1/2, 1/4, none, Drill 1/2, 3/4, Wire, shorted to conductor
New	1997	Pirelli	100 m	28.4 mm	Al	XLPE	4.45 mm	1/4	New	SRO	4/7/2004	14:45	Good, Neutrals 3/4, 1/2, 1/4, none, Drill 1/2, 3/4, Wire, shorted to conductor
New	1997	Pirelli	100 m	28.4 mm	Al	XLPE	4.45 mm	3/4	New	SRP	4/8/2004	9:18	Good, Drill 1/2, 3/4, Wire, shorted to conductor
New	1997	Pirelli	100 m	28.4 mm	Al	XLPE	4.45 mm	3/4	New	SRQ	4/8/2004	9:38	Good, Drill 1/2, 3/4, Wire, shorted to conductor
New	1997	Pirelli	100 m	28.4 mm	Al	XLPE	4.45 mm	3/4	New	SRR	4/8/2004	9:56	Good, Drill 1/2, 3/4, Wire, shorted to conductor

Table G. 1 Continued

State	Vintage	Mfg	Length	Size OD	Conductor	Insulation	Thickness	Defect Site	Neutrals	ID	Date	Time Started	Comments
New	1997	Pirelli	100 m	28.4 mm	Al	XLPE	4.45 mm	3/4	New	SRS	4/8/2004	10:14	Good, Neutrals 3/4, 1/2, 1/4, none, Drill 1/2, 3/4, Wire, shorted to conductor
New	1997	Pirelli	100 m	28.4 mm	Al	XLPE	4.45 mm	3/4	New	SRT	4/8/2004	10:48	Good, Neutrals 3/4, 1/2, 1/4, none, Drill 1/2, 3/4, Wire, shorted to conductor
New	1997	Pirelli	100 m	28.4 mm	Al	XLPE	4.45 mm	3/4	New	SRU	4/8/2004	1233	Good, Neutrals 3/4, 1/2, 1/4, none, Drill 1/2, 3/4, Wire, shorted to conductor
New	1997	Pirelli	60 m	10.3 mm	Al	XLPE	4.45 mm	1/2	New	CWA	4/12/2004	10:47	Good, Drill 1/2, 3/4, Wire, shorted to conductor
New	1997	Pirelli	60 m	10.3 mm	Al	XLPE	4.45 mm	1/2	New	CWB	4/12/2004	12:05	Good, Drill 1/2, 3/4, Wire, shorted to conductor
New	1997	Pirelli	60 m	10.3 mm	Al	XLPE	4.45 mm	1/2	New	CWC	4/12/2004	12:17	Good, Neutrals 1/2, none, Drill 1/2, 3/4, Wire, shorted to conductor
New	1997	Pirelli	100 m	10.3 mm	Al	XLPE	4.45 mm	1/2	New	CWD	4/12/2004	12:49	Good, Drill 1/2, 3/4, Wire, shorted to conductor
New	1997	Pirelli	100 m	10.3 mm	Al	XLPE	4.45 mm	1/2	New	CWE	4/12/2004	13:06	Good, Drill 1/2, 3/4, Wire, shorted to conductor
New	1997	Pirelli	100 m	10.3 mm	Al	XLPE	4.45 mm	1/2	New	CWN	4/14/2004	10:37	Good, Drill 1/2, 3/4, Wire, shorted to conductor
New	1997	Pirelli	100 m	10.3 mm	Al	XLPE	4.45 mm	1/2	New	CWO	4/14/2004	10:54	Good, Drill 1/2, 3/4, Wire, shorted to conductor
New	1997	Pirelli	100 m	10.3 mm	Al	XLPE	4.45 mm	1/2	New	CWF	4/12/2004	13:22	Good, Neutrals 1/2, none, Drill 1/2, 3/4, Wire, shorted to conductor
New	1997	Pirelli	100 m	10.3 mm	Al	XLPE	4.45 mm	1/2	New	CWP	4/14/2004	12:06	Good, Neutrals 1/2, none, Drill 1/2, 3/4, Wire, shorted to conductor

Table G. 1 Continued

State	Vintage	Mfg	Length	Size OD	Conductor	Insulation	Thickness	Defect Site	Neutrals	ID	Date	Time Started	Comments
New	1997	Pirelli	100 m	10.3 mm	Al	XLPE	4.45 mm	3/4	New	CWG	4/14/2004	8:48	Good both Hipot & Thump, Drill 1/2, 3/4, Wire, shorted to conductor
New	1997	Pirelli	100 m	10.3 mm	Al	XLPE	4.45 mm	3/4	New	CWH	4/14/2004	9:11	Good, Drill 1/2, 3/4, Wire, shorted to conductor
New	1997	Pirelli	100 m	10.3 mm	Al	XLPE	4.45 mm	3/4	New	CWJ	4/14/2004	9:30	Good, Neutrals 1/2, none, Drill 1/2, 3/4, Wire, shorted to conductor
New	1997	Pirelli	100 m	10.3 mm	Al	XLPE	4.45 mm	1/4	New	CWK	4/14/2004	9:53	Good, Drill 1/2, 3/4, Wire, shorted to conductor
New	1997	Pirelli	100 m	10.3 mm	Al	XLPE	4.45 mm	1/4	New	CWL	4/14/2004	10:05	Good, Drill 1/2, 3/4, Wire, shorted to conductor
New	1997	Pirelli	100 m	10.3 mm	Al	XLPE	4.45 mm	1/4	New	CWM	4/14/2004	10:17	Good, Neutrals 1/2, none, Drill 1/2, 3/4, Wire, shorted to conductor
Aged	1971	General	30 m	13 mm	CU	HMWPE	5.59 mm		Ok	CIRA	4/14/2004	12:39	7 kV then 14 kV
Aged	1971	General	30 m	13 mm	CU	HMWPE	5.59 mm		Ok	CIRB	4/14/2004	12:45	7 kV then 14 kV
Aged	1971	General	30 m	13 mm	CU	HMWPE	5.59 mm		Ok	CIRC	4/14/2004	12:48	7 kV then 14 kV
Aged	1971	General	30 m	13 mm	CU	HMWPE	5.59 mm		Ok	CIRD	4/14/2004	12:56	7 kV then 14 kV
Aged	1971	General	30 m	13 mm	CU	HMWPE	5.59 mm		Ok	CIRE	4/14/2004	13:02	7 kV then 14 kV
Aged	1971	General	30 m	13 mm	CU	HMWPE	5.59 mm		Ok	CIRF	4/14/2004	13:05	7 kV then 14 kV
Aged	1978	Pirelli	30 m	10.3 mm	Al	XLPE	4.45 mm		Corroded	CIRG	4/14/2004	13:12	7 kV then 14 kV
Aged	1978	Pirelli	30 m	10.3 mm	Al	XLPE	4.45 mm		Corroded	CIRH	4/14/2004	13:17	7 kV then 14 kV
Aged	1978	Pirelli	30 m	10.3 mm	Al	XLPE	4.45 mm		Corroded	CIRJ	4/14/2004	13:22	7 kV then 14 kV
Aged	1978	Okonite	30 m	10.3 mm	Al	XLPE	4.45 mm		Ok	CIRO	4/14/2004	13:48	7 kV then 14 kV
Aged	1978	Okonite	30 m	10.3 mm	Al	XLPE	4.45 mm		Ok	CIRP	4/14/2004	13:56	7 kV then 14 kV
Aged	1978	Okonite	30 m	10.3 mm	Al	XLPE	4.45 mm		Ok	CIRQ	4/14/2004	13:59	7 kV then 14 kV
Aged	1978	Okonite	30 m	10.3 mm	Al	XLPE	4.45 mm		Open	CIRR	4/14/2004	14:08	7 kV then 14 kV
Aged	1978	Okonite	30 m	10.3 mm	Al	XLPE	4.45 mm		Open	CIRS	4/14/2004	14:11	7 kV then 14 kV

Table G. 1 Continued

State	Vintage	Mfg	Length	Size OD	Conductor	Insulation	Thickness	Defect Site	Neutrals	ID	Date	Time Started	Comments
Aged	1978	Okonite	30 m	10.3 mm	Al	XLPE	4.45 mm		Open	CIRT	4/14/2004	14:14	7 kV then 14 kV
Aged	1978	Okonite	30 m	10.3 mm	Al	XLPE	4.45 mm		Corroded	CIRU	4/14/2004	14:24	7 kV then 14 kV
Aged	1978	Okonite	30 m	10.3 mm	Al	XLPE	4.45 mm		Corroded	CIRV	4/14/2004	14:27	7 kV then 14 kV
Aged	1978	Okonite	30 m	10.3 mm	Al	XLPE	4.45 mm		Corroded	CIRW	4/14/2004	14:30	7 kV then 14 kV
Aged	1978	Okonite	30 m	10.3 mm	Al	XLPE	4.45 mm		Corroded	CIRX	4/15/2004	8:45	7 kV then 14 kV
Aged	1978	Okonite	30 m	10.3 mm	Al	XLPE	4.45 mm		Corroded	CIRY	4/15/2004	8:48	7 kV then 14 kV
Aged	1978	Okonite	30 m	10.3 mm	Al	XLPE	4.45 mm		Corroded	CIRZ	4/15/2004	8:51	7 kV then 14 kV
Aged	1974	General	30 m	4.6 mm	CU	HMWPE	5.59 mm		Corroded	CIRK	4/14/2004	13:28	7 kV then 14 kV
Aged	1974	General	30 m	4.6 mm	CU	HMWPE	5.59 mm		Corroded	CIRL	4/14/2004	13:35	7 kV then 14 kV
Aged	1974	General	30 m	4.6 mm	CU	HMWPE	5.59 mm		Ok	CIRM	4/14/2004	13:40	7 kV then 14 kV
Aged	1974	General	30 m	4.6 mm	CU	HMWPE	5.59 mm		Ok	CIRN	4/14/2004	13:45	7 kV then 14 kV
Aged	1974	General	30 m	4.6 mm	CU	HMWPE	5.59 mm		Corroded	RUND	4/15/2004	9:14	7 kV then 14 kV
Aged	1974	General	30 m	4.6 mm	CU	HMWPE	5.59 mm		Corroded	RUNE	4/15/2004	9:18	7 kV then 14 kV
Aged	1974	General	23 m	4.6 mm	CU	HMWPE	5.59 mm		Corroded	RUNA	4/15/2004	8:59	7 kV then 14 kV
Aged	1974	General	23 m	4.6 mm	CU	HMWPE	5.59 mm		Corroded	RUNB	4/15/2004	9:05	7 kV then 14 kV
Aged	1974	General	23 m	4.6 mm	CU	HMWPE	5.59 mm		Corroded	RUNC	4/15/2004	9:09	7 kV then 14 kV
Aged	1974	General	15 m	4.6 mm	CU	HMWPE	5.59 mm		Corroded	RUNF	4/15/2004	9:28	7 kV then 14 kV
Aged	1974	General	15 m	4.6 mm	CU	HMWPE	5.59 mm		Corroded	RUNG	4/15/2004	9:33	7 kV then 14 kV
Aged	1974	General	15 m	4.6 mm	CU	HMWPE	5.59 mm		Corroded	RUNH	4/15/2004	9:39	7 kV then 14 kV
Aged	1974	General	15 m	4.6 mm	CU	HMWPE	5.59 mm		Corroded	RUNJ	4/15/2004	9:44	7 kV then 14 kV

Table G. 2

Physical Tests

Vintage	Mfg	Size OD (mm)	Conductor Strand(mm)		Insulation Dia.(mm)		ID	No. of Water Trees Detected				Vented Trees (mm)
		(mm)	Max	Min	Max	Min		Bow Tie Size (mm)				
								0-0.62	0.63-1.25	1.26-1.89	1.9-2.6	
1997	Pirelli	28.4	3.26	3.17	39.42	39.37	SRA					
1997	Pirelli	28.4	3.26	3.23	39.62	39.37	SRB					
1997	Pirelli	28.4	3.25	3.22	39.62	39.50	SRC					
1997	Pirelli	28.4	3.25	3.21	39.62	39.42	SRD					
1997	Pirelli	28.4	3.25	3.20	39.62	39.50	SRE					
1997	Pirelli	28.4	3.25	3.17	39.37	39.37	SRF					
1997	Pirelli	28.4	3.25	3.24	39.37	39.24	SRG					
1997	Pirelli	28.4	3.25	3.23	39.50	39.50	SRH					
1997	Pirelli	28.4	3.25	3.24	39.62	39.50	SRJ					
1997	Pirelli	28.4	3.26	3.21	39.62	39.37	SRK					
1997	Pirelli	28.4	3.25	3.23	39.62	39.50	SRL					
1997	Pirelli	28.4	3.27	3.25	39.62	39.37	SRM					
1997	Pirelli	28.4	3.25	3.24	39.88	39.62	SRN					
1997	Pirelli	28.4	3.25	3.20	39.88	39.62	SRO					
1997	Pirelli	28.4	3.25	3.21	39.62	39.37	SRP					
1997	Pirelli	28.4	3.25	3.24	39.62	39.37	SRQ					
1997	Pirelli	28.4	3.25	3.17	39.67	39.37	SRR					
1997	Pirelli	28.4	3.25	3.23	39.62	39.37	SRS					
1997	Pirelli	28.4	3.27	3.25	39.62	39.37	SRT					
1997	Pirelli	28.4	3.25	3.23	39.62	39.37	SRU					
1997	Pirelli	28.4	3.27	3.17	39.62	39.50	SRV					
1997	Pirelli	28.4	3.25	3.23	39.62	39.50	SRW					
1997	Pirelli	28.4	3.25	3.23	39.37	39.12	SRX1					
1997	Pirelli	28.4	3.25	3.24	39.75	39.37	SRX2					
1997	Pirelli	28.4	3.26	3.23	39.37	39.12	SRY1					
1997	Pirelli	28.4	3.25	3.20	39.62	39.50	SRY2					
1997	Pirelli	28.4	3.26	3.23	39.50	39.37	SRZ					
1997	Pirelli	10.3	2.13	2.06	20.57	20.45	CWA					
1997	Pirelli	10.3	2.12	2.06	20.70	20.57	CWB					
1997	Pirelli	10.3	2.07	2.05	20.57	20.45	CWC					
1997	Pirelli	10.3	2.09	2.06	20.57	20.57	CWD					
1997	Pirelli	10.3	2.13	2.07	20.70	20.45	CWE					
1997	Pirelli	10.3	2.13	2.03	20.57	20.32	CWF					
1997	Pirelli	10.3	2.14	2.06	20.57	20.45	CWG					
1997	Pirelli	10.3	2.13	2.08	20.45	20.45	CWH					

Table G. 2 Continued

Vintage	Mfg	Size OD (mm)	Conductor Strand(mm)		Insulation Dia.(mm)		ID	No. of Water Trees Detected				Vented Trees (mm)
		(mm)	Max	Min	Max	Min		Bow Tie Size (mm)				
								0-0.62	0.63-1.25	1.26-1.89	1.9-2.6	
1997	Pirelli	10.3	2.13	2.06	20.57	20.45	CWJ					
1997	Pirelli	10.3	2.13	2.07	20.70	20.57	CWK					
1997	Pirelli	10.3	2.13	2.04	20.57	20.45	CWL					
1997	Pirelli	10.3	2.13	2.06	20.45	20.45	CWM					
1997	Pirelli	10.3	2.13	2.06	20.57	20.45	CWN					
1997	Pirelli	10.3	2.13	2.04	20.57	20.57	CWO					
1997	Pirelli	10.3	2.13	2.06	20.45	20.45	CWP					
1971	General	13	2.69	2.68	26.16	25.91	CIRA	>200	9	6	1	1, .63-1.25
1971	General	13	2.67	2.59	26.29	26.16	CIRB	>200	6	1		2, 1.26-1.89
1971	General	13	2.71	2.62	26.16	25.91	CIRC	>200	5	1	1	
1971	General	13	2.67	2.62	26.16	26.03	CIRD	>200	5	2		1, 1.26-1.89
1971	General	13	2.67	2.62	26.16	25.98	CIRE	>200	1	1		
1971	General	13	2.67	2.62	26.16	26.03	CIRF	>200				2, 1.26-1.89
1978	Pirelli	10.3	2.13	1.98	20.70	20.70	CIRG	>200	8			
1978	Pirelli	10.3	2.16	2.02	20.32	20.32	CIRH	>200	11	4	1	2, .63-1.25
1978	Pirelli	10.3	2.13	1.98	20.70	20.57	CIRJ	>200	8			1, .63-1.25
1978	Okonite	10.3	2.15	2.07	20.57	20.45	CIRO	44				
1978	Okonite	10.3	2.12	2.08	20.57	20.45	CIRP	15				2, 0-.62
1978	Okonite	10.3	2.14	2.10	20.32	20.19	CIRQ	11	1	1		
1978	Okonite	10.3	2.12	2.08	20.32	20.32	CIRR	25	1			
1978	Okonite	10.3	2.13	2.07	20.57	20.45	CIRS	34				
1978	Okonite	10.3	2.11	2.08	20.57	20.32	CIRT	35	2			1, .63-1.25
1978	Okonite	10.3	2.11	2.09	20.70	20.57	CIRU	111	8			
1978	Okonite	10.3	2.12	2.10	20.32	20.32	CIRV	80	6			
1978	Okonite	10.3	2.11	2.08	20.45	20.32	CIRW	71	3			
1978	Okonite	10.3	2.13	2.08	20.45	20.32	CIRX	>200	12			3, 0-.62
1978	Okonite	10.3	2.13	2.12	20.57	20.45	CIRY	>200	5			2, .63-1.25
1978	Okonite	10.3	2.14	2.10	20.45	20.19	CIRZ	186	11	1		
1974	General	4.6	1.93	1.90	18.16	18.03	CIRK	>200	7	1		
1974	General	4.6	1.90	1.83	18.29	18.29	CIRL	76	8			1, 0-.62
1974	General	4.6	1.93	1.92	18.29	18.03	CIRM	>200	12			
1974	General	4.6	1.93	1.92	18.41	18.29	CIRN	134				2, 0-.62
1974	General	4.6	1.93	1.92	18.29	18.16	RUND	>200	4			1, .63-1.25
1974	General	4.6	1.93	1.92	18.16	18.03	RUNE	>200	4	1	1	2, 0-.62
1974	General	4.6	1.94	1.92	18.41	18.29	RUNA	>200	5			
1974	General	4.6	1.91	1.89	18.29	18.16	RUNB	>200	5			
1974	General	4.6	1.93	1.93	18.29	18.29	RUNC	>200	1		1	
1974	General	4.6	1.93	1.93	18.16	18.16	RUNF	10	1			
1974	General	4.6	1.85	1.80	18.41	18.41	RUNG	>200	1	1		2, .63-1.25
1974	General	4.6	1.94	1.93	18.41	18.29	RUNH	>200	1			
1974	General	4.6	1.94	1.93	18.29	18.16	RUNJ	>200				2, .63-1.25